Experimental Study and Thermodynamic Assessment of Multicomponent Salt Systems

Experimentelle Untersuchung und thermodynamische Bewertung von Mehrkomponenten-Salzsystemen

Von der Fakultät für Maschinenwesen der Rheinisch-Westfälischen Technischen Hochschule Aachen zur Erlangung des akademischen Grades eines Doktors der Naturwissenschaften genehmigte Dissertation

vorgelegt von

Amedeo Morsa

Berichter: Priv.-Doz. Dr. rer. nat. Michael Müller
Univ.-Prof. Dr.-Ing. Robert Pitz-Paal

Tag der mündlichen Prüfung: 23.06.2026

Diese Dissertation ist auf den Internetseiten der Universitätsbibliothek online verfügbar.

List of publications

Morsa, A., Yazhenskikh, E., Ziegner, M., Wessel, E., Jacob, R. D., Müller, M., & Sergeev, D. (2025). Experimental study and thermodynamic assessment of the $MgSO_4$-$CaSO_4$ system. *Calphad*, *90*, 102855.

Morsa, A., Yazhenskikh, E., Jacob, R. D., Müller, M., & Sergeev, D. (2025). Thermodynamics of the $MgCl_2$-$MgSO_4$ and $CaCl_2$-$CaSO_4$ systems. *Calphad*, *91*, 102888.

Morsa, A., Yazhenskikh, E., Jacob, R., Müller, M., & Sergeev, D. (2026). Experimental study and thermodynamic assessment of the reciprocal system Mg^{2+}, Ca^{2+} // Cl^-, SO_4^{2-}. *The Journal of Chemical Thermodynamics, 218,* 107681.

Morsa, A., Yazhenskikh, E., Ziegner, M., Keuter, P., Müller, M., & Sergeev, D. (2026). Experimental study and thermodynamic assessment of the reciprocal system Na^+, Ca^{2+} // Cl^-, SO_4^{2-}. *Thermochimica Acta, 761,* 180317.

Morsa, A., Yazhenskikh, E., Keuter, P., Müller, M., & Sergeev, D. Thermodynamic assessment and experimental validation of the Na^+, K^+, Mg^{2+} // Cl^-, SO_4^{2-} system. Submitted to *The Journal of Chemical Thermodynamics* and under review.

Morsa, A., Yazhenskikh, E., Keuter, P., Müller, M., & Sergeev, D. Thermodynamics of the K^+, Ca^{2+} // Cl^-, SO_4^{2-} system in the framework of the complex systems K^+, Mg^{2+}, Ca^{2+} // Cl^-, SO_4^{2-} and Na^+, K^+, Ca^{2+} // Cl^-, SO_4^{2-}. To be submitted.

Abstract

In this work, the multicomponent system Na^+, K^+, Mg^{2+}, Ca^{2+} // Cl^-, SO_4^{2-}, which is of particular interest in the field of thermal energy storage, has been experimentally investigated and thermodynamically assessed with the aim of developing a robust and internally consistent thermodynamic database. This has been achieved by integrating newly acquired experimental data with reliable information available in the literature. A stepwise approach was adopted, starting from the reassessment of pure compounds, where necessary, and extending to the binary and quasi-binary subsystems forming the basis of the complex multicomponent system under study.

Through a combination of thermal, calorimetric, and crystallographic analyses coupled with thermodynamic assessment, the phase diagrams of several subsystems have been constructed, and their thermodynamic properties calculated. Particular attention was given to compositions with high sulphate content, which were often neglected due to their tendency to decompose at elevated temperatures. This work addresses such limitations by proposing effective experimental procedures for measuring phase transitions and thermodynamic properties under these challenging conditions - thereby fulfilling one of the broader goals of the research: not only to screen potential phase change materials (PCMs), but also to identify and validate reliable methodologies for characterising their thermodynamic behaviour.

In the framework of the multicomponent system, and specifically among the six reciprocal systems experimentally investigated in this work, the Mg^{2+}, Ca^{2+} // Cl^-, SO_4^{2-} system represents a major contribution, as it is provided here with a comprehensive thermodynamic description for the first time, supported by an extensive experimental campaign. Within this framework, a significant outcome has been the reassessment of the binary systems $MgSO_4$-$CaSO_4$ and Na_2SO_4-$CaSO_4$. Based on new experimental evidence, these systems have been redefined in terms of phase equilibria, leading to a substantial improvement in their thermodynamic description. More broadly, the phase diagrams of subsystems within the various reciprocal systems that compose the multicomponent matrix have been established, and the thermodynamic properties of eutectic or low-melting mixtures within the most thermodynamically favourable sections - those potentially suitable as PCMs - have been experimentally measured.

By incorporating these results into FactSage software and performing thermodynamic optimisation of key Gibbs energy functions, a robust and comprehensive thermodynamic database has been developed. This database enhances the predictive reliability of thermodynamic properties not only for the investigated multicomponent system, but also for other systems in which the same compounds may play a role.

Kurzfassung

In dieser Arbeit wurde das Mehrkomponentensystem Na^+, K^+, Mg^{2+}, Ca^{2+} // Cl^-, SO_4^{2-}, das im Bereich der thermischen Energiespeicherung von besonderem Interesse ist, experimentell untersucht und thermodynamisch bewertet, mit dem Ziel, eine robuste und in sich konsistente thermodynamische Datenbank zu entwickeln. Dies wurde durch die Integration neu gewonnener experimenteller Daten mit zuverlässigen Informationen aus der Literatur erreicht. Es wurde ein schrittweiser Ansatz gewählt, der bei Bedarf mit der Neubewertung reiner Verbindungen begann und sich auf die binären und quasi-binären Teilsysteme ausweitete, die die Grundlage des untersuchten komplexen Mehrkomponentensystems bilden.

Durch eine Kombination aus thermischen, kalorimetrischen und kristallographischen Analysen in Verbindung mit der thermodynamischen Modellierung wurden die Phasendiagramme mehrerer Teilsysteme erstellt und ihre thermodynamischen Eigenschaften berechnet. Besondere Aufmerksamkeit wurde Zusammensetzungen mit hohem Sulfatgehalt gewidmet, die aufgrund ihrer Neigung zur Zersetzung bei erhöhten Temperaturen oft vernachlässigt wurden. Diese Arbeit adressiert solche Einschränkungen, indem sie effektive experimentelle Verfahren zur Messung von Phasenübergängen und thermodynamischen Eigenschaften unter diesen schwierigen Bedingungen vorschlägt - und damit eines der übergeordneten Ziele der Forschung erfüllt: nicht nur potenzielle Phasenwechselmaterialien (PCMs) zu screenen, sondern auch zuverlässige Methoden zur Charakterisierung ihres thermodynamischen Verhaltens zu identifizieren und zu validieren.

Im betrachteten Mehrkomponentensystem und insbesondere unter den sechs in dieser Arbeit experimentell untersuchten reziproken Systemen stellt das System Mg^{2+}, Ca^{2+} // Cl^-, SO_4^{2-} einen wichtigen Beitrag dar, da es hier erstmals eine umfassende thermodynamische Beschreibung erhält, die durch umfangreiche experimentelle Untersuchungen gestützt wird. In diesem Zusammenhang war die Neubewertung der binären Systeme $MgSO_4$-$CaSO_4$ und Na_2SO_4-$CaSO_4$ ein bedeutendes Ergebnis. Auf Grundlage neuer experimenteller Daten wurden die Phasengleichgewichte dieser Systeme neu bewertet und ihre thermodynamische Beschreibung deutlich verbessert. Zudem wurden die Phasendiagramme relevanter Teilsysteme erstellt und die thermodynamischen Eigenschaften eutektischer bzw. niedrigschmelzender, als PCM geeigneter Gemische experimentell bestimmt.

Durch die Einbindung dieser Ergebnisse in die FactSage-Software und die thermodynamische Optimierung wichtiger Gibbs-Energiefunktionen wurde eine robuste und umfassende thermodynamische Datenbank entwickelt. Diese Datenbank verbessert die Vorhersagegenauigkeit der thermodynamischen Eigenschaften nicht nur für das untersuchte Mehrkomponentensystem, sondern auch für andere Systeme, in denen dieselben Verbindungen eine Rolle spielen können.

Contents

List of publications I
Abstract II
Kurzfassung III
Contents IV
List of figures IX
List of tables XVIII
List of symbols and abbreviations XXI
1 Introduction 1
2 Literature review 4
2.1 Phase Change Materials in Thermal Energy Storage applications 4
2.2 Thermodynamics of salt systems 7
2.2.1 Pure salts 8
2.2.2 Binary systems within reciprocal systems 8
2.2.2.1 Mg^{2+}, Ca^{2+} // Cl^-, SO_4^{2-} system 8
2.2.2.1.1 $MgCl_2$-$CaCl_2$ 8
2.2.2.1.2 $MgSO_4$-$CaSO_4$ 9
2.2.2.1.3 $MgCl_2$-$MgSO_4$ 10
2.2.2.1.4 $CaCl_2$-$CaSO_4$ 11
2.2.2.1.5 $MgCl_2$-$CaSO_4$ 12
2.2.2.1.6 $CaCl_2$-$MgSO_4$ 12
2.2.2.2 Na^+, Mg^{2+} // Cl^-, SO_4^{2-} system 12
2.2.2.2.1 NaCl-$MgCl_2$ 13
2.2.2.2.2 Na_2SO_4-$MgSO_4$ 15
2.2.2.2.3 NaCl-Na_2SO_4 16
2.2.2.2.4 NaCl-$MgSO_4$ 17
2.2.2.2.5 $MgCl_2$-Na_2SO_4 18
2.2.2.3 Na^+, Ca^{2+} // Cl^-, SO_4^{2-} system 18
2.2.2.3.1 NaCl-$CaCl_2$ 19
2.2.2.3.2 Na_2SO_4-$CaSO_4$ 20
2.2.2.3.3 NaCl-$CaSO_4$ 22
2.2.2.3.4 $CaCl_2$-Na_2SO_4 23
2.2.2.4 K^+, Mg^{2+} // Cl^-, SO_4^{2-} system 24
2.2.2.4.1 KCl-$MgCl_2$ 25

2.2.2.4.2 K_2SO_4-$MgSO_4$ 26
2.2.2.4.3 KCl-K_2SO_4 27
2.2.2.4.4 KCl-$MgSO_4$ 27
2.2.2.4.5 $MgCl_2$-K_2SO_4 28
2.2.2.5 K^+, Ca^{2+} // Cl^-, SO_4^{2-} system 29
2.2.2.5.1 KCl-$CaCl_2$ 30
2.2.2.5.2 K_2SO_4-$CaSO_4$ 31
2.2.2.5.3 KCl-$CaSO_4$ 32
2.2.2.5.4 $CaCl_2$-K_2SO_4 33
2.2.2.6 Na^+, K^+ // Cl^-, SO_4^{2-} system 34
2.2.2.6.1 NaCl-KCl 35
2.2.2.6.2 Na_2SO_4-K_2SO_4 36
2.2.2.6.3 NaCl-K_2SO_4 37
2.2.2.6.4 KCl-Na_2SO_4 38
2.2.3 Ternary systems 39
2.2.3.1 NaCl-KCl-$MgCl_2$ 39
2.2.3.2 NaCl-KCl-$CaCl_2$ 40
2.2.3.3 NaCl-$MgCl_2$-$CaCl_2$ 41
2.2.3.4 KCl-$MgCl_2$-$CaCl_2$ 42
2.2.3.5 Na_2SO_4-K_2SO_4-$MgSO_4$ 43
2.2.3.6 Na_2SO_4-K_2SO_4-$CaSO_4$ 44
2.2.3.7 Na_2SO_4-$MgSO_4$-$CaSO_4$ 45
2.2.3.8 K_2SO_4-$MgSO_4$-$CaSO_4$ 46
3 Experimental 48
3.1 Samples 48
3.2 Instruments 49
3.2.1 Differential Thermal Analysis/Thermogravimetry (DTA/TG) 49
3.2.2 Differential Scanning Calorimetry (DSC) 51
3.2.2.1 Self-referencing calibration method (SRCM) 52
3.2.3 X-Ray Diffractometry/High Temperature X-Ray Diffractometry (HT-XRD) 55
3.2.4 Microanalysis by Electron Microscopy and Energy Dispersive X-ray Spectroscopy 56
4 Thermodynamic Modelling 58
4.1 Thermodynamic background 59
4.2 Pure compound phases 61
4.3 Solution phases 62
4.3.1 Liquid 63

4.3.2 Solid solutions 64
4.4 Assessment of Gibbs energy parameters 67
5 Experimental results 69
5.1 Mg^{2+}, Ca^{2+} // Cl^-, SO_4^{2-} system 70
5.1.1 $MgCl_2$ 71
5.1.2 $MgSO_4$ 72
5.1.2.1 Transition temperatures 72
5.1.2.2 Heat capacity and enthalpy increment 72
5.1.3 $CaSO_4$ 73
5.1.3.1 Transition temperatures 73
5.1.3.2 Heat capacity and enthalpy increment 74
5.1.4 $CaMg_2(SO_4)_3$ 75
5.1.4.1 Transition temperature 79
5.1.4.2 Heat capacity and enthalpy increment 81
5.1.5 $MgSO_4$-$CaSO_4$ 82
5.1.6 $CaMg(SO_4)_2$ 87
5.1.7 $MgCl_2$-$CaCl_2$ 90
5.1.7.1 Thermodynamic properties of the eutectic mixture 91
5.1.8 $MgCl_2$-$MgSO_4$ 92
5.1.8.1 Thermodynamic properties of the eutectic mixture 95
5.1.9 $CaCl_2$-$CaSO_4$ 96
5.1.9.1 Thermodynamic properties of the eutectic mixture 98
5.1.10 $MgCl_2$-$CaSO_4$ 99
5.1.10.1 Thermodynamic properties of the low-melting mixture 101
5.1.11 $CaCl_2$-$MgSO_4$ 102
5.1.12 $MgCl_2$-$CaMg_2(SO_4)_3$ 103
5.1.13 $CaCl_2$-$CaMg_2(SO_4)_3$ 105
5.2 Na^+, Mg^{2+} // Cl^-, SO_4^{2-} system 106
5.2.1 NaCl-$MgSO_4$ 106
5.2.1.1 Thermodynamic properties of the eutectic mixture 108
5.2.2 $MgCl_2$-Na_2SO_4 113
5.3 Na^+, Ca^{2+} // Cl^-, SO_4^{2-} system 114
5.3.1 Na_2SO_4-$CaSO_4$ 114
5.3.1.1 XRD/HT-XRD 114
5.3.1.1.1 RT-XRD 116
5.3.1.1.2 HT-XRD 119

5.3.1.2 DTA/DSC analysis 129
5.3.2 $NaCl-CaSO_4$ 133
5.3.2.1 Thermodynamic properties of the low-melting mixture 134
5.3.3 $CaCl_2-Na_2SO_4$ 135
5.4 $K^+, Mg^{2+} // Cl^-, SO_4^{2-}$ system 137
5.4.1 $KCl-MgSO_4$ 137
5.4.2 $MgCl_2-K_2SO_4$ 139
5.5 $K^+, Ca^{2+} // Cl^-, SO_4^{2-}$ system 141
5.5.1 $KCl-CaSO_4$ 141
5.5.1.1 Thermodynamic properties of the eutectic mixture 142
5.5.2 $CaCl_2-K_2SO_4$ 144
5.6 $Na^+, K^+ // Cl^-, SO_4^{2-}$ system 145
5.6.1 $NaCl-K_2SO_4$ 145
5.6.2 $KCl-Na_2SO_4$ 147
5.6.2.1 Thermodynamic properties of the low-melting mixture 148
6 Modelling results 150
6.1 $Mg^{2+}, Ca^{2+} // Cl^-, SO_4^{2-}$ system 155
6.1.1 $MgSO_4$ 155
6.1.2 $CaSO_4$ 156
6.1.3 $CaMg_2(SO_4)_3$ 157
6.1.4 $CaMg(SO_4)_2$ 158
6.1.5 $MgSO_4-CaSO_4$ 158
6.1.6 $MgCl_2-CaCl_2$ 160
6.1.7 $MgCl_2-MgSO_4$ 162
6.1.8 $CaCl_2-CaSO_4$ 164
6.1.9 $MgCl_2-CaSO_4$ 165
6.1.10 $CaCl_2-MgSO_4$ 167
6.1.11 The reciprocal system 167
6.2 $Na^+, Mg^{2+} // Cl^-, SO_4^{2-}$ system 170
6.2.1 $Na_2SO_4-MgSO_4$ 170
6.2.2 $NaCl-MgSO_4$ 171
6.2.3 $MgCl_2-Na_2SO_4$ 172
6.2.4 The reciprocal system 173
6.3 $Na^+, Ca^{2+} // Cl^-, SO_4^{2-}$ system 174
6.3.1 $Na_2SO_4-CaSO_4$ 174
6.3.2 $NaCl-CaSO_4$ 177

6.3.3 $CaCl_2$-Na_2SO_4 178
6.3.4 The reciprocal system 180
6.4 K^+, Mg^{2+} // Cl^-, SO_4^{2-} system 181
6.4.1 K_2SO_4-$MgSO_4$ 181
6.4.2 KCl-$MgSO_4$ 181
6.4.3 $MgCl_2$-K_2SO_4 182
6.4.4 The reciprocal system 183
6.5 K^+, Ca^{2+} // Cl^-, SO_4^{2-} system 185
6.5.1 KCl-$CaSO_4$ 185
6.5.2 $CaCl_2$-K_2SO_4 186
6.5.3 The reciprocal system 186
6.6 Na^+, K^+ // Cl^-, SO_4^{2-} system 188
6.6.1 NaCl-K_2SO_4 188
6.6.2 KCl-Na_2SO_4 189
6.6.3 The reciprocal system 190
6.7 Ternary systems 191
6.7.1 NaCl-$MgCl_2$-$CaCl_2$ 192
6.7.2 KCl-$MgCl_2$-$CaCl_2$ 193
6.7.3 Na_2SO_4-K_2SO_4-$MgSO_4$ 193
6.7.4 Na_2SO_4-K_2SO_4-$CaSO_4$ 194
6.7.5 Na_2SO_4-$MgSO_4$-$CaSO_4$ 195
6.7.6 K_2SO_4-$MgSO_4$-$CaSO_4$ 196
6.8 Na^+, K^+, Mg^{2+}, Ca^{2+} // Cl^-, SO_4^{2-} system 197
6.8.1 Validation of the developed database 202
7 Implications for applications: identifying PCM candidates for TES 204
8 Conclusions 208
Acknowledgements 210
References 211
Appendix A 224
Appendix B 237

List of figures

Figure 1-1 Graphical representation of the Na^+, K^+, Mg^{2+}, Ca^{2+} // Cl^-, SO_4^{2-} multi-component system: **a** cubic representation with visualisation of (pseudo)binary systems under analysis; **b** alternative representation of the multi-component system made of four six-component systems. 3
Figure 2-1 Heat vs. temperature during phase transitions in PCMs. 6
Figure 2-2 Enthalpy of fusion as a function of the melting temperature of salts of interest in PCM-Screening-2 project, from Reis [48]. 6
Figure 2-3 Graphical bidimensional representation of the four six-component systems from Rowe et al. [49]. 7
Figure 2-4 Graphical representation of the Mg^{2+}, Ca^{2+} // Cl^-, SO_4^{2-} reciprocal system from Rowe et al. [49]. 8
Figure 2-5 Phase diagram of $MgCl_2$-$CaCl_2$ system from Robelin et al. [55]. 9
Figure 2-6 Phase diagram of $MgSO_4$-$CaSO_4$ system from Yazhenskikh et al. [39] with experimental data from Rowe et al. [58]. 10
Figure 2-7 Phase diagram of $MgCl_2$-$MgSO_4$ system from Jänecke [62]. 11
Figure 2-8 Phase diagram of $CaCl_2$-$CaSO_4$ system from Rowe et al [49] with experimental data from Golubeva et al. [69]. 12
Figure 2-9 Phase diagram of Na^+, Mg^{2+} // Cl^-, SO_4^{2-} system from Speranskaya [63]. 13
Figure 2-10 Phase diagram of NaCl-$MgCl_2$ system from the PCM2 database [4] with experimental data: Speranskaya [63], Klemm and Weiss [75], Grijotheim et al. [77], Menge [50], Matiašovský [52], Abramov [89], Scholich [80], Seifert and Thiel [78]. 14
Figure 2-11 Phase diagram of Na_2SO_4-$MgSO_4$ system from Yazhenskikh et al. [39] with experimental data: Ginsberg [65], Nacken [64], Rowe et al. [58], Speranskaya [63], Bandaranayake and Mellander [90]. 16
Figure 2-12 Phase diagram of NaCl-Na_2SO_4 system from the PCM2 database [4] with experimental data: Wolters [97], Jänecke [108], Nagornyi and Zimina [101], Sackur [98], Klochko [104], Bergman and Sementsova [99], Mukimov [103], Akopov and Bergman [102], Flood at al. [96]. 17
Figure 2-13 Phase diagram of Na_2Cl_2-$MgSO_4$ system from Rowe et al. [49], originally from Speranskaya [63]. 17
Figure 2-14 Phase diagram of $MgCl_2$-Na_2SO_4 system from Speranskaya [63]. 18
Figure 2-15 Phase diagram of Na^+, Ca^{2+} // Cl^-, SO_4^{2-} system from Rowe et al. [49], originally from Zimina et al. [71]. 19
Figure 2-16 Phase diagram of NaCl-$CaCl_2$ system from Reis [48] with experimental data: Tokareva et al. [120], Seltveit and Flood [114], Qiao et al. [118], Igarashi et al. [110], Borovkova et al. [119]. 20
Figure 2-17 Phase diagram of Na_2SO_4-$CaSO_4$ system from Yazhenskikh et al. [39] with experimental data: Kobertz et al. [126], Coursol et al. [125], Bandaranayake et al. [90], Freyer et al. [122, 130], Müller [123], Speranskaya et al. [124]. 22
Figure 2-18 Phase diagram of NaCl-$CaSO_4$ system from Rowe et al. [49]. 23
Figure 2-19 Phase diagram of $CaCl_2$-Na_2SO_4 system from Rowe et al. [49], originally from Palkin [70]. 24
Figure 2-20 Phase diagram of K^+, Mg^{2+} // Cl^-, SO_4^{2-} system from Jänecke [62]. 24
Figure 2-21 Phase diagram of KCl-$MgCl_2$ system from the PCM2 database [4] with experimental data: Klemm et al. [76], Grjotheim et al. [77], Perry and Fletcher [136]. 25
Figure 2-22 Phase diagram of K_2SO_4-$MgSO_4$ system from Yazhenskikh et al. [39] with experimental data: Nacken [64], Rowe et al. [58], Grahmann [144], Mukimov et al. [145]. 26

Figure 2-23 Phase diagram of KCl-K_2SO_4 system from the PCM2 database [4] with experimental data: Jänecke [108], Sackur [98], Bergman et al. [99], Akopov et al. [102], Mukimov [103], Bergman et al. [154], Akopov et al. [149], Sementsova et al. [150], Bergman et al. [151], Nagornyi et al. [153]..... 27
Figure 2-24 Phase diagram of KCl-$MgSO_4$ system From Rowe [49], originally from Jänecke [62]. 28
Figure 2-25 Phase diagram of $MgCl_2$-K_2SO_4 system From Rowe et al. [49], originally from Jänecke [62]. 29
Figure 2-26 Phase diagram of K^+, Ca^{2+} // Cl^-, SO_4^{2-} system from Golubeva and Bergman [69]. 30
Figure 2-27 Phase diagram of KCl-$CaCl_2$ system from Reis [48] with experimental data: Clark and Reinhardt [157], Menge [50], Seifert et al. [141]. 31
Figure 2-28 Phase diagram of K_2SO_4-$CaSO_4$ system from Yazhenskikh et al. [39] with experimental data: Kobertz et al. [126], Rowe et al. [74], Bellanca [128], Mukimov et al. [145], Müller [123]..... 32
Figure 2-29 Phase diagram of K_2Cl_2-$CaSO_4$ system From Rowe et al. [49] with experimental data: Jänecke and Mühlhäusser [68], Golubeva and Bergman [69] and Rubleva and Bergman [135]. 33
Figure 2-30 Phase diagram of $CaCl_2$-K_2SO_4 system from Rowe et al. [49] with experimental data: Jänecke and Mühlhäusser [68] and Golubeva and Bergman [69]. 34
Figure 2-31 Phase diagram of Na^+, K^+ // Cl^-, SO_4^{2-} system from Akopov and Bergman [169]. 35
Figure 2-32 Phase diagram of NaCl-KCl system from Sergeev et al. [37] with experimental data: Akopov et al. [102]; Bergman et al. [178]; Bergman et al. [177]; Coleman et al. [170]; Pelton et al. [172]; Vesnin et al. [182]; Sergeev et al. [41]..... 36
Figure 2-33 Phase diagram of Na_2SO_4-K_2SO_4 system from Yazhenskikh et al. [39] with experimental data: Kobertz et al. [126], Eysel [183, 187], Nacken [184], Forland et al. [185], Bellanca [128], Jänecke [108], Akopov and Bergman [102], Mofaddel et al. [188], Koštenská and Fellner [189]. 37
Figure 2-34 Phase diagram of NaCl-K_2SO_4 from Rowe et al. [49] with experimental data: Jänecke [108], Akopov and Bergman [102]. 38
Figure 2-35 Phase diagram of KCl-Na_2SO_4 from Rowe et al. [49] with experimental data: Jänecke [108], Akopov and Bergman [105]. 38
Figure 2-36 Phase diagram of NaCl-KCl-$MgCl_2$ ternary system from the PCM2 database [4]..... 40
Figure 2-37 Phase diagram of NaCl-KCl-$CaCl_2$ ternary system from Reis [48]. 41
Figure 2-38 Phase diagram of NaCl-$MgCl_2$-$CaCl_2$ ternary system from Chartrand and Pelton [54]. 42
Figure 2-39 Phase diagram of KCl-$MgCl_2$-$CaCl_2$ ternary system from Chartrand and Pelton [54]..... 43
Figure 2-40 Phase diagram of Na_2SO_4-K_2SO_4-$MgSO_4$ ternary system from Yazhenskikh et al. [201]. .. 44
Figure 2-41 Phase diagram of Na_2SO_4-K_2SO_4-$CaSO_4$ ternary system from Yazhenskikh et al. [201] and Bellanca [128]. 45
Figure 2-42 Phase diagram of Na_2SO_4-$MgSO_4$-$CaSO_4$ ternary system from Yazhenskikh et al. [201]. . 46
Figure 2-43 Phase diagram of K_2SO_4-$MgSO_4$-$CaSO_4$ ternary system from Yazhenskikh et al. [201], and Rowe et al. [58]. 47
Figure 3-1 Schematic diagram and drawing of DTA sample holder, with A and B denoting the different legs of thermocouples. 51
Figure 3-2 Schematic diagram and drawing of DSC sample holder, with A and B denoting the different legs of thermocouples. 52
Figure 3-3 Custom sealed platinum tube (**a**) in platinum sample holder (**b**) for investigation in Setaram mHTC 96 calorimeter (**c**)..... 53
Figure 3-4 Schematic representation of the stepwise approach in the self-referencing calibration method (SRCM). 54
Figure 3-5 Comparison of experimental data in open alumina liner and sealed Pt tube in Pt crucible of $BaCO_3$ for Self-referencing calibration method: **a** molar heat capacity; **b** enthalpy increment. 55
Figure 4-1 Relationship between G-X and T-X plots illustrating phase equilibria [220]. 60
Figure 4-2 Stepwise modelling approach: from simple to complex systems. 68

Figure 5-1 Experimental values of molar heat capacity of $MgSO_4$ measured by DSC Setaram by applying SRCM method. 73
Figure 5-2 Experimental values of molar heat capacity of $CaSO_4$ measured by DSC Setaram by applying SRCM method. 75
Figure 5-3 HTXRD pattern of $CaMg_2(SO_4)_3$ under vacuum: **a** HT1 (T = 350 °C); **b** HT2 (T = 500 °C); **c** zoomed HT2 (T = 500 °C). 76
Figure 5-4 a Visualisation of peak splitting due to lattice parameter differences of $CaMg_2(SO_4)_3$ phases; **b** Temperature dependence of lattice parameters a (top) and c (bottom); **c** Characteristic reflections: ß = β-$CaMg_2(SO_4)_3$, ▼ = $CaSO_4$, ▼ = "unknown phase" (orthorhombic?), "H" = presumed hydrate phase, "?" = two additional not-identified phases, "S" = alumina sample holder (Intensity in square root scaling). 78
Figure 5-5 HTXRD $CaMg_2(SO_4)_3$; appearance and disappearance of the unknown phase according to temperature. 79
Figure 5-6 TG curve of $CaMg_2(SO_4)_3$ in open alumina crucible. 81
Figure 5-7 Experimental values of molar heat capacity of $CaMg_2(SO_4)_3$ as $MgSO_4$(66.7 mol%)-$CaSO_4$(33.3 mol%): **a** C_p of solid phase measured by two DSC devices and comparison with calculated values from databases [39, 259]; **b** C_p of solid and liquid phases measured by DSC Setaram by applying SRCM method. 82
Figure 5-8 DTA crucible selection for investigation of $MgSO_4$-$CaSO_4$ binary system. 84
Figure 5-9 Phase diagram of $MgSO_4$-$CaSO_4$, comparison of experimental data of this work with Rowe et al. [58] and Yazhenskikh et al. [39]. 86
Figure 5-10 Heat flow vs. temperature curves of mixtures ($CaSO_4$ mol%) in the $MgSO_4$-$CaSO_4$ binary system tested in DSC Setaram in sealed platinum tubes. 87
Figure 5-11 SEM-Images (Back Scatter Electrons) showing the grains and phases of $MgSO_4$(70 mol%)-$CaSO_4$(30 mol%) across the sample surface, highlighting areas analysed by Energy Dispersive X-Ray Spectroscopy (EDX). 89
Figure 5-12 XRD of $MgSO_4$-$CaSO_4$ with a 1:1 stochiometric ratio: **a** sample subjected to heat treatment at 900 °C, followed by rapid cooling to room temperature; **b** sample subjected to heat treatment at 900 °C, followed by controlled cooling at a rate of 5 K/min. 90
Figure 5-13 DTA curves of $MgCl_2$-$CaCl_2$ mixtures, expressed in molar percentage of $CaCl_2$: **a** heating curves; **b** cooling curves. 91
Figure 5-14 Experimental values of molar heat capacity of $MgCl_2$(52.81 mol%)-$CaCl_2$(47.19 mol%). 92
Figure 5-15 DTA curves of $MgCl_2$-$MgSO_4$ mixtures, expressed in molar percentage of $MgSO_4$: **a** heating curves; **b** cooling curves. 94
Figure 5-16 Experimental values of molar heat capacity for solid and liquid phases of the $MgCl_2$(72.0 mol%)-$MgSO_4$(28.0 mol%) mixture measured by two DSC devices. 96
Figure 5-17 DTA curves of $CaCl_2$-$CaSO_4$ mixtures. expressed in molar percentage of $CaSO_4$: **a** heating curves; **b** cooling curves. 97
Figure 5-18 Experimental values of molar heat capacity for solid and liquid phases of the $CaCl_2$(86.01 mol%)-$CaSO_4$(13.99 mol%) mixture measured by two DSC devices. 99
Figure 5-19 DTA curves of $MgCl_2$-$CaSO_4$ mixtures, expressed in molar percentage of $CaSO_4$: **a** heating curves; **b** cooling curves. 100
Figure 5-20 Experimental values of molar heat capacity of $MgCl_2$(78.34 mol%)-$CaSO_4$(21.66 mol%). 102
Figure 5-21 DTA curves of $CaCl_2$-$MgSO_4$ mixtures. expressed in molar percentage of $MgSO_4$: **a** heating curves; **b** cooling curves. 103
Figure 5-22 DTA curves of $MgCl_2$-$CaMg_2(SO_4)_3$ mixtures, expressed in molar percentage of $CaMg_2(SO_4)_3$: **a** heating curves; **b** cooling curves. 105

Figure 5-23 DTA curves of $CaCl_2$-$CaMg_2(SO_4)_3$ mixtures. expressed in molar percentage of $CaMg_2(SO_4)_3$: **a** heating curves; **b** cooling curves. 106
Figure 5-24 DTA curves of NaCl-$MgSO_4$ mixtures, expressed in molar percentage of $MgSO_4$: **a** heating curves; **b** cooling curves. 108
Figure 5-25 Experimental values of molar heat capacity for solid and liquid phases of the NaCl(100-x mol%)-$MgSO_4$(x mol%) mixtures (x= 31.96, 32.34, 33.56, 35.20), measured by DSC Setaram during heating and cooling cycles. Inset: zoomed view of the cooling curves highlighting the peak region. 110
Figure 5-26 Phase diagram and corresponding Tamman plot of NaCl-$MgSO_4$ system. 111
Figure 5-27 Enthalpy increment (left) and enthalpy of transition (right) of the NaCl(100-x mol%)-$MgSO_4$(x mol%) mixtures (x= 31.96, 32.34, 33.56, 35.20) obtained from DSC results. 112
Figure 5-28 DTA curves of $MgCl_2$-Na_2SO_4 mixtures, expressed in molar percentage of Na_2SO_4: **a** heating curves; **b** cooling curves. 113
Figure 5-29 X-ray diffractogram of Na_2SO_4(75 mol%)-$CaSO_4$(25 mol%), i.e., $Na_6Ca(SO_4)_4$ mixture: **a** $Na_6Ca(SO_4)_4$ A (T=800°C t=60h); **b** $Na_6Ca(SO_4)_4$ B (T=800°C t=100h); **c** $Na_6Ca(SO_4)_4$ C (T=900°C t=72h). 117
Figure 5-30 X-ray diffractogram of Na_2SO_4(67 mol%)-$CaSO_4$(33 mol%), i.e., $Na_4Ca(SO_4)_3$ mixture: **a** $Na_4Ca(SO_4)_3$ A (T=800°C t=72h); **b** $Na_4Ca(SO_4)_3$ B (T=800°C t=72h). 118
Figure 5-31 X-ray diffractogram of Na_2SO_4(88 mol%)-$CaSO_4$(12 mol%) mixture at room temperature. 119
Figure 5-32 X-ray diffractogram of Na_2SO_4(50 mol%)-$CaSO_4$(50 mol%) mixture at room temperature. 119
Figure 5-33 High temperature X-ray diffractogram of Na_2SO_4(75 mol%)-$CaSO_4$(25 mol%), i.e., $Na_6Ca(SO_4)_3$ mixture. 121
Figure 5-34 High temperature X-ray diffractogram of Na_2SO_4(88 mol%)-$CaSO_4$(12 mol%) mixture: **a** HT1 from 300 °C to 150 °C; **b** HT3 (190→220→190→220→275→175 °C); **c** HT4 from 25 °C to 600 °C and back to 25 °C. 123
Figure 5-35 High temperature X-ray diffractogram of Na_2SO_4(50 mol%)-$CaSO_4$(50 mol%) mixture. . 124
Figure 5-36 DTA curves of Na_2SO_4-$CaSO_4$ mixture, expressed in molar percentage of $CaSO_4$: **a** heating curves; **b** cooling curves. 131
Figure 5-37 Phase diagram of Na_2SO_4-$CaSO_4$ system with experimental data: this work and Kobertz et al. [126]; Coursol et al. [125]; Bandaranayake et al. [90]; Freyer et al. [122, 130]; Müller [123]; Speranskaya et al. [124]; and Yazhenskikh et al. [39]. 132
Figure 5-38 DTA curves of NaCl-$CaSO_4$ mixtures, expressed in molar percentage of $CaSO_4$: **a** heating curves; **b** cooling curves. 134
Figure 5-39 Experimental values of molar heat capacity for solid and liquid phases of the NaCl(83.10 mol%)-$CaSO_4$(16.90 mol%) mixture measured by DSC Setaram. 135
Figure 5-40 DTA curves of $CaCl_2$-Na_2SO_4 mixtures, expressed in molar percentage of Na_2SO_4: **a** heating curves; **b** cooling curves. 136
Figure 5-41 DTA curves of KCl-$MgSO_4$ mixtures, expressed in molar percentage of $MgSO_4$: **a** heating curves; **b** cooling curves. 138
Figure 5-42 X-ray diffractogram of KCl-$MgSO_4$ mixtures at room temperature: **a** KCl(49.71 mol%)-$MgSO_4$(50.28 mol%) (T=800 °C, t=60 h); **b** KCl(50.75 mol%)-$MgSO_4$(49.25 mol%) (T=700 °C, t=96 h). 139
Figure 5-43 DTA curves of $MgCl_2$-K_2SO_4 mixtures, expressed in molar percentage of K_2SO_4: **a** heating curves; **b** cooling curves. 140
Figure 5-44 DTA curves of KCl-$CaSO_4$ mixtures. expressed in molar percentage of $CaSO_4$: **a** heating curves; **b** cooling curves. 142

Figure 5-45 Experimental values of molar heat capacity of the KCl(80.48 mol%)-$CaSO_4$(19.52 mol%). 144
Figure 5-46 DTA curves of $CaCl_2$-K_2SO_4 mixtures. expressed in molar percentage of K_2SO_4: **a** heating curves; **b** cooling curves. 145
Figure 5-47 DTA curves of NaCl-K_2SO_4 mixtures, expressed in molar percentage of K_2SO_4: **a** heating curves; **b** cooling curves. 146
Figure 5-48 DTA curves of KCl-Na_2SO_4 mixtures. expressed in molar percentage of Na_2SO_4: **a** heating curves; **b** cooling curves. 147
Figure 5-49 Experimental values of molar heat capacity of KCl(58.44 mol%)-Na_2SO_4(41.56 mol%) mixture. 149
Figure 6-1 Enthalpy increment of $MgSO_4$ obtained from DSC results in comparison with the current database and the commercial databases FTSalt [218] and SGPS [228]. 156
Figure 6-2 Enthalpy increment of $CaSO_4$ obtained from DSC results in comparison with the current database and the commercial databases FTSalt [218] and SGPS [228]. 157
Figure 6-3 Enthalpy increment of $CaMg_2(SO_4)_3$ obtained from DSC results in comparison with the current database. 158
Figure 6-4 Phase diagram of the $MgSO_4$-$CaSO_4$ system: comparison of the developed database with experimental data from the present work and Rowe et al. [58]. 159
Figure 6-5 Phase diagram of $MgCl_2$-$CaCl_2$ system: comparison of the developed database with experimental data from the present work and Menge [50], Ivanov [51], Matiašovský [52], Grjotheim et al. [53]. 160
Figure 6-6 Enthalpy increment of the $MgCl_2$(52.81 mol%)-$CaCl_2$(47.19 mol%) mixture obtained from DSC results in comparison with the current database and the commercial databases FTsalt [218]. 161
Figure 6-7 Calculated activity of $MgCl_2$ in the liquid phase at 800 °C in comparison with Karakaya and Thompson [56]. 161
Figure 6-8 Calculated enthalpy of mixing of the liquid phase at 800 °C in comparison with Karakaya and Thompson [57]. 162
Figure 6-9 Phase diagram of the $MgCl_2$-$MgSO_4$ system: comparison of the developed database with experimental data from the present work and Jänecke [62], and Speranskaya [63]. 163
Figure 6-10 Enthalpy increment of the $MgCl_2$(72.0 mol%)-$MgSO_4$(28.0 mol%) mixture obtained from DSC results in comparison with the current database and the commercial database FTsalt [218]. 163
Figure 6-11 Phase diagram of the $CaCl_2$-$CaSO_4$ system: comparison of the developed database with experimental data from the present work and Sackur [66], Pichugin [67], Golubeva et al. [69], Zimina et al. [71], Arbukhanova et al. [72]. 164
Figure 6-12 Enthalpy increment of the $CaCl_2$(86.01 mol%)-$CaSO_4$(13.99 mol%) mixture obtained from DSC results in comparison with the current database and the commercial database FTsalt [218]. 165
Figure 6-13 Phase diagram of the $MgCl_2$-$CaSO_4$ system: comparison of the developed database with experimental data from the present work. 166
Figure 6-14 Enthalpy increment of the $MgCl_2$(78.34 mol%)-$CaSO_4$(21.66 mol%) mixture obtained from DSC results in comparison with the current database and the commercial database FTsalt [218]. 166
Figure 6-15 Phase diagram of the $CaCl_2$-$MgSO_4$ system: comparison of the developed database with experimental data from the present work. 167
Figure 6-16 Comparison of experimental and calculated phase diagram of: **a** $MgCl_2$-$CaMg_2(SO_4)_3$; **b** $CaCl_2$-$CaMg_2(SO_4)_3$ system. 169
Figure 6-17 Liquidus surface of the reciprocal system Mg^{2+}, Ca^{2+} // Cl^-, SO_4^{2-} calculated with the developed database. 169

Figure 6-18 Phase diagram of Na_2SO_4-$MgSO_4$ system: comparison of the developed database with experimental data from Ginsberg [65], Nacken [64], Rowe et al. [58], Speranskaya [63], Bandaranayake and Mellander [90]. 170
Figure 6-19 Phase diagram of NaCl-$MgSO_4$ system: comparison of the developed database with experimental data from the present work and Speranskaya [63]. 172
Figure 6-20 Phase diagram of $MgCl_2$-Na_2SO_4 system: comparison of the developed database with experimental data from the present work and Speranskaya [63]. 173
Figure 6-21 Liquidus surface of the reciprocal system Na^+, Mg^{2+} // Cl^-, SO_4^{2-} calculated with the developed database, and experimental data of Speranskaya [63]. 174
Figure 6-22 Phase diagram of Na_2SO_4-$CaSO_4$ system: comparison of the developed database with experimental data from the present work and Kobertz et al. [126], Coursol et al. [125], Bandaranayake et al. [90], Freyer et al. [122, 130], Müller [123], Speranskaya et al. [124]. 176
Figure 6-23 Phase diagram of NaCl-$CaSO_4$ system: comparison of the developed database with experimental data from this work and Byé et al. [134], Bergman and Pichugin in [133], Rubleva and Bergman [135]. 178
Figure 6-24 Enthalpy increment of the NaCl(83.10 mol%)-$CaSO_4$(16.90 mol%) mixture obtained from DSC results in comparison with the current database and the commercial database FTsalt [218]... 178
Figure 6-25 Phase diagram of $CaCl_2$-Na_2SO_4 system: comparison of the developed database with experimental data from the present work and Palkin [70]. 179
Figure 6-26 Liquidus surface of the reciprocal system Na^+, Ca^{2+} // Cl^-, SO_4^{2-} calculated with the developed database, and experimental data of Zimina et al. [71]. 180
Figure 6-27 Phase diagram of K_2SO_4-$MgSO_4$ system: comparison of the developed database with experimental data from Nacken [64], Rowe et al. [58], Grahmann [144], Mukimov et al. [145]. 181
Figure 6-28 Phase diagram of KCl-$MgSO_4$ system: comparison of the developed database with experimental data from the present work with Rowe et al. [49], Jänecke [62], and Bergman et al. [109]. 182
Figure 6-29 Phase diagram of $MgCl_2$-K_2SO_4 system: comparison of the developed database with experimental data from the present work and Jänecke [62]. 183
Figure 6-30 Liquidus surface of the reciprocal system K^+, Mg^{2+} // Cl^-, SO_4^{2-} calculated with the current database, and experimental data of Jänecke [62]. 184
Figure 6-31 Phase diagram of KCl-$CaSO_4$ system: comparison of the developed database with experimental data from the present work with Voskresenskaya [133], Jänecke and Mühlhäusser [68], Golubeva and Bergman [69], Rubleva and Bergman [135], and Rowe et al. [49]. 185
Figure 6-32 Phase diagram of $CaCl_2$-K_2SO_4 system: comparison of the developed database with experimental data from the present work and Jänecke [68], Golubeva and Bergman [69]. 186
Figure 6-33 Liquidus surface of the reciprocal system K^+, Ca^{2+} // Cl^-, SO_4^{2-} calculated with the current database, and experimental data of Jänecke and Mühlhäusser [68] and Golubeva and Bergman [69]. 187
Figure 6-34 Phase diagram of NaCl-K_2SO_4 system: comparison of the developed database with experimental data from the present work with Akopov and Bergman[102], Jänecke [108], Sackur [66], and Rowe et al. [49]. 188
Figure 6-35 Phase diagram of KCl-Na_2SO_4 system: comparison of the developed database with experimental data from the present work with Akopov and Bergman[102], Jänecke [108], Sackur [66]. 190
Figure 6-36 Enthalpy increment of the KCl(58.44 mol%)-Na_2SO_4(41.56 mol%) mixture obtained from DSC results in comparison with the current database and the commercial database FTsalt [218]... 190
Figure 6-37 Liquidus surface of the reciprocal system Na^+, K^+ // Cl^-, SO_4^{2-} calculated with the developed database, and experimental data of Jänecke [5] and Akopov and Bergman [102]. 191

Figure 6-38 Phase diagram of NaCl-$MgCl_2$-$CaCl_2$ ternary system from the developed database. 192
Figure 6-39 Phase diagram of KCl-$MgCl_2$-$CaCl_2$ ternary system from the developed database. 193
Figure 6-40 Phase diagram of Na_2SO_4-K_2SO_4-$MgSO_4$ ternary system from the developed database 194
Figure 6-41 Phase diagram of Na_2SO_4-K_2SO_4-$CaSO_4$ ternary system from the developed database. 195
Figure 6-42 Phase diagram of Na_2SO_4-$MgSO_4$-$CaSO_4$ ternary system from the developed database. 196
Figure 6-43 Phase diagram of K_2SO_4-$MgSO_4$-$CaSO_4$ ternary system from the developed database. . 197
Figure 6-44 Graphical representation of the calculated Na^+, K^+, Mg^{2+}, Ca^{2+} // Cl^-, SO_4^{2-} multi-component system with the developed database: **a** cubic representation with visualization of six reciprocal systems under analysis; **b** alternative representation of the multi-component system made of four six-component systems. 201
Figure 6-45 Graphical bidimensional representation of the four quaternary reciprocal salt systems from the developed database..... 202
Figure 7-1 Enthalpy of transition as a function of the transition temperature of selected quasi-binary mixtures as potential PCMs. 205
Figure 7-2 Enthalpy of transition as a function of the transition temperature of selected mixtures as potential PCMs..... 207

Figure A 1 Heating and cooling DTA curves of $MgCl_2$ in sealed platinum tube. 224
Figure A 2 Comparison of heat capacity of the $MgCl_2$ from the experimental DSC measurements and the PCM2 database [4]. 224
Figure A 3 TG curve of $MgSO_4$ in open alumina crucible. 224
Figure A 4 X-ray diffractogram of $MgSO_4$ at room temperature: **a)** as purchased ($MgSO_4$ bottle); **b)** dried in furnace at 150 °C ($MgSO_4$ furnace)..... 225
Figure A 5 TG curve of $CaSO_4$ in open alumina crucible. 225
Figure A 6 DTA curve of $CaSO_4$ in sealed platinum tube. 226
Figure A 7 HTXRD $CaMg_3(SO_4)_4$. Weight ratio $CaMg_2(SO_4)_3$:$CaSO_4$ = 85:15. Lattice parameters of main phase: a = 8.349 Å, c = 7.158 Å, V = 432.09 $Å^3$ (sg P63/m). 226
Figure A 8 Temperature profile of HTXRD of $CaMg_2(SO_4)_3$: **a)** HT1 (25 °C → 350 °C); **b)** HT2 (25 °C → 500 °C). 227
Figure A 9 Diffractogram of $CaMg_2(SO_4)_3$ (HT1): initial state after placing in oven chamber (T = 25 °C / vacuum). 227
Figure A 10 Presumed formation of a hydrate phase after contact with ambient air in $CaMg_2(SO_4)_3$ (HT1)..... 228
Figure A 11 SEM-Images (Back Scatter Electrons) showing the grains and phases of $MgSO_4$(70 mol%)-$CaSO_4$(30 mol%) across the sample surface, highlighting areas analysed by Energy Dispersive X-Ray Spectroscopy (EDX). The areas analysed differ from those shown in **Figure 5-11**. 228
Figure A 12 SEM-Images (Back Scatter Electrons) showing the grains and phases of $MgSO_4$(49.91 mol%)-$CaSO_4$(50.09 mol%) across the sample surface, highlighting areas analysed by Energy Dispersive X-Ray Spectroscopy (EDX). 229
Figure A 13 DTA curves of $MgCl_2$-$MgSO_4$ mixtures in alumina crucibles, expressed in molar percentage of $MgSO_4$: heating curves (red); cooling curves (blue). 230
Figure A 14 X-ray diffractogram of $MgCl_2$-$MgSO_4$ mixtures at room temperature: **a** $MgCl_2$(72 mol%)-$MgSO_4$(28 mol%); **b** $MgCl_2$(50 mol%)-$MgSO_4$(50 mol%); **c** $MgCl_2$(10 mol%)-$MgSO_4$(90 mol%). 231
Figure A 15 DTA curves of $CaCl_2$-$CaSO_4$ mixtures in alumina crucibles, expressed in molar percentage of $CaSO_4$: heating curves (red); cooling curves (blue)..... 232
Figure A 16 X-ray diffractogram of $CaCl_2$(86.01 mol%)-$CaSO_4$(13.99 mol%) mixture at room temperature..... 232

Figure A 17 X-ray diffractogram of $MgCl_2$(30.80 mol%)-$CaSO_4$(69.20 mol%) mixture at room temperature. 233
Figure A 18 X-ray diffractogram of $CaCl_2$(71.70 mol%)-$MgSO_4$(28.30 mol%) mixture at room temperature. 233
Figure A 19 Latent heat as a function of composition, derived from cooling DSC curves for NaCl(100-x mol%)-$MgSO_4$(x mol%) mixtures (x= 31.96, 32.34, 33.56, 35.20). 234
Figure A 20 High temperature X-ray diffractogram of Na_2SO_4(75 mol%)-$CaSO_4$(25 mol%), i.e., $Na_6Ca(SO_4)_3$ mixture: **a** HT1-cycle 1 from 25 °C to 400 °C; **b** HT1-cycle 1 from 400 °C to 25 °C; **c** HT1-cycle 2 from 25 °C to 400 °C; **d** HT1-cycle 2 from 400 °C to 25 °C. 234
Figure A 21 High temperature X-ray diffractogram of Na_2SO_4(50 mol%)-$CaSO_4$(50 mol%) mixture: **a** HT1 from 25 °C to 600 °C; **b** HT1 from 25 °C to 600 °C (intensity magnified); **c** HT1 from 600 °C to 25 °C. 235
Figure A 22 X-ray diffractogram of NaCl(83.10 mol%)-$CaSO_4$(16.90 mol%) mixture at room temperature. 235
Figure A 23 X-ray diffractogram of KCl(66.67 mol%)-$CaSO_4$(33.33 mol%) mixture at room temperature. 236
Figure A 24 Liquidus surface of the reciprocal system Na^+, Mg^{2+} // Cl^-, SO_4^{2-} calculated with the developed database, and experimental data of Speranskaya [63] (sections IV-IX). 237
Figure A 25 Phase diagrams of sections IV-IX in the frame of Na^+, Mg^{2+} // Cl^-, SO_4^{2-} system: comparison of the experimental points from Speranskaya [63] and the developed database. Sections **IV,VI**: (1-a)Na_2SO_4(a)$MgSO_4$-Na_2Cl_2 (with a: 0.5, 0.356); Sections **V**: (0.5)Na_2Cl_2(0.5)Na_2SO_4-$MgSO_4$; Sections **VII-IX**: (1-a-b)Na_2Cl_2(a)Na_2SO_4(b)$MgSO_4$ (with a: 0, 0, 0.25; b: 0.234, 0.631, 0.55). 238
Figure A 26 Phase diagram of NaCl-K_2SO_4-$MgSO_4$ system from the developed database and experimental points from Rowe et al. [49]. 238
Figure A 27 Phase diagram of NaCl-$K_2Mg_2(SO_4)_3$ system from the developed database and experimental points from Rowe et al. [49]. 239
Figure A 28 Phase diagram of $(NaCl)_2$-$(KCl)_2$-$MgSO_4$ system from the developed database and experimental points from Bergman and Selivanova (1938) in Voskresenskaya [133]. 239
Figure A 29 Phase diagram of $(NaCl)_2$-KCl·$MgSO_4$ system from the developed database and experimental points from Bergman and Selivanova (1938) in Voskresenskaya [133]. 240
Figure A 30 Phase diagram of $(NaCl)_2$-$(KCl)_2$-$CaSO_4$ system from the developed database and experimental points of sections I-IX from Rubleva and Bergman [135]. 240
Figure A 31 Phase diagrams of sections I-IX in the frame of $(NaCl)_2$-$(KCl)_2$-$CaSO_4$ system: comparison of the experimental points from Rubleva and Bergman [135] and the developed database. Sections **I-VII**: (100-a)K_2Cl_2(a)Na_2Cl_2-$CaSO_4$ (with a: 75, 60, 53, 50, 42.5, 25, 15 mol%); Sections **VIII-IX**: (100-a)$CaSO_4$(a)K_2Cl_2-Na_2Cl_2 (with a: 72, 62.5 mol%). 241
Figure A 32 Phase diagram of NaCl-K_2SO_4-$CaSO_4$ system from the developed database and experimental points from Rowe et al. [49]. 241
Figure A 33 Phase diagram of NaCl-$K_2Ca_2(SO_4)_3$ system from the developed database and experimental points from Rowe et al. [49]. 242
Figure A 34 Phase diagram of NaCl-$MgSO_4$-$CaSO_4$ system from the developed database and experimental points from Rowe et al. [49]. 242
Figure A 35 Phase diagram of NaCl-$CaMg_3(SO_4)_4$ system from the developed database and experimental points from Rowe et al. [49]. 243
Figure A 36 Phase diagram of NaCl-$K_2Mg_2(SO_4)_3$-$K_2Ca_2(SO_4)_3$ system from the developed database and experimental points from Rowe et al. [49]. 243
Figure A 37 Phase diagram of NaCl-(0.637)$K_2Mg_2(SO_4)_3$(0.363)$K_2Ca_2(SO_4)_3$ system from the developed database and experimental points from Rowe et al. [49]. 244

Figure A 38 Phase diagram of 40-percent NaCl plane in the NaCl-K_2SO_4-$MgSO_4$-$CaSO_4$ system from the developed database and experimental points from Rowe et al. [49]. 244

List of tables

Table 2-1 Good criteria for PCMs. 6
Table 2-2 Calculated invariant points in the NaCl-KCl-$MgCl_2$ system. 40
Table 5-1 Transition data of pure compounds. 69
Table 5-2 Lattice parameters of $CaMg_2(SO_4)_3$. 77
Table 5-3 Experimental values of phase transition temperatures (°C) in the $MgSO_4$-$CaSO_4$ system in sealed platinum tubes. 85
Table 5-4 Molar percentages of elements detected in the analysed regions of the sample by SEM-EDX. 89
Table 5-5 Experimental DTA values of phase transition temperatures (°C) in the $MgCl_2$-$CaCl_2$ system. 91
Table 5-6 Experimental DTA values of phase transition temperatures (°C) in the $MgCl_2$-$MgSO_4$ system. 94
Table 5-7 Coefficients of the second-order equation of molar heat capacity ($J \cdot mol^{-1} \cdot K^{-1}$) $C_p° = A + B \cdot T + C \cdot T^{-2} + D \cdot T^2$ for the $MgCl_2$(72.0 mol%)-$MgSO_4$(28.0 mol%) mixture taken from DSC measurements. . 96
Table 5-8 Experimental DTA values of phase transition temperatures (°C) in the $CaCl_2$-$CaSO_4$ system. 97
Table 5-9 Coefficients of the second-order equation of molar heat capacity ($J \cdot mol^{-1} \cdot K^{-1}$) $C_p° = A + B \cdot T + C \cdot T^{-2} + D \cdot T^2$ for the $CaCl_2$(86.01 mol%)-$CaSO_4$(13.99 mol%) mixture taken from DSC measurements. 99
Table 5-10 Experimental DTA values of phase transition temperatures (°C) in the $MgCl_2$-$CaSO_4$ system. 100
Table 5-11 Experimental DTA values of phase transition temperatures (°C) in the $CaCl_2$-$MgSO_4$ system. 103
Table 5-12 Experimental DTA values of phase transition temperatures (°C) in the $MgCl_2$-$CaMg_2(SO_4)_3$ system. 105
Table 5-13 Experimental DTA values of phase transition temperatures (°C) in the $CaCl_2$-$CaMg_2(SO_4)_3$ system. 106
Table 5-14 Experimental DTA values of phase transition temperatures (°C) in the NaCl-$MgSO_4$ system. 108
Table 5-15 Experimental DTA values of phase transition temperatures (°C) in the $MgCl_2$-Na_2SO_4 system. 114
Table 5-16 Thermal treatment conditions of synthesis of Na_2SO_4(100-x mol%)-$CaSO_4$(x mol%). 115
Table 5-17 Lattice parameters of identified phases in $Na_6Ca(SO_4)_4$ A, B, C. 117
Table 5-18 Lattice parameters of identified phases in $Na_4Ca(SO_4)_3$ A, B. 118
Table 5-19 Onset temperatures of the monoclinic/hexagonal phase transition. 125
Table 5-20 Semiquantitative evaluation of investigated samples. 128
Table 5-21 Experimental DTA values of phase transition temperatures (°C) in the Na_2SO_4-$CaSO_4$ system. 131
Table 5-22 Transition temperatures and enthalpies of Na_2SO_4-$CaSO_4$ mixtures from DSC experiments (heating curves). 132
Table 5-23 Experimental DTA values of phase transition temperatures (°C) in the NaCl-$CaSO_4$ system. 134
Table 5-24 Experimental DTA values of phase transition temperatures (°C) in the $CaCl_2$-Na_2SO_4 system. 136
Table 5-25 Experimental DTA values of phase transition temperatures (°C) in the KCl-$MgSO_4$ system. 138

Table 5-26 Lattice parameters of KCl·$MgSO_4$ mixtures. 139
Table 5-27 Experimental DTA values of phase transition temperatures (°C) in the $MgCl_2$-K_2SO_4 system. 140
Table 5-28 Experimental DTA values of phase transition temperatures (°C) in the KCl-$CaSO_4$ system. 142
Table 5-29 Coefficients of the second-order equation of molar heat capacity ($J \cdot mol^{-1} \cdot K^{-1}$) $C_p° = A + B \cdot T + C \cdot T^{-2} + D \cdot T^2$ for the KCl(80.48 mol%)-$CaSO_4$(19.52 mol%) mixture taken from DSC measurements. 144
Table 5-30 Experimental DTA values of phase transition temperatures (°C) in the $CaCl_2$-K_2SO_4 system. 145
Table 5-31 Experimental DTA values of phase transition temperatures (°C) in the NaCl-K_2SO_4 system. 146
Table 5-32 Experimental DTA values of phase transition temperatures (°C) in the KCl-Na_2SO_4 system. 148
Table 6-1 Thermodynamic data of stochiometric compounds used in the present work. 150
Table 6-2 Calculated invariant points, expressed in equivalent fractions, in the reciprocal system Mg^{2+}, Ca^{2+} // Cl^-, SO_4^{2-}. 169
Table 6-3 Calculated invariant points in the Na_2SO_4-$MgSO_4$ system. 170
Table 6-4 Calculated and experimental invariant points, expressed in equivalent fractions, in the reciprocal system Na^+, Mg^{2+} // Cl^-, SO_4^{2-} 174
Table 6-5 Invariant points in the Na_2SO_4-$CaSO_4$ system 176
Table 6-6 Calculated invariant points in the $CaCl_2$-Na_2SO_4 system 179
Table 6-7 Calculated and experimental invariant points, expressed in equivalent fractions, in the reciprocal system Na^+, Ca^{2+} // Cl^-, SO_4^{2-}. 180
Table 6-8 Calculated and experimental invariant points, expressed in equivalent fractions, in the reciprocal system K^+, Mg^{2+} // Cl^-, SO_4^{2-}. 184
Table 6-9 Calculated and experimental invariant points, expressed in equivalent fractions, in the reciprocal system K^+, Ca^{2+} // Cl^-, SO_4^{2-}. 187
Table 6-10 Calculated invariant points in the NaCl-$MgCl_2$-$CaCl_2$ system. 192
Table 6-11 Calculated invariant points in the KCl-$MgCl_2$-$CaCl_2$ system. 193
Table 6-12 Calculated invariant points in the Na_2SO_4-K_2SO_4-$MgSO_4$ system. 194
Table 6-13 Calculated invariant points in the Na_2SO_4-K_2SO_4-$CaSO_4$ system. 195
Table 6-14 Calculated invariant points in the Na_2SO_4-$MgSO_4$-$CaSO_4$ system. 196
Table 6-15 Calculated invariant points in the Na_2SO_4-$MgSO_4$-$CaSO_4$ system. 197
Table 6-16 Thermodynamic descriptions of the liquid and solid solution phases. 198
Table 7-1 Experimental transition temperature and transition enthalpy of selected quasi-binary mixtures as potential PCMs. 205
Table 7-2 Calculated transition temperature and transition enthalpy of selected multi-component mixtures as potential PCMs. 206

Table A 1 Experimental conditions of HTXRD measurements of $CaMg_2(SO_4)_3$. 226
Table A 2 Molar percentages of elements detected in the analysed regions of the sample $MgSO_4$(70 mol%)-$CaSO_4$(30 mol%) by SEM-EDX. 228
Table A 3 Molar percentages of elements detected in the analysed regions of the sample $MgSO_4$(49.91 mol%)-$CaSO_4$(50.09 mol%) by SEM-EDX. 229
Table A 4 Lattice parameters of $MgCl_2$(50 mol%)-$MgSO_4$(50 mol%) mixture. 231
Table A 5 Lattice parameters of $CaCl_2$(86.01mol%)-$CaSO_4$(13.99mol%) eutectic mixture 232
Table A 6 Lattice parameters of MgCl2(30.80 mol%)-CaSO4(69.20 mol%) mixture. 233

Table A 7 Lattice parameters of CaCl2(71.70 mol%)-MgSO4(28.30 mol%).....233
Table A 8 Calculated invariant points in the NaCl-K_2SO_4-$MgSO_4$ system. 238
Table A 9 Calculated and experimental invariant points in the $(NaCl)_2$-$(KCl)_2$-$MgSO_4$ system.....239
Table A 10 Calculated temperature minimum in the Na_2Cl_2-K_2Cl_2-$CaSO_4$ system.....240
Table A 11 Calculated invariant points in the NaCl-K_2SO_4-$CaSO_4$ system.....242
Table A 12 Calculated invariant points in the NaCl-$MgSO_4$-$CaSO_4$ system.....242
Table A 13 Calculated invariant points in the NaCl-$K_2Mg_2(SO_4)_3$-$K_2Ca_2(SO_4)_3$ system.....243

List of symbols and abbreviations

Chemical formula	
Ag	Silver
Ag_2SO_4	Silver sulphate
Al	Aluminium
Al_2O_3	Aluminium oxide
AlkCl(ss)	Solid solution: $(Na^{1+}, K^{+}, Ca^{2+}, Va^{0})(Cl^{-})$
Au	Gold
$BaCO_3$	Barium carbonate
Bi	Bismuth
C_6H_5COOH	Benzoic acid
Ca^{2+}	Calcium ion
$CaCl_2$	Calcium chloride
CaF_2	Calcium fluoride
$CaSO_4$	Calcium sulphate
Cl^{-}	Chloride ion
CsCl	Caesium chloride
GLAS	Solid solution: $(K^{1+}, Na^{1+})_3(Na^{1+})_1(SO_4^{2-})_2$
HEXA	Solid solution: $(Na^{1+}, K^{1+}, Mg^{2+}, Ca^{2+}, Va^{0})_2(SO_4^{2-})_1$
In	Indium
K^{+}	Potassium ion
K_2CrO_4	Potassium chromate
K_2SO_4	Potassium sulphate
KCl	Potassium chloride
$KClO_4$	Potassium perchlorate
LANGBEINITE	Solid solution: $(K^{1+})_2(Ca^{2+}, Mg^{2+})_2(SO_4^{2-})_3$
MCl2	Solid solution: $(Mg^{2+}, Ca^{2+})_1(Cl^{-})_2$
Mg^{2+}	Magnesium ion
$MgCl_2$	Magnesium chloride
MgF_2	Magnesium fluoride
$MgSO_4$	Magnesium sulphate
Na^{+}	Sodium ion
Na_2SO_4	Sodium sulphate
NaCl	Sodium chloride
NaLT	Solid solution: $(Na^{1+}, K^{1+})_2(SO_4^{2-})_2$
Na-ortho-MT	Solid solution: $(Na^{1+}, K^{1+}, Mg^{2+}, Ca^{2+}, Va^{0})_2(SO_4^{2-})_1$
Ni	Nickel
Pt	Platinum
$RbNO_3$	Rubidium nitrate
Sn	Tin
SO_4^{2-}	Sulphate ion
Zn	Zinc
Symbols	
(g)	Gas
(l)	Liquid
(s)	Solid
$\Delta_f H^0_{298}$	Standard enthalpy of formation [J/mol]
ΔG_{mix}	Gibbs free energy of mixing [J]
ΔH	Enthalpy increment [J]

ΔH_{tr}	Enthalpy of tranisition [kJ/mol]
$\Delta_m H$	Melting enthalpy [J]
ΔS_{mix}	Entropy of mixing [J]
$°G_i$	Molar Gibbs free energy of component I [J/mol]
a, b, c, α, β, V	Lattice parameters [Å, °, Å^3]
b	Baseline
C_p	Heat capacity [J/K]
$C_{p(r)}^{\circ}$	Referemce molar heat capacity [J/(mol·K)]
$C_{p(s)}^{\circ}$	Sample molar heat capacity [J/(mol·K)]
C_p°	Molar heat capacity [J/(mol·K)]
d	Interplanar spacing [Å]
$^{ex}G_m$	Excess molar Gibbs free energy [J/mol]
G	Gibbs free energy [J]
G_m	Molar Gibbs free energy [J/mol]
H	Enthalpy [J]
H_f	Final state enthalpy [J]
H_i	Initial state enthalpy [J]
H^{ref}	Reference enthalpy [J]
H_T	Enthalpy at temperature T [J]
$^{id}G_m$	Ideal molar Gibbs free energy [J/mol]
$L_{ij}^{(v)}$; $L_{i,j,k}{}^k$	Interaction parameters
m	Mass [g]
M	Molar mass [g/mol]
mol%	Molar percentage
m_r	Mass of reference [g]
m_s	Mass of sample [g]
n_i	Molar number of component i
P	Pressure [Pa]
q_i	Extensive variable
r	Reference
R	Universal gas constant [8.1345 J/(mol·K)]
$^{ref}G_m$	Reference molar Gibbs free energy [J/mol]
s	Sample
S	Entropy [J/K]
$S^0{}_{298}$	Standard molar entropy [J/(mol·K)]
S^{ref}	Reference entropy [J/K]
T	Temperature [K; °C]
T_f	Final temperature [K; °C]
T_i	Initial temperature [K; °C]
T_m	Melting temperature [K; °C]
T_{tr}	Transition temperature [K; °C]
U	Internal energy [J]
V	Volume [m^3]
Va	Vacancy
vol%	Volume percentage
wt%	Weight percentage
X	Molar ratio
x_i	Mole fraction of component i
y_i	Site fraction of component i
θ	Diffraction angle [°]
λ	X-ray wavelength [Å]

μ_i	Chemical potential of component i
Φ_i	Thermodynamic potential

Abbreviations

CEF	Compound Energy Formalism
CSP	Concentrated solar power plant
DSC	Differential scanning calorimetry
DTA	Differential thermal analysis
EDX	Energy dispersive X-ray spectroscopy
exp	Experimental
FTsalt	FactSage Thermodynamic Database for Molten Salts
GTOx	GTT Oxide Database
HT	High-temperature modification
HT(n)	The nth HT-XRD cycle
HT-XRD	High temperature X-ray diffractometry
ICDD	International Centre of Diffraction Data
ICSD	Inorganic Crystal Structure Database
IMD-1	Institute of Energy Materials and Devices, Structure and Function of Materials
LH-TES	Latent heat thermal energy storage
Liq	Liquid
LT	Low-temperature modification
MT	Medium-temperature modification
PCM	Phase change material
PCM2	Phase Change Material Screening 2 Database
PDF	Powder Diffraction File
SEM	Scanning electron microscopy
SGPS	Scientific Group Thermodata Europe - Pure Substances
SRCM	Self-referencing calibration method
SRO	Short range ordering
TES	Thermal energy storage
TG	Thermogravimetry
XRD	X-ray diffractometry

1 Introduction

The multicomponent salt system consisting of Na^+, K^+, Mg^{2+}, Ca^{2+} // Cl^-, SO_4^{2-} has wide-ranging applications, particularly in the field of thermal energy storage [1], where it is being evaluated as a promising framework from which suitable phase change material (PCM) candidates for medium-to-high temperature applications may be derived. The study of these salt mixtures is crucial due to their relevance in concentrated solar power (CSP) plants, which require efficient and reliable PCMs to improve energy storage and conversion processes [2, 3].

This work is part of the PCM-Screening-2 project (FKZ 03EN6005D) [4] funded by the Federal Ministry for Economic Affairs and Climate Action (Bundesministerium für Wirtschaft und Klimaschutz), which was aimed at identifying suitable PCMs for thermal energy storage. The focus of the present study is to investigate the salt system involving the cations Na^+, K^+, Mg^{2+}, Ca^{2+} in combination with the anions Cl^- and SO_4^{2-}. Such a system includes:

- eight pure salts: NaCl, KCl, $MgCl_2$, $CaCl_2$, Na_2SO_4, K_2SO_4, $MgSO_4$, and $CaSO_4$;
- twenty-eight (pseudo)binary systems, including both binary systems with the same cation or anion (MX-NX or MX-MY) and sections with different cations and anions (MX-NY);
- fifty-six (pseudo)ternary systems, including both ternary systems (MX-NX-PX) and planes (e.g. MX-NX-PY) defined within higher-order multicomponent systems;
- seventy (pseudo)quaternary systems, including two quaternary systems (MX-NX-PX-QX), six reciprocal systems (MX-NY-MY-NX) and sixty-two non-planar quadrilateral combinations (e.g. MX-NX-PX-MY).

The multicomponent system can be visualised either as a cube or, equivalently, as four trigonal-based prisms sharing one or more faces (**Figure 1-1**). The prisms represent four reciprocal quaternary systems (Na^+,K^+,Mg^{2+}//Cl^-,SO_4^{2-}; Na^+,K^+,Ca^{2+}//Cl^-,SO_4^{2-}; Na^+,Mg^{2+},Ca^{2+}//Cl^-,SO_4^{2-}; K^+,Mg^{2+},Ca^{2+}//Cl^-,SO_4^{2-}), and their quadrilateral faces correspond to six reciprocal ternary systems (Na^+,K^+//Cl^-,SO_4^{2-}; Na^+,Mg^{2+}//Cl^-,SO_4^{2-}; Na^+,Ca^{2+}//Cl^-,SO_4^{2-}; K^+,Mg^{2+}//Cl^-,SO_4^{2-}; K^+,Ca^{2+}//Cl^-,SO_4^{2-}, Mg^{2+},Ca^{2+}//Cl^-,SO_4^{2-}). The terms “ternary” and “quaternary” refer to the number of independent end-members required to thermodynamically describe the system. It is important to note that, although the system is thermodynamically described in terms of ionic components, the diagram is plotted in the space of electrically neutral end-member compounds.

As highlighted by Jänecke [5], the internal phase equilibria of a complex reciprocal salt system can be reconstructed with reasonable accuracy by analysing its boundary surfaces and diagonal section of the complex system. He compared this process to inferring the internal layout of a house when the facades, the ground-floor plan, the sloped roof, and the staircase are known:

«Aus den Grenzflächen und der Diagonalfläche […] kann man mit ziemlicher Genauigkeit das Zustandsbild im Innern des komplizierten Systems konstruieren, ähnlich wie bei einem Haus, von dem die Fassaden, der Grundriß des Erdgeschosses, das äußere Dach und das Treppenhaus bekannt sind, die Angabe des Inneren mit einiger Wahrscheinlichkeit möglich ist.»[1]

Similarly, by examining the binary, ternary and quaternary subsystems that define the outer structure, one can extrapolate the phase relationships within the interior of the prisms or the cube (**Figure 1-1**).

This research, with a focus on energy-related applications, aims to define and present methodologies for the investigation of selected salt systems and the expansion of a dedicated thermodynamic database. By applying advanced thermodynamic modelling techniques and incorporating newly acquired experimental data, the study enables a broader and more reliable screening of candidate materials, facilitating the identification and selection of those meeting the most promising criteria for thermal energy applications. The goal of this thesis is to develop a robust thermodynamic database (PCM2) for the multicomponent salt system, allowing for more accurate predictions of phase equilibria and thermodynamic properties. This will enhance the understanding and utilisation of these systems in CSP and other high-temperature applications.

The structure of this work is organised as follows. Chapter 2 provides a literature review and is structured according to the classification of the previously mentioned reciprocal systems A^{m+}, B^{n+} // X^{p-}, Y^{q-}. Chapter 3 describes the experimental techniques adopted in this study, while Chapter 4 outlines the thermodynamic modelling approach and the software tools employed. Chapters 5 and Chapter 6 present the experimental and modelling results, respectively, and are also structured according to the same classification of reciprocal systems, starting with the reciprocal system Mg^{2+}, Ca^{2+} // Cl^-, SO_4^{2-}, which represented both the chronological and conceptual starting point of this work. Chapter 7 discusses potential applications of the most promising compositions, and Chapter 8 presents the general conclusions and future perspectives.

[1] E. Jänecke, *Über das Schmelz-und Erstarrungsbild des doppelt-ternären Systemes (K_2· Na_2· Mg)(Cl_2· SO_4)*, Zeitschrift für anorganische Chemie 261(3-4) (1950) p. 220.

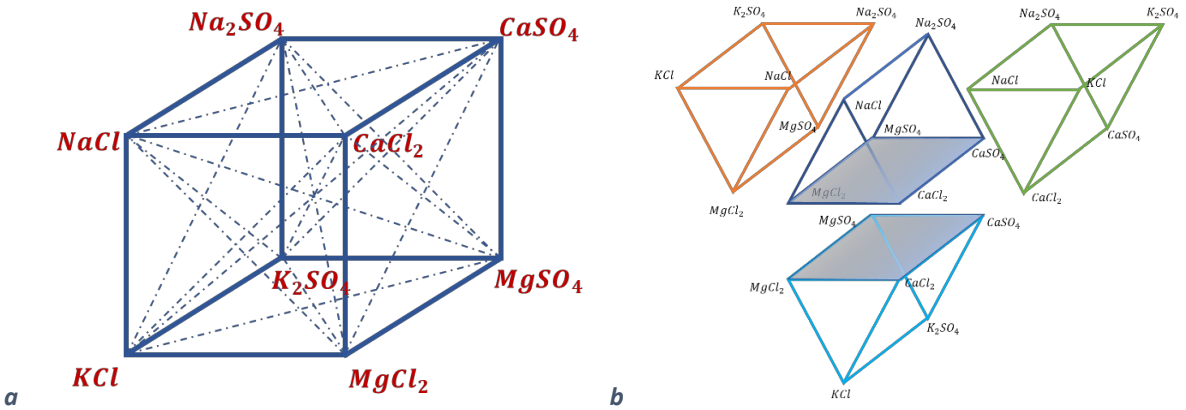


Figure 1-1 *Graphical representation of the Na^+, K^+, Mg^{2+}, Ca^{2+} // Cl^-, SO_4^{2-} multi-component system:* ***a*** *cubic representation with visualisation of (pseudo)binary systems under analysis;* ***b*** *alternative representation of the multi-component system made of four six-component systems.*

2 Literature review

The following chapter provides a literature review of potential applications of molten salts in thermal energy storage, as well as a review of compounds and systems under study. This serves as a necessary foundation for the experimental work and subsequent thermodynamic modelling. For clarity and ease of reference, the subsystems that constitute the multicomponent system are organised into six subsections, each corresponding to one of the six reciprocal systems A^{m+}, B^{n+} // Cl^-, SO_4^{2-}. As shown in **Figure 1-1**, some of the reciprocal systems share common binary edges (i.e., subsystems); therefore, each shared subsystem is presented only once, specifically in the first subsection in which it appears in sequence.

2.1 Phase Change Materials in Thermal Energy Storage applications

Renewable energy technologies are an urgent need in order to tackle catastrophic climate changes, global warming and the depletion of fossil fuel reserves [6, 7]. Among these, concentrating solar power (CSP) technologies are able to solve problems concerning electricity production because they use the sun's heat, an unrestricted and daily available energy source [2]. CSP technology, when integrated with thermal energy storage (TES), provides dispatchable energy, enabling the alignment of energy availability with demand by storing solar heat during daylight hours for later use [8, 9]. TES is achieved through three primary methods [1, 10-13]: sensible heat storage, latent heat storage, and thermochemical storage. Latent heat thermal energy storage (LH-TES) involves using materials that undergo phase transformations (solid-solid, solid-liquid and liquid-gas), known as Phase Change Materials (PCM). When PCMs are heated to their phase change point, they absorb substantial energy, which can then be released as they cool, as illustrated in **Figure 2-1** and described in **Equation 1**. This makes PCMs well-suited for efficient energy storage, though they must meet specific requirements to be effective in TES applications [14-16], as schematically summarised in **Table 2-1**, together with health hazard considerations and cycling stability [17].

$$H_f^0 - H_i^0 = \int_{T_i}^{Tm} C_P dT + \Delta_m H + \int_{T_m}^{T_f} C_P dT + \ldots \qquad \textit{Equation 1}$$

Equation 1 represents the total enthalpy change ($H_f^0 - H_i^0$) between the initial and final states, where T_i and T_f are the initial and final temperatures. It is obtained by integrating the heat capacity C_P over temperature in both the solid and liquid regions and comprises three contributions: the first sensible heat term between T_i and the melting temperature T_m, the enthalpy of fusion at the melting point ($\Delta_m H$), and the second sensible heat term between T_m and T_f.

PCMs can be categorised by type, such as organic and inorganic, and by specific applications. A large number of materials are identified as suitable PCMs [3, 10, 15, 18-27], among them inorganic salts [28, 29]. Despite challenges such as phase separation and corrosion [30], inorganic PCMs generally offer higher thermal conductivity and energy storage capacity than organic counterparts [31]. In particular, eutectic phase change materials (EPCMs), and especially molten salt-based systems, show superior performance in TES applications compared to single-component PCMs, due to their broader phase change temperature range and higher phase stability [32]. Inorganic salts and their eutectic mixtures are promising candidates for medium-to-high temperature PCMs, thanks to their high latent heat of fusion, wide melting temperature ranges, and elevated solid-state densities. Eutectic compositions are especially attractive, as they often combine favourable thermal properties and compositional tunability, enabling the design of tailored PCM systems. To address the inherently low thermal conductivity of many inorganic materials, several strategies have been employed to improve heat transfer and overall performance, including the use of fins, encapsulation, and multiple or cascaded PCM configurations [10, 31, 33].

Investigating systems containing alkali and alkaline-earth chlorides and sulphates is of paramount importance in the pursuit of efficient PCMs for CSP and TES applications. Alkali- and alkaline-earth-based salts have attracted increasing attention in the literature as promising PCM candidates, due to their low cost, availability, and favourable thermal properties [34-36] (**Figure 2-2**). Several studies have previously focused on nitrates, chlorides, carbonates and sulphates, aiming to establish a robust and comprehensive thermodynamic database for high-temperature thermal energy storage applications [34, 37-46]. The present study contributes further to this ongoing effort by providing new thermodynamic data specifically related to chloride- and sulphate-containing systems. These materials could therefore be of interest for latent heat thermal energy storage, which, beyond solar power applications, is relevant for waste heat recovery, thermal management in automotive and electronic systems, and for building heating and air-conditioning [47].

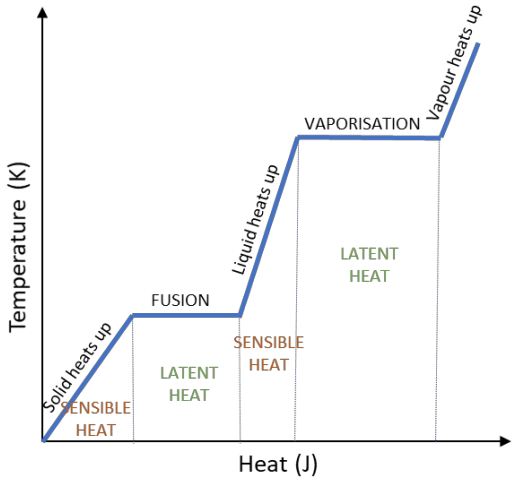


Figure 2-1 *Heat vs. temperature during phase transitions in PCMs.*

Table 2-1 *Good criteria for PCMs.*

THERMODYNAMIC CRITERIA	KINETIC CRITERIA	CHEMICAL CRITERIA	ECONOMIC CRITERIA
A melting point in the desired operating temperature range	Little or no supercooling during cooling	Chemical stability	Available in large quantities
High latent heat of fusion per unit mass		No chemical decomposition	Inexpensive
High density		Non-corrosiveness to construction materials	
High specific heat		Non-poisonous	
High thermal conductivity		Non-flammable	
Congruent melting		Non-explosive	
Small volume changes during phase transition			

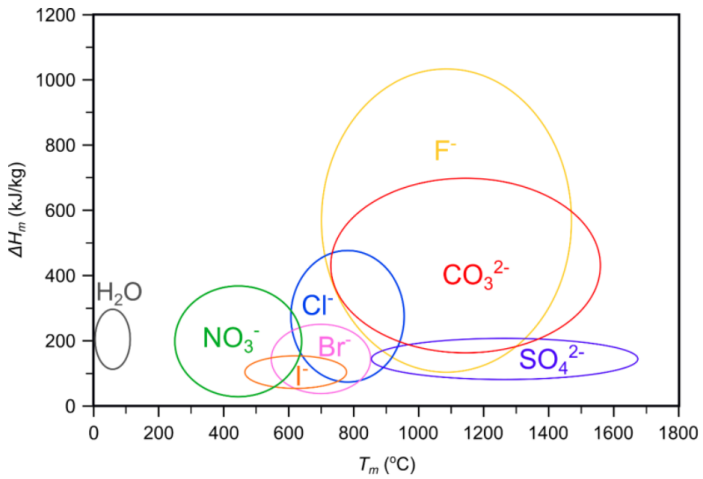
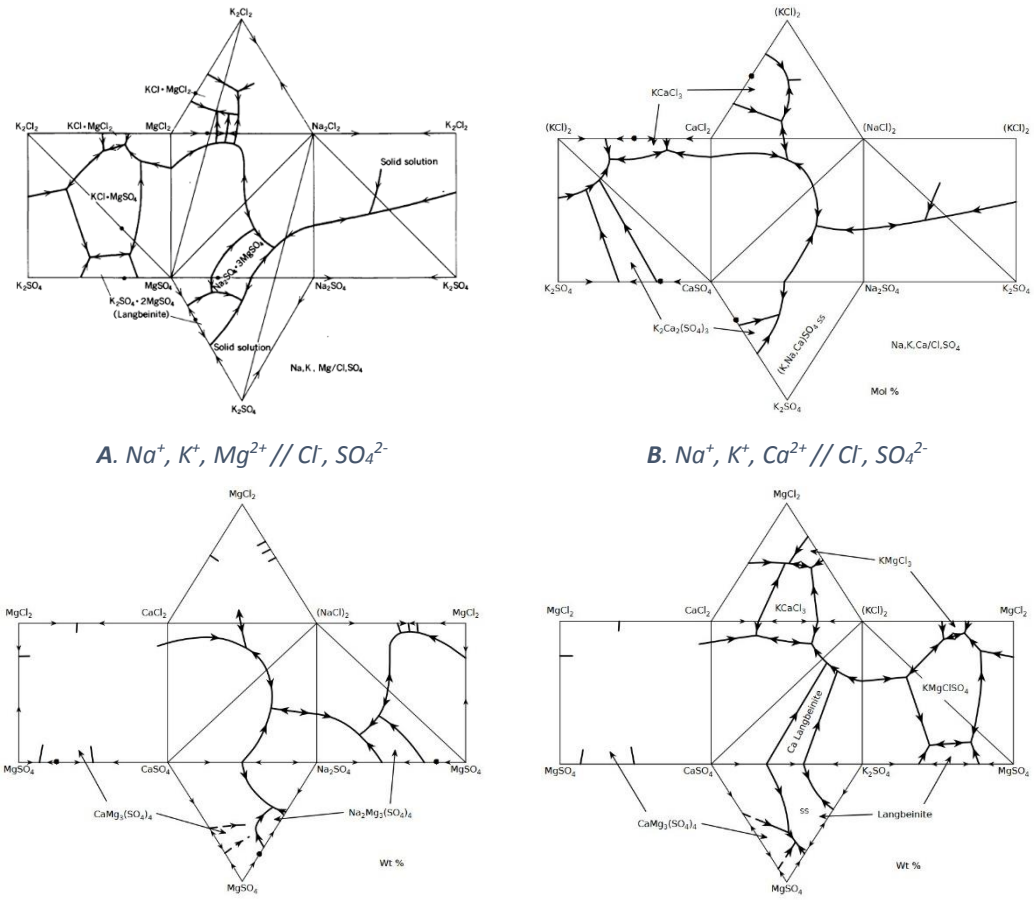


Figure 2-2 *Enthalpy of fusion as a function of the melting temperature of salts of interest in PCM-Screening-2 project, from Reis [48].*

2.2 Thermodynamics of salt systems

The current understanding of the six-component reciprocal systems takes as its starting point the schematic two-dimensional diagrams proposed by Rowe et al. [49] (**Figure 2-3**), which provide an overall view of the prisms shown in **Figure 1-1b**, here depicted in a planar representation. In this section, a comprehensive review of the literature on (pseudo)binary systems, classified within the subsections dedicated to the six reciprocal systems, is presented. This review aims to provide a clear overview of the current knowledge and developments in these systems, serving as a foundational basis for the work presented in this dissertation. The evident lack of comprehensive experimental data in the literature - highlighted, for instance, by diagrams **C** and **D** in **Figure 2-3** - justified the decision to initially focus the experimental campaign on the reciprocal system Mg^{2+}, Ca^{2+} // Cl^-, SO_4^{2-}. Accordingly, the following section presents the available literature data within the framework of reciprocal systems, starting with the first system of interest. This structure mirrors the logic adopted in the experimental study discussed in Chapter 5 and in the thermodynamic modelling results presented in Chapter 6.



A. *Na^+, K^+, Mg^{2+} // Cl^-, SO_4^{2-}* ***B***. *Na^+, K^+, Ca^{2+} // Cl^-, SO_4^{2-}*

C. *Na^+, Mg^{2+}, Ca^{2+} // Cl^-, SO_4^{2-}* ***D***. *K^+, Mg^{2+}, Ca^{2+} // Cl^-, SO_4^{2}*

Figure 2-3 *Graphical bidimensional representation of the four six-component systems from Rowe et al. [49].*

2.2.1 Pure salts

The relevant thermodynamic properties for each pure compound involved in the multicomponent system - both from literature sources and as implemented in the thermodynamic database developed in this work - have been reviewed, and are presented at the beginning of Chapter 5. As the thermodynamic properties of these pure compounds have already been extensively studied, they are not discussed in detail in the present work. Any new experimental findings or database modifications related to the pure components are presented in the relevant experimental and modelling sections.

2.2.2 Binary systems within reciprocal systems

2.2.2.1 Mg^{2+}, Ca^{2+} // Cl^-, SO_4^{2-} system

There are no studies specifically addressing the Mg^{2+}, Ca^{2+} // Cl^-, SO_4^{2-} reciprocal system as a whole, as schematically represented in **Figure 2-4**, extracted from the six-component diagram by Rowe et al. [49]. However, research has been conducted on the related binary subsystems that form its components, as detailed below. The system consists of four binary subsystems ($MgCl_2$-$CaCl_2$, $MgSO_4$-$CaSO_4$, $MgCl_2$-$MgSO_4$ and $CaCl_2$-$CaSO_4$) and two diagonals representing the exchange reaction ($MgCl_2$-$CaSO_4$ and $CaCl_2$-$MgSO_4$).

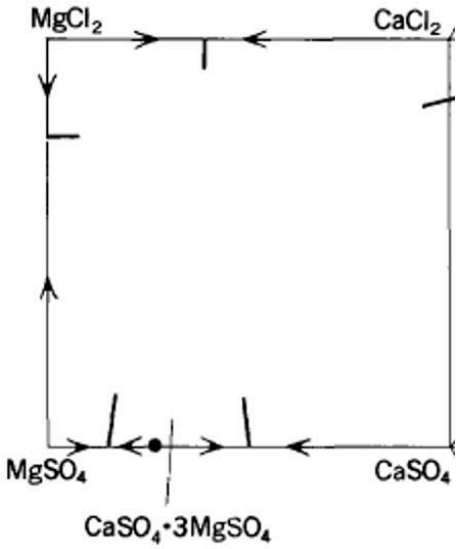


Figure 2-4 *Graphical representation of the Mg^{2+}, Ca^{2+} // Cl^-, SO_4^{2-} reciprocal system from Rowe et al. [49].*

2.2.2.1.1 $MgCl_2$-$CaCl_2$

The $MgCl_2$-$CaCl_2$ system was first investigated experimentally by Menge [50] and later by Ivanov [51] and Matiašovský [52]. These earlier works described the system as a single eutectic phase diagram, with a reported solid solubility of $MgCl_2$ in $CaCl_2$ within a composition range of 10-15 mol%

$MgCl_2$. In these studies [50-52] the determination of solid solubilities was based on plotting the time of thermal arrest as a function of composition. A more comprehensive re-examination was subsequently carried out by Grjotheim et al. [53], who aimed to verify and refine the earlier findings [50-52]. Their investigation employed a combination of techniques, including thermal analysis, differential thermal analysis, quenching technique with microscopic and X-ray examination of quenched samples, and high-temperature X-ray diffraction. The eutectic parameters reported in the literature show some variability. Menge [50] identified a eutectic at 39.1 mol% $CaCl_2$ and 621 °C, with a solid solution of 14.7 mol% $MgCl_2$. Ivanov [51] reported a eutectic composition of 47.2 mol% $CaCl_2$ at 611 °C with a solid solution of approximately 10 mol% $MgCl_2$. Similarly, Matiašovský [52] found a eutectic at 46.7 mol% $CaCl_2$ and 614 °C, and a solid solution larger than 11.5 mol% $MgCl_2$. Grjotheim et al. [53] revised these values, determining a eutectic at 47.2 mol% $CaCl_2$ and 620 °C with a solid solubility of up to 17.2 mol% $MgCl_2$ in $CaCl_2$. The phase diagram was later thermodynamically modelled by Chartrand et al. [54] and Robelin et al. [55] (**Figure 2-5**). Their assessment resulted in a calculated eutectic temperature of 617 °C and a solubility of $MgCl_2$ in solid $CaCl_2$ of less than 18 mol% $MgCl_2$. Their optimisation [54, 55] was based on the phase diagram data by Grjotheim et al. [53], supplemented with the activity data of $MgCl_2$ in the melt derived from electromotive force (emf) measurements by Karakaya and Thompson [56] and the enthalpy of mixing of the liquid phase [57].

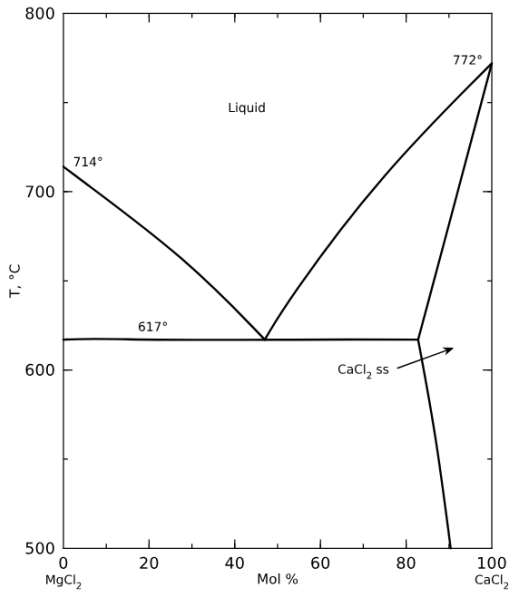


Figure 2-5 *Phase diagram of $MgCl_2$-$CaCl_2$ system from Robelin et al. [55].*

2.2.2.1.2 $MgSO_4$-$CaSO_4$

The binary system $MgSO_4$-$CaSO_4$ was experimentally investigated only by Rowe et al. [58], due to decomposition of sulphates of alkaline earth metals at high temperatures. Ramsdell [59] and

Mukimov et al. [60] considered the system to be a simple eutectic without the formation of intermediate compounds. In contrast, Rowe et al. [58] reported the existence of an intermediate phase, $CaSO_4 \cdot 3MgSO_4$, which was found to melt congruently at 1201 $\pm$ 4 °C. According to Rowe et al. [58], the phase diagram consists of a simple eutectic system with two eutectics: one at 13.5 mol% (temperature not reported) and another at 52 mol% of $CaSO_4$ (at 1116 °C). The liquidus temperatures were determined by sealed tube quenching experiments, whereas the sub-solidus reactions were studied through long-term annealing below the decomposition temperatures. The calculated phase diagrams of this system [39, 61] show good agreement with the experimental data of Rowe et.al. [58]. Du [61] included the congruent-melting compound $CaMg_3(SO_4)_4$ in their assessment, calculating the eutectic points at 1069 °C and 6.4 mol% and at 1116 °C and 52 mol% $CaSO_4$. Similarly, Yazhenskikh et al. [39] calculated a eutectic between $CaSO_4$ and $CaMg_3(SO_4)_4$ at 1117 °C and 53.0 mol% $CaSO_4$, and another eutectic between $MgSO_4$ and $CaMg_3(SO_4)_4$ at 1071 °C and 5.5 mol% $CaSO_4$ (**Figure 2-6**). In Yazhenskikh et al.'s study [39] the heat capacity of $CaMg_3(SO_4)_4$ was generated from the corresponding pure sulphates using Neumann-Kopp rule, and modified in order to avoid unnecessary peaks on heat capacity curve.

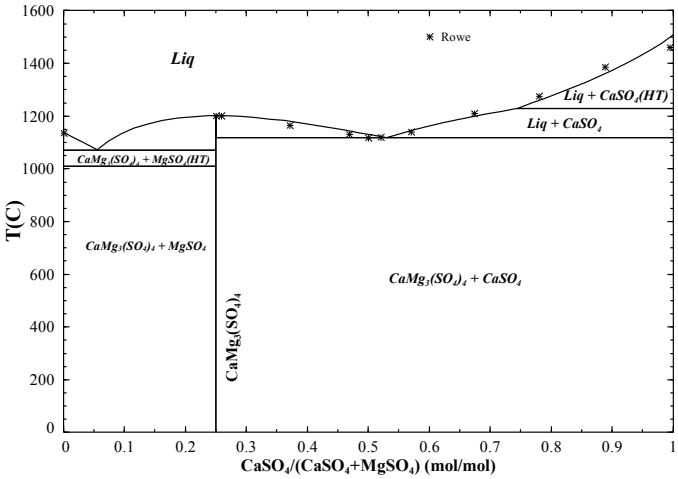


Figure 2-6 *Phase diagram of $MgSO_4$-$CaSO_4$ system from Yazhenskikh et al. [39] with experimental data from Rowe et al. [58].*

2.2.2.1.3 $MgCl_2$-$MgSO_4$

The $MgCl_2$-$MgSO_4$ system was first studied by Jänecke [62] (**Figure 2-7**), who reported a simple eutectic phase diagram with a eutectic at 20 mol% $MgSO_4$ and 667 °C. Speranskaya [63] presented the eutectic at 22.5 mol% $MgSO_4$ and at 656 °C. It should be noted that neither of these studies provided data for high compositions of $MgSO_4$, due to the decomposition of sulphate above 1000 °C [58, 64, 65], preventing experimental investigation in this compositional range.

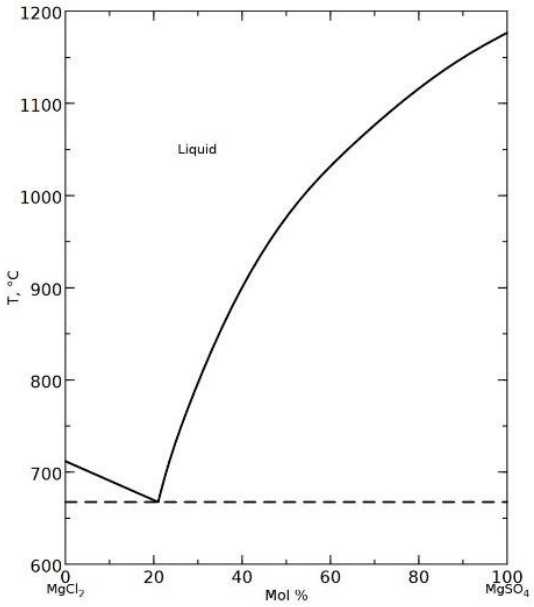


Figure 2-7 *Phase diagram of $MgCl_2$-$MgSO_4$ system from Jänecke [62].*

2.2.2.1.4 $CaCl_2$-$CaSO_4$

The $CaCl_2$-$CaSO_4$ system was investigated by several authors [66-72], who described it as a single eutectic system; however, a complete binary phase diagram covering the entire compositional range is still not available. Sackur [66] reported a minimum of the liquidus curve at 14.4 mol% $CaSO_4$ and 727 °C. Pichugin [67], who studied the system in the composition range 0-25 mol% of $CaSO_4$, identified a eutectic at 15 mol% $CaSO_4$ and 718 °C. In the broader study of the reciprocal system K^+, Ca^{2+} // Cl^-, SO_4^{2-}, Jänecke et al. [68] only noted that the eutectic is located near the $CaCl_2$-rich side of the phase diagram. Golubeva et al. [69] reported a eutectic at 12.5 mol% $CaSO_4$ and 706 °C (**Figure 2-8**), a composition later confirmed by Palkin [70] and Zimina et al. [73], who measured a eutectic temperature of 712 °C. Arbukhanova et al. [72], in their investigation of the ternary system CaF_2-$CaCl_2$-$CaSO_4$, confirmed the same eutectic composition with a temperature of 708 °C. The available experimental data provide only a partial description of the phase diagram, as measurements at higher $CaSO_4$ compositions were limited by the thermal decomposition of $CaSO_4$ above 1200 °C [58, 74].

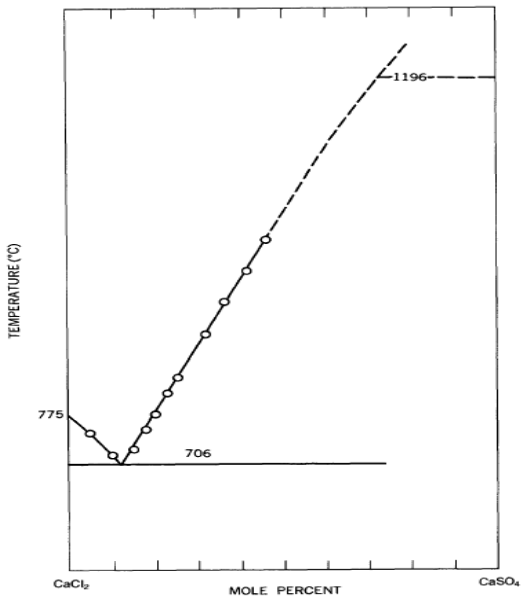


Figure 2-8 *Phase diagram of $CaCl_2$-$CaSO_4$ system from Rowe et al [49] with experimental data from Golubeva et al. [69].*

2.2.2.1.5 $MgCl_2$-$CaSO_4$

The system has not been previously investigated, and no phase diagram data or thermodynamic properties of potential eutectic compositions are available in literature. The lack of data highlights the need for an experimental campaign to investigate the thermodynamic behaviour of the system.

2.2.2.1.6 $CaCl_2$-$MgSO_4$

The system remains unexplored, with no phase diagram information or thermodynamic data reported in the literature. This lack of characterisation suggests the necessity of targeted experimental investigations to clarify its thermodynamic behaviour within the framework of the reciprocal system.

2.2.2.2 Na^+, Mg^{2+} // Cl^-, SO_4^{2-} system

The reciprocal system Na^+, Mg^{2+} // Cl^-, SO_4^{2-} has been previously investigated by Speranskaya [63], Jänecke [5] and Rowe et al. [49]. It is defined by four binary subsystems NaCl-$MgCl_2$, Na_2SO_4-$MgSO_4$, NaCl-Na_2SO_4 and $MgCl_2$-$MgSO_4$, forming the edges of the quaternary system, and two diagonals representing the exchange reaction Na_2Cl_2-$MgSO_4$ and $MgCl_2$-Na_2SO_4. To ensure electroneutrality in the thermodynamic description, NaCl is treated as a dimer (Na_2Cl_2) in the reciprocal system assessment. Based on the phase diagram proposed by Speranskaya [63] (**Figure 2-9**), the system is characterised by seven phase fields of primary crystallisation: Na_2SO_4, Na_2SO_4-$3MgSO_4$, NaCl, $MgSO_4$, $MgCl_2$, NaCl-$2MgCl_2$, and 2NaCl-$MgCl_2$. Speranskaya [63], confirmed later by Jänecke [5],

reported the invariant points at the following temperatures: 435 °C, 546 °C, 465 °C, 560 °C (568 °C [5]), 634 °C (626 °C [5]), and the eutectic between NaCl and $MgSO_4$ at 642 °C. In addition, Speranskaya [63] investigated several quasi-binary sections within the reciprocal system, thereby providing a valuable experimental dataset.

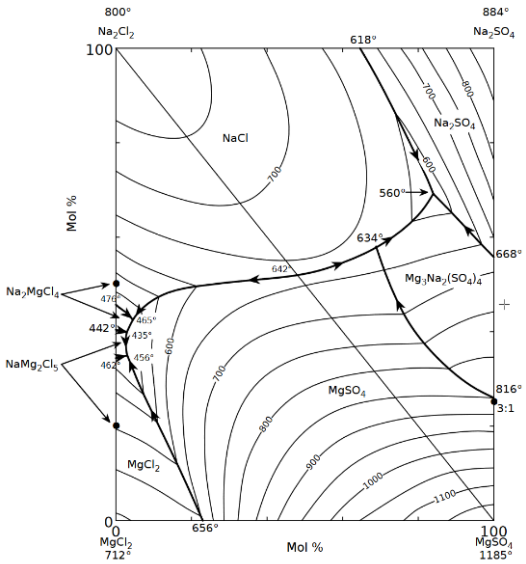


Figure 2-9 *Phase diagram of Na^+, Mg^{2+} // Cl^-, SO_4^{2-} system from Speranskaya [63].*

2.2.2.2.1 NaCl-$MgCl_2$

The NaCl-$MgCl_2$ phase diagram has been extensively investigated through thermal analysis and X-ray diffraction by several authors [50, 52, 63, 75-78]. Early work by Menge [50] reported only one compound, NaCl·$MgCl_2$, within the system. Later studies refined this picture, identifying two incongruently melting compounds; 2NaCl·$MgCl_2$ (melting point between 464 °C and 488 °C) and NaCl·$MgCl_2$ (melting point at 445 °C and 468 °C). Klemm and Weiss [75], using X-ray diffraction, confirmed the existence of these two phases, while Bondarenko [79] supported these findings and located a eutectic at 450 °C and 62 mol% NaCl. In contrast, Scholich [80] and Speranskaya [63] reported two compounds, 2NaCl·$MgCl_2$ (melting point at 476 °C) and NaCl·$2MgCl_2$ (melting point at 462 °C), with a eutectic at 444 °C and 53 mol% NaCl. However, Klemm and Weiss [75] demonstrated that NaCl·$2MgCl_2$ was not a distinct compound but rather a mixture of NaCl·$MgCl_2$ and $MgCl_2$. The phase relations were later confirmed by Grjotheim et al. [77] by DTA and XRD on quenched melts, reporting melting temperatures of 468 °C for NaCl·$MgCl_2$ and 485 °C for 2NaCl·$MgCl_2$, with a eutectic at 445 °C and 41.5 mol% $MgCl_2$, consistent with [75]. Some additional phases, Na_6MgCl_8 and $Na_2Mg_3Cl_8$, were proposed by Seifert and Thiel [78], but their existence was not supported by other investigations [50, 52, 54, 75, 77].

The system is characterised by two peritectic and one eutectic reaction: the first peritectic (Liquid + NaCl ⇌ Na_2MgCl_4) observed between 35.6-39.4 mol% $MgCl_2$ and 464-488 °C; the second peritectic (Liquid + $MgCl_2$ ⇌ $NaMgCl_3$) occurring between 46.9-49.0 mol% $MgCl_2$ and 445-468 °C; the eutectic (Liquid ⇌ Na_2MgCl_4 + $NaMgCl_3$) located between 39.9-44.0 mol% $MgCl_2$ and 430-451 °C.

Calorimetric investigations were carried out for both liquid [81-83] and solid phases [83]. Kleppa and McCarty [81] measured the enthalpy of mixing of the liquid phase at 810 °C. The liquid activities of NaCl and $MgCl_2$ in the system were determined using the electromotive force (emf) method across several studies [56, 84-87], showing good consistency across studies. The phase diagram was calculated by Chartrand et al. [54] and Yin et al. [88], both confirming the two incongruently melting compounds, 2NaCl·$MgCl_2$ (melting point at 475 °C [54] or 471 °C [88]) and NaCl·$MgCl_2$ (melting point at 466 °C [54] or 464 °C [88]), and the eutectic at 459 °C [88] and 44.5 mol% $MgCl_2$ [54] or 43.3 mol% $MgCl_2$ [88]. Finally, the system was assessed by the project partner GTT-Technologies, within the framework of the PCM-Screening-2 project [4], incorporating all available experimental data. The updated thermodynamic database predicts 2NaCl·$MgCl_2$, with a melting temperature of 474 °C, and NaCl·$MgCl_2$, which melts at 464 °C and exhibits a eutectic reaction at 460 °C with a composition of 44.13 mol% $MgCl_2$. The calculated phase diagram is shown in **Figure 2-10** and the optimised interaction parameters $L_{ij}^{(\nu)}$ in the liquid phase are adopted in the present work (**Table 6-16**).

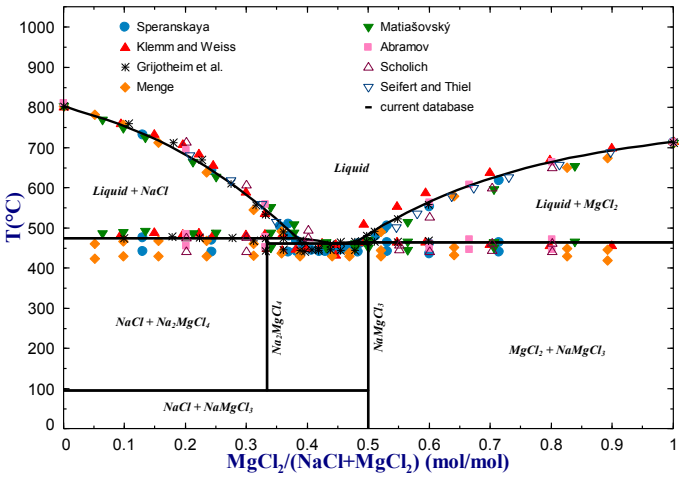


Figure 2-10 *Phase diagram of NaCl-$MgCl_2$ system from the PCM2 database [4] with experimental data: Speranskaya [63], Klemm and Weiss [75], Grijotheim et al. [77], Menge [50], Matiašovský [52], Abramov [89], Scholich [80], Seifert and Thiel [78].*

2.2.2.2.2 Na_2SO_4-$MgSO_4$

The binary sulphate system was experimentally studied [58, 63-65, 90] and assessed [39, 61]. Nacken [64] reported two intermediate compounds with Na_2SO_4:$MgSO_4$ ratio of 3:1 ($Na_6Mg(SO_4)_4$) and 1:3 ($Na_2Mg_3(SO_4)_4$), respectively. In addition to them, Ginsberg [65] identified a third compound $Na_2Mg(SO_4)_2$ (ratio 1:1). $Na_6Mg(SO_4)_4$, known as vanthoffite, was reported to decompose at 490 °C [64]. $Na_2Mg_3(SO_4)_4$, known as anti-vanthoffite, was reported to melt congruently at 813 °C and to take part in two eutectic reactions, one with $MgSO_4$ (77 mol% $MgSO_4$, 808 °C) and one with the solid solution based on the high temperature modification of Na_2SO_4 (48 mol% $MgSO_4$, 665 °C). $Na_2Mg(SO_4)_2$ undergoes two solid-solid transitions before decomposing peritectoidally at 603 °C [64]. That compound was reported also by Mukimov et al. [60]. Additional confirmation of these phase relations was provided by Bandaranayake and Mellander [90], who, through DSC and XRD analyses, verified the existence of $Na_2Mg(SO_4)_2$ and $Na_2Mg_3(SO_4)_4$, and classified $Na_6Mg(SO_4)_4$ as metastable. The phase diagram description of Speranskaya [63] was consistent with the previous studies [64, 65]. The system was thermodynamically assessed by Du [61] and later re-evaluated by Yazhenskikh et al. [39]. In contrast with the work of Du [61], Yazhenskikh et al. [39] incorporated all three compounds observed experimentally, $Na_6Mg(SO_4)_4$, $Na_2Mg(SO_4)_2$ and $Na_2Mg_3(SO_4)_4$ (ratio Na_2SO_4:$MgSO_4$ 3:1, 1:1 and 1:3, respectively), as illustrated in **Figure 2-11**. The heat capacities of these intermediates were estimated via the Neumann-Kopp rule, based on the C_p values of the corresponding pure sulphates [39]. The optimised standard enthalpy of formation of $Na_6Mg(SO_4)_4$ reported in the same study is in good agreement with literature data [91, 92]. The thermodynamic data of the three double sodium-magnesium sulphates, together with the interaction parameters in the solid solution based on the high-temperature modification of alkali sulphates (HEXAGONAL), optimised in Yazhenskikh et al.'s assessment [39] have been incorporated into the PCM2 database and used in the present work (**Table 6-1** and **Table 6-16**).

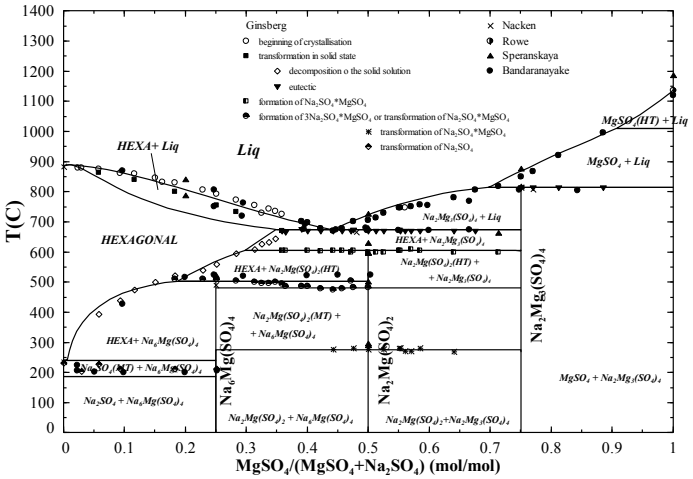


Figure 2-11 *Phase diagram of Na_2SO_4-$MgSO_4$ system from Yazhenskikh et al. [39] with experimental data: Ginsberg [65], Nacken [64], Rowe et al. [58], Speranskaya [63], Bandaranayake and Mellander [90].*

2.2.2.2.3 NaCl-Na_2SO_4

NaCl-Na_2SO_4 system has been experimentally investigated by thermal analysis and visual-polythermal methods [5, 63, 93-106], and later thermodynamically assessed [45, 107]. Experimental studies consistently indicated a simple eutectic phase diagram, with no evidence of intermediate compounds or solid solutions. They reported the eutectic composition between 45 and 48 mol% Na_2SO_4, with a corresponding melting temperature ranging from 624-634 °C. No direct measurements of the thermodynamic properties of the liquid phase have been reported. Lindberg et al. [107] calculated the eutectic point at 46.7 mol% Na_2SO_4 and 625.9 °C, in agreement with experimental findings [99, 101, 102, 104]. Based on the available data in literature, a thermodynamic assessment has been conducted by GTT-Technologies in the frame of the PCM-Screening-2 project, and the interaction parameters $L_{ij}^{(\nu)}$ in the liquid phase of the binary system NaCl-Na_2SO_4 are included in PCM2 database and used in this work (**Table 6-16**). The calculated eutectic point has a composition of 47.4 mol% Na_2SO_4 and a melting temperature of 624.1 °C. The corresponding phase diagram is shown in **Figure 2-12**.

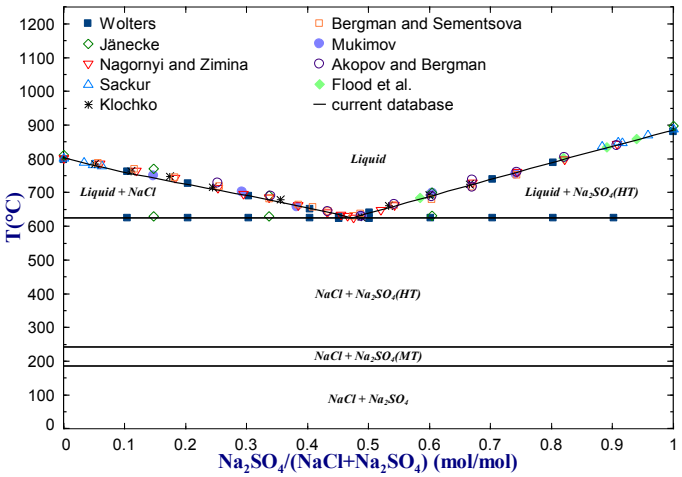


Figure 2-12 *Phase diagram of NaCl-Na_2SO_4 system from the PCM2 database [4] with experimental data: Wolters [97], Jänecke [108], Nagornyi and Zimina [101], Sackur [98], Klochko [104], Bergman and Sementsova [99], Mukimov [103], Akopov and Bergman [102], Flood at al. [96].*

2.2.2.2.4 NaCl-$MgSO_4$

The first investigation of the system was carried out by Speranskaya [63], who identified Na_2Cl_2-$MgSO_4$ as the stable diagonal in the reciprocal system. According to their results, the phase relations correspond to a simple eutectic diagram, with the eutectic located at 642 °C and 48.5 mol% $MgSO_4$ (equivalent to 32.01 mol% in the NaCl-$MgSO_4$ system), as illustrated in **Figure 2-13**. Subsequent studies by Bergman and Golubeva [109] and Rowe et al. [49] corroborated both the eutectic composition and the liquidus topology proposed by Speranskaya, although their experiments were hindered by sulphate decomposition and chloride volatilisation, which complicated the determination of phase boundaries.

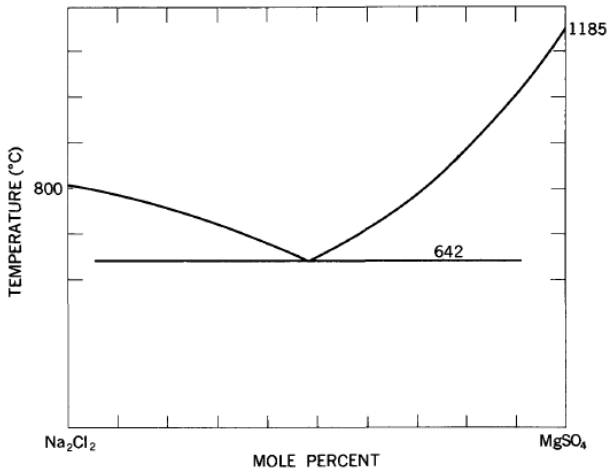


Figure 2-13 *Phase diagram of Na_2Cl_2-$MgSO_4$ system from Rowe et al. [49], originally from Speranskaya [63].*

2.2.2.2.5 $MgCl_2$-Na_2SO_4

Speranskaya [63] examined the section $MgCl_2$-Na_2SO_4 of the reciprocal system, reporting crystallisation temperature of several compositions. Based on these measurements, a clear trend in the liquidus behaviour was outlined. Starting from the melting point of the sulphate (884 °C), the liquidus decreases sharply with increasing $MgCl_2$ to Na_2SO_4, reaching approximately 575 °C at around 81 mol% Na_2SO_4. As the composition moves further into the $MgCl_2$ field, the liquidus temperature rises, attaining a maximum of 662 °C at about 60 mol% Na_2SO_4 as it passes through the primary NaCl field. Beyond this point, the liquidus declines again until it reaches the $MgSO_4$-NaCl boundary at 642 °C (51 mol% Na_2SO_4) where $MgSO_4$ becomes the primary phase up to the $MgCl_2$-$MgSO_4$ boundary at 588 °C (14 mol% Na_2SO_4), after which the liquidus rises to the melting point of $MgCl_2$ at 712 °C. The system experiences solid-solid transitions, with regions of mixed-phase coexistence identified through crystallisation points from the melts, as illustrated in **Figure 2-14**.

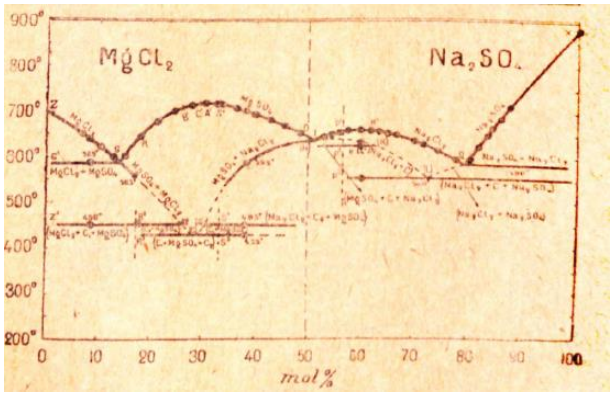


Figure 2-14 *Phase diagram of $MgCl_2$-Na_2SO_4 system from Speranskaya [63].*

2.2.2.3 Na^+, Ca^{2+} // Cl^-, SO_4^{2-} system

The Na^+, Ca^{2+} // Cl^-, SO_4^{2-} system was previously investigated by Palkin [70], Zimina et al. [71], and Rowe et al. [49]. The system consists of four binary systems NaCl-$CaCl_2$, Na_2SO_4-$CaSO_4$, NaCl-Na_2SO_4 and $CaCl_2$-$CaSO_4$ and two sections representing the exchange reaction Na_2Cl_2-$CaSO_4$ and $CaCl_2$-Na_2SO_4, where NaCl is considered as a dimer (Na_2Cl_2) to maintain electroneutrality. In their study, Zimina et al. [71] reported no ternary compounds, a eutectic point at 485 °C in the ternary system Na_2Cl_2-$CaCl_2$-$CaSO_4$ and a sulphate solid solution in the Na_2Cl_2-Na_2SO_4-$CaSO_4$, with a minimum at 634 °C, as presented in **Figure 2-15**.

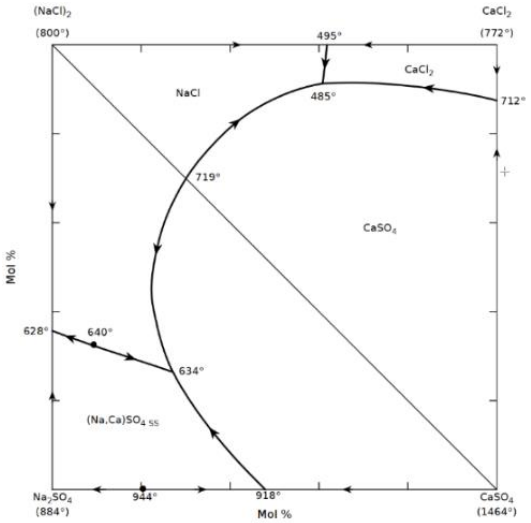


Figure 2-15 *Phase diagram of Na^+, Ca^{2+} // Cl^-, SO_4^{2-} system from Rowe et al. [49], originally from Zimina et al. [71].*

2.2.2.3.1 NaCl-$CaCl_2$

The NaCl-$CaCl_2$ system has been extensively investigated through thermal analysis and X-ray diffraction [50, 110-120]. Menge [50] and Seltveit and Flood [114] reported the existence of an intermediate compound, Na_4CaCl_6; however, other studies challenged this finding, instead indicating a significant solid solubility of $CaCl_2$ in NaCl, up to 20 mol% $CaCl_2$ [114, 119]. The eutectic composition has been estimated to lie between 51 to 53 mol% $CaCl_2$, while reported eutectic temperatures vary slightly among studies: approximately 492 °C [119], 500 °C [118], 506 °C [80], and 510 °C [110]. Østvold [86] measured the heat of mixing at 10 mol% intervals, whereas Sem et al. [121] collected data at broader intervals of about 25 mol%; despite the different resolutions, their results are in good agreement. Østvold [86] and Egan and Bracker [87] reported consistent values for the NaCl activity in the liquid phase, despite performing measurements at temperatures differing by around 25 °C. Based on available experimental data, the phase diagram was calculated and optimised by Chartrand and Pelton [54] and by Yin et al. [43]. The system under investigation was already part of the screening phase within the PCM Screening 1 project (FKZ 03ET1441D) conducted by Reis [48]. In that study, to describe the solubility of $CaCl_2$ in NaCl, the solid solution of NaCl and KCl (referred to as MCl in [48]) was expanded by incorporating two additional species in the first sublattice: Ca^{2+} and Va^0, representing the calcium ion and an electroneutral vacancy, respectively. In that model, each molecule of $CaCl_2$ is assumed to dissociate into $CaCl^+$ and $VaCl^-$, ensuring the solution remains electroneutral. The interaction parameters for the MCl solid solution in the NaCl-$CaCl_2$ system, as well as the interaction parameters for the liquid phase $L_{ij}^{(\nu)}$ were optimised. The final eutectic transition was calculated at 52.34 mol% $CaCl_2$ with a temperature of 499 °C and enthalpy of fusion of 16.34 kJ/mol. The evaluation

performed by Reis [48] has been integrated into the construction of the database utilised in this study. Their calculated phase diagram is displayed in **Figure 2-16**.

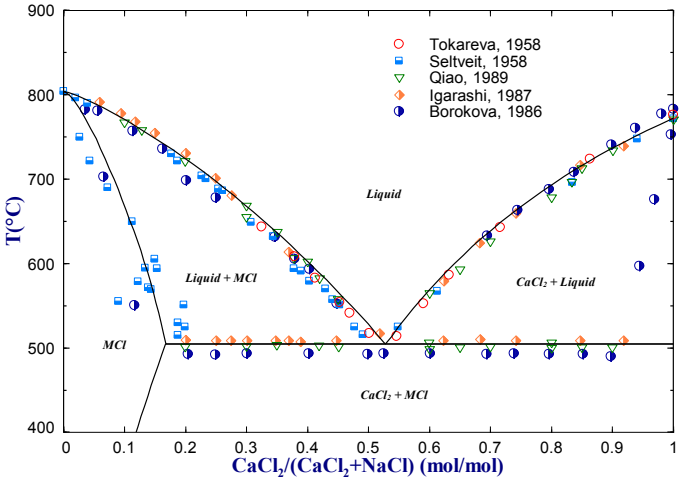


Figure 2-16 *Phase diagram of NaCl-$CaCl_2$ system from Reis [48] with experimental data: Tokareva et al. [120], Seltveit and Flood [114], Qiao et al. [118], Igarashi et al. [110], Borovkova et al. [119].*

2.2.2.3.2 Na_2SO_4-$CaSO_4$

The Na_2SO_4-$CaSO_4$ system has been extensively investigated through thermal analysis and X-ray diffraction [60, 71, 90, 122-130], and subsequently assessed thermodynamically [39, 61]. Early studies by Kommissarova et al. [127] and Freyer et al. [122, 130] reported the formation of an intermediate compound with a Na_2SO_4-$CaSO_4$ ratio 1:1 ($Na_2Ca(SO_4)_2$), known as glauberite. Previously, Müller [123] observed the segregation of a compound with a Na_2SO_4-$CaSO_4$ ratio 4:1, coexisting with $CaSO_4$. Kobertz et al. [126] excluded the possibility of glauberite formation by crystallisation from the melt but identified a compound with a Na_2SO_4-$CaSO_4$ ratio 3:1, $Na_6Ca(SO_4)_4$, instead of the previously suggested 2:1 ratio, as a result of melt segregation. The existence of $Na_6Ca(SO_4)_4$ was further confirmed by XRD analysis of four different compositions (18, 22, 78 and 82 mol% $CaSO_4$) subjected to various heat treatments [126]. XRD investigations also confirmed the presence of two compounds, $Na_6Ca(SO_4)_4$ (3:1) and $Na_2Ca(SO_4)_2$ (1:1), while revealing negligible solubility of calcium in the solid high-temperature Na_2SO_4 (Na_2SO_4-HT), in contrast to findings by other authors [90, 124].

Eysel et al. [131] investigated the Na_2SO_4 crystal structures and the solid solutions in the Na_2SO_4-$CaSO_4$ system. Four solid solution phases were described, namely the hexagonal high-temperature solid solution phase with Na_2SO_4-I crystal structure (structure type: α-K_2SO_4(HT), space group: P63/mmc, e.g. ICSD collection code 81503) and three sodium-rich solid solution phases: the orthorhombic medium temperature solid solution phase with Na_2SO_4-III crystal structure (space group Cmcm, lattice parameters of pure Na_2SO_4 at room temperature: a = 5.6274 Å, b = 8.9664 Å, c = 9.9737

Å and V = 354.88 Å^3 (ICSD 66554)) and two phases with crystal structures related to the orthorhombic Na_2SO_4-III, but with a slight monoclinic distortion. One monoclinic solid solution phase with the approximate chemical composition $(Na_{0.9}Ca_{0.05})_2SO_4$ is reported with the following lattice parameters at room temperature: a ≈ 9.27 Å, b ≈ 5.35 Å, c ≈ 7.12 Å, β ≈ 92.4° and V ≈ 352.5 Å^3 (ICDD PDF 29-1291 (Zn-stabilised)). The other sodium-rich solid solution phase with the approximate chemical composition $(Na_{0.8}Ca_{0.1})_2SO_4$ has a different monoclinic angle, which is now α instead of β. Its lattice parameters at room temperature are as follows: a ≈ 9.25 Å, b ≈ 5.34 Å, c ≈ 7.13 Å, α ≈ 91.4° and V ≈ 352.0 Å^3 (ICDD PDF 29-1296). The exact crystal structure of the two monoclinic phases is not known yet.

A significant contribution to the understanding of the Na_2SO_4-$CaSO_4$ system was provided by Freyer et al. [122], who investigated the formation and transformation of metastable solid solutions obtained by quenching molten mixtures and their subsequent conversion into stable phases. Samples included both freshly quenched melts and long-term annealed solids, enabling a detailed analysis of phase stability. Using XRD and DTA, they characterised structural and thermal behaviour across a wide composition range. Their findings identified glauberite ($Na_2SO_4 \cdot CaSO_4$) as the only stable intermediate compound in the system, existing up to 520 °C, above which it decomposes. A low-temperature phase, thenardite (Na_2SO_4 V), was reported as stable, while the hexagonal Na_2SO_4 I phase was recognised as the only stable solid solution. The thermal events between 230 °C and 280 °C were attributed to reversible transformations between hexagonal and monoclinic lattice structures within the metastable region of the phase diagram, challenging earlier interpretations [90, 124, 128], which had considered these effects as equilibrium transformations. Freyer et al. [122] also identified three distinct metastable solid solutions, whose formation depends on the $CaSO_4$ content: solid solution A (up to 4 mol% $CaSO_4$), associated with stabilised Na_2SO_4 III (orthorhombic); solid solution B (4 and 20 mol% $CaSO_4$), related to stabilised Na_2SO_4 I (hexagonal); solid solution C (33 and 40 mol% $CaSO_4$), a metastable phase resembling $2Na_2SO_4 \cdot CaSO_4$. Solid solution B corresponds to the two phases with monoclinic distorted Na_2SO_4-III structure, which were consolidated by Freyer et al. [122] as one phase. The study determined the limiting concentrations of $CaSO_4$ for these metastable phases and proposed a transformation scheme describing their conversion into stable phases, with glauberite and thenardite predominating at low temperatures. The crystal structure of solid solution C, $Na_4Ca(SO_4)_3$, was later published by Shablinskii et al. [132] (trigonal, space group R3, lattice parameters: a = 15.7278 Å, c = 22.0037Å, V = 4713.7 Å^3, ICSD 143077).

A comprehensive reinvestigation of the binary system was later conducted by Kobertz et al. [126], who combined DTA and XRD analyses. Their DTA work included 15 measurements in Al_2O_3 crucibles in air, 13 measurements in sealed quartz crucibles under vacuum (<10^{-1} mbar) up to 1200

°C, 5 measurements in open Al_2O_3 crucibles with a gas mixture containing 14 vol% CO_2, 6 vol% O_2, 2 vol% SO_2, and the balance N_2, and 12 measurements in Pt crucibles with lids in air. They reported that $Na_6Ca(SO_4)_4$ melts congruently at 950 °C and participates in two eutectic reactions with eutectic points at 46 mol% $CaSO_4$ and 925 °C and at 1-2 mol% $CaSO_4$ and 882 °C. Additionally, $Na_2Ca(SO_4)_2$ was reported to decompose peritectoidally into $Na_6Ca(SO_4)_4$ and $CaSO_4$ at 910 °C.

The phase diagram was subsequently assessed by Du [61] and Yazhenskikh et al. [39]. Unlike Du's work [61], Yazhenskikh et al. [39] incorporated 1:1 $Na_2Ca(SO_4)_2$ and 3:1 $Na_6Ca(SO_4)_4$ compounds, relying heavily on the experimental work of Kobertz et al. [126]. Their assessment [39] provided optimised thermodynamic properties of these double sulphates. The heat capacity data were derived either from the corresponding data of pure sulphates using the Neumann-Kopp rule or from available calorimetric data [130]. According to this latest assessment [39] (**Figure 2-17**), $Na_6Ca(SO_4)_4$ melts congruently at 949.2 °C and is involved in two eutectic reactions. The first occurs with Na_2SO_4 (HT) at 2 mol% $CaSO_4$ and 882.7 °C, while the second involves $CaSO_4$ at 50.4 mol% $CaSO_4$ and 925.6 °C.

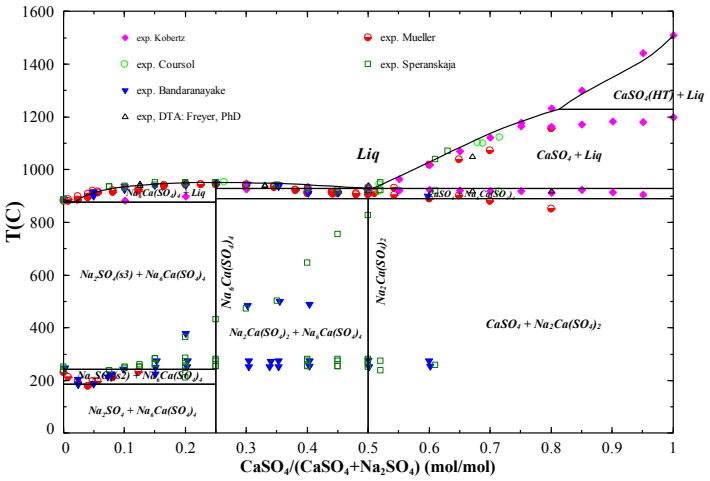


Figure 2-17 *Phase diagram of Na_2SO_4-$CaSO_4$ system from Yazhenskikh et al. [39] with experimental data: Kobertz et al. [126], Coursol et al. [125], Bandaranayake et al. [90], Freyer et al. [122, 130], Müller [123], Speranskaya et al. [124].*

2.2.2.3.3 NaCl-$CaSO_4$

The stable diagonal of the reciprocal system was first examined by Bergman and Pichugin in 1932 as reported in [133], who identified a eutectic point at 31.7 equiv% $CaSO_4$ (16.61 mol%) and 721 °C. Subsequent investigations yielded slightly different results: Byé et al. [134] reported a eutectic at 37 wt% $CaSO_4$ in Na_2Cl_2-$CaSO_4$ (20.13 mol% in NaCl-$CaSO_4$) at 725 °C; whereas Palkin [70] and Rubleva and Bergman [135] placed the eutectic at 30 wt% (17.45 mol% in NaCl-$CaSO_4$). Using a visual-polythermal method within the broader Ba^{2+}, Ca^{2+}, Na^+ // Cl^-, SO_4^{2-} system, Zimina et al. [71] confirmed

a eutectic temperature of 719 °C. Rowe [49] experimentally verified the eutectic thermal effect at 725 °C (**Figure 2-18**). Despite these studies, the available experimental phase diagram data only partially cover the full composition range, primarily due to the thermal decomposition of calcium sulphate, which limited high-temperature investigations.

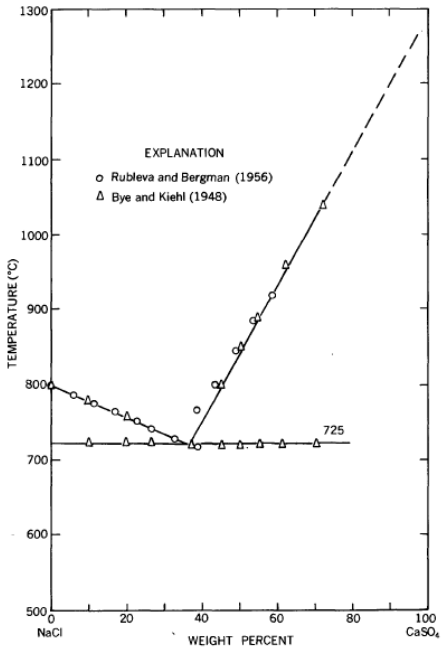


Figure 2-18 *Phase diagram of NaCl-$CaSO_4$ system from Rowe et al. [49].*

2.2.2.3.4 $CaCl_2$-Na_2SO_4

The pseudo-binary system was studied by Palkin [70] who reported the liquidus curve shown in **Figure 2-19**. Although no specific experimental data or temperatures were provided, it was noted that adding $CaCl_2$ to Na_2SO_4 results in a reduction of the liquidus temperature from 884 °C until reaching the composition boundary where $CaSO_4$ becomes the primary crystallising phase. As the system moves further, the $CaSO_4$ field is traversed, and eventually, $CaCl_2$ emerges as the primary phase. The liquidus temperature subsequently increases, reaching the melting point of $CaCl_2$ at 775 °C. The section was studied by Zimina et al. [71], in the frame of the complex system Ba^{2+}, Ca^{2+}, Na^+ // Cl^-, SO_4^{2-}, but they did not provide detailed phase diagram data.

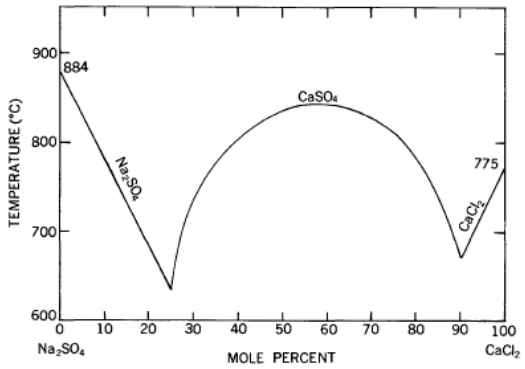


Figure 2-19 *Phase diagram of $CaCl_2$-Na_2SO_4 system from Rowe et al. [49], originally from Palkin [70].*

2.2.2.4 K^+, Mg^{2+} // Cl^-, SO_4^{2-} system

The reciprocal system K^+, Mg^{2+} // Cl^-, SO_4^{2-} was first investigated by Jänecke [5, 62] and later by Rowe et al. [49]. In its quadrilateral representation, the system is defined by four binary subsystems KCl-$MgCl_2$, K_2SO_4-$MgSO_4$, KCl-K_2SO_4 and $MgCl_2$-$MgSO_4$ forming the edges of the diagram. The two diagonals correspond to the exchange reaction, K_2Cl_2-$MgSO_4$ and $MgCl_2$-K_2SO_4, where KCl is considered as a dimer (K_2Cl_2) in order to preserve electroneutrality. The reciprocal system presents seven fields of primary crystallisation: the four pure compounds and the binary compounds $K_2SO_4 \cdot 2MgSO_4$ (langbeinite), $KCl \cdot MgCl_2$ (anhydrocarnallite) and possibly $KCl \cdot MgSO_4$ (anhydrokainite), as presented in **Figure 2-20**. Jänecke [62] proposed the compound $KCl \cdot MgSO_4$ and reported it to melt congruently at 920 °C. In addition, they investigated internal sections, some involving this intermediate compound, either as end-member ($MgCl_2$-$KMgClSO_4$, K_2SO_4-$KMgClSO_4$) or as part of the section $KMgCl_3$-$K_2Mg_2(SO_4)_3$, as well as the $KMgCl_3$-$MgSO_4$ section. Jänecke [62] reported six invariant points: five eutectic points at 418, 433, 605, 620 and 845 °C, and an additional transition at 460 °C.

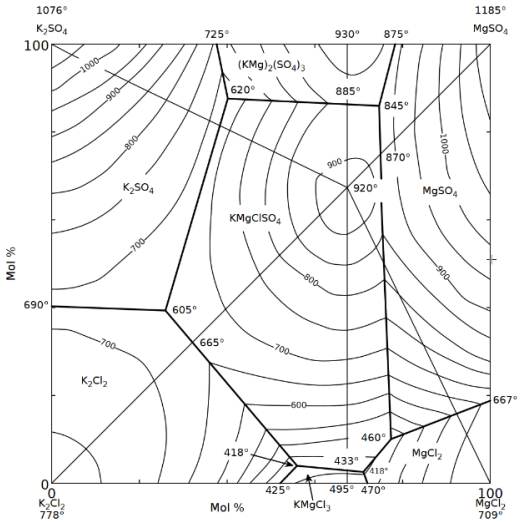


Figure 2-20 *Phase diagram of K^+, Mg^{2+} // Cl^-, SO_4^{2-} system from Jänecke [62].*

2.2.2.4.1 KCl-$MgCl_2$

The binary system KCl-$MgCl_2$ has been subjected to numerous experimental and thermodynamic studies. Early investigations using thermal analysis and XRD [50, 62, 76-78, 80, 85, 89, 136, 137] identified several intermediate compounds, namely K_2MgCl_4, $KMgCl_3$, $K_3Mg_2Cl_7$ and K_4MgCl_6. However K_4MgCl_6 was later discarded in the comprehensive experimental work of Perry and Fletcher [136], which also provided new measurements and a systematic comparison with earlier results. In addition to phase equilibria, various thermodynamic data are available in the literature: calorimetric data [81, 138] and activities in the liquid for KCl [87, 139, 140] and $MgCl_2$ [84, 85] are provided; and for the abovementioned intermediate compounds, the enthalpies of reaction at room temperature from pure chlorides [54, 137, 141] and enthalpies of fusion [54, 142] were measured and optimised. These datasets have formed the basis for previous assessments of the system [54, 143]. For the present work, the Gibbs energy description of the liquid phase has been adopted from the PCM2 database, developed by GTT-Technologies on the basis of the available literature. The interaction parameters for the liquid phase $L_{ij}^{(\nu)}$ (**Table 6-16**) were optimised and adopted in the present work. The phase diagram, presented in **Figure 2-21**, is characterised by three eutectic reactions, which, according to the current database calculations, occur as follows: Liquid ⇌ KCl + K_2MgCl_4 at 30.8 mol% $MgCl_2$ and 429.8 °C; Liquid ⇌ K_2MgCl_4 + $K_3Mg_2Cl_7$ at 34.3 mol% $MgCl_2$ and 431.7 °C; Liquid ⇌ $KMgCl_3$(HT) + $MgCl_2$ at 58.2 mol% $MgCl_2$ and 478.5 °C. The optimised thermodynamic properties of the intermediate compounds adopted in this study are summarised in **Table 6-1**.

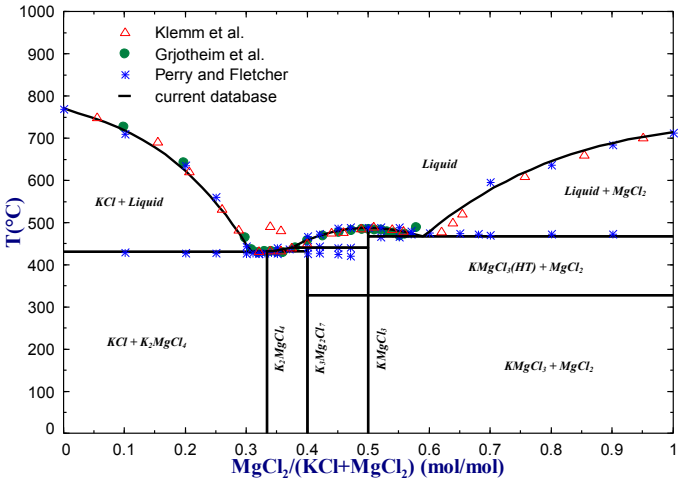


Figure 2-21 *Phase diagram of KCl-$MgCl_2$ system from the PCM2 database [4] with experimental data: Klemm et al. [76], Grjotheim et al. [77], Perry and Fletcher [136].*

2.2.2.4.2 K_2SO_4-$MgSO_4$

The binary system K_2SO_4-$MgSO_4$ has been investigated experimentally in several studies [49, 58, 64, 144-147] and subsequently modelled thermodynamically [39, 61]. A congruent melting double sulphate with stoichiometry $K_2Mg_2(SO_4)_3$, commonly referred to as magnesium langbeinite, was reported in multiple works [49, 58, 64, 144, 145]. Its melting temperature has been measured at 930 °C [64, 144, 145] or slightly higher at 943 °C [148]. Magnesium langbeinite is involved in two eutectic equilibria: the first with the high-temperature modification of potassium sulphate (hexagonal phase) at 38 mol% $MgSO_4$ and 747 °C, and the second with $MgSO_4$ at 78 mol% $MgSO_4$ and 884 °C [64]. The extent of solid solubility between the end-members has also been discussed. A solubility of $MgSO_4$ in the high-temperature modification of potassium sulphate was reported to be up 6 mol% $MgSO_4$ at the eutectic temperature of 747 °C. However, this feature was not confirmed in later studies by Rowe et al. [49, 58], leaving its existence uncertain. Complementary thermodynamic measurements have been provided in the form of heat capacity data for magnesium langbeinite, determined independently by Robie et al. [146] and Boerio-Goates et al. [147]. On the basis of these experimental datasets, Yazhenskikh et al. [39] carried out a comprehensive thermodynamic assessment of the system. Their optimisation included Gibbs energy functions for the liquid phase and the solid solution based on the high-temperature hexagonal modification of the alkali sulphate (K_2SO_4), as well as interaction parameters $L_{ij}^{(\nu)}$ for both liquid and solid solution phases. The calculated phase diagram (**Figure 2-22**) reproduces the key phase equilibria, yielding the first eutectic reaction at 37.1 mol% $MgSO_4$ and 750.5 °C, and the second one at 82.0 mol% $MgSO_4$ and 886.6 °C.

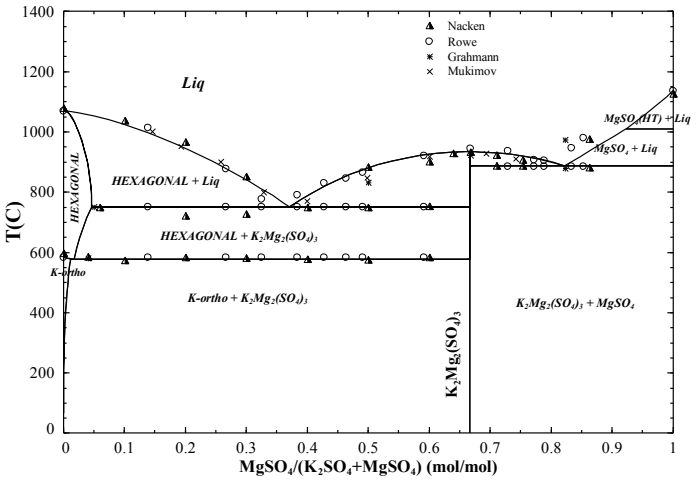


Figure 2-22 *Phase diagram of K_2SO_4-$MgSO_4$ system from Yazhenskikh et al. [39] with experimental data: Nacken [64], Rowe et al. [58], Grahmann [144], Mukimov et al. [145].*

2.2.2.4.3 KCl-K_2SO_4

The binary system KCl-K_2SO_4 has been experimentally investigated by thermal analysis and visual-polythermal methods [98-100, 102, 103, 149-154]. These studies consistently indicate that the system is characterised by a simple eutectic phase diagram, without intermediate compounds or extended solid solubility. The eutectic composition was measured between 23 and 29 mol% K_2SO_4 with a melting temperature in the range 688-694 °C. No measurements of thermodynamic data of the liquid phase have been reported in literature. A first thermodynamic description was provided by Lindberg et al. [107], who optimised the parameters in the liquid phase and located the eutectic point at 25.6 mol% K_2SO_4 and 690.5 °C. More recently, the system was reassessed by GTT-Technologies within the framework of the PCM-screening-2 project, and the optimised interaction parameters $L_{ij}^{(\nu)}$ in the liquid phase have been included into the PCM2 database and adopted for this work (**Table 6-16**). The calculated phase diagram based on the PCM2 database is shown in **Figure 2-23**, with the eutectic point located at 26.5 mol% K_2SO_4 and 690.7 °C.

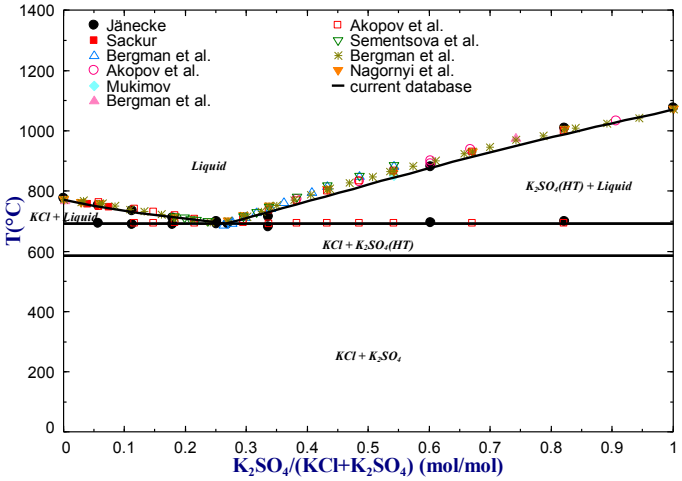


Figure 2-23 *Phase diagram of KCl-K_2SO_4 system from the PCM2 database [4] with experimental data: Jänecke [108], Sackur [98], Bergman et al. [99], Akopov et al. [102], Mukimov [103], Bergman et al. [154], Akopov et al. [149], Sementsova et al. [150], Bergman et al. [151], Nagornyi et al. [153].*

2.2.2.4.4 KCl-$MgSO_4$

Within the reciprocal system, the KCl-$MgSO_4$ section is considered to be the stable diagonal [133]. Early studies by Jänecke [62] proposed the existence of an intermediate compound KCl·$MgSO_4$, known as anhydrokainite, reported to melt congruently at 920 °C. In their phase diagram, a eutectic between $(KCl)_2$ and KCl·$MgSO_4$ was placed at 30 wt% (33.3 mol%) $MgSO_4$ and 665 °C, while a second eutectic between KCl·$MgSO_4$ and $MgSO_4$ was assumed to occur at 870 °C, as shown in **Figure 2-24**. Similar results were obtained by Bergman et al. [109], who confirmed the eutectic between $(KCl)_2$ and

$KCl{\cdot}MgSO_4$ at 33.3 equiv% $MgSO_4$ and 665 °C, and the eutectic between $KCl{\cdot}MgSO_4$ and $MgSO_4$ at 74 equiv% $MgSO_4$ and 870 °C. Subsequent investigations, however, cast doubt on the stability of the proposed intermediate compound. Rowe et al. [49], studying the reciprocal system, performed some XRD experiments on the potential intermediate compound $KCl{\cdot}MgSO_4$; the study reported X-ray diffraction patterns corresponding to phases such as langbeinite $K_2Mg_2(SO_4)_3$, KCl and $MgCl_2$ or $KCl{\cdot}MgCl_2$, but not to the supposed anhydrokainite phase. In addition to that, heating-cooling curves of the composition KCl-$MgSO_4$ indicated thermal effects at 418, 490, 610 and 885 °C, which do not align with the phase relations suggested by [62, 109]. In addition, Linstedt [155], using gravimetric analysis, also questioned the existence of $KCl{\cdot}MgSO_4$, and instead identified only langbeinite from the KCl-$MgSO_4$ composition.

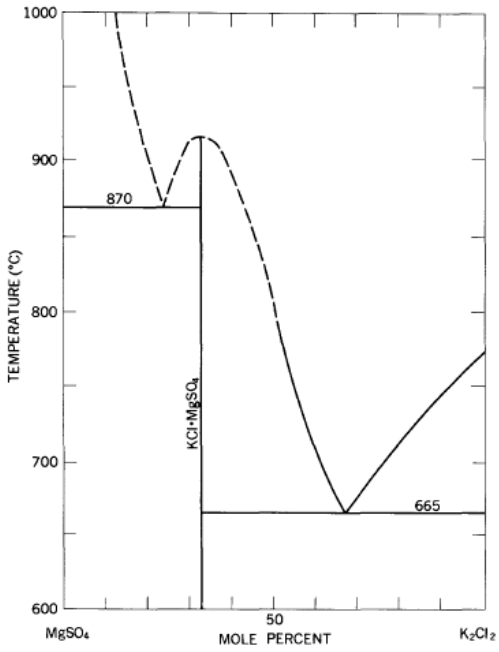


Figure 2-24 *Phase diagram of KCl-$MgSO_4$ system From Rowe [49], originally from Jänecke [62].*

2.2.2.4.5 $MgCl_2$-K_2SO_4

The $MgCl_2$-K_2SO_4 diagonal of the reciprocal system was examined exclusively by Jänecke [5, 62]. In these studies, the author reported the presence of the aforementioned intermediate compound $KCl{\cdot}MgSO_4$, anhydrokainite, which participates in the phase equilibria of the reciprocal system. The corresponding phase diagram reported by Jänecke [62] is presented in **Figure 2-25**. According to this diagram, the liquidus line displays a sequence of phase equilibria as $MgCl_2$ is progressively added to K_2SO_4. Starting from pure K_2SO_4, the liquidus decreases from 1069 °C to approximately 650 °C at a composition of 33 mol% (21 wt%) $MgCl_2$, where the $KCl{\cdot}MgSO_4$ emerges as the primary crystallising compound. With further addition of $MgCl_2$, the liquidus rises to around 790 °C as the anhydrokainite phase becomes stable. At 650 °C and 76 mol% (63 wt%) $MgCl_2$, $MgSO_4$ enters

as the primary phase field. Beyond this composition, the system shifts into the $MgCl_2$ field at 87 mol% (79 wt%) $MgCl_2$ and 580 °C, after which the liquidus increases steadily until it reaches the melting point of $MgCl_2$, reported at 712 °C.

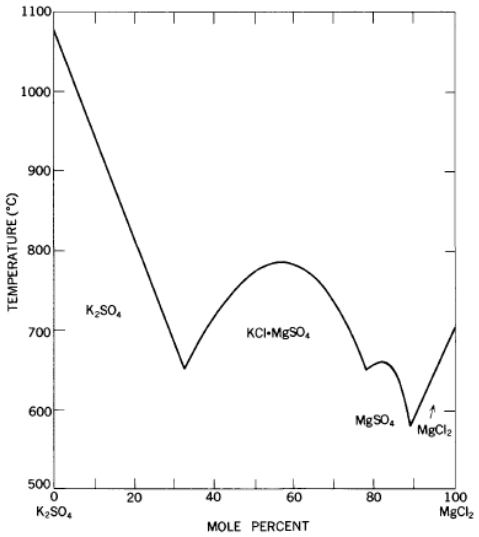


Figure 2-25 *Phase diagram of $MgCl_2$-K_2SO_4 system From Rowe et al. [49], originally from Jänecke [62].*

2.2.2.5 K^+, Ca^{2+} // Cl^-, SO_4^{2-} system

The reciprocal system K^+, Ca^{2+} // Cl^-, SO_4^{2-} has been investigated in several early studies, including those of Jänecke and Mühlhäusser [68], Golubeva and Bergman [69], Rowe et al. [49], and Finkel´shtein et al. [156] in the frame of K^+, Ca^{2+}, Ba^{2+} // Cl^-, SO_4^{2-}. The system consists of four binary subsystems KCl-$CaCl_2$, K_2SO_4-$CaSO_4$, KCl-K_2SO_4 and $CaCl_2$-$CaSO_4$ as edges of its quadrilateral representation, and two sections representing the exchange reaction K_2Cl_2-$CaSO_4$ and $CaCl_2$-K_2SO_4 as diagonals, where KCl is considered as a dimer (K_2Cl_2) to maintain electroneutrality. Jänecke and Mühlhäusser [68] identified several ternary eutectic reactions. These include equilibria at 646 °C (liquid ⇌ KCl + K_2SO_4·2$CaSO_4$ + K_2SO_4), at 680 °C (liquid ⇌ KCl + K_2SO_4·2$CaSO_4$ + $CaSO_4$), and at 582 °C (liquid ⇌ KCl + $CaSO_4$ +KCl·$CaCl_2$). A further eutectic (liquid ⇌ $CaCl_2$ + KCl·$CaCl_2$ + $CaSO_4$) was also suggested but not fully characterised. Golubeva and Bergman [69], in a complementary study, reported that the reciprocal system contains multiple phase fields of binary compounds. In addition to calcium langbeinite, they identified the presence of $2K_2SO_4$·3$CaSO_4$, and a chloride-sulphate phase with a proposed stoichiometry of either KCl·$CaSO_4$ or 2KCl·$CaSO_4$, as shown in **Figure 2-26**. They identified seven invariant points, reported in the frame of the ternary systems K_2Cl_2-K_2SO_4-$CaSO_4$ and K_2Cl_2-$CaCl_2$-$CaSO_4$. These includes four eutectics: at 580 °C and K_2Cl_2(58 mol%)-$CaCl_2$(38 mol%)-$CaSO_4$(4 mol%), at 604 °C and K_2Cl_2(14 mol%)-$CaCl_2$(79.5 mol%)-$CaSO_4$(6.5 mol%), at 644 °C and K_2Cl_2(41 mol%)-K_2SO_4(40 mol%)-$CaSO_4$(19 mol%), and at 675 °C and K_2Cl_2(65 mol%)-K_2SO_4(5 mol%)-$CaSO_4$(30 mol%).

In addition, one peritectic was identified at 653 °C and K_2Cl_2(65 mol%)-$CaCl_2$(19 mol%)-$CaSO_4$(16 mol%), together with two additional transitions at 676 °C and K_2Cl_2(54 mol%)-K_2SO_4(20 mol%)-$CaSO_4$(26 mol%), and at 748 °C and K_2Cl_2(51 mol%)-K_2SO_4(11.5 mol%)-$CaSO_4$(37.5 mol%).

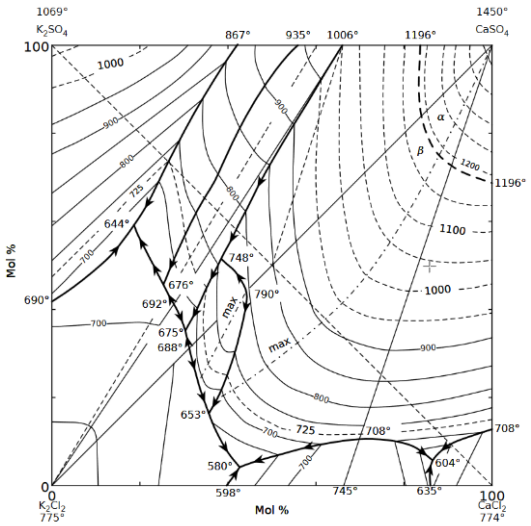


Figure 2-26 *Phase diagram of K^+, Ca^{2+} // Cl^-, SO_4^{2-} system from Golubeva and Bergman [69].*

2.2.2.5.1 KCl-$CaCl_2$

The phase diagram of the system KCl-$CaCl_2$ has been experimentally investigated in several studies [50, 87, 116, 121, 139, 141, 157-162] and in the frame of PCM Screening 1 project [48]. All studies reported the presence of an intermediate congruent melting compound $KCaCl_3$. Seifert et al. [141] determined two phase transitions at 543 and 634 °C for $KCaCl_3$. The transition temperatures, validated in the frame of the project PCM Screening 1, of 554 °C and 637 °C respectively, are in agreement with those reported in [141]. The phase diagram consists of two eutectic compositions: one that is $CaCl_2$-rich (between 22 and 26 mol% KCl) and the other that is KCl-rich (between 73 and 78 mol% KCl). Clark and Reinhardt [157] determined the temperature of the $CaCl_2$-rich eutectic to be 615 ± 2 °C, whereas other sources reported slightly higher values, ranging from 631 °C [48] to 644 °C [50]. On the KCl-rich side, however, the eutectic temperature is more consistent across sources at 595 ± 5 °C. Solid solubility has been reported [157], but it is either considered non-existent or, if present, only to a very limited extent. Østvold [139] and Sem et al. [121] reported the heat of mixing of the liquid phase; while Egan and Bracker [87] and Emons et al. [159] provided activity data of KCl in the liquid phase at 785 °C [87] and at 825 °C [159]. Additional calorimetric measurements have been conducted in the frame of the project PCM Screening 1, by using differential scanning calorimetry technique. The study provided enthalpy increment and heat capacity data of $KCaCl_3$ from room temperature up to 927 °C. The phase diagram has been calculated from Chartrand and Pelton [54], Yin et al. [43] and Reis

[48]. Reis [48] optimised thermodynamic properties ($\Delta_f H^0_{298}$, S^0_{298}, T_{tr}, $\Delta_{tr}H$ and C_p) of α, β and γ phases of $KCaCl_3$ and interaction parameters $L_{ij}^{(\nu)}$ of the liquid solution of the binary system KCl-$CaCl_2$ with the eutectic points placing at 24.8 mol% KCl and 631 °C and 76.2 mol% KCl and 596 °C (**Figure 2-27**). The assessment conducted by Reis [48] is incorporated into the development of the database relevant to this work.

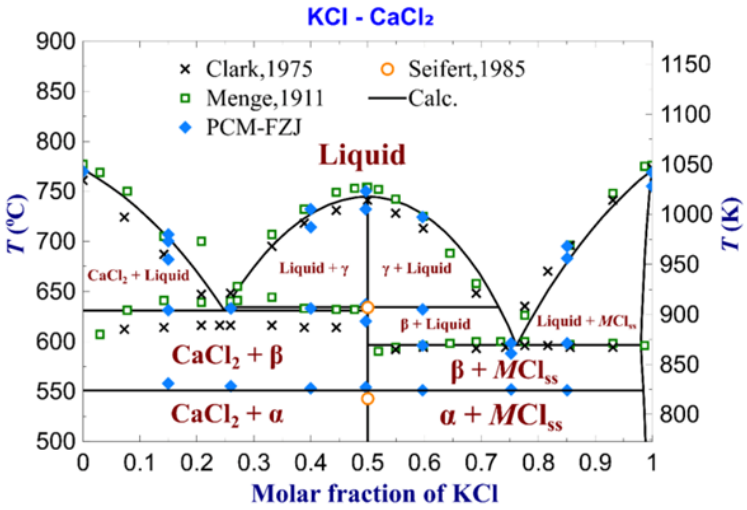


Figure 2-27 *Phase diagram of KCl-$CaCl_2$ system from Reis [48] with experimental data: Clark and Reinhardt [157], Menge [50], Seifert et al. [141].*

2.2.2.5.2 K_2SO_4-$CaSO_4$

The phase diagram was experimentally studied [74, 123, 126, 128, 144, 145, 163-167] and assessed [39, 61]. The experimental investigations [74, 123, 126, 128, 144] reported a double potassium-calcium sulphate with composition 1:2, $K_2Ca_2(SO_4)_3$, known as calcium langbeinite. It melts incongruently with $CaSO_4$ as the solid phase; the reported melting temperature is in the range 1004-1020 °C (1004 °C [123, 144], 1011 °C [74, 163], 1020 °C [128]). Mukimov et al. [145] reported additionally compounds with stoichiometry K_2SO_4:$CaSO_4$ 1:1, 2:1 and 3:1, but XRD investigation conducted by Rowe et al. [74] did not confirm their existence. Calcium langbeinite undergoes two solid-solid transitions [123, 163-165]; the enthalpy of transition of the low-temperature polymorphic transition (201.5 °C) is available in the literature [144]. The activity of the components of the liquid phase were determined by Knudsen effusion mass spectrometry by Marquez [166] and Armatys et al. [167]. A limited solid solution of $CaSO_4$ in the high-temperature modification K_2SO_4(HT) was reported up to 18 mol% $CaSO_4$ and 875 °C [74] or 867 °C [144] or up to 24 mol % $CaSO_4$ and 876 °C [128]. Thermodynamic properties and interaction parameters $L_{ij}^{(\nu)}$ in the liquid phase and in the solid solution based on the high-temperature modification of alkali sulphates (HEXAGONAL) in the K_2SO_4-$CaSO_4$ system, optimised in Yazhenskikh et al.'s study [39], have been adopted into the PCM2 database

and used in the present work (**Table 6-1** and **Table 6-16**). The calculated phase diagram (**Figure 2-28**) presents a eutectoid point at 7 mol% $CaSO_4$ and 538.5 °C, the solubility limit of $CaSO_4$ into the HEXAGONAL solid solution at 23.1 mol% $CaSO_4$ and 867.7 °C, a eutectic at 40.5 mol% $CaSO_4$ and 867.7 °C, and a peritectic point at 64.4 mol% $CaSO_4$ and 1012 °C.

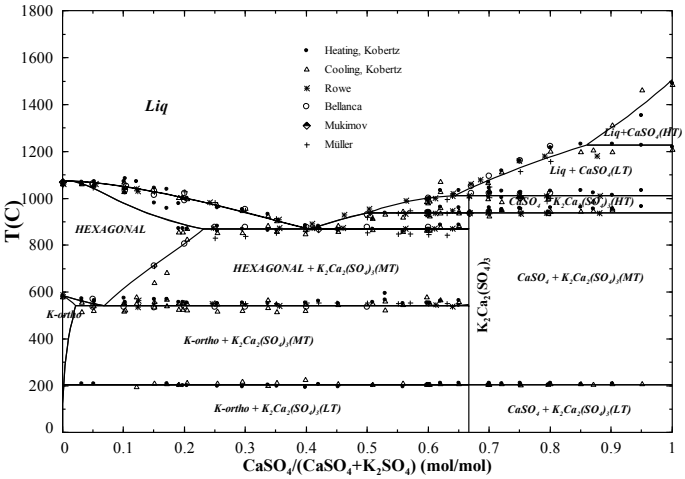


Figure 2-28 *Phase diagram of K_2SO_4-$CaSO_4$ system from Yazhenskikh et al. [39] with experimental data: Kobertz et al. [126], Rowe et al. [74], Bellanca [128], Mukimov et al. [145], Müller [123].*

2.2.2.5.3 KCl-$CaSO_4$

In the frame of the K^+, Ca^{2+} // Cl^-, SO_4^{2-}, KCl-$CaSO_4$ is the stable diagonal. Jänecke and Mühlhäusser [68] reported a eutectic at 685 °C and 31 mol% of $CaSO_4$ in the phase diagram $(KCl)_2$-$CaSO_4$. In an earlier study by Bergman - unavailable in the open literature but cited by Voskresenskaya [133] - several phase transitions were reported across different compositions, including a eutectic between KCl and KCl·$CaSO_4$ at 32.8 equiv% $CaSO_4$ and 685 °C. The observations may also imply the presence of a compound with stoichiometry KCl·$CaSO_4$. Golubeva and Bergman [69], in a later work, reported that the eutectic is at 688 °C and 32 mol% $CaSO_4$; they reported also an incongruently melting compound, 2KCl·$CaSO_4$, with a peritectoid at 790 °C and 44.5 mol% $CaSO_4$. According to the work of Rubleva and Bergman [135] the eutectic is located at 687 °C and 30.5 mol% $CaSO_4$, and the peritectoid at 827 °C and 47.5 mol% $CaSO_4$. Jänecke and Mühlhäusser [68] and Rowe et al. [49] denied the presence of the intermediate compound mentioned above. Jänecke and Mühlhäusser [68] detected a thermal effect at 688 °C for a 60 mol% $CaSO_4$ composition; and XRD investigation conducted by Rowe et al. [49] on a composition containing 52 mol% $CaSO_4$ showed only KCl and $CaSO_4$ and the corresponding heating-cooling study indicated a thermal effect at 685 °C which coincides with the eutectic temperature of the quasi-binary system. Therefore, 2KCl·$CaSO_4$ is not considered in their studies. The KCl-$CaSO_4$ phase diagram is shown in **Figure 2-29**.

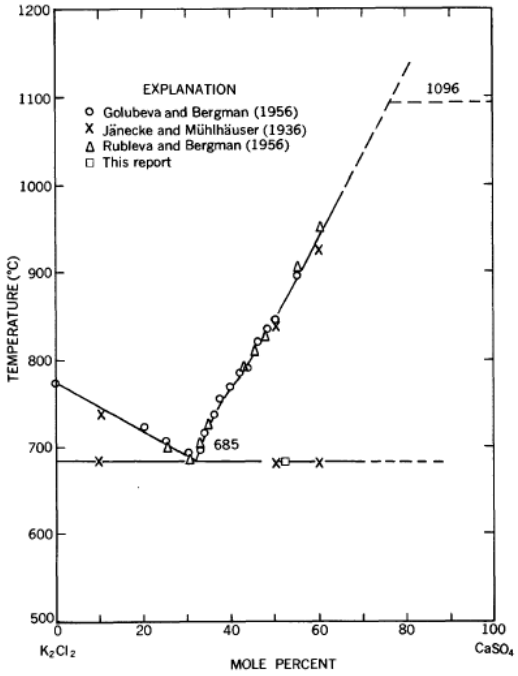


Figure 2-29 *Phase diagram of K_2Cl_2-$CaSO_4$ system From Rowe et al. [49] with experimental data: Jänecke and Mühlhäusser [68], Golubeva and Bergman [69] and Rubleva and Bergman [135].*

2.2.2.5.4 $CaCl_2$-K_2SO_4

The pseudo-binary system $CaCl_2$-K_2SO_4 was examined by Jänecke and Mühlhäusser [68], revealing that adding $CaCl_2$ to K_2SO_4 decreases the liquidus temperature from 1069 °C to approximately 770 °C near 26 mol% $CaCl_2$, at which point calcium langbeinite, $K_2Ca_2(SO_4)_3$, becomes the primary phase. As the system continues through the calcium langbeinite field, the liquidus rises to 790 °C at 43.5 mol% $CaCl_2$, where $CaSO_4$ becomes the primary phase. The temperature then fluctuates as the liquidus crosses the $CaSO_4$ region before reaching the boundary of the $CaCl_2$ field, where it increases to the melting point of $CaCl_2$ at 779 °C (**Figure 2-30**). The section of the system with high $CaCl_2$ content was not directly studied but was extrapolated from the relative binary information. Golubeva and Bergman [69] reported that the diagonal intersects five phase fields in the reciprocal system: $CaCl_2$, $CaSO_4$, $K_2SO_4{\cdot}2CaSO_4$ (calcium langbeinite), $2K_2SO_4{\cdot}3CaSO_4$, and K_2SO_4. These fields are crossed at specific points, as shown in **Figure 2-26**: at 720 °C and 26.5 mol% $CaCl_2$, at 785 °C and 42.5 mol% $CaCl_2$, and at 645 °C and 90 mol% $CaCl_2$.

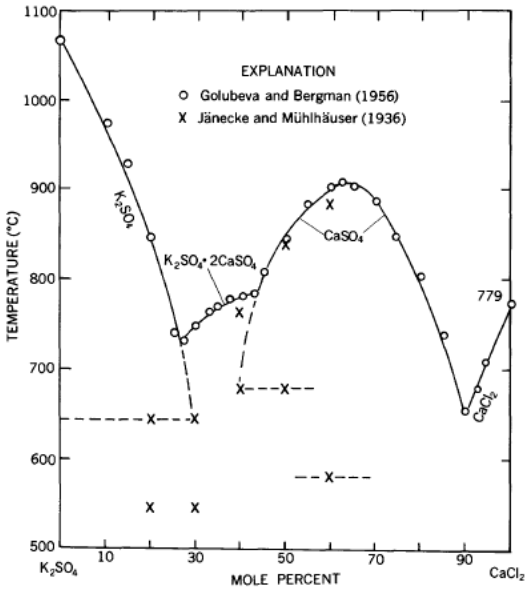


Figure 2-30 *Phase diagram of $CaCl_2$-K_2SO_4 system from Rowe et al. [49] with experimental data: Jänecke and Mühlhäusser [68] and Golubeva and Bergman [69].*

2.2.2.6 Na^+, K^+ // Cl^-, SO_4^{2-} system

Investigations of the reciprocal system Na^+, K^+ // Cl^-, SO_4^{2-} have been carried out by several authors, Akopov and Bergman [93, 105, 168], Jänecke [5, 108] and Rowe et al. [49]. In its quadrilateral representation, the four edges correspond to the binary subsystems NaCl-KCl, Na_2SO_4-K_2SO_4, NaCl-Na_2SO_4 and KCl-K_2SO_4, while the two diagonals represent the exchange reaction, NaCl-K_2SO_4 and KCl-Na_2SO_4. To preserve electroneutrality, both NaCl and KCl are expressed as dimers (Na_2Cl_2 and K_2Cl_2). Different authors provided contrasting interpretations of the phase relations. Jänecke [5, 108] proposed a relatively simple phase diagram, dominated by two extensive solid solutions: (Na,K)Cl and $(Na,K)_2SO_4$. Their description includes a liquidus minimum at 515 °C and 20.6 wt% NaCl, 19.8 wt% KCl, 16.0 wt% Na_2SO_4 and 43.6 wt% K_2SO_4. In contrast, Akopov and Bergman [93, 102, 105, 168, 169] suggested a more complex system, strongly influenced by the stability of three Na_2SO_4-K_2SO_4 double compounds. These phases, together with their mutual solid solutions and interactions with the other components of the system, introduce additional fields into the phase diagram, as illustrated in **Figure 2-31**. In an earlier study [102], a eutectic point was reported at 514 °C (518 °C [169]), with the composition expressed in ternary coordinates as K_2Cl_2(39 equiv%)-Na_2Cl_2(2.5 equiv%)-Na_2SO_4(58.5 equiv%). In [102], two additional invariant points were identified: one at 534 °C between NaCl, Na_2SO_4 and phase X, and another at 538 °C between KCl, K_2SO_4 and phase X, where phase X was presumed to correspond to either $3Na_2SO_4 \cdot K_2SO_4$ or $2Na_2SO_4 \cdot K_2SO_4$. By contrast, in [169], the phase equilibria are described in terms of three sulphate-based solid solutions (I, II, and III), reporting invariant points at 538, 534, 550 and 576 °C (**Figure 2-31**).

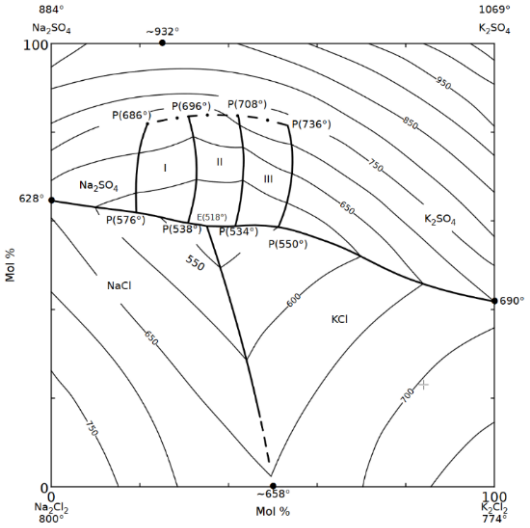


Figure 2-31 *Phase diagram of Na^+, K^+ // Cl^-, SO_4^{2-} system from Akopov and Bergman [169].*

2.2.2.6.1 NaCl-KCl

The phase diagram of the binary system NaCl-KCl has been extensively investigated experimentally [41, 93, 102, 170-178]. It consists of a continuous chloride-based solid solution phase and exhibits a miscibility gap at low temperatures. Kurnakow and Żemczużnyj [174] reported that NaCl and KCl form a complete series of solid solutions which unmix at lower temperatures. The liquidus temperatures have been studied by several authors [102, 170, 172, 179]. The miscibility gap was studied, using X-ray diffraction methods, by Bunk and Tichelaar [180] and by Nguyen-BChanh [181] who determined the upper consolute temperature as 500 ± 5 °C at 69.5 mol% KCl; this result was later confirmed by Vesnin and Zakovryashin [182] and Sergeev et al. [41]. The mixing enthalpy was measured by Hersh and Kleppa [173] and from Sergeev et al. [41]. On the basis of these experimental data, the phase diagram was previously assessed [37, 48] and the Gibbs energy of the liquid phase and solid solution has been incorporated in the PCM2 database. These assessments, consistent with the overall aim of developing a reliable thermodynamic database, are adopted in the present work. The calculated phase diagram (**Figure 2-32**), obtained with the PCM2 database, displays a liquidus minimum at 657 °C and 48.8 mol% NaCl, as well as a solid-solid miscibility gap with a minimum at 515 °C and 58.7 mol% NaCl. The thermodynamic properties of NaCl-KCl system will therefore be used as such in the present work (**Table 6-16**).

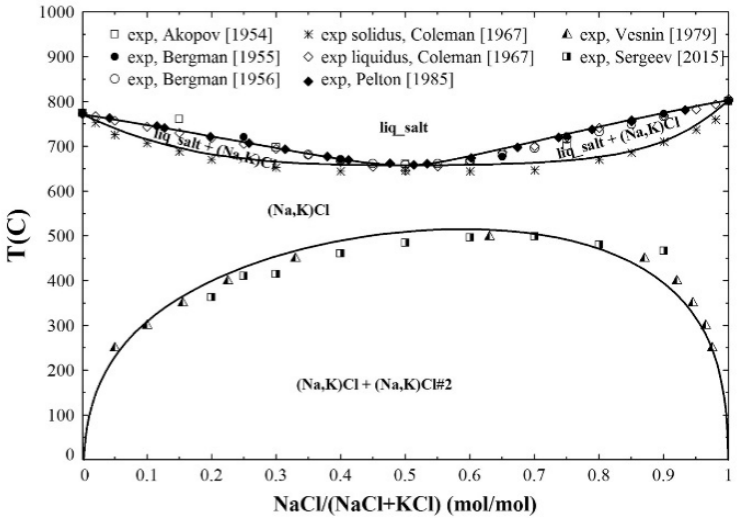


Figure 2-32 *Phase diagram of NaCl-KCl system from Sergeev et al. [37] with experimental data: Akopov et al. [102]; Bergman et al. [178]; Bergman et al. [177]; Coleman et al. [170]; Pelton et al. [172]; Vesnin et al. [182]; Sergeev et al. [41].*

2.2.2.6.2 Na_2SO_4-K_2SO_4

The binary system Na_2SO_4-K_2SO_4 has been the subject of numerous experimental [102, 108, 128, 166, 183-191] and thermodynamic studies [39, 61, 192, 193]. Its phase diagram is characterised by an azeotropic minimum on the liquidus and the presence of several solid solutions. These include a continuous solid solution based on the high-temperature hexagonal modification of the alkali sulphates, an intermediate phase known as glaserite, and terminal solid solutions derived from the orthorhombic polymorphs of Na_2SO_4 and K_2SO_4. The experimental data for the liquidus and the solidus boundaries were obtained through thermal analysis [98, 108, 128, 184] and visual-polythermal methods [102, 186]; while the subsolidus equilibria were studied through a combination of thermal analysis [108, 128, 183-185] and X-ray diffraction [128, 183, 187]. The work of Kobertz et al. [126], based on combined DTA and XRD measurements, confirmed the existence of the intermediate glaserite phase and supported earlier findings. Additional thermodynamic measurements include: the enthalpy of mixing of the liquid phase at 1080 °C from Østvold and Kleppa [190], the chemical activities of Na_2SO_4 and K_2SO_4 in the liquid phase at 1077 °C derived from KEMS measurements of Armatys et al. [191], and the activity of alkali sulphates in the hexagonal phase from KEMS studies by Marquez [166]. Building upon these datasets, several thermodynamic assessments have been carried out. Du [61] and Dessureault et al. [192] described the liquid and solid solutions using sublattice models, while Lindberg et al. [193] employed the modified quasi-chemical model [194] for the liquid phase and the Compound Energy Formalism (CEF) [195] for the solid solutions. More recently, Yazhenskikh et al. [39] re-optimised the system, incorporating both the existing experimental data and the new results of Kobertz et al. [126]. Their assessment located the azeotropic minimum on the liquidus line at 70.4

mol% Na_2SO_4 and 835.8 °C, in agreement with earlier estimates (80 mol% Na_2SO_4 and 830 °C [128], and 73 mol% Na_2SO_4 and 832 °C [102]). The glaserite phase was modelled using a three-sublattice formulation to capture compositional asymmetry, and its congruent transition to the hexagonal phase was calculated at 43.5 mol% Na_2SO_4 and 471.7 °C. The Na_2SO_4-rich and K_2SO_4-rich orthorhombic solid solutions (Na-ortho-MT, Na-ortho-LT and K-ortho in **Figure 2-33**) were described as three separate terminal solutions. The optimised thermodynamic description, including Gibbs energy functions and interaction parameters $L_{ij}^{(\nu)}$ for both the liquid and solid phases from Yazhenskikh et al. [39], have been incorporated into the PCM2 database and are adopted in the present work (**Table 6-16**).

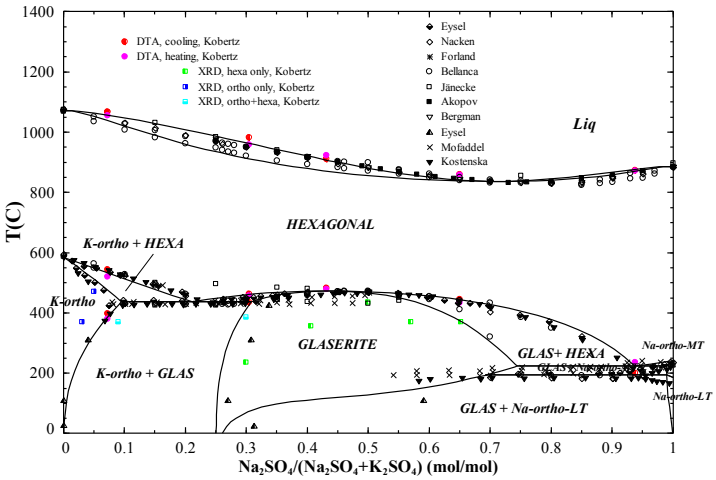


Figure 2-33 *Phase diagram of Na_2SO_4-K_2SO_4 system from Yazhenskikh et al. [39] with experimental data: Kobertz et al. [126], Eysel [183, 187], Nacken [184], Forland et al. [185], Bellanca [128], Jänecke [108], Akopov and Bergman [102], Mofaddel et al. [188], Koštenská and Fellner [189].*

2.2.2.6.3 NaCl-K_2SO_4

Within the Na^+, K^+ // Cl^-, SO_4^{2-} reciprocal system, the NaCl-K_2SO_4 section has been interpreted differently by various authors. Jänecke [5, 108] treated it as an independent binary system and reported a eutectic at 540 °C and 65 mol% K_2SO_4. Later studies, however, proposed a more complex description. Rowe et al. [49], consistent with the visual-polythermal observations of Akopov and Bergman [93, 102, 105, 168], interpreted this section as a pseudo-binary diagonal intersecting several phase fields. According to their results, it passes successively through NaCl, (Na,K)Cl solid solution, KCl, $(Na,K)_2SO_4$ solid solution and K_2SO_4, as illustrated in **Figure 2-34**. Only limited data exist for the NaCl-rich side: Sackur [66] measured a few high-NaCl compositions using cooling curves obtained with a calibrated thermocouple and a recording millivoltmeter.

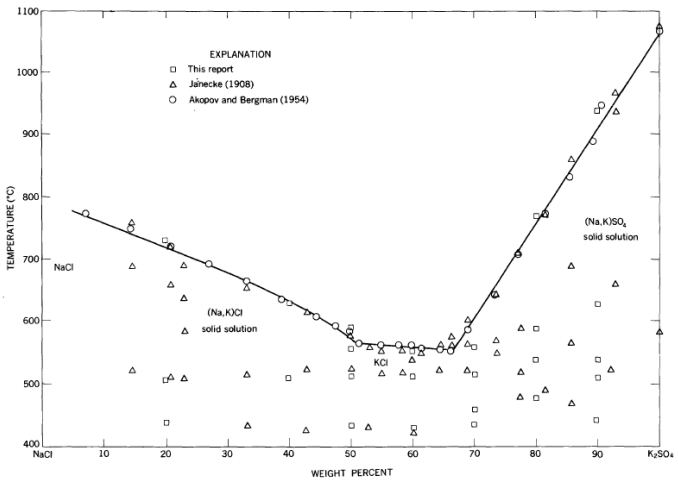


Figure 2-34 *Phase diagram of NaCl-K_2SO_4 from Rowe et al. [49] with experimental data: Jänecke [108], Akopov and Bergman [102].*

2.2.2.6.4 KCl-Na_2SO_4

The KCl-Na_2SO_4 section has been studied by thermal analysis [108] and by visual-polythermal method [93, 102, 105, 168]. Akopov and Bergman [102] reported that this diagonal of the Na^+, K^+ // Cl^-, SO_4^{2-} reciprocal system intersects the stability field of a compound, most likely $2Na_2SO_4 \cdot K_2SO_4$, formed as a result of the decomposition of the $(Na,K)_2SO_4$ solid solution. In a subsequent and detailed study [105], the same authors described the pseudo-binary diagonal as extending from Na_2SO_4 through the $(Na,K)_2SO_4$ solid solution field, then crossing two of the three compounds produced by the decomposition of this solution, and reaching a minimum temperature of 525 °C. Beyond this point, the diagonal passes through the (Na,K)Cl solid solution field before terminating at KCl, as illustrated in **Figure 2-35**.

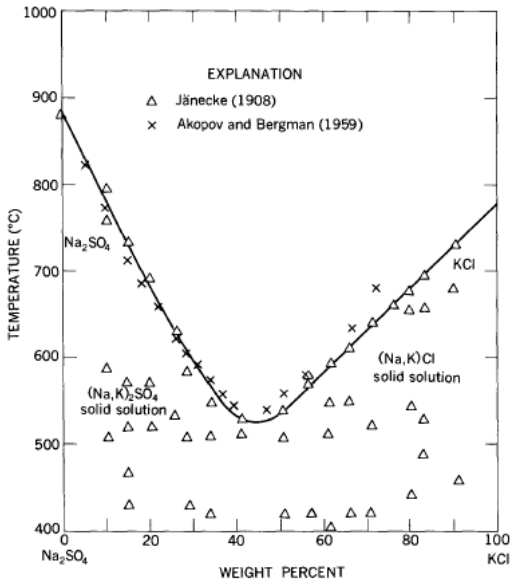


Figure 2-35 *Phase diagram of KCl-Na_2SO_4 from Rowe et al. [49] with experimental data: Jänecke [108], Akopov and Bergman [105].*

2.2.3 Ternary systems

2.2.3.1 NaCl-KCl-$MgCl_2$

The liquidus projection of the ternary system has been presented by Scholich [80], and Jänecke [5]. Scholich [80], based on cooling-curve analysis and microscopic observations, reported a eutectic point in the $KCl{\cdot}MgCl_2$-NaCl section at 410 °C, corresponding to a composition of 41 mol% $MgCl_2$, 41 mol% KCl, and 18 mol% NaCl. In the ternary system, two additional eutectic points were identified: the first at 393 °C with a composition of 47 mol% $MgCl_2$, 19 mol% KCl, and 32 mol% NaCl, involving the solid phases $KCl{\cdot}MgCl_2$, $NaCl{\cdot}2MgCl_2$, and $2NaCl{\cdot}MgCl_2$; the second at 404 °C with a composition of 34 mol% $MgCl_2$, 45 mol% KCl, and 11 mol% NaCl, where the solid phases were $KCl{\cdot}MgCl_2$ and solid solutions based on KCl and NaCl. Abramov [89], through visual interpretation of cooling curves and photomicrographic analysis of solidified melts under polarised light, identified three eutectic points in the NaCl-KCl-$MgCl_2$ system. The first was located at 400 °C with a composition of 35 mol% $MgCl_2$, 47 mol% KCl, and 18 mol% NaCl, involving the solid phases $KCl{\cdot}MgCl_2$ and solid solutions based on $2KCl{\cdot}MgCl_2$ and NaCl. The second eutectic was found at 395 °C with a composition of 46 mol% $MgCl_2$, 22 mol% KCl, and 32 mol% NaCl, and consisted of the solid phases $KCl{\cdot}MgCl_2$, $NaCl{\cdot}2MgCl_2$, and $2NaCl{\cdot}MgCl_2$. The third eutectic was identified at 400 °C with a composition of 39 mol% $MgCl_2$, 42.5 mol% KCl, and 18.5 mol% NaCl, with the solid phases $KCl{\cdot}MgCl_2$, $2NaCl{\cdot}MgCl_2$, and a NaCl-based solid solution. Orekhova et al. [196] investigated the ternary system by XRD, TGA/DSC and conductivity analysis. They reported three ternary eutectic points and six ternary peritectic points in the ternary system, and a ternary compound $NaKMgCl_4$ with a melting temperature of 398 °C. The first eutectic occurs at 385 °C, with a composition of 46 mol% $MgCl_2$, 22 mol% KCl, and 32 mol% NaCl, and involves the equilibrium solid phases $KMgCl_3$, $NaMgCl_3$, and Na_2MgCl_4. The second eutectic is located at 390 °C, corresponding to 39 mol% $MgCl_2$, 25 mol% KCl, and 36 mol% NaCl, with the solid phases $KMgCl_3$, $KNaMgCl_4$, and a (Na,K)Cl solid solution. The third eutectic also appears at 390 °C, at 31.5 mol% $MgCl_2$, 56 mol% KCl, and 12.5 mol% NaCl, and is characterised by the equilibrium of $K_3Mg_2Cl_7$, K_2MgCl_4, and a (Na,K)Cl solid solution. The activity of $MgCl_2$ in the liquid was measured by emf techniques by Neil et al. [85]. Chartrand and Pelton [54], based on the existing data, modelled the ternary system using a regular model for describing the solid solutions $(Na,K)MgCl_3$ and $(Na,K)_2MgCl_4$.

Based on the thermodynamic assessments carried out by the project partners (GTT-Technologies) on the three constituting binary systems, the ternary NaCl-KCl-$MgCl_2$ system was modelled by the same group using both these optimised binaries and the available experimental information from the literature. The assessment included the modelling of the liquid phase, and no ternary compounds or solid solutions were considered. The resulting calculated ternary phase diagram is presented in **Figure 2-36**, and the calculated invariant points listed in **Table 2-2**. The thermodynamic

properties of this optimised ternary system have been incorporated into the database under development in the present work and have been employed for the subsequent calculations presented in this thesis.

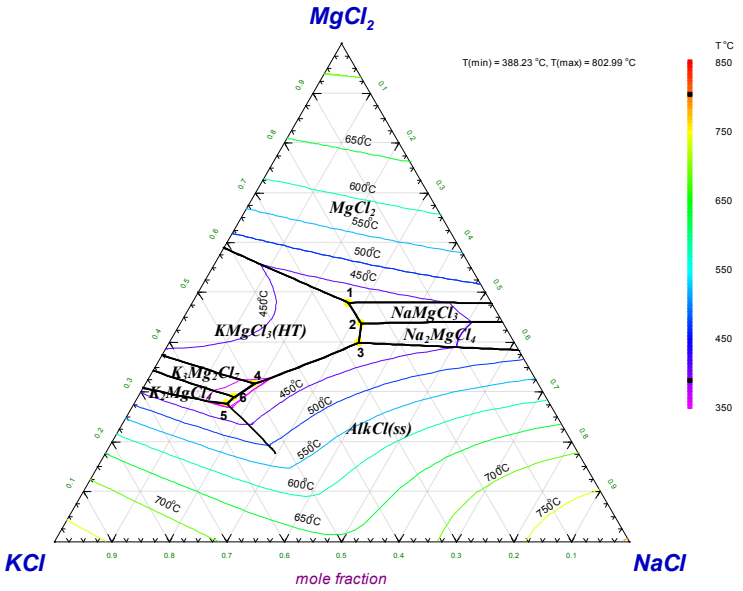


Figure 2-36 *Phase diagram of NaCl-KCl-$MgCl_2$ ternary system from the PCM2 database [4].*

Table 2-2 *Calculated invariant points in the NaCl-KCl-$MgCl_2$ system.*

	$MgCl_2$, mol%	KCl, mol%	NaCl, mol%	T, °C	Solid phase
1	47.87	24.85	27.28	405.1	$MgCl_2$, $NaMgCl_3$, $KMgCl_3$(HT)
2	43.70	24.68	31.62	400.0	$NaMgCl_3$, Na_2MgCl_4, $KMgCl_3$(HT)
3	39.85	27.09	33.05	399.8	Na_2MgCl_4, $KMgCl_3$(HT), AlkCl(ss)
4	31.60	49.31	19.09	392.5	$K_3Mg_2Cl_7$, $KMgCl_3$(HT), AlkCl(ss)
5	27.56	56.13	16.31	389.2	$K_3Mg_2Cl_7$, K_2MgCl_4, AlkCl(ss)
6	28.93	54.19	16.88	388.2	K_2MgCl_4, AlkCl(ss)

2.2.3.2 NaCl-KCl-$CaCl_2$

The ternary system was studied by Scholich [80] who reported three eutectic points and three fields of primary crystallisation, involving the solid solution between NaCl and KCl, the compound $KCl{\cdot}CaCl_2$ and the pure chloride $CaCl_2$. Sem et al. [197] determined the enthalpy of mixing of liquid at 810 °C for three ratios of X_K/X_{Ca}= 1, 1/3 and 3 (or X_{Na}/X_{Ca}= 1, 1/3 and 3) using a high-temperature Calvet microcalorimeter. Plyushchev and Kovalev [198] confirmed the results of Scholich [199], but reported the eutectic to be at 465 °C, instead of 504 °C [199]. The system was modelled by Chartrand and Pelton [54], Yin et al. [43] and Reis [48]. On the basis of the experimental data available in literature and own data of phase diagram of the isopleth NaCl-$KCaCl_3$ and enthalpy increment and heat capacity of NaCl(60 mol%)-$KCaCl_3$(40 mol%), Reis [48] modelled the ternary system by introducing ternary interaction parameters of the liquid phase. They reported three ternary eutectic points: NaCl(41.63

mol%)-KCl(6.59 mol%)-$CaCl_2$(51.79 mol%), NaCl(28.94mol%)-KCl(52.92 mol%)-$CaCl_2$(18.14 mol%), NaCl(43.08 mol%)-KCl(27.82 mol%)-$CaCl_2$(29.10 mol%) at 481 °C, 507 °C and 567 °C, respectively (**Figure 2-37**).

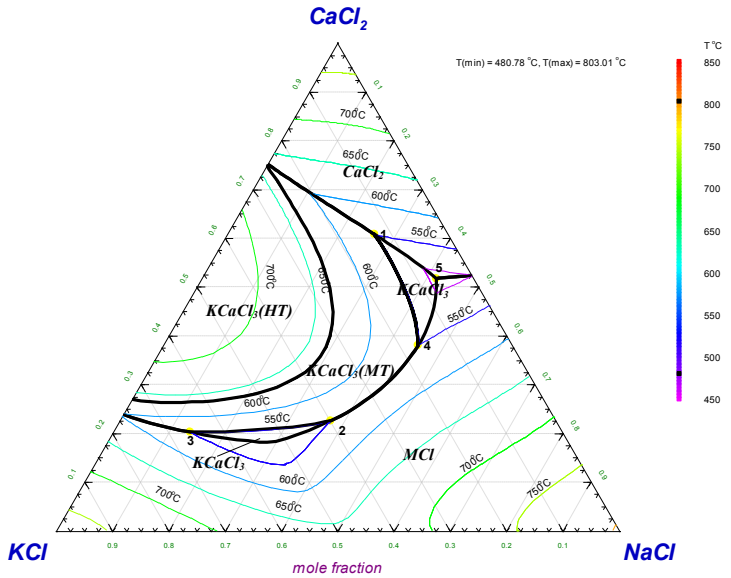


Figure 2-37 *Phase diagram of NaCl-KCl-$CaCl_2$ ternary system from Reis [48].*

2.2.3.3 NaCl-$MgCl_2$-$CaCl_2$

The liquidus projection of the ternary system has not been experimentally provided. Østvold [139] measured the activity of NaCl in the liquid at 850 °C using an emf technique for several ratios $X_{MgCl2}/(X_{MgCl2}+X_{CaCl2})$ = 0.129, 0.344, 0.517, 0.718, 0.796. Karakaya and Thompson [57] measured by emf technique the activity of $MgCl_2$ in the liquid at 800 °C for three ratios $X_{NaCl}/(X_{NaCl}+X_{CaCl2})$ = 0.25, 0.50, 0.75. Chartrand and Pelton [54], in the framework of thermodynamic assessment of alkali and alkaline earth metal chlorides, calculated the ternary system (**Figure 2-38**) without introducing any ternary parameters but only on the basis of the assessed subsystems.

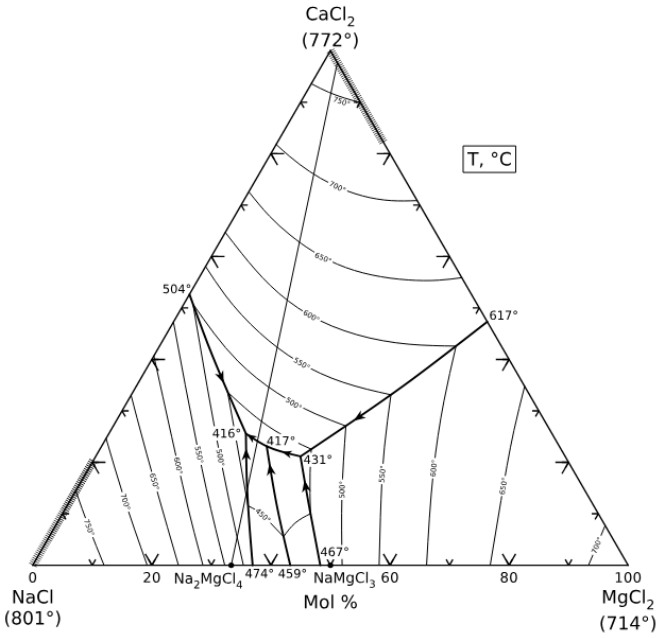


Figure 2-38 *Phase diagram of NaCl-$MgCl_2$-$CaCl_2$ ternary system from Chartrand and Pelton [54].*

2.2.3.4 KCl-$MgCl_2$-$CaCl_2$

The liquidus projection of the ternary system was first presented by Ivanov [51], showing the fields of primary crystallisation defined by pure chlorides and KCl·$CaCl_2$, KCl·$MgCl_2$, 2KCl·$MgCl_2$, and reporting two eutectic points (28.0wt% KCl, 49.0wt% $MgCl_2$, 23.0wt% $CaCl_2$ at 440 °C; 62.0wt% KCl, 35.0wt% $MgCl_2$, 3.0wt% $CaCl_2$ at 434 °C) and two peritectic points (26.0wt% KCl, 49.0wt% $MgCl_2$, 25.0wt% $CaCl_2$ at 446 °C; 59.0wt% KCl, 38.5wt% $MgCl_2$, 2.5wt% $CaCl_2$ at 437 °C). Ivanov [51] investigated seventeen internal sections, including, for example, $MgCl_2$-KCl·$CaCl_2$, KCl·$CaCl_2$-KCl·$MgCl_2$, $CaCl_2$-KCl·$CaCl_2$. Zhu et al. [200] measured the activity of $MgCl_2$ in the liquid at 720 °C and 840 °C, using an emf technique, for the molar ratios X_{KCl}/X_{CaCl2} of 0.5 and 2. Chartrand and Pelton [54] modelled the ternary diagram introducing a subregular model to describe a solid solution between the compounds $KMgCl_3$ and $KCaCl_3$. The calculated phase diagram is shown in **Figure 2-39**.

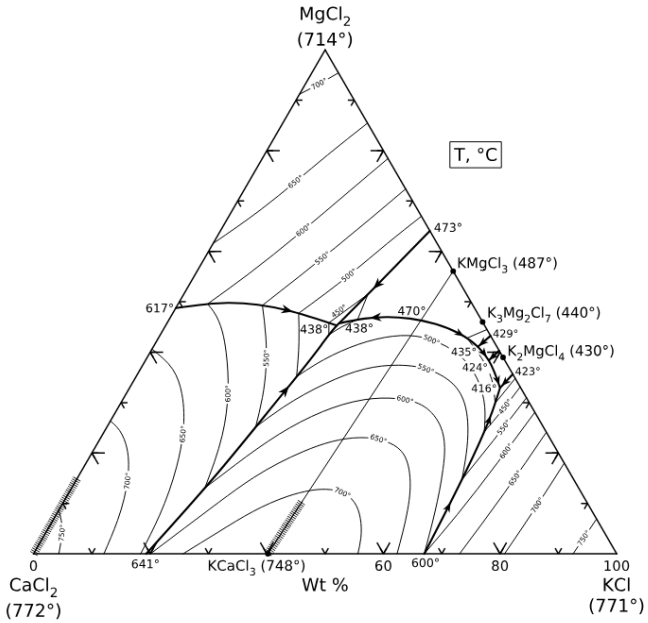


Figure 2-39 *Phase diagram of KCl-$MgCl_2$-$CaCl_2$ ternary system from Chartrand and Pelton [54].*

2.2.3.5 Na_2SO_4-K_2SO_4-$MgSO_4$

The phase diagram of the ternary system was reported by Jänecke [5] and Mukimov et al. [60], showing a different description of phase equilibria. Mukimov et al. [60] identified four primary crystallisation fields - a solid solution between Na_2SO_4 and K_2SO_4 (HEXAGONAL), $MgSO_4$, $Na_2Mg_3(SO_4)_4$, and $K_2Mg_2(SO_4)_3$ - with the lowest melting point reported at 645 °C, albeit without exact compositional data. Jänecke's diagram [5], constructed from binary subsystems, suggested a eutectic temperature below 700 °C, consistent with Mukimov's proposal [60] but lacking direct experimental confirmation. Yazhenskikh et al. [201] investigated the ternary eutectic composition Na_2SO_4(53 mol%)-K_2SO_4(12 mol%)-$MgSO_4$(35 mol%) proposed by Mukimov et al. [60] within the temperature range of 600-650 °C, and reported a melting temperature of 676 °C - significantly higher than that originally indicated by Mukimov et al. [60]. The ternary system was assessed by Du [61] and Yazhenskikh et al. [201]. Du [61] performed a calculation based on an extrapolation from the known binary subsystems, without direct experimental validation. In contrast, Yazhenskikh et al. [201] optimised the ternary interaction parameters by combining their own experimental results with thermodynamic modelling. The resulting phase diagram, presented in **Figure 2-40**, includes a calculated ternary eutectic point at Na_2SO_4(51.9 mol%)-K_2SO_4(7.2 mol%)-$MgSO_4$(40.9 mol%) and 674 °C, as well as a peritectic point at 799 °C.

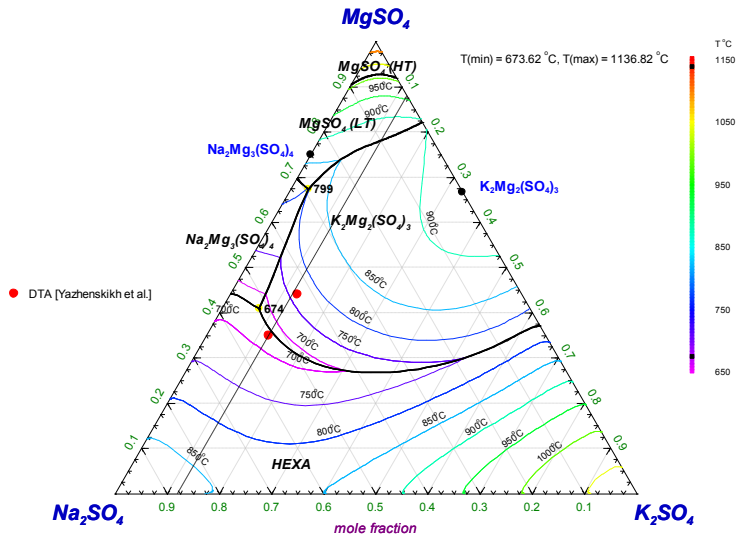


Figure 2-40 *Phase diagram of Na_2SO_4-K_2SO_4-$MgSO_4$ ternary system from Yazhenskikh et al. [201].*

2.2.3.6 Na_2SO_4-K_2SO_4-$CaSO_4$

The ternary system was experimentally studied by Bellanca [128] and Yazhenskikh et al. [201]. Bellanca [128] found the ternary eutectic point to be at Na_2SO_4(29 mol%)-K_2SO_4(29.5 mol%)-$CaSO_4$(41.5 mol%) and 775 °C. Yazhenskikh et al. [201] confirmed through DTA analysis that composition to be eutectic with a melting point of 774 °C. Their DTA study also included three additional compositions, which were analysed to refine the understanding of phase equilibria within the system. The ternary system was assessed by Du [61] and Yazhenskikh et al. [201]. Du [61] calculated the phase diagram based on an extrapolation from the binary subsystems. Yazhenskikh et al. [201] modelled the phase diagram introducing a ternary interaction parameter in the liquid phase. The calculated phase diagram agreed with experimental data (**Figure 2-41**), and reported a ternary eutectic point at Na_2SO_4(29 mol%)-K_2SO_4(30 mol%)-$CaSO_4$(41 mol%) and 770 °C. The reassessment of Na_2SO_4-$CaSO_4$ system in their study with the reported intermediate compounds $Na_6Ca(SO_4)_4$ and $Na_2Ca(SO_4)_2$ determined a different description of the crystallisation fields of the primary phases compared to [128, 201].

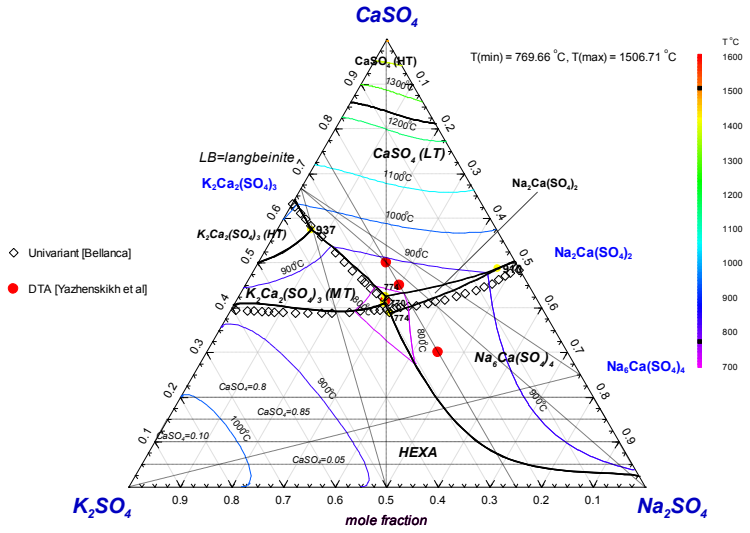


Figure 2-41 *Phase diagram of Na_2SO_4-K_2SO_4-$CaSO_4$ ternary system from Yazhenskikh et al. [201] and Bellanca [128].*

2.2.3.7 Na_2SO_4-$MgSO_4$-$CaSO_4$

The ternary system was experimentally studied by Mukimov and Filippova [60] and Yazhenskikh et al. [201]. Mukimov and Filippova [60] identified via visual-polythermal method a ternary eutectic point at Na_2SO_4(53 mol%)-$MgSO_4$(40 mol%)-$CaSO_4$(7 mol%) and 650 °C. Their analysis was based on the assumption that the $MgSO_4$-$CaSO_4$ and Na_2SO_4-$CaSO_4$ subsystems behave as simple mono-eutectic systems. Yazhenskikh et al. [201] analysed the same composition by DTA, along with another composition within the ternary system, and identified four thermal effects. Among them, the eutectic transition was observed at 653 °C, and the liquidus at 766 °C. Based on the reassessed binary subsystems by Yazhenskikh et al. [201], the ternary eutectic point was calculated at Na_2SO_4(55.3 mol%)-$MgSO_4$(44.1 mol%)-$CaSO_4$(0.6 mol%) and 672 °C, involving the phases Na_2SO_4 (hexagonal), $Na_6Ca(SO_4)_4$ and $Na_2Mg_3(SO_4)_4$, which were introduced into their thermodynamic database, as illustrated in **Figure 2-42**.

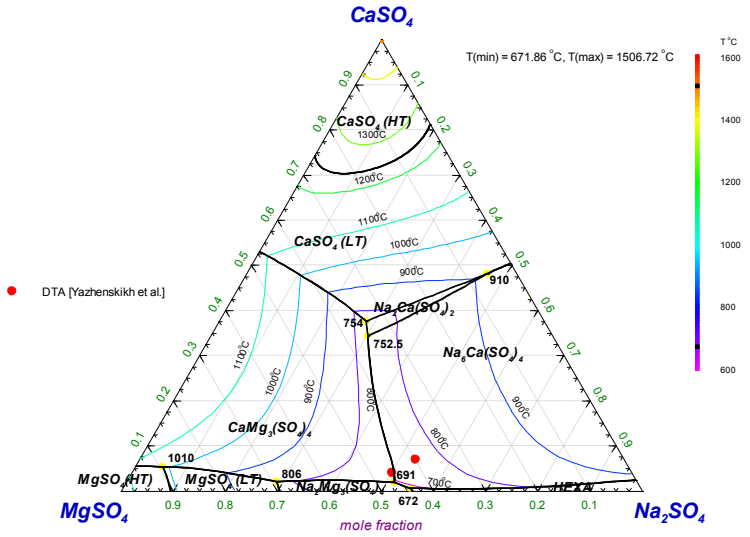


Figure 2-42 *Phase diagram of Na_2SO_4-$MgSO_4$-$CaSO_4$ ternary system from Yazhenskikh et al. [201].*

2.2.3.8 K_2SO_4-$MgSO_4$-$CaSO_4$

The ternary system was first studied by Rowe et al. [58] and then by Yazhenskikh et al. [201]. Rowe et al. [58] using several methods (heating-cooling curves, DTA, optical methods, HT-XRD, quenching techniques) reported a composition of K_2SO_4(61 mol%)-$MgSO_4$(32 mol%)-$CaSO_4$(7 mol%) with the minimum melting temperature of 740 °C. Yazhenskikh et al. [201] validated by DTA that composition finding two thermal events at 563 °C and 754 °C, related to solid-solid and solid-liquid transitions, respectively. The ternary system was assessed by Du [61] who introduced a ternary parameter in the liquid phase and treated langbeinite as a solid phase. Yazhenskikh et al. [201] modelled the ternary system, after assessing all subsystems [39], showing in the liquidus surface five fields of crystallisation, involving the three pure sulphates, the solid solution phase langbeinite, and the compound $CaSO_4 \cdot 3MgSO_4$ (**Figure 2-43**). According to Rowe et al. [58] a ternary eutectic involving langbeinite, $MgSO_4$, and $CaSO_4 \cdot 3MgSO_4$ is located near the K_2SO_4-langbeinite isopleth and occurs at approximately 882 °C, at the composition K_2SO_4(20 mol%)-$MgSO_4$(75 mol%)-$CaSO_4$(5 mol%). The corresponding calculated eutectic by Yazhenskikh et al. [201] is at K_2SO_4(18 mol%)-$MgSO_4$(77 mol%)-$CaSO_4$(5 mol%) at 863 °C.

A second ternary eutectic is also reported at 882 °C [58] or 873 °C [201], where liquid coexists with $CaSO_4$, langbeinite, and a ternary phase rich in $MgSO_4$.

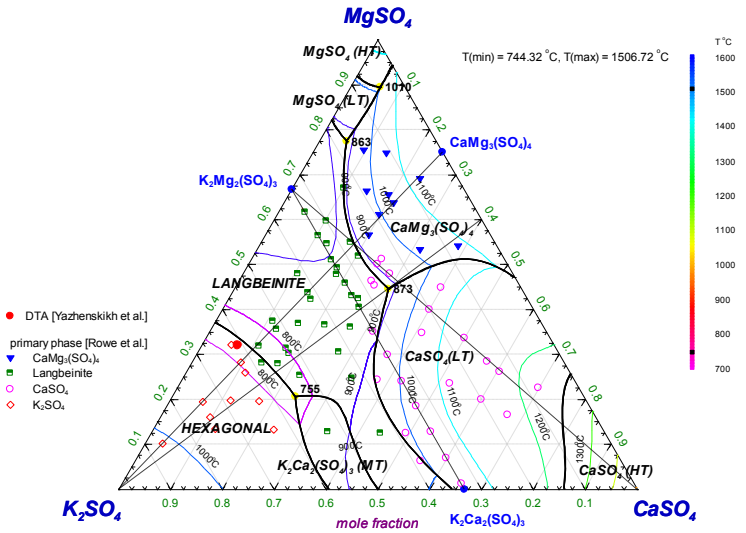


Figure 2-43 *Phase diagram of K_2SO_4-$MgSO_4$-$CaSO_4$ ternary system from Yazhenskikh et al. [201], and Rowe et al. [58].*

3 Experimental

In the following chapter, the selection of materials and the preparation of samples will be discussed. The methods employed, including differential thermal analysis coupled with thermogravimetric analysis (DTA/TG), differential scanning calorimetry (DSC), high-temperature X-ray diffractometry (HT-XRD), and scanning electron microscopy coupled with energy dispersive X-ray spectroscopy (SEM-EDX) will be detailed. These techniques are utilised to carry out the experimental investigation of the systems under study, with the objective of providing phase equilibrium data and thermodynamic properties for the development of an accurate thermodynamic database.

3.1 Samples

The pure salts NaCl (Thermo Fisher Scientific, anhydrous 99.998%), KCl (Thermo Fisher Scientific, anhydrous 99.997%), $MgCl_2$ (Sigma-Aldrich, anhydrous 99.99%), $CaCl_2$ (Alfa Aesar, anhydrous 99.99%), Na_2SO_4 (Thermo Fisher Scientific, anhydrous 99.9955%), K_2SO_4 (Alfa Aesar, anhydrous 99.99%), $MgSO_4$ (VWR Chemicals, anhydrous ≥99%, metal basis) and $CaSO_4$ (Alfa Aesar, anhydrous 99.993%) were utilised in the appropriate stoichiometric ratios to prepare the mixtures under investigation. Alkali and alkaline earth metal chlorides and sulphates were stored in a glovebox under argon to avoid contact with moisture. Prior to use, the salts were tested via differential thermal analysis and X-ray diffraction to confirm their purity and any potential water content. The chlorides were dehydrated in a furnace within the glovebox at temperatures below 300 °C to remove any water of crystallisation (both primary and secondary). In contrast, for the sulphates, pre-treatment dehydration was less sensitive to temporary atmospheric exposure; therefore, drying was performed in a vacuum furnace at 150 °C. Further DTA and XRD analyses confirmed their suitability for use. Intermediate compounds were prepared *in situ* by mixing the end-members in the appropriate stoichiometric ratios and placing the mixture in a quartz ampoule within the glovebox. The ampoule was sealed under vacuum using a hydrogen-oxygen flame, with the vacuum level achieved by a rotary pump (10^{-1}-10^{-3} mbar). The mixture was then heated to temperatures 100 °C below the melting point to facilitate the solid-state reaction. The thermal treatment involved three heating and cooling steps, with intermediate stages where the ampoule was opened, and the mixture was ground in an agate mortar within the glovebox to enhance homogeneity. The final mixture was tested using DTA and XRD to determine phase transition temperatures and crystallographic properties. Eutectic mixtures from the pseudo-binary systems were synthesised in a similar manner, with thermal treatment in quartz ampoules consisting of a single step at temperatures slightly above their melting points. Further details will be provided in the section dedicated to DSC measurements. Details regarding the

investigated mixtures will be provided in the respective subsections dedicated to each system under consideration.

3.2 Instruments

3.2.1 Differential Thermal Analysis/Thermogravimetry (DTA/TG)

Differential Thermal Analysis coupled with Thermogravimetric Analysis (DTA/TG) is used to measure the temperature difference between a sample and a reference under controlled and programmed thermal cycles. It enables the measurement of phase transition temperatures and mass changes during the heating and cooling processes. The schematic diagram of a DTA sample holder is shown in **Figure 3-1**. During measurements, two crucibles are utilised: one containing the sample and the other for a reference. The sample or reference thermocouple temperatures are determined by the voltage difference between thermocouple legs *A* and *B* for each crucible, with appropriate cold junction compensation. The signal is obtained by shorting the *B* legs and measuring the voltage between the *A* legs [202]. DTA/TG measurements are performed using a STA 449 C Jupiter (Netzsch), i.e. a simultaneous thermal analysis instrument, with a silicon carbide oven (RT-1600 °C) and a perpendicular sample holder with type S thermocouple (Pt/(Pt10Rh)). All phase transitions temperatures are determined with Proteus Analysis software from Netzsch. The results show good reproducibility from the second heating-cooling cycle. In this work, the phase transformation temperature is defined from the heating cycle and more specifically, the eutectic transformation is taken as the onset temperature, and the maximum peak temperature of further transformations is taken as the liquidus temperature or solid-solid transformation temperature. In general, three heating and cooling cycles were performed for each measured sample. The first cycle serves to form the mixture, as incomplete mixing or poor contact between the sample and crucible wall can influence heat transfer and the curve slope. Additionally, the mixing enthalpy of components may cause deviations in the first cycle. However, once the salt melts during the first cycle, these effects are mitigated, and the results from the second and third cycles are generally reproducible. If discrepancies persist, an additional cycle is conducted to ensure reliable data. While heating curves are generally used for peak detection and determining phase transition temperatures, cooling curves can occasionally reveal additional thermal arrests that are undetectable during heating. This is likely due to kinetic effects that make certain transitions, such as crystallisation events, more apparent during cooling. For this reason, both heating and cooling curves are analysed where necessary to obtain comprehensive information of phase transitions.

The selection of crucibles was guided by the specific behaviour of the studied system. Open crucibles, e.g. made of alumina or platinum, were deemed unsuitable at high temperatures due to

volatilisation of chlorides and decomposition of sulphates. These processes result in significant mass loss during measurements in open crucibles, indicating changes in the system's composition. Consequently, the analysed output would no longer correspond to the initial loaded composition. Due to the decomposition of sulphates, the experimentally observed melting temperatures of pure sulphate compounds should be considered as minimum values. This is because the potential formation of metal oxides MO (M = Mg, Ca) can lower the liquidus temperature as the system becomes quasi-binary (MO-MSO_4) [125]. The same principle applies to the mixtures within the binary systems MCl_2-MSO_4, which would in turn become ternary MCl_2-MO-MSO_4, or in case of sulphate-based binary and pseudo-binary systems, high-order systems may form as a result. Prior and subsequent to DTA experiments on pure sulphates and their selected mixtures, X-ray diffraction investigations were conducted in order to be able to assess the percentage of alkaline metal oxide formed and to evaluate the extent of partial decomposition of the corresponding sulphates.

To address mass loss issues, sealed platinum crucibles were used to minimise mass loss and ensure the integrity of the composition during measurements. The crucible was closed after filling the sample (50-100 mg) under dry argon in a glove box and then welded outside the box in a hydrogen/oxygen flame. A more detailed discussion of crucible selection for specific systems, such as $MgSO_4$-$CaSO_4$, is provided in Section 5.1.5. When the maximum temperature remained below approximately 700 °C and no significant mass loss was observed, measurements were conducted in open alumina crucibles where feasible.

The temperature calibration was conducted using the phase transition temperatures of In (156.6 °C), Sn (231.9 °C), Bi (271.4 °C), Zn (419.5 °C), Al (660.3 °C), Ag (961.8 °C), Au (1064.2 °C), and Ni (1454.0 °C) in alumina crucibles and C_6H_5COOH (122.5 °C), $RbNO_3$ (164.2 °C), $KClO_4$ (300.8 °C), Ag_2SO_4 (462.2 °C), CsCl (470.0 °C), K_2CrO_4 (668.0 °C), $BaCO_3$ (808.0 °C), K_2SO_4 (1069 °C), and CaF_2 (1418 °C) in sealed platinum tubes placed within alumina DTA crucibles. The resulting accuracy of transition temperature measurements is ±5 °C. The experiments were carried out with a heating rate of 5 K/min and three cycles of heating and cooling under an Ar atmosphere with a flow rate of 20 ml/min.

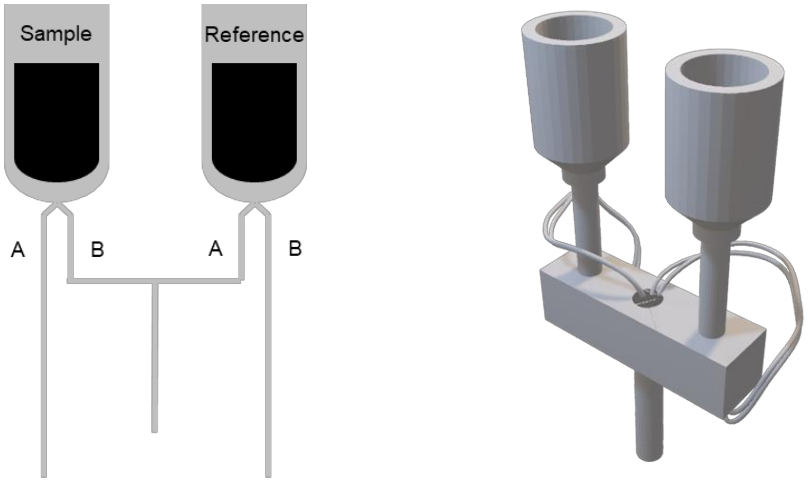


Figure 3-1 *Schematic diagram and drawing of DTA sample holder, with A and B denoting the different legs of thermocouples.*

3.2.2 Differential Scanning Calorimetry (DSC)

Differential Scanning Calorimetry (DSC) works by measuring the difference in temperature between a sample and a reference as a function of heat flux. This heat flux is directly proportional to the energy absorbed or released by the sample during thermal events, such as phase transitions. The connecting metal strip, positioned between the sample and the reference, is often used as an active sensing element to obtain the differential signal by measuring the voltage between the *B* legs of the thermocouple [202]. A schematic diagram illustrating this setup is shown in **Figure 3-2**. From measurements, heat capacity and enthalpy changes can be accurately calculated.

Two different differential scanning calorimeters were used for the determination of thermodynamic properties. A differential scanning calorimeter DSC 404 Pegasus (Netzsch) with a Pt oven (RT-1500 °C) and type S thermocouple (Pt/(Pt10Rh)) was used to determine the heat capacity of selected compositions at temperatures below decomposition points of sulphates and under conditions ensuring no mass loss. The temperature calibration was performed with the pure compounds C_6H_5COOH (122.5 °C), $RbNO_3$ (164.2 °C), $KClO_4$ (300.8 °C), Ag_2SO_4 (462.2 °C), CsCl (470.0 °C), K_2CrO_4 (668.0 °C), $BaCO_3$ (808.0 °C), K_2SO_4 (1069 °C), and CaF_2 (1418 °C). The average temperature deviation was ±2 °C. Ar atmosphere with gas flow of 20 ml/min was used. The sample powder of 30-40 mg, loaded in alumina liner within the platinum pan, was subjected to a heating rate of 10 K/min. A Calvet-type DSC calorimeter, model mHTC 96 (Setaram), was used for determination of heat capacity of the selected mixtures. Two distinct types of measurements were conducted: one in the low-temperature range, where no mass loss is observed, and the other one at high temperatures. In the first measurement, a sample powder of 200-300 mg, was loaded in alumina liner and platinum crucibles. In the second measurement, a specimen of 50-100 mg was loaded into a sealed platinum tube in a platinum sample holder. A heating rate of 4 K/min under He with a flow of 5 ml/min was

applied. Temperature and enthalpy calibration for the first measurement type were performed using pure metals In (156.6 °C), Sn (231.9 °C), Pb (327,5 °C), Zn (419.5 °C), Al (660.3 °C) and Ag (961.8 °C). For the second measurement type, calibration was done with pure salts $BaCO_3$ (808.0 °C), Na_2SO_4 (241 °C and 884 °C), K_2SO_4 (584 °C and 1069 °C), and MgF_2 (1263 °C). The three-step ratio method [203] with sapphire (α-Al_2O_3, NIST Standard Reference Material SRM720, purity 99.95%, metal basis) [204] as a reference was applied for the determination of the heat capacity (C_p°, J·mol^{-1}·K^{-1}) according to the following equation:

$$C_{p(s)}^{\circ} = \frac{m_r}{m_s} \cdot \frac{DSC_s - DSC_b}{DSC_r - DSC_b} \cdot C_{p(r)}^{\circ} \qquad \textit{Equation 2}$$

where m is the mass of the substance (g), DSC is the signal of thermopile (µV), and subscripts b, r and s stand for baseline, reference and sample respectively. Baseline and reference measurements were performed for each measured sample separately. The sapphire reference used in the experiments varied based on the specific instrument and setup. For the Netzsch DSC, the sapphire reference was a disc-shaped specimen of mass comparable to that of the sample mass under analysis. For the Setaram DSC, two configurations were used depending on the crucible type. When a platinum crucible with an alumina liner was used, stacked sapphire discs were employed as reference. Alternatively, when platinum tubes were used as crucibles, small sapphire cylinders with a diameter of approximately 1 mm were used.

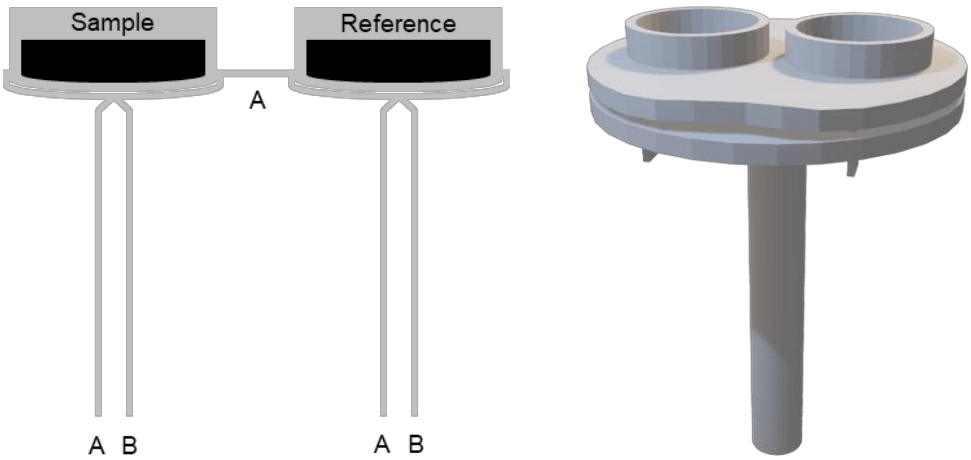


Figure 3-2 *Schematic diagram and drawing of DSC sample holder, with A and B denoting the different legs of thermocouples.*

3.2.2.1 Self-referencing calibration method (SRCM)

To extend DSC measurements to a wide temperature range up to the melting of pure compounds and selected mixtures, experiments can be carried out using fully sealed crucibles in DSC

Setaram mHTC 96. A custom-made platinum crucible, fabricated in-house, was initially employed for this purpose. The crucible consisted of a platinum tube whose ends were folded into a book-like shape and sealed by flame welding. The sealed tube containing the investigated mixture was then inserted into a cylindrical platinum sample holder and placed in the DSC furnace (**Figure 3-3**). However, it was found that the three-step ratio method is sensitive to variations in the positioning and shape of the sealed platinum tube between baseline, reference and sample runs. As a result, the calculated heat capacity curve exhibited an anomalous trend, although still providing useful information.

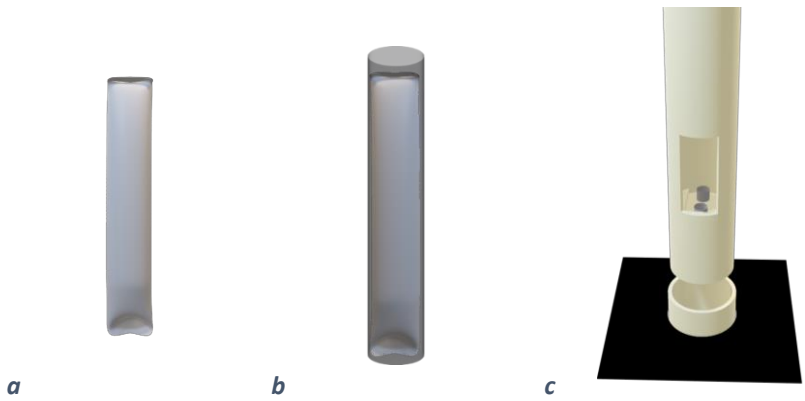


Figure 3-3 *Custom sealed platinum tube (**a**) in platinum sample holder (**b**) for investigation in Setaram mHTC 96 calorimeter (**c**).*

Since the anomalous trend observed in the C_p curves is most likely attributable to purely practical issues related to sample handling and positioning, a novel procedure for correcting experimental heat capacity curves was introduced. Initially proposed by the author in [205], this procedure is here further discussed. The method, referred to as the self-referencing calibration method (SRCM), is based on the assumption that reliable C_p data can be obtained for the same compound in a temperature range below its decomposition point, where measurements can safely be performed in open containers. In this stable range, the C_p curve can be accurately described by a polynomial function, which is assumed to remain valid over a broader temperature range, including the high-temperature region accessible only with sealed crucibles [41]. The SRCM consists of four sequential steps (**Figure 3-4**). First, high-temperature DSC measurements are performed using a fully sealed platinum tube placed in a platinum sample holder, yielding the experimental heat capacity curve, $C_{p,exp}$. Second, low-temperature measurements are carried out in an open alumina liner placed in a platinum sample holder, providing a reliable polynomial representation of the C_p curve, hereafter referred to as the correction baseline, $C_{p,correction}$. Third, the deviation between the high-temperature experimental data and the expected polynomial trend is quantified as a temperature-dependent function, $\Delta C_p(T) = C_{p,exp}(T) - C_{p,correction}(T)$. Finally, this correction factor is applied across the entire

temperature range to reconstruct the corrected heat capacity curve, $C_{p,corrected}$, which restores a physically consistent trend even in the high-temperature region where sealed crucibles are required. This method was validated using a well-known standard, $BaCO_3$, confirming its reliability (**Figure 3-5**). In addition to the three curves involved in the SRCM procedure, the figure shows a direct comparison between the corrected C_p curve obtained in the sealed platinum tube ($C_{p,corrected}$) and that measured under standard DSC conditions (alumina liner in a platinum sample holder), which also serves as the correction baseline ($C_{p,correction}$). $BaCO_3$ was selected as a reference material because it allows comparable measurements in both crucibles over the same temperature range, without undergoing mass loss. The enthalpy increment curves (**Figure 3-5b**), derived from the respective C_p data (**Figure 3-5a**), overlap almost perfectly, thus demonstrating the validity of the proposed method.

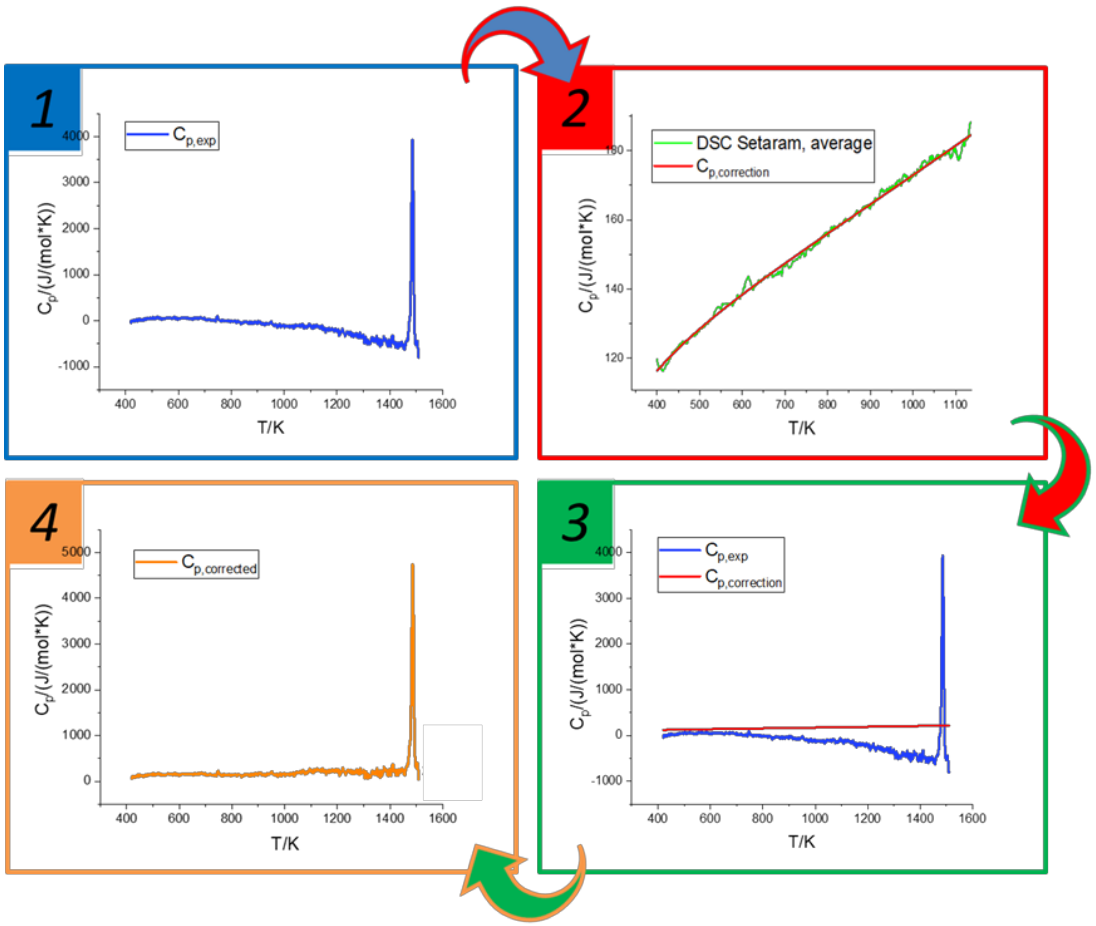


Figure 3-4 *Schematic representation of the stepwise approach in the self-referencing calibration method (SRCM).*

By applying the method proposed in this work, heat capacity curves can be reliably obtained over a wide temperature range without mass losses caused by the decomposition of sulphates. Moreover, the method enables the determination of the C_p values of the liquid phase, which would otherwise be inaccessible. Although enthalpy increment (ΔH vs T) curves can, in principle, be derived

by integrating experimental C_p data, this procedure is significantly affected by the anomalous trends of the uncorrected curves, which fail to provide the sharp vertical steps required for accurately calculating transition enthalpies. This limitation underscores the advantages of the proposed approach. Through appropriate calibration with standard salts measured in fully sealed platinum tubes, it is possible to determine transition enthalpies directly from the areas under the peaks and to compare these values with those obtained from enthalpy increment curves derived by integrating the corrected C_p data ($C_{p,corrected}$). The method proposed here can also be applied using the C_p polynomial available in the literature, derived from available databases or other experimental studies, as a baseline ($C_{p,correction}$), rather than necessarily deriving it from *in situ* experiments. While this approach is less precise, it may still be useful for estimating thermodynamic properties that would otherwise be unobtainable.

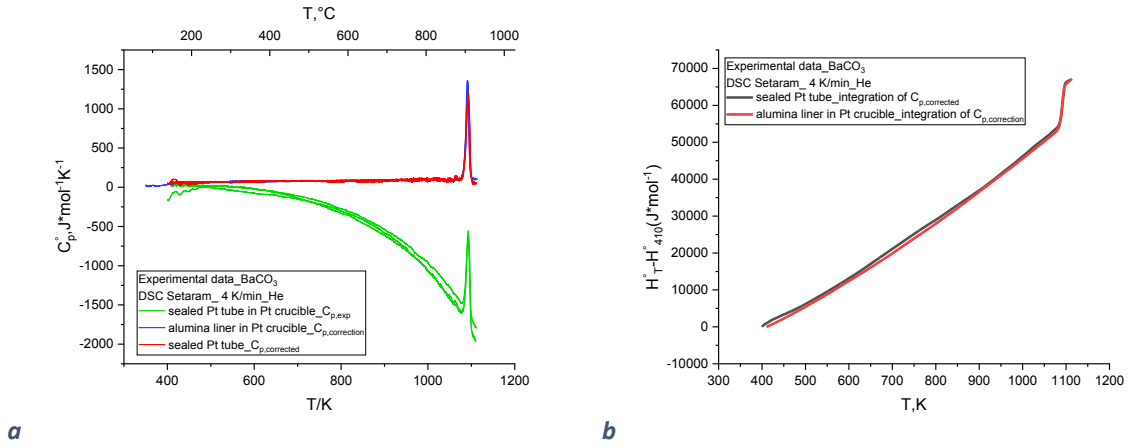


Figure 3-5 *Comparison of experimental data in open alumina liner and sealed Pt tube in Pt crucible of $BaCO_3$ for Self-referencing calibration method:* ***a*** *molar heat capacity;* ***b*** *enthalpy increment.*

3.2.3 X-Ray Diffractometry/High Temperature X-Ray Diffractometry (HT-XRD)

X-ray Diffractometry (XRD) is an essential technique for investigating material properties such as phase composition, structure, and texture in powder, solid, or even liquid samples [206]. The wavelength of X-rays is comparable to the distances between atoms in a crystal lattice. When X-rays interact with the periodic arrays of atoms in a crystal, diffraction occurs, producing constructive interference at specific angles. This scattering generates a diffraction pattern that provides detailed information about the arrangement of atoms within the crystal. The fundamental principle governing X-ray diffraction is Bragg's Law, expressed as $n\lambda = 2d \sin\vartheta$, where n is the diffraction order, λ is the X-ray wavelength, d is the interplanar spacing, and ϑ is the diffraction angle. Bragg's law explains how constructive interference arises when the path difference between X-rays scattered by parallel planes of atoms equals an integer multiple of the wavelength. This principle underpins XRD analysis, allowing

the determination of crystal structures, lattice parameters, and phase composition. Identification of phases is achieved by comparing the X-ray diffraction pattern of an analysed sample with reference patterns from databases such as the ICDD (International Centre of Diffraction Data) [207, 208] and ICSD (Inorganic Crystal Structure Database) [209, 210]. Additionally, custom reference databases can be built from experimental diffraction patterns of pure phases or data published in the literature. High-Temperature X-ray Diffractometry (HTXRD) extends these capabilities to elevated temperatures, enabling the analysis of structural and phase changes as a function of temperature. HT-XRD is particularly effective for observing phase transitions, determining temperature-dependent lattice parameters, and studying changes in crystal symmetry or composition over a wide temperature range. This makes HT-XRD an invaluable tool for understanding the thermal behaviour and stability of materials.

Room- and high-temperature measurements were conducted by the analytical department of IMD-1 at Forschungszentrum Jülich using an Empyrean diffractometer from Malvern PANalytical equipped with a Cu-LFF X-ray tube (operated at 40 kV and 40 mA), BBHD mirror, a PIX-cel3D detector and a high temperature oven chamber Anton Paar HTK 1200 N. A continuous flow of synthetic air was applied during the experiment. Lattice parameters and amounts of secondary phases were determined through Rietveld refinement using the profile analysis software TOPAS version 6 from Bruker AXS. The uncertainty for molar volume was estimated to be ±0.02 cm^3/mol and for temperature ±2 K. XRD investigations were performed on selected compositions chosen to provide a comprehensive overview of phase relations. These included eutectic mixtures, confirmed and potential intermediate compounds, and specifically designed mixtures prepared to verify phase stability and possible reactions among components. These samples were synthesised *in situ* under experimental conditions tailored to the specific system under study, as described in the relevant experimental sections. Stoichiometric amounts of anhydrous pure compounds were thoroughly mixed and ground in an agate mortar. The resulting mixture was then placed in a sealed quartz ampoule and heated to a predetermined temperature. During the heating process, the procedure was briefly interrupted one to three times to regrind the charges, ensuring homogeneity of the sample. The final powder obtained after the thermal treatment was analysed using X-ray diffraction to characterise the crystalline phases and assess the structural properties of the synthesised material.

3.2.4 Microanalysis by Electron Microscopy and Energy Dispersive X-ray Spectroscopy

Morphology and phase distribution were analysed by the analytical department of IMD-1 with scanning electron microscopy using a Merlin (Zeiss Microscopy, Oberkochen, Germany) field emission scanning electron microscope (SEM) operated at 10 kV accelerating voltage and 0.5 nA probe current.

SEM is specifically employed in this work to study and analyse the phases present in the $MgSO_4$-$CaSO_4$ system. This technique serves as a complementary method to support and validate additional experimental findings, providing detailed insights into the morphology and phase distribution within the system. Pellets of $CaSO_4$ and $MgSO_4$ were pressed and sintered for the EDX analysis. The non-conductive samples were sputter coated with Ir using a Q150T coater (Quorum Technologies, Laughton, UK) prior to SEM investigation. Images were acquired using an Everhart-Thornley secondary electron (SE) detector or a four-segment solid-state backscattered electron (BSE) detector. The local chemical composition was investigated by energy-dispersive X-ray (EDX) spectroscopy. Spectra were recorded using an X-max 80 silicon drift detector (Oxford Instruments, High Wycombe, UK). The AZtec software package (Oxford Instruments) was used for data acquisition and analysis. For the EDX analysis, areas were selected that were sufficiently large and had a flat surface.

4 Thermodynamic Modelling

The pioneering work of J. Willard Gibbs [211] introduced the concept of free energy, revolutionising the understanding of spontaneous processes and the feasibility of chemical reactions. This theoretical framework enabled scientists to predict reaction outcomes without experimental trials, provided that the thermodynamic properties of the substances involved were well-characterised. Building on this foundation, the CALPHAD (CALculation of PHAse Diagrams) method emerged as a robust computational approach for predicting phase diagrams, phase equilibria, and thermodynamic properties, as first introduced by Kaufman and Bernstein [212]. The technique has been refined through collaborative efforts by leading research institutions worldwide, resulting in sophisticated algorithms for Gibbs energy minimisation and accurate determination of phase boundaries [213-215]. Over time, this methodology has become indispensable in materials chemistry and engineering. Although its initial applications were largely focused on metallic systems, significant progress has also been made in non-metallic systems, including oxides and salts, which are now considered in many energy-related and industrial applications worldwide. A key factor for obtaining reliable calculations and predictions is the quality, completeness, and internal consistency of the thermodynamic database used. In addition, appropriate software is required to perform thermodynamic modelling and to calculate phase equilibria and thermodynamic properties under equilibrium conditions. Several software packages have been developed by different institutions worldwide, such as Thermo-Calc and Pandat. Thanks to the contributions of groups such as GTT-Technologies and Thermfact, the widely-used FactSage software [216-220] was developed, and it is the one employed in the present work.

The commercial databases available in existing thermochemical software tools do not always provide reliable phase equilibria and thermodynamic property descriptions across the full compositional and temperature ranges of salt systems. Therefore, the development of a dedicated and rigorously evaluated thermodynamic database is required.

Based on the experimental data and findings obtained in this work, as well as studies available in the literature, the objective of this thesis is to develop a consistent thermodynamic database (PCM2). This database aims to include the appropriate thermodynamic properties of Na^+, K^+, Mg^{2+}, Ca^{2+} // Cl^-, SO_4^{2-} system and serves as a foundation for predicting the properties of other multicomponent systems involving the studied systems. For the development of the PCM2 database, the assessment of the Gibbs free energy of various phases is performed using the CALPHAD method. This is conducted through the FactSage software, specifically utilising the Calphad Optimizer module [221] available from version FactSage 8.2 onwards. This module replaces the Optisage module present in earlier versions, providing enhanced capabilities for thermodynamic modelling and optimisation. This

chapter delves into the theoretical underpinnings of thermodynamic calculations, examines the models utilised for the representation of Gibbs free energy, and elaborates on the systematic approach adopted for thermodynamic optimisation.

4.1 Thermodynamic background

The fundamental principle of thermodynamic equilibria is the minimisation of the Gibbs free energy of a system [222-224]. The stability of phases is defined by the condition that, under identical temperature and pressure, the system with the lowest Gibbs free energy is the thermodynamically stable one. Gibbs free energy is a state function and it can be expressed as follows:

$$G = U + PV - TS = H - TS \qquad \textit{Equation 3}$$

and, for an arbitrary infinitesimal change in state, the change in Gibbs free energy is

$$dG = dU + PdV + VdP - TdS - SdT \qquad \textit{Equation 4}$$

or

$$dG = VdP - SdT + \sum \mu_i dn_i \qquad \textit{Equation 5}$$

where U is the internal energy, P is the pressure, V is the volume, T is the temperature, H is the enthalpy, S is the entropy, μ_i and n_i are the chemical potential and molar number of components i, respectively. Equation 5 represents a statement of the combined first and second laws of thermodynamics.

Under thermodynamic equilibrium, the Gibbs-Duhem relation (Equation 6) serves as a key tool for analysing the interdependence of thermodynamic variables. It can be expressed in terms of specific thermodynamic potentials Φ_i and their extensive conjugate variables q_i. These transformations are crucial for systematically understanding and predicting the behaviour of diverse thermodynamic systems.

$$\sum q_i d\Phi_i = 0 \qquad \textit{Equation 6}$$

Determining the minimum Gibbs energy of a system under specific conditions requires knowledge of the Gibbs energy of each phase involved. The stability fields of these phases can be visualised through equilibrium maps and phase diagrams. One commonly used representation in this context is the temperature-composition (T-X) phase diagram, which illustrates the stability regions of specific phases as functions of temperature and composition. These stability fields can also be interpreted using Gibbs energy-composition (G-X) plots, where the regions in the T-X diagram

correspond to configurations that minimise the system's Gibbs energy, as shown in **Figure 4-1**. In these diagrams, the Gibbs free energy is plotted against the mole fraction of one component at a fixed temperature and pressure. The stability domains are identified by the minima of the Gibbs energy and by the construction of the common tangent, which connects phases in equilibrium.

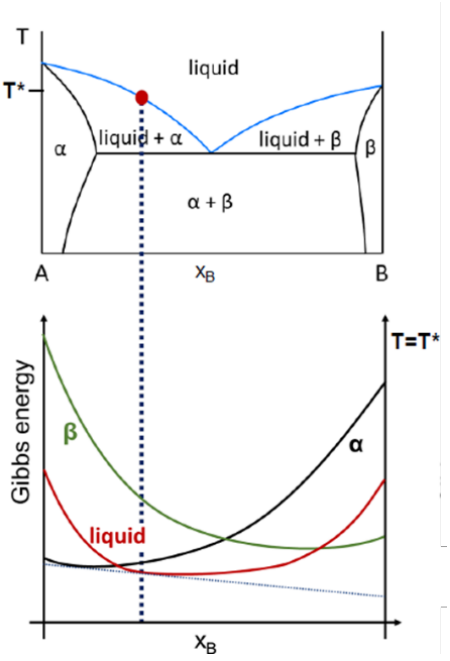


Figure 4-1 *Relationship between G-X and T-X plots illustrating phase equilibria [220].*

In thermodynamic modelling, it is necessary to define the molar Gibbs free energy of all phases involved in the system [225, 226]. The molar Gibbs free energy is typically expressed as the sum of several contributions, as shown in Equation 7:

$$G_m = {}^{ref}G_m + {}^{id}G_m + {}^{ex}G_m \qquad \textit{Equation 7}$$

The first term corresponds to the reference term, representing the mechanical mixture of the pure end-member constituents without any interaction - essentially a non-reactive sum of the constituent Gibbs energies. The second term accounts for the ideal contribution, assuming random mixing of the components and describing the configurational entropy of mixing ΔS_{mix}. The third term represents the excess Gibbs energy, which captures deviations from ideality and allows for the description of real solution behaviour, including short-range ordering (SRO), clustering, or repulsion effects among species.

4.2 Pure compound phases

For pure compounds, the Gibbs free energy is described solely by the first term in Equation 7, as these are fixed-composition phases whose thermodynamic behaviour depends exclusively on temperature and pressure. As outlined in Equation 3, the Gibbs free energy is function of enthalpy and entropy. Both of these thermodynamic properties can, in turn, be expressed as functions of the heat capacity, as shown in Equation 8 and Equation 9.

$$H = H^{ref} + \int_{T_{ref}}^{T} C_p dT \qquad \textit{Equation 8}$$

$$S = S^{ref} + \int_{T_{ref}}^{T} \frac{C_p}{T} dT \qquad \textit{Equation 9}$$

In these equations, H^{ref} and S^{ref} represent the reference enthalpy and entropy, respectively. According to the Standard Element Reference (SER) convention, these reference values are defined relative to the stable state of the element at 1 atm and 298 K. Accordingly, H^{ref} corresponds to the standard enthalpy of formation $\Delta_f H^0_{298}$, while S^{ref} represents the absolute entropy at standard conditions S^0_{298}.

The heat capacity C_p is typically represented by a temperature-dependent polynomial, as given in Equation 10. In most cases, this expression is truncated after the *D* coefficient, neglecting higher-order terms.

$$C_p = A + B \cdot T + C \cdot T^{-2} + D \cdot T^2 + E \cdot T^3 + \cdots \qquad \textit{Equation 10}$$

By combining Equation 3, Equation 8 and Equation 9 with Equation 10, the thermodynamic functions *G*, *H*, *S* can all be derived consistently as functions of temperature, mirroring the structure of the C_p expression. Heat capacity data can be determined experimentally; however, when direct measurement is not feasible, the Neumann-Kopp rule is often applied [215, 227]. According to this approximation, the heat capacity of a compound is estimated as the stoichiometric sum of the heat capacities of its constituent species, weighted by their respective molar ratios.

Thermodynamic data (standard enthalpy of formation $\Delta_f H^0_{298}$, standard entropy S^0_{298}, and heat capacity as function of temperature $C_p(T)$ for pure solid and liquid compounds) are summarised in **Table 6-1**, along with transition temperatures and heats of transitions. While this work does not primarily focus on the detailed Gibbs energy modelling of pure compounds, a major emphasis is placed on the Gibbs energy optimisation of liquid solution, which constitutes a key aspect of this study. This

modelling approach, based on the Calphad method [215], is implemented using the FactSage software [218, 220].

In cases where experimental evidence leads to modifications of the thermodynamic database, including the substitution and/or introduction of a new stoichiometric compound, the species is introduced using the 'Mixer' function within the 'Compound' module of FactSage. This function allows the creation of a compound by combining the thermodynamic data of existing and stored end-members, based on the Neumann-Kopp rule. Such an update of the database under development, based on experimental evidence confirming the existence of a given phase, leads to a more accurate thermodynamic description of the investigated system. As a result, it provides an improvement over commercial databases [217, 218, 228].

4.3 Solution phases

In the case of solution phases, all contributions in Equation 7 must be considered, since these phases exhibit compositional variability without structural transitions. Several models are available for the thermodynamic representation of solutions. The simplest of these is the ideal solution model, which assumes random mixing of components and does not include any adjustable parameters. In this model, the enthalpy of mixing is zero, and the entropy of mixing corresponds to that of an ideal mixture. Consequently, the model cannot distinguish between different solution phases having the same composition at a given temperature. A more advanced representation is provided by the regular solution model, which retains the entropy of mixing of an ideal solution (i.e., zero excess entropy), but introduces a non-zero enthalpy of mixing that depends on composition. Thus, the excess Gibbs free energy is equal to the enthalpy of mixing, implying that it is a function of composition but independent of temperature.

As outlined in Equation 7, the molar Gibbs free energy of a solution phase is composed of three contributions - reference, ideal mixing, and excess terms - which are detailed in the following expression:

$$G_m = \sum x_i {}^\circ G_i + RT \sum x_i ln x_i + \sum \sum_{i<j} x_i x_j \sum_{v=0} L_{ij}^{(v)} \left(x_i - x_j\right)^v \qquad \textit{Equation 11}$$

where x_i is the mole fraction of phase constituent i (including the associate species), ${}^\circ G_i$ is the molar Gibbs energy of the pure phase constituent i and $L_{ij}^{(v)}$ with v = 0, 1, 2 are the interaction coefficients between components i and j, according to the Redlich-Kister polynomial [229]. ${}^\circ G_i$ and $L_{ij}^{(v)}$ are temperature dependent in the same way according to Equation 12:

$$^{\circ}G_i, L_{ij}^{(v)} = A + BT + CTln(T) + DT^2 + ET^3 + F/T \qquad \textit{Equation 12}$$

This solution model becomes regular for v = 0 and subregular for v = 1.

The quasi-chemical model for short-range ordering was developed to account for non-random mixing in the solution. It assumes that the energy of the system resides in interactions between neighbouring atoms or molecules, and that these bond energies are composition-independent. When bond energies are allowed to vary with composition, the model leads to the so-called subregular solution model. In contrast, non-regular or real solution models account for both composition and temperature dependence of the excess Gibbs energy (or, equivalently, the enthalpy of mixing). These models are required to describe complex behaviours such as ordering, clustering, or significant asymmetry in phase equilibria.

Additional models include the sublattice model, which employs the compound energy formalism (CEF) [195] to represent sublattice configurations, as well as the modified quasi-chemical model (MQM) [143, 194, 230-232] and the modified associate species model (MAM) [233], both commonly used to describe liquid phases with strong interactions and short-range ordering (SRO). The formation of associates from the constituents reflects the tendency of certain species to exhibit SRO within the solution.

The following sections present the thermodynamic models adopted in this work to describe the liquid and solid solution phases of the inorganic salt systems under investigation.

4.3.1 Liquid

The Gibbs energy of the liquid phase in the studied system was modelled using the modified non-ideal associate species model (MAM) proposed by Besmann et al. [233], which has demonstrated applicability for complex oxide and salt liquids [38, 39, 234]. To account for short-range ordering (SRO) in solutions, the model introduces associate species as additional constituents. For example, if a solution of A and B exhibits ordering around 50 mol% B, SRO can be represented by adding a new constituent with the stoichiometry AB. The inclusion of such a species requires the definition of its corresponding standard Gibbs energy. Accordingly, the standard enthalpy of formation and standard entropy of the species become parameters of the model, while its heat capacity is typically estimated using the Neumann-Kopp rule. In the present work, the liquid phase is considered as an oxide solution to keep consistence with the general oxide database GTOx [235]. The pure compounds, MCl_2 and MSO_4 (M = Na_2, K_2, Mg and Ca), in liquid phase, are taken as solution components. The interactions between them are responsible for the thermodynamic properties of the liquid phase. To provide equal weighting of each associate species with regard to its entropic contribution in the ideal mixing term in

the oxide database, each species contains a total of two non-oxygen atoms per formula unit according to the model used in Besmann et al. [233]. For sodium, potassium, magnesium and calcium chlorides and sulphates, this is represented by NaCl, KCl, ($MgCl_2$):1.5, ($CaCl_2$):1.5, (Na_2SO_4):1.5, (K_2SO_4):1.5, $MgSO_4$ and $CaSO_4$, meaning that each atom stoichiometry for alkaline-earth chlorides and alkali sulphates is divided by 1.5. This aims to provide compatibility with the general oxide database GTOx [235]. In addition, interactions between associate species are introduced in order to fine tune the thermodynamic description. Typically, in Equation 12, the optimisation process focuses primarily on the coefficients A and B for $L_{ij}^{(v)}$.

When dealing with ternary systems, it is necessary to account for ternary interaction parameters in the excess Gibbs free energy contribution. Several geometric models have been proposed to estimate the thermodynamic properties of ternary systems from those of the corresponding binary subsystems, as noted by Pelton [236], with the Muggianu model being one of the most widely used. This implies that the excess Gibbs energy term in Equation 11 must also include the ternary interaction parameters, resulting in the modified form of Equation 11 reported below:

$$G_m = \sum x_i {}^{\circ}G_i + RT \sum x_i ln x_i + \sum \sum_{i<j} x_i x_j \sum_{v=0} L_{ij}^{(v)} \left(x_i - x_j\right)^v + \sum \sum_{i<j} \sum_{j<k} x_i x_j x_k \left[L_{i,j,k}^{i} \left(x_i + \frac{1 - x_i - x_j - x_k}{3} \right) + L_{i,j,k}^{j} \left(x_j + \frac{1 - x_i - x_j - x_k}{3} \right) + L_{i,j,k}^{k} \left(x_k + \frac{1 - x_i - x_j - x_k}{3} \right) \right] \quad \text{Equation 13}$$

The subregular ternary interaction parameters $L_{i,j,k}^{i}$, $L_{i,j,k}^{j}$ and $L_{i,j,k}^{k}$ are expressed as temperature-dependent functions, formulated analogously to those defined for the binary interactions in Equation 12.

4.3.2 Solid solutions

In this work, the solid solutions are modelled using the sublattice model within the compound energy formalism (CEF) [195], which is based on the assumption that the constituents of the solution can be distributed over one or more sublattices. A simple case of this is the ideal substitutional solution model, where all species are randomly distributed over a single lattice, representing an ideal mixing of end-members. To describe real solutions, as previously discussed, interaction parameters between end-members must be introduced - typically expressed as shown in Equation 12. A more advanced configuration is represented by the two-sublattice model, expressed as $(A,B)_a(C,D)_c$, where *A* and *B* are the species occupying the first sublattice, *C* and *D* those of the second, *a* and *c* are the stoichiometric coefficients associated with each sublattice, corresponding to the stoichiometry of the

compound. To calculate the Gibbs free energy of such a solution phase, the concept of site fractions y_i must be introduced. Site fractions represent the molar fraction of each constituent within its respective sublattice, and they are essential for correctly evaluating the Gibbs energy of the solution.

By redefining the terms in Equation 11 as functions of the site fractions, the Gibbs energy of the solution [215] can be expressed as follows:

$$\begin{aligned} G_m = & \sum_i \sum_{j>i} y_i^I \, y_j^{II} {}^\circ G_{ij} + aRT \sum y_i^I ln y_i^I + cRT \sum y_j^{II} ln y_j^{II} \\ & + \sum_i y_i^I \sum_j \sum_{k>j} y_j^{II} y_k^{II} \sum_{v=0} L_{i:j,k}^{(v)} \left(y_j^{II} - y_k^{II}\right)^v \\ & + \sum_i y_i^{II} \sum_j \sum_{k>j} y_j^I y_k^I \sum_{v=0} L_{i,j:k}^{(v)} \left(y_j^I - y_k^I\right)^v \end{aligned} \qquad \textit{Equation 14}$$

where I and II refer to the first and the second sublattices, respectively. The indices i, j and k represent the end-members occupying the sublattices. In the $i{:}\,j,k$ notation a colon (:) is used to separate the sublattices, while a comma (,) separates the mixing constituents within each sublattice.

The solid solubilities based on alkali and alkaline-earth chlorides (AlkCl(ss) and MCl2, respectively) were both described in this work using a two sublattice model. For the alkali chlorides, the formulation proposed by Reis [48] was adopted. In this model, one sublattice is assigned to alkali cations, while the second is designated for chloride anions: $(Na^{1+}, K^{1+}, Ca^{2+}, Va^{0})_1(Cl^{1-})_1$. In that model, each molecule of $CaCl_2$ was assumed to dissociate into $CaCl^+$ and $VaCl^-$, ensuring the solution remains electroneutral. The molar Gibbs energy of AlkCl(ss) solution is described by the following expression:

$$\begin{aligned} G_m = & \, y_{Na^{1+}}^I {}^\circ G_{NaCl} + y_{K^{1+}}^I {}^\circ G_{KCl} + y_{Ca^{2+}}^I {}^\circ G_{CaCl} + y_{Va^0}^I {}^\circ G_{VaCl^-} \\ & + RT\left(y_{Na^{1+}}^I ln y_{Na^{1+}}^I + y_{K^{1+}}^I ln y_{K^{1+}}^I + y_{Ca^{2+}}^I ln y_{Ca^{2+}}^I \right. \\ & \left. + y_{Va^0}^I ln y_{Va^0}^I\right) \\ & + \left[y_{Me1}^I \cdot y_{Me2}^I \cdot \sum_{k=0}^{n} L_{(Me1,Me2:Cl^-)}^k (y_{Me1}^I - y_{Me2}^I)^k\right] \end{aligned} \qquad \textit{Equation 15}$$

The modelling of alkaline-earth chloride solubility MCl2 was developed in the present work, using the sublattice model. One sublattice accommodates the alkaline earth cations (Mg^{2+}, Ca^{2+}), while the other contains the chloride anion (Cl^-), and the solution phase is represented as $(Mg^{2+}, Ca^{2+})_1(Cl^{1-})_2$. The molar Gibbs energy is expressed as follows:

$$\begin{aligned} G_m = & \, y_{Mg^{2+}}^I {}^\circ G_{MgCl_2} + y_{Ca^{2+}}^I {}^\circ G_{CaCl_2} + RT\left(y_{Mg^{2+}}^I ln y_{Mg^{2+}}^I + y_{Ca^{2+}}^I ln y_{Ca^{2+}}^I\right) \\ & + \left[y_{Mg^{2+}}^I \cdot y_{Ca^{2+}}^I \cdot \sum_{v=0} L_{MgCl_2,CaCl_2}^{(v)} \left(y_{Mg^{2+}}^I - y_{Ca^{2+}}^I\right)^v\right] \end{aligned} \qquad \textit{Equation 16}$$

Various sulphate-based solid solutions were implemented to accurately represent the phase equilibria observed in binary and reciprocal systems, and had already been incorporated into the thermodynamic database under development [39, 201]. The hexagonal phase HEXA (referred to as HEXAGONAL in [39, 201]) was introduced to model the unlimited mutual solubility between the high-temperature modifications of Na_2SO_4 (HT) and K_2SO_4 (HT), while accounting for the limited solubility with alkaline earth sulphates such as $MgSO_4$ and $CaSO_4$. This solid solution was described using the model proposed by Du [61], based on the general formula $(Na^{1+}, K^{1+}, Mg^{2+}, Ca^{2+}, Va^0)_2(SO_4^{2-})_1$, where the introduction of vacancies (Va) in the cation sublattice ensures electroneutrality in the presence of mixed-valence species. To describe the mutual solubility of the low- and medium-temperature polymorphs of alkali sulphates, two solid solutions were implemented: Na-ortho-MT as combination of the two solid solutions referred to in [39] as K-ortho, based on on K_2SO_4 (LT), and Na-ortho-MT related to Na_2SO_4 (MT); and the solid solution based on Na_2SO_4 (LT), referred to as NaLT (denoted as Na-ortho-LT in [39]). These solid solutions were described using a sublattice formalism in accordance with the thermodynamic models developed by Lindberg et al. [193], expressed as $(Na^{1+}, K^{1+}, Mg^{2+}, Ca^{2+}, Va^0)_2(SO_4^{2-})_1$.

The molar Gibbs energy of Na-ortho-MT and HEXA is expressed as follows:

$$\begin{aligned} G_m = {} & y^I_{Na^{1+}} {}^\circ G_{Na_2SO_4} + y^I_{K^{1+}} {}^\circ G_{K_2SO_4} + y^I_{Mg^{2+}} {}^\circ G_{Mg_2SO_4^{2+}} + y^I_{Ca^{2+}} {}^\circ G_{Ca_2SO_4^{2+}} \\ & + y^I_{Va^0} {}^\circ G_{VaSO_4^{2-}} \\ & + 2RT \left(y^I_{Na^{1+}} ln y^I_{Na^{1+}} + y^I_{K^{1+}} ln y^I_{K^{1+}} + y^I_{Mg^{2+}} ln y^I_{Mg^{2+}} \right. \\ & \left. + y^I_{Ca^{2+}} ln y^I_{Ca^{2+}} + y^I_{Va^0} ln y^I_{Va^0} \right) \\ & + \left[y^I_{Me1} \cdot y^I_{Me2} \cdot \sum_{k=0}^{n} L^k_{(Me1,Me2:SO_4^{2-})} \left(y^I_{Me1} - y^I_{Me2}\right)^k \right] \end{aligned} \qquad \textit{Equation 17}$$

In Equation 17, the square brackets denote the molar excess Gibbs energy contribution G_m^{ex}, within which ternary interaction parameters can be incorporated in the modelling of ternary systems to enhance the description of phase equilibria. The molar Gibbs energy of the NaLT solution phase, represented as $(Na^{1+}, K^{1+})_2(SO_4^{2-})_1$, is expressed using a formulation equivalent to that in Equation 17.

Additionally, the glaserite phase (GLAS), a solid solution in the subsolidus region of the Na_2SO_4-K_2SO_4 system, was adopted from the assessments by Du [61] and Lindberg et al. [193]. It was modelled using a three-sublattice approach, with the composition $(K^{1+}, Na^{1+})_3(Na^{1+})_1(SO_4^{2-})_2$, to capture the asymmetric one-phase field observed in the corresponding phase diagram. The molar Gibbs energy of GLAS is given, as reported in [39], by the following expression:

$$G_m = y^I_{K^{1+}} {}^\circ G_{K_3Na(SO_4)_2} + y^I_{Na^{1+}} {}^\circ G_{Na_3Na(SO_4)_2} + 3RT\left(y^I_{Na^{1+}} ln y^I_{Na^{1+}} + y^I_{K^{1+}} ln y^I_{K^{1+}}\right) + \left[y^I_{K^{1+}} \cdot y^I_{Na^{1+}} \cdot L^0_{(K^{1+},Na^{1+}:Na^{1+}:SO_4^{2-})} + y^I_{K^{1+}} \cdot y^I_{Na^{1+}} \cdot L^1_{(K^{1+},Na^{1+}:Na^{1+}:SO_4^{2-})}\left(y^I_{K^{1+}} - y^I_{Na^{1+}}\right)\right] \quad \textit{Equation 18}$$

The langbeinite solid solution between $K_2Mg_2(SO_4)_3$ and $K_2Ca_2(SO_4)_3$, named as LANG, is also considered in this work. This phase was first reported by Morey et al. [148] and later incorporated into thermodynamic assessments by Rowe et al. [58]. The solid solution has been modelled using the three-sublattice approach proposed by Du [61], expressed as $(K^{1+})_2(Ca^{2+}, Mg^{2+})_2(SO_4^{2-})_3$, and the corresponding molar Gibbs energy as the following expression:

$$G_m = y^{II}_{Ca^{2+}} {}^\circ G_{K_2Ca_2(SO_4)_3} + y^{II}_{Mg^{2+}} {}^\circ G_{K_2Mg_2(SO_4)_3} + 2RT\left(y^{II}_{Ca^{2+}} ln y^{II}_{Ca^{2+}} + y^{II}_{Mg^{2+}} ln y^{II}_{Mg^{2+}}\right) + \left[y^{II}_{Ca^{2+}} \cdot y^{II}_{Mg^{2+}} \cdot L^0_{(K^{1+}:Ca^{2+},Mg^{2+}:SO_4^{2-})} + y^{II}_{Ca^{2+}} \cdot y^{II}_{Mg^{2+}} \cdot L^1_{(K^{1+}:Ca^{2+},Mg^{2+}:SO_4^{2-})}\left(y^{II}_{Ca^{2+}} - y^{II}_{Mg^{2+}}\right)\right] \quad \textit{Equation 19}$$

4.4 Assessment of Gibbs energy parameters

The assessment of the sub-systems investigated in this study was conducted by combining the experimental results obtained in the present work with available literature data on phase diagrams and thermodynamic properties. The standard enthalpy of formation $\Delta_f H^0_{298}$ and the standard entropy S^0_{298} of some double sulphates and some pure compounds, along with the various binary and ternary interaction parameters ($L^{(\nu)}_{ij}$) between species in the liquid and in the solid solutions were optimised. The C_p functions of all substances were assessed before the optimisation and kept constant.

As with the experimental campaign, the thermodynamic modelling follows a stepwise approach (**Figure 4-2**). It begins with the definition of the thermodynamic properties of pure compounds and proceeds through the modelling of binary and quasi-binary systems within the framework of reciprocal systems. Once the binary systems have been assessed, the modelling extends to ternary subsystems. The final objective is to describe the full multicomponent system and to provide an updated thermodynamic database capable of predicting the thermodynamic behaviour of even more complex systems.

In this work, several modules available in the FactSage software [218, 220] are employed. The 'Compound' and 'Solution' modules allow for the definition and modification of thermodynamic properties of pure substances and intermediate compounds, and solution phases (both solid and liquid), respectively. The 'Reaction', 'Equilib', and 'Phase Diagram' modules are used to calculate

thermodynamic properties under various conditions. Among them, the 'Phase Diagram' module is extensively utilised to compute phase diagrams, which are typically represented as temperature-composition (T-X) plots for binary systems, and as polythermal liquidus projection plots for ternary and reciprocal systems. The 'Calphad Optimizer' module [221] is employed to refine and optimise the Gibbs energy parameters of the phases, based on both literature and newly acquired experimental data. Following optimisation, the comparison between the calculated phase equilibria and thermodynamic properties and the corresponding experimental results serves as a critical validation step, confirming the reliability and predictive capability of the updated thermodynamic database.



Figure 4-2 *Stepwise modelling approach: from simple to complex systems.*

5 Experimental results

This chapter presents the experimental investigations conducted in this study, which aimed to provide comprehensive insights into the phase diagrams and thermodynamic properties of the selected compounds and systems. A combination of analytical techniques was employed, including differential thermal analysis (DTA) coupled with thermogravimetry (TG), differential scanning calorimetry (DSC), X-ray diffraction (XRD) and high-temperature XRD (HT-XRD), as well as scanning electron microscopy coupled with energy dispersive X-ray spectroscopy (SEM-EDX). The chapter is structured into dedicated sections, each focusing on one of the six reciprocal systems investigated. Within each section, the discussion is further divided into subsections that specifically address the binary and pseudo-binary subsystems relevant to the reciprocal system in question, and that have been subjected to experimental study. However, as some of these binary subsystems are shared among multiple reciprocal systems - analogous to the way cube faces share common edges - the experimental details of these binary systems are presented only in the first instance in which they appear. **Table 5-1** provides a summary of the transition temperatures and associated enthalpy values for pure chloride and sulphate compounds, obtained from the literature and from experimental results of this study. These data have been subsequently integrated into the thermodynamic database.

Table 5-1 *Transition data of pure compounds.*

Reaction	Reaction Type	Temperature of transition		Heat of transition	
		T_{tr}, °C (K)	Ref.	ΔH_{tr}, kJ/mol	Ref.
NaCl					
NaCl ↔ liquid	melting	800.6 (1073.8)	[228, 237]	28.158	[228, 237]
		800 (1073)	[238]	27.99	[238]
		800. 4 (1073.6)	[129, 239]		
		809.8 (1083)	[a]		
KCl					
KCl ↔ liquid	melting	771 (1044)	[228, 237]	26.28	[228, 237]
		770 (1043)	[238]	26.53	[238]
		770.3 (1043.5)	[239]		
		777.7 (1050.9)	[a]		
$MgCl_2$					
$MgCl_2$ ↔ liquid	melting	714 (987)	[92, 237, 240, 241]	43.095	[92, 237, 240, 241]
		712.7 (985.9)	[53]		
		719.4 (992.5)	[a]		
		716.7 (989.9)	[b]	43.1	[b]
$CaCl_2$					
$CaCl_2$ ↔ liquid	melting	772 (1045)	[242-244]	28.543	[242-244]
		771.7 (1044.9)	[53]		
		776 (1049)	[a]		
Na_2SO_4					
Na_2SO_4 (LT) ↔ Na_2SO_4 (MT)	solid↔solid	185 (458)	[245]	0.314	[245]
		185 (458)	[39, 228]	0.3	[39, 228]
		195.3 (468.5)	[a]		
Na_2SO_4 (MT) ↔ Na_2SO_4 (HT)	solid↔solid	241 (514)	[39, 228, 245]	10.9	[39, 228, 245]
		246.4 (519.6)	[a]		
Na_2SO_4 (HT) ↔ liquid	melting	883 (1156)	[64]	23.35	[246]
		884 (1157)	[65]	24.1	[247]
		884 (1157)	[248]	23.7	[248]
		884 (1157)	[249]	24.3	[249]
		884 (1157)	[183]	23.7	[183]

		887 (1163) ± 5	[126]	24.58 ± 0.1	[126]
		884 (1157)	[39, 228]	23.5	[39, 228]
		886.8 (1160)	[a]		
K_2SO_4					
K_2SO_4 (LT) ↔ K_2SO_4 (HT)	solid↔solid	595 (868)	[64]		
		583 (856)	[250]	8.95	[250]
		583 (856)	[251]	8.11	[251]
		595 (868)	[185]	8.03	[185]
		586 (859)	[163]	7.23	[163]
		589 (872)	[126]	7.04 ± 2.7	[126]
		584 (867)	[39, 228]	8.45	[39, 228]
		581.2 (854.4)	[a]		
K_2SO_4 (HT) ↔ liquid	melting	1076 (1349)	[64]	36.65	[251]
		1069 (1342)	[250]	37.9	[250]
		1069 (1342)	[74, 163]	21.12	[163]
		1070 (1343)	[126]	29.3 ± 2.1	[126]
		1069 (1342)	[39, 228]	34.39	[39, 228]
		1076.2 (1349.4)	[a]		
$MgSO_4$					
$MgSO_4$ (LT) ↔ $MgSO_4$ (HT)	solid↔solid	1010 (1373)	[252]		
		997-1095 (1270-1368)	[58]		
		1010 (1283)	[39, 218, 228]	3	[92, 218, 228]
		1027.1 (1300.3)	[a]		
		1029.9 (1303.1)	[b]	14.6	[b]
$MgSO_4$ (HT) ↔ liquid	melting	1124 (1397)	[64]		
		1120 (1393)	[65]		
		1185 (1458)	[5]		
		1136 (1409)	[58]		
		1137 (1410)	[39, 92, 228]	14.6	[39, 228]
		1137 (1410)	[218]	23.6	[218]
		1135.6 (1408.8)	[a]		
		1135.7 (1408.9)	[b]	43.4	[b]
$CaSO_4$					
$CaSO_4$ (LT) ↔ $CaSO_4$ (HT)	solid↔solid	1196 (1469)	[144]		
		1195 (1468)	[58, 74, 128]		
		1199 (1472)	[253]	29.43	[253]
		1211 (1484)	[254]		
		1201 (1474)	[163]	9.12	[163]
		1200 (1473)	[218, 228]	5	[218, 228]
		1227.4 (1500.6)	[39, 126]	17.61	[39, 126]
		1220.4 (1493.6)	[a]		
		1222.6 (1495.8)	[b]	17.7	[b]
$CaSO_4$ (HT) ↔ liquid	melting	1380 (1653)	[128]		
		1450 (1723)	[144]		
		1462 (1735)	[74]		
		1528 (1801)	[125]		
		1506.8 (1779.9)	[126]		
		1460 (1733)	[228]	25.4	[228]
		1527 (1800)	[218]	36.84	[218]
		1506.8 (1779.9)	[39, 126]	16	[39, 126]
		1510.4 (1783.6)	[a]		

[a] This work, DTA in sealed Pt tube.
[b] This work, DSC in sealed Pt tube.

5.1 Mg^{2+}, Ca^{2+} // Cl^-, SO_4^{2-} system

In this section dedicated to the experimental results of the reciprocal system, the subsections are generally organised following a logical progression: starting from the investigated pure compounds, then addressing the binary systems, and subsequently the pseudo-binary ones. This order is occasionally altered to better reflect the narrative flow of the experimental campaign, aligning the

presentation of results with the actual sequence of measurements and the motivations or research inputs that prompted specific investigations and scientific findings.

5.1.1 $MgCl_2$

In the present study, the melting temperature of the pure magnesium chloride was determined by DTA measurements to validate the experimental results and compare them with existing literature data. The experiments, carried out in sealed platinum tubes, yielded a melting temperature of 719 °C (992 K), with the corresponding heating and cooling DTA curves shown in **Figure A 1**. The heat capacity C_p of $MgCl_2$ was measured using the Setaram DSC instrument. Two measurements were performed in alumina liners in platinum crucibles covered with platinum lids. No mass loss was observed over the investigated temperature range, from room temperature to 780 °C. The melting temperature obtained from DSC measurements was 717 °C (990 K). The experimentally measured heat capacity curves are presented in **Figure A 2**. Integration of the experimental C_p curves yielded an enthalpy of fusion of pure $MgCl_2$ of 44.4 kJ/mol, while the value obtained from enthalpy calibration was 41.9 kJ/mol. Taking the average of the two, the resulting enthalpy of fusion is 43.1 ± 1.3 kJ/mol, which shows good agreement with literature data [92, 237, 240, 241] (see **Table 5-1**). As the calorimetric measurements obtained in this study are in good agreement with the values previously reported in the literature and already implemented in the PCM2 thermodynamic database, they serve as an experimental validation of the existing thermodynamic properties. Consequently, no changes to the database were required.

A comparison between the experimentally determined heat capacity values and those adopted in the thermodynamic database used in this work - based on the SGPS database [228] - revealed a deviation, with the experimental measurements consistently yielding higher C_p values of about 11 J/(mol·K) (**Figure A 2**). The DSC measurements performed in this study primarily aimed to validate the enthalpy of fusion of magnesium chloride. Due to the observed disagreement and the limited possibility of performing further investigations to revise the C_p polynomials currently employed in the database, no modifications have been introduced. Nevertheless, this discrepancy is noteworthy, as it may contribute to deviations in the calculated C_p values of selected mixtures, especially when applying the Neumann-Kopp rule in systems where $MgCl_2$ is one of the end-members. This behaviour may indeed be observed in eutectic compositions involving $MgCl_2$-$CaCl_2$ and $MgCl_2$-$MgSO_4$, where the temperature-dependent enthalpy increments might appear to be affected.

5.1.2 $MgSO_4$

5.1.2.1 Transition temperatures

Magnesium sulphate is thermally unstable at high temperatures, decomposing before reaching its melting point [64, 65]. Differential thermal and thermogravimetric analyses (DTA/TG) carried out in an open alumina crucible (**Figure A 3**) showed that decomposition starts at approximately 1000 °C, producing magnesium oxide MgO and sulphur trioxide SO_3. The recorded mass loss of 66.90% confirms the complete conversion of sulphate to metal oxide, as it is in excellent agreement with the theoretical value of 66.51%. To avoid decomposition and accurately determine phase transitions, additional DTA measurements were performed in sealed platinum tubes. These experiments revealed a solid-solid transition at 1028 °C (1301 K), and a solid-liquid transition at 1136 °C (1409 K). A comparison of the present results with literature data is provided in **Table 5-1**. The measured melting point agrees with the value reported by Rowe et al. [58] and adopted in the SGPS database [228]. However, the solid-solid transition temperature determined in this work differs from the 1010 °C (1283 K) reported by Dewing and Richardson [252] and in use in SGPS database [228]. The transition temperatures were further confirmed by DSC analysis in sealed platinum tubes, which yielded consistent results: 1030 °C (1303 K) for the solid-solid and 1136 °C (1409 K) for the solid-liquid transition.

5.1.2.2 Heat capacity and enthalpy increment

Due to the decomposition of $MgSO_4$ into MgO at temperatures above 1000 °C (1273 K), DSC measurements in an open crucible are prevented over a wider temperature range up to the melting temperature. In this work, DSC experiments were nonetheless carried out in open platinum crucibles lined with alumina to determine heat capacity values of the solid phase and compare them with literature data [92, 250, 255]. Measurements were performed between 298 and 1050 K - below the onset of decomposition - using two DSC instruments (described in section 3.2.2) operated at heating rates of 4 and 10 K/min. The mass loss observed after heating to 1050 K was less than 0.5%.

To overcome the decomposition issue and reach the melting temperature, the self-referencing calibration method SRCM (section 3.2.2.1) was applied. The final curves $C_{p,corrected}$ are presented in **Figure 5-1**. The enthalpy of solid-solid transition and of fusion are summarised in **Table 5-1**. The enthalpy of the solid-solid transition was determined to be 14.6 kJ/mol based on energy calibration, as described in section 3.2.2, and 14.7 kJ/mol from the integration of C_p curves. For the fusion enthalpy, values of 41.4 kJ/mol and 45.3 kJ/mol were obtained from calibration and integration, respectively. Ideally, both methods should provide identical results; however, for the fusion enthalpy an approximately 9% discrepancy was observed, most likely due to experimental uncertainties in heat-

flow measurements performed in sealed platinum tubes. Calibration against standards is known to be more sensitive to such issues. Consequently, the final experimental enthalpies are reported as the average of both methods: 14.6 ± 0.4 kJ/mol for the solid-solid transition and 43.4 ± 2.0 kJ/mol for the fusion. Unlike the DSC curves obtained in open crucibles, an additional endothermic peak appeared at approximately 780 K during heating, but was absent on cooling. XRD analysis (**Figure A 4**) detected no impurities in either the as-purchased chemical or in the sample dried in a furnace at 150 °C. This peak is plausibly linked to some impurities, as a similar feature was observed only during the first heating cycle in open crucible tests. Further drying at 600 °C was attempted to eliminate potential moisture interference; however, subsequent DTA and DSC analyses still showed the peak. Its enthalpic contribution is considered negligible and has therefore been excluded from the thermodynamic assessment.

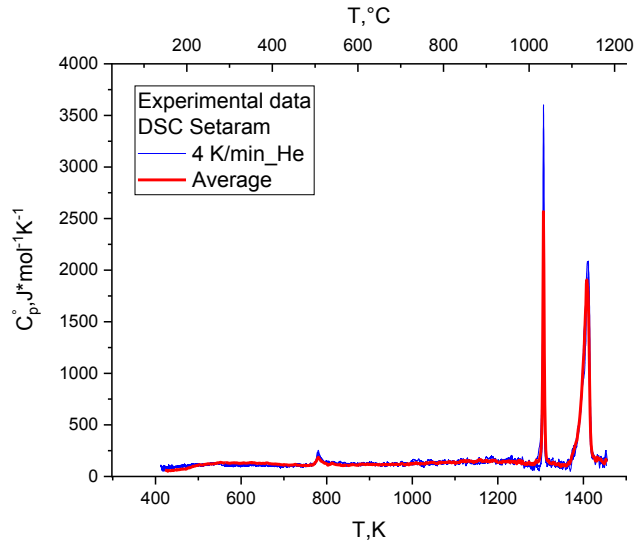


Figure 5-1 *Experimental values of molar heat capacity of $MgSO_4$ measured by DSC Setaram by applying SRCM method.*

5.1.3 $CaSO_4$

5.1.3.1 Transition temperatures

$CaSO_4$ decomposes into CaO at temperatures above 1200 °C, prior to reaching its melting point, making direct determination of its melting temperature challenging, as noted in [58]. DTA/TG measurements conducted in open alumina crucibles (**Figure A 5**) showed a weight loss of 60.85%, consistent with the complete decomposition of the sulphate to calcium oxide (theroretical value: 58.81%). As a result, the compound shifts into the $CaSO_4$-CaO binary system, preventing the observation of its actual melting temperature. Consequently, experimental melting temperatures reported in the literature [74] should be regarded as minimum estimates, equal to or lower than the true melting point [58, 125]. The earlier thermodynamic assessment by Yazhenskikh et al. [39] relied

on the DTA results obtained by Kobertz and Müller [126]. In the present work, DTA and DSC analyses were performed in sealed platinum tubes to validate the transition temperatures and overcome decomposition issues. The solid-solid transition was observed at 1220 °C (1493 K) by DTA and at 1223 °C (1496 K) by DSC, while the melting point was determined to be 1510 °C (1783 K) from DTA measurements. The experimental values slightly differ from the previous DTA analysis [126], which reported transitions at 1227 °C (1550 K) and 1507 °C (1780 K).

5.1.3.2 Heat capacity and enthalpy increment

Three DSC measurements were performed in the temperature range 298-1350 K, using alumina liners in platinum crucibles with both instruments described in section 3.2.2. The results are consistent with literature data [146]. Additional three high-temperature DSC measurements were carried out in sealed platinum tubes using platinum crucibles in DSC Setaram (**Figure 5-2**). According to the DSC Setaram settings using type B sample holder, the maximum measurable temperature was 1673 K (1400 °C), preventing access to the melting point of the compound. Consequently, only the solid-solid transition enthalpy is reported in this study. The enthalpy of the solid-solid transition was determined to be 16.7 kJ/mol from energy calibration and 18.6 kJ/mol from C_p integration, giving an average value of 17.7 ± 1.0 kJ/mol. This result is in excellent agreement with the value of 17.61 kJ/mol reported in the previous thermodynamic database [39], originally derived from DTA measurements by [126]. **Table 5-1** compares the present findings with other literature data [218, 228]. Given the consistency of the solid-solid transition enthalpy and the experimental limitations preventing a reliable determination of the enthalpy of fusion, the previously published fusion enthalpy value has been retained in this work for the assessment of sulphate-containing systems. DTA tests, which reached temperatures up to 1600 °C, qualitatively confirmed that the enthalpy of fusion is lower than that of the solid-solid transition (**Figure A 6**). However, quantitative DTA-derived enthalpy values were not considered reliable due to intrinsic limitations of the technique, including baseline drifts, heat-flow inaccuracies, and calibration challenges at high temperatures in sealed platinum tubes. These factors can introduce significant uncertainties, making DSC-derived values more trustworthy for thermodynamic assessments.

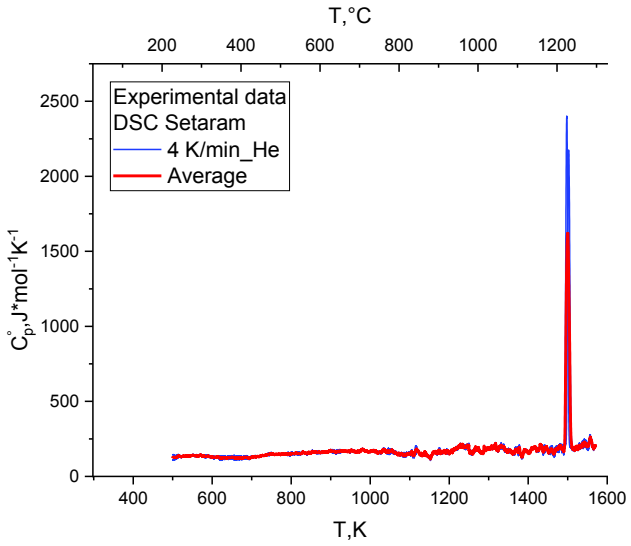


Figure 5-2 *Experimental values of molar heat capacity of $CaSO_4$ measured by DSC Setaram by applying SRCM method.*

5.1.4 $CaMg_2(SO_4)_3$

The calculated phase diagram [39, 61], following the interpretation of Rowe [58], proposed the existence of an intermediate compound with the stoichiometry $CaMg_3(SO_4)_4$. However, Smith et al. [256] demonstrated that this stoichiometry was incorrect, and density calculations indicated that the actual composition corresponds to $CaMg_2(SO_4)_3$. Weil [257] determined the crystal structure of this double sulphate, reporting hexagonal symmetry ($P6_3/m$) with lattice parameters: a = 8,3072 Å, c = 7,3057 Å, V = 436,62 Å^3. To clarify the composition of the intermediate phase - and to verify whether more than one double sulphate exists - several DTA and XRD experiments were conducted on both $CaSO_4{\cdot}3MgSO_4$ and $CaSO_4{\cdot}2MgSO_4$. Several *in situ* synthesised samples with these nominal compositions were specifically investigated. High-temperature XRD tests on $CaSO_4{\cdot}3MgSO_4$ revealed diffraction patterns nearly identical to those of $CaMg_2(SO_4)_3$ across the sample (**Figure A 7**), indicating a strong structural similarity. These results support the conclusion of Smith et al. [256] that only one intermediate compound is stable. Despite the initial 1:3 composition, the sample showed two main phases: one consistent with $CaMg_2(SO_4)_3$ and the other with $CaSO_4$. The absence of detectable $MgSO_4$, which would be expected based on the starting composition, is likely due to partial vaporisation of $MgSO_4$ or incomplete equilibration during synthesis.

The sample $CaMg_2(SO_4)_3$ has been synthesised by solid state reaction. The stoichiometric amount of anhydrous $MgSO_4$ and $CaSO_4$ were thoroughly mixed, grinded in an agate mortar and heated up to 900 °C for 72 hours in a sealed quartz ampoule. The heating was interrupted three times to regrind the mixture, after which the final product was analysed by X-ray diffraction. Three high temperature experiments were performed under different conditions: in vacuum ($P<10^{-4}$ mbar) up to

350 °C (HT1); in vacuum (P<10^{-4} mbar) up to 500 °C (HT2); in synthetic air up to 500 °C (HT3). The experimental conditions for HT1-3 are summarised in **Table A 1** and **Figure A 8**. The diffractograms collected at the highest temperatures in the HT1 and HT2 experiments are presented in **Figure 5-3**. HT3 was conducted to assess the influence of the atmospheric conditions; however, no significant differences were observed compared to HT1 and HT2.

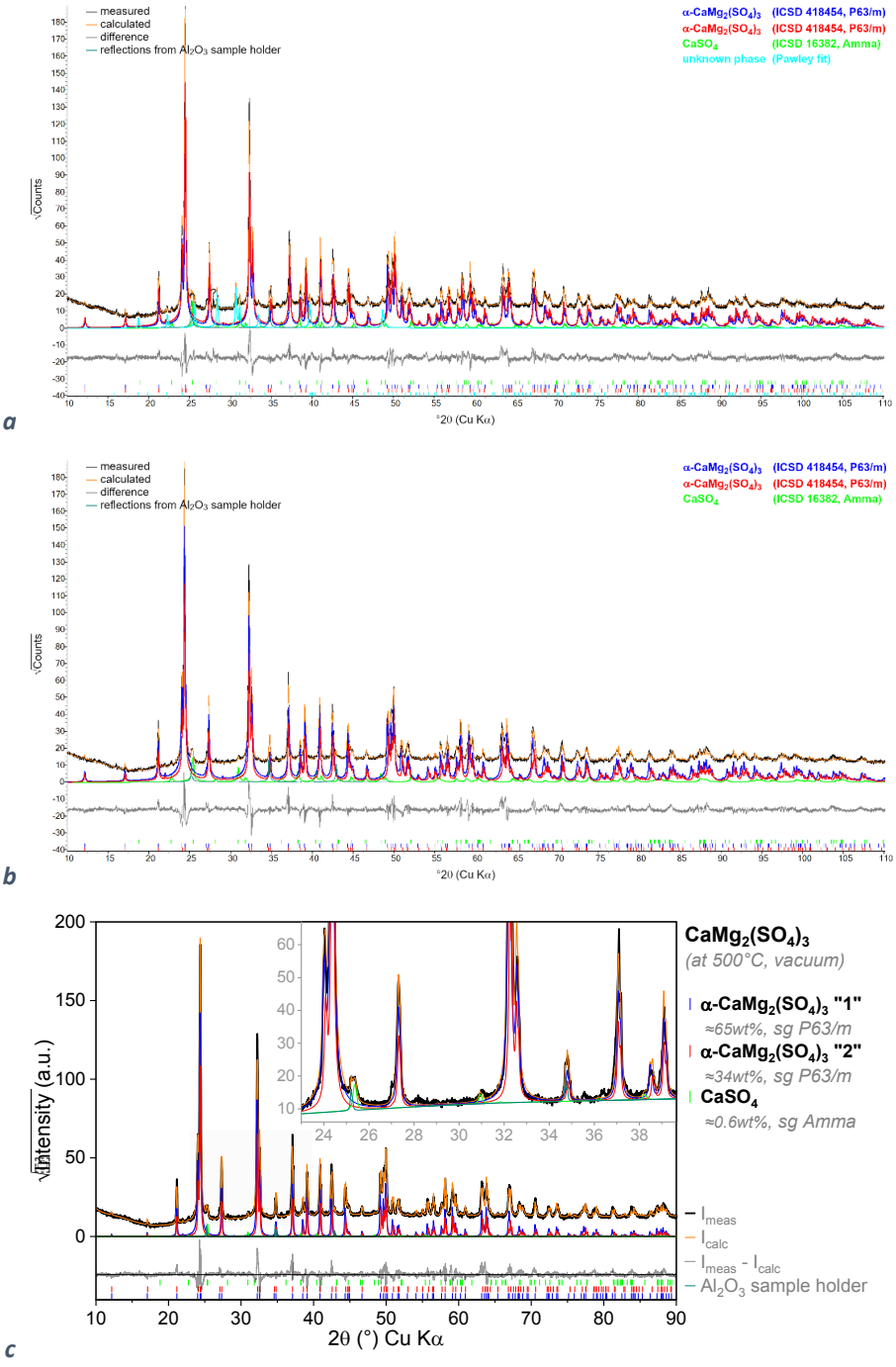


Figure 5-3 *HTXRD pattern of $CaMg_2(SO_4)_3$ under vacuum:* ***a*** *HT1 (T = 350 °C);* ***b*** *HT2 (T = 500 °C);* ***c*** *zoomed HT2 (T = 500 °C).*

The targeted compound $CaMg_2(SO_4)_3$ tended to form multiple similar phases with only minor differences in lattice parameters. Two hexagonal $CaMg_2(SO_4)_3$ polymorphs were identified. The first, referred to here as α-$CaMg_2(SO_4)_3$, crystallises in space group P63/m (176) with following lattice parameters at room temperature: a ≈7.3 Å and c ≈ 8.3 Å [257]. The second polymorph, designated β-$CaMg_2(SO_4)_3$, crystallises in space group P63 (173) with a c-lattice parameter similar to α-$CaMg_2(SO_4)_3$ but doubled a-lattice parameter [258] (**Figure 5-4**). Lattice parameters of both polymorphs are listed in **Table 5-2**.

The thermal history strongly influences both the number of $CaMg_2(SO_4)_3$ phases formed and their degree of crystallinity (**Figure 5-4**). The diffraction patterns can be relatively well described by just two $CaMg_2(SO_4)_3$ phases, even if there are still some Bragg reflections not well fitted in the Rietveld refinement. At high temperatures (500 °C) the lattice parameters of the two phases converge, making them appear as a single phase, even when analysed with a high-resolution diffractometer. In contrast, at lower temperatures, the splitting of diffraction peaks becomes evident due to lattice parameter differences (**Figure 5-4a)**. The two polymorphs can be distinguished by the additional superstructure reflections characteristic of β-$CaMg_2(SO_4)_3$, the most intense occurring at approximately 38.3° 2θ (hkl: 113). These reflections disappear above 300 °C. At higher temperatures the diffraction patterns can instead be interpreted as originating from two α-$CaMg_2(SO_4)_3$ phases (**Figure 5-3c**). Rietveld analyses suggests that only one of these α-phases, here referred to as α-$CaMg_2(SO_4)_3$ "2", transforms into β-$CaMg_2(SO_4)_3$ However, an alternative interpretation is possible: with increasing temperature, the intensities of the β superstructure reflections may approach zero as the atomic positions shift closer to special positions characteristic of the α structure. In such a case, no true phase transition would occur, and α and β structures would be indistinguishable at high temperature. The other phase (α-$CaMg_2(SO_4)_3$ "1") remains in α-$CaMg_2(SO_4)_3$ structure over the whole investigated temperature range. Phase "2" consistently shows a larger a-lattice parameter and a smaller c-lattice parameter than phase "1" (**Figure 5-4b**).

Table 5-2 *Lattice parameters of $CaMg_2(SO_4)_3$.*

T (°C)	phase	a (Å)	c (Å)	c/a	V (Å^3)
500	α-$CaMg_2(SO_4)_3$ "1"	8.390	7.403	0.882	451.3
	α-$CaMg_2(SO_4)_3$ "2"	8.390	7.381	0.880	449.9
25	α-$CaMg_2(SO_4)_3$ "1"	8.287	7.370	0.889	438.1
	β-$CaMg_2(SO_4)_3$ "2"	16.635	7.342		1758
	Recalculated for comparison	*8.317*	*7.342*	*0.883*	*439.6*

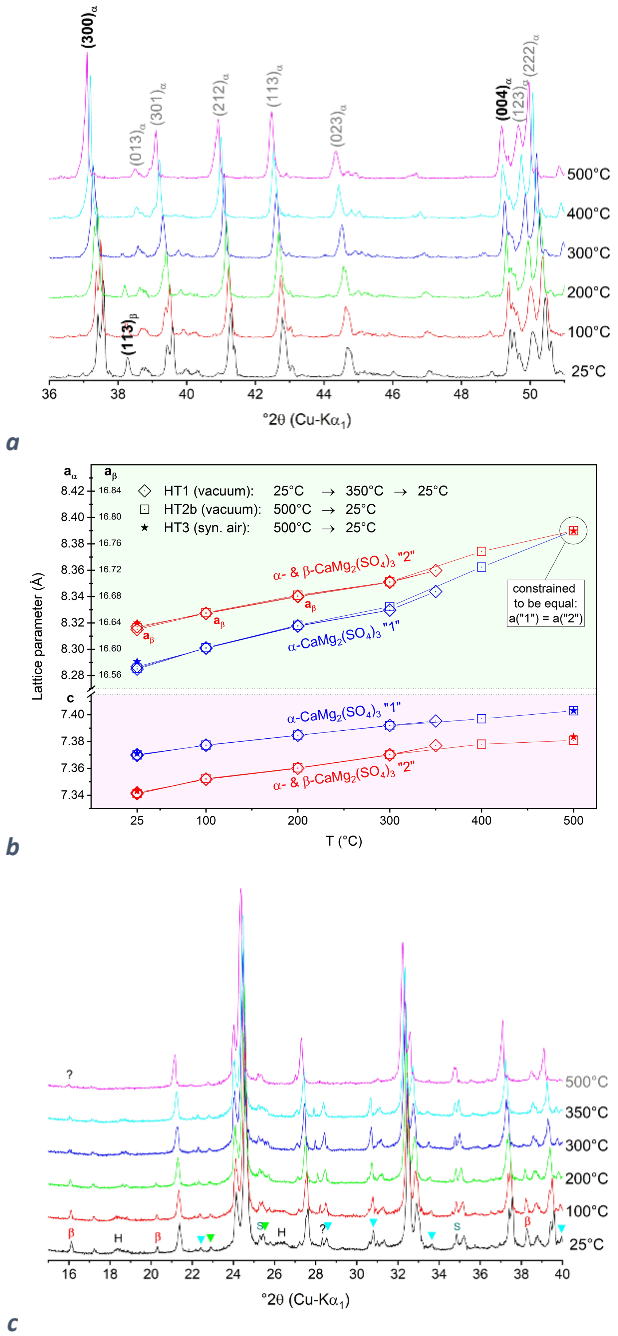


Figure 5-4 a *Visualisation of peak splitting due to lattice parameter differences of $CaMg_2(SO_4)_3$ phases;* ***b*** *Temperature dependence of lattice parameters* a *(top) and* c *(bottom);* ***c*** *Characteristic reflections: ß = ß-$CaMg_2(SO_4)_3$, ▼ = $CaSO_4$, ▼ = "unknown phase" (orthorhombic?), "H" = presumed hydrate phase, "?" = two additional not-identified phases, "S" = alumina sample holder (Intensity in square root scaling).*

The sample contains approximately 1 wt% of $CaSO_4$. No changes in concentration were observed during the investigation. An unknown phase was detected, likely due to the sample's exposure to ambient air during mounting in the oven chamber (HT1) (**Figure A 9**). The compound is known to be moisture-sensitive, and although care was taken, the sample remained in contact with air for approximately one minute. This brief exposure appears to have led to the formation of a

hydrate phase, as indicated by two broad peaks observed between 18°-19° and 26°-27° 2θ. These features, marked with 'H' in **Figure A 10**, could not be matched to any known phase in the ICDD database. Upon heating the sample to 200 °C, both peaks disappeared, supporting the hypothesis of a transient hydrate formation, which therefore did not interfere with the HTXRD analysis. Additionally, reflections attributable to an unknown phase were detected and are marked in cyan in **Figure 5-4c** and **Figure 5-5**. Nine characteristic peaks were identified at 18.4°, 22.4°, 25.8°, 28.5°, 30.8°, 31.3°, 33.6°, 39.9°, and 48.9° 2θ at room temperature. An attempt was made to index these reflections in order to derive plausible lattice parameters and a Bravais lattice. The preliminary indexing suggests an orthorhombic base-centred symmetry with lattice parameters at room temperature of a = 9.41 Å, b = 7.37 Å, and c = 6.91 Å. While this solution accounts for the observed reflections reasonably well across the investigated temperature range, it is acknowledged that the reliability of the indexing remains questionable due to the limited number of reflections and significant peak overlap with the primary phases. Nonetheless, this tentative model was employed to represent the unknown phase in the Rietveld plots using a Pawley fit approach, wherein the intensities of the nine identified reflections were freely refined against the measured data, with their positions constrained by the proposed lattice parameters. All other reflections associated with this hypothetical phase were manually set to zero intensity. The unknown phase was observed to disappear upon heating above 425 °C and reappear upon cooling (**Figure 5-5**). Due to the lack of structural information, quantitative analysis is not feasible; however, its content is estimated to be below 5 wt%.

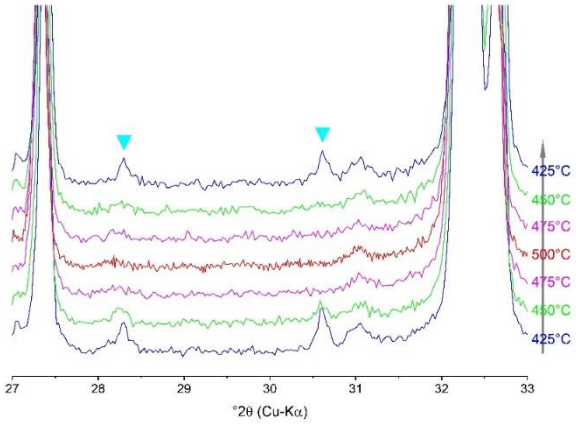


Figure 5-5 *HTXRD $CaMg_2(SO_4)_3$; appearance and disappearance of the unknown phase according to temperature.*

5.1.4.1 Transition temperature

DTA measurements in open crucibles are hindered by the decomposition of sulphate into oxides, as described by Equation 20. DTA/TG analyses in an open platinum tube demonstrated that $CaMg_2(SO_4)_3$ remains stable up to 900 °C. Beyond this temperature, the system exhibits a mass loss of

62.44%, consistent with the complete decomposition of the 2:1 sulphate mixture into metal oxides and sulphur dioxide, as predicted by Equation 20. Based on the stoichiometry of the decomposition reaction, the residual mass fraction of metal oxides is calculated to be 36.27%.

$$CaMg_2(SO_4)_3(s,l) = CaO(s,l) + 2MgO(s,l) + 3SO_2(g) + 3/2\ O_2(g) \qquad \textit{Equation 20}$$

The decomposition of $CaMg_2(SO_4)_3$ proceeds through two distinct stages, as described in Equation 21 and illustrated in **Figure 5-6**. The first stage, between 900 °C and 1100 °C, involves partial decomposition of $CaMg_2(SO_4)_3$ with the formation of magnesium oxide. This step is marked by an experimental mass loss of 42.17%, closely matching the theoretical prediction of 42.49%. The second stage, above 1100 °C, corresponds to the further decomposition of the remaining compound $CaSO_4$, yielding calcium oxide and an additional mass loss of 20.27%, in good agreement with the theoretical value of 21.22%. The overall mass loss, 62.44%, aligns well with the calculated total decomposition value of 63.71%. These results highlight the stepwise thermal decomposition behaviour of $CaMg_2(SO_4)_3$ and provide crucial insights for understanding its stability under high-temperature conditions.

$$\begin{aligned} CaMg_2(SO_4)_3(s,l) &\xrightarrow{1^{st}step} 2MgO(s,l) + CaSO_4(s,l) + 2SO_2(g) + O_2(g) \\ &\xrightarrow{2^{nd}step} 2MgO(s,l) + CaO(s,l) + 3SO_2(g) + 3/2\ O_2(g) \end{aligned} \qquad \textit{Equation 21}$$

In order to overcome the problem of decomposition and to measure the melting temperature, DTA investigations were successfully performed in sealed platinum tubes in a temperature range of 25-1300 °C. These analyses confirmed that the sample undergoes congruent melting at 1213 °C (1486 K), with no additional phase transitions detected. Three DTA measurements were conducted on samples prepared via solid-state reaction of the 2:1 mixture. Additional tests were carried out by preparing the mixture directly inside platinum tubes for DTA analysis, allowing the compound to form during the first heating-cooling cycle. In these cases, extra peaks appeared in the thermograms, likely due to incomplete equilibration or slight compositional deviations from the stoichiometric intermediate phase, causing a shift in its position within the phase diagram. The melting temperature was independently validated by DSC measurements in sealed platinum tubes using DSC Setaram. Three DSC experiments yielded a melting temperature of 1210 °C (1483 K), in excellent agreement with the DTA results.

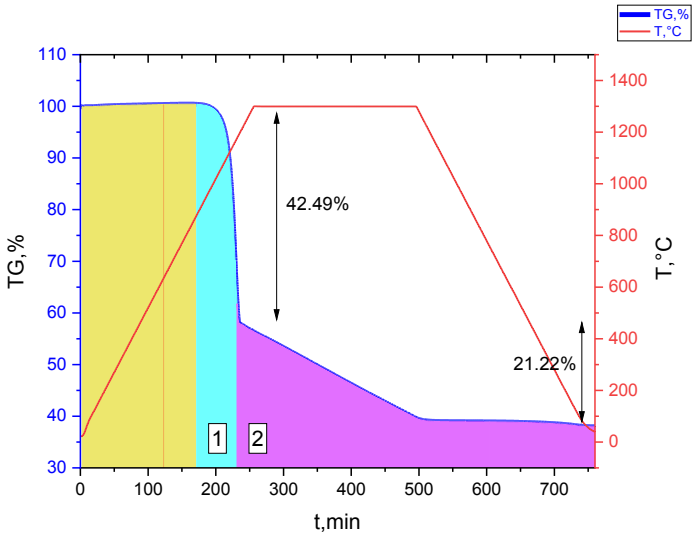
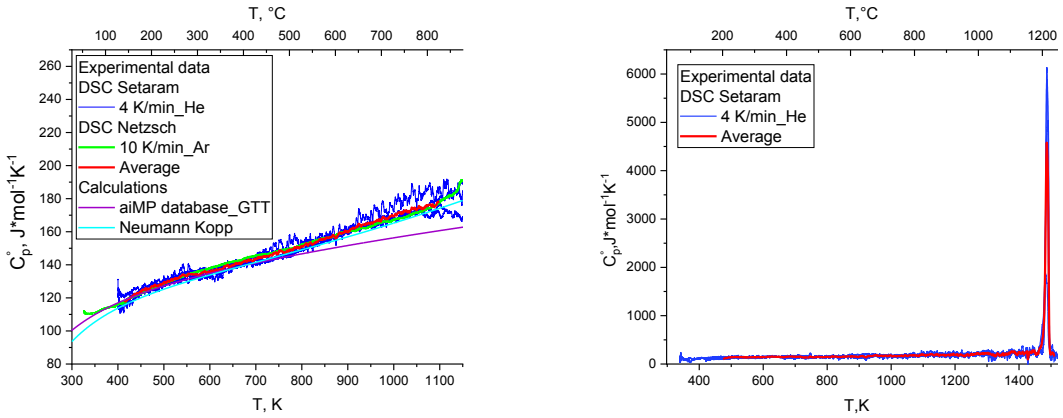


Figure 5-6 *TG curve of $CaMg_2(SO_4)_3$ in open alumina crucible.*

5.1.4.2 Heat capacity and enthalpy increment

The thermodynamic properties of the intermediate compound $CaMg_2(SO_4)_3$ were investigated for the first time in this study. Six DSC measurements were performed: three using a Netzsch DSC and three with a Setaram DSC, all conducted up to 1173 K (900 °C) with a final mass loss below 1 wt%. The experiments were carried out in platinum pan with alumina liner covered by a platinum lid. **Figure 5-7a** compares the C_p curves obtained by DSC with those predicted by Neumann-Kopp rule and ab-initio calculations (aiMP) [259]. The curves represent C_p of $CaMg_2(SO_4)_3$, considering its composition as $MgSO_4$(66.7 mol%)-$CaSO_4$(33.3 mol%), i.e., $Ca_{0.33}Mg_{0.67}SO_4$.

To extend the investigated temperature range and determine the enthalpy of fusion experimentally, additional measurements were carried out using the Setaram DSC in sealed platinum tubes. The C_p curves were corrected according to the SRCM methodology described in section 3.2.2.1, and are presented in **Figure 5-7b**. Three measurements were conducted for this purpose, which yielded an enthalpy of fusion value of 47.2 kJ/mol from calibration method and 49.7 kJ/mol from integration method, resulting in an average value of 48.5 ± 1.3 kJ/mol, which is here adopted. The melting and crystallisation enthalpies showed excellent reproducibility, with values of 47.4 and 47.0 kJ/mol, respectively, meeting one of the key requirements for phase change materials [14-16]. Based on its stoichiometry, the experimental enthalpy of fusion of $CaMg_2(SO_4)_3$ corresponds to 145.5 kJ/mol.



a *b*

Figure 5-7 *Experimental values of molar heat capacity of $CaMg_2(SO_4)_3$ as $MgSO_4$(66.7 mol%)-$CaSO_4$(33.3 mol%): **a** C_p of solid phase measured by two DSC devices and comparison with calculated values from databases [39, 259]; **b** C_p of solid and liquid phases measured by DSC Setaram by applying SRCM method.*

5.1.5 $MgSO_4$-$CaSO_4$

Experimental investigation of $MgSO_4$-$CaSO_4$ system in open crucibles was hampered by the decomposition of both sulphates above 1000 °C [64, 65, 74]. DTA/TG tests in open alumina crucibles of $MgSO_4$ and $CaSO_4$ showed a mass loss of 65.78 % and 58.80 %, respectively. Alumina DTA crucibles with alumina lids were tested not only with the two end-members but also with their mixtures. The observed mass loss was not negligible and would have effectively transformed the original binary sulphate system into a quaternary system involving sulphates and oxides of the constituent metals. Hence, there is a need to use closed containers to analyse such sulphate system. Several attempts have been carried out in order to find the most suitable crucible for such a system, as illustrated in **Figure 5-8**.

Sealed quartz DTA crucibles were tested, as they were considered suitable for studying systems prone to decomposition [37, 260]. They reacted with the specimen and did not allow to reach high temperatures without causing breakage. Sealed platinum tubes with various wall thickness (3 and 6 mm) and shapes (tubes with welded flat-section ends and cylinder-shaped 6 mm thick tubes) were prepared. Platinum tubes were prepared by welding the lower section, shaped in a 'V' cross-section, followed by loading the sample and sealing the upper part in a manner analogous to the lower section. Thick-walled cylindrical tubes were fabricated by welding three distinct components: a 2-3 mm thick disk-shaped base, compacted using a press to ensure structural integrity; a hollow cylindrical tube; and a conical lid, formed *in situ* by pressing and polishing to achieve the desired shape. The conical lid enabled mechanical sealing of the tube after sample insertion, achieved through hammering, followed by flame welding. These methods were particularly effective for creating closed systems; however,

their success was not always guaranteed. In the system under investigation, multiple tests revealed leakage at the tube walls or the formation of perforations, compromising the analysis.

Various closed alumina crucibles were tested for their suitability in studying the system, but all exhibited mass loss, making them unsuitable. The first approach involved a hybrid design, where an alumina crucible was encapsulated within a sealed glass ampoule. This configuration aimed to achieve proper sealing while preventing direct contact between the salts and the glass. The crucibles were specifically designed and fabricated for this purpose, but the temperature limitations of the glass ampoule led to the consideration of fully alumina-based alternatives. To address this, an alumina crucible with a screw-on cap was designed and produced in the workshop to maintain a closed system at higher temperatures. However, since proper sealing tools could not be used without risking damage to the ceramic crucible, the closure had to be done manually. This method did not ensure a completely airtight seal, leading to mass loss during the experiments.

Another approach involved capped alumina crucibles sealed with coarse-grained castable materials. Ceramic-based glues were used to promote more effective sealing in both capped alumina crucibles and those with screw-on caps. Two coarse grain castable materials, with good moisture and alkali resistance, have been tested in the laboratory: alumina based Ceramacast 510 (T_{max}= 1760 °C; binder TiO_2-CaO) and zirconium silicate based Ceramabond 586 (T_{max}= 1535 °C; binder MgO-P_2O_5). Both required a drying time of about three hours at 120 °C, directly in DTA/TG with a mass loss check. Unfortunately, due to the still porous nature of ceramic adhesives (<7,0% and <2,0%, respectively), a mass loss was recorded which prevented the sulphate mixtures from being studied. An attempt was made to enhance the effectiveness by testing a double coating approach - applying the adhesive and allowing it to dry twice before analysing the mixture. Regrettably, this method also proved unsuccessful. An individually sealed double-walled platinum tube, henceforth referred to as a double Pt tube, has been successfully tested for investigating sulphates mixtures.

Two different platinum tubes have been used: the inner one with diameter of 5 mm and thickness of 0.3 mm, the outer with diameter of 6 mm and thickness of 0.2 mm. The stoichiometric ratio mixture is loaded into the inner tube in glove box and the tube is sealed using an oxygen-hydrogen flame. Subsequently the inner tube is encapsulated into the outer shell, also performed in glovebox, and sealed once more. It has been proven that the double Pt tube does not experience mass loss after three-cycle DTA experiments, making it suitable for studying the system of interest. The success of such custom crucibles is attributed to their double-layer design, where the outer layer protects and ensures sealing even in the event of leakage from the inner layer. As a drawback, the resulting heavier crucible and the bigger number of layers between the thermocouple and the sample considerably decrease the experimental sensitivity. The peaks are broad and flat, and consequently

difficult to detect. To circumvent this issue, measurements were performed using a DSC instrument provided by Setaram, which is characterised by higher sensitivity due to the thermocouples surrounding the cylindrical sample holder. However, not every mixture could be tested in the DSC device due to the limited size of the sample holder and the potential expansion of the double Pt tube under high vapor pressure. This expansion could either damage the instrument or cause the tube to become stuck. Therefore, before performing DSC tests on double Pt tubes, they needed to be tested in a DTA or high temperature furnace. Only tubes that did not experience expansion during these preliminary tests could be safely tested in the DSC. Unfortunately, many mixtures exhibited expansion, limiting the number of samples that could be analysed using DSC.

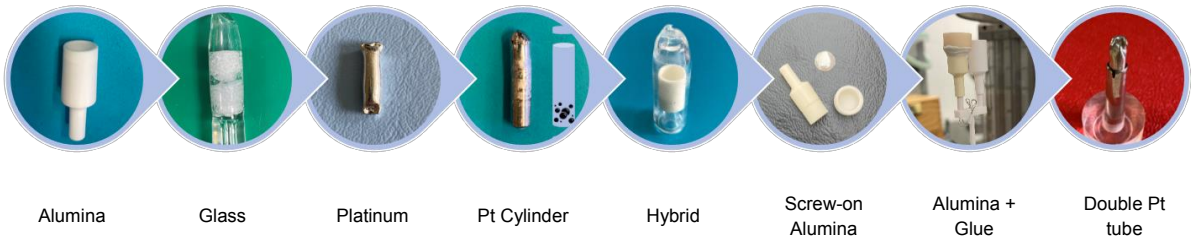


Figure 5-8 *DTA crucible selection for investigation of $MgSO_4$-$CaSO_4$ binary system.*

The most effective solution was found to be sealed single-walled platinum tubes (with diameter of 5 mm, thickness of 0.3 mm and length of 2-2.5 cm) containing the mixtures in their stoichiometric ratios. Initial attempts to synthesise the target compositions by directly heating the two end-members in DTA crucibles were unsuccessful, resulting in mass losses and incomplete reactions. More reliable DTA investigations were achieved using mixtures that had been pre-prepared by thoroughly mixing the end-members, annealing them at 1000-1100 °C for 48-72 hours in sealed quartz ampoules, and subsequently re-mixing before testing. Mixtures with a high content of $MgSO_4$ were particularly prone to failure due to leakage through the crucible walls. Given the presence of the intermediate compound with congruent melting, a revised experimental strategy was adopted. The $MgSO_4$-$CaSO_4$ binary system was treated as two sub-systems: $MgSO_4$-$CaMg_2(SO_4)_3$ and $CaMg_2(SO_4)_3$-$CaSO_4$. Study mixtures were prepared by mixing $CaMg_2(SO_4)_3$ with either $MgSO_4$ or $CaSO_4$. This approach was motivated by both the need to reliably form the compositions of interest and by experimental evidence showing that direct synthesis from pure sulphates frequently failed. Indeed, long-term annealing experiments demonstrated that samples prepared from pure sulphates were far more susceptible to crucible degradation at temperatures above 1300 °C, whereas mixtures containing the intermediate compound were more stable. The underlying reasons are not fully understood, but it is likely that

equilibration from pure sulphates requires longer times and harsher conditions, making sample preparation more problematic than when using double-sulphate precursors.

The experimental DTA data points for $MgSO_4$-$CaSO_4$ mixtures are summarised in **Table 5-3** and displayed in **Figure 5-9**. The experimental data are compared with the phase diagram calculated using the previous assessment [39]. Unlike Rowe et al.'s data [58], the present study did not confirm the eutectic composition near 50 mol% $CaSO_4$; instead, additional thermal effects were observed. Mixtures in this composition range yielded experimental results that deviated significantly from previous reports, suggesting alternative interpretations of the phase equilibria and the possible presence of previously unidentified phases. The DTA results of mixtures with compositions (47.63, 50.03, 53.85, 61.33, 72.10, 72.82 mol% $CaSO_4$) prepared by combining end-members revealed distinct thermal effects. An initial thermal event at approximately 1020 °C was initially attributed to the solid–solid transition of residual $MgSO_4$ within partially equilibrated mixtures. Repeated DTA measurements, including specific heat treatments to promote equilibration, produced consistent results, indicating that the observed thermal effect was reproducible.

To verify that this thermal event was intrinsic to the tested compositions and not caused by residual $MgSO_4$, additional DTA tests were performed on mixtures prepared using $CaMg_2(SO_4)_3$ and $CaSO_4$ as starting materials, thereby avoiding the presence of $MgSO_4$. These mixtures (42.21, 60.48, 66.10 mol% $CaSO_4$ in the system $MgSO_4$-$CaSO_4$, alternatively 36.54, 67.06, 74.36 mol% $CaSO_4$ in the system $CaMg_2(SO_4)_3$-$CaSO_4$) confirmed the presence of a consistent thermal event at around 1020 °C. This strongly suggests that the observed effect is related to new phase formation, rather than to the solid-solid transition of $MgSO_4$.

Table 5-3 *Experimental values of phase transition temperatures (°C) in the $MgSO_4$-$CaSO_4$ system in sealed platinum tubes.*

$CaSO_4$ (mol)	$CaSO_4$ (wt%)	1st	2nd	3rd	Method
0	0	1027	1136		DTA
0.0413	4.65	1010	1141	1161	DTA
0.0556	6.24	1140	1171		DTA
0.0989	11.04	1122	1189		DTA
0.1530	16.96	1018	1128	1178	DTA [a]
0.2003	22.08	1199			DTA
0.2070	22.79	1098	1216		DTA
0.2222	24.42	1174	1195		DTA
0.2498	27.36	1026	1202		DTA
0.2916	31.77	1105	1176	1208	DTA [a]
0.3333	36.12	1213			DTA
0.4000	42.99	1210	1249		DTA
0.4000	42.99	1215	1247		DSC
0.4221	45.24	1013	1216	1273	DTA [b]
0.4221	45.24	1014	1246		DSC [b]
0.4763	50.71	1023	1210		DTA
0.4802	51.10	1209	1282		DTA
0.4802	51.10	1212	1267		DSC
0.5000	53.07	1034	1224	1309	DTA
0.5199	55.05	1216	1251		DTA

0.5385	56.89	1022	1213	1302	DTA
0.6048	63.38	1037	1214	1241	DTA [b]
0.6048	63.38	1025	1216	1232	DSC [b]
0.6133	64.21	1018	1212	1268	DSC
0.6610	68.80	1033	1195	1230	DTA [b]
0.7210	74.51	1040	1215		DTA
0.7282	75.19	1030	1234		DTA
0.7820	80.23	1222	1232		DTA
0.8589	87.32	1219	1230	1367	DTA
0.9279	93.57	1218	1226	1419	DTA
1	100	1220	1510		DTA

[a] prepared as mixture $MgSO_4$-$CaMg_2(SO_4)_3$
[b] prepared as mixture $CaMg_2(SO_4)_3$-$CaSO_4$

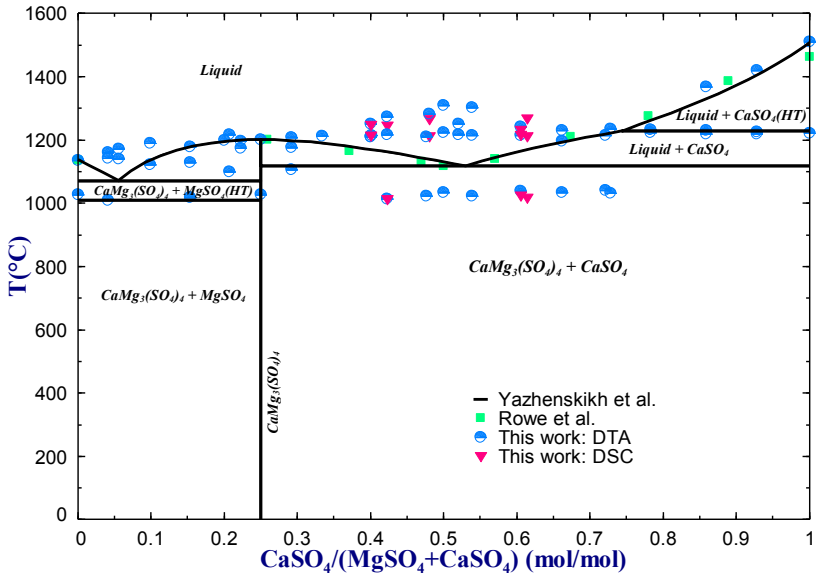


Figure 5-9 *Phase diagram of $MgSO_4$-$CaSO_4$, comparison of experimental data of this work with Rowe et al. [58] and Yazhenskikh et al. [39].*

To gain a clearer understanding of the phase transitions in mixtures containing 40-75 mol% $CaSO_4$, and to resolve discrepancies with the data reported by Rowe et al. [58], samples in sealed platinum tubes were tested using a Setaram DSC. This approach was employed to validate the transition temperatures obtained from DTA measurements and to provide more detailed information on their enthalpic contributions. The DSC analysis of samples (40.00, 42.21, 47.63, 48.02, 60.48, 61.33, and 72.82 mol% $CaSO_4$) revealed a prominent thermal peak between 1010 °C and 1030 °C in several cases, with an enthalpic contribution significantly higher than that of the second peak, which appeared at temperatures above 1200 °C (**Figure 5-10**). These results indicate that the mixtures were properly formed and had reached equilibrium. If equilibration had not been achieved, a low-temperature peak corresponding to the solid-solid transition of residual $MgSO_4$, would be expected, which would be much weaker due to the small amount of unreacted sulphate and would diminish further as the composition shifted towards the $CaSO_4$-rich side.

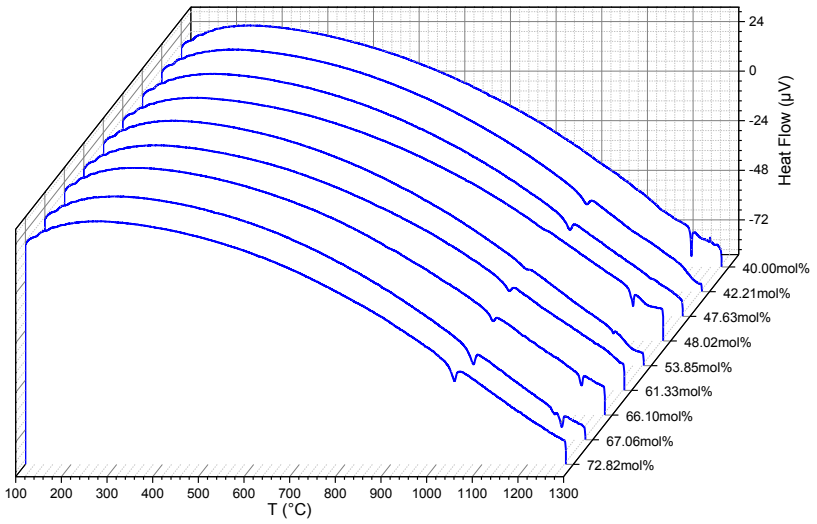


Figure 5-10 *Heat flow vs. temperature curves of mixtures ($CaSO_4$ mol%) in the $MgSO_4$-$CaSO_4$ binary system tested in DSC Setaram in sealed platinum tubes.*

5.1.6 $CaMg(SO_4)_2$

The phase equilibria (**Figure 5-9**) reveal a more complex behaviour than suggested by the initially proposed phase diagram, indicating the possible formation of a previously unreported compound with a 1:1 $MgSO_4$:$CaSO_4$ stoichiometry. This new phase may explain the distinct thermal effects observed in the studied mixtures.

Support for this hypothesis was provided by Scanning Electron Microscopy (SEM) analysis of sulphate mixtures. Several sulphate mixtures were initially planned for SEM investigation, as this technique can reveal whether the mixtures are homogeneous or composed of distinct phases of the pure compounds, thereby providing valuable insights into the phase equilibria. As discussed elsewhere [261], SEM is particularly useful for identifying eutectic compositions and for qualitatively assessing how far a given composition deviates from the eutectic mixture. However, preparing the mixtures as pellets suitable for SEM analysis proved challenging. Among the tested compositions, the specimen with 70 mol% $MgSO_4$ and 30 mol% $CaSO_4$ is presented here as a representative case, as it provided the clearest microstructural evidence supporting the hypothesis of the existence of the 1:1 phase. This choice is also related to the greater difficulty in pelletising sulphate mixtures with higher $CaSO_4$ content. The specimen with a composition of $MgSO_4$(70 mol%)-$CaSO_4$(30 mol%) was synthesised via a solid-state reaction. The synthesis involved a three-stage heat treatment (stage 1: 1050 °C for 72 hours; stage 2: 950 °C for 45 hours; stage 3: 1050 °C for 48 hours), with intermittent grinding in an agate mortar between stages. The resulting powder was then pelletised (100 mg, 5 mm diameter, 2 mm height) using a hydraulic press at 15 kN and subsequently annealed in air at 600 °C for 24 hours.

SEM analysis confirmed the presence of phases with $MgSO_4$:$CaSO_4$ ratios of 1:1, 2:1, and 0:1, as shown in **Figure 5-11** and summarised in **Table 5-4**, despite the initial overall composition. All identified phases were enriched in $CaSO_4$, suggesting a more complex reaction mechanism or incomplete equilibration of the starting mixture - issues that fall beyond the scope of this study. Nonetheless, these findings strongly support the existence of an intermediate 1:1 compound, initially suggested by the DTA results. Moreover, they corroborate the presence of the 2:1 compound, discussed in detail in section 5.1.4, and further illustrated in **Figure A 11** and **Table A 2**.

A specimen with a $MgSO_4$:$CaSO_4$ ratio of 1:1 was synthesised by heating the mixture in a sealed quartz ampoule at 900 °C for 15 days, followed by rapid quenching to room temperature. XRD analysis identified $CaMg_2(SO_4)_3$ as the primary phase, with $CaSO_4$ as the secondary phase in an approximate 3:1 ratio. In addition, an unknown orthorhombic phase was detected, representing 5-10 wt%, together with other minor unidentified secondary phases, as presented in **Figure 5-12a**. Although present in small quantities relative to the initial stoichiometry, the detection of this orthorhombic phase supports the hypothesis of a 1:1 compound. Its limited abundance is likely due to kinetic constraints, such as incomplete reaction or slow nucleation and growth rates, which may have hindered full phase formation under the applied experimental conditions. Furthermore, the thermodynamic stability of this phase might be restricted to a narrow temperature or compositional range, favouring the preferential formation of competing phases.

To investigate further, a separate sample with the same 1:1 composition, $MgSO_4$(49.91 mol%)-$CaSO_4$(50.09 mol%), underwent heat treatment at 900 °C for 15 days, followed by controlled cooling at a rate of 5 K/min. XRD analysis of this sample identified 53 wt% $CaSO_4$, 43 wt% $MgSO_4$ and 4 wt% $CaMg_2(SO_4)_3$, with no evidence of the orthorhombic phase, as illustrated in **Figure 5-12b**. Two pellets were produced and sintered at 600 °C for 60 hours under a nitrogen atmosphere. Pelletisation proved more challenging due to the friable nature of the mixture and its tendency to form thin, separated disc-like pellets. SEM-EDX results confirmed the presence of $CaSO_4$ and the 2:1 compound, but no evidence of the 1:1 phase was observed, contrary to expectations. A probable explanation for this outcome is that the 1:1 compound is stable within a narrow temperature range, and the preparation conditions did not favour its formation. The results of elemental analysis for the examined spots are presented in the following figures and tables (**Figure A 12** and **Table A 3**).

The variation in phase composition observed among the 1:1 samples subjected to different heat treatments, together with the SEM results (**Figure 5-11**) and DTA data (**Figure 5-9**), indicates that the $MgSO_4{\cdot}CaSO_4$ compound is likely a transient phase. This intermediate phase appears to be metastable, decomposing at relatively low temperatures into fine-grained exsolution structures of $MgSO_4$ and $CaSO_4$, as evidenced by distinct microstructural features in the SEM images.

Additional evidence for the existence of the 1:1 phase is provided by DTA analysis of an in-situ synthesised 1:1 mixture, which displayed three distinct thermal events. The final thermal effect corresponds to the congruent melting of the intermediate compound at approximately 1309 °C (1582 K). This finding supports the hypothesis that the $CaMg(SO_4)_2$ phase is thermally stable only within a defined temperature range, existing as a distinct phase between roughly 1000 °C and its melting point. Outside this range, it either decomposes or transforms into other phases, confirming its limited thermal stability. In the phase diagram, the compound $CaMg(SO_4)_2$ is suggested to be stable from the low-temperature limit up to the congruent melting point. This transient behaviour highlights its intermediate nature and provides new insights into the phase equilibria of the $MgSO_4$-$CaSO_4$ system.

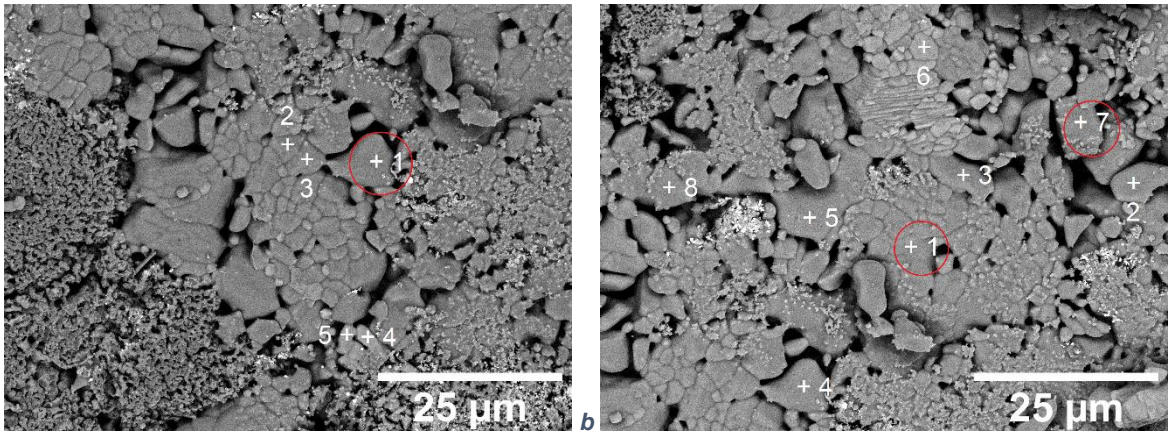


Figure 5-11 *SEM-Images (Back Scatter Electrons) showing the grains and phases of $MgSO_4$(70 mol%)-$CaSO_4$(30 mol%) across the sample surface, highlighting areas analysed by Energy Dispersive X-Ray Spectroscopy (EDX).*

Table 5-4 *Molar percentages of elements detected in the analysed regions of the sample by SEM-EDX.*

	Spectrum Label	O	Mg	S	Ca	Total (mol%)	$MgSO_4$:$CaSO_4$
Figure 5-11a	Spectrum 1	67.7	8.3	17.7	6.3	100.0	1:1
	Spectrum 2	66.8	11.0	16.8	5.5	100.0	2:1
	Spectrum 3	66.6	11.2	16.6	5.6	100.0	2:1
	Spectrum 4	66.6	0.6	16.6	16.2	100.0	0:1
	Spectrum 5	66.9	0.6	15.6	15.6	100.0	0:1
Figure 5-11b	Spectrum 1	68.3	6.3	18.3	7.1	100.0	1:1
	Spectrum 2	67.0	10.4	17.0	5.6	100.0	2:1
	Spectrum 3	66.7	10.8	16.7	5.8	100.0	2:1
	Spectrum 4	67.0	10.3	17.0	5.8	100.0	2:1
	Spectrum 5	66.8	10.6	16.8	5.8	100.0	2:1
	Spectrum 6	66.7	0.4	16.7	16.3	100.0	0:1
	Spectrum 7	67.8	7.4	17.8	7.0	100.0	1:1
	Spectrum 8	67.4	9.4	17.4	5.9	100.0	2:1

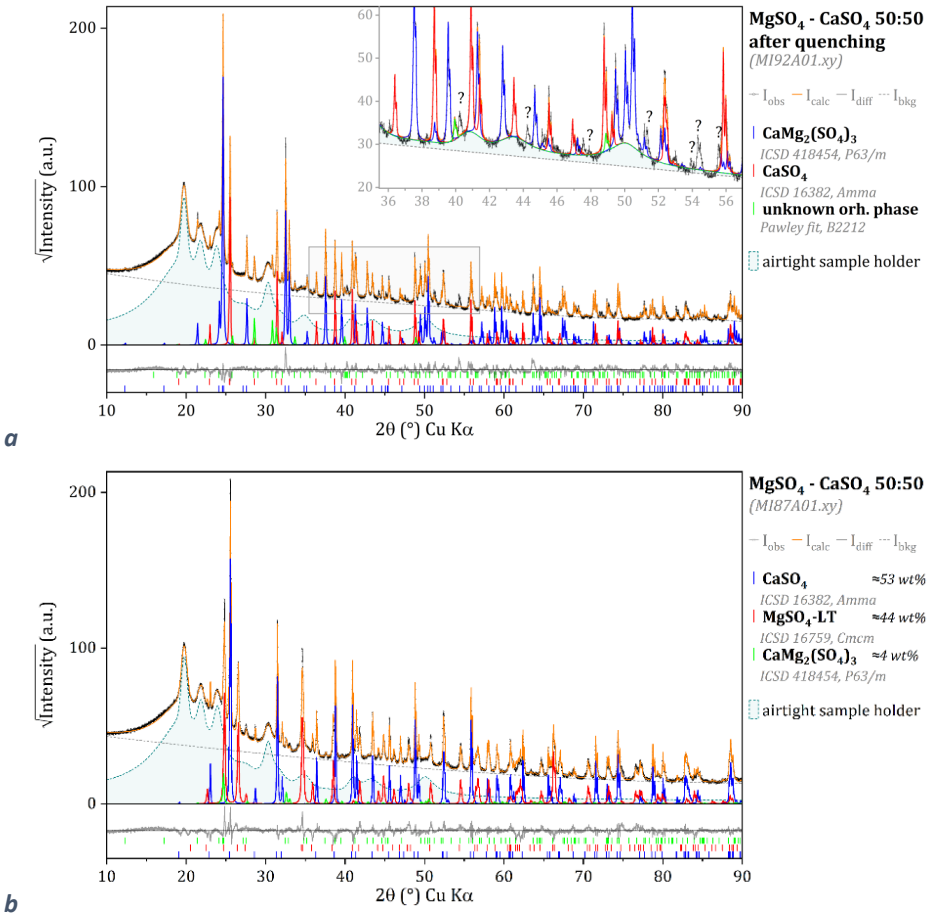


Figure 5-12 *XRD of $MgSO_4$-$CaSO_4$ with a 1:1 stochiometric ratio:* ***a*** *sample subjected to heat treatment at 900 °C, followed by rapid cooling to room temperature;* ***b*** *sample subjected to heat treatment at 900 °C, followed by controlled cooling at a rate of 5 K/min.*

5.1.7 $MgCl_2$-$CaCl_2$

In light of previous experimental studies [50, 51, 53] and the consistency of their data, selected mixtures were investigated in order to validate their reported transition temperatures. Two mixtures in the eutectic region (46.94 and 47.42 mol% $CaCl_2$) were analysed with DTA in alumina crucibles, and seven compositions with medium-to-high $CaCl_2$ content (47.19, 72.75, 79.93, 82.89, 88.48, 89.51, and 93.11 mol% $CaCl_2$) were examined in sealed platinum tubes. The DTA tests on the mixtures within the eutectic region both exhibited a single thermal event during both heating and cooling cycles, leading to the conclusion that the eutectic composition lies within this compositional range. The DTA analysis of mixtures with high $CaCl_2$ content partially confirmed the solubility of $CaCl_2$ in $MgCl_2$, showing reasonable agreement with the data reported by Grjotheim et al. [53]. DTA curves are displayed in **Figure 5-13**, and the corresponding temperature transitions are listed in **Table 5-5**. The experimental points derived from these transitions are later plotted in the phase diagram and compared with the calculated one, as discussed in the thermodynamic modelling results section (**Figure 6-5**).

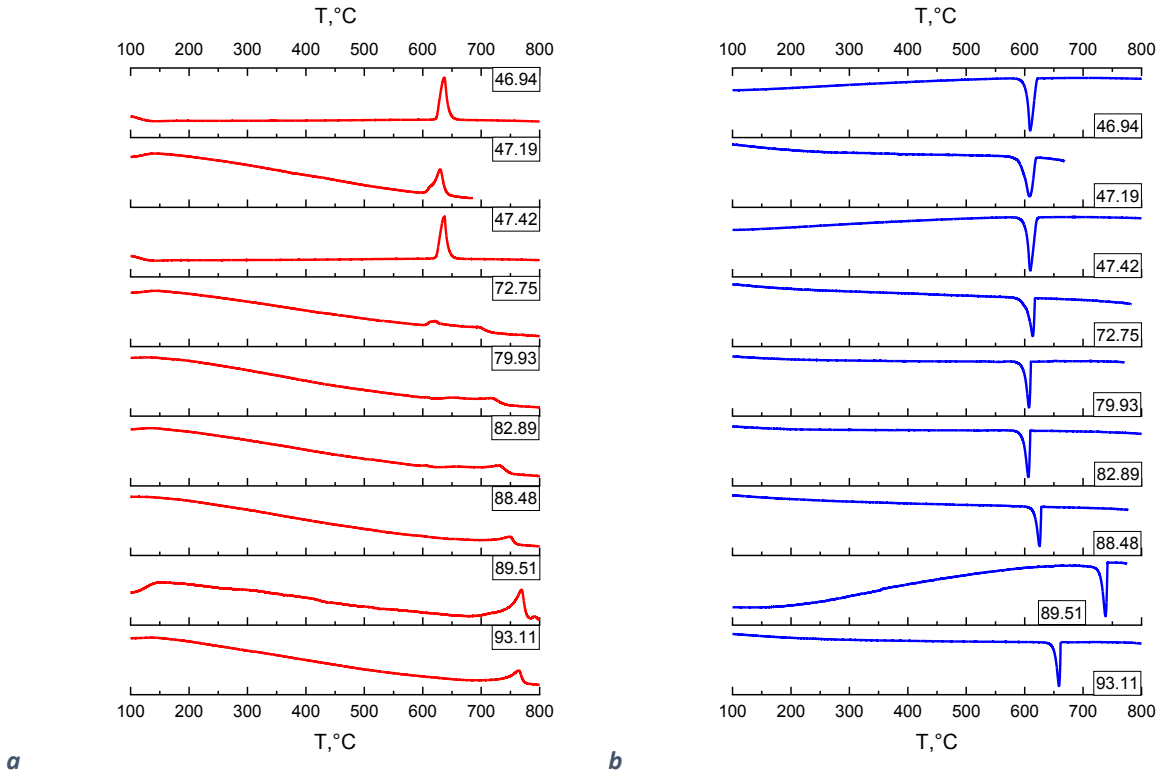


Figure 5-13 *DTA curves of $MgCl_2$-$CaCl_2$ mixtures, expressed in molar percentage of $CaCl_2$:* ***a*** *heating curves;* ***b*** *cooling curves.*

Table 5-5 *Experimental DTA values of phase transition temperatures (°C) in the $MgCl_2$-$CaCl_2$ system.*

$CaCl_2$ (mol)	$CaCl_2$ (wt%)	1st	2nd	3rd	DTA crucible
0	0	719			Sealed Pt tube
0.4694	50.77	624			Al_2O_3
0.4719	51.02	615			Sealed Pt tube
0.4742	51.25	623			Al_2O_3
0.7275	75.68	606	621	699	Sealed Pt tube
0.7993	82.23	607	649	717	Sealed Pt tube
0.8289	84.96	605	658	730	Sealed Pt tube
0.8848	89.95	595	674	750	Sealed Pt tube
0.8951	90.86	651	749		Sealed Pt tube
0.9311	94.03	459	764		Sealed Pt tube
1	100	776			Sealed Pt tube

5.1.7.1 Thermodynamic properties of the eutectic mixture

The eutectic composition of the system was experimentally established in this study as 47.19 mol% $CaCl_2$. To prepare the eutectic mixture for DSC analysis, the pure end-member compounds were accurately weighed according to the stoichiometric ratio[2], thoroughly homogenised, and sealed in an evacuated quartz ampoule. The ampoule underwent heat treatment at 750 °C for 72 hours in a furnace. After cooling to room temperature, the solidified mixture was retrieved inside a glove box

[2] For all calculations the molar mass M = 102.65 g/mol of the $MgCl_2$(52.81 mol%)-$CaCl_2$(47.19 mol%) mixture was used.

and ground in an agate mortar to produce a fine, homogeneous powder suitable for calorimetric testing. Two DSC measurements were performed using platinum tubes closed with platinum lids in the Setaram DSC instrument. A post-measurement mass loss less than 4 wt% was recorded; while this value is not negligible, the results are still regarded as reliable based on the overall consistency of the measurements. The eutectic melting temperature was determined as 624 °C (897 K). The specific heat capacity curve in the temperature region close to the melting point is shown in **Figure 5-14**. At lower temperatures, the C_p curve displayed irregularities and unusually high values; therefore, only the high-temperature region - where the data are more consistent and relevant to the fusion process - is reported here. The primary objective of this measurement was to determine, for the first time in the literature, the enthalpy of fusion of the eutectic mixture. A full reassessment of the entire C_p profile may be required in future studies but falls outside the scope of the present work. By integrating the experimental C_p curves, the enthalpy of fusion was determined to be 33.4 kJ/mol, while an independent calibration method provided a value of 32.9 ± 1.5 kJ/mol. The average value 33.2 ± 0.3 kJ/mol is proposed here as the experimental enthalpy of fusion of the eutectic composition of the binary system.

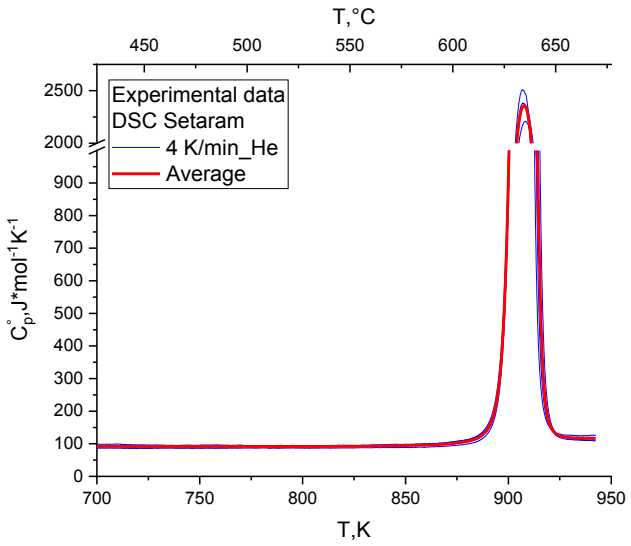


Figure 5-14 *Experimental values of molar heat capacity of $MgCl_2$(52.81 mol%)-$CaCl_2$(47.19 mol%).*

5.1.8 $MgCl_2$-$MgSO_4$

The phase diagram of the $MgCl_2$-$MgSO_4$ system was experimentally determined in this work using DTA and compared with previously published data [62, 63]. The use of sealed platinum crucibles was crucial, as it allowed overcoming issues related to the thermal decomposition of sulphates and the influence of moisture, thereby enabling investigation across the entire composition range, including the high-sulphate-content region that had not been examined in earlier studies [62, 63]. As

a preliminary step, DTA measurements were performed in open alumina crucibles on five mixtures with low sulphate contents, close to the expected eutectic composition. These tests revealed only minor mass losses (below 5-10 wt%) up to a maximum temperature of 900 °C, which is below the decomposition temperature of $MgSO_4$, confirming the need to conduct experiments in sealed systems to avoid artefacts. The corresponding DTA curves are provided in **Figure A 13**. During heating, the thermal events associated with the eutectic and liquidus transitions were not well resolved, whereas during cooling, both transitions appeared clearly separated. However, the cooling curves exhibited significant undercooling, resulting in transition temperatures lower than those observed on heating.

For the construction of the phase diagram of the $MgCl_2$-$MgSO_4$ system the experimental transition temperatures were determined from the second heating of the DTA experiments. Thirteen mixtures covering the entire composition range were analysed in sealed platinum tubes in alumina sample holders. The resulting DTA curves are presented in **Figure 5-15** and the corresponding transition temperatures are summarised in **Table 5-6**. In general, heating and cooling temperatures agreed within ±5 °C, confirming the absence of supercooling in most compositions. In the eutectic region, however, it was not possible to distinguish whether a sample corresponded exactly to the eutectic composition from the heating curves alone; only the cooling curves displayed a split signal into two peaks, corresponding to the eutectic and liquidus transitions. At high sulphate contents, the liquidus peak became progressively broader, weaker, and less well-defined in the heating curves, while appearing sharper and more intense during cooling. Nevertheless, heating curves were used as the primary reference for determining transition temperatures, as cooling curves tend to underestimate them due to supercooling. Mixtures rich in sulphates also exhibited slightly lower eutectic temperatures compared with low-sulphate mixtures. An additional weak endothermic peak around 500 °C was observed in some high-sulphate compositions, appearing exclusively during heating and absent during cooling. Subsequent tests demonstrated that when mixtures were analysed in open crucibles, allowing contaminant evaporation below the melting point, this peak disappeared entirely after the first heating/cooling cycle.

To further investigate, X-ray diffraction analyses were conducted on three selected compositions (28, 50 and 90 mol% $MgSO_4$), to check for intermediate compounds or secondary phases potentially responsible for this anomaly. The detailed XRD patterns are provided in the Appendix A. The analyses revealed no significant contaminants attributable to $MgSO_4$ and only a negligible presence of MgO (0.2 wt%, **Figure A 14**), insufficient to account for either the extra thermal peak at 500 °C or the approximately 10 °C reduction in the eutectic temperature. These events were therefore interpreted as artefacts caused by removable contamination and excluded from consideration in the final phase-diagram assessment.

DTA measurements indicate that the eutectic point is located at a composition near 28 mol% $MgSO_4$ and at 668 °C (941 K). This eutectic composition is shifted towards higher sulphate contents compared with the values reported by previous authors [62, 63], resulting in a corresponding depression of the liquidus line (liquid ⇌ liquid + $MgSO_4$) at lower temperatures.

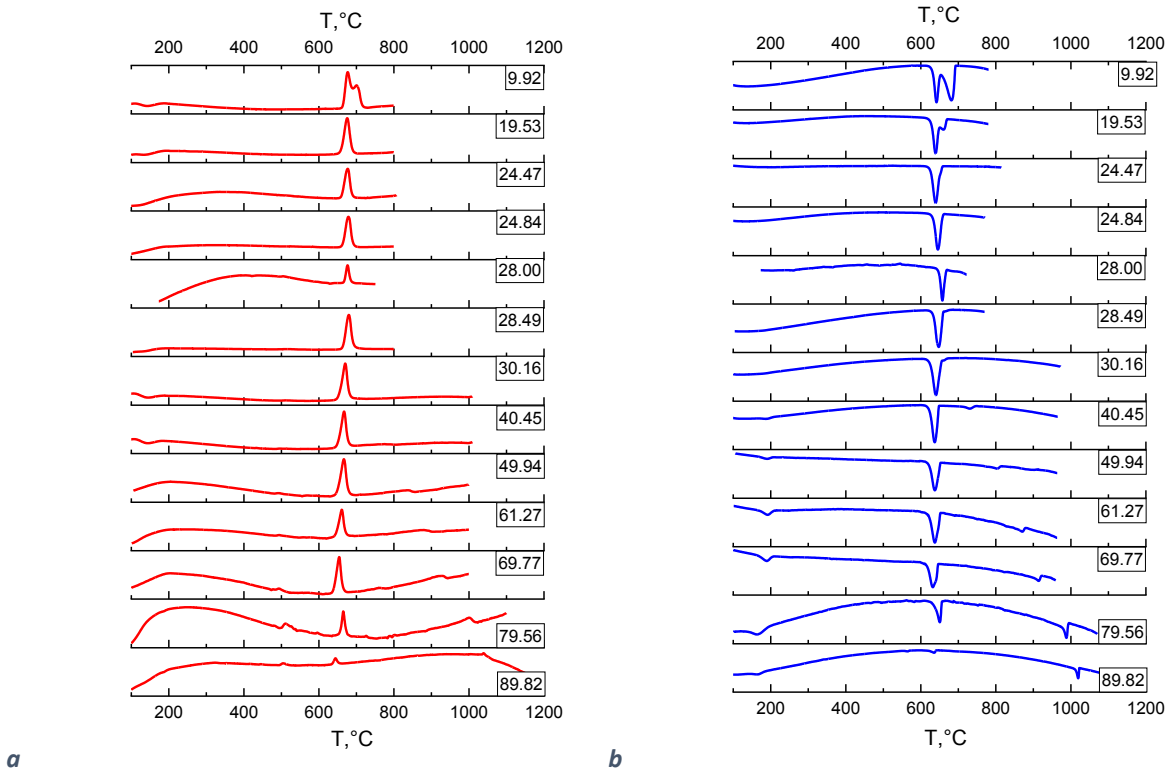


Figure 5-15 *DTA curves of $MgCl_2$-$MgSO_4$ mixtures, expressed in molar percentage of $MgSO_4$:* ***a*** *heating curves;* ***b*** *cooling curves.*

Table 5-6 *Experimental DTA values of phase transition temperatures (°C) in the $MgCl_2$-$MgSO_4$ system.*

$MgSO_4$ (mol)	$MgSO_4$ (wt%)	1st	2nd
0	0	719	
0.0992	12.22	664	700
0.1953	23.48	659	669 [a]
0.2447	29.06	650	658
0.2484	29.47	664	
0.2800	32.96	668	
0.2849	33.50	665	
0.3016	35.31	654	674
0.4045	46.20	651	744 [a]
0.4994	55.78	651	827
0.6127	66.67	647	878
0.6977	74.48	641	930
0.7956	83.11	657	979
0.8982	91.77	636	1035
1	100	1027	1136

[a] from cooling curves

5.1.8.1 Thermodynamic properties of the eutectic mixture

The assumed eutectic mixture $MgCl_2$(72.0 mol%)-$MgSO_4$(28.0 mol%), as identified from DTA measurements, was further investigated by DSC to determine its heat capacity and enthalpy of fusion. The mixture was synthesised *in situ* by thoroughly mixing stoichiometric amounts of anhydrous $MgCl_2$ (72.0 mol%) and $MgSO_4$ (28.0 mol%)[3] in an agate mortar in glove box under argon atmosphere. The mixture was then sealed in a quartz ampoule and heat-treated at 800 °C for 60 hours. After cooling, the resulting powder was ground to a fine, homogeneous state and loaded into platinum crucibles for calorimetric tests. The heat capacity was measured in the temperature range 50-750 °C using the two DSC devices (described in section 3.2.2) with different heating rates (10 and 4 K/min). A total of ten samples were analysed: three heated up to 700 °C and seven up to 750 °C until complete melting. The observed mass loss after heating up to 750 °C remained below 4.2%.

The first heating cycle was excluded from the analysis because it primarily served to remove residual moisture and water of crystallisation, as evidenced by an anomalous endothermic peak around 220 °C (493 K), which disappeared in subsequent runs. Although the samples were prepared under dry conditions, slight moisture absorption during handling is likely. Therefore, only the second and third heating cycles were considered for C_p evaluation. As already discussed in section 5.1.8, DTA analyses revealed an unexplained endothermic peak around 500 °C in certain compositions; this feature was also detected in the eutectic mixture by DSC. Unlike DTA, which only revealed this peak in medium- to high-sulphate-content mixtures, DSC was sensitive enough to detect it in the eutectic composition, which has a lower sulphate content. The peak appeared only during heating and was absent on cooling. Its origin remains unclear: decomposition of $MgSO_4$ is unlikely, as this occurs only above 1000 °C, and XRD analysis of the eutectic mixture (**Figure A 14a**) confirmed the presence of only the pure end-members in their expected weight ratios. The appearance of this peak is thus interpreted as an artefact, probably linked to trace contaminants removable during heating.

The eutectic melting temperature obtained from DSC analysis was 663 °C (936 K), in good agreement with the value of 667 °C determined by DTA. The C_p curves (**Figure 5-16**) show that, as noted elsewhere [34], different heating rates influence the apparent width of the phase-transition region; however, the heat capacities of the solid and liquid phases remain consistent between devices. The coefficients obtained from C_p measurements are reported in **Table 5-7**.

The enthalpy of fusion was determined by integrating the phase-transition peaks. The DSC 404C (10 K/min) yielded a value of 37.12 kJ/mol, whereas the mHTC 96 (4 K/min) provided 39.25 kJ/mol. This discrepancy, previously experienced in our laboratories [34], may be attributed to the design of the sample holder of the DSC 404C, which employs only two thermocouples and may

[3] For all calculations the molar mass M = 102.26 g/mol of the $MgCl_2$(72.0 mol%)-$MgSO_4$(28.0 mol%) mixture was used.

underestimate phase-transition enthalpies. Consequently, the value measured by mHTC 96, equipped with a Calvet-type thermocouple, is considered more reliable. That device enables energy calibration through the determination of the area under the phase transition curve of suitable reference metals. Using this method, the average enthalpy of fusion across five samples was 37.6 ± 2.7 kJ/mol, which is in close agreement with the value obtained from C_p integration across both DSC devices (38.2 ± 1.1 kJ/mol). The resulting average value of the two, considered in this work as the final experimental value of enthalpy of fusion of the eutectic point, is 37.9 ± 1.0 kJ/mol.

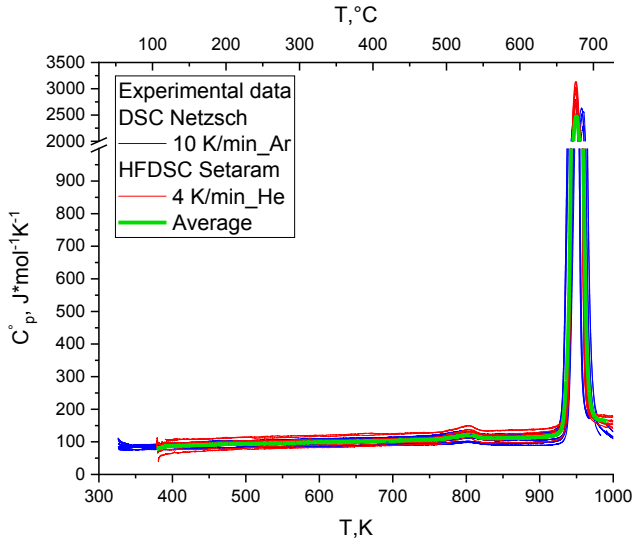


Figure 5-16 *Experimental values of molar heat capacity for solid and liquid phases of the $MgCl_2$(72.0 mol%)-$MgSO_4$(28.0 mol%) mixture measured by two DSC devices.*

Table 5-7 *Coefficients of the second-order equation of molar heat capacity ($J \cdot mol^{-1} \cdot K^{-1}$) $C_p° = A + B \cdot T + C \cdot T^{-2} + D \cdot T^2$ for the $MgCl_2$(72.0 mol%)-$MgSO_4$(28.0 mol%) mixture taken from DSC measurements.*

Temperature range/K	A	B	C	D
298 - 936	48.96872	$7.975 \cdot 10^{-2}$	$1.167316 \cdot 10^{6}$	$-1.72591 \cdot 10^{-5}$
936 - 1050	165.1			

5.1.9 $CaCl_2$-$CaSO_4$

The $CaCl_2$-$CaSO_4$ system has been experimentally investigated by several authors [66-72]; however, none of these studies provided a complete phase diagram extending into the high-sulphate region. In this study, DTA was primarily performed using sealed platinum crucibles to prevent sulphate decomposition, enable measurements at high temperatures, and cover the full compositional range of the system. Preliminary DTA experiments were first conducted in open alumina crucibles on near-eutectic mixtures, up to a maximum temperature of 900 °C (**Figure A 15**). These tests exhibited mass losses below 3 wt%, demonstrating that partial investigation of the system in open crucibles is possible

without significant interference from mass loss. Nevertheless, to achieve better resolution of thermal events and to ensure consistency and reliability of the data, only results from sealed platinum crucibles are presented and discussed in this work. Seventeen compositions were analysed and the resulting DTA curves are shown in **Figure 5-17**, with their corresponding temperatures of phase transitions listed in **Table 5-8**. The DTA experimental data showed good agreement with literature data reported by Golubeva et al. [69].

The eutectic transition appeared as a strong and well-defined peak in both heating and cooling curves for all mixtures. In contrast, the liquidus transition was poorly resolved on heating, appearing as small and broad peaks, but could be more clearly identified in the cooling curves, despite the occurrence of undercooling. For mixtures containing more than 50 mol% of $CaSO_4$, no undercooling was observed at the liquidus transition, and the transition temperatures in heating and cooling cycles coincided within ±5 °C, except for the eutectic transition, which still showed undercooling effect. The eutectic mixture was also examined by XRD solely to confirm the absence of any secondary or intermediate phases. These XRD results are provided in **Figure A 16** and **Table A 5**.

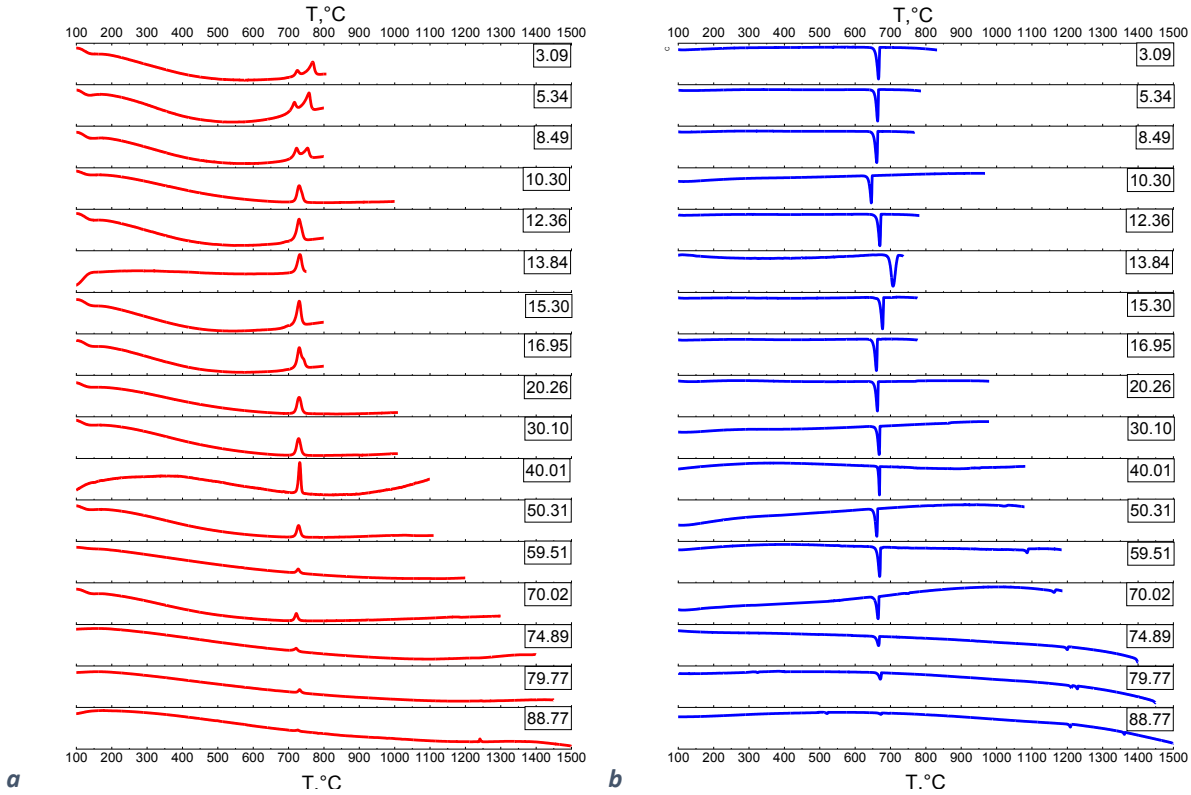


Figure 5-17 *DTA curves of $CaCl_2$-$CaSO_4$ mixtures. expressed in molar percentage of $CaSO_4$: **a** heating curves; **b** cooling curves.*

Table 5-8 *Experimental DTA values of phase transition temperatures (°C) in the $CaCl_2$-$CaSO_4$ system.*

$CaSO_4$ (mol)	$CaSO_4$ (wt%)	1st	2nd	3rd
0	0	776		
0.0309	3.76	716	768	
0.0534	6.47	717	758	

0.0849	10.22	720	752	
0.1030	12.35	719	738	
0.1236	14.75	717		
0.1384	16.46	718		
0.1530	18.14	716	737	
0.1695	20.02	719	744	
0.2026	23.76	718	809	
0.3010	34.57	717	894	
0.4001	45.00	717	970	
0.5031	55.40	718	1030	
0.5951	64.32	715	1100	
0.7002	74.13	714	1176	
0.7489	78.53	712	1209	
0.7977	82.87	724	1233	1290
0.8877	90.65	721	1240	1379
1	100	1220	1510	

5.1.9.1 Thermodynamic properties of the eutectic mixture

The eutectic composition identified from DTA measurements, $CaCl_2$ (86.01 mol%)-$CaSO_4$ (13.99 mol%)[4], was investigated by DSC in order to determine heat capacity and enthalpy of fusion. The preparation of the eutectic mixture followed the same procedure described in section 5.1.8.1. A total of ten DSC measurements were conducted: five within the lower temperature range (50-690 °C), below the melting point, and five extending beyond it, up to 790 °C, with the recorded mass loss remaining below 1%. The resulting C_p curves are presented in **Figure 5-18**, and the corresponding polynomial coefficients derived from the measurements are listed in **Table 5-9**. The eutectic melting temperature determined by DSC was 724 °C (997 K), in good agreement with the value of 718 °C (991 K) obtained from DTA measurements.

The enthalpy of fusion was determined by integrating the phase-transition peak areas. The values obtained were 30.7 kJ/mol from DSC 404C (10 K/min) and 29.8 kJ/mol from mHTC 96 (4 K/min), yielding an average of 30.2 ± 0.5 kJ/mol. Additionally, the energy calibration method available in the mHTC 96 provided a consistent value of 30.2 ± 0.5 kJ/mol. The resulting average value, presented in this work as the final experimental enthalpy of fusion, is 30.2 ± 0.4 kJ/mol.

[4] For all calculations the molar mass M = 114.50 g/mol of the $CaCl_2$(86.01 mol%)-$CaSO_4$(13.99 mol%) mixture was used.

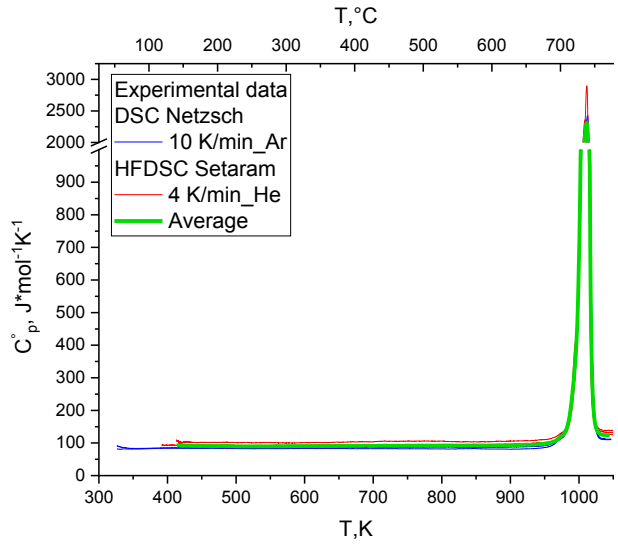


Figure 5-18 *Experimental values of molar heat capacity for solid and liquid phases of the $CaCl_2$(86.01 mol%)-$CaSO_4$(13.99 mol%) mixture measured by two DSC devices.*

Table 5-9 *Coefficients of the second-order equation of molar heat capacity ($J \cdot mol^{-1} \cdot K^{-1}$) $C_p° = A + B \cdot T + C \cdot T^{-2} + D \cdot T^2$ for the $CaCl_2$(86.01 mol%)-$CaSO_4$(13.99 mol%) mixture taken from DSC measurements.*

Temperature range/K	A	B	C	D
298 - 997	78.983	$1.810 \cdot 10^{-3}$	$1.208 \cdot 10^{5}$	$1.749 \cdot 10^{-5}$
997 - 1050	124.22			

5.1.10 $MgCl_2$-$CaSO_4$

According to the thermodynamic data available in the PCM2 database, the $MgCl_2$-$CaSO_4$ system is thermodynamically stable with respect to the ion-exchange reaction of the reciprocal system. However, no experimental investigations had previously been reported for this system. The present work therefore aims to clarify its phase equilibria through targeted experimental analysis. The system was studied using DTA, conducted in sealed platinum tubes to prevent sulphate decomposition at high temperatures. A total of twelve mixtures were analysed, with no detectable mass loss up to 1250 °C. The corresponding heating and cooling curves are shown in **Figure 5-19**, and the identified thermal events are summarised in **Table 5-10**. Multiple well-defined thermal effects were observed, indicating the occurrence of several phase equilibria, consistent with the presence of different phases and intermediate compounds already reported in related binary systems, such as $MgSO_4$-$CaSO_4$. These findings constitute the first experimental evidence for the reciprocal system, filling a significant gap in previous knowledge.

To further investigate the possible formation of intermediate phases, a mixture with the composition $MgCl_2$(30.80 mol%)-$CaSO_4$(69.20 mol%) was synthesised by solid-state reaction. Stoichiometric amounts of the pure compounds were mixed, sealed in an evacuated quartz ampoule, and heat-treated at 900 °C for 60 hours. After cooling, the mixture was ground in an agate mortar and

analysed by X-ray diffraction analysis. The results revealed three major phases - $CaMg_2(SO_4)_3$, $CaSO_4$, and $CaCl_2$ - as well as an unknown orthorhombic phase associated with $CaMg(SO_4)_2$, previously reported in section 5.1.6. The detailed XRD results are provided in **Figure A 17** and **Table A 6**. These identified phases correlate well with the thermal events detected by DTA, confirming that no additional intermediate compounds are present in the $MgCl_2$-$CaSO_4$ system under the investigated conditions.

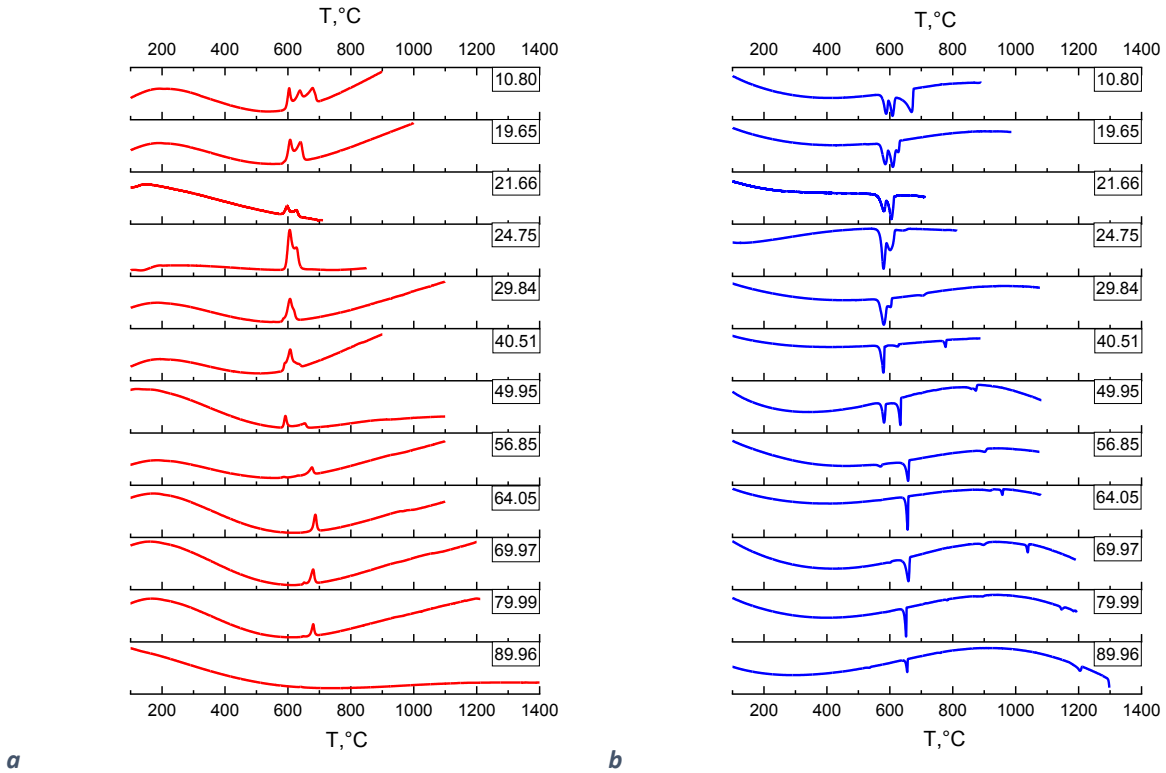


Figure 5-19 *DTA curves of $MgCl_2$-$CaSO_4$ mixtures, expressed in molar percentage of $CaSO_4$: **a** heating curves; **b** cooling curves.*

Table 5-10 *Experimental DTA values of phase transition temperatures (°C) in the $MgCl_2$-$CaSO_4$ system.*

$CaSO_4$ (mol)	$CaSO_4$ (wt%)	1st	2nd	3rd	4th	5th
0	0	719				
0.1080	14.76	587	631	671		
0.1965	25.91	581	600	633		
0.2166	28.33	587	627			
0.2475	32.10	588	616	659 [a]		
0.2984	37.82	574	599	632 [a]	707 [a]	
0.4051	49.33	578	601	618	630	797 [a]
0.4995	58.80	578	647	869 [a]		
0.5685	65.32	572	626	670	901 [a]	
0.6405	71.81	670	919 [a]	952 [a]		
0.6997	76.91	639	673	900 [a]	1032 [a]	
0.7999	85.11	636	673	892 [a]	1146 [a]	
0.8996	92.76	670	1202	1215		
1	100	1220	1510			

[a] from cooling curves

5.1.10.1 Thermodynamic properties of the low-melting mixture

To improve the thermodynamic description of the system under investigation, a calorimetric study was performed on the mixture $MgCl_2$(78.34 mol%)-$CaSO_4$(21.66 mol%)[5], corresponding to the minimum of the liquidus line as suggested by DTA measurements. The main objective of this analysis was to obtain additional experimental thermodynamic data, essential for refining the thermodynamic assessment and improving the accuracy of the thermodynamic optimisation and database development for the reciprocal system. The mixture was prepared following the same procedure as for the previously investigated compositions: the pure end-members were weighed in the appropriate stoichiometric ratio, thoroughly mixed, sealed in an evacuated quartz ampoule, and subjected to heat treatment at 700 °C for 48 hours. After cooling, the sample was retrieved and subsequently subjected to DSC measurements. Both Netzsch and Setaram calorimeters were used, with three independent samples from the same batch measured in each instrument. The resulting C_p curves displayed two distinct thermal events at 591 °C (864 K) and at 632 °C (905 K), as shown in **Figure 5-20**. These two transitions occurred in close succession and, under the experimental conditions adopted, appeared as partially overlapping peaks, which may have affected the accuracy of enthalpy determination by simple peak integration. A mathematical deconvolution of the overlapping signals allowed separation of the contributions, yielding enthalpies of 13.8 kJ/mol for the first transition and 19.0 kJ/mol for the second. The initial aim of this calorimetric investigation was to identify and characterise the thermodynamic properties of a potential eutectic composition, which could be considered as a candidate phase change material. However, the experimental results, in combination with DTA data, demonstrated that this composition does not correspond to an invariant eutectic point. Despite this, the measurements provide new and valuable thermodynamic data, improving the understanding of the phase behaviour of the reciprocal system and contributing to the refinement and extension of the thermodynamic database.

[5] For all calculations the molar mass M = 104.08 g/mol of the $MgCl_2$(78.34 mol%)-$CaSO_4$(21.66 mol%) mixture was used.

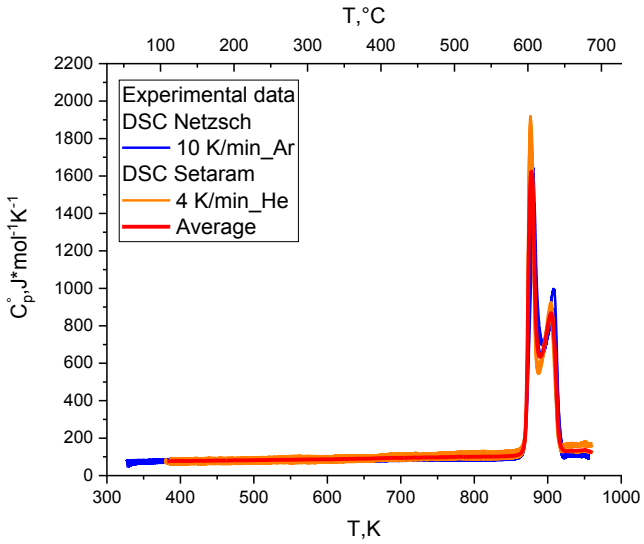


Figure 5-20 *Experimental values of molar heat capacity of $MgCl_2$(78.34 mol%)-$CaSO_4$(21.66 mol%).*

5.1.11 $CaCl_2$-$MgSO_4$

A total of fifteen mixtures, covering the entire compositional range, were investigated by DTA in sealed platinum tubes, with no detectable mass loss up to 1300 °C. The corresponding DTA heating and cooling curves for all studied mixtures are presented in **Figure 5-21**, and the identified phase-transition temperatures are summarised in **Table 5-11**.

To further clarify the phase equilibria of the system and assess the possible formation of intermediate compounds, a selected mixture with the composition $CaCl_2$(71.70 mol%)-$MgSO_4$(28.30 mol%) was synthesised in-situ and analysed by XRD. The preparation followed the standard protocol: the pure compounds were mixed in their stoichiometric ratio, sealed within an evacuated quartz ampoule, and subjected to heat treatment, in this case at 900 °C for 60 hours in a furnace. The resulting room temperature diffraction results are summarised in **Figure A 18** and **Table A 7**. The analysis confirmed the presence of $CaCl_2$ and $CaMg_2(SO_4)_3$ as the main crystalline phases. This finding provided additional evidence regarding the phase fields within the corresponding regions of the phase diagram, and confirmed the absence of other multicomponent chloride-sulphate phases.

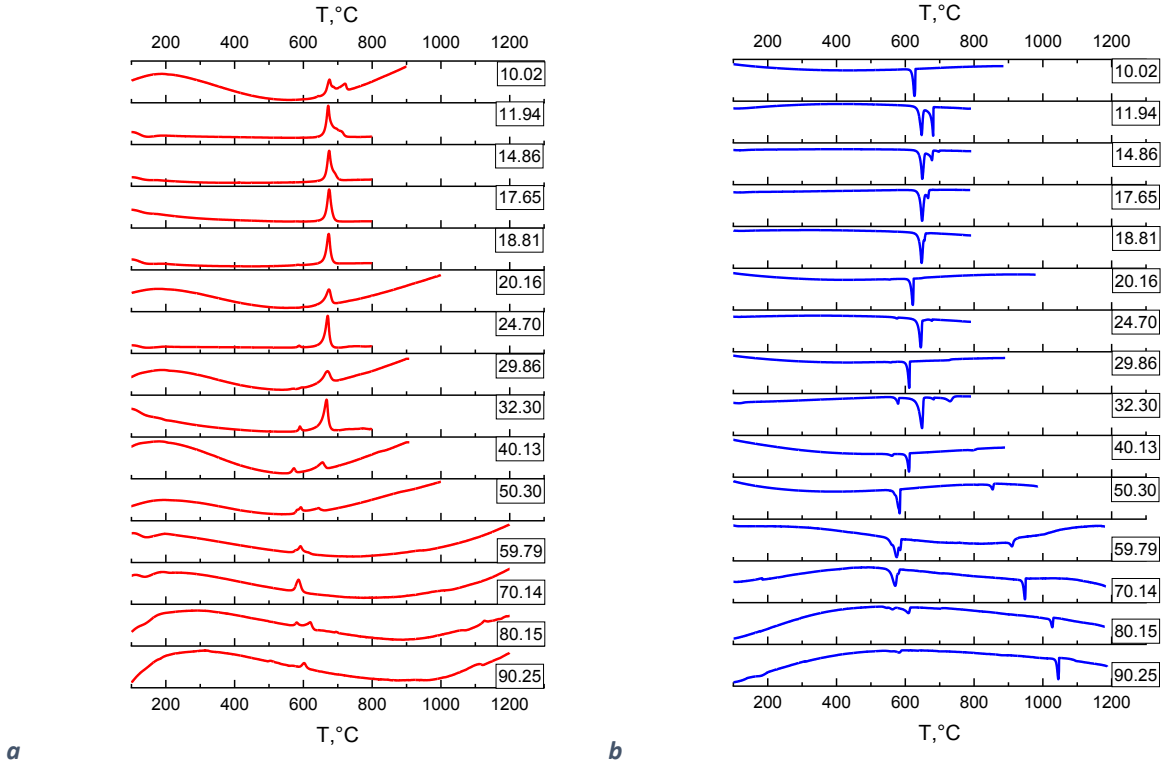


Figure 5-21 *DTA curves of $CaCl_2$-$MgSO_4$ mixtures. expressed in molar percentage of $MgSO_4$:* ***a*** *heating curves;* ***b*** *cooling curves.*

Table 5-11 *Experimental DTA values of phase transition temperatures (°C) in the $CaCl_2$-$MgSO_4$ system.*

$MgSO_4$ (mol)	$MgSO_4$ (wt%)	1st	2nd	3rd	4th
0	0	776			
0.1002	10.78	642	675	689	721
0.1194	12.82	664	702		
0.1486	15.92	657 [a]	681 [a]	689 [a]	
0.1765	18.86	658 [a]	669 [a]		
0.1881	20.08	653 [a]	659 [a]		
0.2016	21.50	562	604	673	
0.2470	26.24	579 [a]	649 [a]	678 [a]	
0.2986	31.59	575	597	670	735 [a]
0.3230	34.10	582 [a]	653 [a]	677 [a]	746 [a]
0.4013	42.10	561	656	828	
0.5030	52.33	574	592	643	863 [a]
0.5979	61.73	577	591	615	940
0.7014	71.81	572	586 [a]	1001	
0.8015	81.41	573	618	1055	
0.9025	90.94	573 [a]	587 [a]	1065 [a]	
1	100	1027	1136		

[a] from cooling curves

5.1.12 $MgCl_2$-$CaMg_2(SO_4)_3$

The identification of the intermediate compound $CaMg_2(SO_4)_3$ within the binary system $MgSO_4$-$CaSO_4$ enabled the investigation of two additional chloride-containing sections: $MgCl_2$-$CaMg_2(SO_4)_3$ and $CaCl_2$-$CaMg_2(SO_4)_3$. An experimental effort to study these systems is driven by the objective of gaining a deeper understanding of the phase equilibria within the reciprocal system and

its thermodynamic description. The mixtures $MgCl_2$-$CaMg_2(SO_4)_3$ intended to be studied were prepared by directly mixing the end-members of the quasi-binary systems or equivalently by mixing the three pure compounds ($MgCl_2$, $MgSO_4$, $CaSO_4$) involved in the appropriate molar ratios. Interestingly, the high-sulphate mixtures in the system $MgCl_2$-$CaMg_2(SO_4)_3$ showed a mass loss at temperatures above 1200 °C when prepared by directly mixing the pure compounds ($MgCl_2$, $MgSO_4$, $CaSO_4$), whereas they showed no mass loss when the same mixtures were prepared by mixing the two end-members. Ten mixtures have been investigated in DTA/TG in sealed platinum tubes. The DTA heating and cooling curves for the mixtures under study are displayed in **Figure 5-22**, and the transition temperatures are listed in **Table 5-12**. The transition temperatures observed during the heating cycles exhibit broad and low-intensity peaks, whereas the cooling curves display sharper and more intense peaks, allowing for better discrimination of the thermal events. However, the cooling cycles also show a systematic shift of approximately 20 °C towards lower temperatures, attributable to undercooling effects, which introduces greater uncertainty in the determination of the transition temperatures. Therefore, in this work, the transition temperatures derived from the heating curves are reported. In proximity to the composition corresponding to the liquidus minimum, the discrimination of this minimum is more evident in the cooling curves, where the thermal event appears as two distinct and well-separated peaks. In contrast, such peak splitting is not clearly detectable during the heating cycle, where only a single thermal event is observed at 666 °C for the composition containing 20.63 mol% $CaMg_2(SO_4)_3$. On the other hand, the cooling curve reveals two distinct transitions at 641 °C and 655 °C, respectively. To account for the proximity to the eutectic (or minimum-liquidus) composition - while acknowledging that the analysed composition does not exactly coincide with it - the transition temperatures identified from the cooling curve are reported for that composition.

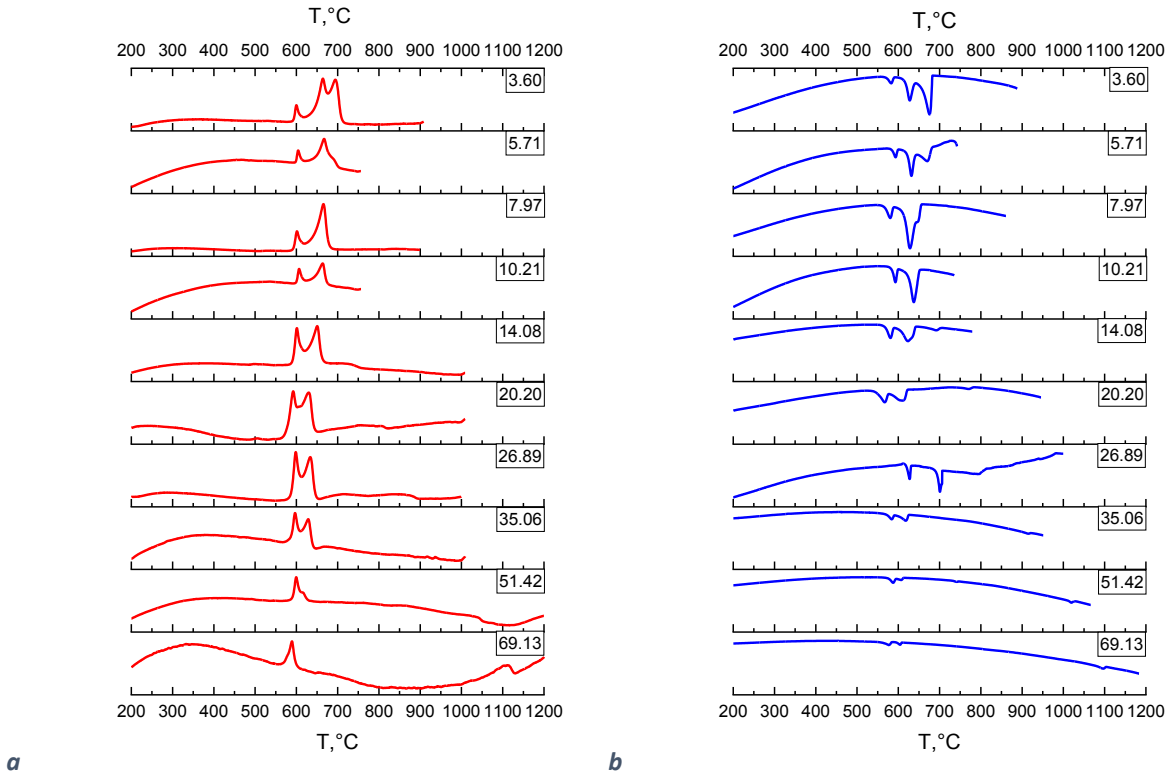


Figure 5-22 *DTA curves of $MgCl_2$-$CaMg_2(SO_4)_3$ mixtures, expressed in molar percentage of $CaMg_2(SO_4)_3$:* ***a*** *heating curves;* ***b*** *cooling curves.*

Table 5-12 *Experimental DTA values of phase transition temperatures (°C) in the $MgCl_2$-$CaMg_2(SO_4)_3$ system.*

$CaMg_2(SO_4)_3$ (mol)	$CaMg_2(SO_4)_3$ (wt%)	1st	2nd	3rd
0	0	719		
0.0360 [a]	12.88	593	664	693
0.0571 [b]	19.33	599	668	691
0.0797 [a]	25.54	593	641 [c]	655 [c]
0.1021 [b]	31.04	600	664	
0.1408 [a]	39.35	592	650	732
0.2020 [a]	50.06	576	629	801
0.2689 [a]	59.32	588	633	884
0.3506 [b]	68.12	587	628	937
0.5142 [b]	80.73	591	619	1041
0.6913 [b]	89.86	580	646	1104
1	100	1213		

[a] mixing $MgCl_2$, $MgSO_4$ and $CaSO_4$
[b] mixing $MgCl_2$ and $CaMg_2(SO_4)_3$
[c] from cooling curves

5.1.13 $CaCl_2$-$CaMg_2(SO_4)_3$

The system $CaCl_2$-$CaMg_2(SO_4)_3$ was investigated through DTA thermal analysis using sealed platinum tubes to determine the phase diagram. To this end, nine mixtures covering the entire compositional range, with a 10 mol% interval in composition, were analysed. The resulting DTA curves are presented in **Figure 5-23**, while the corresponding experimental transition temperatures are shown in **Table 5-13**. Thermal events were distinctly observed in both heating and cooling cycles. In

mixtures with a high proportion of the double sulphate, these events were less pronounced during heating; however, crystallisation during cooling was more evident, offering clearer indications for determining the liquidus temperature.

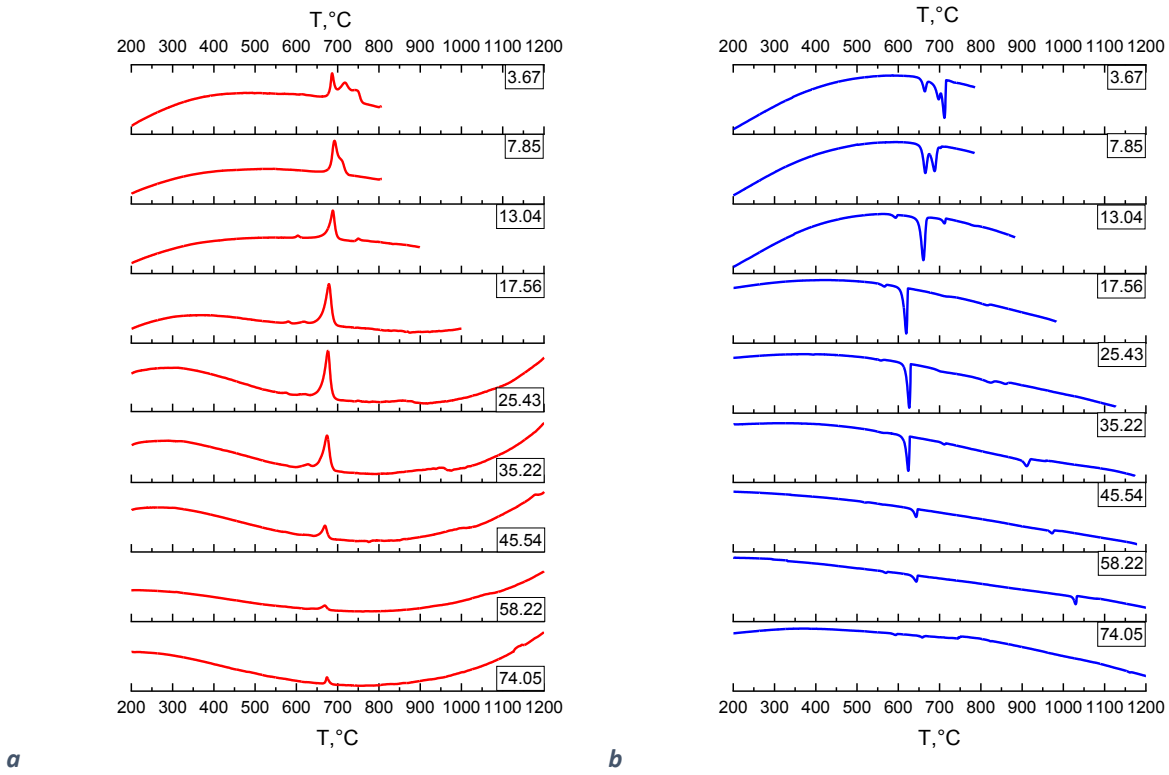


Figure 5-23 *DTA curves of $CaCl_2$-$CaMg_2(SO_4)_3$ mixtures. expressed in molar percentage of $CaMg_2(SO_4)_3$: **a** heating curves; **b** cooling curves.*

Table 5-13 *Experimental DTA values of phase transition temperatures (°C) in the $CaCl_2$-$CaMg_2(SO_4)_3$ system.*

$CaMg_2(SO_4)_3$ (mol)	$CaMg_2(SO_4)_3$ (wt%)	1st	2nd	3rd	4th
0	0	776			
0.0367	11.45	679	720	739	
0.0785	22.44	681	710	744	
0.1304	33.74	596	676	729 [a]	773 [a]
0.1756	41.98	581	678	726 [a]	823 [a]
0.2543	53.66	564 [a]	662	834 [a]	887
0.3522	64.87	624	661	920 [a]	960
0.4554	73.96	669	1006		
0.5822	82.56	663	1072		
0.7405	90.61	669	1127		
1	100	1213			

[a] from cooling curves

5.2 Na^+, Mg^{2+} // Cl^-, SO_4^{2-} system

5.2.1 $NaCl$-$MgSO_4$

The stable diagonal of the reciprocal Na^+, Mg^{2+} // Cl^-, SO_4^{2-} system was experimentally investigated by DTA in sealed platinum tubes in order to avoid any mass loss. The primary aim of these

measurements was to validate experimental data previously reported in the literature [63], which provide only the liquidus temperatures, and to achieve a more detailed understanding of the phase equilibria within the corresponding binary system. For this purpose, fifteen compositions (9.88, 18.07, 25.76, 29.60, 30.98, 31.89, 32.97, 34.50, 40.29, 49.20, 57.22, 65.09, 71.36, 83.99, and 93.81 mol% $MgSO_4$) were analysed, whose DTA curves are displayed in **Figure 5-24** and their phase transition temperatures are listed in **Table 5-14**. In the medium-high sulphate composition range, the present results revealed thermal events not reported by Speranskaya [63]. These additional effects suggest the possibility of more complex phase relations than those expected for a simple eutectic diagram, potentially involving the formation of an intermediate compound, $Na_2Mg_3(SO_4)_4$. For instance, a peak at 683.8 °C was observed for a mixture containing 49.20 mol% $MgSO_4$. This transition, however, is not visible in measurements of mixtures with higher sulphate content. Because of its isolated occurrence, this event was not considered reliable and was excluded from the dataset used for subsequent thermodynamic modelling. Another recurrent feature was the appearance of a peak near 500 °C, which is likely attributed to $MgSO_4$, as previously discussed (section 5.1). This anomaly was detected only during heating cycles, while absent upon cooling, and its origin remains unclear. Given its uncertain nature and lack of reproducibility, this transition was also disregarded in the final assessment and not incorporated into the thermodynamic database. As a general rule, phase transitions in DTA are interpreted from heating curves. Nevertheless, in several cases the thermal effects were much more pronounced in the cooling cycles, where peaks were broader and more intense, while the corresponding heating signals appeared flattened and noisy. Under such conditions, the transition temperatures derived solely from heating curves may be misleading, and therefore complementary evaluation of cooling curves was necessary for consistent interpretation.

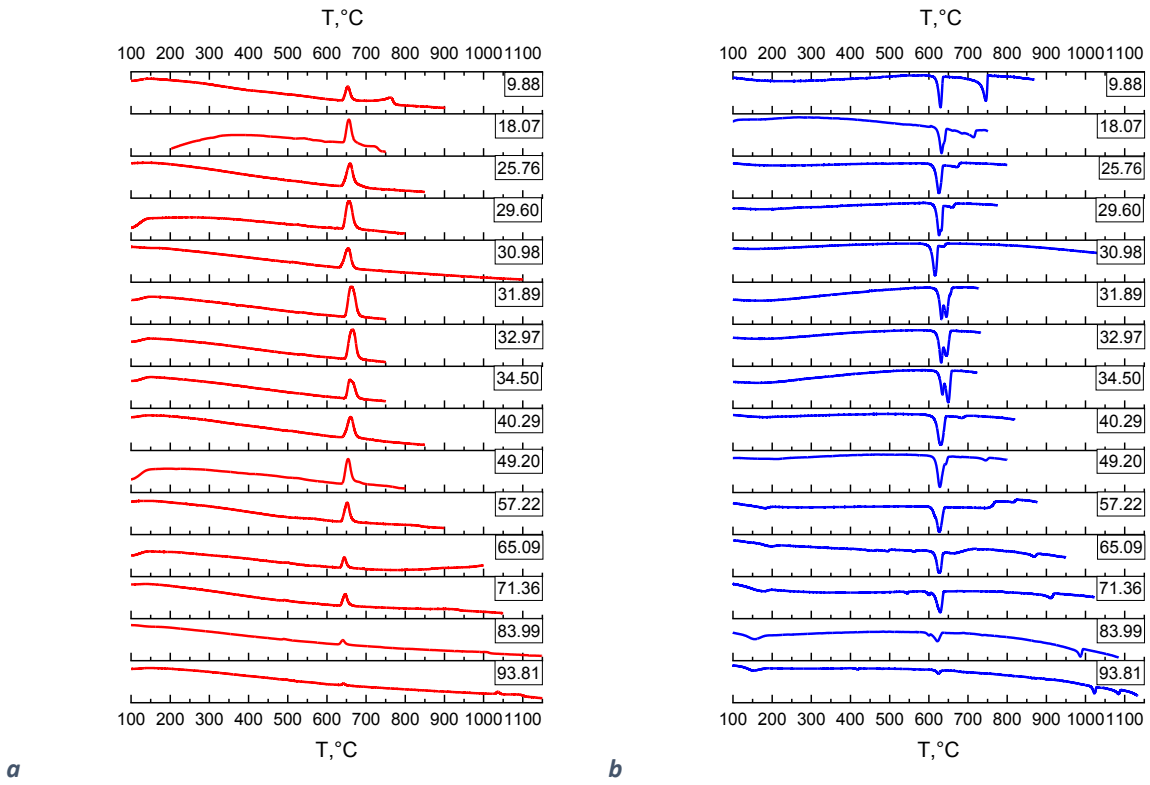


Figure 5-24 *DTA curves of NaCl-$MgSO_4$ mixtures, expressed in molar percentage of $MgSO_4$:* ***a*** *heating curves;* ***b*** *cooling curves.*

Table 5-14 *Experimental DTA values of phase transition temperatures (°C) in the NaCl-$MgSO_4$ system.*

$MgSO_4$ (mol)	$MgSO_4$ (wt%)	$MgSO_4$ (mol) [a]	1st	2nd	3rd
0	0	0	810		
0.0988	18.42	0.1798	641	762	
0.1807	31.24	0.3061	644	725	
0.2576	41.68	0.4097	641	680	
0.2960	46.77	0.4604	642	668 [b]	
0.3098	48.04	0.4731	637 [b]	644 [b]	
0.3189	49.09	0.4836	640	654 [b]	
0.3297	50.32	0.4959	641	659 [b]	
0.3450	52.04	0.5131	641 [b]	661 [b]	
0.4029	58.15	0.5743	643	695 [b]	
0.4920	66.61	0.6595	641	754	
0.5722	73.37	0.7279	638	826	
0.6509	79.34	0.7885	636	877 [b]	
0.7136	83.69	0.8328	568	636	920
0.8399	91.53	0.9130	632	1010	
0.9381	96.90	0.9681	637	1030	1085
1	100	1	1027	1136	

[a] in the $(NaCl)_2$-$MgSO_4$ system
[b] from cooling curves

5.2.1.1 Thermodynamic properties of the eutectic mixture

The DTA experiments did not allow for an unambiguous identification of the eutectic composition suitable for detailed calorimetric measurements. This limitation arose from the presence of a single peak in the heating curves of near-eutectic mixtures (30.98, 31.89, 32.97, and 34.50 mol%

$MgSO_4$), which could be associated with the eutectic transition, in contrast to the corresponding cooling curves, where the peak exhibited splitting (**Figure 5-24**). The latter behaviour indicated proximity to the eutectic composition but not its precise location. To obtain more accurate and detailed information on the eutectic composition, additional DSC measurements were therefore performed.

For the DSC measurements, four mixtures (31.96, 32.34, 33.56, and 35.20 mol% $MgSO_4$) were prepared by mixing the pure compounds in the appropriate stoichiometric ratios within a quartz ampoule inside a glove box to prevent contamination. The ampoules were then vacuum-sealed by flame and subjected to high-temperature treatment at 650-700 °C for several days to ensure complete homogenisation and melting. After the thermal treatment, the molten salts were solidified, subsequently ground in an agate mortar under controlled conditions within a glove box, and finally used for DSC measurements. The analyses were conducted in a Setaram DSC instrument, with the samples placed in platinum crucibles. DSC measurements were conducted in order to refine the determination of the eutectic composition and evaluate the enthalpy of the eutectic transition, as the enthalpy contribution is expected to be maximal at the true eutectic point [261]. To achieve this, Tamman diagram can be constructed by plotting the enthalpy contributions associated with eutectic melting [262]. Typically, these diagrams incorporate data from heating cycles across the entire compositional range. However, in this study, the selected mixtures were all within the near-eutectic region, as the objective was to prepare samples within this range and identify the exact eutectic composition. In this region, heating curves displayed a single peak, while cooling curves revealed a splitting of peaks, corresponding to the eutectic and liquidus transitions. **Figure 5-25** presents a comparison of the experimental heat capacity curves for the compositions under investigation. For each composition, the curves represent the average of multiple measurements, separately for the heating and cooling cycles. The figure highlights both the differences among the various compositions and the thermal behaviour observed between heating and cooling. Notably, while the heating curves consistently exhibit a single endothermic peak, the corresponding cooling curves reveal two overlapping but distinguishable exothermic peaks. It should be emphasised that the cooling curves are shown here not for accurate C_p determination - as thermal lag, baseline instability, and kinetic effects during cooling may compromise the precision of heat capacity values - but solely to illustrate the peak splitting and the associated crystallisation behaviour.

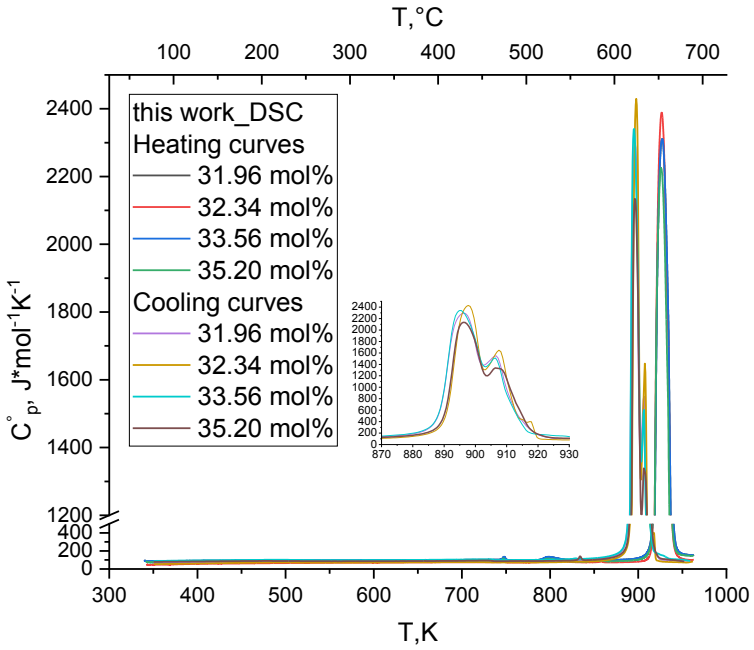


Figure 5-25 *Experimental values of molar heat capacity for solid and liquid phases of the NaCl(100-x mol%)-$MgSO_4$(x mol%) mixtures (x= 31.96, 32.34, 33.56, 35.20), measured by DSC Setaram during heating and cooling cycles. Inset: zoomed view of the cooling curves highlighting the peak region.*

The peak separation in cooling complicates the use of heating peaks for constructing Tamman diagrams. Nevertheless, in theory, the method could still be applied using the first peak at the lower temperature in the cooling curves, which corresponds to the eutectic transition. However, undercooling effects in the cooling curves can introduce deviations, potentially compromising the construction of Tamman diagram. To mitigate these challenges, a deconvolution of the overlapping peaks in the cooling curves was performed to differentiate and quantify the respective enthalpy contributions. The resulting plot is shown in **Figure A 19**. However, no clear intersection point indicative of the precise eutectic composition was identified, as the expected trend of two intersecting lines at the highest enthalpy value - corresponding to the true eutectic composition - was not observed. This finding led to a reconsideration of the composition range, extending the analysis to a broader set of mixtures in order to better evaluate the enthalpy contribution of the eutectic transition. To achieve this, DTA measurements were utilised for a Tamman diagram construction. For this purpose, compositions in the near-eutectic region were excluded. This decision was made because, in this compositional range, the integrated peak areas in the heating curves represent the combined effect of both the eutectic and liquidus transitions, making it difficult to separate their individual contributions. The results of the linear fitting performed on two distinct compositional segments - one for sub-eutectic and one for super-eutectic compositions - are illustrated in **Figure 5-26**. The intersection-point of these two linear segments provided an estimated eutectic composition of 34.1

mol% $MgSO_4$. The Tamman diagram remains a reliable tool for approximating the eutectic composition, with an estimated uncertainty of ±3 mol%. For the purposes of this study, the estimation of the enthalpy of fusion of the eutectic mixture was carried out to provide a key thermodynamic property for use in thermodynamic modelling. This estimation contributes to the refinement of the thermodynamic database and aligns with the broader objective of identifying potential Phase Change Materials, which represents the overarching goal of the project. Given the ±3 mol% compositional range, the identification of a eutectic mixture within this interval remains within an acceptable uncertainty margin for the intended thermodynamic assessment. While additional experimental efforts could further refine this estimation, they fall beyond the scope of this work.

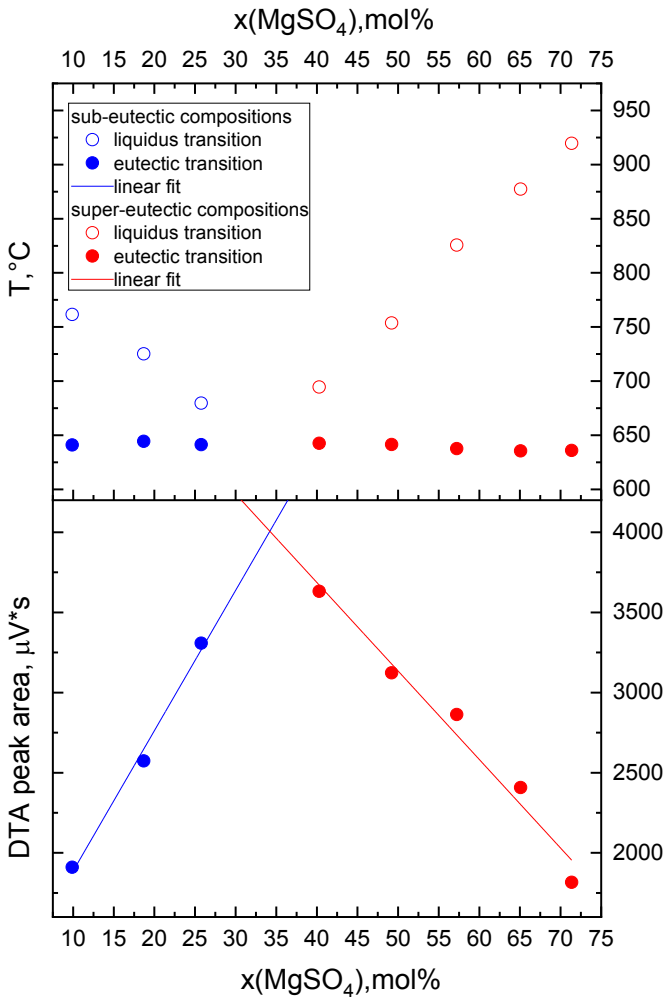


Figure 5-26 *Phase diagram and corresponding Tamman plot of NaCl-$MgSO_4$ system.*

The determination of the enthalpy of fusion of the eutectic mixture cannot therefore be provided with absolute certainty, but only as an estimate. As shown in **Figure 5-27**, the integration of DSC heating curves for the composition proposed as eutectic (34.1 mol% $MgSO_4$) does not exhibit a

distinct maximum in the enthalpy of fusion, as would be expected from a classical Tamman plot. This observation reflects the difficulty previously described in unambiguously identifying the eutectic composition. Instead, the results provide an approximate estimate of the enthalpic contribution, yielding a value of about 42 ± 3 kJ/mol - better interpreted as an energy window rather than a sharply defined maximum. However, this estimate may represent an overestimation, as the broad peak observed in heating likely corresponds to the convolution of multiple closely spaced transitions. Conversely, deconvolution of the cooling curves suggested a substantially lower enthalpy of around 21 kJ/mol (see **Figure A 19**), which is considered an underestimation due to the artificial splitting of latent heat between distinct peaks. These two effects highlight the limitations of both approaches: heating curves tend to overestimate the enthalpy by merging thermal events, while cooling curves underestimate it by distributing the latent heat. Importantly, such a low value (~21 kJ/mol) is not consistent with thermodynamic expectations, since no comparable enthalpic contribution would be anticipated for eutectic-related transitions, whereas the real eutectic composition is expected to yield the maximum enthalpic content. This consideration supports discarding the value derived from the deconvoluted cooling peaks. Taking these factors into account, the most reasonable outcome is to consider the enthalpy of fusion of the eutectic mixture as lying within this range, with the heating-derived value (~42 kJ/mol) providing the more reliable experimental estimate. It should be noted that additional measurements aimed at refining and more accurately determining the latent heat of the eutectic composition of the studied system would be desirable; however, such an investigation falls beyond the scope of the present work.

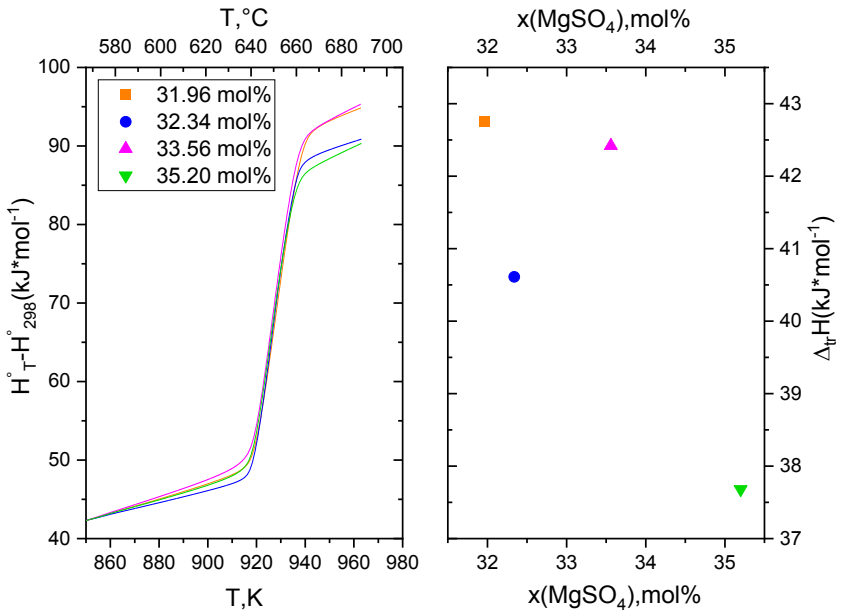


Figure 5-27 *Enthalpy increment (left) and enthalpy of transition (right) of the NaCl(100-x mol%)-$MgSO_4$(x mol%) mixtures (x= 31.96, 32.34, 33.56, 35.20) obtained from DSC results.*

5.2.2 $MgCl_2$-Na_2SO_4

To validate the experimental data of Speranskaya [63] and to extend the phase diagram description of the $MgCl_2$-Na_2SO_4 system, a series of DTA measurements was carried out. Twelve compositions (9.92, 10.63, 19.91, 21.20, 29.95, 38.21, 50.00, 60.06, 67.09, 70.95, 80.30, and 86.59 mol% Na_2SO_4) were analysed in sealed platinum tubes, which allowed the required temperature range to be reached without mass loss. The observed transition temperatures derived from the DTA curves (**Figure 5-28**) are summarised in **Table 5-15**. The present study complements the work of Speranskaya [63], with which it is consistent in describing the liquidus curve on the basis of the melting temperatures of the analysed mixtures. However, the DTA analyses performed in this study revealed additional thermal events not described in that work. These effects are attributed to phase transitions involving double sulphates and chlorides of sodium and magnesium. For mixtures with a high chloride content, the DTA curves exhibited multiple thermal effects, some of which were difficult to attribute to specific phase transitions. Consequently, not all observed thermal events will be considered in the phase diagram calculations and database development. In sulphate-rich compositions, additional thermal effects - absent in [63] - can be attributed to phase equilibria involving sulphate-based solid solutions.

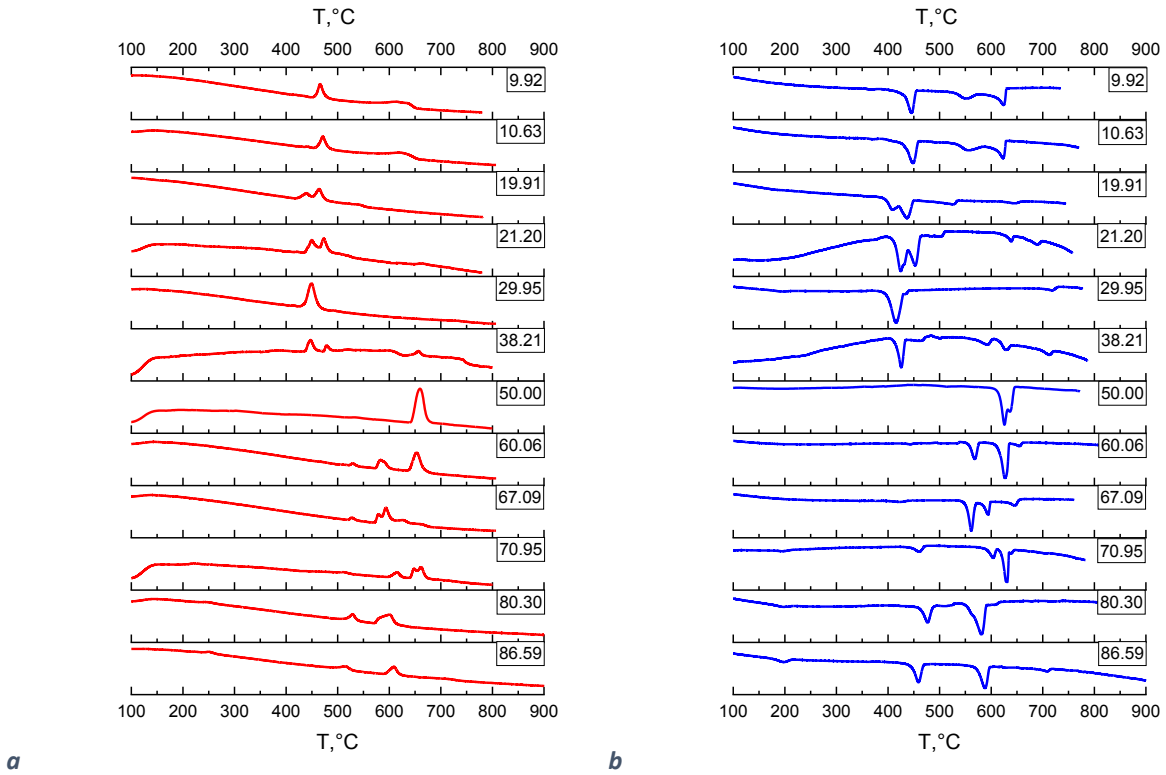


Figure 5-28 *DTA curves of $MgCl_2$-Na_2SO_4 mixtures, expressed in molar percentage of Na_2SO_4:* ***a*** *heating curves;* ***b*** *cooling curves.*

Table 5-15 *Experimental DTA values of phase transition temperatures (°C) in the $MgCl_2$-Na_2SO_4 system.*

Na_2SO_4 (mol)	Na_2SO_4 (wt%)	1st	2nd	3rd	4th	5th	6th
0	0	719					
0.0992	14.11	418	436	457	573 [a]	637	
0.1063	15.07	424	441	460	586 [a]	628 [a]	
0.1991	27.05	422	439	464	544	660 [a]	
0.2120	28.64	422	439	466	522	662	698 [a]
0.2995	38.94	414	449	494	729 [a]		
0.3821	47.99	438	479	518	602	654	721 [a]
0.5000	59.87	593	631	644			
0.6006	69.17	523	575	593	639	673	
0.6709	75.26	521	573	594	626	660	
0.7095	78.46	223	512	600	634 [a]	644 [a]	
0.8030	85.88	231	518	572	601	625	
0.8659	90.60	216	247	495	592	609	721
1	100	195	246	887			

[a] from cooling curves

5.3 Na^+, Ca^{2+} // Cl^-, SO_4^{2-} system

5.3.1 Na_2SO_4-$CaSO_4$

The experimental investigation of the binary Na_2SO_4-$CaSO_4$ system aimed to re-examine the phase diagram using differential thermal analysis, differential scanning calorimetry and high-temperature X-ray diffraction, addressing discrepancies in the literature and resolving disagreements regarding the existence of potential intermediate compounds in the system. It primarily focused on validating and gaining a deeper understanding of the intermediate compound $Na_6Ca(SO_4)_4$, previously proposed by Kobertz et al. [21]. Due to the lack of consensus in subsequent studies, the proposed intermediate compound and other selected compositions were synthesised.

5.3.1.1 XRD/HT-XRD

To acquire information on potential intermediate compounds through XRD and/or HT-XRD analysis, four Na_2SO_4-$CaSO_4$ mixtures (12.0, 25.0, 33.3, and 50.0 mol% $CaSO_4$) were synthesised *in situ* and subjected to XRD investigation. The preparation of the mixtures was carried out with particular care to ensure stoichiometric accuracy and homogeneity. The end-member compounds were combined in their respective molar ratios and subjected to a solid-state reaction procedure. Initially, the pure reagents were finely ground in an agate mortar inside a glovebox to avoid contamination and moisture uptake. The homogenised powders were then transferred into quartz ampoules, which were evacuated and sealed under vacuum using a hydrogen/oxygen flame. The sealed ampoules were subsequently heated in a high-temperature furnace at controlled conditions. Annealing was performed at temperatures below the melting point of the system - typically not exceeding 1000 °C - to prevent deformation or fracture of the quartz walls. After the heat treatment, the ampoules were opened inside the glovebox, and the partially reacted powders were recovered. The mixtures were

reground to further enhance homogeneity and then resealed in new quartz ampoules for additional annealing cycles. This iterative process of grinding, sealing, and annealing was repeated until satisfactory reaction progress was achieved. The thermal history proved to be a critical factor in obtaining the desired phase assemblages. X-ray diffraction analyses performed on intermediate products consistently revealed the coexistence of residual unreacted starting materials alongside newly formed compounds, highlighting the stepwise nature of the solid-state reaction pathway. These intermediate checks provided essential feedback to guide the subsequent synthesis steps and ensure the reliability of the final mixtures.

The Na_2SO_4(75 mol%)-$CaSO_4$(25 mol%) mixture, corresponding to the stoichiometry $Na_6Ca(SO_4)_4$, underwent a sequence of three thermal treatments, referred to as stages A, B, and C. During stage A, the sample was annealed at 800 °C for 60 hours, with a controlled heating rate of 5 K/min and subsequently cooled at the same rate. Stage B consisted of heating the mixture to 800 °C for 100 hours under identical heating and cooling conditions. The final stage C involved heating the sample to 900 °C for 72 hours at a rate of 5 K/min, followed by rapid quenching in air.

The mixture Na_2SO_4(66.7 mol%)-$CaSO_4$(33.3 mol%), corresponding to the stoichiometry $Na_4Ca(SO_4)_3$, was subjected to two distinct thermal stages. The first stage (labelled A) involved treatment at 800 °C for 72 hours, with heating and cooling rates maintained at 5 K/min. The subsequent stage, B, saw the sample annealed at 800 °C for 72 hours, employing the same heating and cooling parameters.

For the Na_2SO_4(50 mol%)-$CaSO_4$(50 mol%) mixture, the synthesis was carried out using two specific thermal steps. Initially, the sample was held at 900 °C for 60 hours with a ramp rate of 5 K/min. In the second stage, the mixture was annealed at 850 °C for 72 hours under controlled conditions, maintaining a consistent heating and cooling rate throughout.

Finally, the Na_2SO_4(88 mol%)-$CaSO_4$(12 mol%) mixture was synthesised using a two-step process to investigate the behaviour of a mixture with high Na_2SO_4 content and explore the potential presence of solid solutions within this compositional region. The initial step required annealing at 800 °C for 72 hours with a steady heating and cooling rate of 5 K/min. The subsequent stage employed treatment at 800 °C for 72 hours, ensuring thermal stability and uniformity throughout the process.

These precise thermal protocols, summarised in **Table 5-16**, allowed for the careful formation and analysis of the targeted mixtures, optimising phase stability and composition reproducibility.

Table 5-16 *Thermal treatment conditions of synthesis of Na_2SO_4(100-x mol%)-$CaSO_4$(x mol%).*

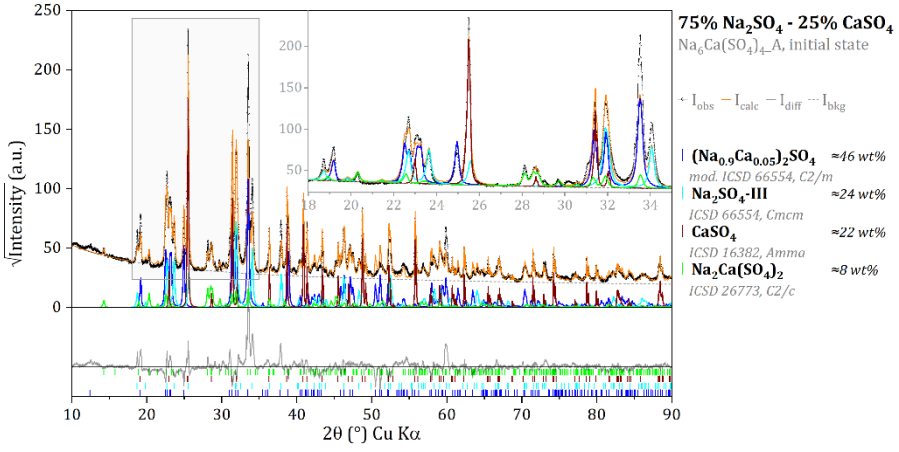
Composition	Thermal treatment (5 K/min)		
	A	B	C
Na_2SO_4(88 mol%)-$CaSO_4$(12 mol%)	800 °C; 72 h	800 °C; 72 h	
Na_2SO_4(75 mol%)-$CaSO_4$(25 mol%)	800 °C; 60 h	800 °C; 100 h	900 °C; 72 h *

i.e., $Na_6Ca(SO_4)_4$			
Na_2SO_4(67 mol%)-$CaSO_4$(33 mol%) i.e., $Na_4Ca(SO_4)_3$	800 °C; 72 h	800 °C; 72 h	
Na_2SO_4(50 mol%)-$CaSO_4$(50 mol%) i.e., $Na_2Ca(SO_4)_2$	900 °C; 60 h	850 °C; 72 h	

*quenched in air

5.3.1.1.1 RT-XRD

The initial experiments were conducted on the $Na_6Ca(SO_4)_4$ specimen to validate its existence, as supported by previous studies [126]. This hypothesis could be motivated by the presence of $Na_6Mg(SO_4)_4$ in Na_2SO_4-$MgSO_4$ system, considering that Mg and Ca belong to the same group of alkaline earth metals, and similarities in their phase diagrams could therefore be expected. The predominant phase identified was $(Na_{0.9}Ca_{0.05})_2SO_4$, which, as previously mentioned, corresponds to a monoclinic distorted Na_2SO_4-III structure (Na_2SO_4(MT)) with a β angle slightly above 90° (**Figure 5-29**). Although the lattice parameters and space group are listed in the ICDD database [263], the actual structure remains unpublished. The orthorhombic Na_2SO_4-III structure (ICSD 66554) was adjusted to fit the monoclinic symmetry using the reported lattice parameters, while keeping the atomic coordinates unchanged. This modification yielded a reasonably good match with the measured data, enabling a rough quantification with an estimated relative error of 10-20%. Additionally, $Na_2Ca(SO_4)_2$ was identified as a secondary intermediate phase. The lattice parameters and relative amounts of identified phases are summarised in **Table 5-17** and **Table 5-19**. From specimen A to C, the initially persistent amounts of pure compounds in A, indicating incomplete formation of the intended phases, gradually decreased, demonstrating the progressive formation of the desired mixture. However, an unidentified secondary phase appeared, with reflections at 12.4° and 21.9° 2θ (**Figure 5-29**). Discrepancies between calculated and observed intensities, particularly for $Na_4Ca(SO_4)_3$, suggested that deviations could be attributed to differences in the structural model versus the actual structure, such as atomic positions, thereby impacting the accuracy of the quantification.



a

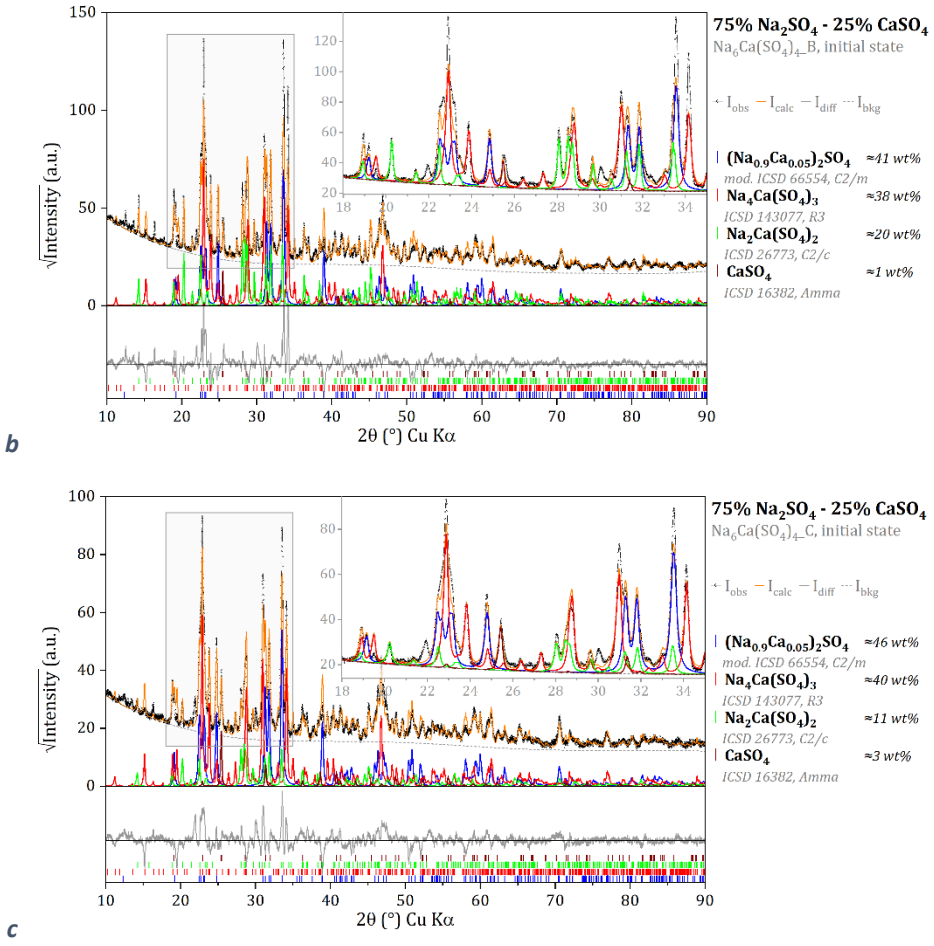


Figure 5-29 *X-ray diffractogram of Na_2SO_4(75 mol%)-$CaSO_4$(25 mol%), i.e., $Na_6Ca(SO_4)_4$ mixture:* ***a*** *$Na_6Ca(SO_4)_4$ A (T=800°C t=60h);* ***b*** *$Na_6Ca(SO_4)_4$ B (T=800°C t=100h);* ***c*** *$Na_6Ca(SO_4)_4$ C (T=900°C t=72h).*

Table 5-17 *Lattice parameters of identified phases in $Na_6Ca(SO_4)_4$ A, B, C.*

$Na_6Ca(SO_4)_4$ A								
Phase	**Na_2SO_4:$CaSO_4$**	**ICSD**	**wt%**	**SG**	**a (Å)**	**b (Å)**	**c (Å)**	**β (°)**
$CaSO_4$	0:1	16382	22	Amma	7.001	6.994	6.240	
Na_2SO_4-III	1:0	66554	24	Cmcm	5.598	8.963	6.974	
$Na_2Ca(SO_4)_2$	1:1	26773	8	C2/c	10.154	8.297	8.526	112.26
$(Na_{0.9}Ca_{0.05})_2SO_4$	9:1	66554, mod.	46	C2/m	9.286	5.349	7.156	91.99
$Na_6Ca(SO_4)_4$ B								
Phase	**Na_2SO_4:$CaSO_4$**	**ICSD**	**wt%**	**SG**	**a (Å)**	**b (Å)**	**c (Å)**	**β (°)**
$CaSO_4$	0:1	16382	2	Amma	7.002	6.993	6.241	
$Na_2Ca(SO_4)_2$	1:1	26773	29	C2/c	10.148	8.307	8.544	112.32
$Na_4Ca(SO_4)_3$	2:1	143077	36	R3	15.756		22.387	
$(Na_{0.9}Ca_{0.05})_2SO_4$	9:1	66554, mod.	41	C2/m	9.262	5.338	7.177	91.90
$Na_6Ca(SO_4)_4$ C								
Phase	**Na_2SO_4:$CaSO_4$**	**ICSD**	**wt%**	**SG**	**a (Å)**	**b (Å)**	**c (Å)**	**β (°)**
$CaSO_4$	0:1	16382	3	Amma	7.002	6.993	6.241	
$Na_2Ca(SO_4)_2$	1:1	26773	11	C2/c	10.150	8.307	8.519	112.23
$Na_4Ca(SO_4)_3$	2:1	143077	40	R3	15.748		22.372	
$(Na_{0.9}Ca_{0.05})_2SO_4$	9:1	66554, mod.	46	C2/m	9.265	5.336	7.178	91.90

The predominant presence of $Na_4Ca(SO_4)_3$, presumably corresponding to dobrovolskyite [132], prompted the synthesis of a 2:1 mixture for comparative XRD analysis against the 3:1 mixture.

The corresponding X-ray diffractograms are displayed in **Figure 5-30**, with the lattice parameters listed in **Table 5-18**, The experimental results are not sufficient to either confirm or refute the presence of the 3:1 compound, nor to definitively establish the existence of the 2:1 compound.

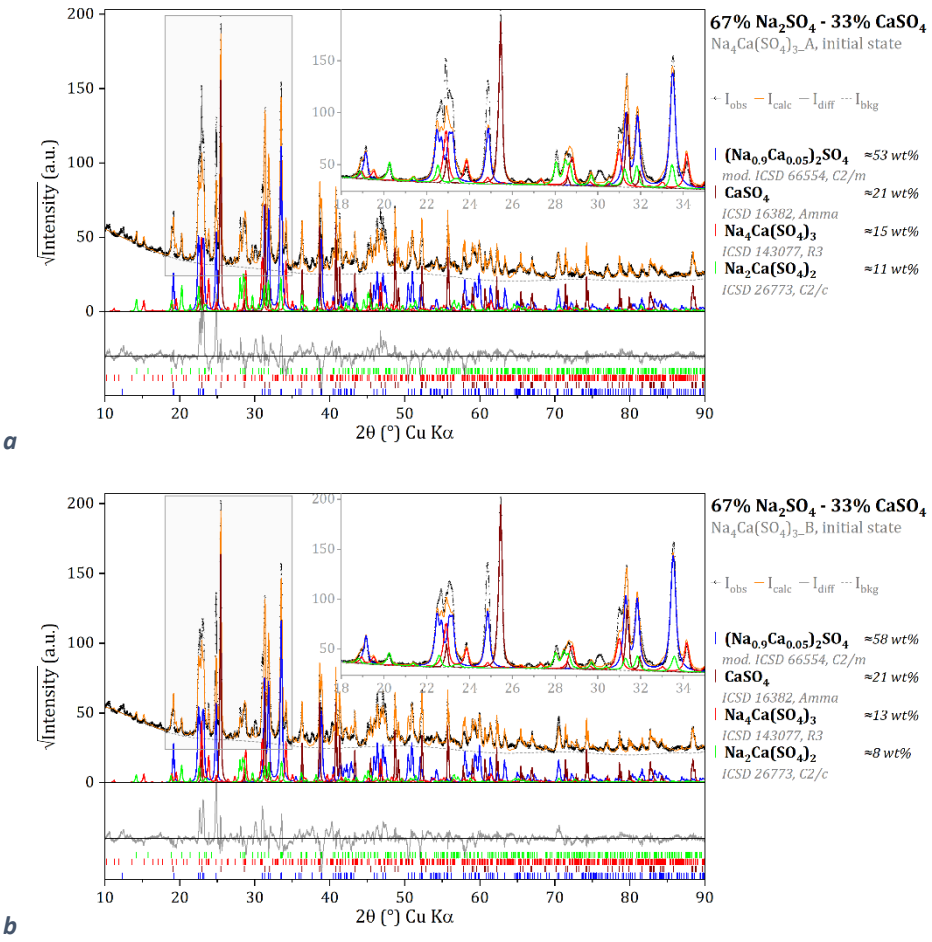


Figure 5-30 *X-ray diffractogram of Na_2SO_4(67 mol%)-$CaSO_4$(33 mol%), i.e., $Na_4Ca(SO_4)_3$ mixture:* ***a*** *$Na_4Ca(SO_4)_3$ A (T=800°C t=72h);* ***b*** *$Na_4Ca(SO_4)_3$ B (T=800°C t=72h).*

Table 5-18 *Lattice parameters of identified phases in $Na_4Ca(SO_4)_3$ A, B.*

$Na_4Ca(SO_4)_3$ A								
Phase	**Na_2SO_4:$CaSO_4$**	**ICSD**	**wt%**	**SG**	**a (Å)**	**b (Å)**	**c (Å)**	**β (°)**
$CaSO_4$	0:1	16382	21	Amma	7.000	6.993	6.241	
$Na_2Ca(SO_4)_2$	1:1	26773	11	C2/c	10.155	8.308	8.531	112.33
$Na_4Ca(SO_4)_3$	2:1	143077	15	R3	15.745		22.369	
$(Na_{0.9}Ca_{0.05})_2SO_4$	9:1	66554, mod.	53	C2/m	9.279	5.343	7.164	91.97
$Na_4Ca(SO_4)_3$ B								
Phase	**Na_2SO_4:$CaSO_4$**	**ICSD**	**wt%**	**SG**	**a (Å)**	**b (Å)**	**c (Å)**	**β (°)**
$CaSO_4$	0:1	16382	21	Amma	7.000	6.994	6.242	
$Na_2Ca(SO_4)_2$	1:1	26773	8	C2/c	10.185	8.310	8.500	112.20
$Na_4Ca(SO_4)_3$	2:1	143077	13	R3	15.744		22.367	
$(Na_{0.9}Ca_{0.05})_2SO_4$	9:1	66554, mod.	58	C2/m	9.273	5.340	7.169	91.94

XRD measurements on Na_2SO_4(88 mol%)-$CaSO_4$(12 mol%) mixture additionally show the diffraction pattern of $Na_2Ca(SO_4)_2$ (in red, **Figure 5-31**). The reflection near 20° 2θ together with the

three reflections near 28° 2θ are characteristic for this phase even with low content as overlapping with other phases is less severe.

For the secondary phase $Na_4Ca(SO_4)_3$, observed in Na_2SO_4(50 mol%)-$CaSO_4$(50 mol%) mixture (in green, **Figure 5-32**), the two reflections near 24° 2θ and 34° 2θ are characteristic and rarely overlapped. The 2θ range from 18° to 35° used in the insets will also be used for the 3D surface plots of the HT-XRD experiments in this work. The identification of all above mentioned phases is relatively easy in this range and peak overlapping is less severe.

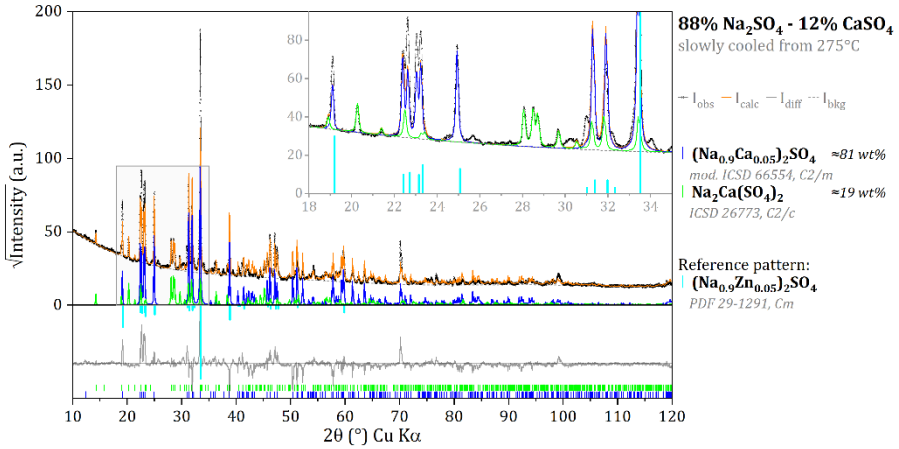


Figure 5-31 *X-ray diffractogram of Na_2SO_4(88 mol%)-$CaSO_4$(12 mol%) mixture at room temperature.*

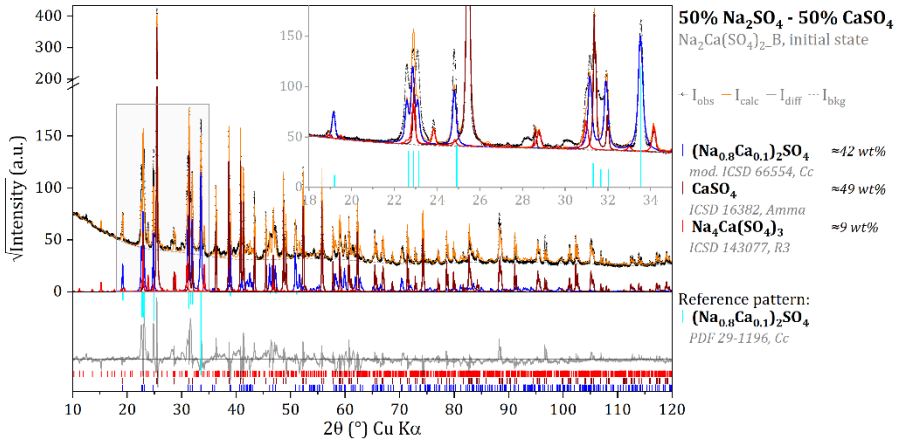


Figure 5-32 *X-ray diffractogram of Na_2SO_4(50 mol%)-$CaSO_4$(50 mol%) mixture at room temperature.*

5.3.1.1.2 HT-XRD

The results of high-temperature X-ray diffraction measurements for the samples Na_2SO_4(100-x mol%)-$CaSO_4$(x mol%) with x = 12, 25 and 50 are presented, providing an evaluation of the phases present and a semi-quantitative analysis. Specifically, 3D surface plots with projections are used to

visualise the data. The Bragg reflections of the hexagonal high temperature solid solution phase Na_2SO_4-I are marked with ◆ and the according hkl index. On cooling, this phase transforms to the monoclinic $(Na_{0.9}Ca_{0.05})_2SO_4$ solid solution phase or $(Na_{0.8}Ca_{0.1})_2SO_4$ solid solution phase or a mixture of both (apparently depending on cooling conditions). The hexagonal 101 and 102 reflections split then into three to four reflections. The reflections of the monoclinic phase are marked with I. For other phases, only the strongest reflections with low peak overlapping are marked as follows: $Na_2Ca(SO_4)_2$ with ◆, $Na_4Ca(SO_4)_3$ with ◆, Na_2SO_4-III with ◆ and $CaSO_4$ with ◆.

The mixture Na_2SO_4(75 mol%)-$CaSO_4$(25 mol%), here indicated as $Na_6Ca(SO_4)_4$ C, was analysed by XRD at high temperature. Two cycles of heating from 25 °C to 400 °C and cooling to 25 °C were performed in synthetic air with 2 K/min heating/cooling rate between XRD measurements. **Figure 5-33** presents the high-temperature X-ray diffraction pattern as an overall dataset, whereas **Figure A 20** displays the diffraction patterns corresponding to the individual steps of the heating and cooling cycles. Fast scans (2 min overall) were performed at 5 K intervals, long scans (1 hour overall) at 50 K intervals. Between scans, a heating/cooling rate of 2 K/min was applied, which, taking in account short scans, resulted in a rate of 1 K/min and a dwell time of 1 hour every 50 K. The sample $Na_6Ca(SO_4)_4$ C initially consisted of the monoclinic $(Na_{0.8}Ca_{0.1})_2SO_4$ solid solution phase, $Na_4Ca(SO_4)_3$, $Na_2Ca(SO_4)_2$, $CaSO_4$ and a small amount of Cristobalite (SiO_2, residual of a quartz ampoule, marked with ◆). The Cristobalite transformation from the cubic β high temperature modification to tetragonal α takes place at similar temperature as the transformation of hexagonal to monoclinic solid solution phase. $Na_4Ca(SO_4)_3$ was observed in several samples after synthesis. In HT-XRD experiments, it disappeared upon heating during the transformation of monoclinic to hexagonal solid solution phase and did not reappear. The room temperature stable phase Na_2SO_4-V (Na-LT, Thenardite, space group Fddd, ICSD 81506) was occasionally formed after exposure to ambient air for several days (not shown here).

In order to find regular kinetic effects, variations in cooling rates and prolonged annealing times at certain temperature were applied in later experiments.

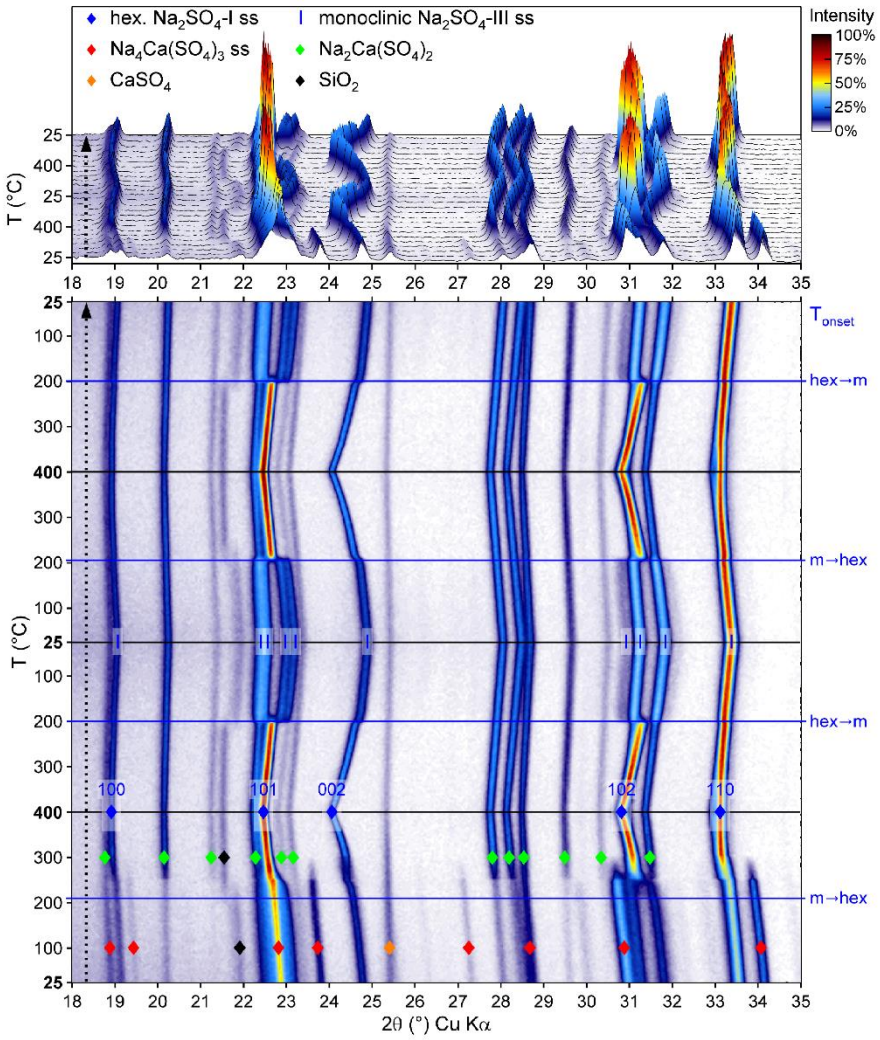
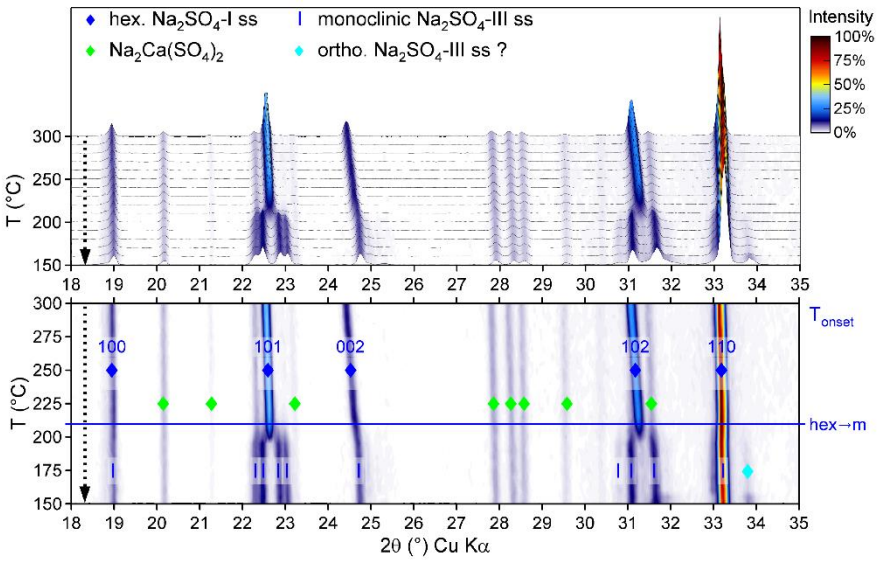


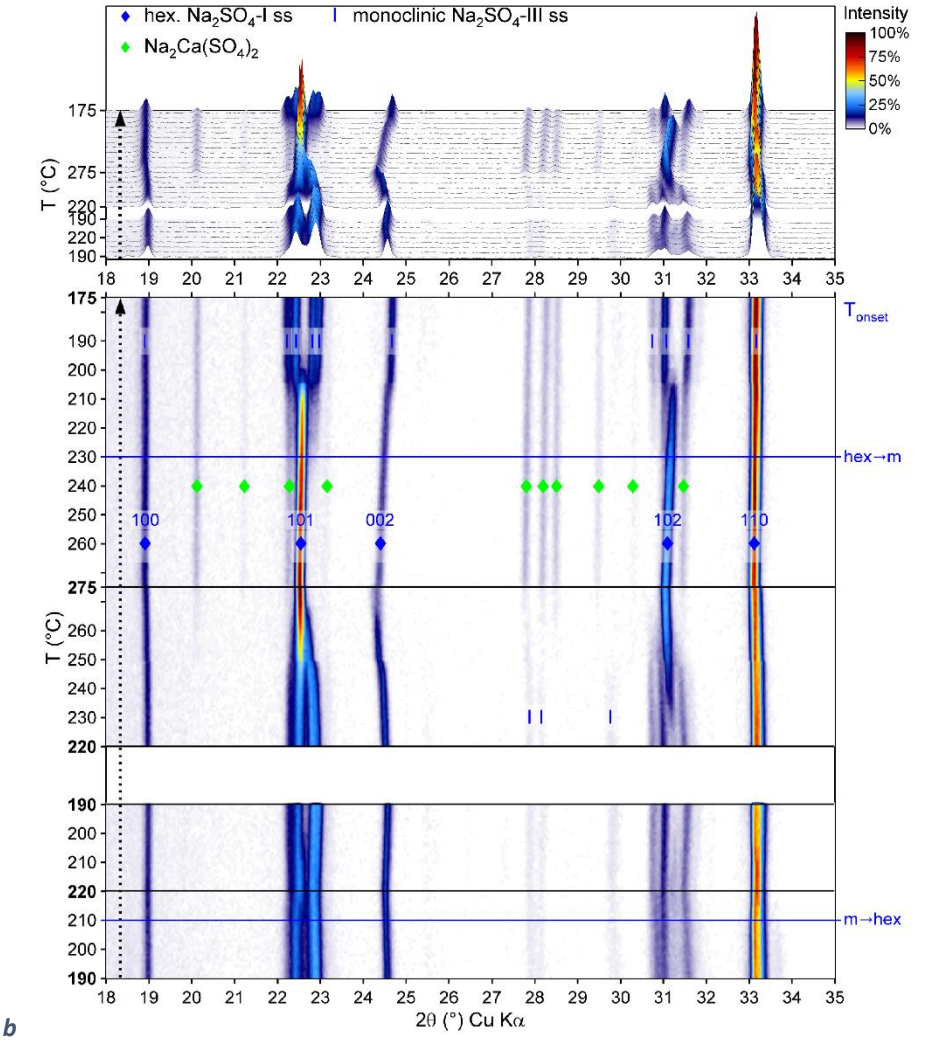
Figure 5-33 *High temperature X-ray diffractogram of Na_2SO_4(75 mol%)-$CaSO_4$(25 mol%), i.e., $Na_6Ca(SO_4)_3$ mixture.*

The mixture Na_2SO_4(88 mol%)-$CaSO_4$(12 mol%) was subjected to four HT-XRD experiments, and the corresponding diffraction patterns are presented in **Figure 5-34**. The first high temperature experiment (HT1) was performed under high vacuum. After annealing at 300 °C for 5 h, the sample was cooled to 150 °C with approximately 1 K/min and 1 hour annealing (long scans) in 25 K intervals. The atmosphere was switched to synthetic air before cooling to 25 °C. The second experiment (HT2) was a quenching test. The sample was cooled fast from 500 °C to 70 °C and heated to 175 °C without measurements. The achieved average cooling rates were 30 K/min from 500 °C to 200 °C and 10 K/min from 200 °C to 100 °C. No changes were observed in the sample during 10 h of annealing at 175 °C under continuous monitoring. The phase assemblage consisted of approximately equal amounts of the two monoclinic solid phases, $(Na_{0.9}Ca_{0.05})_2SO_4$ and $(Na_{0.8}Ca_{0.1})_2SO_4$, together with a minor fraction of Na_2SO_4-III, which remains questionable. The sample was subsequently homogenised, reheated to 175 °C under vacuum, and maintained at this temperature in synthetic air for five days, yet no further

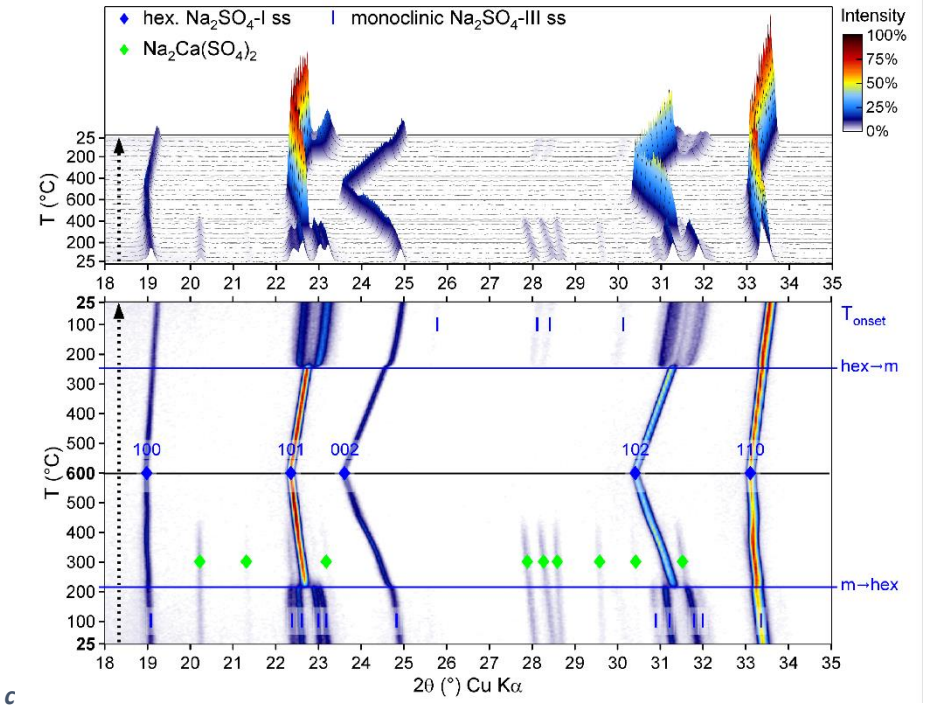
transformations were detected. The subsequent set of experiments (HT3a-3d) was focused to investigate the phase behaviour around the hexagonal to monoclinic transition. In the first stage (HT3a), the sample was heated to 220 °C and cooled to 190 °C at a rate of 0.25 K/min, with 1 h annealing at 5 K intervals. Under these conditions, the amount of $(Na_{0.9}Ca_{0.05})_2SO_4$ increased at cost of $(Na_{0.8}Ca_{0.1})_2SO_4$. Although the beginning formation of the hexagonal solid solution phase was already observed at 225 °C in experiment HT3bc (0.25 K/min heating and 1 hour annealing at 250 °C), the monoclinic low temperature solid solution phase was still detectable up to 260 °C. Around this point the formation of $Na_2Ca(SO_4)_2$ started. Experiment HT3d involved the slow cooling from 275 °C to 150 °C (0.25 K/min cooling rate, with 1 h annealing at 250 °C, 225 °C, 205 °C, 200 °C, 195 °C, 190 °C, 175 °C, and 150 °C). Under these conditions, the reappearance of $(Na_{0.8}Ca_{0.1})_2SO_4$ was suppressed. The hexagonal Na_2SO_4-I transformed only to $(Na_{0.9}Ca_{0.05})_2SO_4$, and no change in the content of $Na_2Ca(SO_4)_2$ was observed. During the experiment HT4 the sample was heated from 25 °C to 600 °C and cooled to 25 °C in order to investigate the stability range of $Na_2Ca(SO_4)_2$. During heating (HT4a, 0.8 K/min heating rate, without annealing) $Na_2Ca(SO_4)_2$ disappeared at around 440 °C. However, upon cooling to 25 °C (HT4b, 1 K/min cooling rate, 1 hour annealing at 50 K intervals) $Na_2Ca(SO_4)_2$ did not re-form. The hexagonal Na_2SO_4-I transformed to approximately equal amounts of $(Na_{0.9}Ca_{0.05})_2SO_4$ and $(Na_{0.8}Ca_{0.1})_2SO_4$.



a



b



c

Figure 5-34 *High temperature X-ray diffractogram of Na_2SO_4(88 mol%)-$CaSO_4$(12 mol%) mixture:* ***a*** *HT1 from 300 °C to 150 °C;* ***b*** *HT3 (190→220→190→220→275→175 °C);* ***c*** *HT4 from 25 °C to 600 °C and back to 25 °C.*

The mixture Na_2SO_4(50 mol%)-$CaSO_4$(50 mol%) was subjected to HT-XRD analysis, with the corresponding 3D plots shown in **Figure 5-35** (and in **Figure A 21**). Although, $Na_2Ca(SO_4)_2$ was the intended targeted phase, it was absent in the initial state of the sample. Its first appearance was observed during experiment HT1 (25 °C → 600 °C → 25 °C, 0.8 K/min heating/cooling rate, 1 h annealing at 50 K intervals, 2 h annealing at 600 °C), where $Na_2Ca(SO_4)_2$ began to form upon heating at approximately 250 °C, concomitant with the formation of the Na_2SO_4-I solid solution. However, no re-formation of $Na_2Ca(SO_4)_2$ was detected during subsequent cooling. A small amount was again observed on reheating to 400 °C. The sample was kept then for 3 days at 400 °C and 4 days at 300 °C (HT2). Under these conditions, the $Na_2Ca(SO_4)_2$ content gradually increased and reached 21 wt%, alongside 44 wt% Na_2SO_4-I and 36 wt% $CaSO_4$.

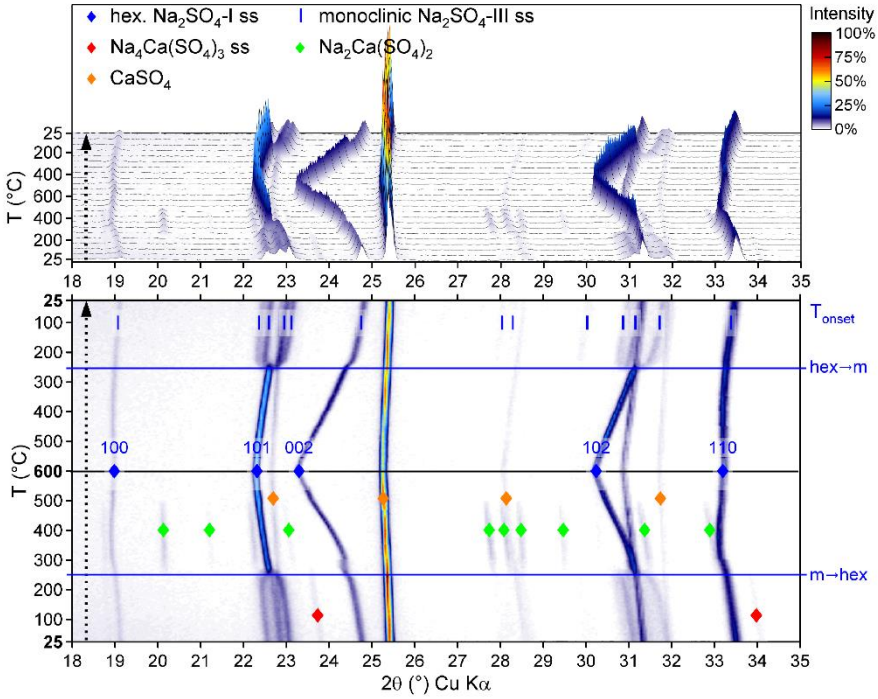


Figure 5-35 *High temperature X-ray diffractogram of Na_2SO_4(50 mol%)-$CaSO_4$(50 mol%) mixture.*

The high-temperature experiments conducted revealed the monoclinic-to-hexagonal phase transition [$(Na_{0.9}Ca_{0.05})_2SO_4$ / $(Na_{0.8}Ca_{0.1})_2SO_4$ ⇆ Na_2SO_4-I] at the onset temperatures specified below for the respective compositions analysed. These values are summarised in **Table 5-19**, corresponding to the different thermal cycles or measurements performed. For the Na_2SO_4(75 mol%)-$CaSO_4$(25 mol%) C sample, during the first heating cycle from 25 °C to 400 °C, the onset temperature was recorded at 225 °C, while during the cooling cycle, it was observed at 200 °C. In the second cycle, also from 25 °C to 400 °C, the onset temperature was noted at 215 °C during heating and 185 °C during cooling. For the composition Na_2SO_4(88 mol%)-$CaSO_4$(12 mol%), multiple cycles were performed. In

the first cycle (HT1), during cooling from 300 °C to 150 °C, the onset temperature was recorded as 210 °C. In the subsequent measurement (HT3abc), consisting of an initial heating from 190 °C to 220 °C, followed by cooling from 220 °C to 190 °C and a final heating from 190 °C to 275 °C, the onset temperature was again detected at 210 °C, with the monoclinic solid solution phase detectable up to 260 °C. In measurement HT3d, during cooling from 275 °C to 150 °C, the onset temperature was 230 °C. In this case, no significant increase in the monoclinic solid solution was observed during annealing for 1 hour at 225 °C; however, a marked increase was noted during annealing for 1 hour at 205 °C. This finding raises questions about the existence of a two-phase region, warranting further investigation. In measurement HT4a, during heating from 25 °C to 600 °C, the onset temperature was recorded at 210 °C, while during cooling, it was observed at 245 °C. No phases other than the monoclinic and hexagonal solid solutions were detected in this experiment. In the final high-temperature measurement on the Na_2SO_4(50 mol%)-$CaSO_4$(50 mol%) composition, performed from 25 °C to 600 °C, the onset temperature during heating was 250 °C, while during cooling it was 260 °C. However, the onset temperature during heating was challenging to determine due to peak overlap with $CaSO_4$. These observations underline the variability in phase transitions and suggest complexities in the phase behaviour, particularly regarding the potential presence of a two-phase region that merits further exploration.

Table 5-19 *Onset temperatures of the monoclinic/hexagonal phase transition.*

Composition	Experiment conditions		T_{onset} (°C)
Na_2SO_4(75 mol%)-$CaSO_4$(25 mol%) C	HT1, Cycle 1	25 °C → 400 °C	210
	HT1, Cycle 1	400 °C → 25 °C	200
	HT1, Cycle 2	25 °C → 400 °C	205
	HT1, Cycle 2	400 °C → 25 °C	200
Na_2SO_4(88 mol%)-$CaSO_4$(12 mol%)	HT1	300 °C → 150 °C	210
	HT3abc	190 °C → 220 °C → 190 °C → 275 °C	210
	HT3d	275 °C → 150 °C	230
	HT4a	25 °C → 600 °C	210
	HT4b	600 °C → 25 °C	245
Na_2SO_4(50 mol%)-$CaSO_4$(50 mol%) B	HT1	25 °C → 600 °C	250
	HT1	600 °C → 25 °C	260

To elucidate the crystallographic phases identified across the various experiments conducted and to better interpret the results of XRD measurements performed at either room temperature or high temperatures, a recap of the pure compounds and solid solution phases - previously characterised in the literature [122, 126, 130, 131] and/or determined through internal analysis - are listed below:

- Na_2SO_4-V, known as Thenardite, is the low-temperature modification (Na_2SO_4(LT)) which is stable up to 473 K in pure Na_2SO_4. The phase was only observed after exposing the two samples

"$Na_6Ca(SO_4)_4$ C" (initial state) and "$Na_6Ca(SO_4)_4$ C" (after HT-XRD) for several days to ambient air. It did not occur in sample "Na_2SO_4(88 mol%)-$CaSO_4$(12 mol%)" (initial state) during storage at room temperature and ambient air for one month. In Freyer et al. [122, 130], Na_2SO_4-V and $Na_2Ca(SO_4)_2$ were considered the stable Na-rich phases at room temperature, proved by storing over several months.

- Na_2SO_4-I, hexagonal high temperature solid solution phase (Na_2SO_4(HT)). As demonstrated by Eysel [131] for Na_2SO_4-$NiSO_4$ and Na_2SO_4-$Y_2(SO_4)_3$, the lattice parameters change with increasing Ca content to smaller *a* and larger *c* at constant temperature. This effect can be easily recognised in the 3D surface plots presented above by following the shift of the 002 reflection (23°-25° 2θ) and the 110 reflection (33°-34° 2θ) when the Na-Ca ratio in Na_2SO_4-I changes, for example due to formation or decomposition of $Na_2Ca(SO_4)_2$ (**Figure 5-33** and **Figure 5-34**).
- β-$CaSO_4$, known as Anhydrite (ICSD 16382: space group Amma, a = 7.006 Å, b = 6.998 Å, c = 6.245 Å).
- $Na_2Ca(SO_4)_2$, known as Glauberite (ICSD 26773: a = 10.158 Å, b = 8.333 Å, c = 8.551 Å, β = 112.33°). $Na_2Ca(SO_4)_2$ was found in all samples in initial state, but astonishingly not in "Na_2SO_4(50 mol%)-$CaSO_4$(50 mol%) B", where it was the targeted phase, but it was only 8 wt% in "Na_2SO_4(50 mol%)-$CaSO_4$(50 mol%) A".

Solid solution phases $(Na_{1-x}Ca_{x/2})_2SO_4$ (0<x<0.5) are listed as follows:

- $Na_4Ca(SO_4)_3$. The crystal structure was published by Shablinskii et al. [132] (ICSD 143077, space group R3, a = 15.7278 Å, c = 22.0037 Å). It corresponds to an idealised composition of a mineral with the actual composition $(Na_{3.90}K_{0.10})(Ca_{0.45}Mg_{0.16}Cu_{0.12}Na_{0.10})(SO_4)_3$. In Freyer et al. [122] the solid solution phase was called "solid solution C" with 0.32<x<0.4. Experimentally, it was found in all samples tested in the initial state with the exception of "$Na_6Ca(SO_4)_4$ A" and "Na_2SO_4(88 mol%)-$CaSO_4$(12 mol%)". The phase disappeared after heating to around 250 °C with the formation of the hexagonal Na_2SO_4-I solid solution phase and $Na_2Ca(SO_3)_2$ and was never formed during a HT-XRD experiment.
- $(Na_{0.98}Ca_{0.02})_2SO_4$. The phase has the structure of Na_2SO_4-III (orthorhombic, space group Cmcm), and considered stable between 473 K and 503 K in pure Na_2SO_4 (ICSD 66554: a = 5.6274 Å, b = 8.9664 Å, c = 6.9737 Å at 298 K). It was found in "$Na_6Ca(SO_4)_4$ A" (**Figure 5-29a**) and "Na_2SO_4(88 mol%)-$CaSO_4$(12 mol%)" in initial state as secondary phase. In Freyer et al. [122] the solid solution phase was called "solid solution A" with 0<x<0.04, corresponding to stabilised Na_2SO_4-III. It could also be present in "Na_2SO_4(88 mol%)-$CaSO_4$(12 mol%)" after high temperature-XRD (HT1) (slowly cooled from 300 °C) and after quenching from 500 °C (HT2), but more likely in a different structural modification, as some diffraction peaks were missing (**Figure 5-34**).

- $(Na_{0.9}Ca_{0.05})_2SO_4$. In Eysel et al.'s study [131], it was reported a monoclinic distorted Na_2SO_4-III with a = 9.27 Å, b = 5.35 Å, c = 7.12 Å and β = 92.4° (values shown only for Zn stabilised, but reported with Zn^{2+}, Ca^{2+} and Y^{3+}). The phase was probably present in all samples below 200 °C and was often the phase with the highest content. A monoclinic structural model has been made based on the orthorhombic Na_2SO_4-III, which described most observed reflections quite well. But additional reflections, mostly very week, were measured. Therefore, it was probably not just a simple monoclinic distortion. Quantifications using the Rietveld method are based on this imperfect model.
- $(Na_{0.8}Ca_{0.1})_2SO_4$. In Eysel et al.'s work [131], it was reported a monoclinic distorted Na_2SO_4-III with a = 9.25 Å, b = 5.34 Å, c = 7.13 Å and α = 91.4° (if $CaSO_4$ > 9 mol%. For the standardised crystallographic setting with β instead of α being the monoclinic angle, the axes a and b have to be switched: a = 5.34 Å, b = 9.25 Å, c = 7.13 Å, β = 91.7°). A relatively high content was observed in "Na_2SO_4(88 mol%)-$CaSO_4$(12 mol%)" after quenching (**Figure 5-34**) and "Na_2SO_4(50 mol%)-$CaSO_4$(50 mol%) B" (**Figure 5-35**). It seems to form only with higher cooling rates and could be present in most samples in initial state as secondary phase besides $(Na_{0.9}Ca_{0.05})_2SO_4$. A transformation to $(Na_{0.9}Ca_{0.05})_2SO_4$ and $Na_2Ca(SO_4)_2$ has been observed several times during slowly cooling or annealing around 200 °C.

In the study of Freyer et al. [122] no differentiation between $(Na_{0.9}Ca_{0.05})_2SO_4$ and $(Na_{0.8}Ca_{0.1})_2SO_4$ has been made, although referring to the Eysel et al.'s work [131]. The phase was named as "solid solution B" with 0.04<x<0.2 [122], or also called as stabilised Na_2SO_4-I with monoclinic lattice, which is misleading. The exact crystal structures of the solid solution phases $(Na_{0.9}Ca_{0.05})_2SO_4$ and $(Na_{0.8}Ca_{0.1})_2SO_4$ are unknown. During the investigations, both phases never occurred as a single phase. $(Na_{0.9}Ca_{0.05})_2SO_4$ occurred as main phase together with a small amount of $Na_2Ca(SO_4)_2$ and only moderate peak overlapping in sample "Na_2SO_4(88 mol%)-$CaSO_4$(12 mol%)" after experiment at high temperature (HT3d. **Figure 5-34**). A Pawley fit with a monoclinic distorted unit cell of Na_2SO_4-III as suggested by Eysel et al. [131] (PDF 29-1291), with the approximate lattice parameters a = 9.3 Å, b = 5.4 Å, c = 7.1 Å and β = 92°, matched well with measurement, as shown in (**Figure 5-31**). However, some weak measured reflections, which were always accompanied with this phase, were not explained. This could be an additional unknown secondary phase. However, as the intensity ratio of the explained (by Pawley fit) and unexplained reflections appears at least similar in several measurements, it seems more likely that they all belong to the same phase. An explanation could be an incommensurable modulated structure with monoclinic distorted Na_2SO_4-III being the average structure, similar to the structurally related Na_2CO_3 with β-Na_2CO_3 (space group C2/m, a ≈ 9.0 Å, b ≈ 5.2 Å, c ≈ 6.3 Å, β ≈ 98°. ICSD 80988) being the average structure of the incommensurable modulated

γ-Na_2CO_3 (C2/m(α0γ)0s) [40]. Testing for possible space groups led to the following three possibilities: C2 (5), Cm (8) and C2/m (12). Eysel et al. [131] suggested Cm and, as mentioned above, the structurally related β-Na_2CO_3 adopts the C2/m space group. Even more difficult to verify was the $(Na_{0.8}Ca_{0.1})_2SO_4$ solid solution phase as there was only one experiment (Na_2SO_4(50 mol%)-$CaSO_4$(50 mol%) B, initial state (**Figure 5-32**)), where it was observed without or with only a low amount of $(Na_{0.9}Ca_{0.05})_2SO_4$. Unfortunately, its reflections were partly overlapped by $CaSO_4$. $(Na_{0.8}Ca_{0.1})_2SO_4$ and $CaSO_4$ have comparable amounts, plus a minor amount of $Na_4Ca(SO_4)_3$. The Pawley fit with a metric of the unit cell as suggested by Eysel et al. [131] leaves unexplained reflection similar to the Pawley fit of $(Na_{0.9}Ca_{0.05})_2SO_4$. An incommensurable modulated structure might be a possible explanation again. Both phases can be distinguished by some small differences in their diffraction patterns due to their different monoclinic angles. For example $(Na_{0.9}Ca_{0.05})_2SO_4$ forms a group of four peaks between 22° and 24° 2θ. Whereas, $(Na_{0.8}Ca_{0.1})_2SO_4$ has only three peaks at that position.

A summary of the semi-quantitative evaluation of the phases identified in the experiments, conducted at either room temperature or high temperature is provided in **Table 5-20**, with estimated weight percentage ranges. While the values offer a useful approximation, they remain subject to potential uncertainties.

Table 5-20 *Semiquantitative evaluation of investigated samples.*

Sample	Conditions	Na_2SO_4-III	$(Na_{0.9}Ca_{0.05})_2SO_4$	$(Na_{0.8}Ca_{0.1})_2SO_4$	$Na_4Ca(SO_4)_3$	$Na_2Ca(SO_4)_2$	$CaSO_4$
Na_2SO_4(75mol%)-$CaSO_4$(25mol%) or $Na_6Ca(SO_4)_4$ A	RT	+	+	?		--	+
Na_2SO_4(75mol%)-$CaSO_4$(25mol%) or $Na_6Ca(SO_4)_4$ B	RT		+	?	+	+	--
Na_2SO_4(75mol%)-$CaSO_4$(25mol%) or $Na_6Ca(SO_4)_4$ C	RT		++	?	+	-	--
Na_2SO_4(67mol%)-$CaSO_4$(33mol%) or $Na_4Ca(SO_4)_3$ A	RT		++	?	-	-	+
Na_2SO_4(67mol%)-$CaSO_4$(33mol%) or $Na_4Ca(SO_4)_3$ B	RT		++	?	-	-	+
Na_2SO_4(75mol%)–$CaSO_4$(25mol%) or $Na_6Ca(SO_4)_4$ C	initial state 25 °C		++	?	+	-	--
Na_2SO_4(75mol%)-$CaSO_4$(25mol%) or $Na_6Ca(SO_4)_4$ C	final state 25 °C, after two cycles with T_{max}=400 °C		+			+	--
Na_2SO_4(88mol%)-$CaSO_4$(12mol%)	initial state 25 °C	-	+++	?		--	
Na_2SO_4(88mol%)-$CaSO_4$(12mol%)	150 °C / vacuum, slowly cooled from 300 °C	--?	+++			+	
Na_2SO_4(88mol%)-$CaSO_4$(12mol%)	25 °C / synthetic air	-?	+++			-	
Na_2SO_4(88mol%)-$CaSO_4$(12mol%)	175 °C, fast cooled from 500 °C to 70 °C	--?	++	++			

Na_2SO_4(88mol%)-$CaSO_4$(12mol%)	Slowly cooled from 275 °C to 150 °C		+++			+	
Na_2SO_4(88mol%)-$CaSO_4$(12mol%)	Slowly cooled from 600 °C to 25 °C		++	++			
Na_2SO_4(50mol%)-$CaSO_4$(50mol%) A	Initial state		-	?	-	--	++
Na_2SO_4(50mol%)-$CaSO_4$(50mol%) B	Initial state			++	--		++
Na_2SO_4(50mol%)-$CaSO_4$(50mol%) B	Slowly heated to 600 °C, slowly cooled to 25 °C		++	?			++

"--" <10 wt%; "-" =10 wt%; "+" =20-40 wt%; "++" =40-60 wt%; "+++" >60 wt%; "?" phase identification questionable

The quantifications are made utilising the Rietveld method which requires the crystal structure of each phase. As already mentioned, the actual crystal structures of $(Na_{0.9}Ca_{0.05})_2SO_4$ and $(Na_{0.8}Ca_{0.1})_2SO_4$ are not known, but are assumed [131] to be monoclinic distorted Na_2SO_4-III (Na_2SO_4-MT). Therefore, the crystal structure of the orthorhombic Na_2SO_4-III (ICSD 66554) was adapted to monoclinic symmetry without changing atomic positions or site occupancies, as the low data quality due to overlaps with other phases does not allow it. This imperfect structural model matches the measured data well enough to enable an at least semiquantitative evaluation.

A question mark in the $(Na_{0.8}Ca_{0.1})_2SO_4$ column of **Table 5-20** indicates that it might be present together with a larger amount of $(Na_{0.9}Ca_{0.05})_2SO_4$, but peak overlapping prevents a proper identification. A question mark in the Na_2SO_4-III column of **Table 5-20** indicates the absence of distinct, non-overlapping reflections typically associated with this phase. This suggests the possibility of a different, as yet unknown, structural modification.

5.3.1.2 DTA/DSC analysis

To refine the understanding of phase equilibria in the binary system, twelve mixtures (4.84, 7.93, 12.00, 14.90, 19.72, 25.00, 33.33, 39.72, 50.04, 60.12, 70.39, and 85.14 mol% $CaSO_4$) were analysed by DTA using sealed platinum tubes. The resulting thermograms are presented in **Figure 5-36**, with transition temperatures listed in **Table 5-21**. The experimental liquidus temperatures derived from these measurements align well with previous literature data [60, 71, 90, 122-130], as illustrated in **Figure 5-37**. At lower temperatures, however, the present results deviate from those reported by [126] but are consistent with the findings of [90] and [124], particularly with regard to two distinct transitions at about 250 °C and 280 °C. These transitions are also supported by the HT-XRD data (**Table 5-19**). According to DTA results, the maximum of the liquidus line lies at a composition of approximately 25 mol% $CaSO_4$, corresponding to the stoichiometry of the intermediate compound $Na_6Ca(SO_4)_4$ proposed by [126]. A preliminary interpretation of the DTA data would suggest the presence of this congruently melting intermediate compound with a melting temperature of 956.5 °C.

Nevertheless, XRD analysis does not provide definitive evidence for its stability: while it does not entirely exclude the existence of $Na_6Ca(SO_4)_4$, it fails to unambiguously confirm it. Within the compositional range of 15-70 mol% $CaSO_4$, the two low-temperature peaks detected by DTA decrease in intensity with increasing sulphate content. Furthermore, for samples with 25.0 and 33.4 mol%, an additional thermal event was identified near 500 °C in the heating curves. In several other compositions, a comparable transition was observed exclusively in the cooling cycles. The nature of this feature remains uncertain: it may reflect the decomposition of glauberite $Na_2Ca(SO_4)_2$ or indicate the stability region of a solid solution. At higher temperatures, certain transitions (e.g., for the 4.84 and 50.04 mol% $CaSO_4$ mixtures) were identified from the heating curves, where peak splitting was evident, enabling the distinction of two separate thermal events.

To clarify some ambiguous signals, four compositions (12.0, 25.0, 33.3, and 50.0 mol% $CaSO_4$), previously characterised by XRD, were subjected to DSC analysis. The tests were conducted in sealed platinum tubes using platinum sample holders in a Setaram DSC. The objectives of this complementary study were to assess whether the transitions could be detected with greater sensitivity and resolution, and to determine the enthalpy content of the events after calibration. The underlying assumption was that the true intermediate compound would correspond to the composition exhibiting the largest enthalpy of transition, while off-stoichiometric mixtures would display diminished values.

The phase transition temperatures and enthalpy values are summarised in **Table 5-22**, where the four analysed mixtures are labelled as 1 to 4. The values refer to transitions observed in heating curves, which were used for the comparison of enthalpy content. However, some low-temperature transitions in the mixture containing 12 mol% $CaSO_4$ and high-temperature transitions in the mixture with 50 mol% $CaSO_4$ were taken from cooling curves, as they exhibited peak splitting that was not visible in heating (see **Table 5-21** and **Figure 5-37**). This splitting provides additional information on the stability fields within the phase diagram. The sample with 12 mol% $CaSO_4$ exhibited only a single transition near 260 °C, associated with a moderate enthalpy content - approximately an order of magnitude larger than those of the other mixtures. In contrast, the $Na_4Ca(SO_4)_3$ mixture displayed a clear transition at 562 °C, with an enthalpy of 8.22 kJ/mol.

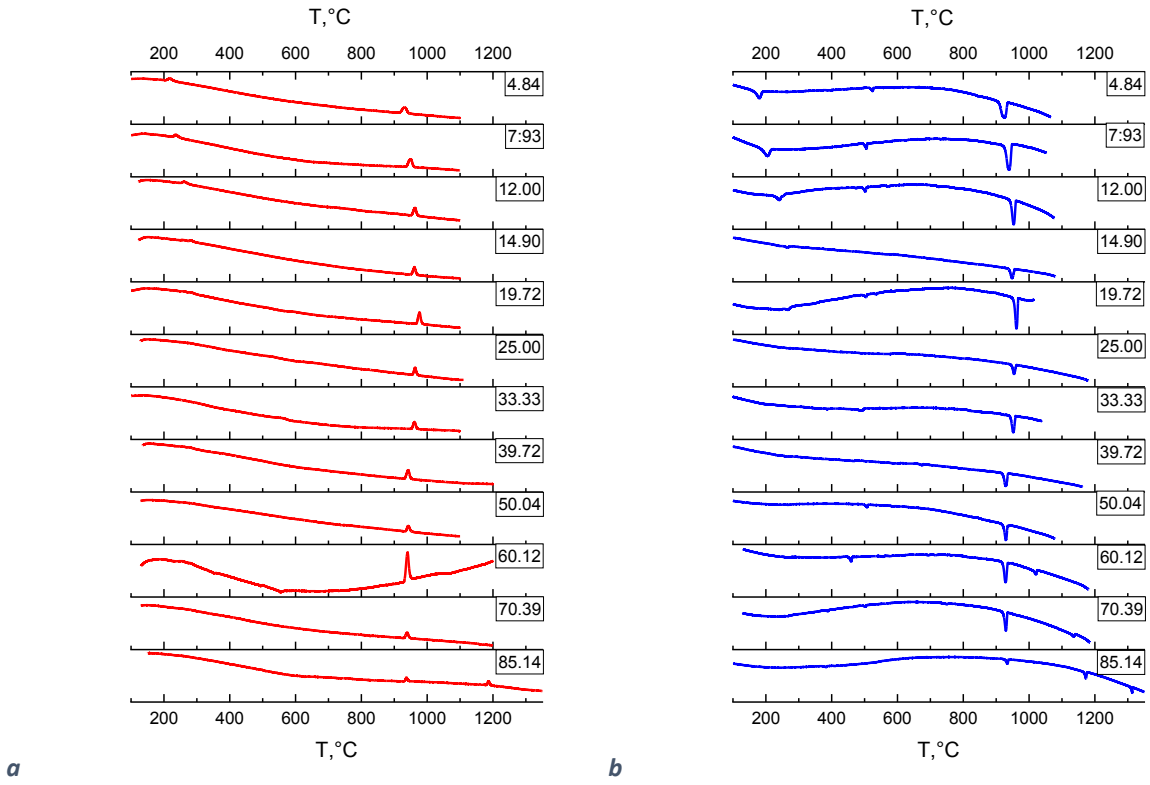


Figure 5-36 *DTA curves of Na_2SO_4-$CaSO_4$ mixture, expressed in molar percentage of $CaSO_4$:* ***a*** *heating curves;* ***b*** *cooling curves.*

Table 5-21 *Experimental DTA values of phase transition temperatures (°C) in the Na_2SO_4-$CaSO_4$ system.*

$CaSO_4$ (mol)	$CaSO_4$ (wt%)	1st	2nd	3rd	4th	5th	Method
0	0	195	246	887			DTA
0.0484	4.65	206	506 [a]	918	931 [a]		DTA
0.0793	7.63	228	508 [a]	937	950		DTA
0.1200	11.56	249 [a]	261 [a]	506 [a]	953		DTA
0.1200	11.56	258	269	950			DSC
0.1490	14.37	245	276	952			DTA
0.1972	19.06	250	277	365 [b]	508 [a]	968	DTA
0.2500	24.21	249	276	536	957		DTA
0.2500	24.21	253	278	519	959		DSC
0.3333	32.39	261	282	564	953		DTA
0.3333	32.39	562	948				DSC
0.3972	38.71	259	281	609 [a]	933		DTA
0.5000	48.94	258	281	918	927		DSC
0.5004	48.98	260	283	511 [a]	935	944 [a]	DTA
0.6012	59.10	256	282	501	932	1024	DTA
0.7039	69.50	254	279	931	1140		DTA
0.8514	84.60	254	522	932	1183	1317 [a]	DTA
1	100	1220	1510				DTA

[a] from cooling curves

[b] from heating curves 1 K/min

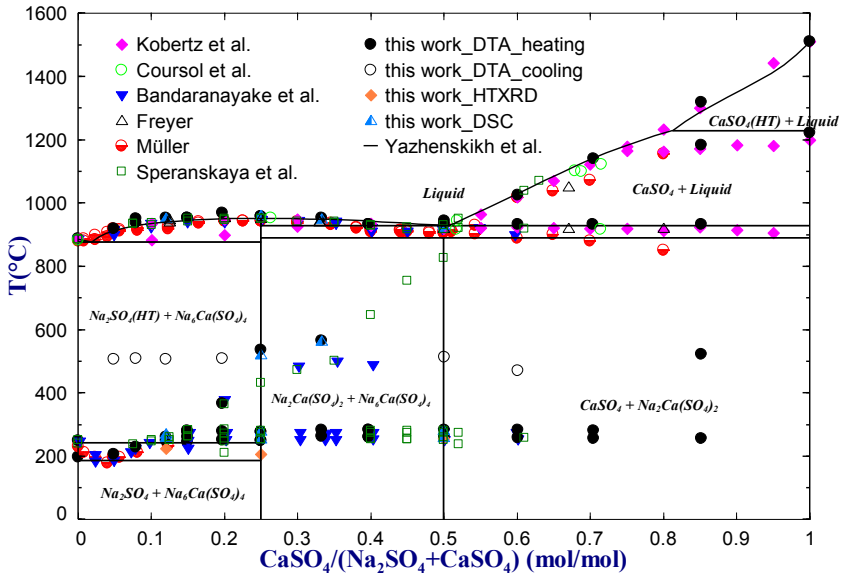


Figure 5-37 *Phase diagram of Na_2SO_4-$CaSO_4$ system with experimental data: this work and Kobertz et al. [126]; Coursol et al. [125]; Bandaranayake et al. [90]; Freyer et al. [122, 130]; Müller [123]; Speranskaya et al. [124]; and Yazhenskikh et al. [39].*

Table 5-22 *Transition temperatures and enthalpies of Na_2SO_4-$CaSO_4$ mixtures from DSC experiments (heating curves).*

	1st transition		2nd transition		3rd transition		4th transition	
$CaSO_4$, mol%	T, °C	ΔH, kJ/mol	T, °C	ΔH, kJ/mol	T, °C	ΔH, kJ/mol	T, °C	ΔH, kJ/mol
12.0	259	2.8 ± 0.5					950	15.1 ± 0.9
25.0	253	0.14 ± 0.13	278	0.53 ± 0.06	519	3.43 ± 0.09	959	18.8 ± 0.7
33.3					562	8.22 ± 0.06	948	19.3 ± 1.0
50.0	258	0.125 ± 0.005	281	0.33 ± 0.17			929	18.9 ± 0.6

The combined DTA/DSC analyses, coupled with XRD studies, provide significant insights into the binary system. The experimental results provide no evidence for the existence of the intermediate compound $Na_6Ca(SO_4)_4$ proposed by [126]. In particular, the absence of eutectic transitions in both DTA and DSC measurements argues against its stability: if such an intermediate were present, two eutectic reactions involving this phase would be expected. The results indicate that $Na_2Ca(SO_4)_2$ is stable within a narrow temperature range, between 280 °C and its decomposition at about 500 °C. The transition observed at approximately 250 °C in DTA curves was likely associated with the decomposition of $Na_4Ca(SO_4)_3$. In the low-$CaSO_4$ region, DTA also revealed evidence of a eutectoid reaction. The equilibrium line between Na_2SO_4-I solid solution and $CaSO_4$ was not well defined by DTA, but appeared to follow a trend similar to that proposed in previous studies [90, 122, 124, 130]. The observed splitting of certain liquidus peaks for low $CaSO_4$-mixtures, mainly in cooling curves, along with supporting data from Kobertz et al. [126], suggested the possible presence of azeotropic points, as proposed in earlier literature [90, 122, 124, 130]. At 50 mol% $CaSO_4$, DTA experiments showed

pronounced peak splitting during cooling, a feature even more clearly resolved in DSC. This behaviour is consistent with the coexistence of eutectic and liquidus transitions, placing the eutectic composition between 40 and 50 mol% $CaSO_4$. At lower concentrations, the oblique line defining the Na_2SO_4-I solid solution stability field, indicated by some DTA measurements (25.0 and 33.3 mol% $CaSO_4$) may have extended to higher temperatures, broadly following the tendency proposed by Speranskaya et al.'s data [124]. At high sulphate contents DTA (80-90 mol% $CaSO_4$) the two low-temperature transitions were only partially confirmed, as their intensity diminished significantly. The 500 °C transition, expected to correspond to phase decomposition, was unexpectedly weak or absent in the 50 mol% $CaSO_4$ mixture on heating, although its presence was evident in cooling cycles. Nevertheless, HTXRD data (see **Figure 5-35** and **Figure A 21a-b**) clearly defined the stability range of this phase, lending support to the overall phase equilibria interpretation. On the basis of these results, the phase relations in the 12-33 mol% $CaSO_4$ region can be described by four principal transitions: the first, occurring at the lowest temperature, corresponds to a solid-solid transformation of pure Na_2SO_4; the second is associated with the eutectoid reaction; the third corresponds to the decomposition of $Na_4Ca(SO_4)_3$; and the fourth marks the formation of $Na_2Ca(SO_4)_2$. This interpretation, derived from experimental data, provided the basis for the thermodynamic modelling.

5.3.2 NaCl-$CaSO_4$

The phase diagram of the NaCl-$CaSO_4$ system was analysed in this work by DTA using sealed platinum tubes, which effectively prevented the decomposition of calcium sulphate and the evaporation of sodium chloride, allowing reliable acquisition of new experimental data. The study targeted the low-to-medium $CaSO_4$ region to validate existing literature data and extended into the high-$CaSO_4$ region, scarcely explored due to the experimental difficulties associated with sulphate decomposition. Seven compositions (9.49, 16.90, 18.81, 32.74, 55.14, 74.76, and 87.95 mol% of $CaSO_4$) were analysed, covering the entire composition range. The DTA results for chloride-rich compositions are in excellent agreement with previously published data [133-135], confirming their reliability and indicating that no additional measurements with narrower composition intervals are required in this region. Thus, the existing literature data are considered robust and suitable for use in the assessment. In addition to previous investigations [133-135], the DTA measurements performed in this study consistently detected an additional thermal event at around 630 °C across all analysed compositions. The heating and cooling DTA curves are presented in **Figure 5-38** and the corresponding phase transition temperatures are summarised in **Table 5-23**.

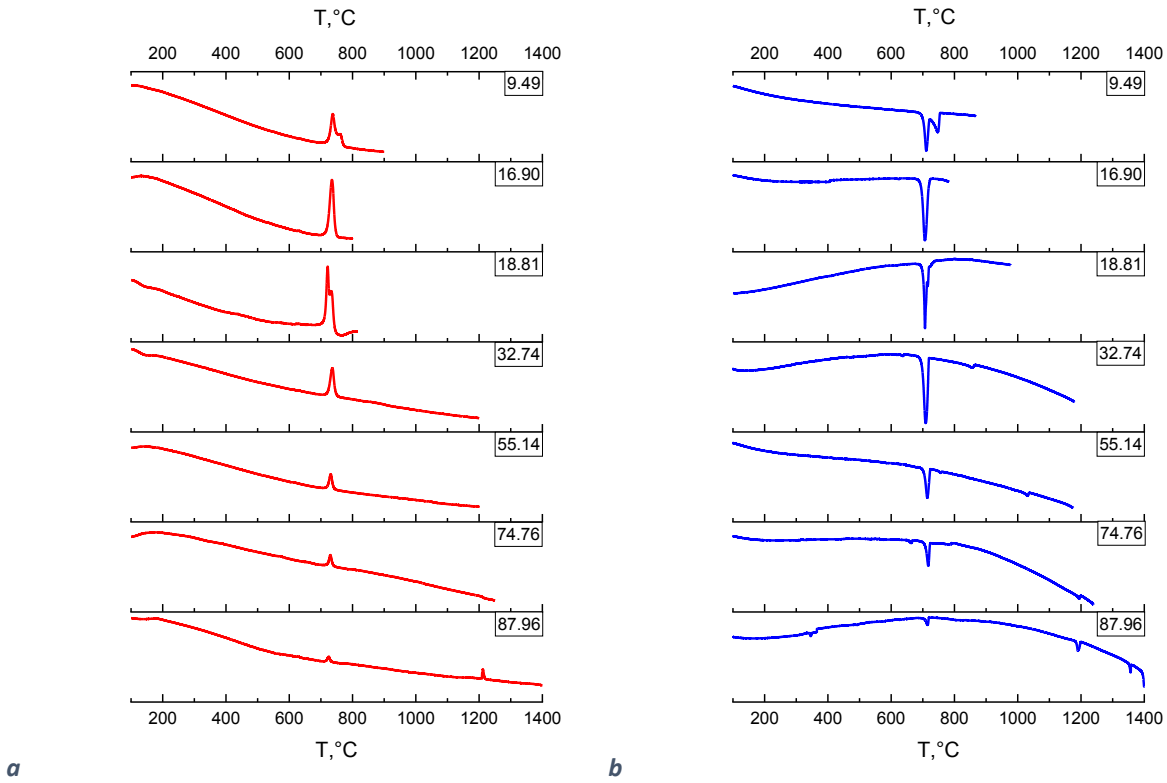


Figure 5-38 *DTA curves of NaCl-$CaSO_4$ mixtures, expressed in molar percentage of $CaSO_4$:* ***a*** *heating curves;* ***b*** *cooling curves.*

Table 5-23 *Experimental DTA values of phase transition temperatures (°C) in the NaCl-$CaSO_4$ system.*

$CaSO_4$ (mol)	$CaSO_4$ (wt%)	$CaSO_4$ (mol) [a]	1st	2nd	3rd	4th
0	0	0	810			
0.0949	19.63	0.1734	633	725	760	
0.1690	32.15	0.2892	627	720		
0.1881	35.05	0.3166	622	721	733	
0.3274	53.14	0.4933	630	722	865	
0.5514	74.12	0.7108	613	721	1051	
0.7476	87.34	0.8555	654	722	1199	
0.8795	99.44	0.9359	628	724	1209	1358 [b]
1	100	1	1220	1510		

[a] in the $(NaCl)_2$-$CaSO_4$ system
[b] from cooling curves

5.3.2.1 Thermodynamic properties of the low-melting mixture

To gain further thermodynamic insights into the system under investigation - and considering that the DTA results indicated a liquidus minimum composition at 16.9 mol% $CaSO_4$ - a mixture with a nominal composition of NaCl(83.10 mol%)-$CaSO_4$(16.90 mol%)[6] was prepared. The synthesis was carried out by thoroughly mixing the weighed pure components, sealing them in an evacuated quartz ampoule, and heating at 750 °C for 30 hours to ensure equilibration. Three samples from the same batch were analysed using DSC Setaram, and the resulting heat capacity curves are displayed in **Figure**

[6] For all calculations the molar mass M = 71.57 g/mol of the NaCl(83.10 mol%)-$CaSO_4$(16.90 mol%) mixture was used.

5-39. The experimentally determined heat capacity of the liquid phase was assumed constant at 138.2 J/(mol·K). Consistent with the DTA findings, an additional thermal event was detected in the DSC runs, appearing as a small peak at 633 °C, just before melting, with an associated enthalpy of approximately 0.52 kJ/mol. This peak is likely attributed to the melting of the sulphate-based solid solution HEXA, based on a preliminary qualitative comparison with the current (pre-optimisation) thermodynamic dataset. According to the DSC analysis, the eutectic mixture melts at 724 °C (997 K) with an enthalpy of fusion of 39.3 kJ/mol, obtained by integrating the C_p curves.

To verify the phase assemblage, the synthesised mixture was also characterised by XRD analysis. The diffraction patterns confirmed the exclusive presence of pure chloride and sulphate phases, with no evidence of additional phases or intermediate compounds (**Figure A 22**).

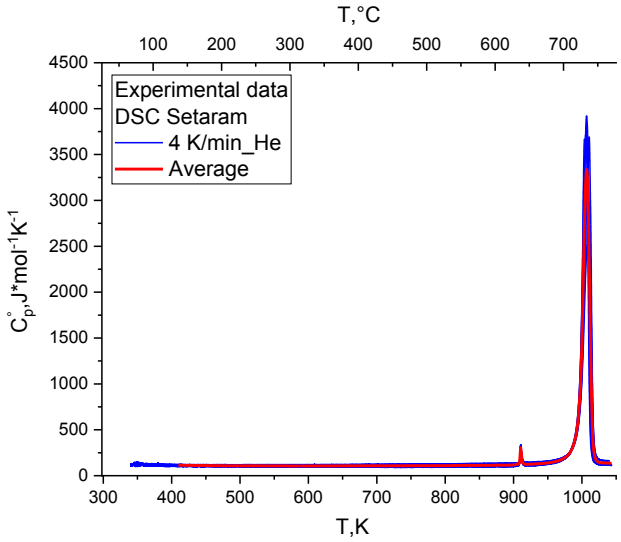


Figure 5-39 *Experimental values of molar heat capacity for solid and liquid phases of the NaCl(83.10 mol%)-$CaSO_4$(16.90 mol%) mixture measured by DSC Setaram.*

5.3.3 $CaCl_2$-Na_2SO_4

The $CaCl_2$-Na_2SO_4 system was originally explored by Palkin [70], who primarily reported liquidus curves without detailed information or solid-state transformation data. In the present work, DTA investigations were carried out in sealed platinum tubes to both validate these earlier findings and gain new insights into possible phase transitions. To this end, a total of eleven compositions (9.47, 16.32, 24.92, 40.59, 49.84, 61.05, 69.09, 76.37, 79.93, 85.44, and 94.33 mol% Na_2SO_4) were systematically analysed. The corresponding DTA curves are presented in **Figure 5-40** and the identified transitions are summarised in **Table 5-24**. For compositions with high Na_2SO_4 content, two distinct transitions were detected at approximately 255 °C and 280 °C. These transitions are interpreted as the decomposition of $Na_4Ca(SO_4)_3$ and the formation of $Na_2Ca(SO_4)_2$, respectively. Their occurrence aligns

with observations in the Na_2SO_4-$CaSO_4$ system (section 5.3.1), providing additional experimental confirmation of the phase equilibria proposed for this system.

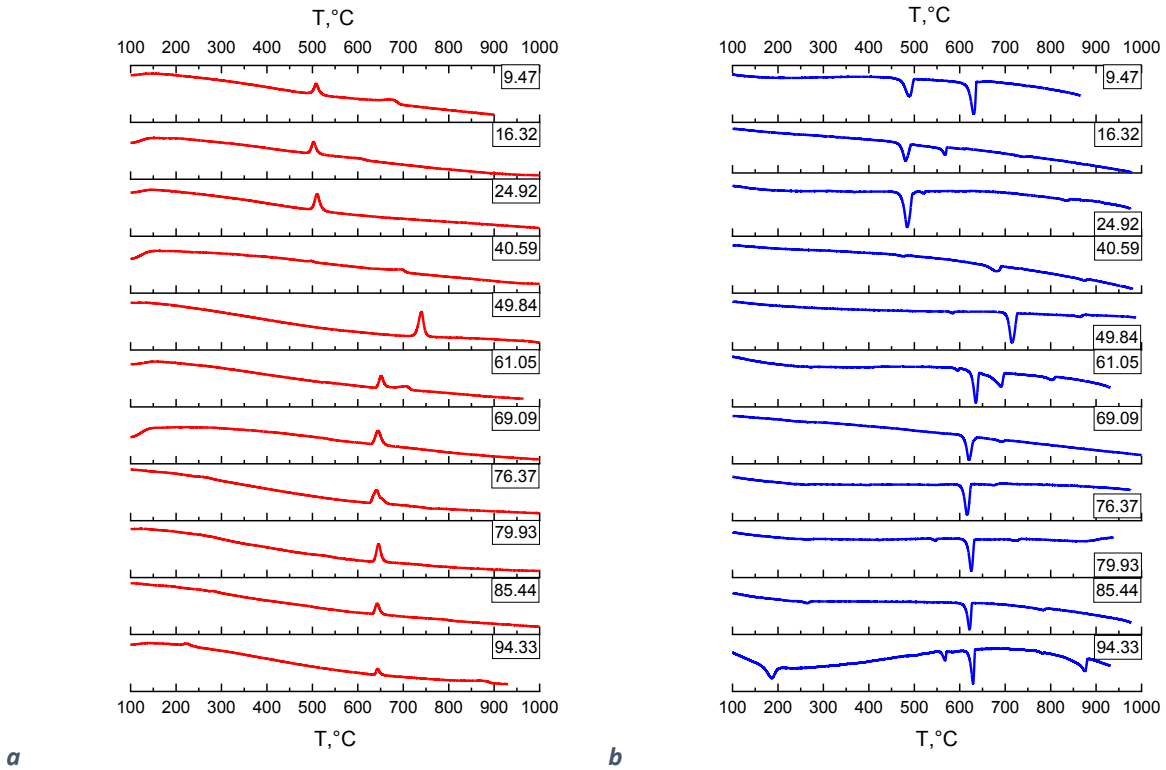


Figure 5-40 *DTA curves of $CaCl_2$-Na_2SO_4 mixtures, expressed in molar percentage of Na_2SO_4:* ***a*** *heating curves;* ***b*** *cooling curves.*

Table 5-24 *Experimental DTA values of phase transition temperatures (°C) in the $CaCl_2$-Na_2SO_4 system.*

Na_2SO_4 (mol)	Na_2SO_4 (wt%)	1st	2nd	3rd	4th	5th	6th
0	0	776					
0.0947	11.81	499	673				
0.1632	19.98	493	606	757			
0.2492	29.81	494	506	843			
0.4059	46.65	491	692	877			
0.4984	55.98	604	727	875			
0.6105	66.73	636	700	811			
0.6909	74.10	255	279	629	636	701	780
0.7637	80.53	255	268	628	652	702	
0.7993	83.60	258	283	529	636	739	
0.8544	88.25	255	280	634	790		
0.9433	95.51	211	571 [a]	638	881		
1	100	195	246	887			

[a] from cooling curves

5.4 K^+, Mg^{2+} // Cl^-, SO_4^{2-} system

5.4.1 KCl-$MgSO_4$

The sub-system KCl-$MgSO_4$ in the reciprocal system K^+, Mg^{2+} // Cl^-, SO_4^{2-} was experimentally investigated in this work using DTA. The measurements were designed to cover the entire compositional range in order to characterise the phase equilibria, with particular emphasis on the sulphate-rich region, where literature data are scarce or entirely lacking. DTA analyses were carried out in sealed platinum tubes to account for both sulphate decomposition and chloride volatilisation, in line with the experimental strategy adopted throughout this thesis. A total of eleven mixtures were analysed via DTA (10.50, 20.11, 28.39, 29.76, 34.89, 44.01, 50.00, 58.43, 72.78, 85.26, and 90.79 mol% $MgSO_4$), and the resulting heating and cooling curves are presented in **Figure 5-41**. The observed phase transition temperatures are summarised in **Table 5-25**. In the sulphate-poor region, the results of this study show reasonable agreement with the data reported by Jänecke [62] and Bergman et al. [109]. Notably, all analysed mixtures exhibited two phase transitions within the 400-500 °C range, which were not reported in prior studies [62, 109], but only for the 1:1 composition from [49]. Jänecke [62] reported the presence of an intermediate compound KCl·$MgSO_4$ with a melting temperature of 920 °C. However, a single DTA experiment cannot provide conclusive evidence for or against its existence. To investigate this further and evaluate the possible stability of such a compound, a stoichiometric 1:1 mixture of the end members was synthesised *in situ* via solid-state reaction. The reagents were combined in their stoichiometric ratio, sealed in a quartz ampoule, and annealed for more than three days. After annealing, the sample was recovered in a glovebox, ground in an agate mortar, and subsequently analysed by X-ray diffraction. Two equimolar samples were prepared, subjected to slightly different thermal treatments (800 °C for 60 h; 700 °C for 96 h) prior to XRD analysis, to examine the role of thermal history. The diffraction results, presented in **Figure 5-42**, revealed that phase formation and the relative amounts of crystalline products are strongly influenced by the annealing protocol. Both samples contained pure sulphate, the mixed sulphate $K_2Mg_2(SO_4)_3$, and two mixed chlorides K_2MgCl_4 and $K_3Mg_2Cl_7$. Lattice parameters and phase percentages are summarised in **Table 5-26**. These findings are largely consistent with the observations of Rowe et al. [49], who reported the presence of $K_2Mg_2(SO_4)_3$, KCl, and $MgCl_2$ or the compound KCl·$MgCl_2$. The transition temperatures determined for the equimolar mixture (see **Table 5-25**) are in good agreement with the literature data [49], namely 418, 490, 610, and 885 °C, and further confirm the occurrence of two transitions in the 400-500 °C range. Overall, the present results do not support the stability of the intermediate compound KCl·$MgSO_4$ proposed by Jänecke [62] and later considered by Bergman et al. [109]. Instead, they corroborate the conclusions of Rowe et al. [49] and Linstedt [155],

who likewise questioned its existence. Further investigations were considered beyond the scope of the present study.

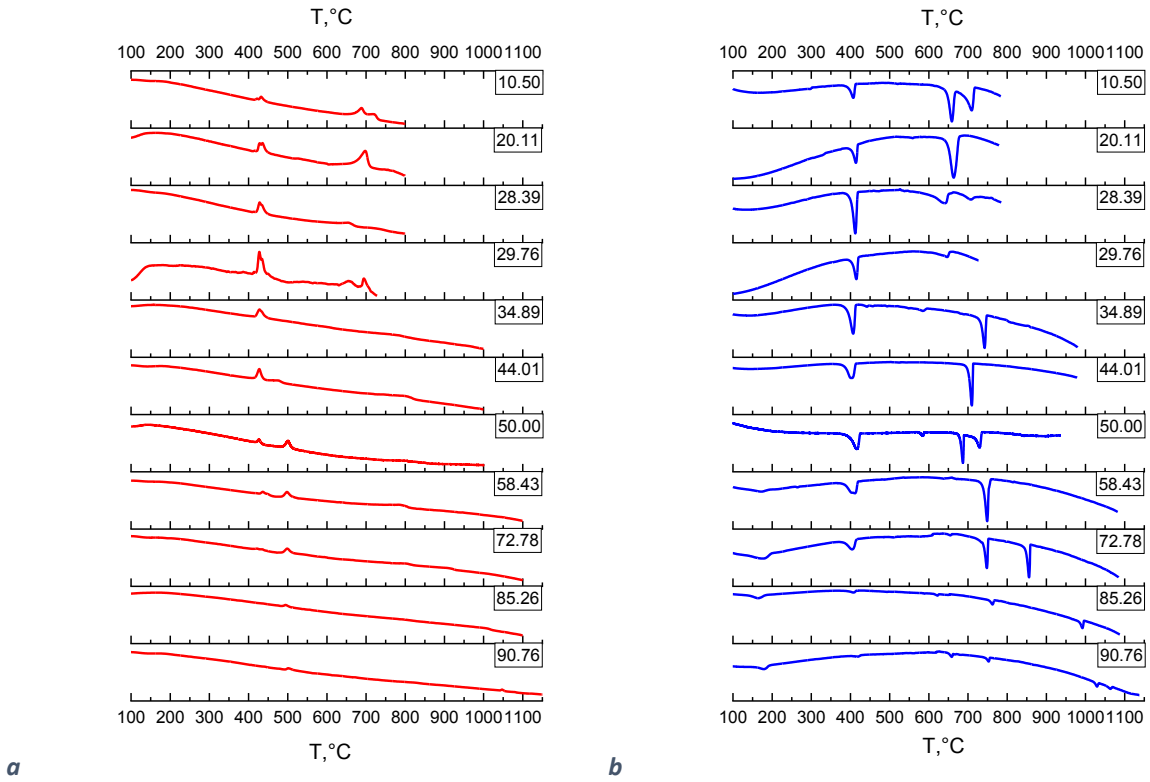


Figure 5-41 *DTA curves of KCl-$MgSO_4$ mixtures, expressed in molar percentage of $MgSO_4$:* ***a*** *heating curves;* ***b*** *cooling curves.*

Table 5-25 *Experimental DTA values of phase transition temperatures (°C) in the KCl-$MgSO_4$ system.*

$MgSO_4$ (mol)	$MgSO_4$ (wt%)	$MgSO_4$ (mol) [a]	1st	2nd	3rd	4th	5th
0	0	0	778				
0.1050	15.93	0.1901	416	432	688	717	
0.2011	28.90	0.3349	411	428	435	673	
0.2839	39.03	0.4423	414	429	434	654	702
0.2976	40.62	0.4587	414	428	434	656	695
0.3489	46.39	0.5174	417	433	599	754 [b]	
0.4401	55.93	0.6112	418	477	789		
0.5000	61.75	0.6666	420	489	690 [b]	836	
0.5843	69.41	0.7376	415	435	489	784	803
0.7278	81.19	0.8424	412	434	804	907	
0.8526	90.33	0.9205	436	487	798	1011	
0.9079	94.09	0.9517	442	494	822	1042	1080
1	100	1	1027	1136			

[a] in the $(KCl)_2$-$MgSO_4$ system
[b] from cooling curves

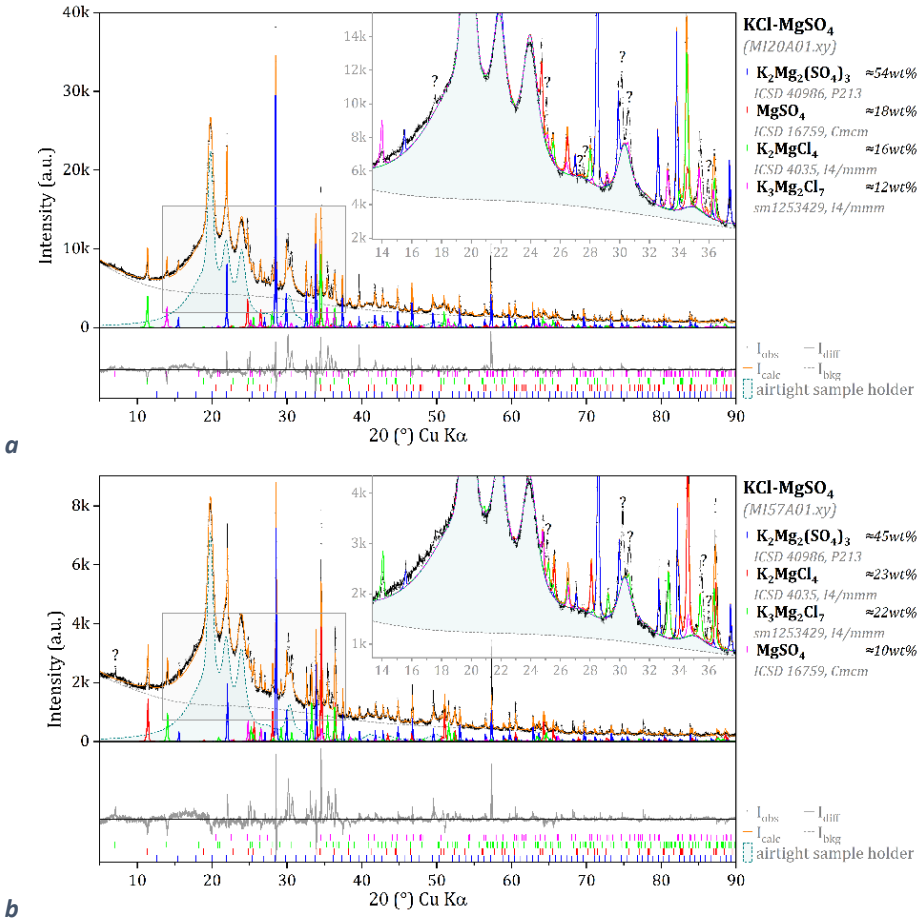


Figure 5-42 *X-ray diffractogram of KCl-$MgSO_4$ mixtures at room temperature:* ***a*** *KCl(49.71 mol%)-$MgSO_4$(50.28 mol%) (T=800 °C, t=60 h);* ***b*** *KCl(50.75 mol%)-$MgSO_4$(49.25 mol%) (T=700 °C, t=96 h).*

Table 5-26 *Lattice parameters of KCl·$MgSO_4$ mixtures.*

Phase	ICSD	wt%		SG	a (Å)	b (Å)	c (Å)
		a	b				
$K_2Mg_2(SO_4)_3$	10986	54	45	P213	9.922		
K_2MgCl_4	4035	16	23	I4/mmm	4.942		15.602
$MgSO_4$	16759	18	22	Cmcm	5.184	7.883	6.499
$K_3Mg_2Cl_7$	Sm1253429*	12	10	I4/mmm	4.953		25.409

* Springer materials Dataset ID 1253429

5.4.2 $MgCl_2$-K_2SO_4

The $MgCl_2$-K_2SO_4 system was investigated in this study through thermal analysis. A total of nine compositions (10.15, 20.00, 29.12, 40.74, 43.63, 51.20, 67.92, 79.68, and 90.75 mol% K_2SO_4) were prepared and analysed using DTA in sealed platinum tubes, covering nearly the entire compositional range. The experimental data, with DTA curves presented in **Figure 5-43**, are summarised in **Table 5-27**. The present study confirms the liquidus temperatures with a good degree of consistency with the literature data reported by Jänecke [62], whose study remains the only experimental work available for direct comparison, and additionally identifies further phase transitions, offering valuable

insights into phase equilibria. Jänecke [62] previously interpreted the phase equilibria on the basis of the involvement of the proposed 1:1 intermediate compound, $KCl{\cdot}MgSO_4$. However, as discussed in the preceding section regarding the $KCl\text{-}MgSO_4$ system (section 5.4.1), the combined DTA and XRD analysis conducted in this study provided no evidence for the existence of this intermediate compound. Consequently, the phase equilibria in the $MgCl_2\text{-}K_2SO_4$ system must also be explained based on chloride- and sulphate-based compounds rather than the hypothesised 1:1 compound. Certain high-temperature transitions were more effectively discriminated in the cooling curves, as the associated thermal effects were sharper and more intense than the weak and broadened signals detected upon heating. The DTA analysis carried out in this study, aimed at validating existing experimental data and providing additional information where necessary to describe the reciprocal system, is considered sufficient for a comprehensive thermodynamic assessment.

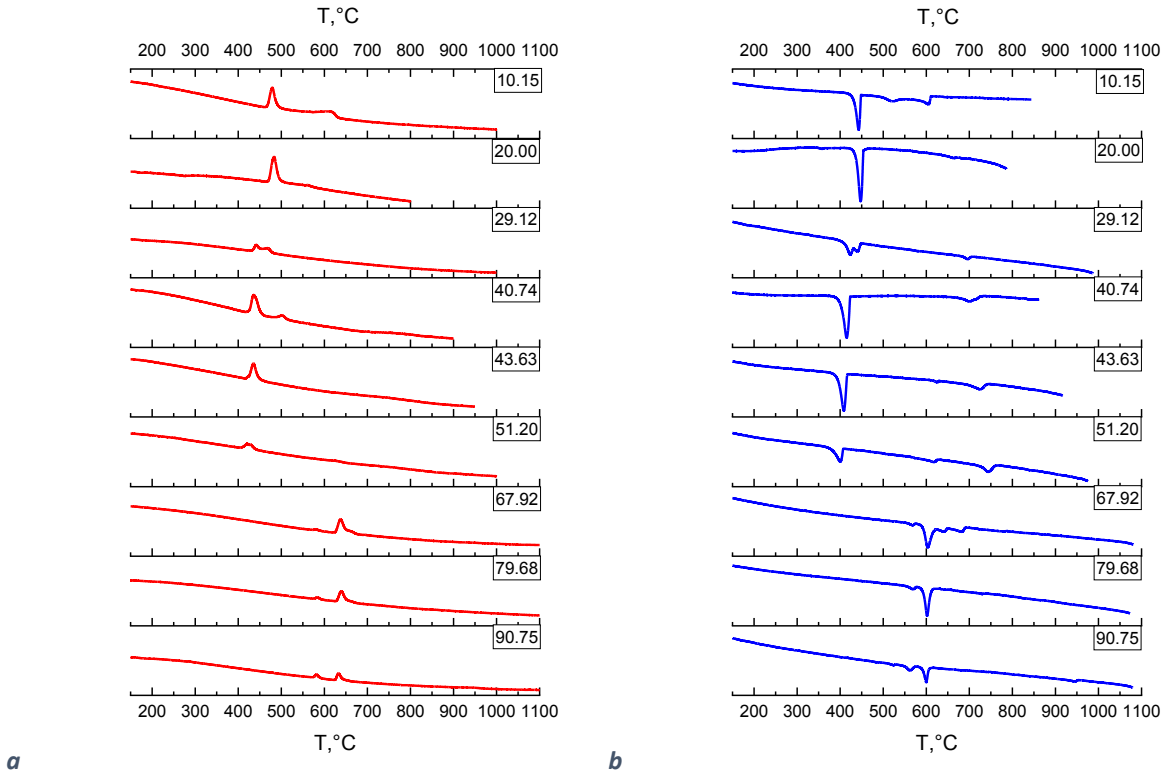


Figure 5-43 *DTA curves of $MgCl_2\text{-}K_2SO_4$ mixtures, expressed in molar percentage of K_2SO_4:* ***a*** *heating curves;* ***b*** *cooling curves.*

Table 5-27 *Experimental DTA values of phase transition temperatures (°C) in the $MgCl_2\text{-}K_2SO_4$ system.*

K_2SO_4 (mol)	K_2SO_4 (wt%)	1st	2nd	3rd	4th
0	0	719			
0.1015	17.13	468	541 [a]	611 [a]	
0.2000	31.39	362 [a]	471	668 [a]	
0.2912	42.92	433	468	704 [a]	
0.4074	55.71	426	502	708 [a]	725 [a]
0.4363	58.62	420	435	629 [a]	739 [a]
0.5120	65.76	409	428	630	760 [a]

0.6792	79.49	575	626	664	693
0.7968	87.77	577	629	662	735 [a]
0.9075	94.72	575	626	653	949
1	100	581	1076		

[a] from cooling curves

5.5 K^+, Ca^{2+} // Cl^-, SO_4^{2-} system

5.5.1 KCl-$CaSO_4$

The stable diagonal KCl-$CaSO_4$ of the reciprocal system K^+, Ca^{2+} // Cl^-, SO_4^{2-} was investigated through a combined analysis of DTA, DSC, and XRD. The DTA study aimed to validate and assess the agreement with existing experimental data, with particular attention to sulphate-rich compositions. This was essential for completing the phase diagram description, as high-sulphate compositions are underrepresented in the literature [68, 69, 133, 135] due to thermal decomposition at elevated temperatures. To overcome this limitation, six compositions (10.12, 19.67, 30.73, 61.84, 76.69, and 90.55 mol% $CaSO_4$) were analysed using DTA in sealed platinum tubes, allowing measurements at high temperatures without mass loss. The results demonstrated strong agreement with existing literature data [68, 69, 133, 135], leading to the selection of three compositions in the near-eutectic region and three additional compositions with medium-to-high sulphate content to address the data gap. The DTA curves are presented in **Figure 5-44**, while the observed phase transition temperatures are summarised in **Table 5-28**. The experimental data of this study align well with previous findings, and the newly acquired sulphate-rich data points naturally extend the liquidus curve described in earlier works [68, 69, 133, 135]. Golubeva and Bergman [69] previously reported an incongruently melting compound, $2KCl{\cdot}CaSO_4$, which was later refuted by Jänecke and Mühlhäusser [68] and Rowe et al. [49]. To further investigate these findings, the KCl(66.67 mol%)-$CaSO_4$(33.33 mol%) composition, i.e. $2KCl{\cdot}CaSO_4$, was synthesised in the laboratory by mixing pure components in their stoichiometric ratios, sealing them in glass ampoules, and annealing at 700 °C for 96 hours. The resulting mixture was recovered, ground in an agate mortar under a controlled atmosphere in glovebox, and analysed by XRD at room temperature. The XRD results, shown in **Figure A 23**, confirmed the exclusive presence of pure chloride and sulphate phases, supporting the conclusions of Rowe et al. [49].

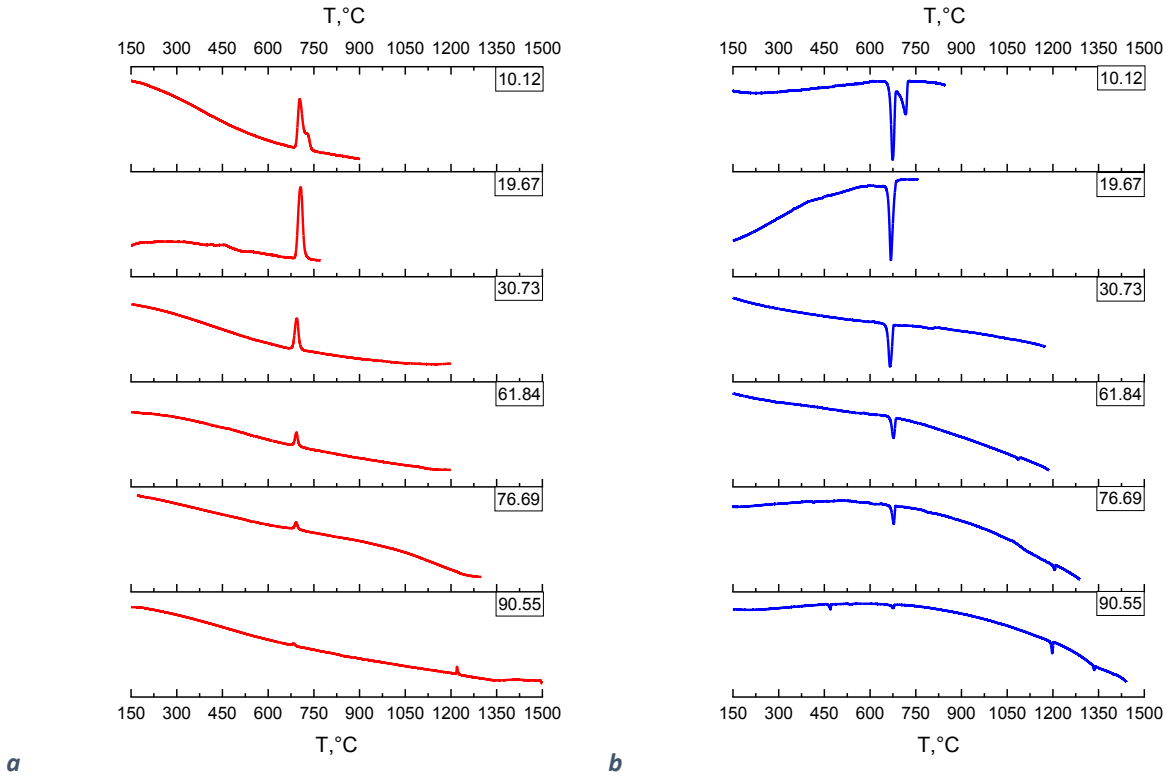


Figure 5-44 *DTA curves of KCl-$CaSO_4$ mixtures. expressed in molar percentage of $CaSO_4$:* ***a*** *heating curves;* ***b*** *cooling curves.*

Table 5-28 *Experimental DTA values of phase transition temperatures (°C) in the KCl-$CaSO_4$ system.*

$CaSO_4$ (mol)	$CaSO_4$ (wt%)	$CaSO_4$ (mol) [a]	1st	2nd	3rd
0	0	0	778		
0.1012	21.70	0.4702	692	728	
0.1967	30.90	0.2329	691		
0.3073	44.75	0.3287	681	817	
0.6184	74.74	0.4701	684	1092	
0.7669	85.73	0.7642	683	1209 [b]	
0.9055	94.59	0.8681	677	1217	1350 [b]
1	100	1	1220	1510	

[a] in the $(KCl)_2$-$CaSO_4$ system
[b] from cooling curves

5.5.1.1 Thermodynamic properties of the eutectic mixture

To obtain further thermodynamic insights into the reciprocal system, a DSC analysis was conducted on the eutectic composition of the KCl-$CaSO_4$ system. This investigation aimed to provide additional experimental data for thermodynamic assessment and contribute to the development and refinement of the thermodynamic database. Based on the DTA analysis, its agreement with literature data [68, 69, 133, 135], and an initial estimation derived from the existing thermodynamic database prior to optimisation, a eutectic composition of approximately 20 mol% $CaSO_4$ was suggested.

Consequently, the KCl(80.48 mol%)-$CaSO_4$(19.52 mol%)[7] composition was synthesised in the laboratory by mixing pure components in a glovebox. The mixture was sealed in quartz ampoules using a hydrogen-oxygen flame and subjected to thermal treatment at 700 °C for 70 hours to promote the formation of a homogeneous phase. After annealing, the sample was retrieved under an inert atmosphere in a glovebox, finely ground in an agate mortar, and subsequently used for calorimetric analysis. Three samples from the same batch were analysed using a Setaram DSC instrument, employing platinum crucibles with alumina liners and platinum caps. The resulting experimental C_p curves for the eutectic mixture are presented in **Figure 5-45**. The calorimetric measurements of the eutectic mixture enabled the determination of a melting temperature of 690 °C (963 K), in agreement with the 691 °C (964 K) value obtained from DTA analysis. From the experimental data, and specifically from the average heat capacity curve derived from multiple measurements, it was possible to establish a polynomial function describing the molar heat capacity of the solid phase over the temperature range extending from room temperature (extrapolated) to the melting point at 690 °C, as listed in **Table 5-29**. Additionally, the heat capacity of the liquid phase was estimated as a constant value of 131.5 J/(mol·K). These findings provide essential thermodynamic properties that contribute not only to the characterisation of the KCl-$CaSO_4$ system but also to the broader understanding of the entire reciprocal system. Through appropriate integration of the C_p curves, the enthalpy of fusion for the eutectic composition was determined to be 37.0 kJ/mol. This value does not align with the value derived from calibration using standard references, which yielded 28.7 ± 0.2 kJ/mol. Considering the consistency of the raw C_p data and their integration, and given the significant discrepancy between the two approaches, the enthalpy value of 37.0 kJ/mol - directly obtained from the experimental C_p curves - was retained as the experimental reference value for the eutectic composition, while acknowledging the lower value derived from calibration.

[7] For all calculations the molar mass M = 86.57 g/mol of the KCl(80.48 mol%)-$CaSO_4$(19.52 mol%) mixture was used.

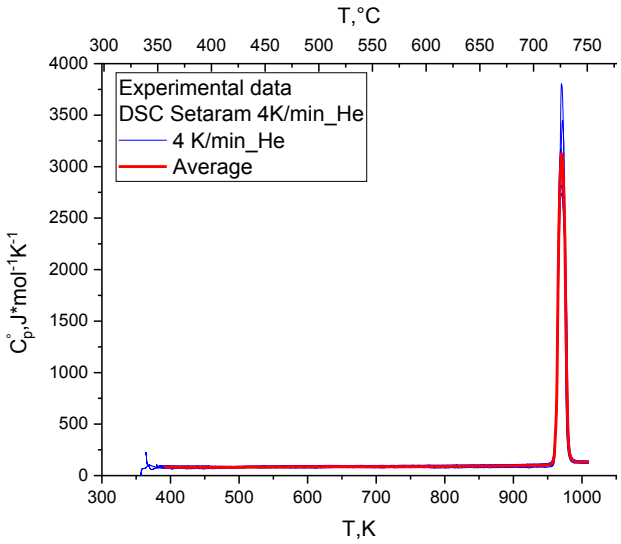


Figure 5-45 *Experimental values of molar heat capacity of the KCl(80.48 mol%)-$CaSO_4$(19.52 mol%).*

Table 5-29 *Coefficients of the second-order equation of molar heat capacity ($J \cdot mol^{-1} \cdot K^{-1}$) $C_p° = A + B \cdot T + C \cdot T^{-2} + D \cdot T^2$ for the KCl(80.48 mol%)-$CaSO_4$(19.52 mol%) mixture taken from DSC measurements.*

Temperature range/K	A	B	C	D
298 - 963	265.44	-0.39386	$-1.219 \cdot 10^7$	$2.472 \cdot 10^{-4}$
963 - 1020	131.5			

5.5.2 $CaCl_2$-K_2SO_4

The other section of the reciprocal system, $CaCl_2$-K_2SO_4, was also investigated in this study through differential thermal analysis. A total of eight compositions (10.52, 20.53, 30.46, 44.15, 54.77, 69.92, 74.00, and 85.52 mol% K_2SO_4) were analysed using DTA in sealed platinum tubes, with the objective of covering the entire compositional range and determining the phase transitions within the phase diagram. The resulting DTA curves are presented in **Figure 5-46**, while the corresponding thermal event temperatures are summarised in **Table 5-30**. Golubeva and Bergman's work [69] reported only the liquidus curve, which has been validated in this study with a good agreement within a ±10 °C window. Moreover, the present DTA analysis has provided additional insights into previously unreported phase transitions involved in the phase equilibria of the system under investigation, partially confirming those described by Jänecke and Mühlhäusser [68]. When considered collectively, the data obtained in this study, along with the available literature data, provide a sufficient basis for the thermodynamic assessment and the prediction of thermodynamic properties of the system.

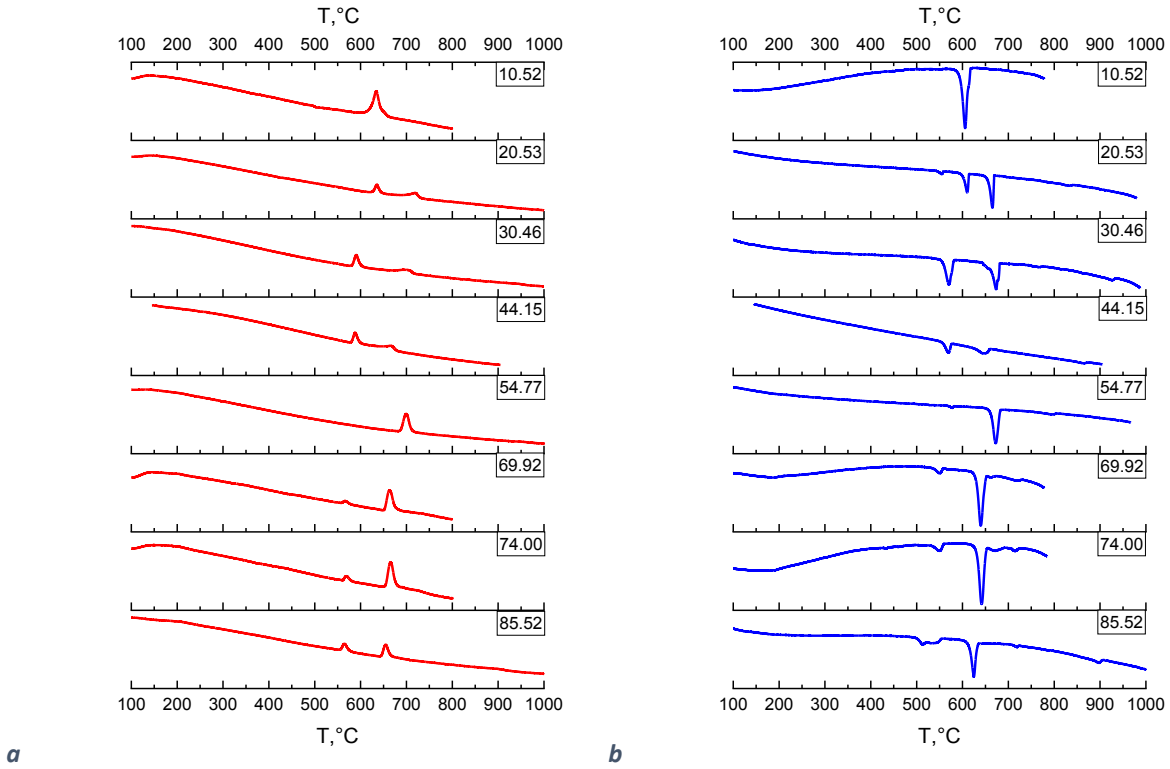


Figure 5-46 *DTA curves of $CaCl_2$-K_2SO_4 mixtures. expressed in molar percentage of K_2SO_4:* ***a*** *heating curves;* ***b*** *cooling curves.*

Table 5-30 *Experimental DTA values of phase transition temperatures (°C) in the $CaCl_2$-K_2SO_4 system.*

K_2SO_4 (mol)	K_2SO_4 (wt%)	1st	2nd	3rd	4th	5th
0	0	776				
0.1052	15.58	621	652			
0.2053	28.86	558	627	719	834 [a]	
0.3046	40.75	555	583	671	704	942 [a]
0.4415	55.38	580	666	875		
0.5477	65.53	212	597	688	805	
0.6992	78.49	205	559	653	671	734
0.7400	81.72	204	562	655	690	728
0.8552	90.27	210	556	645	701	896
1	100	581	1076			

[a] from cooling curves

5.6 Na^+, K^+ // Cl^-, SO_4^{2-} system

5.6.1 NaCl-K_2SO_4

Experimental studies available in the literature [49, 66, 102, 108] for the NaCl-K_2SO_4 phase diagram show a generally consistent picture of the phase equilibria. The present work was undertaken to evaluate the reliability of these data and to validate them through independent measurements. To this end, nine mixtures (19.88, 24.03, 29.56, 33.48, 36.97, 40.43, 45.39, 50.89, and 89.46 mol% K_2SO_4) were analysed in sealed platinum tubes by DTA, with a specific focus on compositions with low-to-medium K_2SO_4 content. This investigation was designed to clarify the phase relations in this

composition range, where multiple phases coexist and several equilibria and transitions are observed (see **Figure 2-34**). The corresponding DTA curves from this work are presented in **Figure 5-47**, and the phase transition temperatures are summarised in **Table 5-31**. The measurements reproduced the key transitions already documented in earlier studies, while also revealing an additional thermal effect near 200 °C, which is likely attributable to pure Na_2SO_4. A detailed analysis of this feature, which could provide further insight into the system's equilibria, was not pursued within the scope of the present work. Nevertheless, the combination of the new DTA results with literature data provides a consistent and reliable basis for describing the phase relations in the NaCl-K_2SO_4 system.

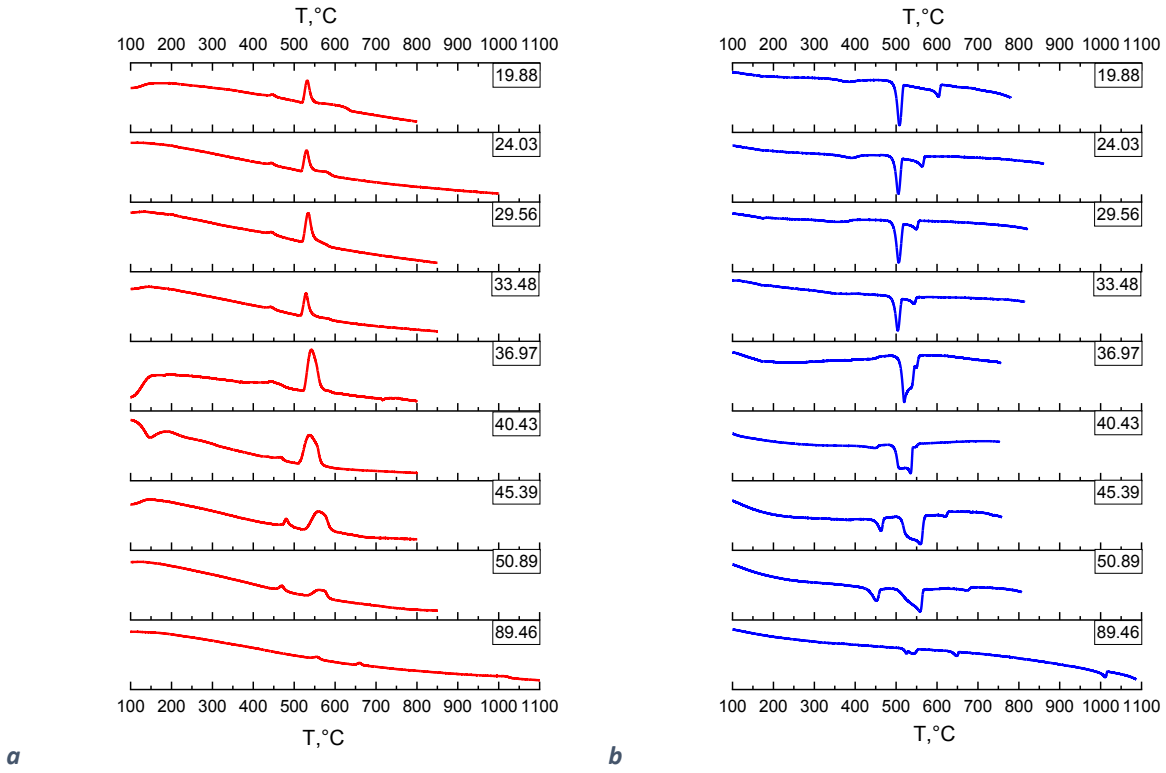


Figure 5-47 *DTA curves of NaCl-K_2SO_4 mixtures, expressed in molar percentage of K_2SO_4:* ***a*** *heating curves;* ***b*** *cooling curves.*

Table 5-31 *Experimental DTA values of phase transition temperatures (°C) in the NaCl-K_2SO_4 system.*

K_2SO_4 (mol)	K_2SO_4 (wt%)	K_2SO_4 (mol) [a]	1st	2nd	3rd	4th	5th
0	0	0	810				
0.1988	42.71	0.3333	199	439	521	615	
0.2403	48.54	0.3875	201	436	519	580	
0.2956	55.58	0.4563	201	434	522	566	
0.3348	60.01	0.5016	202	432	518	585	
0.3697	63.62	0.5398	196	445	525	556	589
0.4043	66.93	0.5758	431	467	513	557	
0.4539	71.25	0.6244	473	530	578	627	
0.5089	75.55	0.6745	459	530	576	681	
0.8946	96.20	0.9444	394 [b]	529 [b]	553 [b]	649	1010
1	100	1	581	1076			

[a] in the $(NaCl)_2$-K_2SO_4 system
[b] from cooling curves

5.6.2 KCl-Na_2SO_4

To examine the stable diagonal of the reciprocal Na^+, K^+ // Cl^-, SO_4^{2-} system, DTA measurements were carried out on mixtures sealed in platinum tubes to prevent mass loss, following the same procedure adopted for the other subsystems in this study. Nine compositions spanning the full compositional range (14.75, 28.42, 38.75, 41.56, 44.22, 53.40, 70.13, 78.00, and 89.76 mol% Na_2SO_4) were analysed. The resulting DTA curves are presented in **Figure 5-48**, with the corresponding transition temperatures reported in **Table 5-32**. The experimental results indicate a liquidus minimum near 41.5 mol% Na_2SO_4. In addition to the melting points of the analysed mixtures, further phase transitions were identified prior to melting. These include, for example, the low-temperature solid-solid transformation of Na_2SO_4 and a transition at approximately 440 °C, previously reported by Jänecke [108], which corresponds to a phase transition involving sodium and potassium sulphates. Unlike the study of Akopov and Bergman [102], which reported only the melting temperatures of the investigated compositions to describe the liquidus curve, the present work provides complementary information to that of Jänecke [108] by documenting all detectable phase transitions. The DTA results clearly demonstrate that the system exhibits a relatively complex set of equilibria, rather than a simple mono-eutectic phase diagram.

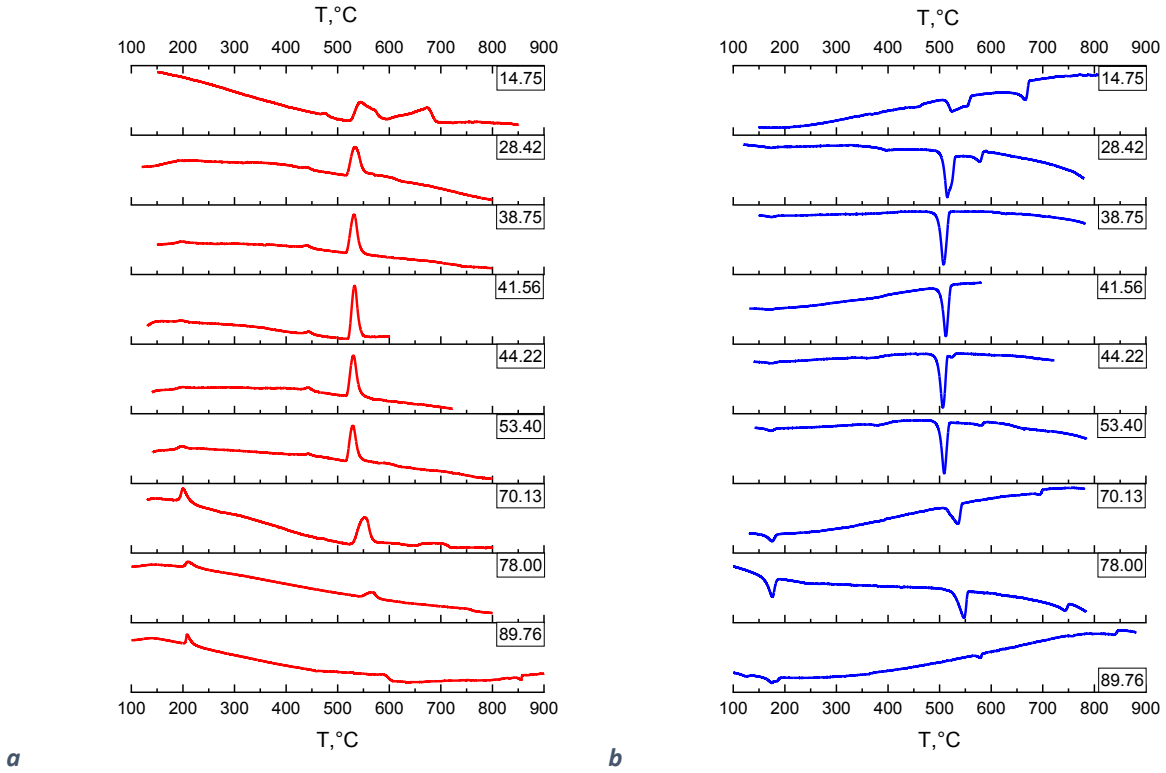


Figure 5-48 *DTA curves of KCl-Na_2SO_4 mixtures. expressed in molar percentage of Na_2SO_4: **a** heating curves; **b** cooling curves.*

Table 5-32 *Experimental DTA values of phase transition temperatures (°C) in the KCl-Na_2SO_4 system.*

Na_2SO_4 (mol)	Na_2SO_4 (wt%)	Na_2SO_4 (mol) [a]	1st	2nd	3rd	4th	5th
0	0	0	778				
0.1475	24.79	0.2571	468	527	573	673	
0.2842	43.07	0.4426	195	439	520	531 [b]	585 [b]
0.3875	54.66	0.5586	198	440	519		
0.4156	57.54	0.5872	197	442	522		
0.4422	60.17	0.6133	198	441	519	532 [b]	
0.5340	68.59	0.6963	197	434	518	590	
0.7013	81.73	0.8244	193	395 [b]	530	554	700
0.7800	87.11	0.8765	202	546	567	756	
0.8976	94.35	0.9460	180	191	586	840	
1	100	1	195	246	887		

[a] in the $(KCl)_2$-Na_2SO_4 system
[b] from cooling curves

5.6.2.1 Thermodynamic properties of the low-melting mixture

The DTA results obtained in this study, together with literature data [102, 108], indicated a liquidus minimum at 41.56 mol% Na_2SO_4. To gain further thermodynamic insight into the binary system, this composition was synthesised and subjected to DSC analysis. The sample KCl(58.44 mol%)-Na_2SO_4(41.56 mol%)[8] was prepared by mixing the pure end members in their stoichiometric ratio inside sealed quartz ampoules, followed by annealing above the melting point at 580 °C for 60 h. After thermal treatment, the solidified mixture was recovered, ground in a glovebox, and analysed using a Setaram DSC with platinum crucibles lined with alumina and covered by platinum lids. The measured heat capacity values are displayed in **Figure 5-49**. By integration of the C_p curves the enthalpy of fusion was determined as 20.0 kJ/mol, while enthalpy calibration yielded a slightly higher value of 24.9 ± 1 kJ/mol, corresponding to a melting temperature of 521 °C (794 K). The enthalpic contributions of the first transition at 193 °C (466 K) was estimated at 0.37 kJ/mol from integration and 0.32 ± 0.02 from calibration. The second transition, observed at 435 °C (708 K), showed enthalpy values of 1.55 kJ/mol from integration and 1.5 ± 0.3 kJ/mol from calibration. As discussed in section 5.5.1.1, the value obtained from the integration of the experimental C_p curves is here presented as the experimental result to be used in the comparison with the thermodynamic dataset. Nevertheless, further measurements would be desirable to verify and consolidate this experimental value.

[8] For all calculations the molar mass M=113.99 g/mol of the KCl(58.44 mol%)-Na_2SO_4(41.56 mol%) mixture was used.

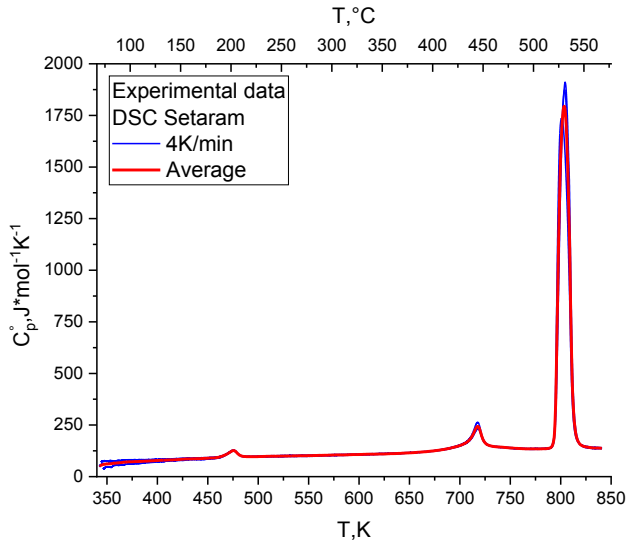


Figure 5-49 *Experimental values of molar heat capacity of KCl(58.44 mol%)-Na_2SO_4(41.56 mol%) mixture.*

6 Modelling results

This chapter presents the results of the thermodynamic modelling carried out in this thesis, based on the experimental data obtained in this study and, where available, complemented by literature data. The chapter is structured into sections dedicated to each of the six reciprocal systems, which are further divided into subsections focusing on the respective subsystems analysed. Only those systems that were thermodynamically assessed as part of this work are discussed. In cases where certain systems were not modelled here and their thermodynamic properties optimised in previous studies were used instead, they are not described again in this chapter, as they are already reviewed and summarised in the corresponding sections of the Literature review chapter. Furthermore, since some binary systems are shared among the six reciprocal diagrams, when such systems have already been discussed earlier in the chapter, they are not repeated in subsequent sections. Instead, the reader is asked to consult the first paragraph where the respective binary system was originally introduced and analysed.

Table 6-1 *Thermodynamic data of stochiometric compounds used in the present work.*

Compound	$\Delta H^0_{298,f}$ J/mol	S^0_{298} J/(mol·K)	T (K)	C_p, J/(mol·K)	Ref.
NaCl (solid)	-411120 [228]	72.132 [242]	1-20	$0.08112742793394T - 0.01041590551383T^2 + 0.000524656971697T^3$	[48]
			20-116	$-10.6712089631739 + 0.6130440076047T - 5.0146910679\cdot10^{-4}T^2 - 9.09935974\cdot10^{-6}T^3$	[48]
			116-298	$12.937383161886 + 0.33737791631461T - 1.08663138387\cdot10^{-3}T^2 + 1.26668694\cdot10^{-6}T^3$	[48]
			298-900	$56.304 - 0.0130328T - 342570T^{-2} - 2.18749998\cdot10^{-5}T^2$	[48, 228]
			900-1076	$59.853 - 0.0194622T - 688110T^{-2} - 2.51622\cdot10^{-5}T^2$	[48, 228]
NaCl (liquid)	-391305 [a]	82.493 [a]	S→L ΔH_{tr} = 28.2 kJ/mol at 1076 K (803 °C)		[48, 228]
			1-20	$0.08112742793394T - 0.01041590551383T^2 + 0.000524656971697T^3$	[48]
			20-116	$-10.6712089631739 + 0.6130440076047T - 5.0146910679\cdot10^{-4}T^2 - 9.09935974\cdot10^{-6}T^3$	[48]
			116-178	$12.937383161886 + 0.33737791631461T - 1.08663138387\cdot10^{-3}T^2 + 1.26668694\cdot10^{-6}T^3$	[48]
			178-3000	68.45	[48]
KCl (solid)	-436684 [242]	82.555 [242]	1-20	$0.00394175357143 - 0.01478181559524T + 1.86488757143\cdot10^{-3}T^2 + 3.7952896667\cdot10^{-4}T^3$	[a]
			20-130	$-16.9844632541827 + 1.08979287666386T - 6.54977319151\cdot10^{-3}T^2 + 1.341381559\cdot10^{-4}T^3$	[a]
			130-298	$28.3889438596798 + 0.15841492508822T - 3.693196603\cdot10^{-4}T^2 + 3.1975681\cdot10^{-7}T^3$	[a]
			298-700	$50.47661 + 0.005924377T - 144173.9T^{-2} + 7.496682\cdot10^{-6}T^2$	[228]
			700-1044	$143.5698 - 0.1680399T - 8217836T^{-2} + 9.9657018\cdot10^{-5}T^2$	[228]
KCl (liquid)	-421789 [a]	86.658 [a]	S→L ΔH_{tr} = 26.3 kJ/mol at 1044 K (771 °C)		[228]
			1-20	$0.00394175357143 - 0.01478181559524T + 1.86488757143\cdot10^{-3}T^2 + 3.7952896667\cdot10^{-4}T^3$	[a]
			20-130	$-16.9844632541827 + 1.08979287666386T - 6.54977319151\cdot10^{-3}T^2 + 1.341381559\cdot10^{-4}T^3$	[a]
			130-250	$28.3889438596798 + 0.15841492508822T - 3.693196603\cdot10^{-4}T^2 + 3.1975681\cdot10^{-7}T^3$	[a]
			250-3000	73.59656	[a]
$MgCl_2$ (solid)	-644300 [228]	89.62 [228]	1-40	$0.01578312T - 0.00540726797T^2 + 6.88028004\cdot10^{-4}T^3 - 2.6046278\cdot10^{-5}T^4 + 5.53055764\cdot10^{-7}T^5 - 4.56290219\cdot10^{-9}T^6$	[264], [a]
			40-298	$214.15146 - 1.3637537T + 204423.51T^{-2} + 0.0083405079T^2 - 2.53029383\cdot10^{-5}T^3 - 2.90946621\cdot10^{-8}T^4 - 11675.506/T$	[a]

			298-987	$75.65277 + 0.009980036T - 643923.9T^{-2} - 3.198664\cdot10^{-9}T^2$	[228]
			987-2900	84.782	[a]
$MgCl_2$ (liquid)	-609584.64 [a]	117.243 [a]	S→L ΔH_{tr} = 43.1 kJ/mol at 987 K (714 °C)		[a]
			1-40	$0.01578312T - 0.00540726797T^2 + 6.88028004\cdot10^{-4}T^3 - 2.6046278\cdot10^{-5}T^4 + 5.53055764\cdot10^{-7}T^5 - 4.56290219\cdot10^{-9}T^6$	[a]
			40-117	$214.15146 - 1.3637537T + 204423.51T^{-2} + 0.0083405079T^2 - 2.53029383\cdot10^{-5}T^3 - 2.90946621\cdot10^{-8}T^4 - 11675.506/T$	[a]
			117-2900	92.048	[a]
$CaCl_2$ (solid)	-795797 [237]	104.602 [237]	1-50	$0.78155423 - 0.12359292T + 0.0306270316T^2 - 3.49282014\cdot10^{-4}T^3$	[48]
			50-180	$-16.732490 + 1.1686419T - 6.02988655\cdot10^{-3}T^2 + 1.1662759\cdot10^{-5}T^3$	[48]
			180-600	$43.925204 + 0.17176775T - 3.10281876\cdot10^{-4}T^2 + 1.97728035\cdot10^{-7}T^3$	[48]
			600-1045	$77.936089 - 0.00630254569T + 6.57695848\cdot10^{-6}T^2 + 7.52474113\cdot10^{-9}T^3$	[48]
			1045-3000	87.12	[48]
$CaCl_2$ (liquid)	-786860.75 [48]	104.602 [48]	S→L ΔH_{tr} = 28.543 kJ/mol at 1045 K (772 °C)		[237]
			1-50	$0.78155423 - 0.12359292T + 0.0306270316T^2 - 3.49282014\cdot10^{-4}T^3$	[48]
			50-180	$-16.732490 + 1.1686419T - 6.02988655\cdot10^{-3}T^2 + 1.1662759\cdot10^{-5}T^3$	[48]
			180-486	$43.925204 + 0.17176775T - 3.10281876\cdot10^{-4}T^2 + 1.97728035\cdot10^{-7}T^3$	[48]
			486-3000	116.0	[48]
Na_2MgCl_4	-1466400 [a]	240.945 [a]	1-40	$0.00542290420587499T - 0.00352251575673869T^2 + 9.93818776938874\cdot10^{-4}T^3 - 2.03142124845626\cdot10^{-5}T^4 + 4.77073775377446\cdot10^{-7}T^5 - 5.85664934270221\cdot10^{-9}T^6$	[a]
			40-298	$604.88136550599 - 3.94403453339611T + 477804.657730018T^{-2} + 0.0212022524873058T^2 - 5.87085199527924\cdot10^{-5}T^3 + 6.39602890667231\cdot10^{-8}T^4 - 29801.338587285/T$	[a]
			298-773	$135 + 0.1125T$	[a]
$NaMgCl_3$	-1055400 [a]	168.611 [a]	1-40	$-0.00663995599511934T - 0.00130194941574864T^2 + 3.07349307982698\cdot10^{-4}T^3 + 1.03232608047322\cdot10^{-5}T^4 - 2.64274300354774\cdot10^{-7}T^5 - 7.96852286746871\cdot10^{-10}T^6$	[a]
			40-298	$403.698207521254 - 2.6675079453525T + 297316.750118745T^{-2} + 0.0143477362359946T^2 - 3.99198856695826\cdot10^{-5}T^3 + 4.39813847497758\cdot10^{-8}T^4 - 19168.6925345792/T$	[a]
			298-1000	$90 + 0.075T$	[a]
$KMgCl_3$ (LT)	-1091276 [a]	182.91 [a]	1-40	$0.01434000756073l5T - 0.00609339716120444T^2 + 0.00107324960492649T^3 - 3.48425291441905\cdot10^{-5}T^4 + 8.0398011970119\cdot10^{-7}T^5 - 7.79100435267131\cdot10^{-9}T^6$	[a]
			40-298	$453.844447306611 - 2.93044154420064T + 378545.792230591T^{-2} + 0.016211967322187T^2 - 4.61482545825587\cdot10^{-5}T^3 + 5.14251895056537\cdot10^{-8}T^4 - 23024.173528421/T$	[a]
			298-5000	$123.710790568024 + 0.0270730210924837T - 2169.44177994039T^{-2} - 2.24274957859515\cdot10^{-6}T^2$	[a]
$KMgCl_3$ (HT)	-1090020 [a]	185.002 [a]	LT→HT ΔH_{tr} = 1.3 kJ/mol at 600 K (326.9 °C)		[228]
			1-40	$0.0144833564109219T - 0.00615431661079951T^2 + 0.00108398067041603T^3 - 3.51908905019105\cdot10^{-5}T^4 + 8.12018591634669\cdot10^{-7}T^5 - 7.86890394310494\cdot10^{-9}T^6$	[a]
			40-298	$475.619686088299 - 3.06804778907046T + 400207.653359349\ T^{-2} + 0.0163649022958513T^2 - 4.44532897508209\cdot10^{-5}T^3 + 4.69325956527989\cdot10^{-8}T^4 - 24221.9341726372/T$	[a]
			298-5000	$123.710790568024 + 0.0270730210924837T - 2169.44177994039T^{-2} - 2.24274957859515\cdot10^{-6}T^2$	[a]
K_2MgCl_4	-1530010 [a]	265 [a]	1-40	$0.0208789187619569T - 0.0088719478824875T^2 - 0.0088719478824875T^3 - 5.073054656934\cdot10^{-5}T^4 + 1.17059133744953\cdot10^{-6}T^5 - 1.13436726859226\cdot10^{-8}T^6$	[a]
			40-298	$659.052172236215 - 4.25581683704046T + 549348.028446282T^{-2} + 0.0236063355328872T^2 - 6.74138595798356\cdot10^{-5}T^3 + 7.53878154267351\cdot10^{-8}T^4 - 33425.0601851172/T$	[a]

			298-5000	176.341638735329 + 0.0410241443105296T + 304829.811924281T^{-2} - 3.5840156614721·$10^{-6}T^2$	[a]
$K_3Mg_2Cl_7$	-2622310 [a]	448.535 [a]	1-40	0.035104012556746T - 0.0149165387665822T^2 + 0.00262730497773045T^3 - 8.52940440098243·$10^{-5}T^4$ + 1.96813328499584 ·$10^{-6}T^5$ - 1.90722973241753·$10^{-8}T^6$	[a]
			40-298	1095.6129966755 - 7.07692430726866T + 910714.022343872T^{-2} + 0.0396944919011202T^2 – 1.14894508040871·$10^{-4}T^3$ + 1.30357145560559·$10^{-7}T^4$ - 55498.9903296159/T	[a]
			298-5000	295.78963584469 + 0.0701460293601505T + 627551.683475232T^{-2} - 5.9875787327355·$10^{-6}T^2$	[a]
$KCaCl_3$ (LT)	-1252154 [48]	191.275 [48]	1-20	0.02042140607144 - 0.08102903517857T + 0.01260697757143T^2 + 0.00072166465T^3	[48]
			20-130	-28.1569247085101 + 1.97133832624177T - 0.009273469389867T^2 + 1.357783207·$10^{-5}T^3$	[48]
			130-420	59.2329660663033 + 0.45102019096191T - 0.001097496778687T^2 + 9.9799118·$10^{-7}T^3$	[48]
			420-824	97.4303735543922 + 0.0883721089112T - 3.572031881·$10^{-5}T^2$ + 1.129553·$10^{-8}T^3$	[48]
			824-907	97.0096327351631 + 0.07398639190124T - 1.920371333·$10^{-5}T^2$ + 4.48214·$10^{-9}T^3$	[48]
			907-1018	93.802702727389 + 0.07154056076401T - 1.85688798·$10^{-5}T^2$ + 4.33397·$10^{-9}T^3$	[48]
$KCaCl_3$ (MT)	-1251634 [48]	191.906 [48]	LT→MT ΔH_{tr} = 0.52 kJ/mol at 824 K (550.8 °C), C_p like $KCaCl_3$ (LT)		[48]
$KCaCl_3$ (HT)	-1251414 [48]	192.149 [48]	MT→HT ΔH_{tr} = 0.52 kJ/mol at 907.2 K (634 °C), C_p like $KCaCl_3$ (LT)		[48]
Na_2SO_4 (LT)	-1387900 [228]	149.58 [228]	1-34	2.86·$10^{-4}T^3$	[39]
			34-298	60.363842 + 0.3702618T + 37895.87535T^{-2} - 3.6413037·$10^{-4}T^2$ - 3197.4504/T	[39]
			298-458	80.81543 + 0.1586519T	[228]
			458-514	93.34096 + 0.1313035T	[228]
			514-1157	161.54872 + 0.01536T - 4636382.93347T^{-2} + 3.31857·$10^{-5}T^2$	[39]
			1157-3500	197.033	[228], [39]
Na_2SO_4 (MT)	-1387600 [228]	150.235 [228]	LT→MT ΔH_{tr} = 0.3 kJ/mol at 458 K (185 °C), C_p like Na_2SO_4 (LT)		[228]
Na_2SO_4 (HT)	-1378105 [39]	168.233 [39]	MT→HT ΔH_{tr} = 10.9 kJ/mol at 514 K (241 °C)		[228]
			1-34	2.86·$10^{-4}T^3$	[39]
			34-298	60.363842 + 0.3702618T + 37895.87535T^{-2} - 3.6413037·$10^{-4}T^2$ - 3197.4504/T	[39]
			298-514	62.99363 + 0.21808T	[39]
			514-1157	208.1015 - 0.1314436T + 1485.492T^{-2} + 1.323406·$10^{-4}T^2$	[228]
			1157-3500	197.033	[228], [39]
Na_2SO_4 (liquid)	-1365585 [39]	158.177 [39]	HT→L ΔH_{tr} = 23.5 kJ/mol at 1157 K (884 °C)		[228]
			1-34	2.86·$10^{-4}T^3$	[39]
			34-265	60.363842 + 0.3702618T + 37895.87535T^{-2} - 3.6413037·$10^{-4}T^2$ - 3197.4504/T	[39]
			265-3500	197.033	[228], [39]
K_2SO_4 (LT)	-1437710 [228]	175.544 [228]	1-36	4.93196231·$10^{-4}T^3$	[39]
			36-298	110.03412 + 0.10558283T + 53579.32526T^{-2} + 5.6608246·$10^{-5}T^2$ - 4741.22424 /T	[39]
			298-857	108.173 + 0.105551T - 837910T^{-2} + 1.27682·$10^{-5}T^2$	[228]
			857-1342	114.287 + 0.0814451T + 1290T^{-2} - 1.1245·$10^{-5}T^2$	[228]
			1342-1500	201.46	[228]
K_2SO_4 (HT)	-1423818 [39]	193.415 [39]	LT→HT ΔH_{tr} = 8.5 kJ/mol at 857 K (583.9 °C), C_p like K_2SO_4 (LT)		[228], [39]
K_2SO_4 (liquid)	-1409976 [39]	175.553 [39]	HT→L ΔH_{tr} = 34.4 kJ/mol at 1342 K (1068.9 °C)		[228]
			1-36	4.93196231·$10^{-4}T^3$	[39]
			36-315	110.03412 + 0.10558283T + 53579.32526T^{-2} + 5.6608246·$10^{-5}T^2$ - 4741.22424 /T	[39]
			315-1500	201.46	[39]

$MgSO_4$ (LT)	-1288800 [228]	91.6 [228]	1-42	$8.73213058 \cdot 10^{-5}T^3$	[39]
			42-298	$10.582036 + 0.44690916T + 34086.236T^{-2} - 4.7507286 \cdot 10^{-4}T^2 - 1740.55857/T$	[39]
			298-1283	$85.18297 + 0.08756883T - 1167240T^{-2} - 1.982192 \cdot 10^{-5}T^2$	[228]
			1283-2000	155	[228]
$MgSO_4$ (HT)	-1274200 [a]	102.828 [a]	$LT \rightarrow HT\ \Delta H_{tr}$ = 14.6 kJ/mol at 1300.3 K (1027.1 °C), C_p like $MgSO_4$ (LT)		[a]
$MgSO_4$ (liquid)	-1238766 [a]	120.880 [a]	$HT \rightarrow L\ \Delta H_{tr}$ = 43.4 kJ/mol at 1410.2 K (1137.0 °C)		[228], [a]
			1-42	$8.73213058 \cdot 10^{-5}T^3$	[39]
			42-298	$10.582036 + 0.44690916T + 34086.236T^{-2} - 4.7507286 \cdot 10^{-4}T^2 - 1740.55857/T$	[39]
			298-1283	$85.18297 + 0.08756883T - 1167240T^{-2} - 1.982192 \cdot 10^{-5}T^2$	[228]
			1283-2000	155	[228]
$CaSO_4$ (LT)	-1437622 [228]	107.492 [146]	1-39	$1.58639676 \cdot 10^{-4}T^3$	[39]
			39-298	$60.2427676 + 0.22021804T + 73416.5259T^{-2} - 1.3048247 \cdot 10^{-4}T^2 - 4185.07635/T$	[39]
			298-1784	$100.854288 + 0.06896988T - 1736052.08T^{-2} - 8.6603105 \cdot 10^{-6}T^2$	[39]
			1784-2000	195.63	[a]
$CaSO_4$ (HT)	-1420012 [39]	119.282 [39]	$LT \rightarrow HT\ \Delta H_{tr}$ = 17.6 kJ/mol at 1493.6 K (1220.4 °C), C_p like $CaSO_4$ (LT)		[39], [a]
$CaSO_4$ (liquid)	-1425938 [39]	107.714 [a]	$HT \rightarrow L\ \Delta H_m$ = 16 kJ/mol at 1783.6 K (1510.4 °C)		[39], [a]
			1-39	$1.58639676 \cdot 10^{-4}T^3$	[39]
			39-298	$60.2427676 + 0.22021804T + 73416.5259T^{-2} - 1.3048247 \cdot 10^{-4}T^2 - 4185.07635/T$	[39]
			298-795	$100.854288 + 0.06896988T - 1736052.08T^{-2} - 8.6603105 \cdot 10^{-6}T^2$	[39]
			795-2000	195.63	[39]
$Na_6Mg(SO_4)_4$	-5475977 [a]	555.06 [39]	1-40	$0.0967225949075733T - 0.0291776237831126T^2 + 0.00326319051205519T^3 - 0.000108922525821161T^4 + 2.0321941793195 \cdot 10^{-6}T^5 - 1.47050844266121 \cdot 10^{-8}T^6$	[264], [a]
			40-298	$1117.51413153541 - 7.19388975961303T + 1160043.61054648T^{-2} + 0.0535009723706019T^2 - 0.000182194933644599T^3 + 2.25886612239128 \cdot 10^{-7}T^4 - 63770.1302778353T^{-1}$	[264], [a]
			298-780	$301.28724 + 0.73896511T - 1081383.89T^{-2} - 2.89072633 \cdot 10^{-4}T^2$	[39]
$Na_2Mg(SO_4)_2$ (LT)	-2684197 [a]	254.4 [a]	1-40	$0.0424705237362021T - 0.0124021173781477T^2 + 0.00134815835330562T^3 - 4.24482690007059 \cdot 10^{-5}T^4 + 7.50864769573235 \cdot 10^{-7}T^5 - 5.13350584277551 \cdot 10^{-9}T^6$	[264], [a]
			40-298	$493.448593241483 - 3.19272619256448T + 520434.041046126T^{-2} + 0.0246869034295407T^2 - 8.54485737404076 \cdot 10^{-5}T^3 + 1.06738318792183 \cdot 10^{-7}T^4 - 28399.3078588106T^{-1}$	[264], [a]
			298-880	$158.48514 + 0.29826393T - 1143672.89\ T^{-2} - 1.03443711 \cdot 10^{-4}T^2$	[39]
$Na_2Mg(SO_4)_2$ (MT)	-2680710 [39]	257.18 [39]	$LT \rightarrow MT\ \Delta H_{tr}$ = 1.647 kJ/mol at 548 K (275 °C)		[39]
			1-40	$0.0452582752555805T - 0.0136527441676933T^2 + 0.00152690657084644T^3 - 5.09668273245906 \cdot 10^{-5}T^4 + 9.50900361044361 \cdot 10^{-7}T^5 - 6.88077332405548 \cdot 10^{-9}T^6$	[264], [a]
			40-298	$536.080690096592 - 3.44906377096178T + 556460.301132334T^{-2} + 0.0250287389114654T^2 - 8.36118545341094 \cdot 10^{-5}T^3 + 1.01881787953935 \cdot 10^{-7}T^4 - 30578.4014420163T^{-1}$	[264], [a]
			298-880	$158.48514 + 0.29826393T - 1143672.89\ T^{-2} - 1.03443711 \cdot 10^{-4}T^2$	[39]
$Na_2Mg(SO_4)_2$ (HT)	-2678445 [39]	260.19 [39]	$MT \rightarrow HT\ \Delta H_{tr}$ = 2.265 kJ/mol at 753 K (480 °C)		[39]
			1-40	$0.0452582752555805T - 0.0136527441676933T^2 + 0.00152690657084644T^3 - 5.09668273245906 \cdot 10^{-5}T^4 + 9.50900361044361 \cdot 10^{-7}T^5 - 6.88077332405548 \cdot 10^{-9}T^6$	[264], [a]
			40-298	$536.05364435053 - 3.44875348353241T + 556442.807507352T^{-2} + 0.0250269327732739T^2 - 8.36067369851824 \cdot 10^{-5}T^3 + 1.01876203846262 \cdot 10^{-7}T^4 - 30577.2756677046T^{-1}$	[264], [a]

			298-880	158.48514 + 0.29826393T-1143672.89 T^{-2} - 1.03443711·$10^{-4}T^2$	[39]
$Na_2Mg_3(SO_4)_4$	-5260974 [a]	456.68 [39]	1-40	0.0671421354401656T - 0.0180645656739119T^2 + 0.00182964247027248T^3 - 4.68605402988581·$10^{-5}T^4$ + 6.59081899507656·$10^{-7}T^5$ - 3.24665849200665·$10^{-9}T^6$	[264], [a]
			40-298	804.714539202214 - 5.28197097625234T + 875925.373876772T^{-2} + 0.0448262723762568T^2 - 0.000161055179855131T^3 + 2.04971963131772·$10^{-7}T^4$ - 47108.8041097587T^{-1}	[264], [a]
			298-1100	338.84422 + 0.42565089T - 3520610.75T^{-2} - 9.65937193·$10^{-5}T^2$	[39]
$Na_2Ca(SO_4)_2$	-2851669 [a]	257.072 [a]	1-40	0.0404823106512207T - 0.011386782654179T^2 + 0.00119850154098668T^3 - 3.47493555383553·$10^{-5}T^4$ + 5.66348660882418·$10^{-7}T^5$ - 3.50955711217862·$10^{-9}T^6$	[264], [a]
			40-298	485.770729051669 - 3.16102420452602T + 520131.07491148T^{-2} + 0.0250441741230522T^2 - 8.70656764614227·$10^{-5}T^3$ + 1.08439154194594·$10^{-7}T^4$ - 28176.9046664479T^{-1}	[264], [a]
			298-1183	199.01893 + 0.22177562T - 2559395.63T^{-2} - 6.90796848·$10^{-5}T^2$	[39]
$Na_4Ca(SO_4)_3$	-4216029 [a]	406.652 [a]	34-39	120.727684 + 0.7405236T + 75791.7507T^{-2} + 0.00072826074T^2 - 0.000158639676T^3 - 6394.9008T^{-1}	[a]
			39-298	180.9704516 + 0.96074164T + 149208.2766T^{-2} - 0.00085874321T^2 - 10579.97715T^{-1}	[a]
			298-458	262.485148 + 0.386273682T - 1736052.08T^{-2} - 8.6603105·$10^{-5}T^2$	[a]
			458-514	287.536208 + 0.331576882T - 1736052.08T^{-2} - 8.6603105·$10^{-5}T^2$	[a]
			514-1157	423.951728 + 0.099689882T - 11008817.94694T^{-2} + 5.77110895·$10^{-5}T^2$	[a]
			1157-1780	494.920288 + 0.068969882T - 1736052.08T^{-2} - 8.6603105·$10^{-5}T^2$	[a]
			1780-3500	589.699423117135	[a]
$K_2Mg_2(SO_4)_3$	-4058580 [a]	378.244 [39]	1-25	0.00118508166T^3	[39]
			25-298	118.721426 + 0.9851507T + 60448.1877T^{-2} - 0.000846977431T^2 - 5536.7453T^{-1}	[39]
			298-1220	294.328177 + 0.30094091T - 818237.98T^{-2} - 0.00012192163T^2	[39]
$K_2Ca_2(SO_4)_3$ (LT)	-4309500 [39]	405.4 [39]	1-25	0.00147050569T^3	[39]
			25-298	156.14367 + 0.91747523T + 79864.2962T^{-2} - 0.00076792723T^2 - 7082.26024T^{-1}	[39]
			298-1283	318.26342 + 0.25842548T - 4707432.4T^{-2} - 5.09715831·$10^{-5}T^2$	[39]
$K_2Ca_2(SO_4)_3$ (MT)	-4307380 [39]	409.854 [39]	LT→MT ΔH_{tr} = 2.12 kJ/mol at 476 K (202.8 °C), C_p like $K_2Ca_2(SO_4)_3$ (LT)		[39]
$K_2Ca_2(SO_4)_3$ (HT)	-4273380 [39]	437.953 [39]	MT→HT ΔH_{tr} = 34 kJ/mol at 1210 K (936.8 °C), C_p like $K_2Ca_2(SO_4)_3$ (LT)		[39]
$CaMg(SO_4)_2$	-2678290 [a]	249.173 [a]	1-39	2.459609818·$10^{-4}T^3$	[a]
			39-42	60.2427676 + 0.22021804T + 73416.5259T^{-2} - 1.3048247·$10^{-4}T^2$ - 4185.07635/T + 8.73213058·$10^{-5}T^3$	[a]
			42-298	70.8248036 + 0.6671272T + 107502.76145T^{-2} - 6.0555533·$10^{-4}T^2$ - 5925.63492/T	[a]
			298-1800	181.98396 + 0.17561T - 3004485.32926T^{-2} - 4.59679·$10^{-5}T^2$	[a]
$CaMg_2(SO_4)_3$	-4054080 [a]	281.088 [a]	1-39	3.332822876·$10^{-4}T^3$	[a]
			39-42	60.2427676 + 0.22021804T + 73416.5259T^{-2} - 1.3048247·$10^{-4}T^2$ - 4185.07635/T + 1.746426116·$10^{-4}T^3$	[a]
			42-298	81.4068396 + 1.11403636T + 141588.997T^{-2} - 1.08062819·$10^{-3}T^2$ - 7666.19349/T	[a]
			298-1800	394.68198 - 0.01296T - 10918147.69689T^{-2} + 1.249221·$10^{-5}T^2$	[a]

[a] PCM2 database, in the frame of the database development of PCM-Screening-2 project [4]

6.1 Mg^{2+}, Ca^{2+} // Cl^-, SO_4^{2-} system

6.1.1 $MgSO_4$

The low-temperature heat capacity of $MgSO_4$, previously assessed by Yazhenskikh et al. [39] on the basis of data from [228, 255] had already been incorporated into the thermodynamic database. For temperature above 505 K (Kauzmann's temperature), the C_p of the liquid phase was assumed to remain constant. The standard formation enthalpy and standard entropy were adopted from the SGPS database [228] and retained unchanged in the assessment [39]. A summary of the thermodynamic properties of $MgSO_4$ is reported in **Table 6-1**.

In the present work, DSC measurements confirmed the validity of the heat capacity polynomial presented elsewhere [39]. The value of C_p of the liquid phase obtained experimentally by the SRCM method, and considered constant, is 154.5 J/(mol·K). This result is consistent with the value adopted in the current database of 155 J/(mol·K) [218, 228], which, therefore, can be considered experimentally validated in the present work. Accordingly, no modifications to the C_p values have been introduced in the updated database (**Table 6-1**).

In the previous assessment [39], the enthalpy of fusion was adopted from the SGPS database [228] and Glushko's reference book [92]. In this work, the DSC experiments - performed with proper sensitivity calibration and by integration of the C_p curves - enabled the determination of the enthalpies of the phase transitions, both for the solid-solid transition and for melting. These new experimental values differ significantly from those reported in the commercial databases [218, 228], as illustrated in **Figure 6-1** and summarised in **Table 6-1**. Based on these new experimental findings, the current database was updated in order to improve thermodynamic description of systems containing $MgSO_4$. The following values are proposed: 14.6 kJ/mol for the enthalpy of solid-solid transition and 43.4 kJ/mol for the enthalpy of fusion. The experimentally measured melting temperature agrees with values reported in the databases [218, 228], and thus remains unchanged. However, the experimental evidence indicates a different solid-solid transition temperature, compared to the values reported elsewhere [218, 228]; consequently, a value of 1027.1 °C has been introduced into the developed database.

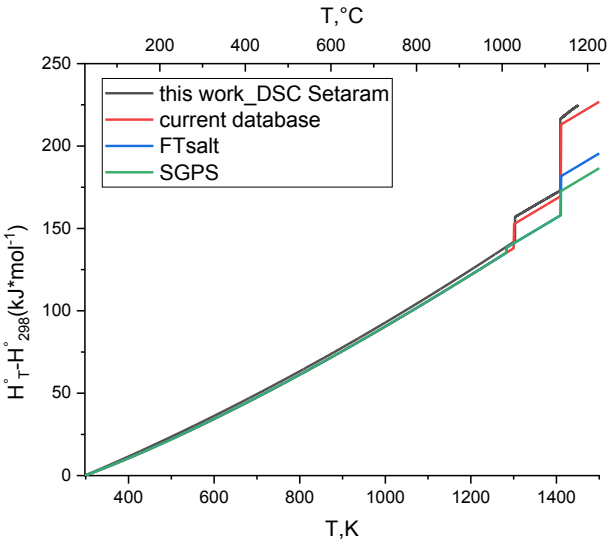


Figure 6-1 *Enthalpy increment of $MgSO_4$ obtained from DSC results in comparison with the current database and the commercial databases FTSalt [218] and SGPS [228].*

6.1.2 $CaSO_4$

The present study expands upon the thermodynamic assessment carried out by Yazhenskikh et al. [39], where new heat capacity polynomials were developed for the temperature range from 0 K to the melting point, based on experimental data [146]. The standard enthalpy and entropy values were adopted from the SGPS database [228] and the work of Robie et al. [146]. The C_p of the liquid phase was assumed to remain constant above the temperature at which the liquid and the solid entropies converge, and was extrapolated to temperatures below the melting point [39]. Experimental validation in the present work confirmed the values for heat capacity and solid-solid phase transition enthalpy (17.7 kJ/mol), resulting in no modifications to the database from the previous assessment (**Figure 6-2**). Therefore, enthalpy values of 17.6 and 16.0 kJ/mol obtained in [126] and used in the previous assessment [39] are considered for solid-solid and solid-liquid phase transitions, respectively. However, new experimental measurements provided slightly revised phase-transition temperatures compared with earlier literature data [126, 218, 228]. The updated values, 1220 °C for the solid-solid transition and 1510°C for melting, have been incorporated into the thermodynamic database.

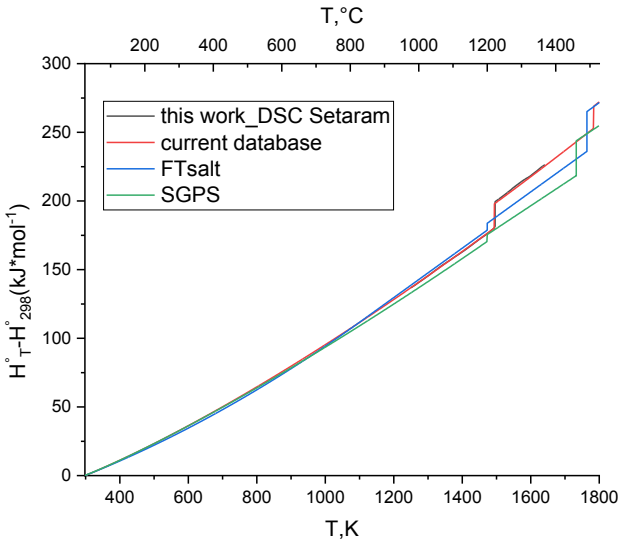


Figure 6-2 *Enthalpy increment of $CaSO_4$ obtained from DSC results in comparison with the current database and the commercial databases FTSalt [218] and SGPS [228].*

6.1.3 $CaMg_2(SO_4)_3$

Experimental evidence confirming the existence of an intermediate compound with a $MgSO_4$:$CaSO_4$ stoichiometric ratio of 2:1, rather than the previously assumed 3:1, has resulted in the replacement of the former compound in the current thermodynamic database. The values of standard formation enthalpy and standard entropy of the new compound were initially introduced based on the Neumann-Kopp rule, while the heat capacity and solid-liquid transition enthalpy values were introduced according to experimental data. **Figure 5-7** compares the C_p curves determined in this study with those calculated using the Neumann-Kopp rule and ab-initio calculations [265]. **Figure 6-3** presents the comparison between enthalpy increments obtained experimentally by DSC and those calculated using the current database. For the intermediate compound, the C_p of the solid phase was derived from experimental results and implemented in the database accordingly. Furthermore, the values of $\Delta_f H^0_{298}$ and S^0_{298}, were optimised to describe the solid-liquid equilibria in the binary system, as summarised in **Table 6-1**.

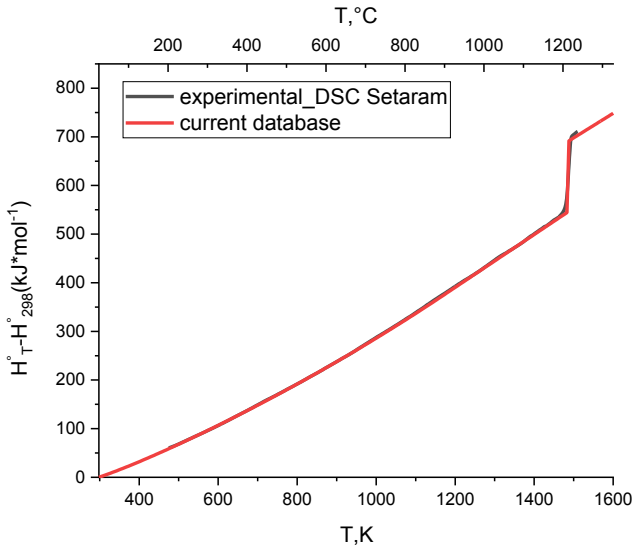


Figure 6-3 *Enthalpy increment of $CaMg_2(SO_4)_3$ obtained from DSC results in comparison with the current database.*

6.1.4 $CaMg(SO_4)_2$

The intermediate compound with a stoichiometric ratio of $MgSO_4$:$CaSO_4$ 1:1 was incorporated into the thermodynamic database, based on the experimental evidence presented in this study. The standard formation enthalpy $\Delta_f H^0_{298}$ and standard entropy S^0_{298}, as well as the heat capacity, were initially estimated using the Neumann-Kopp rule, derived from the thermodynamic properties of the pure sulphate components. The C_p values were kept unchanged. However, the experimental data detailed in section 5.1.6 indicate that this compound exhibits thermal stability in the narrow temperature range. To account for this behaviour, the initially estimated thermodynamic parameters ($\Delta_f H^0_{298}$ and S^0_{298}) were subsequently optimised. The final optimised values, summarised in **Table 6-1**, were determined to achieve better agreement between the calculated phase equilibria and the experimental observations, allowing for a more accurate representation of the compound's thermal decomposition behaviour and stability limits within the binary system.

6.1.5 $MgSO_4$-$CaSO_4$

A comprehensive re-assessment of the $MgSO_4$-$CaSO_4$ system was undertaken in this study, integrating new experimental phase equilibria data and calorimetric measurements. The thermodynamic database was revised to incorporate updated information for the pure sulphates and the two newly confirmed intermediate compounds with stoichiometries of 2:1, $CaMg_2(SO_4)_3$, and 1:1, $CaMg(SO_4)_2$.

The interaction parameters between $MgSO_4$ and $CaSO_4$ in the liquid phase were optimised using all available data obtained in this work (**Table 6-16**). The introduction of two intermediate compounds of different stoichiometry significantly modified the liquidus curve compared with the earlier assessment [39]. The phase diagram calculated using the new dataset is shown in **Figure 6-4**. It presents overall good agreement with the experimental observations, with minor discrepancies in the $MgSO_4$-rich region, likely due to the experimental difficulties associated with high-$MgSO_4$ compositions. These deviations, however, do not compromise the overall reliability of the dataset. The melting temperatures of the intermediate compounds, $CaMg_2(SO_4)_3$ and $CaMg(SO_4)_2$, were calculated at 1212.2 °C and 1313.3 °C, respectively. In addition, the eutectic point between $MgSO_4$ and $CaMg_2(SO_4)_3$ was predicted at 9.7 mol% $CaSO_4$ at 1089.2 °C. The eutectic between $CaMg_2(SO_4)_3$ and $CaMg(SO_4)_2$ was calculated to be very close to the congruent melting point of $CaMg(SO_4)_2$, 33.5 mol% $CaSO_4$ at 1213.0 °C. The calculated eutectic between $CaMg(SO_4)_2$ and $CaSO_4$ (71.5 mol% $CaSO_4$ at 1214.0 °C) was found in a good agreement with the data from [58] and the present measurements (71.5 mol% $CaSO_4$ at 1214.0 °C).

The calculated enthalpy of melting of the compound $CaMg_2(SO_4)_3$ (146.3 kJ/mol at 1212.2 °C) agrees very well with the measured values (145.5 kJ/mol at 1212.7 °C) (**Figure 6-3**).

Overall, the optimised interaction parameters deliver an enhanced thermodynamic description of the $MgSO_4$-$CaSO_4$ system, accurately reproducing the experimental phase transitions and providing a more robust representation of its phase equilibria and thermal stability.

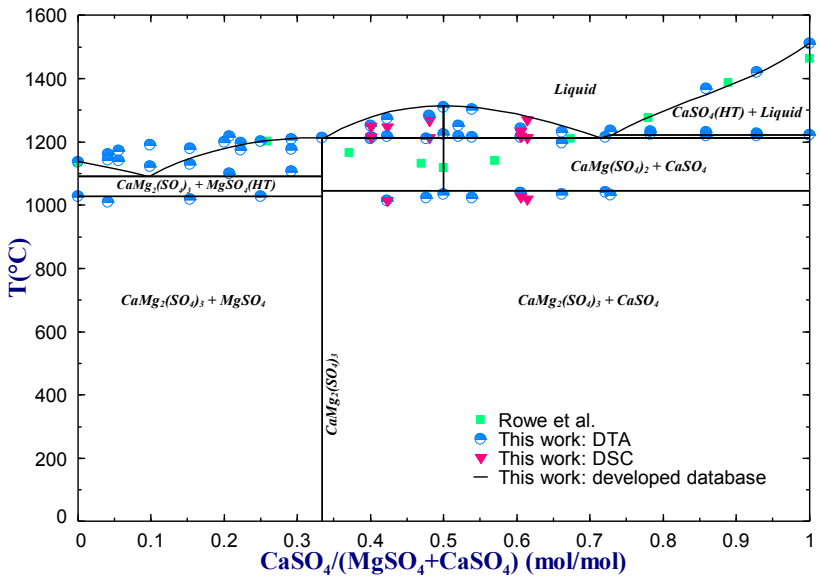


Figure 6-4 *Phase diagram of the $MgSO_4$-$CaSO_4$ system: comparison of the developed database with experimental data from the present work and Rowe et al. [58].*

6.1.6 $MgCl_2$-$CaCl_2$

The first thermodynamic optimisation of the phase diagram was carried out by Chartrand et al. [54], based on the experimental work of Grjotheim et al. [53]. Their assessment reported a eutectic temperature of 617 °C and a solid solubility of $MgCl_2$ in solid $CaCl_2$ below 18 mol% $MgCl_2$. This optimisation incorporated the activity of $MgCl_2$ in the molten phase, derived from electromotive force (emf) measurements [56], as well as the enthalpy of mixing in the liquid phase [57].

In the present study, a new optimisation of the binary system was conducted, integrating both literature data - specifically phase equilibria [53], activity of $MgCl_2$ at 800 °C [56] and enthalpy of mixing of the liquid at 800 °C [57] - with newly acquired experimental data. The latter include some transition temperature data of selected compositions and the determination of the latent enthalpy of fusion for the eutectic composition (47.19 mol% $CaCl_2$), measured as 33.2 kJ/mol at 624 °C (897 K). The sublattice model [266] was used to describe the solubility of $MgCl_2$ in $CaCl_2$, as mentioned in section 4.2.1.

The optimised interaction parameters are summarised in **Table 6-16**. **Figure 6-5** displays the recalculated phase diagram with a eutectic at 47.1 mol% $CaCl_2$ and 619.1 °C (892.3 K), and the limited solubility of $MgCl_2$ in $CaCl_2$ is up to 17.0 mol% at 619.1 °C. The calculated enthalpy of fusion for the eutectic mixture is 31.2 kJ/mol, in good agreement with the experimental value determined in this work, as displayed in **Figure 6-6**. The calculated activity of $MgCl_2$ in the liquid phase at 800 °C and enthalpy of mixing of the liquid at 800 °C are presented in **Figure 6-7** and **Figure 6-8**, respectively.

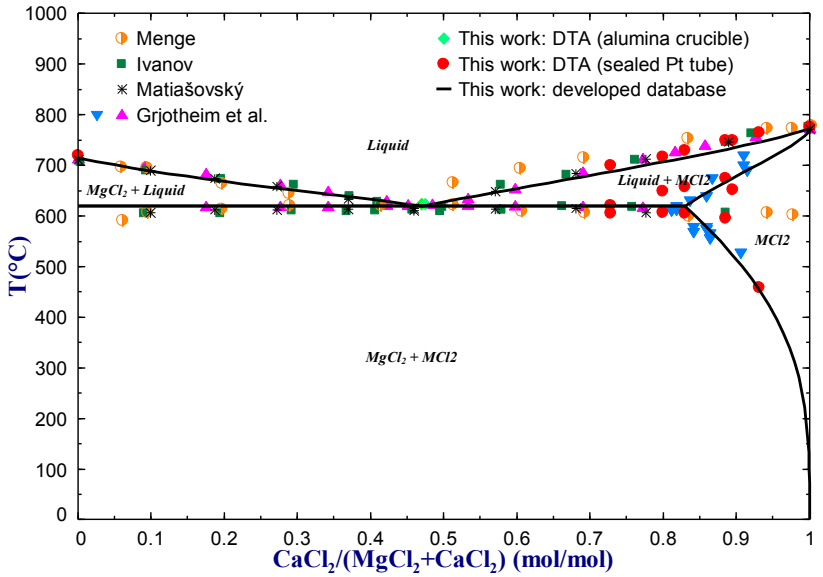


Figure 6-5 *Phase diagram of $MgCl_2$-$CaCl_2$ system: comparison of the developed database with experimental data from the present work and Menge [50], Ivanov [51], Matiašovský [52], Grjotheim et al. [53].*

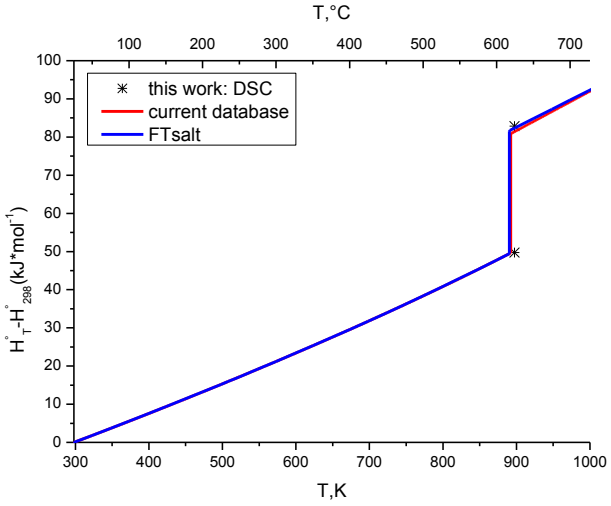


Figure 6-6 *Enthalpy increment of the $MgCl_2$(52.81 mol%)-$CaCl_2$(47.19 mol%) mixture obtained from DSC results in comparison with the current database and the commercial databases FTsalt [218].*

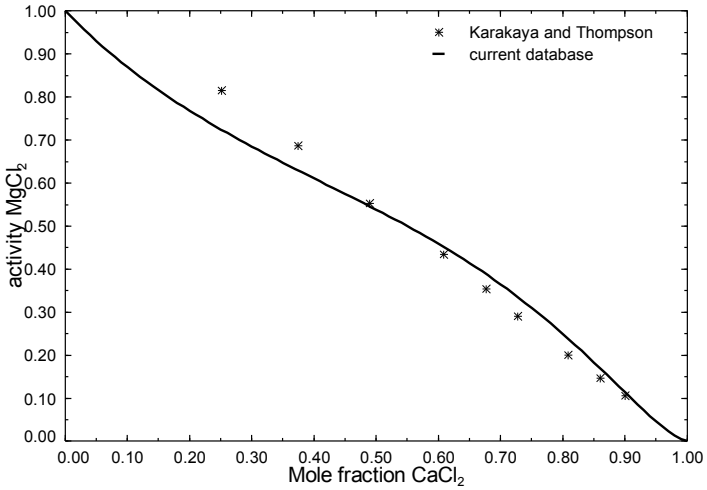


Figure 6-7 *Calculated activity of $MgCl_2$ in the liquid phase at 800 °C in comparison with Karakaya and Thompson [56].*

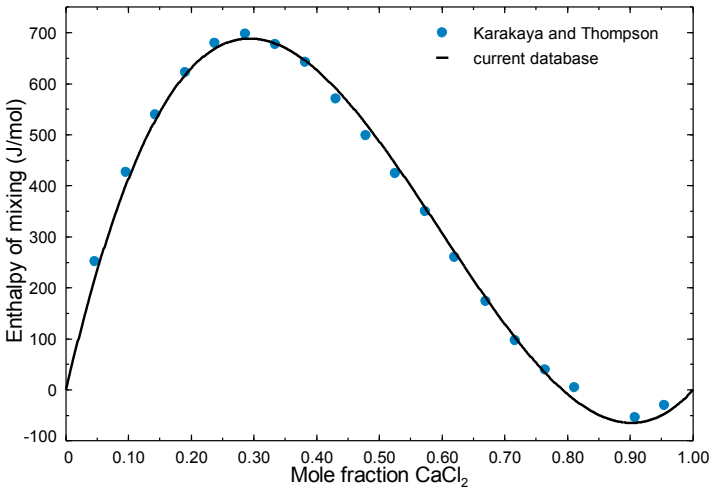


Figure 6-8 *Calculated enthalpy of mixing of the liquid phase at 800 °C in comparison with Karakaya and Thompson [57].*

6.1.7 $MgCl_2$-$MgSO_4$

In the present study, a comprehensive thermodynamic re-assessment of the binary system $MgCl_2$-$MgSO_4$ has been carried out by combining the new experimental data generated within this work with additional information from the literature. This re-assessment considered phase transitions determined by DTA, calorimetric data obtained by DSC on the eutectic composition, as well as transition temperatures and enthalpies of the pure sulphates. The thermodynamic data on the solution components and the interaction parameters are summarised in **Table 6-16**, and the corresponding calculated phase diagram, obtained with the updated thermodynamic database, is presented in **Figure 6-9**. The reassessed phase diagram exhibits a good agreement with the experimental results from this study, whereas discrepancies with earlier measurements reported in the literature [62, 63] justified the need for this re-evaluation and the subsequent database update. The eutectic composition was calculated at 27.9 mol% $MgSO_4$ with a melting temperature of 663.0 °C (936.2 K), which closely matches the experimental value determined in this work, 28.0 mol% $MgSO_4$ at 663.0 °C (936.2 K). The calculated enthalpy of fusion for the eutectic composition is 37.25 kJ/mol, showing good agreement with the experimentally measured average value of 37.92 kJ/mol. **Figure 6-10** compares these values with that obtained from the commercial FTsalt database [218], clearly demonstrating the substantial improvements in thermodynamic consistency and phase-equilibria prediction achieved through this re-assessment. A slight misalignment of the enthalpy increment curves at high temperatures between the experimental results and those calculated from the updated database can be attributed to the previously mentioned discrepancies in the heat capacity curves, most likely arising from inconsistencies in the reported C_p values of $MgCl_2$ (section 5.1.1). In this work,

however, the primary objective was to determine an accurate experimental value for the latent enthalpy of fusion of the eutectic mixture, as this property represents one of the key parameters for optimising the thermodynamic description of the system and for developing a reliable and internally consistent database. Furthermore, this value was considered essential to assess the potential suitability of the eutectic composition as PCM candidate. The noted discrepancies in the high-temperature enthalpy increments are therefore acknowledged but are considered beyond the scope of the present study. A more detailed investigation of this aspect is recommended for future work.

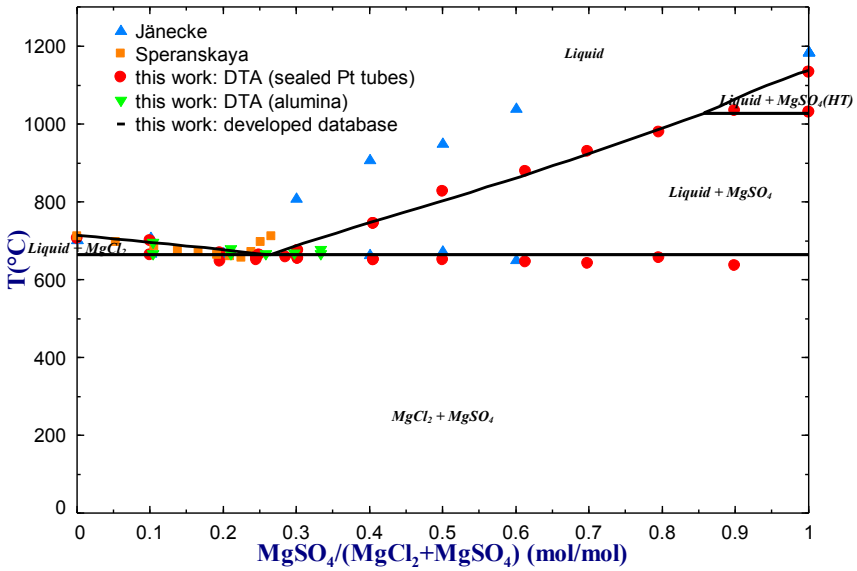


Figure 6-9 *Phase diagram of the $MgCl_2$-$MgSO_4$ system: comparison of the developed database with experimental data from the present work and Jänecke [62], and Speranskaya [63].*

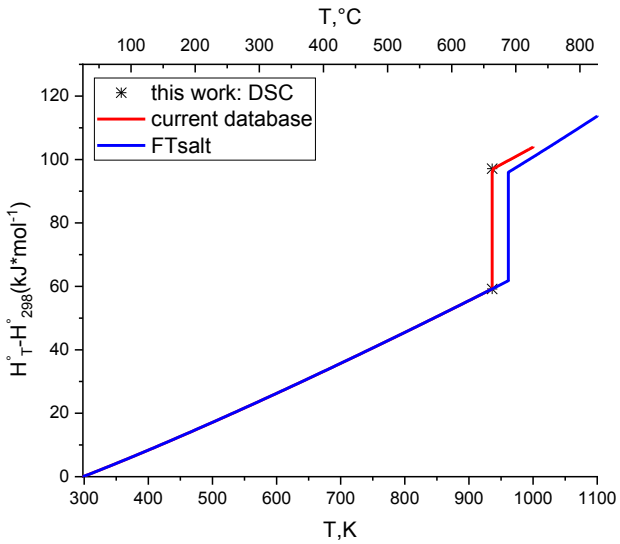


Figure 6-10 *Enthalpy increment of the $MgCl_2$(72.0 mol%)-$MgSO_4$(28.0 mol%) mixture obtained from DSC results in comparison with the current database and the commercial database FTsalt [218].*

6.1.8 $CaCl_2$-$CaSO_4$

The binary system $CaCl_2$-$CaSO_4$ was thermodynamically re-assessed by integrating the new experimental data generated in this study with relevant information previously reported in the literature. In particular, phase transition temperatures determined by DTA and enthalpic data from DSC on the eutectic composition were incorporated into the optimisation. The data were implemented in FactSage, and the thermodynamic properties were optimised using the Calphad Optimizer module. The optimised interaction parameters for the liquid phase are reported in **Table 6-16**, while the resultant phase diagram computed using the revised database is displayed in **Figure 6-11**. The calculated phase diagram exhibits excellent agreement with both the new experimental data presented here and earlier findings from the literature [67, 69]. The eutectic composition was calculated at 14.20 mol% $CaSO_4$, with a melting point of 721.5 °C (994.7 K), which is in very close agreement with the experimental composition of 13.99 mol% $CaSO_4$ at 721.5 °C (994.7 K). The calculated eutectic enthalpy of fusion is 30.07 kJ/mol, closely aligning with the experimental value of 30.21 kJ/mol. A direct comparison with the commercial FTsalt database [218], presented in **Figure 6-12**, highlights the significant improvements in the thermodynamic description achieved through this revised optimisation.

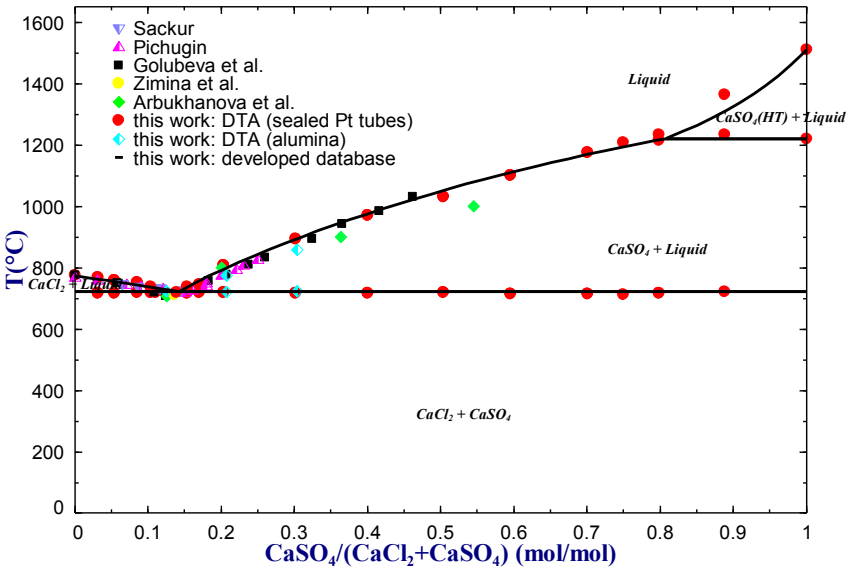


Figure 6-11 *Phase diagram of the $CaCl_2$-$CaSO_4$ system: comparison of the developed database with experimental data from the present work and Sackur [66], Pichugin [67], Golubeva et al. [69], Zimina et al. [71], Arbukhanova et al. [72].*

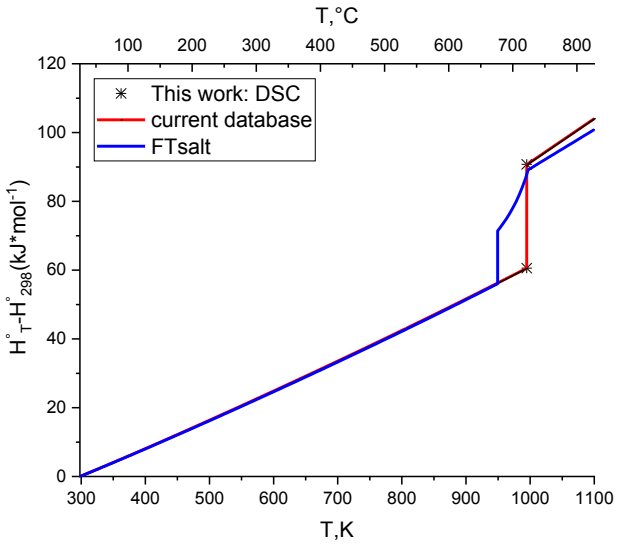


Figure 6-12 *Enthalpy increment of the $CaCl_2$(86.01 mol%)-$CaSO_4$(13.99 mol%) mixture obtained from DSC results in comparison with the current database and the commercial database FTsalt [218].*

6.1.9 $MgCl_2$-$CaSO_4$

The thermodynamic assessment of the $MgCl_2$-$CaSO_4$ system was primarily based on the phase transition temperatures determined by DTA measurements, as these represent the only experimental data currently available in the literature. The optimised interaction parameters of the liquid phase are reported in **Table 6-16**. The calculated phase diagram and its comparison with the experimental data are shown in **Figure 6-13**. Overall, the optimised thermodynamic description provides a reliable representation of the phase equilibria of the system. In addition to the DTA results, the calorimetric data on the $MgCl_2$(78.34 mol%)-$CaSO_4$(21.66 mol%) mixture were also incorporated into the thermodynamic assessment to further constrain and validate the optimisation. **Figure 6-14** presents the comparison between the experimentally determined enthalpy increments as a function of temperature, obtained by integration of the measured heat capacity curves, and those calculated from the updated database. The updated dataset predicts a liquidus minimum at 20.4 mol% $CaSO_4$ and 621.7 °C (894.9 K), corresponding to the transition Liquid ⇌ $MgCl_2$ + $CaMg_2(SO_4)_3$ + Liquid. At this composition a low-temperature thermal effect, corresponding to the transition Liquid + $MgCl_2$ + $CaMg_2(SO_4)_3$ ⇌ $CaCl_2$ + $MgCl_2$ + $CaMg_2(SO_4)_3$, is calculated at 577.8 °C (851.0 K). The observed agreement between experimental and calculated data (**Figure 6-14**) confirms the internal consistency of the optimised thermodynamic parameters and supports their predictive capability for phase equilibria modelling, further demonstrating the improved reliability of the database developed in this work compared to the commercial FTsalt database [218]. In particular, the present calculations correctly reproduce the presence of two transitions, whereas the FTsalt database predicted only one. The small temperature difference between calculated and measured transition points is acceptable

and arises from the need to use a single, transferable set of parameters that consistently reproduces phase equilibria and thermodynamic properties not only in this subsystem, but also across the other subsystems and the overall reciprocal system.

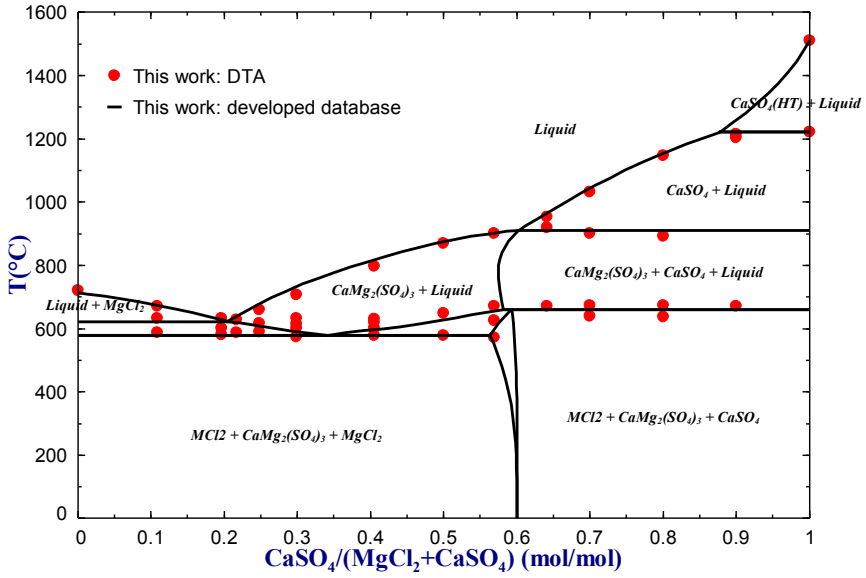


Figure 6-13 *Phase diagram of the $MgCl_2$-$CaSO_4$ system: comparison of the developed database with experimental data from the present work.*

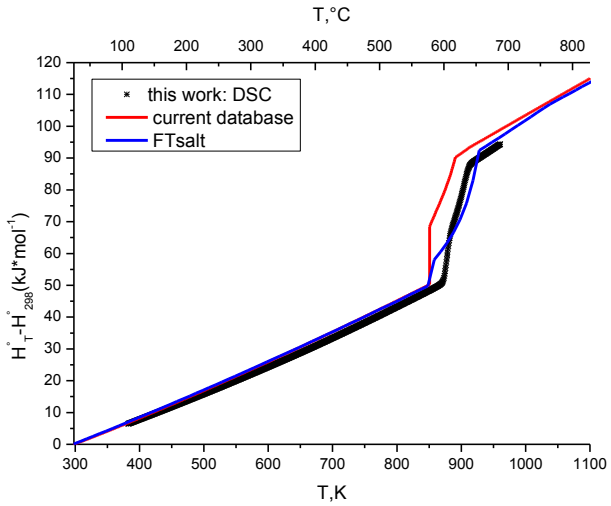


Figure 6-14 *Enthalpy increment of the $MgCl_2$(78.34 mol%)-$CaSO_4$(21.66 mol%) mixture obtained from DSC results in comparison with the current database and the commercial database FTsalt [218].*

6.1.10 $CaCl_2$-$MgSO_4$

The thermodynamic modelling of the $CaCl_2$-$MgSO_4$ binary system was performed based on the phase equilibria information acquired in this work. The phase transition temperatures determined experimentally by DTA served as the primary basis for optimising the liquid-phase description within the Calphad Optimizer module. The optimised interaction parameters are summarised in **Table 6-16** while the resulting calculated phase diagram, plotted together with the experimental data points, is presented in **Figure 6-15**. The updated thermodynamic description provides a consistent and reliable representation of the phase behaviour of the system and constitutes the first thermodynamic assessment available in the literature. The optimised dataset predicts a liquidus minimum at 20.2 mol% $MgSO_4$ and 658.0 °C (931.2 K), corresponding to the transition Liquid ⇌ $CaCl_2$ + $CaMg_2(SO_4)_3$ + Liquid.

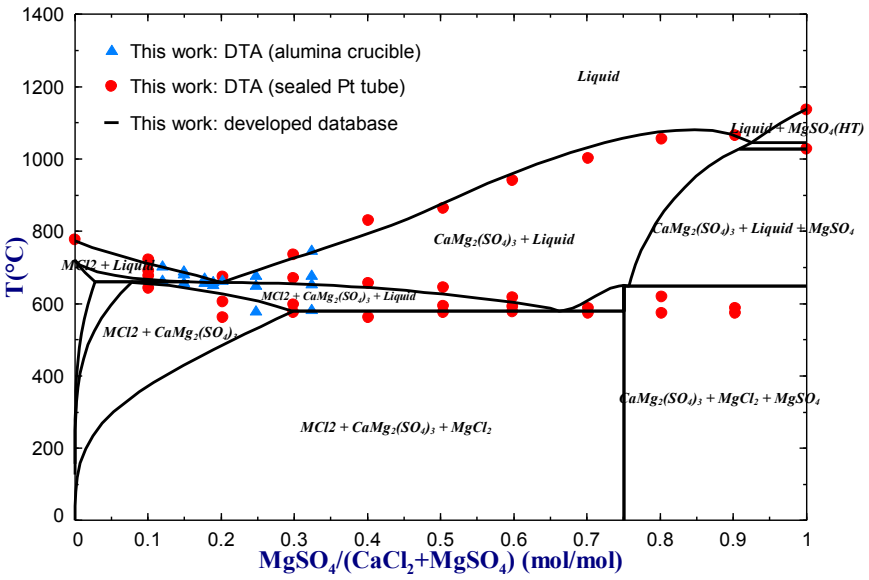


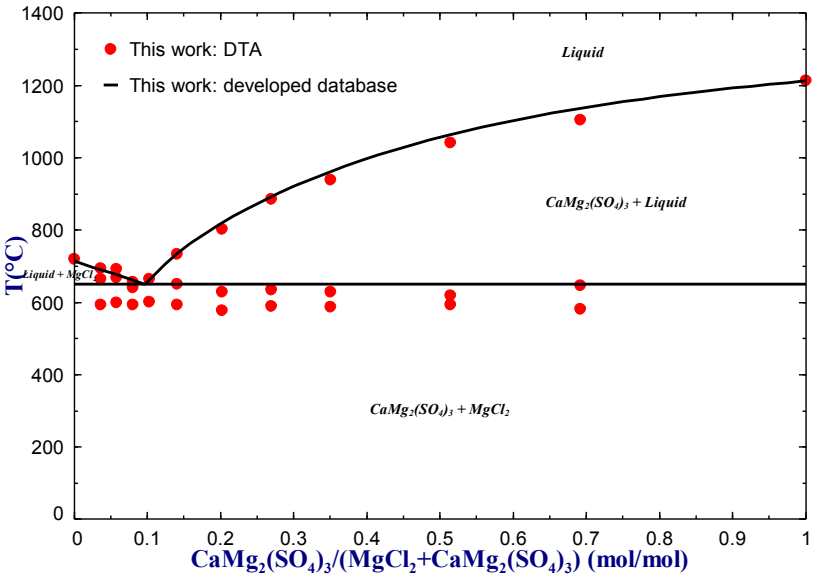
Figure 6-15 *Phase diagram of the $CaCl_2$-$MgSO_4$ system: comparison of the developed database with experimental data from the present work.*

6.1.11 The reciprocal system

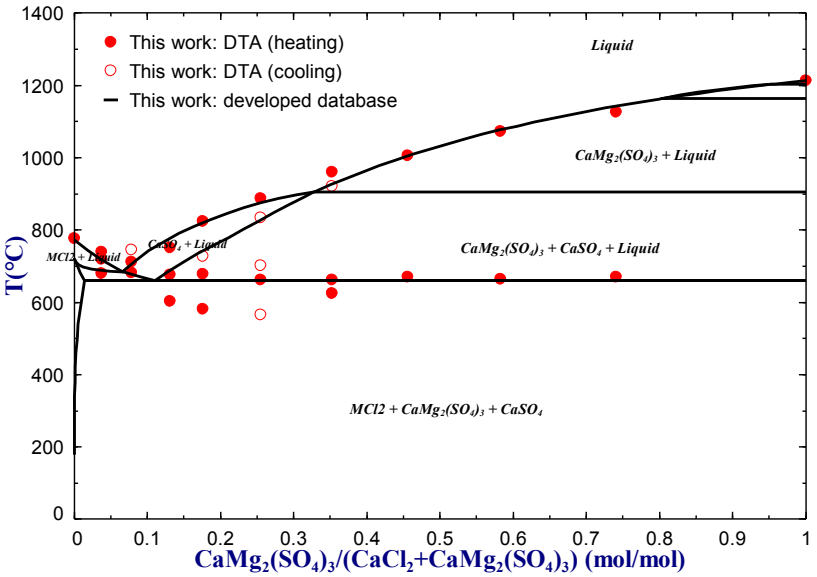
The thermodynamic assessment of the reciprocal system was performed by combining the experimental data obtained in this study with relevant literature data, following a stepwise approach progressing from simpler to progressively more complex subsystems. The optimisation was primarily based on the thermodynamic description of four key binary systems and two quasi-binary sections representative of the ion-exchange reaction. Each of the binary subsystems was individually assessed according to the available experimental evidence, as detailed in the preceding sections. In contrast,

the optimisation of the reciprocal system (i.e., the two diagonals) required the simultaneous refinement of the two pairs of interaction parameters, rather than an independent optimisation of each diagonal. This ensured a consistent description of the ion-exchange equilibria across the entire reciprocal system. The experimental investigations on the $MgCl_2$-$CaMg_2(SO_4)_3$ and $CaCl_2$-$CaMg_2(SO_4)_3$ sections served as an independent validation tool of the thermodynamic database. These sections were not included in the optimisation procedure but were instead used *a posteriori* to verify the reliability of the optimised parameters derived from the assessment of the six primary systems. The comparison between the calculated phase equilibria and the experimental observations is shown in **Figure 6-16**, demonstrating the consistency between the optimised database and independent experimental findings.

Based on the thermodynamic optimisation of the binary sub-systems (**Table 6-16**), the reciprocal system was calculated and the liquidus surface is presented in **Figure 6-17**. The calculated phase diagram indicates eight primary crystallisation fields and several minima in the liquidus projections, as listed in **Table 6-2**. These compositions represent promising candidates for future experimental verification and may also be evaluated for their suitability as PCMs for thermal energy storage applications; they could be investigated in a dedicated follow-up experimental campaign.



a



b

Figure 6-16 *Comparison of experimental and calculated phase diagram of:* ***a*** *$MgCl_2$-$CaMg_2(SO_4)_3$;* ***b*** *$CaCl_2$-$CaMg_2(SO_4)_3$ system.*

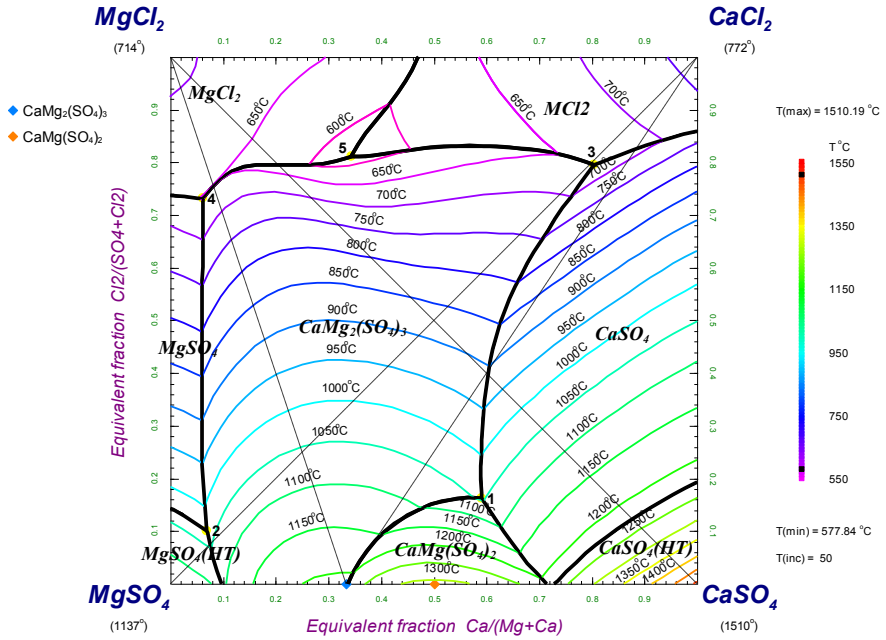


Figure 6-17 *Liquidus surface of the reciprocal system Mg^{2+}, Ca^{2+} // Cl^-, SO_4^{2-} calculated with the developed database.*

Table 6-2 *Calculated invariant points, expressed in equivalent fractions, in the reciprocal system Mg^{2+}, Ca^{2+} // Cl^-, SO_4^{2-}.*

	$\frac{Ca}{Mg+Ca}$	$\frac{Cl_2}{2SO_4+Cl_2}$	T, °C	Solid phase
1	0.5910	0.1624	1044.2	$CaSO_4$, $CaMg(SO_4)_2$, $CaMg_2(SO_4)_3$

2	0.0690	0.1005	1027.2	$MgSO_4$(LT), $MgSO_4$(HT), $CaMg_2(SO_4)_3$
3	0.8045	0.7955	658.6	MCl2, $CaSO_4$, $CaMg_2(SO_4)_3$
4	0.0612	0.7314	648.3	$MgCl_2$, $MgSO_4$(LT), $CaMg_2(SO_4)_3$
5	0.3438	0.8113	577.8	$MgCl_2$, MCl2, $CaMg_2(SO_4)_3$

6.2 Na^+, Mg^{2+} // Cl^-, SO_4^{2-} system

6.2.1 Na_2SO_4-$MgSO_4$

Given the modifications introduced in this work to the pure sulphate $MgSO_4$, specifically regarding the transition temperatures and the corresponding transition enthalpies, a re-assessment of the Na_2SO_4-$MgSO_4$ binary system was carried out within the PCM-Screening-2 project [4]. This re-assessment, based on the thermodynamic modelling by [39], employed the same dataset of thermodynamic values available in the literature [58, 63-65, 90], supplemented with the $MgSO_4$ updated data introduced in this study (**Table 6-1**), including the modified data on double-sulphates. The resulting calculated binary phase diagram is shown in **Figure 6-18**, and the corresponding re-optimised interaction parameters $L_{ij}^{(\nu)}$ for the liquid and solid phase HEXA are summarised in **Table 6-16**. The calculated invariant points of the studied system with the developed database are listed in **Table 6-3**.

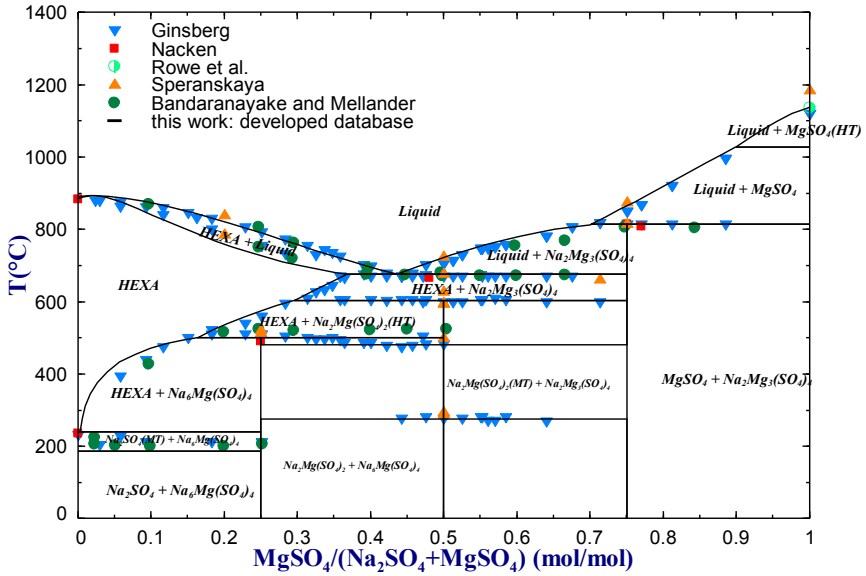


Figure 6-18 *Phase diagram of Na_2SO_4-$MgSO_4$ system: comparison of the developed database with experimental data from Ginsberg [65], Nacken [64], Rowe et al. [58], Speranskaya [63], Bandaranayake and Mellander [90].*

Table 6-3 *Calculated invariant points in the Na_2SO_4-$MgSO_4$ system.*

Reaction	Reaction type	$MgSO_4$, mol (in Liquid)	T, °C

HEXA ↔ $Na_6Mg(SO_4)_4$ + Na-ortho-MT	Eutectoid	0.003	240.3
$Na_6Mg(SO_4)_4$ ↔ HEXA + $Na_2Mg(SO_4)_2$ (HT)	Peritectoid	0.163	499.1
$Na_2Mg(SO_4)_2$ ↔ HEXA + $Na_2Mg_3(SO_4)_4$	Peritectoid	0.296	602.0
Solubility limit of $MgSO_4$ in HEXA		0.367	674.8
Liquid ↔ HEXA + $Na_2Mg_3(SO_4)_4$	Eutectic	0.437	674.8
$Na_2Mg(SO_4)_2$ (LT) ↔ $Na_2Mg(SO_4)_2$ (MT)	Transition		275.0
$Na_2Mg(SO_4)_2$ (MT) ↔ $Na_2Mg(SO_4)_2$ (HT)	Transition		480.0
$Na_2Mg_3(SO_4)_4$ ↔ Liquid + $MgSO_4$	Peritectic	0.702	812.7

6.2.2 NaCl-$MgSO_4$

The thermodynamic modelling of the NaCl-$MgSO_4$ system was carried out based on the experimental evidence obtained in this thesis work, supplemented by additional data available in the literature [63]. Specifically, the experimental data refer to the phase transitions defining the phase diagram, as well as to the enthalpy of fusion of the eutectic composition. As discussed in section 5.2.1.1, particular attention was given to the experimental challenges in identifying the eutectic composition, which ultimately led to its estimation being reported as an experimental value. Aware of this inherent uncertainty, the experimental enthalpy value was considered solely for comparison with the thermodynamic modelling and were not used as input in the optimisation process. The final dataset presented here (see **Table 6-16**) should therefore be regarded as preliminary. The calculated phase diagram reveals a simple mono-eutectic system, in fair agreement with the experimental data (**Figure 6-19**), with a eutectic composition at 30.9 mol% $MgSO_4$ and a melting temperature of 631.1 °C (904.3 K). The enthalpy of fusion of the calculated eutectic mixture is 36.0 kJ/mol. The calculated enthalpy for the proposed experimental composition (34.1 mol% $MgSO_4$) is, as expected, lower (33.8 kJ/mol), since this composition deviates from the eutectic point predicted by the dataset. This outcome highlights both the overall reliability of the dataset description and the need for further refinement.

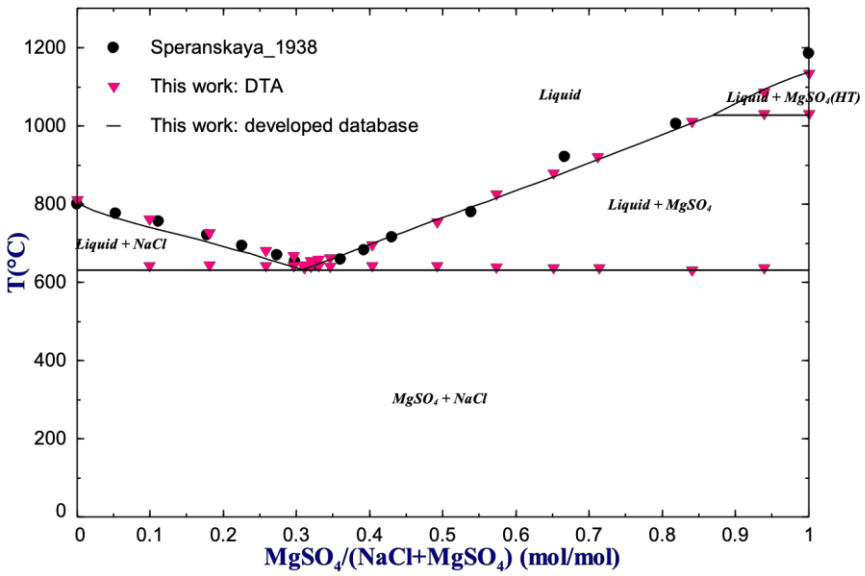


Figure 6-19 *Phase diagram of NaCl-$MgSO_4$ system: comparison of the developed database with experimental data from the present work and Speranskaya [63].*

6.2.3 $MgCl_2$-Na_2SO_4

The phase diagram along the other diagonal of the reciprocal system was also calculated, based on the thermal analysis results obtained in this study and supplemented by literature data [63]. The calculated phase diagram shows good agreement with the phase equilibria observed through DTA measurements, and it is presented in **Figure 6-20**. The system appears to be rather complex, with the presence of multiple phase regions determined by the formation and stability of intermediate compounds involving chlorides and sulphates. The optimised values of the liquid-phase interaction parameters $L_{ij}^{(\nu)}$ are summarised in **Table 6-16**. The dataset presented here provides a consistent description of the experimental data, accurately reproducing the low- and medium-temperature phase equilibria, which, on the basis of the DTA results reported in this work, yield an updated representation of the phase diagram. The description of the liquidus curve slightly deviates from the experimental observations in the low- to medium-sulphate region, exhibiting a maximum temperature of 688 °C compared to the measured value of 728 °C. Given the overall good agreement in the representation of the phase equilibria, the dataset can be considered reliable, although further refinements are desirable.

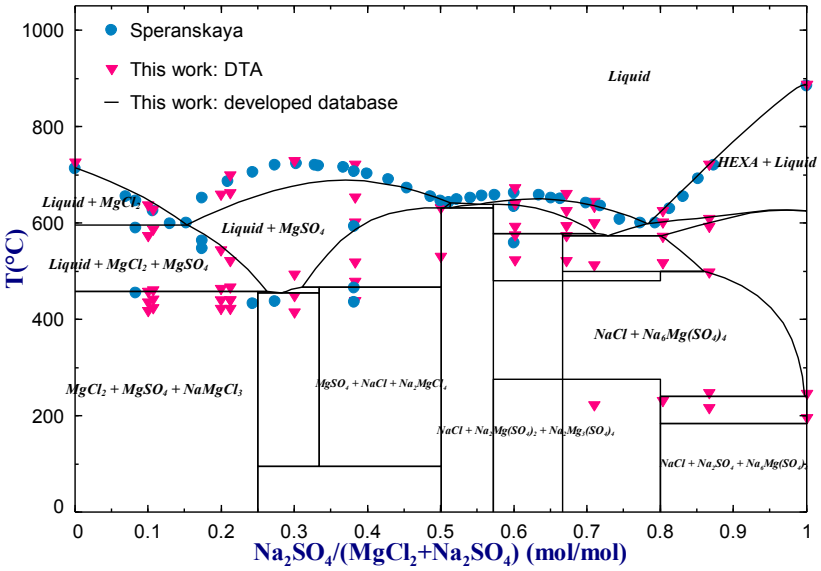


Figure 6-20 *Phase diagram of $MgCl_2$-Na_2SO_4 system: comparison of the developed database with experimental data from the present work and Speranskaya [63].*

6.2.4 The reciprocal system

Based on the modelling of binary and quasi-binary systems conducted in this work - using both original experimental data and values from the literature - and the resulting development and refinement of the thermodynamic database, the reciprocal system was subsequently calculated using this updated database. The introduction of a single reciprocal interaction parameter in the liquid phase, NaCl-$MgSO_4$ (**Table 6-16**), was sufficient to describe the phase equilibria in the entire system. The calculated reciprocal system is presented in **Figure 6-21**. It outlines the stable phase regions corresponding to the following phases: NaCl, $MgCl_2$, $NaMgCl_3$, Na_2MgCl_4, $MgSO_4$, $Na_2Mg_3(SO_4)_4$, $Na_2Mg(SO_4)_2$(HT), and HEXA. In **Table 6-4**, the calculated invariant points are compared with the data reported by Speranskaya [63], originally presented in the context of the ternary systems Na_2Cl_2-$MgCl_2$-$MgSO_4$ and Na_2Cl_2-Na_2SO_4-$MgSO_4$, and here converted to molar fractions for consistency. Speranskaya's work [63] provided several sections within the reciprocal system. In the present study, the experimental data from these sections were used to compare with the current database description and to validate its applicability. The results are presented in Appendix B (**Figure A 24-25**). The excellent agreement obtained demonstrates the reliability of the database developed in this study.

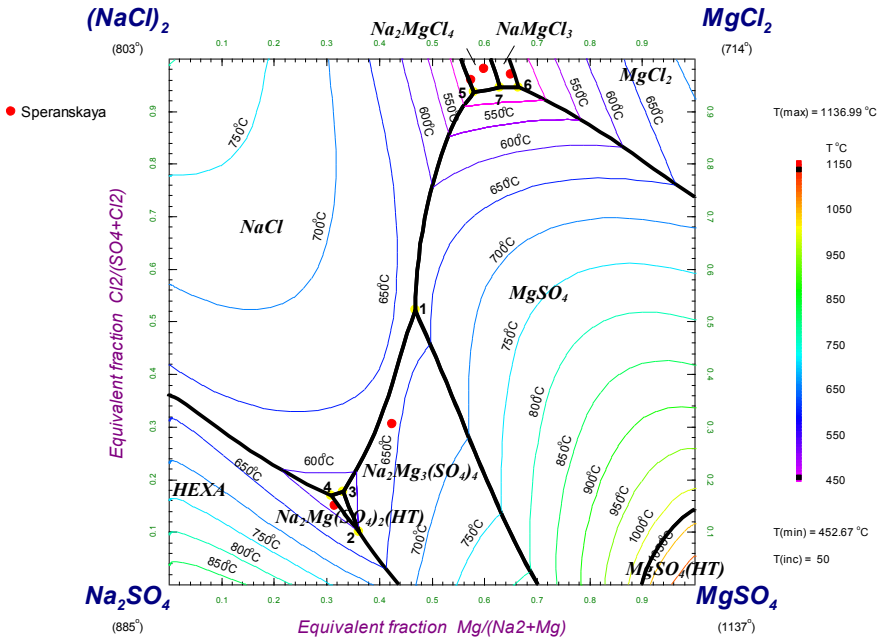


Figure 6-21 *Liquidus surface of the reciprocal system Na^+, Mg^{2+} // Cl^-, SO_4^{2-} calculated with the developed database, and experimental data of Speranskaya [63].*

Table 6-4 *Calculated and experimental invariant points, expressed in equivalent fractions, in the reciprocal system Na^+, Mg^{2+} // Cl^-, SO_4^{2-}.*

	$\frac{Mg}{Na_2 + Mg}$	$\frac{Cl_2}{SO_4 + Cl_2}$	T, °C	Solid phase	Ref.
1	0.4686	0.5213	631.7	NaCl, $MgSO_4$, $Na_2Mg_3(SO_4)_4$	[a]
2	0.3613	0.1015	602.0	$Na_2Mg(SO_4)_2$(HT), $Na_2Mg_3(SO_4)_4$, HEXA	[a]
3	0.3313	0.1771	578.3	NaCl, $Na_2Mg(SO_4)_2$(HT), $Na_2Mg_3(SO_4)_4$	[a]
4	0.3092	0.1693	573.0	NaCl, $Na_2Mg(SO_4)_2$(HT), HEXA	[a]
5	0.5803	0.9359	464.7	NaCl, Na_2MgCl_4, $MgSO_4$	[a]
6	0.6654	0.9453	456.5	$MgCl_2$, $NaMgCl_3$, $MgSO_4$	[a]
7	0.6304	0.9459	452.7	$NaMgCl_3$, Na_2MgCl_4, $MgSO_4$	[a]
1	0.425	0.305	634	NaCl, $MgSO_4$, $Na_2Mg_3(SO_4)_4$	[63]
2	0.315	0.15	560	NaCl, Na_2SO_4, $Na_2Mg_3(SO_4)_4$	[63]
3	0.575	0.96	465	NaCl, $MgSO_4$, Na_2MgCl_4	[63]
4	0.65	0.97	456	$MgCl_2$, $NaMg_2Cl_5$, $MgSO_4$	[63]
5	0.6	0.98	435	Na_2MgCl_4, $NaMg_2Cl_5$, $MgSO_4$	[63]

[a] this work

6.3 Na^+, Ca^{2+} // Cl^-, SO_4^{2-} system

6.3.1 Na_2SO_4-$CaSO_4$

Based on new experimental evidence regarding the sulphate-based binary system, the thermodynamic database has been revised. The previously included $Na_6Ca(SO_4)_4$ compound, which was incorporated based on earlier experimental findings [39, 126], has been excluded. Conversely, the $Na_4Ca(SO_4)_3$ compound has been introduced into the system. Additionally, the thermal stability

window of $Na_2Ca(SO_4)_2$ has been redefined, alongside that of $Na_4Ca(SO_4)_3$, through the optimisation of their thermodynamic properties, specifically their standard formation enthalpy and standard entropy. The optimised thermodynamic properties of the relevant compounds, included in the updated database, are listed in **Table 6-1**. Based on these modifications and the phase transitions identified through DTA analysis in this work, the interaction parameters were subsequently optimised within the PCM-Screening-2 project [4] to accurately describe the phase equilibria. The optimised parameters are summarised in **Table 6-16**, and the phase diagram calculated using the revised database is shown in **Figure 6-22**. The reactions occurring in the system are listed in **Table 6-5**. The updated diagram provides a significantly improved representation of the experimental findings and constitutes an advancement over the previous thermodynamic assessment [39]. A significant $CaSO_4$ solid solubility within the high-temperature modification of Na_2SO_4 (HEXA) has been introduced to the revised dataset. The optimised interaction parameters between sodium and calcium in the first sublattice of HEXA (**Table 6-16**) enabled an accurate description of the solid-liquid transformations across the concentration range of 0-45 mol% $CaSO_4$, including the azeotropic-like point that is characteristic of this system, which replaces the previously assumed congruent melting of the intermediate compound $Na_6Ca(SO_4)_4$. Moreover, the improved database successfully captures the low-temperature experimental observations, approximately between 150 and 600 °C. These include: the decomposition temperature of compound $Na_4Ca(SO_4)_3$, calculated at 260.7 °C; the thermal stability window of compound $Na_2Ca(SO_4)_2$, calculated at 282-507 °C; and the eutectoid transformation involving Na_2SO_4(LT), the solid solution Na-ortho-MT and the compound $Na_4Ca(SO_4)_3$, predicted at 170 °C - representing a substantial improvement over the previous modelling [39]. The HEXA solid solution undergoes congruent melting at a composition of 22.3 mol% $CaSO_4$, which falls well within the composition range of 20-25 mol% reported in the literature [90, 122, 124, 130]. The calculated transition temperature and enthalpy are 970 °C and 17.0 kJ/mol, respectively, which align with DSC measurements indicating a transition temperature of 959 °C and an enthalpy of 18.8 ± 0.7 kJ/mol (see **Table 5-22**) for a comparable $CaSO_4$ concentration of 25 mol%. The eutectic reaction (Liquid ⇌ $CaSO_4$ + HEXA) is calculated at 50.9 mol% $CaSO_4$ and 915 °C, in good agreement with recent literature reports [39, 125]. The calculated transition enthalpy of the eutectic mixture is 16.9 kJ/mol, which compares well with the DSC-measured value of 18.9 ± 0.6 kJ/mol for a composition of 50 mol% $CaSO_4$ (see **Table 5-22**).

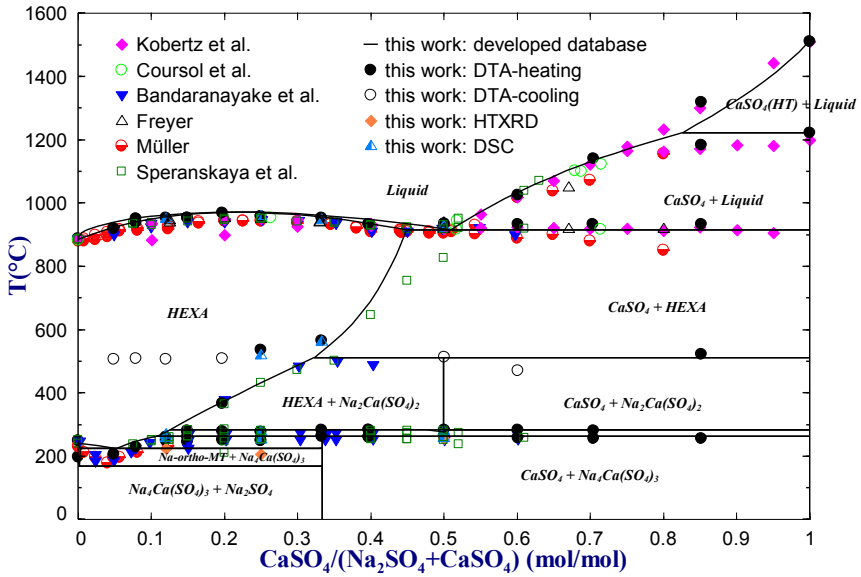


Figure 6-22 *Phase diagram of Na_2SO_4-$CaSO_4$ system: comparison of the developed database with experimental data from the present work and Kobertz et al. [126], Coursol et al. [125], Bandaranayake et al. [90], Freyer et al. [122, 130], Müller [123], Speranskaya et al. [124].*

Table 6-5 *Invariant points in the Na_2SO_4-$CaSO_4$ system*

Reaction	Reaction type	$CaSO_4$, mol (in Liquid)	T, °C	Ref.
Na_2SO_4(LT)+ $Na_4Ca(SO_4)_3$ ↔ Na-ortho-MT	Eutectoid	appr. 0.003	170	[a]
Na-ortho-MT + $Na_4Ca(SO_4)_3$ ↔ HEXA	Eutectoid	0.04	178	[123]
		0.049	185.81	[90]
		0.052	223.31	[a]
HEXA ↔ Liquid (maximum)	Azeotrope	0.20	944	[123]
		0.20-0.25	950	[124]
		appr. 0.25	945	[90]
		0.2	952	[130]
		0.25	949.2	[39] [b]
		0.223	970.0	[a]
HEXA + $CaSO_4$(LT) ↔ $Na_4Ca(SO_4)_3$	Decomposition	0.333	260.70	[a]
HEXA + $CaSO_4$(LT) ↔ Liquid	Eutectic	0.4	913	[123]
		0.47	909	[90]
		0.49	918	[124]
		0.5	916	[125]
		-	919	[122]
		0.46	925	[126]
		0.504	925.6	[39] [b]
		0.509	914.6	[a]
HEXA + $CaSO_4$(LT) ↔ $Na_2Ca(SO_4)_2$	Formation	0.5	282.01	[a]
$Na_2Ca(SO_4)_2$ ↔ HEXA + $CaSO_4$(LT)	Decomposition	0.5	520	[130]
		0.5	910	[126]
		0.5	910.1	[39] [b]
		0.5	507.3	[a]

[a] PCM2 database, in the frame of the database development of PCM-Screening-2 project [4]
[b] in the work of Yazhenskikh et al. [39], the congruent melting compound $Na_6Ca(SO_4)_4$ is considered instead of the solid solution HEXA

6.3.2 NaCl-$CaSO_4$

The stable diagonal of the Na^+, Ca^{2+} // Cl^-, SO_4^{2-} reciprocal system was thermodynamically assessed based on the thermal and calorimetric data presented in this work, along with available literature data [133-135]. The phase diagram was modelled by optimising the liquid phase interaction parameters (**Table 6-16**) mainly using the experimental data obtained in this study, which cover the entire compositional range. Notably, this includes the sulphate-rich region, for which no prior data were available in the literature. The calculated phase diagram is shown in **Figure 6-23** and demonstrates excellent agreement with the experimental results. The calculated liquidus minimum composition is 16.6 mol% $CaSO_4$ at 710.4 °C (983.6 K), which is in close proximity to the experimentally determined value of 16.9 mol% $CaSO_4$ at 724 °C (997 K). The minimum corresponds to the reaction: Liquid ⇌ AlkCl(ss) + $CaSO_4$ + Liquid. The corresponding enthalpy of fusion is calculated as 35.4 kJ/mol, in good agreement with the experimental value of 39.3 kJ/mol (**Figure 6-24**). Additionally, the phase transition (AlkCl(ss) + $CaSO_4$ + Liquid ⇌ AlkCl(ss) + $CaSO_4$ + HEXA) is calculated to occur at 657.2 °C, is higher than the experimental DSC observation of 633 °C, and also above the DTA values ranging from 613-654 °C for the varying compositions (see **Table 5-23**). In the present case, the enthalpy increment-temperature curve does not display a sharp vertical step at the melting point, that would be expected for a single fusion event. Instead, it shows a gradual increase, which can be attributed to the occurrence of an additional transition immediately preceding melting. The latent heat associated with the transition occurring just before melting, combined with the sensible heat due to the locally elevated heat capacity in this temperature interval, results in a progressive enthalpy increment instead of an abrupt discontinuity. Moreover, the invariant reaction involves the solid solution phase based on NaCl, rather than a stoichiometric compound. The presence of a solid solution leads to a distributed melting process over a temperature interval, which further contributes to the observed smooth enthalpy evolution at the transition.

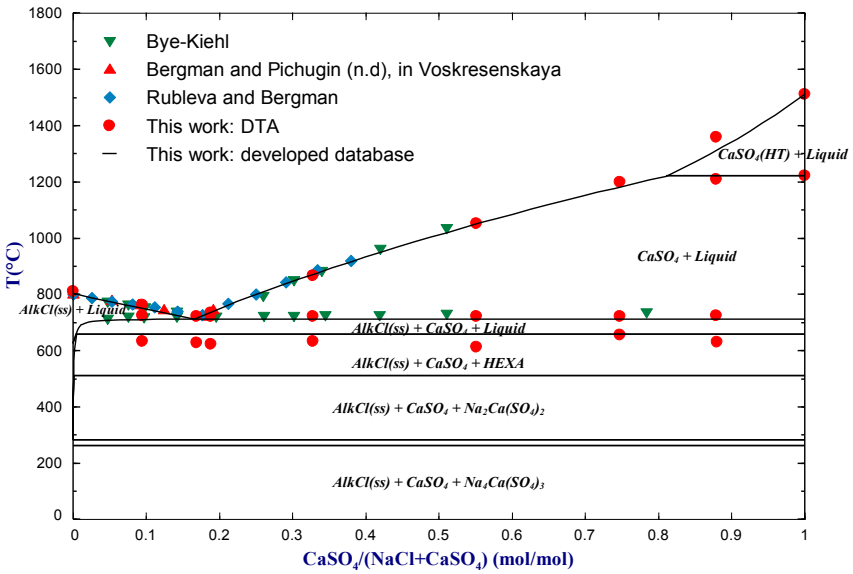


Figure 6-23 *Phase diagram of NaCl-$CaSO_4$ system: comparison of the developed database with experimental data from this work and Byé et al. [134], Bergman and Pichugin in [133], Rubleva and Bergman [135].*

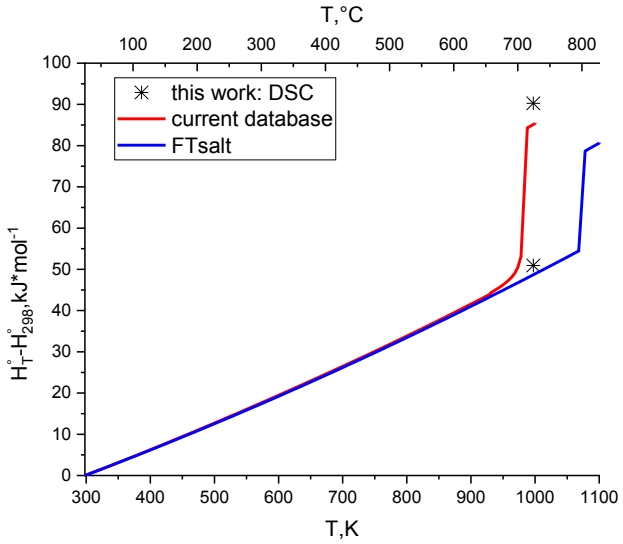


Figure 6-24 *Enthalpy increment of the NaCl(83.10 mol%)-$CaSO_4$(16.90 mol%) mixture obtained from DSC results in comparison with the current database and the commercial database FTsalt [218].*

6.3.3 $CaCl_2$-Na_2SO_4

The $CaCl_2$-Na_2SO_4 system was thermodynamically assessed based on experimental data obtained from DTA analysis. The calculated phase diagram and its comparison with the experimental results are presented in **Figure 6-25**. The re-assessment of the Na_2SO_4-$CaSO_4$ binary system carried

out in this thesis has led to an improved description of the phase equilibria involving sulphate-based phases. This is particularly evident in the characterisation of low-temperature phase transitions within the sulphate-rich composition range, which were experimentally observed and are now accurately captured by the updated thermodynamic database. These transitions involve the intermediate compound $Na_4Ca(SO_4)_3$, introduced and modelled as part of the thermodynamic assessment developed in this study and discussed in Sections 5.3.2 and 6.3.2. These low-temperature transitions are realised in the eutectoid at 223.6 °C. The liquidus curve exhibits two minima, located at 8.84 mol% Na_2SO_4 and 670.8 °C and 71.72 mol% Na_2SO_4 and 699.3 °C, respectively. The other calculated invariant points are summarised in **Table 6-6**. The study of this system also served as additional experimental validation for the thermodynamic description of the Na_2SO_4-$CaSO_4$ system, contributing to the refinement and validation of the developed thermodynamic database. The optimised interaction parameters $L_{ij}^{(\nu)}$ are summarised in **Table 6-16**.

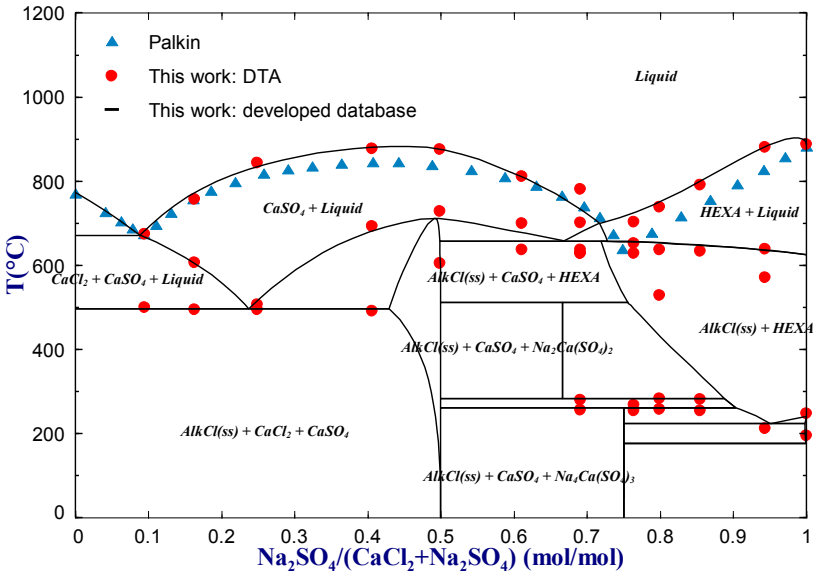


Figure 6-25 *Phase diagram of $CaCl_2$-Na_2SO_4 system: comparison of the developed database with experimental data from the present work and Palkin [70].*

Table 6-6 *Calculated invariant points in the $CaCl_2$-Na_2SO_4 system.*

Reaction	Na_2SO_4, mol (in Liquid)	T, °C
$CaCl_2$ + $CaSO_4$ + Liquid ↔ Liquid	0.0884	670.8
AlkCl(ss) + $CaCl_2$ + $CaSO_4$ ↔ Liquid + $CaSO_4$	0.2374	496.0
AlkCl(ss) + $CaCl_2$ + $CaSO_4$ ↔ AlkCl(ss) + $CaSO_4$ + Liquid	0.4293	496.0
AlkCl(ss) + $CaSO_4$ + HEXA ↔ Liquid + $CaSO_4$	0.6677	657.2
$CaSO_4$ + HEXA + Liquid ↔ Liquid	0.7172	699.3
Na-ortho-MT + AlkCl(ss) + $Na_4Ca(SO_4)_3$ ↔ AlkCl(ss) + HEXA	0.9516	223.6

6.3.4 The reciprocal system

The Na^+, Ca^{2+} // Cl^-, SO_4^{2-} reciprocal system was calculated using the updated thermodynamic database, which incorporates the optimised parameters from the binary and quasi-binary systems modelled in this work, as described above. The thermodynamic properties used for the calculation are summarised in **Table 6-1** and **Table 6-16**. The interaction between NaCl and $CaSO_4$, correspoding to the main diagonal of the reciprocal system, was introduced in the liquid phase in addition to the binary parameters (**Table 6-16**). The resulting reciprocal phase diagram is presented in **Figure 6-26**. It displays the stability regions between $CaCl_2$, $CaSO_4$, $CaSO_4$(HT), AlkCl(ss) and HEXA, providing an updated and refined description compared to the data currently available in the literature, as illustrated in **Figure 2-15**. Two minima in the liquidus surface are calculated at 657 °C (930 K) and 496 °C (769 K). A comparison of the invariant points calculated in this work with those reported by Zimina et al. [71] and those obtained using the FTsalt database [218], based on its constituent binary subsystems, is presented in **Table 6-7**. These compositions may be considered as potential candidates for phase change materials (PCMs) and warrant further investigation in future experimental studies.

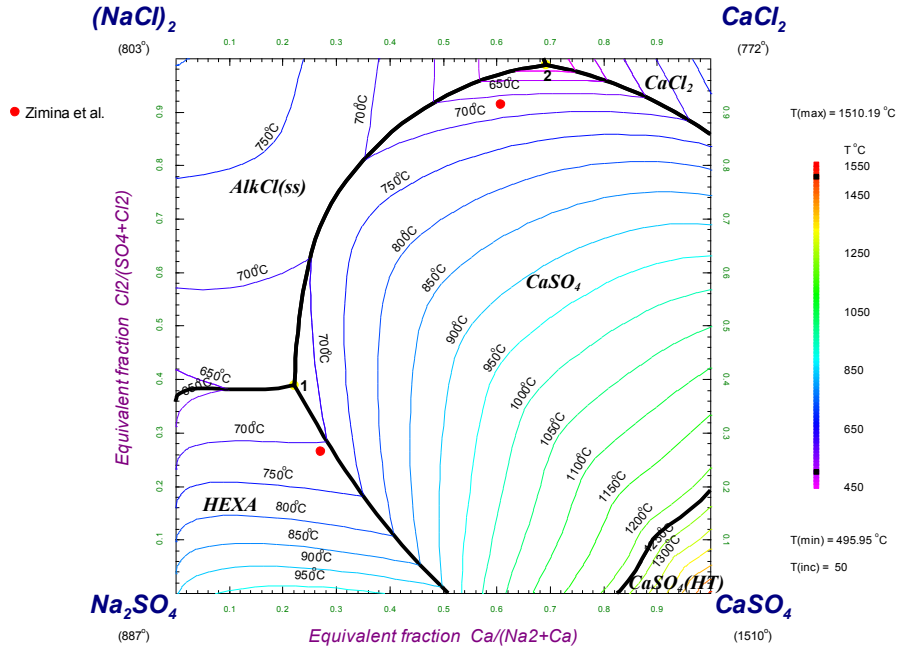


Figure 6-26 *Liquidus surface of the reciprocal system Na^+, Ca^{2+} // Cl^-, SO_4^{2-} calculated with the developed database, and experimental data of Zimina et al. [71].*

Table 6-7 *Calculated and experimental invariant points, expressed in equivalent fractions, in the reciprocal system Na^+, Ca^{2+} // Cl^-, SO_4^{2-}.*

	$\frac{Ca}{Na_2 + Ca}$	$\frac{Cl_2}{SO_4 + Cl_2}$	T, °C	Solid phase	Ref.
1	0.2229	0.3882	657.5	AlkCl(ss), HEXA, $CaSO_4$	[a]
2	0.6925	0.9877	496.0	AlkCl(ss), $CaCl_2$, $CaSO_4$	[a]
1	0.2711	0.2642	634	NaCl, $CaSO_4$, (Na,Ca)SO_4(ss)	[71] [b]

2	0.6077	0.9130	485	NaCl, $CaCl_2$, $CaSO_4$	[71] [b]
1	0.1527	0.2675	596.1	NaCl, Na_2SO_4, $CaSO_4$	[218]
2	0.6841	0.9639	470.7	NaCl, $CaCl_2$, $CaSO_4$	[218]

[a] PCM2 database, in the frame of the database development of PCM-Screening-2 project [4]
[b] digitised data

6.4 K^+, Mg^{2+} // Cl^-, SO_4^{2-} system

6.4.1 K_2SO_4-$MgSO_4$

The modification of the thermodynamic properties of the pure sulphate $MgSO_4$, based on the experimental evidence observed in this work, necessitated the re-assessment of systems involving $MgSO_4$. Consequently, the K_2SO_4-$MgSO_4$ binary system was re-assessed, within the PCM-Screening-2 project [4], using the thermodynamic framework previously established by [39], along with the experimental data considered therein [58, 64, 144, 145], incorporating the updated end-member properties introduced in this study (**Table 6-1**). The resulting calculated phase diagram is shown in **Figure 6-27**, and the corresponding optimised interaction parameters are summarised in **Table 6-16**.

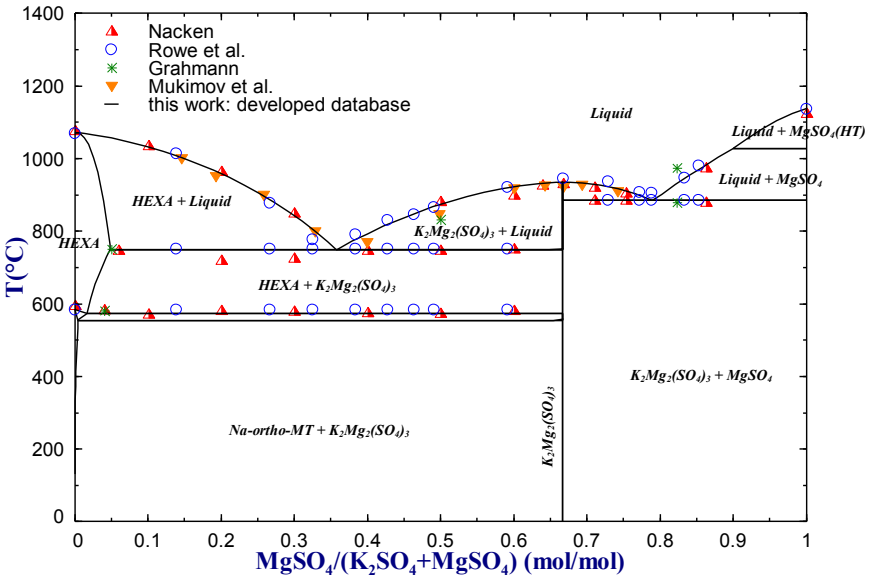


Figure 6-27 *Phase diagram of K_2SO_4-$MgSO_4$ system: comparison of the developed database with experimental data from Nacken [64], Rowe et al. [58], Grahmann [144], Mukimov et al. [145].*

6.4.2 KCl-$MgSO_4$

The thermodynamic assessment of the KCl-$MgSO_4$ system was carried out based on DTA thermal analysis data obtained in this study, which expanded the description of the phase equilibria by providing new evidence for medium- to low-temperature transitions not previously reported in the

literature. Additionally, this work offers the first experimental data for the sulphate-rich region, which was entirely absent in previous studies. The resulting calculated phase diagram is shown in **Figure 6-28**, and the optimised interaction parameters are summarised in **Table 6-16**. The calculated phase diagram accurately reproduces the experimental data presented in this work and provides a reliable description of the phase boundaries defined by the end-members and the intermediate compounds K_2MgCl_4 and $K_2Mg_2(SO_4)_3$ in the reciprocal system K^+, Mg^{2+} // Cl^-, SO_4^{2-}. The two minima are reported at 15.0 mol% $MgSO_4$ and 633.2 °C, and at 59.38 mol% $MgSO_4$ and 809.3 °C, corresponding to the transitions Liquid ⇌ KCl + $K_2Mg_2(SO_4)_3$ + Liquid and Liquid ⇌ $MgSO_4$ + $K_2Mg_2(SO_4)_3$ + Liquid, respectively. A future investigation and further refinement of the database, aimed at improving the description of the two low-temperature thermal effects, would be desirable in subsequent work. Nevertheless, the dataset presented here is considered satisfactory for the thermodynamic description of the system under study.

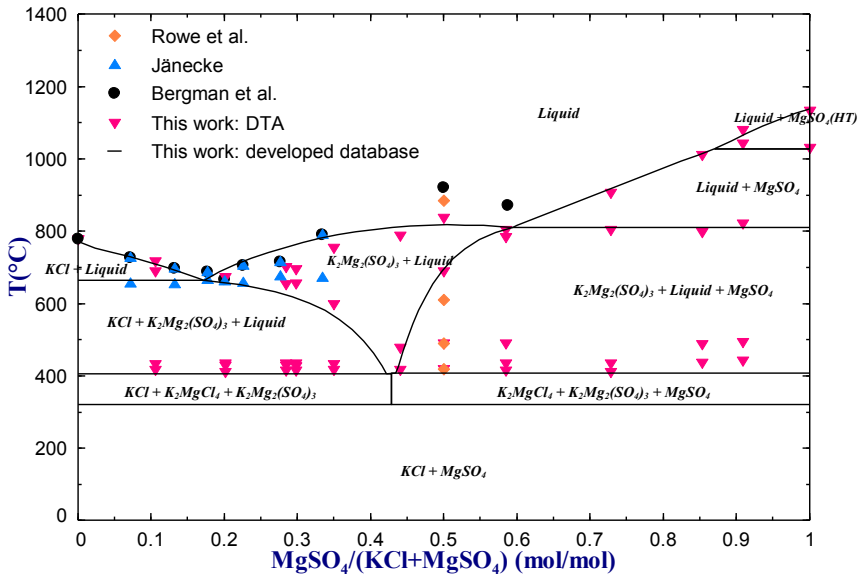


Figure 6-28 *Phase diagram of KCl-$MgSO_4$ system: comparison of the developed database with experimental data from the present work with Rowe et al. [49], Jänecke [62], and Bergman et al. [109].*

6.4.3 $MgCl_2$-K_2SO_4

The phase diagram of the $MgCl_2$-K_2SO_4 system was calculated by optimising the liquid phase interaction parameters, using DTA data obtained in this study. The resulting diagram, shown in **Figure 6-29**, demonstrates good agreement with the experimental data. In addition to the liquidus curve already reported in the literature [62], the present work provides new insights into phase transitions at low and intermediate temperatures, which define the phase regions of the system. These regions,

determined by the phase equilibria of the two end-members and their intermediate compounds ($KMgCl_3$, K_2MgCl_4, $K_2Mg_2(SO_4)_3$), are accurately described by the thermodynamic database developed in this study. The optimised $L_{ij}^{(\nu)}$ interaction parameters are summarised in **Table 6-16**. The dataset has been updated to give greater weight to the new DTA experimental data presented in this work, which differ slightly from those reported by Jänecke [62] and here digitised from the liquidus curve in his study. The resulting phase diagram provides an improved description of the phase equilibria in the medium- to high-sulphate region, but still shows deviations from both the liquidus curve reported in the literature [62] and the behaviour at low- to medium-sulphate contents. The dataset presented here is therefore regarded as improved but not definitive, and should be considered preliminary, with further adjustments to be undertaken in future work.

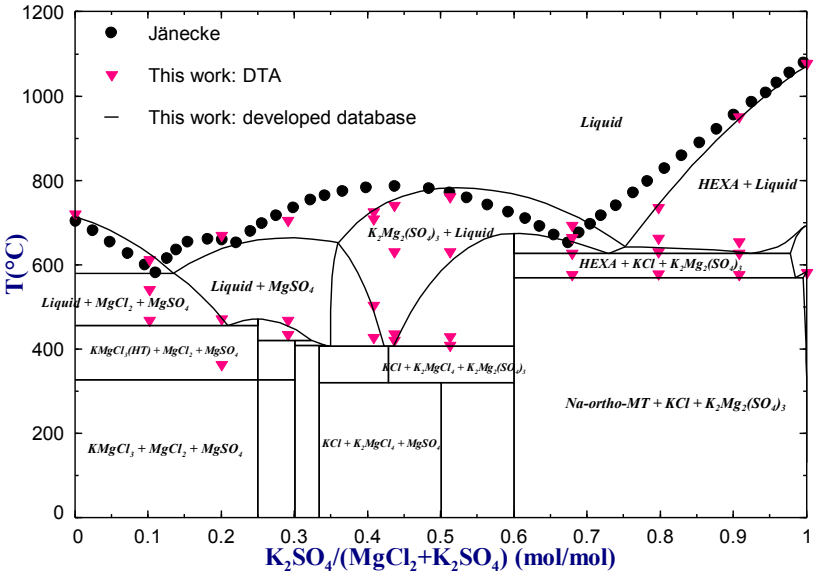


Figure 6-29 *Phase diagram of $MgCl_2$-K_2SO_4 system: comparison of the developed database with experimental data from the present work and Jänecke [62].*

6.4.4 The reciprocal system

The interactions KCl-$MgSO_4$ and K_2SO_4-$MgCl_2$ (**Table 6-16**) were optimised in the liquid phase to describe the phase equilibria of the K^+, Mg^{2+} // Cl^-, SO_4^{2-} system, including the diagonal sections (chapters 6.4.2 and 6.4.3). Based on the updated thermodynamic database - refined through the assessment of the subsystems comprising this system - the full reciprocal system was calculated and is presented in **Figure 6-30**. When compared with **Figure 2-20**, derived from [62], the new diagram provides an updated description of the phase equilibria, incorporating the new experimental evidence introduced in this work. Specifically, the stability field of $K_2Mg_2(SO_4)_3$ is significantly more extended

than in the description provided by Jänecke [62]. **Figure 6-30** shows nine crystallisation fields, given by KCl, $MgCl_2$, $MgSO_4$(LT), $MgSO_4$(HT), K_2MgCl_4, $KMgCl_3$, $K_3Mg_2Cl_7$, $K_2Mg_2(SO_4)_3$ and the solid solution HEXA. The calculated invariant points are compared with those reported by Jänecke [62] in **Table 6-8**. Targeted measurements on the calculated compositions reported for this system may be desirable in order to resolve the inconsistencies discussed in the previous sections and to further refine the thermodynamic database developed in this work. Although preliminary, the present database is deemed adequate for the thermodynamic description of the system.

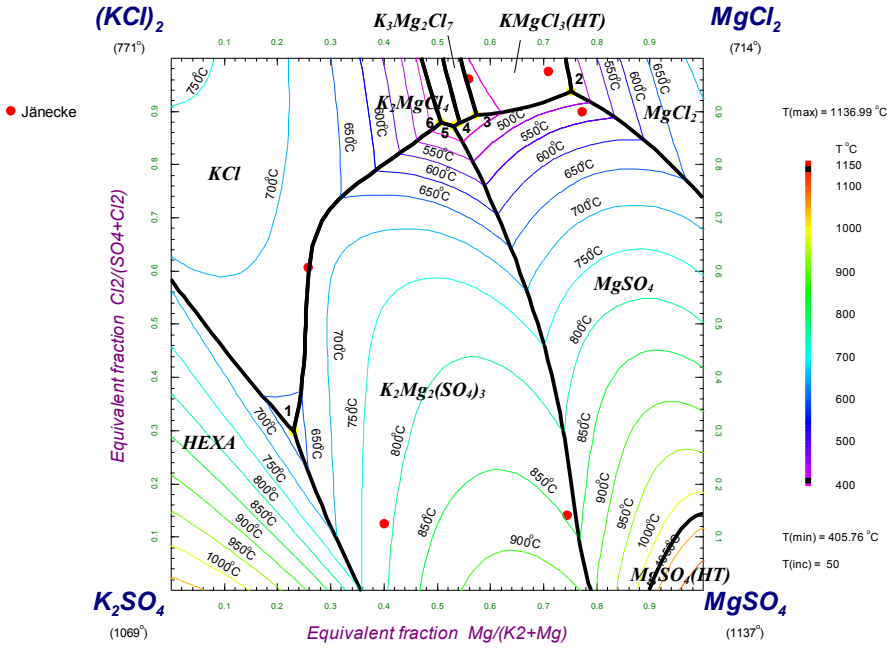


Figure 6-30 *Liquidus surface of the reciprocal system K^+, Mg^{2+} // Cl^-, SO_4^{2-} calculated with the current database, and experimental data of Jänecke [62].*

Table 6-8 *Calculated and experimental invariant points, expressed in equivalent fractions, in the reciprocal system K^+, Mg^{2+} // Cl^-, SO_4^{2-}.*

	$\frac{Mg}{K_2 + Mg}$	$\frac{Cl_2}{SO_4 + Cl_2}$	T, °C	Solid phase	Ref.
1	0.2304	0.2984	625.4	KCl, $K_2Mg_2(SO_4)_3$, HEXA	[a]
2	0.7536	0.9364	455.2	$MgCl_2$, $KMgCl_3$, $K_2Mg_2(SO_4)_3$	[a]
3	0.5744	0.8922	419.7	$KMgCl_3$, $K_3Mg_2Cl_7$, $MgSO_4$	[a]
4	0.5434	0.8785	407.7	K_2MgCl_4, $K_3Mg_2Cl_7$, $MgSO_4$	[a]
5	0.5322	0.8704	405.9	K_2MgCl_4, $MgSO_4$, $K_2Mg_2(SO_4)_3$	[a]
6	0.2304	0.8781	405.8	KCl, K_2MgCl_4, $K_2Mg_2(SO_4)_3$	[a]
1	0.7459	0.1392	845	$MgSO_4$, $K_2Mg_2(SO_4)_3$, KCl·$MgSO_4$	[62] [b]
2	0.4016	0.1238	620	K_2SO_4, $K_2Mg_2(SO_4)_3$, KCl·$MgSO_4$	[62] [b]
3	0.2596	0.6051	605	KCl, K_2SO_4, KCl·$MgSO_4$	[62] [b]
4	0.7736	0.8981	460	$MgCl_2$, $MgSO_4$, KCl·$MgSO_4$	[62] [b]
5	0.7104	0.9737	433	$MgCl_2$, $KMgCl_3$, KCl·$MgSO_4$	[62] [b]
6	0.5606	0.9598	418	KCl, $KMgCl_3$, KCl·$MgSO_4$	[62] [b]

[a] this work

[b] digitised data

6.5 K^+, Ca^{2+} // Cl^-, SO_4^{2-} system

6.5.1 KCl-$CaSO_4$

The KCl-$CaSO_4$ subsystem, corresponding to the stable diagonal of the K^+, Ca^{2+} // Cl^-, SO_4^{2-} reciprocal system, was thermodynamically modelled based on new experimental data presented in this work. Specifically, thermal analysis via DTA provided a comprehensive description of the phase diagram, particularly in the sulphate-rich compositional region - completely absent in the existing literature [49, 68, 69, 135]. Additionally, the eutectic composition was investigated through calorimetric measurements using DSC. The optimisation and refinement of the liquid-phase interaction parameters $L_{ij}^{(v)}$ between KCl and $CaSO_4$ (**Table 6-16**) led to the final phase diagram shown in **Figure 6-31**. Some difficulties were encountered in identifying the most suitable thermodynamic dataset capable of accurately reproducing the phase equilibria of the system, in particular the eutectic composition and temperature, as well as the enthalpy of fusion associated with the eutectic transition. The dataset selected as the most reliable and presented here (**Table 6-16**) displays a simple eutectic-type phase diagram, with the eutectic composition calculated at 19.65 mol% $CaSO_4$ and 669.3 °C (942.5 K), in very good agreement with the experimental value of 19.52 mol% $CaSO_4$, albeit at a slightly lower temperature than the experimental 690 °C (963 K). This discrepancy is also reflected in the enthalpy of fusion, with the calculated value of 27.1 kJ/mol compared to the experimental 37.0 kJ/mol. Despite these deviations, the thermodynamic description achieved is consistent and considered satisfactory, confirming the suitability of the selected dataset. Nevertheless, further refinements are anticipated in order to improve the accuracy of the liquidus temperature and the enthalpy description.

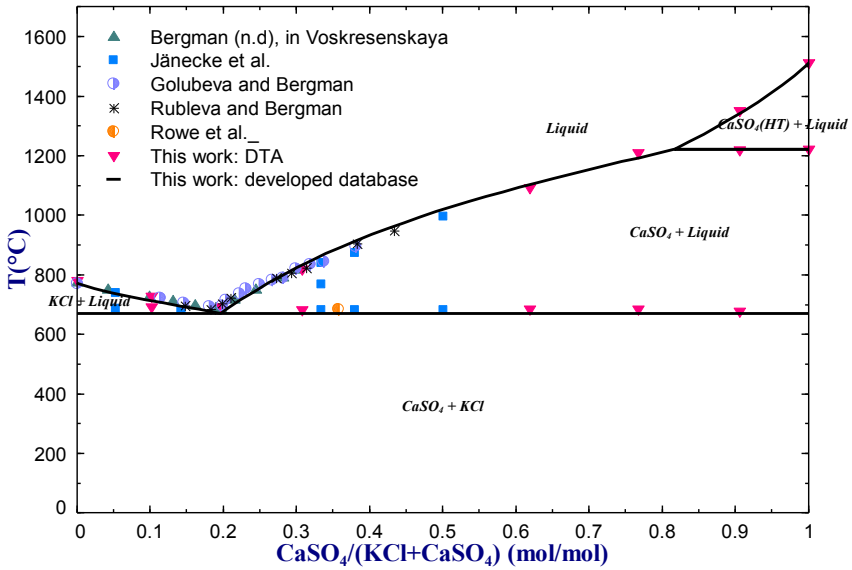


Figure 6-31 *Phase diagram of KCl-$CaSO_4$ system: comparison of the developed database with experimental data from the present work with Voskresenskaya [133], Jänecke and Mühlhäusser [68], Golubeva and Bergman [69], Rubleva and Bergman [135], and Rowe et al. [49].*

6.5.2 $CaCl_2$-K_2SO_4

The phase diagram and thermodynamic properties of the $CaCl_2$-K_2SO_4 system were assessed based on experimental data obtained from DTA analysis, combined with thermodynamic data already available in the literature [68, 69]. The optimised liquid phase interaction parameters are listed in **Table 6-16**, and the calculated phase diagram is presented in **Figure 6-32**, which also includes a comparison with the experimental results. As shown in the figure, the updated thermodynamic database provides an accurate description of the phase equilibria. The DTA results from this study successfully detected the thermal events associated with phase transitions, including those occurring at lower temperatures. Notably, the solid-solid transition of the $K_2Ca_2(SO_4)_3$ compound was clearly identified, further validating the improved database.

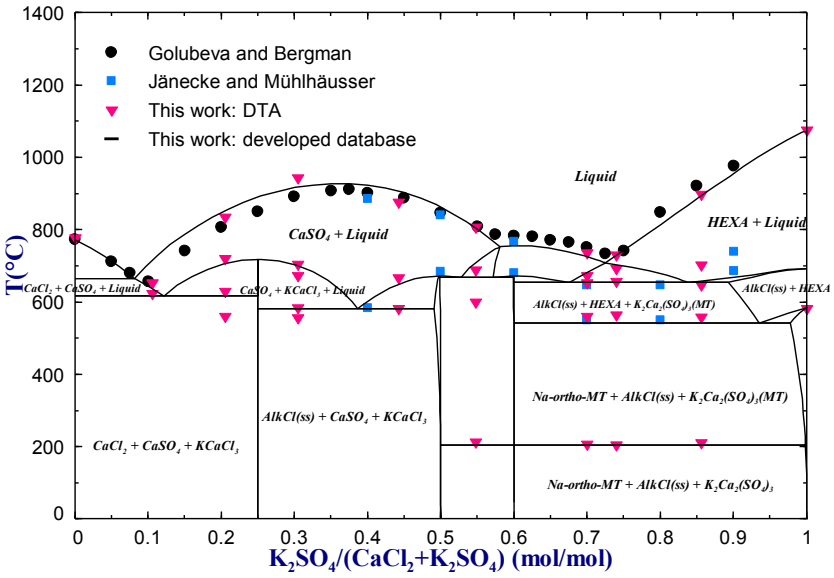


Figure 6-32 *Phase diagram of $CaCl_2$-K_2SO_4 system: comparison of the developed database with experimental data from the present work and Jänecke [68], Golubeva and Bergman [69].*

6.5.3 The reciprocal system

Thanks to the experimental campaign and the thermodynamic assessment of the subsystems constituting the K^+, Ca^{2+} // Cl^-, SO_4^{2-} reciprocal system, the thermodynamic database has been updated. The optimised thermodynamic properties are summarised in **Table 6-1** and **Table 6-16**. Using this updated database, the full reciprocal system was calculated and is presented in **Figure 6-33**. The diagram illustrates the stability regions of the various phases and the resulting invariant points, summarised in **Table 6-9**, which could be considered as potential phase change materials. The table provides a comparison with literature data [68, 69] and the calculated data from this work and from

[218]. Further experimental investigation of these mixtures could provide additional validation of the reliability of the thermodynamic database developed in this work and confirm the suitability of these compositions as promising candidates for thermal energy storage applications.

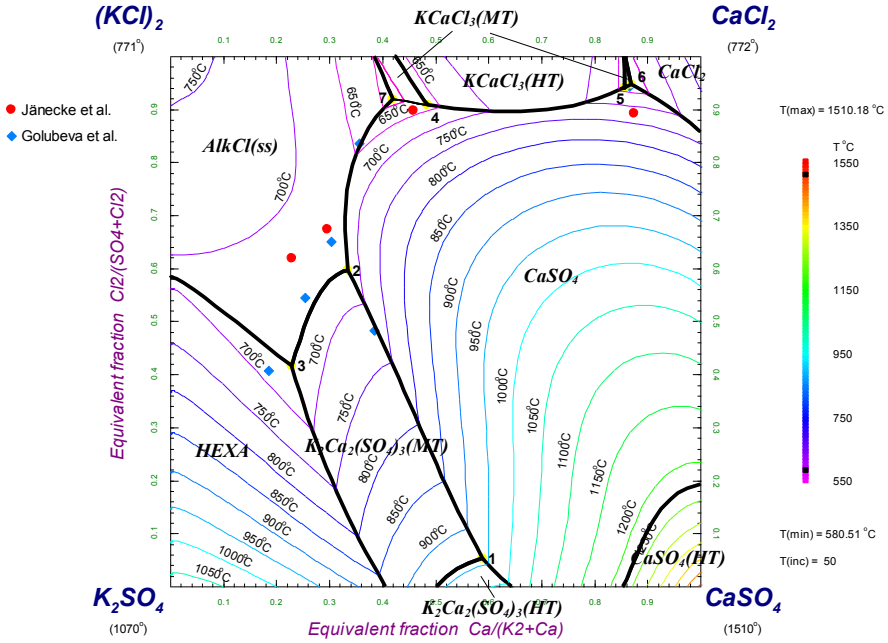


Figure 6-33 *Liquidus surface of the reciprocal system K^+, Ca^{2+} // Cl^-, SO_4^{2-} calculated with the current database, and experimental data of Jänecke and Mühlhäusser [68] and Golubeva and Bergman [69].*

Table 6-9 *Calculated and experimental invariant points, expressed in equivalent fractions, in the reciprocal system K^+, Ca^{2+} // Cl^-, SO_4^{2-}.*

	$\frac{Ca}{K_2 + Ca}$	$\frac{Cl_2}{SO_4 + Cl_2}$	T, °C	Solid phase	Ref.
1	0.5891	0.0529	936.9	$CaSO_4$, $K_2Ca_2(SO_4)_3$(MT), $K_2Ca_2(SO_4)_3$(HT)	[a]
2	0.3347	0.5963	666.8	AlkCl(ss), $CaSO_4$, $K_2Ca_2(SO_4)_3$(MT)	[a]
3	0.2290	0.4159	653.3	AlkCl(ss), HEXA, $K_2Ca_2(SO_4)_3$(MT)	[a]
4	0.4853	0.9085	634.1	$CaSO_4$, $KCaCl_3$(MT), $KCaCl_3$(HT)	[a]
5	0.8573	0.9404	634.0	$CaSO_4$, $KCaCl_3$(MT), $KCaCl_3$(HT)	[a]
6	0.8696	0.9465	616.2	$CaCl_2$, $CaSO_4$, $KCaCl_3$(MT)	[a]
7	0.4205	0.9196	580.5	AlkCl(ss), $CaSO_4$, $KCaCl_3$(MT)	[a]
1	0.2961	0.6745	680	KCl, K_2SO_4, $K_2Ca_2(SO_4)_3$	[68] [b]
2	0.2294	0.6182	646	KCl, $CaSO_4$, $K_2Ca_2(SO_4)_3$	[68] [b]
3	0.4594	0.8984	582	KCl, $KCaCl_3$, $CaSO_4$	[68] [b]
4	0.8748	0.8931	-	$CaCl_2$, $KCaCl_3$, $CaSO_4$	[68] [b]
1	0.3844	0.4834	748	$CaSO_4$, 2KCl·$CaSO_4$, $K_2Ca_2(SO_4)_3$	[69] [b]
2	0.2532	0.5451	676	KCl, $K_2Ca_2(SO_4)_3$, $2K_2SO_4$·$3CaSO_4$	[69] [b]
3	0.3026	0.6500	675	KCl, $K_2Ca_2(SO_4)_3$, 2KCl·$CaSO_4$	[69] [b]
4	0.3566	0.8367	653	KCl, $CaSO_4$, 2KCl·$CaSO_4$	[69] [b]
5	0.1853	0.4078	644	KCl, K2SO_4, $2K_2SO_4$·$3CaSO_4$	[69] [b]
6	0.8659	0.9431	604	$CaCl_2$, $CaSO_4$, $KCaCl_3$	[69] [b]
7	0.4261	0.9586	580	KCl, $CaSO_4$, $KCaCl_3$	[69] [b]
1	0.3883	0.0802	800.1	K_2SO_4(HT), $CaSO_4$, $K_2Ca_2(SO_4)_3$	[218]
2	0.1912	0.4378	657.2	KCl, K_2SO_4(HT), $CaSO_4$	[218]
3	0.4710	0.9517	626.9	$CaSO_4$, $KCaCl_3$(MT), $KCaCl_3$(HT)	[218]

4	0.8642	0.9471	626.9	$CaCl_2$, $KCaCl_3$(MT), $KCaCl_3$(HT)	[218]
5	0.8691	0.8374	626.9	$CaSO_4$, $KCaCl_3$(MT), $KCaCl_3$(HT)	[218]
6	0.8878	0.8500	600.2	$CaCl_2$, $KCaCl_3$(MT), $CaSO_4$	[218]
7	0.4220	0.9678	595.7	KCl, $KCaCl_3$(MT), $CaSO_4$	[218]

[a] this work
[b] digitised data

6.6 Na^+, K^+ // Cl^-, SO_4^{2-} system

6.6.1 NaCl-K_2SO_4

Although the NaCl-K_2SO_4 system has already been experimentally investigated in the literature [49, 66, 102, 108], the present work includes an additional DTA study aimed at validating the available data and providing a more detailed description of phase transitions below the liquidus curve. As reported in Section 5.6.1, the experimental results obtained in this study are in full agreement with those previously published. Both experimental datasets were jointly used as the basis for the thermodynamic modelling. The optimised interaction parameters are summarised in **Table 6-16**, and the resulting calculated phase diagram is shown in **Figure 6-34**. The diagram reveals several phase stability regions, involving not only the end-members but also solid solutions based on chlorides and sulphates. The thermodynamic dataset developed in this work accurately captures the experimental behaviour, especially in the medium- to low-temperature range, where the experimental data provided in this study have been prioritised. The very low-intensity transitions observed near 200 °C, likely arising from residual Na_2SO_4 in the sample, were excluded from the thermodynamic assessment, as they were not deemed to be representative of the primary melting behaviour.

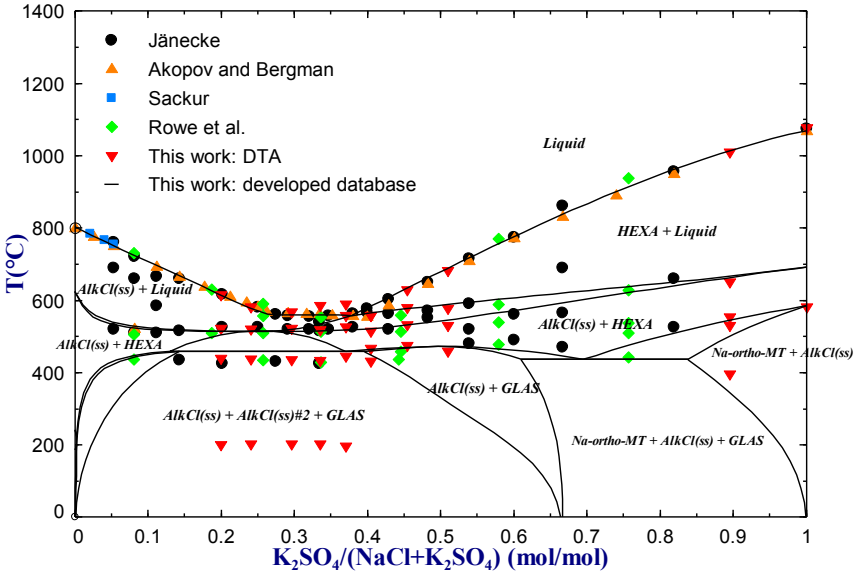


Figure 6-34 *Phase diagram of NaCl-K_2SO_4 system: comparison of the developed database with experimental data from the present work with Akopov and Bergman[102], Jänecke [108], Sackur [66], and Rowe et al. [49].*

6.6.2 KCl-Na_2SO_4

In a similar manner, the KCl-Na_2SO_4 system was experimentally examined in this study to confirm the reliability of the phase equilibria and transition data previously reported in the literature [66, 102, 108]. The phase diagram data obtained in this work, together with selected data from the literature, were used collectively to describe the full compositional range of the phase diagram and served as the basis for the thermodynamic modelling. The resulting optimised interaction parameters are summarised in **Table 6-16**, and the phase diagram calculated using the updated thermodynamic database is shown in **Figure 6-35**. The diagram provides an accurate representation of the phase equilibria suggested by the experimental observations.

As suggested by the phase diagram, prior to the melting of the composition at the liquidus minimum (calculated at 38.0 mol% Na_2SO_4), additional transitions occur. This is evidenced by the absence of a sharp vertical step in the enthalpy increment-temperature plot (**Figure 6-36**), which instead reveals multiple contributions from both latent and sensible heat effects. Indeed, although the integration of the experimental C_p curves invariably yields enthalpy increment curves with a non-vertical rise at the fusion temperature, in this case the effect indicates the coexistence of multiple transitions. The comparison between the calculated and experimental (integrated) enthalpy increment curves, shown in **Figure 6-36**, illustrates this behaviour. According to the current database, the transition between the solid solutions HEXA and GLAS within the miscibility gap of AlkCl(ss) is calculated at 457 °C (730 K) with an enthalpy of 3.6 kJ/mol. The second enthalpy rise, associated with melting, develops between 513 °C (786 K) and 527 °C (800 K), with the melting point occurring at 527 °C, and corresponds to 21.7 kJ/mol, in good agreement with the experimental value of 20.0 kJ mol^{-1} at 521 °C (794 K). The satisfactory agreement between calculated and experimental values supports the conclusion that the dataset presented here provides a reliable description of the phase equilibria.

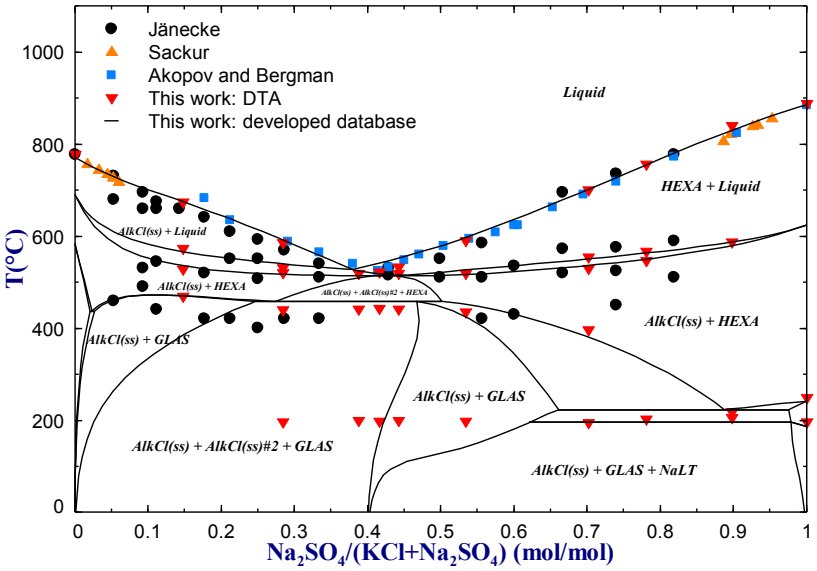


Figure 6-35 *Phase diagram of KCl-Na_2SO_4 system: comparison of the developed database with experimental data from the present work with Akopov and Bergman[102], Jänecke [108], Sackur [66].*

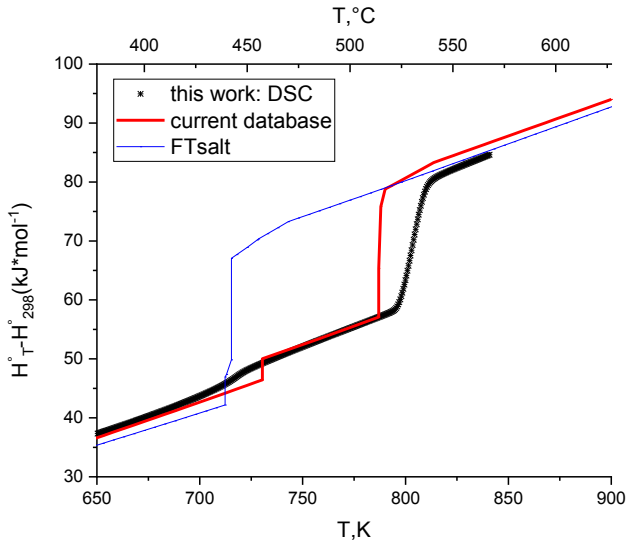


Figure 6-36 *Enthalpy increment of the KCl(58.44 mol%)-Na_2SO_4(41.56 mol%) mixture obtained from DSC results in comparison with the current database and the commercial database FTsalt [218].*

6.6.3 The reciprocal system

The thermodynamic description of the binary subsystems with a common cation or anion was previously developed within the PCM-Screening-1 and PCM-Screening-2 projects, and the corresponding optimised parameters were retained without modification in the present work. In

order to reproduce the experimental phase equilibria and the enthalpies along the diagonal sections, interaction parameters between NaCl and K_2SO_4 and between KCl and Na_2SO_4 were introduced in the liquid phase (**Table 6-16**). Based on the thermodynamic properties included in the database - and in particular on the updated parameters resulting from the experimental investigation conducted on the two previously discussed subsystems - the phase diagram of the reciprocal system was calculated and is presented in **Figure 6-37**. According to the present database, no invariant points are predicted in the liquidus projection. Instead, the diagram shows only a continuous equilibrium line separating the two main phase fields: the chloride-based solid solution, AlkCl(ss), and the sulphate-based solid solution, HEXA, with a minimum temperature of 514.4 °C. This contrasts with the description given by Akopov et al. [102, 169], who reported distinct phase equilibria between the individual chlorides - here replaced by their corresponding solid solution AlkCl(ss) - together with the sulphates and their possible sulphate-based solid solutions (see **Figure 2-31**, with the invariant points represented by blue diamonds in **Figure 6-37**).

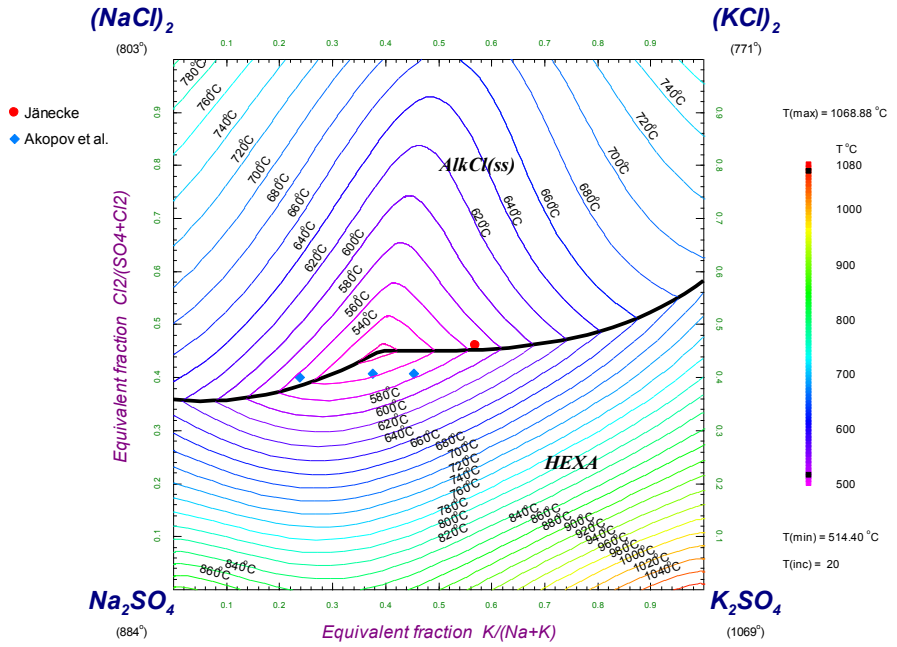


Figure 6-37 *Liquidus surface of the reciprocal system Na^+, K^+ // Cl^-, SO_4^{2-} calculated with the developed database, and experimental data of Jänecke [5] and Akopov and Bergman [102].*

6.7 Ternary systems

The reassessment of binary systems inevitably requires a subsequent reassessment of the corresponding ternary systems, particularly when recent evaluations have led to modifications of pure compounds and/or binary subsystems that have been incorporated into the thermodynamic database. In the present work, no new experimental investigations were carried out on selected

mixtures, isopleths, or internal sections of the ternary systems. The reassessment presented here, as part of the PCM-Screening-2 project [4], is therefore primarily based on the updates and developments introduced in the database for the constituting binary systems. Consequently, only the ternary systems recalculated with the optimised database are discussed in this section, as a result of database refinements introduced in this work. The presentation of the ternary systems is intended to support the visualisation and interpretation of the overall multicomponent system and to demonstrate the improvements achieved in the database reliability.

6.7.1 NaCl-$MgCl_2$-$CaCl_2$

The thermodynamic database was updated based on the reassessment of the thermodynamic properties of the $MgCl_2$-$CaCl_2$ binary system, presented in this work, together with the assessments of NaCl-$CaCl_2$ system by [48] and NaCl-$MgCl_2$ system by GTT-Technologies. Using this updated database, the NaCl-$MgCl_2$-$CaCl_2$ ternary system was recalculated, and no ternary interaction parameters were introduced. The resulting phase diagram, shown in **Figure 6-38**, illustrates the primary crystallisation fields of $MgCl_2$, $NaMgCl_3$, Na_2MgCl_4 and the two chloride-based solid solutions MCl2 and AlkCl(ss), which are involved in the invariant reactions listed in **Table 6-10**.

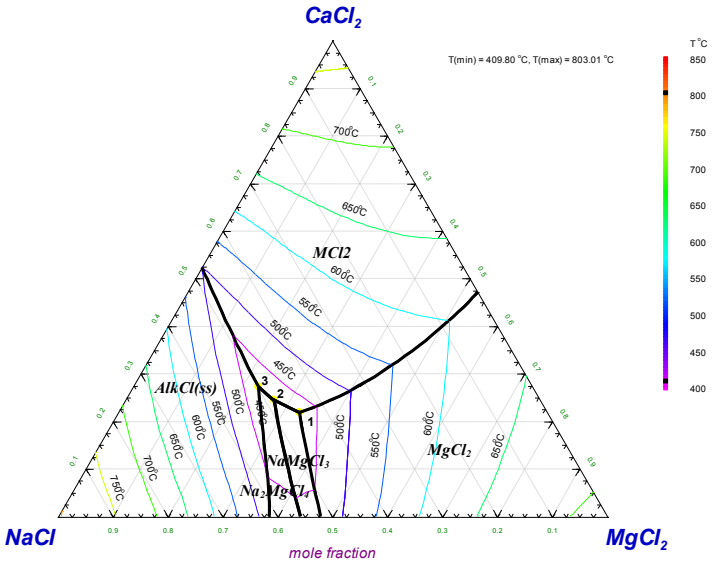


Figure 6-38 *Phase diagram of NaCl-$MgCl_2$-$CaCl_2$ ternary system from the developed database.*

Table 6-10 *Calculated invariant points in the NaCl-$MgCl_2$-$CaCl_2$ system.*

	$CaCl_2$, mol%	NaCl, mol%	$MgCl_2$, mol%	T, °C	Solid phase
1	21.89	45.08	33.04	420.5	$MgCl_2$, $NaMgCl_3$, MCl2
2	24.49	48.43	27.09	410.1	$NaMgCl_3$, Na_2MgCl_4, MCl2
3	27.27	49.84	22.89	409.8	Na_2MgCl_4, MCl2, AlkCl(ss)

6.7.2 KCl-$MgCl_2$-$CaCl_2$

The ternary system was re-evaluated using the updated thermodynamic database, which incorporates the revised description of the $MgCl_2$-$CaCl_2$ binary subsystem, developed in this study, as well as the assessments of the KCl-$CaCl_2$ system [48] and the KCl-$MgCl_2$ system modelled by the project partner GTT-Technologies. No ternary interaction parameters were included. The calculated phase diagram is presented in **Figure 6-39**, while the corresponding invariant points are listed in **Table 6-11**. The system exhibits nine primary crystallisation fields: $MgCl_2$, $KMgCl_3$(HT), $KCaCl_3$(LT), $KCaCl_3$(MT), $KCaCl_3$(HT), K_2MgCl_4, $K_3Mg_2Cl_7$, AlkCl(ss) and MCl2.

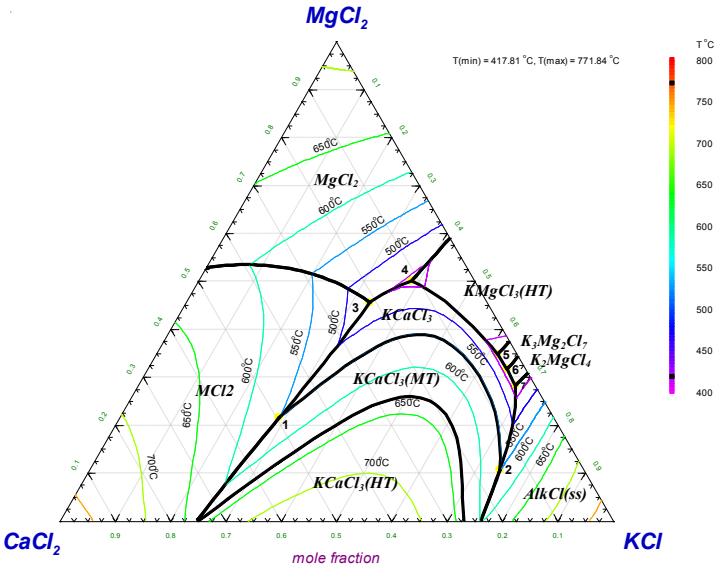


Figure 6-39 *Phase diagram of KCl-$MgCl_2$-$CaCl_2$ ternary system from the developed database.*

Table 6-11 *Calculated invariant points in the KCl-$MgCl_2$-$CaCl_2$ system.*

	$MgCl_2$, mol%	$CaCl_2$, mol%	KCl, mol%	T, °C	Solid phase
1	21.56	49.59	28.90	550.8	$KCaCl_3$, $KCaCl_3$(MT), MCl2
2	10.72	15.02	74.26	550.8	$KCaCl_3$, $KCaCl_3$(MT), AlkCl(ss)
3	45.60	21.15	33.25	454.6	$MgCl_2$, $KCaCl_3$, MCl2
4	50.03	11.43	38.55	437.2	$MgCl_2$, $KCaCl_3$, $KMgCl_3$(HT)
5	34.76	3.46	61.79	428.6	$KCaCl_3$, $KMgCl_3$(HT), $K_3Mg_2Cl_7$
6	31.62	3.32	65.06	420.3	$KCaCl_3$, K_2MgCl_4, $K_3Mg_2Cl_7$,
7	28.19	3.53	68.28	417.8	$KCaCl_3$, K_2MgCl_4, AlkCl(ss)

6.7.3 Na_2SO_4-K_2SO_4-$MgSO_4$

The ternary system was recalculated considering the modifications introduced in the thermodynamic description of magnesium sulphate, specifically the transition temperatures and enthalpies derived from the thermal and calorimetric analyses performed in this work. The binary subsystems forming the ternary system were accordingly reassessed, and the binary interaction

parameters in the liquid phase were optimised. Based on the previous assessment [201], the ternary interaction parameters in the liquid and HEXA phases were re-optimised (**Table 6-16**). Using the updated thermodynamic database, the calculated ternary phase diagram is shown in **Figure 6-40**, and the invariant points are listed in **Table 6-12**. There are five main crystallisation fields, namely $MgSO_4$(LT), $MgSO_4$(HT), $K_2Mg_2(SO_4)_3$, $Na_2Mg_3(SO_4)_4$ and the solid solution HEXA. The ternary eutectic is calculated at Na_2SO_4(52.90 mol%)-K_2SO_4(4.40 mol%)-$MgSO_4$(42.70 mol%) and 667.1 °C, and it agrees well with the ternary eutectic point reported by Mukimov et al. [60]. The peritectic transformation is observed at Na_2SO_4(26.66 mol%)-K_2SO_4(5.35 mol%)-$MgSO_4$(67.99 mol%) and 795.1 °C.

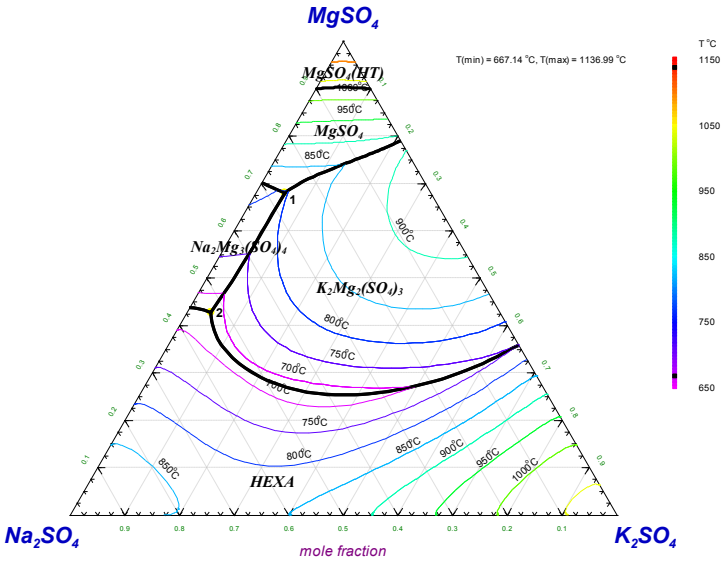


Figure 6-40 *Phase diagram of Na_2SO_4-K_2SO_4-$MgSO_4$ ternary system from the developed database*

Table 6-12 *Calculated invariant points in the Na_2SO_4-K_2SO_4-$MgSO_4$ system.*

	Na_2SO_4, mol%	K_2SO_4, mol%	$MgSO_4$, mol%	T, °C	Solid phase
1	26.66	5.35	67.99	795.1	$MgSO_4$, $K_2Mg_2(SO_4)_3$, $Na_2Mg_3(SO_4)_4$
2	52.90	4.40	42.70	667.1	HEXA, $K_2Mg_2(SO_4)_3$, $Na_2Mg_3(SO_4)_4$

6.7.4 Na_2SO_4-K_2SO_4-$CaSO_4$

The Na_2SO_4-K_2SO_4-$CaSO_4$ ternary system was recalculated based on the experimental evidence presented in this work and the resulting modifications to the thermodynamic properties introduced into the database. These changes stem from the reassessment of the Na_2SO_4-$CaSO_4$ binary subsystem and from the revised phase diagram proposed in this study, which differs from previous assessments and includes the characterisation of the intermediate compounds $Na_4Ca(SO_4)_3$ and $Na_2Ca(SO_4)_2$. **Figure 6-41** shows the calculated liquidus projection obtained using the current version of the database, characterised by five main phase fields: $CaSO_4$(LT), $CaSO_4$(HT), $K_2Ca_2(SO_4)_3$(MT),

$K_2Ca_2(SO_4)_3$(HT) and the solid solution HEXA. The calculated invariant points are summarised in **Table 6-13**.

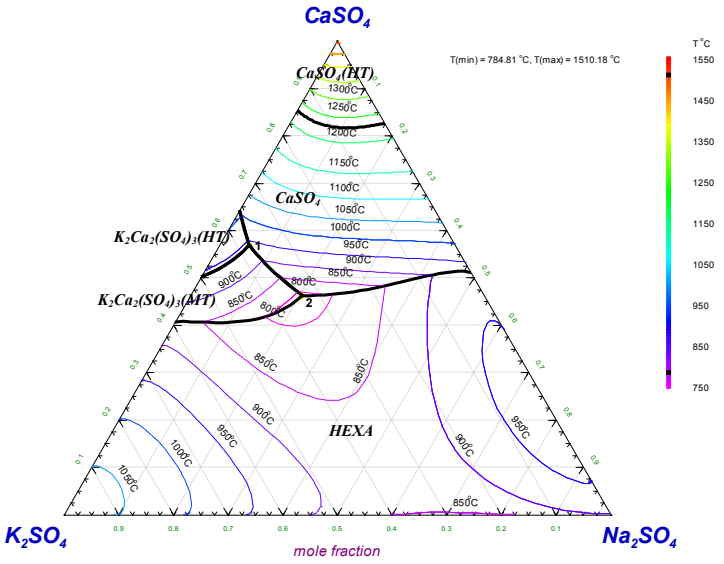


Figure 6-41 *Phase diagram of Na_2SO_4-K_2SO_4-$CaSO_4$ ternary system from the developed database.*

Table 6-13 *Calculated invariant points in the Na_2SO_4-K_2SO_4-$CaSO_4$ system.*

	Na_2SO_4, mol%	K_2SO_4, mol%	$CaSO_4$, mol%	T, °C	Solid phase
1	5.45	37.65	56.91	936.9	$CaSO_4$, $K_2Ca_2(SO_4)_3$(MT), $K_2Ca_2(SO_4)_3$(HT)
2	20.51	33.25	46.25	784.8	$CaSO_4$, $K_2Ca_2(SO_4)_3$(MT), HEXA

6.7.5 Na_2SO_4-$MgSO_4$-$CaSO_4$

The ternary system was reassessed in light of the investigation of the constituent compounds and binary subsystems. Particular attention was given to the revised transition temperatures and enthalpies of $MgSO_4$, as well as to the reassessment of the Na_2SO_4-$CaSO_4$ and $MgSO_4$-$CaSO_4$ binary systems, whose phase diagrams were significantly revised compared to previous studies. These revisions include the introduction of new intermediate compounds and the update of their thermodynamic properties. Based on the experimental results presented in this work, the ternary system was recalculated re-optimising the liquid-phase ternary interaction parameters and introducing additional interaction parameters for the HEXA phase (see **Table 6-16**). The resulting liquidus projection is shown in **Figure 6-42**. The diagram clearly illustrates the crystallisation fields defined by the newly introduced phases, $CaMg(SO_4)_2$, $CaMg_2(SO_4)_3$, together with $MgSO_4$(LT), $MgSO_4$(HT), $CaSO_4$(LT), $CaSO_4$(HT), $Na_2Mg(SO_4)_2$(HT), $Na_2Mg_3(SO_4)_4$ and the solid solution HEXA. The calculated invariant points are listed in **Table 6-14**.

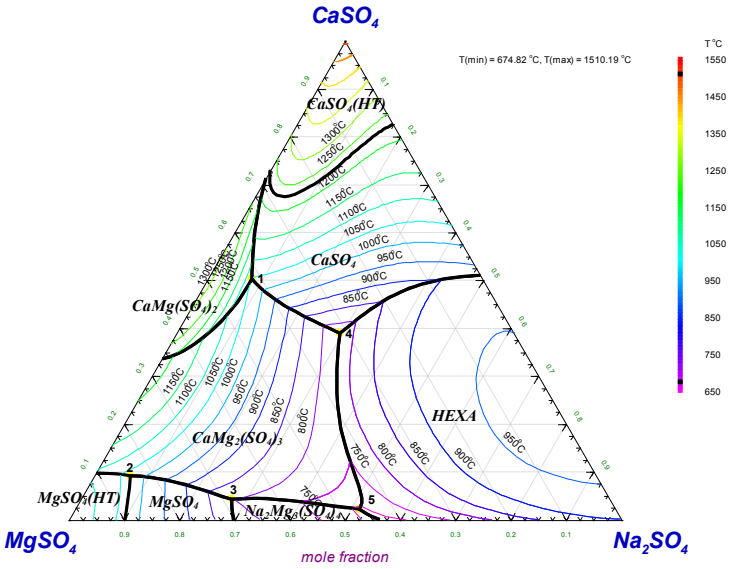


Figure 6-42 *Phase diagram of Na_2SO_4-$MgSO_4$-$CaSO_4$ ternary system from the developed database.*

Table 6-14 *Calculated invariant points in the Na_2SO_4-$MgSO_4$-$CaSO_4$ system.*

	Na_2SO_4, mol%	$MgSO_4$, mol%	$CaSO_4$, mol%	T, °C	Solid phase
1	8.00	41.65	50.35	1044.2	$CaMg(SO_4)_2$, $CaMg_2(SO_4)_3$, $CaSO_4$
2	6.44	84.32	9.24	1027.2	$CaMg_2(SO_4)_3$, $MgSO_4$(LT), $MgSO_4$(HT)
3	27.29	68.46	4.25	801.0	$CaMg_2(SO_4)_3$, $MgSO_4$(LT), $Na_2Mg(SO_4)_2$
4	29.58	31.45	38.97	761.8	$CaMg_2(SO_4)_3$, $CaSO_4$, HEXA
5	51.40	46.32	2.28	690.9	$CaMg_2(SO_4)_3$, $Na_2Mg(SO_4)_2$, HEXA

6.7.6 K_2SO_4-$MgSO_4$-$CaSO_4$

The ternary system was reassessed based on the modifications introduced to the pure compound $MgSO_4$, following calorimetric analysis, and on the subsequent reassessment of the binary systems in which it is involved. Most notably, the revision of the $MgSO_4$-$CaSO_4$ binary system - extensively investigated in this work - led to a redefinition of the phase equilibria and the identification and characterisation of intermediate compounds. Building upon the previous thermodynamic assessment [201], the ternary interaction parameters of the liquid and LANGBEINITE phases were reassessed and re-optimised, with the resulting values summarised in **Table 6-16**. **Figure 6-43** shows the calculated ternary phase diagram obtained using the thermodynamic database developed and updated within this study. The diagram presents the liquidus projection, delineating the primary crystallisation fields of the following phases: $MgSO_4$(LT), $MgSO_4$(HT), $CaSO_4$(LT), $CaSO_4$(HT), $CaMg(SO_4)_2$, $CaMg_2(SO_4)_3$, $K_2Ca_2(SO_4)_3$, and the two solid solutions LANGBEINITE and HEXA. The calculated invariant points are summarised in **Table 6-15**.

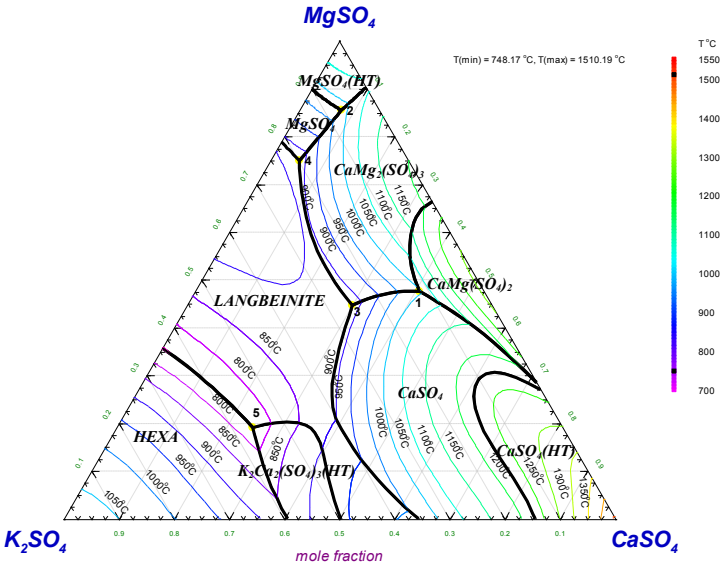


Figure 6-43 *Phase diagram of K_2SO_4-$MgSO_4$-$CaSO_4$ ternary system from the developed database.*

Table 6-15 *Calculated invariant points in the Na_2SO_4-$MgSO_4$-$CaSO_4$ system.*

	K_2SO_4, mol%	$MgSO_4$, mol%	$CaSO_4$, mol%	T, °C	Solid phase
1	11.67	47.65	40.68	1044.2	$CaMg(SO_4)_2$, $CaMg_2(SO_4)_3$, $CaSO_4$
2	6.90	85.53	7.57	1027.2	$CaMg_2(SO_4)_3$, $MgSO_4$(LT), $MgSO_4$(HT)
3	25.29	44.73	29.98	870.2	$CaMg_2(SO_4)_3$, $CaSO_4$, LANGBEINITE
4	19.78	75.00	5.22	870.1	$CaMg_2(SO_4)_3$, LANGBEINITE, $MgSO_4$
5	56.12	19.14	24.74	763.8	HEXA, $K_2Ca_2(SO_4)_3$(HT), LANGBEINITE

6.8 Na^+, K^+, Mg^{2+}, Ca^{2+} // Cl^-, SO_4^{2-} system

Based on the thermodynamic assessment of the subsystems described in the previous sections, the multicomponent system Na^+, K^+, Mg^{2+}, Ca^{2+} // Cl^-, SO_4^{2-} has been thoroughly characterised from a thermodynamic perspective. The work, which combined extensive and targeted experimental efforts with CALPHAD-based thermodynamic modelling, led to the development of a robust and internally consistent thermodynamic database. This database enables the reliable description of the thermodynamic properties of chloride and sulphate systems involving alkali and alkaline earth metals. It represents a solid step towards a comprehensive description of the investigated systems. While the current modelling achieves good agreement with the available experimental data, it remains open to refinement as new experimental results and optimised datasets become available, in line with the progressive nature of thermodynamic database development.

The thermodynamic descriptions of the solid and liquid solution phases, as obtained from the thermodynamic optimisation performed in this work, and more broadly in the framework of PCM-Screening-2 project [4], are summarised in **Table 6-16**.

Table 6-16 *Thermodynamic descriptions of the liquid and solid solution phases.*

Gibbs energy data, J/mol	Ref.
Liquid: (NaCl, KCl, $MgCl_2$/1.5, $CaCl_2$/1.5, Na_2SO_4/1.5, K_2SO_4/1.5, $MgSO_4$, $CaSO_4$)	
$^\circ G_{NaCl} = {}^\circ G_{NaCl(liquid)}$	[48]
$^\circ G_{KCl} = {}^\circ G_{KCl(liquid)}$	[48]
$^\circ G_{MgCl_2} = {}^\circ G_{MgCl_2(liquid)}$	a
$^\circ G_{CaCl_2} = {}^\circ G_{CaCl_2(liquid)}$	[48]
$^\circ G_{Na_2SO_4} = {}^\circ G_{Na_2SO_4(liquid)}$	[39]
$^\circ G_{K_2SO_4} = {}^\circ G_{K_2SO_4(liquid)}$	[39]
$^\circ G_{MgSO_4} = {}^\circ G_{MgSO_4(liquid)}$	a
$^\circ G_{CaSO_4} = {}^\circ G_{CaSO_4(liquid)}$	[39]
Binary interaction parameters	
$L^{(0)}_{CaCl_2,MgCl_2} = 1294.86 + 7.71978 * T$	a
$L^{(1)}_{CaCl_2,MgCl_2} = -2221.13 + 1.70498 * T$	a
$L^{(0)}_{CaSO_4,MgSO_4} = -10697.8 + 0.93 * T$	a
$L^{(1)}_{CaSO_4,MgSO_4} = 5791.59 + 4.94 * T$	a
$L^{(2)}_{CaSO_4,MgSO_4} = 2192.44$	a
$L^{(0)}_{MgSO_4,MgCl_2} = -27772.3 + 18 * T$	a
$L^{(1)}_{MgSO_4,MgCl_2} = -2606.47 - 4.89221 * T$	a
$L^{(0)}_{CaCl_2,CaSO_4} = 35970.8 - 21.371 * T$	a
$L^{(1)}_{CaCl_2,CaSO_4} = -5159.39 - 1.5534 * T$	a
$L^{(0)}_{NaCl,MgCl_2} = -25691.1 + 7.1414 * T$	a
$L^{(1)}_{NaCl,MgCl_2} = 2.3989 * T$	a
$L^{(2)}_{NaCl,MgCl_2} = 4110$	a
$L^{(0)}_{Na_2SO_4,MgSO_4} = -59746.7 + 21.9788 * T$	a
$L^{(1)}_{Na_2SO_4,MgSO_4} = 7167.12$	a
$L^{(2)}_{Na_2SO_4,MgSO_4} = -11429.6$	a
$L^{(0)}_{NaCl,Na_2SO_4} = 3724$	a
$L^{(1)}_{NaCl,Na_2SO_4} = 2198$	a
$L^{(0)}_{NaCl,CaCl_2} = -12778.555786 + 7.259609388 * T$	[48]
$L^{(1)}_{NaCl,CaCl_2} = -438.0466 + 1.047187394 * T$	[48]
$L^{(0)}_{CaSO_4,Na_2SO_4} = -2642.9 - 1.0951 * T$	a
$L^{(1)}_{CaSO_4,Na_2SO_4} = 11282.4 - 1 * T$	a
$L^{(0)}_{KCl,MgCl_2} = -51440.2 + 12.1292 * T$	a
$L^{(1)}_{KCl,MgCl_2} = 2449.01 + 5.25116 * T$	a
$L^{(2)}_{KCl,MgCl_2} = 6021.94$	a
$L^{(0)}_{K_2SO_4,MgSO_4} = -81539.4 + 20.1163 * T$	a
$L^{(1)}_{K_2SO_4,MgSO_4} = -2957.2 + 9.6177 * T$	a
$L^{(2)}_{K_2SO_4,MgSO_4} = -1712$	a
$L^{(0)}_{KCl,K_2SO_4} = 5327.5$	a
$L^{(1)}_{KCl,K_2SO_4} = 3494$	a
$L^{(2)}_{KCl,K_2SO_4} = 1084$	a
$L^{(0)}_{KCl,CaCl_2} = -45676.39234 + 124.93717566 * T - 14.35279 * T * ln(T)$	a
$L^{(1)}_{KCl,CaCl_2} = -247.4455 + 3.0382981 * T$	a
$L^{(0)}_{CaSO_4,K_2SO_4} = -4612 - 4.2 * T$	[39]
$L^{(1)}_{CaSO_4,K_2SO_4} = 8526.5$	[39]
$L^{(0)}_{NaCl,KCl} = -2186 + 0.16478682 * T$	a
$L^{(1)}_{NaCl,KCl} = -136$	a

$L^{(0)}_{K_2SO_4,Na_2SO_4} = -2928.45 - 7.554 * T$ [39]

Ternary interaction parameters

$L^{(CaCl_2)}_{CaCl_2,KCl,NaCl} = -2673.31 + 47.83 * T$ [48]

$L^{(KCl)}_{CaCl_2,KCl,NaCl} = 20915.99 - 95.33 * T$ [48]

$L^{(NaCl)}_{CaCl_2,KCl,NaCl} = -13137.35 + 2.1 * T$ [48]

$L^{(CaSO_4)}_{CaSO_4,K_2SO_4,MgSO_4} = 23000$ a

$L^{(K_2SO_4)}_{CaSO_4,K_2SO_4,MgSO_4} = -28000$ a

$L^{(MgSO_4)}_{CaSO_4,K_2SO_4,MgSO_4} = -107000$ a

$L^{(CaSO_4)}_{CaSO_4,K_2SO_4,Na_2SO_4} = -47538.9$ a

$L^{(K_2SO_4)}_{CaSO_4,K_2SO_4,Na_2SO_4} = -65567.9$ a

$L^{(Na_2SO_4)}_{CaSO_4,K_2SO_4,Na_2SO_4} = -10174.2$ a

$L^{(CaSO_4)}_{CaSO_4,Na_2SO_4,MgSO_4} = -118000$ [201]

$L^{(Na_2SO_4)}_{CaSO_4,Na_2SO_4,MgSO_4} = 122900$ a

$L^{(MgSO_4)}_{CaSO_4,Na_2SO_4,MgSO_4} = -154137$ a

$L^{(K_2SO_4)}_{K_2SO_4,Na_2SO_4,MgSO_4} = -56000$ a

$L^{(Na_2SO_4)}_{K_2SO_4,Na_2SO_4,MgSO_4} = -29000$ a

$L^{(MgSO_4)}_{K_2SO_4,Na_2SO_4,MgSO_4} = 140750$ a

Reciprocal interaction parameters

$L^{(0)}_{CaSO_4,MgCl_2} = -12262 + 6 * T$ a

$L^{(1)}_{CaSO_4,MgCl_2} = 20600$ a

$L^{(0)}_{CaCl_2,MgSO_4} = -13000$ a

$L^{(0)}_{NaCl,MgSO_4} = -12000 - 1.5 * T$ a

$L^{(1)}_{NaCl,MgSO_4} = -6000 + 8.5 * T$ a

$L^{(0)}_{NaCl,CaSO_4} = 78507.2 - 65.8391 * T$ a

$L^{(1)}_{NaCl,CaSO_4} = -13531.4$ a

$L^{(0)}_{KCl,MgSO_4} = -46000 + 19 * T$ a

$L^{(1)}_{KCl,MgSO_4} = -18000 + 18 * T$ a

$L^{(0)}_{K_2SO_4,MgCl_2} = 18000 - 20 * T$ a

$L^{(1)}_{K_2SO_4,MgCl_2} = 10000 + 10 * T$ a

$L^{(0)}_{KCl,CaSO_4} = 6500 - 1.5 * T$ a

$L^{(1)}_{KCl,CaSO_4} = -3500$ a

$L^{(0)}_{NaCl,K_2SO_4} = -16008$ a

$L^{(1)}_{NaCl,K_2SO_4} = 10525$ a

$L^{(0)}_{KCl,Na_2SO_4} = -2680$ a

$L^{(1)}_{KCl,Na_2SO_4} = 13770.7$ a

HEXA: $(Na^{1+}, K^{1+}, Mg^{2+}, Ca^{2+}, Va^{0})_2(SO_4^{2-})_1$

$^\circ G_{Na_2SO_4} = {}^\circ G^{SGPS}_{Na_2SO_4(HT)}$ [228]

$^\circ G_{K_2SO_4} = {}^\circ G^{SGPS}_{K_2SO_4(HT)}$ [228]

$^\circ G_{Mg_2SO_4^{2+}} = 2{}^\circ G_{MgSO_4(HT)} + 7220.2478 + 22.4563 * T$ a

$^\circ G_{Ca_2SO_4^{2+}} = 2{}^\circ G_{CaSO_4(HT)} - 36483.5 + 76.975 * T$ [39]

$^\circ G_{VaSO_4^{2-}} = 0$ [39]

$L^{(0)}_{Ca^{2+},K^{1+}:SO_4^{2-}} = 54322 - 39 * T$ [39]

$L^{(1)}_{Ca^{2+},K^{1+}:SO_4^{2-}} = -29564 + 3 * T$ [39]

$L^{(0)}_{Ca^{2+},Na^{1+}:SO_4^{2-}} = 65007.9 - 63.782 * T$ a

$L^{(0)}_{K^{1+},Mg^{2+}:SO_4^{2-}} = 70714 - 33.1171 * T$ a

$L^{(0)}_{Na^{1+},Mg^{2+}:SO_4^{2-}} = 24122 - 15 * T$ a

$L^{(1)}_{Na^{1+},Mg^{2+}:SO_4^{2-}} = 2897.99$ a

$L^{(0)}_{K^{1+},Na^{1+}:SO_4^{2-}} = 1854 + 5 * T$ [39]

$L^{(1)}_{K^{1+},Na^{1+}:SO_4^{2-}} = -3547.29$	[39]
$L^{(K^{1+})}_{K^{1+},Mg^{2+},Na^{1+}} = 65000$	[201]
$L^{(Mg^{2+})}_{K^{1+},Mg^{2+},Na^{1+}} = 85000$	[201]
$L^{(Na^{1+})}_{K^{1+},Mg^{2+},Na^{1+}} = -55000$	[a]
$L^{(Ca^{2+})}_{Ca^{2+},Mg^{2+},Na^{1+}} = 0$	[a]
$L^{(Mg^{2+})}_{Ca^{2+},Mg^{2+},Na^{1+}} = 0$	[a]
$L^{(Na^{1+})}_{Ca^{2+},Mg^{2+},Na^{1+}} = -179000$	[a]
Na-ortho-MT: $(Na^{1+}, K^{1+}, Mg^{2+}, Ca^{2+}, Va^0)_2(SO_4^{2-})_1$	
$^\circ G_{Na_2SO_4} = {}^\circ G^{SGPS}_{Na_2SO_4(MT)}$	[39]
$^\circ G_{K_2SO_4} = {}^\circ G_{K_2SO_4(LT)}$	[39]
$^\circ G_{Mg_2SO_4^{2+}} = 2{}^\circ G^{SGPS}_{MgSO_4(LT)} + 96151.4$	[a]
$^\circ G_{Ca_2SO_4^{2+}} = 2{}^\circ G_{CaSO_4(LT)} + 100385.65$	[39]
$^\circ G_{VaSO_4^{2-}} = 0$	[39]
$L^{(0)}_{K^{1+},Na^{1+}:SO_4^{2-}} = 33863 - 28.5 * T$	[a]
$L^{(1)}_{K^{1+},Na^{1+}:SO_4^{2-}} = -5800$	[a]
$L^{(0)}_{K^{1+},Mg^{2+}:SO_4^{2-}} = -2600$	[a]
$L^{(0)}_{K^{1+},Ca^{2+}:SO_4^{2-}} = 8800$	[39]
$L^{(0)}_{Ca^{2+},Na^{1+}:SO_4^{2-}} = 29800 - 60 * T$	[a]
$L^{(1)}_{Ca^{2+},Na^{1+}:SO_4^{2-}} = -8000$	[a]
$L^{(0)}_{Mg^{2+},Va^0:SO_4^{2-}} = 80 * T$	[39]
$L^{(0)}_{Ca^{2+},Va^0:SO_4^{2-}} = 80 * T$	[39]
GLAS: $(K^{1+}, Na^{1+})_3(Na^{1+})_1(SO_4^{2-})_2$	
$^\circ G_{K_3Na(SO_4)_2} = 1.5{}^\circ G^{SGPS}_{K_2SO_4(HT)} + 0.5{}^\circ G^{SGPS}_{Na_2SO_4(HT)} - 29933.58 + 27.16 * T$	[39]
$^\circ G_{Na_3Na(SO_4)_2} = 2{}^\circ G^{SGPS}_{Na_2SO_4(HT)} - 1284.8 + 11.75 * T$	[39]
$L^{(0)}_{K^{1+},Na^{1+}:Na^{1+}:SO_4^{2-}} = 12914 - 10 * T$	[39]
$L^{(1)}_{K^{1+},Na^{1+}:Na^{1+}:SO_4^{2-}} = 11560 - 10 * T$	[39]
NaLT: $(Na^{1+}, K^{1+})_2(SO_4^{2-})_2$	
$^\circ G_{Na_2SO_4} = {}^\circ G^{SGPS}_{Na_2SO_4(LT)}$	[39]
$^\circ G_{K_2SO_4} = {}^\circ G^{SGPS}_{K_2SO_4(LT)} + 25300$	[39]
AlkCl(ss): $(Na^{1+}, K^{1+}, Ca^{2+}, Va^0)(Cl^{1-})$	
$^\circ G_{NaCl} = {}^\circ G_{NaCl}$	[48]
$^\circ G_{KCl} = {}^\circ G_{KCl}$	[48]
$^\circ G_{CaCl} = {}^\circ G_{CaCl_2} + 39682.04271405 + 5.11655819225 * T$	[48]
$^\circ G_{VaCl^-} = 0$	[48]
$L^{(0)}_{Na^{1+},K^{1+}:Cl^-} = 15975.6 + 33.08 * T - 5.593 * T * ln(T)$	[48]
$L^{(1)}_{Na^{1+},K^{1+}:Cl^-} = 1650.4$	[48]
$L^{(0)}_{Ca^{2+},Va^0:Cl^-} = -41618.41682$	[48]
MCl2: $(Mg^{2+}, Ca^{2+})_1(Cl^{1-})_2$	
$^\circ G_{MgCl_2} = {}^\circ G_{MgCl_2(liquid)} + 29550.2 + 18.4261$	[54]
$^\circ G_{CaCl_2} = {}^\circ G_{CaCl_2(liquid)}$	[54]
LANGBEINITE: $(K^{1+})_2(Ca^{2+}, Mg^{2+})_2(SO_4^{2-})_3$	
$^\circ G_{K_2Ca_2SO_4} = {}^\circ G_{K_2Ca_2(SO_4)_3(HT)}$	[39]
$^\circ G_{K_2Mg_2SO_4} = {}^\circ G_{K_2Mg_2(SO_4)_3}$	[39]
$L^{(0)}_{K^{1+}:Ca^{2+},Mg^{2+}:SO_4^{2-}} = -5300$	[a]
$L^{(1)}_{K^{1+}:Ca^{2+},Mg^{2+}:SO_4^{2-}} = 22200$	[201]

[a] PCM2 database, in the frame of the database development of PCM-Screening-2 project [4]

The initial objective of the study, as outlined in the introduction, was represented conceptually through the geometry of a cube or as four triangular-based prisms (**Figure 1-1**). Following the results

obtained in this work, the system can now be illustrated by the three-dimensional schematics shown in **Figure 6-44**, which summarise the full thermodynamic description within the developed database. These graphical representations provide a comprehensive overview of the results and clearly demonstrate how the stepwise approach adopted in this study - progressing from unary to binary, ternary, reciprocal, and ultimately higher-order systems - might enable the prediction of thermodynamic properties within the three-dimensional compositional space of the final multicomponent system.

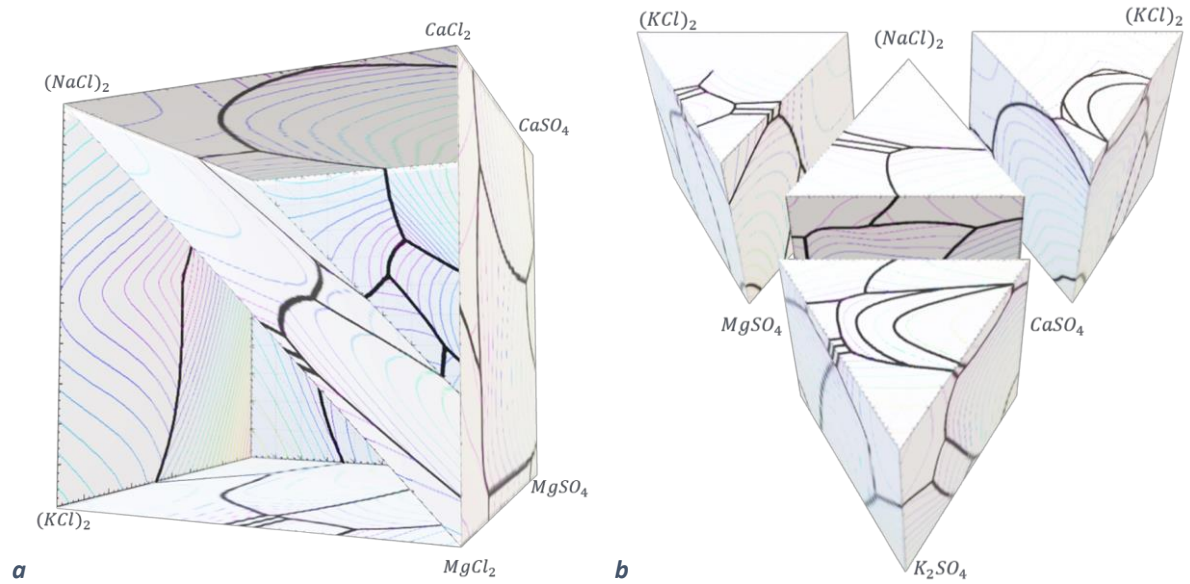
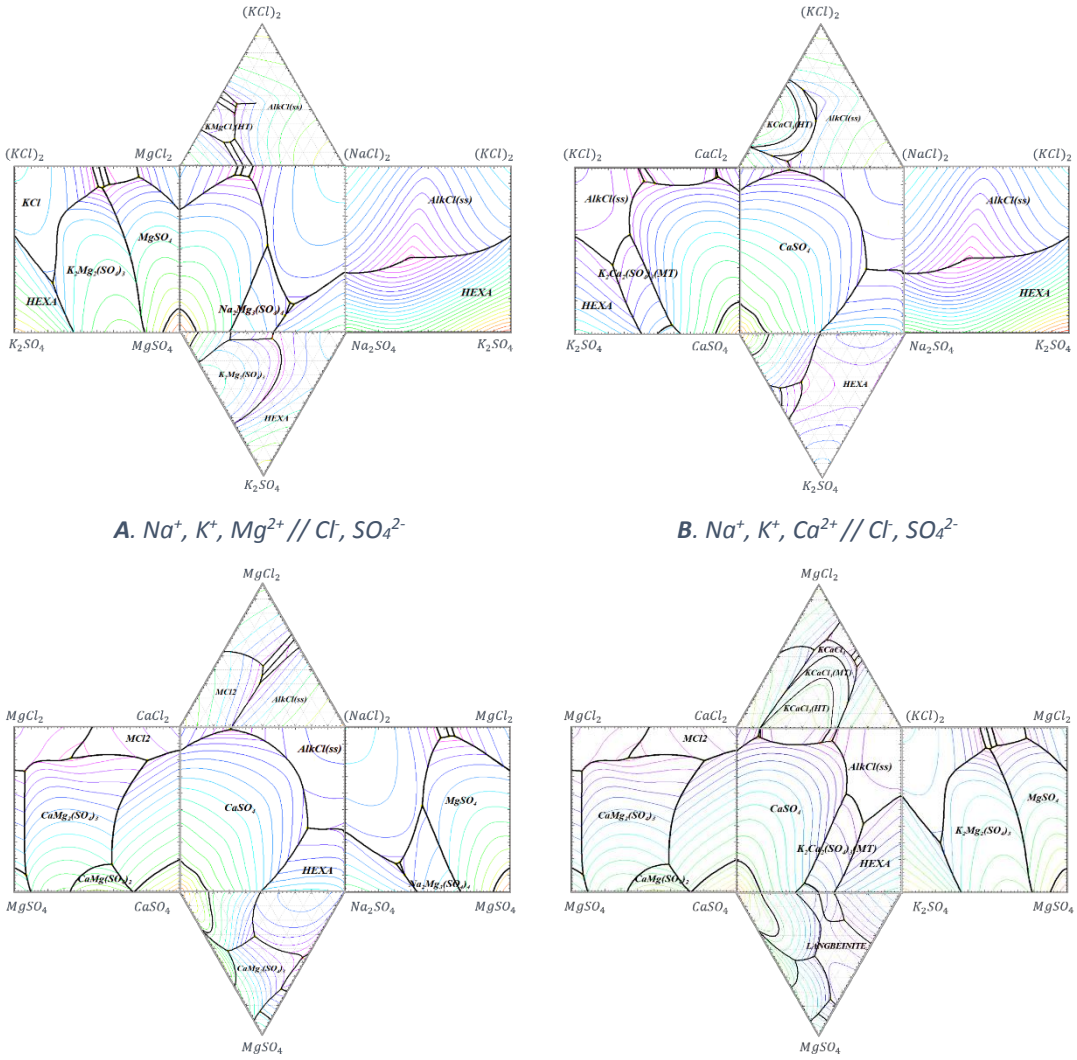


Figure 6-44 *Graphical representation of the calculated Na^+, K^+, Mg^{2+}, Ca^{2+} // Cl^-, SO_4^{2-} multi-component system with the developed database:* ***a*** *cubic representation with visualization of six reciprocal systems under analysis;* ***b*** *alternative representation of the multi-component system made of four six-component systems.*

In **Figure 2-3**, the state of the art from the literature, particularly based on the work of Rowe et al. [49], was shown as a set of four six-component systems. In contrast, **Figure 6-45** presents a two-dimensional schematic of the triangular prisms (comprising three reciprocal and two ternary systems), as calculated using the thermodynamic database developed in this work. This figure serves as the two-dimensional counterpart of the three-dimensional representation shown in **Figure 6-44b**, effectively highlighting the structural coherence and predictive capability achieved through the methodology applied.



A. Na^+, K^+, Mg^{2+} // Cl^-, SO_4^{2-} ***B***. Na^+, K^+, Ca^{2+} // Cl^-, SO_4^{2-}

C. Na^+, Mg^{2+}, Ca^{2+} // Cl^-, SO_4^{2-} ***D***. K^+, Mg^{2+}, Ca^{2+} // Cl^-, SO_4^{2}

Figure 6-45 *Graphical bidimensional representation of the four quaternary reciprocal salt systems from the developed database.*

6.8.1 Validation of the developed database

The thermodynamic database developed in this work, optimised on the basis of the subsystems investigated, demonstrates a high degree of reliability. This section and Appendix B present the validation of the database, which was carried out by comparing the phase equilibria calculated with the present database against available experimental data from the literature [49, 63, 133, 135]. The comparison focuses on subsystems within the multicomponent system Na^+, K^+, Mg^{2+}, Ca^{2+} // Cl^-, SO_4^{2-}, and in particular on ternary sections of quaternary systems, with the aim of demonstrating the overall consistency and predictive capability of the database.

In addition to the validation of the database for the sections investigated by Speranskaya [63] within the reciprocal system Na^+, Mg^{2+} // Cl^-, SO_4^{2-} (see section 6.2.4), further validation was conducted

with reference to ternary planes for which experimental data are reported in the literature. For each system considered, the results of the validation are presented in a consistent format in the Appendix B. First, the calculated ternary phase diagram is shown, followed by a table summarising the corresponding invariant points obtained using the present database. Additionally, selected quasi-binary sections derived from these ternary systems are reported and compared with the available experimental data. This layout allows a direct comparison between calculations and measurements and demonstrates the ability of the thermodynamic database to reproduce the experimental phase equilibria. The NaCl-K_2SO_4-$MgSO_4$ system and its internal section NaCl-$K_2Mg_2(SO_4)_3$, based on the experimental data of Rowe et al. [49], are presented in **Figure A 26** and **Figure A 27**, with the corresponding calculated invariant points summarised in **Table A 8**. Within the $(NaCl)_2$-$(KCl)_2$-$MgSO_4$ system (**Figure A 28**; **Table A 9**), the section $(NaCl)_2$-KCl·$MgSO_4$ was calculated and compared with the experimental data of Bergman and Selivanova [133] (**Figure A 29** and **Figure A 27**). In the frame of the $(NaCl)_2$-$(KCl)_2$-$CaSO_4$ system (**Figure A 30**; **Table A 10**), Rubleva and Bergman [135] provided experimental data for several sections; the comparison of experimental and calculated phase diagrams of sections I-IX - corresponding to (1-a)K_2Cl_2(a)Na_2Cl_2-$CaSO_4$ with a: 75, 60, 53, 50, 42.5, 25, 15 mol% (I-VII), and (1-a)$CaSO_4$(a)K_2Cl_2-Na_2Cl_2 with a: 72, 62.5 mol% (VIII-IX) - is shown in **Figure A 31**. Additionally, other subsystems investigated by Rowe et al. [49] were considered in this work: NaCl-$K_2Ca_2(SO_4)_3$ in the NaCl-K_2SO_4-$CaSO_4$ system (**Figure A 32**; **Table A 11**; **Figure A 33**), NaCl-$CaMg_3(SO_4)_4$ in the NaCl-$MgSO_4$-$CaSO_4$ system (**Figure A 34**; **Table A 12**; **Figure A 35**), NaCl-(0.637)$K_2Mg_2(SO_4)_3$(0.363)$K_2Ca_2(SO_4)_3$ in the NaCl-$K_2Mg_2(SO_4)_3$-$K_2Ca_2(SO_4)_3$ system (**Figure A 36**; **Table A 13**; **Figure A 37**), and the 40 mol% NaCl plane in the NaCl-K_2SO_4-$MgSO_4$-$CaSO_4$ system (**Figure A 38**).

The good agreement between the calculated phase diagrams and the corresponding experimental results confirms the reliability of the database presented here, providing a solid foundation for the description of higher-order systems.

7 Implications for applications: identifying PCM candidates for TES

The thermodynamic study of the multicomponent system presented in this thesis aimed to provide an extended and detailed analysis for the understanding and description of the selected systems from a thermodynamic perspective, with the goal of improving and updating the thermodynamic database. This objective was pursued within the broader framework of the PCM-Screening-2 project [4], which focuses on identifying and evaluating new phase change materials (PCMs) for thermal energy storage (TES) applications. The study presented here primarily contributes to the fundamental scientific understanding of the thermodynamic behaviour of relevant systems, laying the groundwork for future screening activities. A number of compositions were selected and extensively investigated during the experimental campaign. These are mainly eutectic mixtures or low-melting compositions, chosen to expand the thermodynamic dataset and improve the description of the system behaviour. In addition, selected compositions corresponding to known or hypothesised intermediate compounds were studied to better assess their existence, stability, and potential role in the phase diagrams. As discussed throughout the text, potential PCM candidates include multi-component eutectic compositions predicted by the reciprocal phase diagrams and ternary systems derived from the updated and optimised thermodynamic database. Although these specific eutectic mixtures were not directly analysed in this work, they represent a valuable starting point for future experimental screening, which could serve to validate or refute their suitability as TES materials.

Table 7-1 summarises the binary mixtures experimentally investigated in this study using DTA and DSC analyses, sorted by increasing transition temperature. Most of the studied compositions fall within the 600-700 °C temperature window, aligning with the medium-to-high temperature range of TES applications [1, 10]. The DTA/TG analysis provides key insights into the operating temperature of the materials and their thermal stability. Within the investigated temperature range, the materials did not exhibit signs of sulphate decomposition - an issue typically observed at higher temperatures - and also showed no significant vaporisation of chloride phases, supporting the overall chemical stability of the mixtures. The DSC measurements offered essential information on the enthalpy of fusion, a critical property for evaluating PCM performance [3]. The corresponding values are listed in **Table 7-1**, and shown in **Figure 7-1**. High enthalpy values, combined with favourable melting temperatures and stability, make several of the studied compositions promising from a thermodynamic standpoint.

In the selection of good phase change materials, eutectic compositions are generally preferred over liquidus-minimum compositions (indicated as M in **Table 7-1**). While eutectics provide a sharp and well-defined melting transition, the liquidus minima are typically preceded by additional solid-state transformations. Such transitions may interfere with the charging and discharging processes in thermal applications, as the latent heat of fusion may not be fully recovered or may become partially

distributed across multiple transitions. Consequently, eutectic compositions offer a more efficient and reliable thermal response for latent heat storage systems.

Table 7-1 *Experimental transition temperature and transition enthalpy of selected quasi-binary mixtures as potential PCMs.*

System	Mixture (mol%)	T_{tr} (°C) [K]	$\Delta_{tr}H$ (kJ/mol) [J/g]
$KCl\text{-}Na_2SO_4$*	M: 41.6 Na_2SO_4	521 [794]	20.0 [175.5]
$MgCl_2\text{-}CaCl_2$	E: 47.2 $CaCl_2$	624 [897]	33.2 [323.0]
$MgCl_2\text{-}CaSO_4$*	M: 21.7 $CaSO_4$	632 [905]	19.0 [182.6]
$NaCl\text{-}MgSO_4$*	E: 34.1 $MgSO_4$	641 [914]	42.0 [527.9]
$MgCl_2\text{-}MgSO_4$	E: 28.0 $MgSO_4$	663 [936]	37.9 [370.6]
$KCl\text{-}CaSO_4$*	E: 19.5 $CaSO_4$	690 [963]	37.0 [427.4]
$CaCl_2\text{-}CaSO_4$	E: 14.0 $CaSO_4$	724 [997]	30.2 [263.8]
$NaCl\text{-}CaSO_4$*	M: 16.9 $CaSO_4$	724 [997]	39.3 [549.1]
$Na_2SO_4\text{-}CaSO_4$	50 $CaSO_4$ [$Na_2Ca(SO_4)_2$]	929 [1202]	18.9 [135.9]
$Na_2SO_4\text{-}CaSO_4$	25 $CaSO_4$ [$Na_4Ca(SO_4)_3$]	948 [1221]	19.3 [137.8]
$Na_2SO_4\text{-}CaSO_4$	12 $CaSO_4$	950 [1223]	15.1 [106.8]
$Na_2SO_4\text{-}CaSO_4$	25 $CaSO_4$	959 [1232]	18.8 [133.7]
$MgSO_4\text{-}CaSO_4$	$CaMg_2(SO_4)_3$	1212 [1485]	145.5 [386.1]

*stable diagonal of the reciprocal system
E: eutectic composition; M: minimum of liquidus

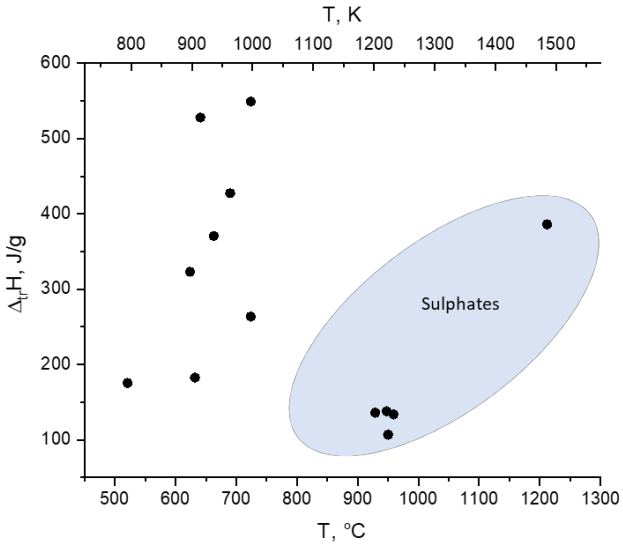


Figure 7-1 *Enthalpy of transition as a function of the transition temperature of selected quasi-binary mixtures as potential PCMs.*

In addition to **Table 7-1**, which reports the experimentally tested compositions, **Table 7-2** lists the melting temperatures and corresponding enthalpies of the invariant reactions calculated using the thermodynamic database developed in this work, for selected compositions of the ternary, reciprocal, and higher-order systems presented in Chapter 6. Only systems actually assessed and presented in the thesis are considered; therefore, the table does not include all possible subsystems or all minima

predicted within the overall six-component system. Furthermore, only compositions exhibiting a discrete latent heat of fusion - consistent with PCM requirements - are listed, while compositions showing a continuous enthalpy increase at melting (i.e., without a distinct latent contribution) are excluded.

All the mixtures listed in **Table 7-1** and **Table 7-2** are plotted in **Figure 7-2**, which displays the melting transition enthalpies as a function of the corresponding transition temperatures. Higher transition temperatures are associated with compositions richer in sulphates, up to fully sulphate-based mixtures. However, no straightforward linear trend is observed between the enthalpy of transition and the alkali/alkaline-earth cation ratio across the investigated systems.

As previously stated, the thermodynamic analysis carried out in this work represents a solid foundation for PCM screening. However, additional investigations into complementary properties - such as material compatibility and corrosion behaviour in contact with container materials, as well as cost analysis - should be considered in future studies. These aspects, while crucial for real-world applications, lie beyond the scope of this thesis and the PCM-Screening-2 project. Nevertheless, this fundamental analysis is not disconnected from potential practical implications. On the contrary, it provides the necessary scientific foundation to guide the rational selection and validation of candidate PCMs for advanced TES systems, potentially leading to market-relevant materials.

Table 7-2 *Calculated transition temperature and transition enthalpy of selected multi-component mixtures as potential PCMs.*

System	Mixture (mol%)			T_{tr} (°C) [K]	$\Delta_{tr}H$ (kJ/mol) [J/g]
Mg^{2+}, Ca^{2+} // Cl^-, SO_4^{2-}	$MgCl_2$	$MgSO_4$	$CaSO_4$		
	73.14	20.75	6.12	648 [921]	42.0 [408.0]
	$MgCl_2$	$CaCl_2$	$CaSO_4$		
	65.61	15.51	18.88	578 [851]	34.5 [327.4]
Na^+, Mg^{2+} // Cl^-, SO_4^{2-}	NaCl	Na_2SO_4	$MgSO_4$		
	68.54	0.66	30.80	632 [905]	36.2 [463.7]
	28.95	44.61	26.44	573 [846]	27.7 [247.1]
	NaCl	$MgCl_2$	$MgSO_4$		
	53.98	42.07	3.95	453 [726]	25.4 [332.7]
Na^+, Ca^{2+} // Cl^-, SO_4^{2-}	NaCl	Na_2SO_4	$CaCl_2$		
	45.59	0.95	53.46	496 [769]	16.9 [193.5]
K^+, Mg^{2+} // Cl^-, SO_4^{2-}	KCl	K_2SO_4	$MgCl_2$		
	12.73	65.70	21.57	625 [898]	37.2 [257.1]
	30.92	5.38	63.70	455 [728]	23.6 [253.6]
	50.20	9.10	40.70	408 [681]	18.5 [201.0]
	50.54	9.69	39.77	406 [679]	18.0 [194.7]
	KCl	K_2SO_4	$CaCl_2$		
	31.49	49.21	19.30	653 [926]	33.0 [252.6]
	66.58	5.36	28.06	581 [854]	21.3 [236.4]
NaCl-KCl-$MgCl_2$	$MgCl_2$	KCl	NaCl		
	43.70	24.68	31.62	400 [673]	21.0 [267.6]
	39.85	27.09	33.05	400 [673]	20.8 [268.6]
	27.56	56.13	16.31	389 [662]	16.8 [216.4]
	28.93	54.19	16.88	388 [661]	17.6 [226.2]
NaCl-KCl-$CaCl_2$	$CaCl_2$	KCl	NaCl		
	29.10	27.82	43.08	567 [840]	22.1 [282.6]

	18.14	52.92	28.94	507 [780]	17.5 [228.8]
	51.79	6.59	41.63	481 [754]	16.5 [190.3]
$NaCl-MgCl_2-CaCl_2$	$CaCl_2$	NaCl	$MgCl_2$		
	24.49	48.43	27.09	410 [683]	20.9 [257.2]
	27.27	49.84	22.89	410 [683]	19.6 [241.4]
$KCl-MgCl_2-CaCl_2$	$MgCl_2$	$CaCl_2$	KCl		
	50.03	11.43	38.55	437 [710]	22.1 [248.2]
	31.62	3.32	65.06	420 [693]	16.6 [201.7]
	28.19	3.53	68.28	418 [691]	16.6 [203.3]
$Na_2SO_4-K_2SO_4-MgSO_4$	Na_2SO_4	K_2SO_4	$MgSO_4$		
	52.90	4.40	42.70	667 [940]	18.3 [136.4]
$Na_2SO_4-K_2SO_4-CaSO_4$	Na_2SO_4	K_2SO_4	$CaSO_4$		
	20.51	33.25	46.25	785 [1058]	19.6 [130.6]
$Na_2SO_4-MgSO_4-CaSO_4$	Na_2SO_4	$MgSO_4$	$CaSO_4$		
	29.58	31.45	38.97	762 [1035]	22.6 [170.0]
	51.40	46.32	2.28	691 [964]	22.3 [169.1]
$K_2SO_4-MgSO_4-CaSO_4$	K_2SO_4	$MgSO_4$	$CaSO_4$		
	25.29	44.73	29.98	870 [1143]	38.7 [279.0]
	19.78	75.00	5.22	870 [1143]	49.2 [373.2]
	56.12	19.14	24.74	764 [1037]	26.4 [170.9]
$Na^+, K^+, Mg^{2+} // Cl^-, SO_4^{2-}$	NaCl	K_2SO_4	$MgSO_4$		
	68.80	0.54	30.66	630 [903]	36.0 [461.2]
	62.88	8.70	28.42	601 [874]	36.5 [423.8]
$Na^+, K^+, Ca^{2+} // Cl^-, SO_4^{2-}$	$(NaCl)_2$	$(KCl)_2$	$CaSO_4$		
	39.34	44.51	16.15	588 [861]	40.2 [299.3]
$Na^+, Mg^{2+}, Ca^{2+} // Cl^-, SO_4^{2-}$	NaCl	$MgSO_4$	$CaSO_4$		
	75.95	10.05	14.00	682 [955]	36.4 [481.9]
	69.08	30.57	0.35	631 [904]	35.6 [458.5]
$Na^+, K^+, Mg^{2+}, Ca^{2+} // Cl^-, SO_4^{2-}$	NaCl	$K_2Mg_2(SO_4)_3$	$K_2Ca_2(SO_4)_3$		
	84.42	14.67	0.91	606 [879]	36.7 [321.1]

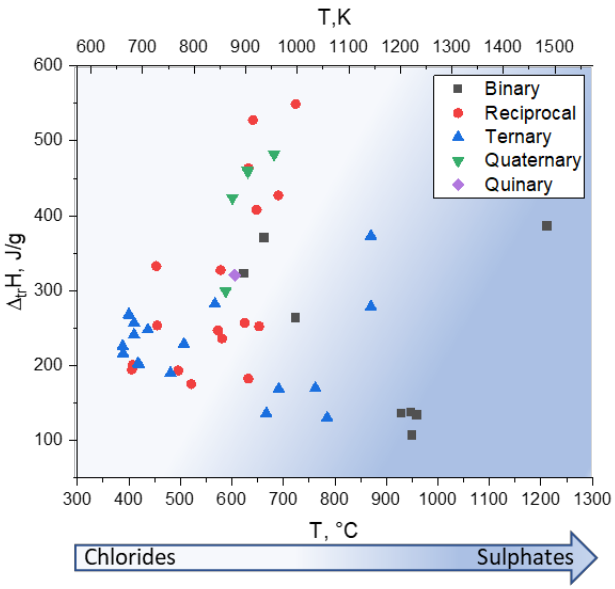


Figure 7-2 *Enthalpy of transition as a function of the transition temperature of selected mixtures as potential PCMs.*

8 Conclusions

The objective of this work was to perform a comprehensive thermodynamic assessment of the multicomponent system Na^+, K^+, Mg^{2+}, Ca^{2+} // Cl^-, SO_4^{2-} through a combined experimental and thermodynamic modelling approach. The ultimate goal was to update and expand the thermodynamic database describing the Gibbs free energies of all relevant phases involved. The experimental campaign employed multiple techniques - including DTA/TG, DSC, HT-XRD, and SEM - to generate reliable experimental evidence supporting the thermodynamic characterisation of the systems under investigation. These data, together with selected, high-quality literature values, provided a robust and consistent dataset that formed the foundation for the thermodynamic modelling carried out using the FactSage software package.

The complex multicomponent system was treated as comprising six reciprocal systems. Each of these was analysed through a stepwise modelling strategy, beginning with unary systems and progressing through binary and quasi-binary subsystems, ultimately leading to the reciprocal systems. This hierarchical approach ensured accurate propagation of thermodynamic consistency across all levels of the model.

Thermal analysis via DTA was performed using sealed platinum crucibles, enabling a comprehensive investigation across the full compositional range. This setup was particularly effective in addressing the decomposition of sulphate-containing mixtures and filling significant gaps in the existing literature. Calorimetric analysis, carried out using two different instruments, was fundamental for determining heat capacities and transition enthalpies of selected compositions. These measurements significantly enriched the thermodynamic understanding of the systems. A key methodological contribution of this thesis was the development and application of the “self-referencing calibration method” (SRCM), designed to measure and correct the heat capacity curves of sulphate-rich mixtures, which are prone to decomposition at high temperatures and cannot be analysed in open crucibles. This innovative approach enabled the determination of reliable C_p curves and associated transition enthalpies, even for pure compounds, and can be applied to a wide range of compositions. Complementary techniques such as high-temperature X-ray diffraction (HT-XRD) and scanning electron microscopy (SEM) were employed both to verify the purity of starting materials and to characterise the crystal structures of selected phases. These methods were particularly valuable in providing critical evidence for redefining the phase equilibria of specific subsystems within the overall multicomponent system. This is especially true for the two sulphate-based systems, $MgSO_4$-$CaSO_4$ and Na_2SO_4-$CaSO_4$, for which the present work introduced, on the basis of experimental evidence, a significantly updated and reliable thermodynamic description, supported by the consistency of the data obtained.

From the experimental standpoint, nineteen (pseudo)binary systems were investigated. For thermodynamically stable sections, selected compositions corresponding to eutectic points or low-melting mixtures along the liquidus curves were examined calorimetrically to determine more detailed thermodynamic properties. In addition, several compositions corresponding to intermediate compounds - either already validated or requiring confirmation - as well as other strategically chosen compositions to better elucidate phase equilibria, were also investigated calorimetrically. In total, sixteen compositions were examined to measure heat capacities and to determine transition enthalpies.

The experimental results enabled either a new thermodynamic assessment or a re-assessment of previously studied systems. Altogether, nineteen subsystems were modelled within the framework of the six reciprocal systems presented in this work. Among these, the Mg^{2+}, Ca^{2+} // Cl^{-}, SO_4^{2-} reciprocal system constitutes one of the major contributions, filling important gaps in the literature and representing one of the first comprehensive studies of this kind. The experimental updates obtained in this work also led to the reassessment of six ternary systems. Finally, the experimental results, together with the methodologies and strategies developed for such an extensive experimental campaign, culminated in the establishment of a broad, updated, and internally consistent thermodynamic database. This database provides an improved and reliable thermodynamic description within the multicomponent Na^{+}, K^{+}, Mg^{2+}, Ca^{2+} // Cl^{-}, SO_4^{2-} system, thereby making a significant contribution to the advancement of thermodynamic knowledge on complex salt systems and establishing a solid foundation for future screening of phase change materials for thermal energy storage applications.

Acknowledgements

I would like to express my deepest gratitude to Prof. Ruth Schweiger and Dr. Michael Müller for giving me the opportunity to carry out my research within the Institute of Energy Materials and Devices, Structure and Function of Materials (IMD-1) at Forschungszentrum Jülich.

My sincere thanks go especially to my supervisor, Dr. Michael Müller, leader of the Thermochemistry group, who has represented an academic father figure for me throughout this journey. I am profoundly grateful for his guidance, scientific wisdom, and for the joyful spirit and collegial atmosphere he created, which greatly contributed to both productivity and personal growth. I would also like to thank all members of the IMD-1 group, whose presence was vital in making me feel at home while at the same time encouraging me to grow as a scientist in an environment full of intellectual stimulation.

A special acknowledgement goes to Dr. Dmitry Sergeev, who during the early stages of this work was an irreplaceable guide, a kind soul, and a constant source of inspiration whose esteem I deeply cherish. I am equally grateful for the support and contributions of Inge Dreger, Dr. Egbert Wessel, and Dr. Rhys Dominic Jacob. I am indebted to Mirko Ziegner for his invaluable assistance with XRD analyses, as well as for his generosity and expertise, which will not be forgotten. I am also grateful to Dr. Philipp Keuter from GTT-Technologies for his support during the final stages of the development of the thermodynamic database presented in this work.

A very special word of thanks goes to Dr. Elena Yazhenskikh. Her expertise in thermodynamic modelling and the use of FactSage has been a continuous source of inspiration and admiration. My gratitude to her as a mentor is immeasurable: I will always remember her intellectual generosity, her emotional intelligence, her meticulous attention, and the grace with which she supported me throughout this work.

Finally, I am endlessly grateful to my parents, who have endured and supported me in this demanding adventure that has challenged me as both a researcher and as a person. This work would not have been possible without my sister, Mariateresa, to whom I owe my deepest recognition. She has shared in every small success and every minor setback, listened to my silence, and read my eyes when words were not enough.

This work was supported by the Federal Ministry for Economic Affairs and Climate Action on the basis of a decision by the German Bundestag within the project PCM-Screening 2 (FKZ 03EN6005D).

References

[1] M.M. Kenisarin, High-temperature phase change materials for thermal energy storage, Renewable and Sustainable Energy Reviews 14(3) (2010) 955-970.
[2] D.A. Baharoon, H.A. Rahman, W.Z.W. Omar, S.O. Fadhl, Historical development of concentrating solar power technologies to generate clean electricity efficiently–A review, Renewable and Sustainable Energy Reviews 41 (2015) 996-1027.
[3] A. Abhat, Low temperature latent heat thermal energy storage: heat storage materials, Solar Energy 30 (1983) 313-332.
[4] https://www.enargus.de/pub/bscw.cgi/?op=enargus.eps2&q=PCM-2&v=10&id=2029269.
[5] E. Jänecke, Über das Schmelz-und Erstarrungsbild des doppelt-ternären Systemes (K_2· Na_2· Mg)(Cl_2· SO_4), Zeitschrift für anorganische Chemie 261(3-4) (1950) 213-225.
[6] IEA, World Energy Outlook 2021, IEA, Paris https://www.iea.org/reports/world-energy-outlook-2021, (2021).
[7] H.E. Murdock, D. Gibb, T. Andre, J.L. Sawin, A. Brown, L. Ranalder, U. Collier, C. Dent, B. Epp, C. Hareesh Kumar, Renewables 2021-global status report, (2021).
[8] M.I. Khan, F. Asfand, S.G. Al-Ghamdi, Progress in technology advancements for next generation concentrated solar power using solid particle receivers, Sustainable Energy Technologies and Assessments 54 (2022) 102813.
[9] T. Kousksou, P. Bruel, A. Jamil, T. El Rhafiki, Y. Zeraouli, Energy storage: Applications and challenges, Solar Energy Materials and Solar Cells 120 (2014) 59-80.
[10] B. Cárdenas, N. León, High temperature latent heat thermal energy storage: Phase change materials, design considerations and performance enhancement techniques, Renewable and Sustainable Energy Reviews 27 (2013) 724-737.
[11] M. Liu, W. Saman, F. Bruno, Review on storage materials and thermal performance enhancement techniques for high temperature phase change thermal storage systems, Renewable and Sustainable Energy Reviews 16(4) (2012) 2118-2132.
[12] T. Kousksou, P. Bruel, A. Jamil, T. El Rhafiki, Y. Zeraouli, Energy storage: Apllications and challenges, Solar Energy Materials and Solar Cells 120 (2014) 59-80.
[13] A. Gil, M. Medrano, I. Martorell, A. Lázaro, P. Dolado, B. Zalba, L.F. Cabeza, State of the art on high temperature thermal energy storage for power generation. Part 1—Concepts, materials and modellization, Renewable and Sustainable Energy Reviews 14(1) (2010) 31-55.
[14] A. Abhat, Low temperature latent heat thermal energy storage: heat storage materials, Solar energy 30(4) (1983) 313-332.
[15] G.A. Lane, Low temperature heat storage with phase change materials, International Journal of Ambient Energy 1(3) (1980) 155-168.
[16] G.A. Lane, Solar heat storage: latent heat materials, CRC press Boca Raton, FL, USA:1983.
[17] L. Miró, C. Barreneche, G. Ferrer, A. Solé, I. Martorell, L.F. Cabeza, Health hazard, cycling and thermal stability as key parameters when selecting a suitable phase change material (PCM), Thermochimica acta 627 (2016) 39-47.
[18] H. Lorsch, K. Kauffman, J. Denton, Thermal energy storage for heating and air conditioning, Future energy production systems: Heat and mass transfer processes 1 (1976) 69-81.
[19] W.R. Humphries, E.I. Griggs, A design handbook for phase change thermal control and energy storage devices, 1977.
[20] S. Farid, M, Khudhair, K, Razack, S, Hallaj,, A review on phase change energy storage: materials and applications, Energy Conversion and Management 45(9-10) (2004) 1597-1615.
[21] B. Zalba, J.M. Marín, L.F. Cabeza, H. Mehling, Review on thermal energy storage with phase change: materials, heat transfer analysis and applications, Applied thermal engineering 23(3) (2003) 251-283.
[22] A. Sharma, V.V. Tyagi, C.R. Chen, D. Buddhi, Review on thermal energy storage with phase change materials and applications, Renewable and Sustainable energy reviews 13(2) (2009) 318-345.

[23] F. Agyenim, N. Hewitt, P. Eames, M. Smyth, A review of materials, heat transfer and phase change problem formulation for latent heat thermal energy storage systems (LHTESS), Renewable and sustainable energy reviews 14(2) (2010) 615-628.
[24] S. Jegadheeswaran, S. Pohekar, T. Kousksou, Exergy based performance evaluation of latent heat thermal storage system: a review, Renewable and Sustainable Energy Reviews 14(9) (2010) 2580-2595.
[25] E. Oró, A. De Gracia, A. Castell, M.M. Farid, L.F. Cabeza, Review on phase change materials (PCMs) for cold thermal energy storage applications, Applied Energy 99 (2012) 513-533.
[26] L.F. Cabeza, A. Castell, C.d. Barreneche, A. De Gracia, A. Fernández, Materials used as PCM in thermal energy storage in buildings: A review, Renewable and sustainable energy reviews 15(3) (2011) 1675-1695.
[27] A. Kürklü, Energy storage applications in greenhouses by means of phase change materials (PCMs): a review, Renewable energy 13(1) (1998) 89-103.
[28] T. Bauer, D. Laing, R. Tamme, Overview of PCMs for concentrated solar power in the temperature range 200 to 350 C, Advances in Science and Technology, Trans Tech Publ, 2010, pp. 272-277.
[29] M. Liu, E.S. Omaraa, J. Qi, P. Haseli, J. Ibrahim, D. Sergeev, M. Müller, F. Bruno, P. Majewski, Review and characterisation of high-temperature phase change material candidates between 500 C and 700° C, Renewable and Sustainable Energy Reviews 150 (2021) 111528.
[30] J.C. Gomez-Vidal, R. Tirawat, Corrosion of alloys in a chloride molten salt (NaCl-LiCl) for solar thermal technologies, Solar energy materials and solar cells 157 (2016) 234-244.
[31] S.A. Mohamed, F.A. Al-Sulaiman, N.I. Ibrahim, M.H. Zahir, A. Al-Ahmed, R. Saidur, B. Yılbaş, A. Sahin, A review on current status and challenges of inorganic phase change materials for thermal energy storage systems, Renewable and Sustainable Energy Reviews 70 (2017) 1072-1089.
[32] M. Sun, T. Liu, H. Sha, M. Li, T. Liu, X. Wang, G. Chen, J. Wang, D. Jiang, A review on thermal energy storage with eutectic phase change materials: Fundamentals and applications, Journal of Energy Storage 68 (2023) 107713.
[33] H. Michels, R. Pitz-Paal, Cascaded latent heat storage for parabolic trough solar power plants, Solar Energy 81(6) (2007) 829-837.
[34] D. Sergeev, B.H. Reis, I. Dreger, M.t. Baben, K. Hack, M. Müller, Thermodynamics of the $Ca(NO_3)_2$–$NaNO_3$ system, Calphad 67 (2019) 101688.
[35] Y. Zhang, X. Zhang, Thermal properties of a new type of calcium chloride hexahydrate-magnesium chloride hexahydrate/expanded graphite composite phase change material and its application in photovoltaic heat dissipation, Solar Energy 204 (2020) 683-695.
[36] K. Nagano, K. Ogawa, T. Mochida, K. Hayashi, H. Ogoshi, Thermal characteristics of magnesium nitrate hexahydrate and magnesium chloride hexahydrate mixture as a phase change material for effective utilization of urban waste heat, Applied Thermal Engineering 24(2-3) (2004) 221-232.
[37] D. Sergeev, E. Yazhenskikh, D. Kobertz, K. Hack, M. Müller, Phase equilibria in the reciprocal NaCl–KCl–$NaNO_3$–KNO_3 system, Calphad 51 (2015) 111-124.
[38] J. Qi, E. Yazhenskikh, M. Ziegner, X. Zhao, G. Wu, M. Müller, D. Sergeev, Experimental study and thermochemical assessment of the reciprocal system Li^+, K^+//Cl^-, CO_3^{2-}, Calphad 83 (2023) 102603.
[39] E. Yazhenskikh, T. Jantzen, D. Kobertz, K. Hack, M. Müller, Critical thermodynamic evaluation of the binary sub-systems of the core sulphate system Na_2SO_4–K_2SO_4–$MgSO_4$–$CaSO_4$, Calphad 72 (2021) 102234.
[40] D. Sergeev, E. Yazhenskikh, P. Haseli, M. Liu, M. Ziegner, F. Bruno, M. Müller, Experimental study of thermodynamic properties and phase equilibria in Na_2CO_3–K_2CO_3 system, Calphad 71 (2020).
[41] D. Sergeev, D. Kobertz, M. Müller, Thermodynamics of the NaCl–KCl system, Thermochimica Acta 606 (2015) 25-33.
[42] J. Qi, E. Yazhenskikh, M. Ziegner, G. Wu, M. Müller, D. Sergeev, Experimental study and thermodynamic assessment of thermodynamic properties of pure Li_2CO_3 and K_2CO_3, Calphad 78 (2022) 102452.

[43] H. Yin, Z. Wang, X. Lai, Y. Wang, Z. Tang, Optimum design and key thermal property of NaCl–KCl–$CaCl_2$ eutectic salt for ultra-high-temperature thermal energy storage, Solar Energy Materials and Solar Cells 236 (2022) 111541.
[44] L. Zhao, J. Wang, L. Cui, B. Li, X. Du, H. Wu, Performance Design of High-Temperature Chloride Salts as Thermal Energy Storage Material, Journal of Thermal Science 33(2) (2024) 479-490.
[45] X. Liu, Z. Kang, J. Zhao, S. Huang, Y. Zhang, M. He, Preparation and thermal property characterization of NaCl–Na_2CO_3–Na_2SO_4 eutectic salt mixed with carbon nanomaterials for heat storage, Solar Energy Materials and Solar Cells 251 (2023) 112173.
[46] M. Kenisarin, K. Mahkamov, Salt hydrates as latent heat storage materials: Thermophysical properties and costs, Solar Energy Materials and Solar Cells 145 (2016) 255-286.
[47] K. Ghaib, Latent heat storage: storage materials, heat transfer, and applications, ChemBioEng Reviews 4(4) (2017) 215-224.
[48] B.H. Reis, Development of a novel thermodynamic database for salt systems with potential as phase change materials, BTU Cottbus-Senftenberg, 2021.
[49] J.J. Rowe, G. Morey, C.S. Zen, The quinary reciprocal salt system Na, K, Mg, Ca/Cl, SO_4. A review of the literature with new data, Geological Survey Professional Paper 741 (1972).
[50] O. Menge, Die binaren systeme von $MgCl_2$ und $CaCl_2$ mit den chloriden der metalle K, Na, Ag, Pb, Cu, Zn, Sn und Cd, Z. Anorg. Allg. Chem.1911.
[51] A.I. Ivanov, Phase diagram of the system KCl-$MgCl_2$-$CaCl_2$ Izvest. Sektora Fiz.-Khim. Anal., Akad. Nauk S.S.S.R 23 (1953) 189-200.
[52] K. Matiašovský, Phase diagrams of some systems important in electrolytic production of magnesium. I. Two-component systems $MgCl_2$-NaCl, $CaCl_2$-NaCl, and $MgCl_2$-$CaCl_2$, Chemical Papers 13(2) (1959) 69-77.
[53] K. Grjotheim, J.L. Holm, J. Malmo, The Phase Diagram of the System $MgCl_2$-$CaCl_2$, and Thermodynamic Properties of Molten Mixtures in this System, Acta Chem. Scand 24 (1970) 77-86.
[54] P. Chartrand, A.D. Pelton, Thermodynamic Evaluation and Optimization of the LiCl-NaCl-KCl-RbCl-CsCl-$MgCl_2$-$CaCl_2$ System Using the Modified Quasi-chemical Model, Metallurgical and Materials Transactions A 32A (2001) 1361-1383.
[55] C. Robelin, P. Chartrand, A.D. Pelton, Thermodynamic evaluation and optimization of the ($MgCl_2$+$CaCl_2$+$MnCl_2$+$FeCl_2$+$CoCl_2$+$NiCl_2$) system, The Journal of Chemical Thermodynamics 36(9) (2004) 793-808.
[56] I. Karakaya, W.T. Thompson, Thermodynamic properties of {(1-x)$MgCl_2$+x$CaCl_2$}(l), J. Chem. Thermodynamics 18 (1986) 859-866.
[57] I. Karakaya, W.T. Thompson, A Thermodynamic Study of the System $MgCl_2$–NaCl–$CaCl_2$, Canadian Metallurgical Quarterly 25(4) (1986) 307-317.
[58] J. Rowe, G. Morey, C. Silber, The ternary system K_2SO_4·$MgSO_4$·$CaSO_4$, Journal of Inorganic and Nuclear Chemistry 29 (1967) 925-942.
[59] L.S. Ramsdell, An X-ray study of the system K_2SO_4-$MgSO_4$-$CaSO_4$, American Mineralogist: Journal of Earth and Planetary Materials 20(8) (1935) 569-574.
[60] S.M. Mukimov, Z.I. Filippova, Reactions in melts of Na, K, Mg, and Ca sulfates, Trudy Inst. Khim., Akad. Nauk Uzbek. SSSR, Inst. Khim 2 (1949) 123-132.
[61] H. Du, Thermodynamic Assessment of the K_2SO_4-Na_2SO_4-$MgSO_4$-$CaSO_4$ System, Journal of Phase Equilibria 21 (2000) 6-18.
[62] E. Jänecke, Über reziproke salzpaare. II. Das Salzpaar K_2Cl_2-$MgSO_4$. $MgCl_2$-K_2SO_4., Z. Phys. Chem. 80 (1912).
[63] E.I. Speranskaya, Exchange decomposition without solvent: irreversible reciprocal system of sodium and magnesium chlorides and sulphates, Bull. Acad. Sci. URSS, Ser. Chim. 2 (1938) 463-487.
[64] R. Nacken, Ueber Langbeinit und Vanthoffit (K_2SO_4. $2MgSO_4$ und $3Na_2SO_4$. $MgSO_4$), Nachrichten von der Gesellschaft der Wissenschaften zu Göttingen, Mathematisch-Physikalische Klasse 1907 (1907) 602-613.

[65] A. Ginsberg, Über die Verbindungen von Magnesium-und Natriumsulfat, Zeitschrift für anorganische Chemie 61(1) (1909) 122-136.
[66] O. Sackur, Geschmolzene Salze als Lösungsmittel: Erwiderung an Herrn WC Bray, Z. Physik. Chem. 80(1) (1912) 254-254.
[67] A.M. Pichugin, Technical Encyclopedia- special communication (n.d.): 7: 192. Appears in: Schmorak J. $CaCl_2$-$CaSO_4$ in Handbook of Solid-Liquid Equilibria in Systems of Anhydrous Inorganic Salts (1970). Volume I: 628. Ed. N. K. Voskresenskaya. Compilers: NK Voskresenskaya, NN Evseeva, SI Berul, IP Vereshchetina. Translated from Russian.
[68] E. Jänecke, W. Mühlhäusser, Das reziproke Salzpaar (K_2-Ca)(Cl_2-SO_4), Zeitschrift für anorganische und allgemeine Chemie 228 (1936) 241-248.
[69] M.S. Golubeva, A.G. Bergman, The ternary reciprocal system of the chlorides and sulfates of potassium and calcium, Russian Jour. General Chemistry 26 (1956) 249-258.
[70] A. Palkin, Evolution of the diagram of state of ternary reciprocal systems in the absence of water, Izvestiya Sektora Fiziko-Khimicheskogo Analiza, Institut Obshchei i Neorganicheskoi Khimii, Akademiya Nauk SSSR 17 (1949) 228-253.
[71] T.D. Zimina, A.G. Bergman, G.I. Nagornyi, The Ba, Ca, Na // Cl, SO_4 reciprocal system, Russian Journal of Inorganic Chemistry 10 (1965) 1167-1171.
[72] P.A. Arbukhanova, Y.A. Dibirov, N.N. Verdiev, A.M. Amadziev, The CaF_2-$CaCl_2$-$CaSO_4$ system, Russian Journal of Inorganic Chemistry 54(6) (2009) 980-982.
[73] T.D. Zimina, A.G. Bergaman, G.I. Nagornyi, Vzaimnaya sistema iz khloridov i sul´fatov natriya. kal´tsiya i bariya, Zhur. Neorg. Khimii 10(9) (1965) 2145-2151.
[74] J. Rowe, G. Morey, I. Hansen, The binary system K_2SO_4-$CaSO_4$, Journal of Inorganic and Nuclear Chemistry 27 (1965) 53-58.
[75] W. Klemm, P. Weiss, Über binäre Systeme aus Halogeniden. I. Das System Natriumchlorid-Magnesiumchlorid, Zeitschrift für anorganische und allgemeine Chemie 245(3) (1940) 279-284.
[76] W. Klemm, K. Beyersdorfer, J. Oryschkewitsch, Über binäre Systeme aus Halogeniden II): Das Verhalten von NaCl, KCl, RbCl, NaJ und KJ zu den entsprechenden Magnesiumhalogeniden, Zeitschrift für anorganische Chemie 256(1-3) (1948) 25-36.
[77] K. Grjotheim, J.L. Holm, M. Rotnes, The Phase Diagrams of the Systems NaCl-$MgCl_2$ and KCl-$MgCl_2$, (1972).
[78] H. Seifert, J. Uebach, Thermodynamic and structural investigations of chlorides in the systems KCl/$MgCl_2$ and KCl/$MnCl_2$, Journal of Solid State Chemistry 59(1) (1985) 86-94.
[79] N. Bondarenko, Equilibrium diagram of the $BaCl_2$-$MgCl_2$-NaCl system, Russian Journal of Inorganic Chemistry 7(6) (1962) 714-717.
[80] K. Scholich, Ternare Systeme aus Kaliumchlorid, Natriumchlorid und den Chloriden zweiwertiger Metalle, Neues Jahrbuch für Mineralogie, Geologie und Paläontologie 43 (1920) 251-262.
[81] O. Kleppa, F. McCarty, Thermochemistry of Charge-Unsymmetrical Binary Fused Halide Systems. II. Mixtures of Magnesium Chloride with the Alkali Chlorides and with Silver Chloride, The Journal of Physical Chemistry 70(4) (1966) 1249-1255.
[82] B. Markov, T. Tishura, A. Budarina, The enthalpy of formation of crystallized melts of individual chlorides of melts of the NaCl-$MgCl_2$ system at a variable composition and from literature data on enthalpy of components and enthalpy of mixing from the thermodynamic cycle, Z. Khim. Ukr 47 (1981) 696-697.
[83] L. Denielou, J. Petitet, C. Tequi, Calorimetric study of MgCl/sub 2/-NaCl mixtures, Rev. Gen. Therm.;(France) 19(220) (1980).
[84] H. Ikeuchi, C. Krohn, Chloride-Alkali Chloride Mixtures, Acta Chemica Scandinavica 23(7) (1969) 2230-2240.
[85] D. Neil, H. Clark, R. Wiswall Jr, Thermodynamic Properties of Molten Solutions of $MgCl_2$-KCl, $MgCl_2$-NaCl, and $MgCl_2$-KCl-NaCl, Journal of Chemical and Engineering Data 10(1) (1965) 21-24.
[86] T. Østvold, Partial free energies of alkali chlorides in fused mixtures with magnesium chloride, Munksgaard INT PUBL LTD 35 Norre Sogade, PO BOX 2148, DK-1016 Copenhagen, 1969, pp. 688-&.

[87] J. Egan, J. Bracker, Thermodynamic properties of some binary fused chloride mixtures obtained from emf measurements, The Journal of Chemical Thermodynamics 6(1) (1974) 9-16.
[88] H. Yin, J. Song, W. Liu, B. Hu, Thermodynamic re-optimization of the ACl_x-$MgCl_2$ (A= Na, K, Rb, Cs and Ca, x= 1 or 2) systems, Calphad 79 (2022) 102476.
[89] G. Abramov, The ternary system KCl-$MgCl_2$-NaCl, Metallurg (Leningrad) 10 (1935) 82-105.
[90] P.W.S.K. Bandaranayake, B.E. Mellander, Electrical conductivity and phase diagram of the Na_2SO_4-$CaSO_4$ system, Solid state ionics 26(1) (1988) 33-36.
[91] F. Capellina, G. Napolitano, Calore di soluzione di alcuni sali alcalini e di magnesio.-Nata I. Influenza della diluizione, Ann. Chim.(Rome) 56 (1966) 30-47.
[92] V. Glushko, Termicheskie konstanty (thermal constants of substances), in: Online Reference Book, Moscow State University, Chemical Department, Moscow, 1982. http://www.chem.msu.ru/cgi-bin/tkv.pl?show=welcome.html (1965-1982).
[93] E. Akopov, A. Bergman, Quaternary Reciprocal Systems Of The Chlorides And Sulfates Of Lithium, Sodium And Potassium, Journal of General Chemistry of the USSR in English Translation (1955) 1.
[94] J. Sangster, A. Pelton, Critical coupled evaluation of phase diagrams and thermodynamic properties of binary and ternary alkali salt systems, Phase diagrams for ceramists. American Ceramic Society (1987).
[95] P.I. Fedorov, K.A. Bol'shakov, The ternary reciprocal system of the chlorides and sulfates of sodium and cobalt, Russian Journal of Inorganic Chemistry 4(4) (1959) 405-407.
[96] H. Flood, T. Forland, A. Nesland, Cryoscopic measurements in fused salts at elevated temperatures, Acta Chemica Scandinavica (Denmark) Divided into Acta Chem. Scand., Ser. A and Ser. B 5 (1951) 1193-1198.
[97] A. Wolters, Neues Jahrb. Min. Geol, Beil. Bd 30 (1911) 55-96.
[98] O. Sackur, Fused Salts as Solvents I, Cryoscopic Investigations. Z. physik. Chem 78 (1912) 550-563.
[99] A. Bergman, A. Sementsova, Troinye sistemy na parallel-to Cl, SO_4, CO_3 ik parallel-to Cl, SO_4, CO_3, Zhurnal Neorganicheskoi Khimii 3(2) (1958) 383-392.
[100] A. Bergman, E. Bakumskaya, Complex-formation and double decomposition in the reciprocal system of chlorides and sulfates of sodium and cadmium, Zhurnal Obshchei Khimii 25 (1955) 2405-2414.
[101] G. Nagornyi, T. Zimina, Nonreversible reciprocal system of sodium and barium chlorides and sulfates, Izvest. Fiz.-Khim. Nauch.-Issledovatel. Inst., Irkutsk. Univ 2 (1953) 31-40.
[102] E. Akopov, A. Bergman, Reversible-adiagonal system of sodium and potassium chlorides and sulfates, Zh. Obshch. Khim 24 (1954) 1524-1532.
[103] S. Mukimov, Double decomposition in the absence of a solvent. XLVII. Property (fusion) diagrams of the ternary systems of sodium and potassium fluorides, chlorides and sulfates, Ann. secteur anal. phys.-chim., Inst. chim. gen.(USSR) 12 (1940) 19-38.
[104] M. Klochko, Double decomposition in the absence of a solvent. XXIV. Irreversible-reciprocal system: sodium chloride-lithium sulfate, Zh. Obshch. Khim 3 (1933) 1026-1039.
[105] E. Akopov, A. Bergman, Fusion Diagrams for the Ternary System of the Sulfates of Lithium, Sodium and Potassium, Zh. Neorg. Khim 4 (1959) 1146-1152.
[106] J. Gabčová, M. Malinovský, Experimental determination and thermodynamic analysis of the phase diagrams of the systems NaCl-Na_2SO_4 and NaCl-NaF, (1986).
[107] D. Lindberg, R. Backman, P. Chartrand, Thermodynamic evaluation and optimization of the (Na_2CO_3 + Na_2SO_4 + Na_2S + K_2CO_3 + K_2SO_4 + K_2S) system, The Journal of Chemical Thermodynamics 39(6) (2007) 942-960.
[108] E. Jänecke, The Reciprocal Salt Couples NaCl-K_2SO_4, KCl-Na_2SO_4, Z. physik. Chem 64 (1909) 343-356.
[109] A. Bergman, M. Golubeva, Complex formation of the double heteroionic salt type (anhydrous kainites) in ternary reciprocal systems, Doklady Akademiia Nauk SSR, 1953, pp. 471-473.

[110] K. Igarashi, H. Ohtani, J. Mochinaga, Phase diagram of the system $LaCl_3$-$CaCl_2$-NaCl, Zeitschrift für Naturforschung A 42(12) (1987) 1421-1424.
[111] K. Nishihara, Y. Shimizu, S. Katori, An Investigation of the Equilibrium Diagram of the CeCl, $CaCl_2$-NaCl System-J, Electrochem. Soc. Japan 18 (1950) 179.
[112] V. Plyushchev, F. Kovalev, I. Shakhno, Reactions of alkali and alkaline earth chlorides in melts I. Ternary system of sodium, rubidium and calcium chlorides, Journal of General Chemistry of the Union of Soviet Socialist Republics 25 (1955) 821.
[113] I.S. Morozov, Z.N. Shevtsova, L.V. Klyukina, Izuchenie diagrammy sostoyaniya sistemy $NdCl_3$-$CaCl_2$-NaCl, Zhur. Nrorg. Khim 2 (1957) 1640-1645.
[114] A. Seltveit, H. Flood, Determination of the solidus curve by a tracer technique. The system $CaCl_2$–NaCl, Acta Chem. Scand 12 (1958) 1030-1041.
[115] A.V. Nikolskii, A.M. Zakharov, V.G. Parshikov, L.G. Vodopyanova, Izv Vyssh Ucheb Zaved Tsv, Metall,, Russian, 1990, pp. 89-94.
[116] F. Landsberry, R. Page, Solidification of metallic chlorides, J. Soc. Chem. Ind. 39 (1920) 37-40.
[117] T. Hattori, H. Ikezawa, R. Hirano, J. Mochinaga, Phase-diagram of ternary $PrCl_3$-$CaCl_2$-NaCl system, Nippon Kagaku Kaishi (6) (1982) 952-955.
[118] Z. Qiao, A. Du, W. Mo, J. Zhi, M. Wang, C. Zheng, S. Duan, Study on the NaCl-$CaCl_2$ binary system, Rare Metals 8(1) (1989) 9-13.
[119] M. Borovkova, A. Orekhova, K. Aleksandrov, T. Puzanova, Study of the calcium chloride-sodium chloride system, Izv. Vysshikh Uchebnykh Zaved. Tsvetnaya Metall 4 (1986) 56-59.
[120] M. Tokareva, A. Bergman, S. Kayalova, Mutual system of sodium and calcium nitrates and chlorides, Zh. Neorg. Khim 3(8) (1958) 1909-1913.
[121] P. Sem, G. Hatem, J.-P. Bros, M. Gaune-Escard, $CaCl_2$ + KCl + NaCl molten-salt mixtures. Experimental and estimated enthalpies of mixing, Journal of the Chemical Society, Faraday Transactions 1: Physical Chemistry in Condensed Phases 80(2) (1984) 297-308.
[122] D. Freyer, W. Voigt, K. Köhnke, The phase diagram of the system Na_2SO_4-$CaSO_4$, European Journal of Solid State and Inorganic Chemistry 35(10-11) (1998) 595-606.
[123] H. Müller, Über binäre Systeme, gebildet aus den Sulfaten der Alkalien und des Calziums, Neues Jahrbuch der Mineralogie, Geologie und Paläontologie 30 (1910) 1-54.
[124] E.I. Speranskaya, I.B. Barskaya, Rentgenograficheskoe i termicheskoe issledovanie splavov sistemy Na_2SO_4-$CaSO_4$, Zhur. Neorg. Khimii, 6 (1961) 1392-1396. (translated in Russian Jour. Inorg. Chemistry, v. 6, no. 6, p. 715-717).
[125] P. Coursol, A. Pelton, P. Chartrand, M. Zamalloa, The $CaSO_4$-Na_2SO_4-CaO phase diagram, Canadian metallurgical quarterly 44(4) (2005) 537-546.
[126] D. Kobertz, M. Müller, Experimental Studies And Re-assessment of the Quasi-Binary Systems Containing the Sulfates Of Sodium, Potassium, and Calcium By Differential Thermal Analysis And X-Ray Diffraction in CALPHAD XL, CALPHAD XL (2011).
[127] L. Komissarova, V. Plyushchev, S. Stepina, The reaction between sodium and calcium sulfate at high temperatures: Moskov, Inst. Tonkol. Khim. Tekhnol. im. MV Lomonosova Trudy (5) (1955) 3-9.
[128] A. Bellanca, L'aftitalite nel sistema ternario K_2SO_4-Na_2SO_4-$CaSO_4$, Periodico di mineralogia 13 (1942) 21-86.
[129] F. Kracek, Melting and transformation temperatures of mineral and allied substance, Handbook of Physical Constants, Geol. Soc. Am., Special Papers (36) (1942) 140-174.
[130] D. Freyer, Untersuchungen zur Phasenbildung und -stabilität im System Na_2SO_4 - $CaSO_4$ - H_2O, in die Fakultät für Chemie und Physik, PhD thesis, Technische Universität Bergakademie Freiberg, Germany, (2000).
[131] W. Eysel, H. Höfer, K. Keester, T. Hahn, Crystal chemistry and structure of Na_2SO_4 (I) and its solid solutions, Acta Crystallographica Section B: Structural Science 41(1) (1985) 5-11.
[132] A.P. Shablinskii, S.K. Filatov, S.V. Krivovichev, L.P. Vergasova, S.V. Moskaleva, E.Y. Avdontseva, A.V. Knyazev, R.S. Bubnova, Dobrovolskyite, $Na_4Ca(SO_4)_3$, a new fumarolic sulfate from the Great

Tolbachik fissure eruption, Kamchatka Peninsula, Russia, Mineralogical Magazine 85(2) (2021) 233-241.
[133] N.K. Voskresenskaya, Spravochnik po plavkosti sistem iz bezvodnykh neorganicheskikh soleĭ. Tom 1. Dvoĭnye sistemy (Handbook on the Fusibility of Anhydrous Inorganic Salt Systems. Volume 1. Binary Systems), 1961.
[134] J. Bye, J. Kiehl, Etude du systeme binaire sulfate de calcium-chlorure de sodium, Bulletin de la societe chimique de France 15(7-8) (1948) 847-848.
[135] V. Rubleva, A. Bergman, Equilibrium diagram of the Na_2Cl_2-K_2Cl_2-$CaSO_4$ system, Zhurnal Obshchei Khimi 26 (1956) 651-655.
[136] G. Perry, H. Fletcher, The magnesium chloride-potassium chloride phase diagram, Journal of phase equilibria 14 (1993) 172-178.
[137] H.J. Seifert, G. Thiel, Lösungskalorimetrische Messungen an Doppelchloriden des Magnesiums, Zeitschrift für anorganische und allgemeine Chemie 436(1) (1977) 237-243.
[138] J.L. Holm, B.J. Holm, B. Rinnan, F. Grønvold, The enthalpies of fusion and the heat capacities of K_2MgCl_4, Rb_2MgCl_4, Cs_2MgCl_4, $KMgCl_3$, $RbMgCl_3$, and $CsMgCl_3$, The Journal of Chemical Thermodynamics 5(1) (1973) 97-106.
[139] T. Østvold, A thermodynamic study of some fused salt mixtures containing alkali and alkaline earth chlorides, bromides and iodides, Institute of Physical Chemistry, University of Trondheim, NTH1971.
[140] W.K. Behl, J.J. Egan, Transference numbers and ionic mobilities from electromotive force measurements on molten salt mixtures, The Journal of Physical Chemistry 71(6) (1967) 1764-1769.
[141] H.J. Seifert, H. Fink, G. Thiel, J. Uebach, Thermodynamische und strukturelle Untersuchungen an den Verbindungen der Systeme KCl/MCl_2 (M= Ca, Cd, Co, Ni), Zeitschrift für anorganische und allgemeine Chemie 520(1) (1985) 151-159.
[142] T. Hattori, K. Igarashi, J. Mochinaga, Enthalpies of Fusion of Intermediate Compounds, $KMgCl_3$, K_2MgCl_4, K_2BaCl_4, $KCaCl_3$, K_2SrCl_4, K_2LaCl_5, K_3PrCl_6, K_3NdCl_6, KGd_3Cl_{10}, and KDy_3Cl_{10}, Bulletin of the Chemical Society of Japan 54(6) (1981) 1883-1884.
[143] A.D. Pelton, S.A. Degterov, G. Eriksson, C. Robelin, Y. Dessureault, The modified quasichemical model I—Binary solutions, Metallurgical and Materials Transactions B 31 (2000) 651-659.
[144] W. Grahmann, Vergleich der Sulfate der Erdalkalien und des Bleis in den Temperatur-Konzentrationsdiagrammen mit Kaliumsulfat unter besonderer Berücksichtigung der Dimorphie von Anhydrit, Colestin, Baryt und Anglesit, Voss1913.
[145] S.M. Mukimov, N.I. Krylova, A.G. Bergman, Reactions in melts of sodium, potassium, magnesium, and calcium sulfates, Tr. Inst. Khim., Akad. Nauk Uzb. SSR 2(Obshchaya i Neorg. Khim.) 2 (1949) 94-112.
[146] R.A. Robie, S. Russell-Robinson, B.S. Hemingway, Heat capacities and entropies from 8 to 1000 K of langbeinite ($K_2Mg_2(SO_4)_3$), anhydrite ($CaSO_4$) and of gypsum ($CaSO_4{\cdot}2H_2O$), Thermochimica acta 139 (1989) 67-81.
[147] J. Boerio-Goates, J.I. Artman, B.F. Woodfield, Heat capacity studies of phase transitions in langbeinites II. $K_2Mg_2(SO_4)_3$, Physics and chemistry of minerals 17 (1990) 173-178.
[148] G. Morey, J. Rowe, R. Fournier, The system $K_2Mg_2(SO_4)_3$ (langbeinite)-$K_2Ca_2(SO_4)_3$ (calcium-langbeinite), Journal of Inorganic and Nuclear Chemistry 26(1) (1964) 53-58.
[149] E. Akopov, E. Korobka, Thermal analysis of potassium chloridepotassium sulfate and lithium chloride-lithium sulfate systems, Zhur. Neorg. Khim 13(8) (1968) 2312-2313.
[150] A. Sementsova, A. Bergman, The ternary system of five ions, Na_2CO_3-K_2Cl_2-K_2SO_4, Zh. Obshch. Khim 26 (1956) 992-996.
[151] A. Bergman, A. Kislova, V. Posypaiko, Investigation of ternary systems of chlorides, sulfates, and tungstates of lithium and potassium. II, Zh. Obshch. Khim 25 (1955) 12-16.
[152] O. Dombrovskaya, Double Decomposition in the Absence of a Solvent: XXIII, Zh. Obshch. Khim. 3(8) (1933) 1017-25.

[153] G. Nagornyi, N. Finkel'stein, Irreversible-reciprocal system of chlorides and sulfates of potassium and barium, Izv. Fiz.-Khim. Nauchn.-Issled. Inst. pri Irkutskom Univ 4(1) (1959) 94-106.
[154] A. Bergman, A. Sementsova, Vnutrennie secheniya cherez prizmu sostava chetvernoi vzaimnoi sistemy Na, K parallel-to-Cl, SO_4, CO_3, Zhurnal Neorganicheskoi Khimii 3(12) (1958) 2740-2750.
[155] H. Linstedt, Application of the gravimetric method to the anhydrokainite problem, Zeitschrift für Physikalische Chemie 199(1) (1952) 345-349.
[156] N. Finkel´shtein , A. Bergman, G. Nagornyi, Interaction of chlorides and sulphates of potassium, calcium, and barium in melts, Russian Journal of Inorganic Chemistry 10(8) (1965) 1031-1034.
[157] R.P. Clark, F.W. Reinhardt, Phase diagrams for the binary systems $CaCl_2$-KCl and $CaCl_2$-$CaCrO_4$, Thermochimica Acta 12(3) (1975) 309-314.
[158] W. Moldenhauer, J. Anderseit, Über die elektrolytische Darstellung von Calciumlegierungen und Calcium, Zeitschrift für Elektrochemie und angewandte physikalische Chemie 19(11) (1913) 444-447.
[159] H. Emons, G. Bräutigam, R. Thomas, Einige thermodynamische Eigenschaften binärer geschmolzener Mischungen aus Erdalkalimetall-und Alkalimetallchloriden, Chem. zvesti 32(6) (1978) 721-733.
[160] V. Plyushchev, F. Kovalev, Reaction be-tween the chlorides of the alkali and alkaline earth elements in melts. IV. The ternary system of the chlorides of lithium, potassium, and calcium, Russ J Inorg Chem 1 (1956) 1013-1018.
[161] E. Dergunov, A. Bergman, On the formation of complex compounds between chlorides of alkali and alkali-earth metals, Doklady Akad. Nauk SSSR, 1950.
[162] B. Korshunov, Y. Podzolko, V. Kerner, S. Krishtul, Melting diagram of $BiCl_3$-$CaCl_2$-KCl system, Russ. J. Non-Ferrous Metals 5 (1975) 147-149.
[163] F. Tesfaye, D. Lindberg, L. Hupa, The K_2SO_4–$CaSO_4$ System and Its Role in Fouling and Slagging During High-Temperature Processes, Materials Processing Fundamentals 2018, Springer, 2018, pp. 133-142.
[164] D. Speer, E. Salje, Phase transitions in langbeinites I: Crystal chemistry and structures of K-double sulfates of the langbeinite type $M^{++} + K_2(SO_4)_3$, M^{++}= Mg, Ni, Co, Zn, Ca, Physics and chemistry of minerals 13 (1986) 17-24.
[165] H. Cao, J. Boerio-Goates, Heat-capacity measurements and thermodynamic functions of langbeinite-type $K_2Cd_2(SO_4)_3$ and $K_2Ca_2(SO_4)_3$ at temperatures from 10K to 340K, The Journal of Chemical Thermodynamics 26(3) (1994) 251-259.
[166] G. Marquez, Chemische und thermodynamische Untersuchung von kreislaufrelevanten Verbindungen bei der Zementherstellung durch Knudsen-Effusionmassenspektrometrie, Institut für Nichtmetallische Werkstoffe, Tech-nische Universität Clausthal, Clausthal-Zellerfeld (2006).
[167] K. Armatys, L. Bencze, M. Miller, A. Wolter, Investigation of potassium sulphate–calcium sulphate binary system by Knudsen effusion mass spectrometry, Thermochimica Acta 575 (2014) 254-261.
[168] E. Akopov, A. Bergman, Complex formation and phase transformations in the reciprocal quaternary system of the chlorides and sulfates of lithium, sodium and potassium, Proceedings of the Academy of Sciences of the USSR.: Chemistry section (1960) 561.
[169] E. Akopov, A. Bergman, Decomposition of the solid solutions in the reciprocal system of the chlorides and sulfates of sodium and potassium, Zhur. Neorg. Khim 4 (1959) 1653-1656.
[170] D. Coleman, P. Lacy, The phase equilibrium diagram for the KCl-NaCl system, Materials research bulletin 2(10) (1967) 935-938.
[171] V. Yu.I, Z. S.P., Decomposition of Solid Solutions KCl-NaCl, Solid State Communications 31(9) (1979) 635-639.
[172] A.D. Pelton, A. Gabriel, J. Sangster, Liquidus measurements and coupled thermodynamic–phase-diagram analysis of the NaCl–KCl system, Journal of the Chemical Society, Faraday Transactions 1: Physical Chemistry in Condensed Phases 81(5) (1985) 1167-1172.

[173] L.S. Hersh, O. Kleppa, Enthalpies of mixing in some binary liquid halide mixtures, The Journal of Chemical Physics 42(4) (1965) 1309-1322.
[174] N. Kurnakow, S. Żemczużnyj, Isomorphismus der Kalium-und Natriumverbindungen, Zeitschrift für anorganische Chemie 52(1) (1907) 186-201.
[175] M. Bhardwaj, R. Roy, Effect of high pressure on crystalline solubility in the system NaCl–KCl, Journal of Physics and Chemistry of Solids 32(7) (1971) 1603-1607.
[176] A.J. Darnell, W.A. McCollum, Polymorphism in the KCI-KF and KCI-NaCI Systems at Elevated Pressures and Temperatures, High Temperature Science 3(1) (1971) 73-80.
[177] A. Bergman, V. Rubleva, Phase diagram of the system Na_2Cl_2–K_2Cl_2–$CaSO_4$, J. Gen. Chem 26 (1956) 747.
[178] A. Bergman, G. Bukhalova, Quaternary reciprocal system of fluorides and chlorides of sodium, potassium, calcium, and barium as a basis of fluxes for remelting secondary light metals, J. Appl. Chem 28 (1955) 1266.
[179] H. Gemsky, Kristallographische und thermische Untersuchung des ternären Systems Bariumchlorid-Kaliumchlorid-Natriumchlorid, (No Title) (1913).
[180] A. Bunk, G. Tichelaar, Investigations in the systems NaCl-KCl, Kon Ned Akad Wetensch Proc B, 1953, pp. 375-384.
[181] Nguyen-Ba-Chanh, Equilibres des systemes binaires dhalogenures de sodium et potassium a letat solide, Journal De Chimie Physique 61(10) (1964) 1428.
[182] Y.I. Vesnin, S.P. Zakovryashin, Decomposition of Solid Solutions KCl-NaCl, Solid State Communications 31(9) (1979) 635-639.
[183] W. Eysel, DTA and DSC of compounds and solid solutions in the system sodium sulfate-potassium sulfate, Therm. Anal., Proc. Int. Conf., 3rd, 1972, pp. 179-192.
[184] R. Nacken, On the formation and inversion of mix-crystals and double salts in the binary systems of the dimorphous sulphates of lithium, sodium, potassium and silver, Neues Jahrb. Mineral. Geol. Beil 24 (1907) 1-68.
[185] T. Förland, J. Krogh-Moe, Transition-point depression and its structural interpretation in the binary system sodium sulfate-potassium sulfate, Acta Chem. Scandinavica 13 (1959) 1051-1063.
[186] A. Bergman, V. Rubleva, A diagonal reciprocal system formed by the fluorides and sulphates of sodium and potassium, Russ. J. Inorg. Chem. 4(1) (1959) 56-58.
[187] W. Eysel, Crystal chemistry of the system Na_2SO_4-K_2SO_4-K_2CrO_4-Na_2CrO_4 of the glaserite phase, American Mineralogist: Journal of Earth and Planetary Materials 58(7-8) (1973) 736-747.
[188] N. Mofaddel, R. Bouaziz, M. Mayer, Le polymorphisme du sulfate de sodium anhydre et les phases intermediaires, glaserite et aphtitalite, dans le binaire Na_2SO_4-K_2SO_4, Thermochimica acta 185(1) (1991) 141-153.
[189] I. Koštenská, P. Fellner, Sub-solid equilibria in the systems Li_2SO_4-Na_2SO_4 and Na_2SO_4-K_2SO_4, Thermochimica acta 188(2) (1991) 207-211.
[190] T. Østvold, O. Kleppa, Enthalpies of Mixing in Binary Liquid Alkali Sulfate Mixture, Acta Chem. Scand. 25 (1971) 919-929.
[191] K. Armatys, M. Miller, A. Matraszek, A. Wolter, Vaporization study of sodium sulphate — potassium sulphate binary system by Knudsen effusion mass spectrometry, Materials Science-Poland 29(2) (2011) 77-85.
[192] Y. Dessureault, J. Sangster, A.D. Pelton, Coupled Phase Diagram/Thermodynamic Analysis of the Nine Common-Ion Binary Systems Involving the Carbonates and Sulfates of Lithium, Sodium, and Potassium, Journal of The Electrochemical Society 137(9) (1990) 2941.
[193] D. Lindberg, R. Backman, P. Chartrand, Thermodynamic evaluation and optimization of the (Na_2SO_4 + K_2SO_4 + $Na_2S_2O_7$ + $K_2S_2O_7$) system, The Journal of Chemical Thermodynamics 38(12) (2006) 1568-1583.
[194] A.D. Pelton, P. Chartrand, G. Eriksson, The modified quasi-chemical model: Part IV. Two-sublattice quadruplet approximation, Metallurgical and Materials Transactions A 32 (2001) 1409-1416.

[195] B. Sundman, J. Ågren, A regular solution model for phases with several components and sublattices, suitable for computer applications, Journal of physics and chemistry of solids 42(4) (1981) 297-301.
[196] A.I. Orekhova, N.P. Podlesnyak, L.K. Kuznetsova, G.G. Arkhipov, N.A. Krasil'nikova, The system $KMgCl_3$−NaCl, Russ. J. Inorg. Chem. 3 (1985) 30-31.
[197] P. Sem, G. Hatem, J.-P. Bros, M. Gaune-Escard, $CaCl_2$ + KCl+ NaCl molten-salt mixtures. Experimental and estimated enthalpies of mixing, Journal of the Chemical Society, Faraday Transactions 1: Physical Chemistry in Condensed Phases 80(2) (1984) 297-308.
[198] V. Plyushchev, F. Kovalev, Interaction of the Chlorides of Alkalies and Alkaline Earths in Melts. 5, Liquidus of the Sodium Chloride Potassium Chloride-Calcium Chloride Ternary System Izvest. Vysshikh Ucheb. Zavedenii, SSSR, Khim. I Khim. Tekhnol 3 (1960) 575.
[199] K. Scholich, Ternäre Systeme aus Kaliumchlorid, Natriumchlorid und den Chloriden zweiwertiger Metalle, Friedrich-Wilhelms-Universität zu Berlin, 1919.
[200] J. Zhu, I. Karakaya, W. Thompson, Partial Molar Properties of $MgCl_2$ in $MgCl_2$-KCl-$CaCl_2$ Melts, Journal of the Electrochemical Society 135(1) (1988) 122.
[201] E. Yazhenskikh, T. Jantzen, Y. Wang, K. Armatys, K. Hack, D. Sergeev, M. Mueller, Thermodynamic description of the ternary systems of the core sulphate system Na_2SO_4–K_2SO_4–$MgSO_4$–$CaSO_4$, Calphad 74 (2021) 102313.
[202] W.J. Boettinger, U.R. Kattner, K.-W. Moon, J.H. Perepezko, DTA and heat-flux DSC measurements of alloy melting and freezing, Methods for phase diagram determination, Elsevier2007, pp. 151-221.
[203] A.S.f.T. Materials, Standard test method for determining specific heat capacity by differential scanning calorimetry, ASTM International2011.
[204] D. Ditmars, S. Ishihara, S. Chang, G. Bernstein, E. West, Enthalpy and heat-capacity standard reference material: synthetic sapphire (α-Al_2O_3) from 10 to 2250 K, Journal of Research of the National Bureau of Standards 87(2) (1982) 159.
[205] A. Morsa, E. Yazhenskikh, M. Ziegner, E. Wessel, R.D. Jacob, M. Müller, D. Sergeev, Experimental study and thermodynamic assessment of the $MgSO_4$-$CaSO_4$ system, Calphad 90 (2025) 102855.
[206] M. Ermrich, D. Opper, X-Ray powder diffraction, XRD for the Analyst, Getting Acquainted with the Principles (2011) 63-85.
[207] S.N. Kabekkodu, A. Dosen, T.N. Blanton, 5+: a comprehensive powder diffraction file™ for materials characterization, Powder Diffraction (2024) 1-13.
[208] S. Gates-Rector, T. Blanton, The powder diffraction file: a quality materials characterization database, Powder Diffraction 34(4) (2019) 352-360.
[209] I. Levin, NIST Inorganic Crystal Structure Database, NIST Standard Reference Database Number 3 (National Institute of Standards and Technology, 2018), Accessed, 2023.
[210] A. Belsky, M. Hellenbrandt, V.L. Karen, P. Luksch, New developments in the Inorganic Crystal Structure Database (ICSD): accessibility in support of materials research and design, Acta Crystallographica Section B: Structural Science 58(3) (2002) 364-369.
[211] J.W. Gibbs, On the equilibrium of heterogeneous substances, American Journal of Science 3(96) (1878) 441-458.
[212] L. Kaufman, H. Bernstein, Computer calculation of phase diagrams. With special reference to refractory metals, (1970).
[213] N. Saunders, A.P. Miodownik, CALPHAD (calculation of phase diagrams): a comprehensive guide, Elsevier1998.
[214] K. Hack, The SGTE casebook: thermodynamics at work, Elsevier2008.
[215] H. Lukas, S.G. Fries, B. Sundman, Computational Thermodynamics: the Calphad Method, Cambridge University Press (2007) 104.

[216] C.W. Bale, P. Chartrand, S. Degterov, G. Eriksson, K. Hack, R.B. Mahfoud, J. Melançon, A. Pelton, S. Petersen, FactSage thermochemical software and databases, Calphad 26(2) (2002) 189-228.
[217] C.W. Bale, E. Bélisle, P. Chartrand, S.A. Decterov, G. Eriksson, K. Hack, I.H. Jung, Y.B. Kang, J. Melançon, A.D. Pelton, C. Robelin, S. Petersen, FactSage thermochemical software and databases — recent developments, Calphad 33(2) (2009) 295-311.
[218] C.W. Bale, E. Bélisle, P. Chartrand, S.A. Decterov, G. Eriksson, A.E. Gheribi, K. Hack, I.H. Jung, Y.B. Kang, J. Melançon, A.D. Pelton, S. Petersen, C. Robelin, J. Sangster, P. Spencer, M.A. Van Ende, FactSage thermochemical software and databases, 2010–2016, Calphad 54 (2016) 35-53.
[219] C.W. Bale, E. Bélisle, P. Chartrand, S. Decterov, G. Eriksson, A.E. Gheribi, K. Hack, I.-H. Jung, Y.-B. Kang, J. Melançon, Reprint of: FactSage thermochemical software and databases, 2010–2016, Calphad 55 (2016) 1-19.
[220] FactSage, Facility for the Analysis of Chemical Thermodynamics, Version 8.3. Available from: http://www.factsage.com/.
[221] B. Reis, F. Tang, P. Keuter, M. to Baben, User-friendly and robust Calphad optimizations using Calphad Optimizer in FactSage, Calphad 88 (2025) 102800.
[222] P.W. Atkins, J. De Paula, J. Keeler, Atkins' physical chemistry, Oxford university press2023.
[223] R. DeHoff, Thermodynamics in materials science, CRC Press2006.
[224] A.D. Pelton, Phase diagrams and thermodynamic modeling of solutions, Academic Press2018.
[225] A.D. Pelton, Thermodynamics and phase diagrams of materials, Phase Transformations in Materials (2001) 1-80.
[226] M. Hillert, Phase equilibria, phase diagrams and phase transformations: their thermodynamic basis, Cambridge university press2007.
[227] J. Leitner, P. Voňka, D. Sedmidubský, P. Svoboda, Application of Neumann–Kopp rule for the estimation of heat capacity of mixed oxides, Thermochimica Acta 497(1-2) (2010) 7-13.
[228] (v13.1), SGPS - SGTE Pure Substances database, 2019.
[229] O. Redlich, A. Kister, Algebraic representation of thermodynamic properties and the classification of solutions, Industrial & Engineering Chemistry 40(2) (1948) 345-348.
[230] A.D. Pelton, P. Chartrand, The modified quasi-chemical model: Part II. Multicomponent solutions, Metallurgical and Materials Transactions A 32 (2001) 1355-1360.
[231] P. Chartrand, A.D. Pelton, The modified quasi-chemical model: Part III. Two sublattices, Metallurgical and Materials Transactions A 32 (2001) 1397-1407.
[232] Y. Dessureault, A. Pelton, Contribution to the quasichemical mode of reciprocai moiten sait solutions, J Chim Phys 8 (1991) 1811-1830.
[233] T.M. Besmann, K.E. Spear, Thermochemical modeling of oxide glasses, Journal of the American Ceramic Society 85(12) (2002) 2887-2894.
[234] E. Yazhenskikh, K. Hack, M. Müller, Critical thermodynamic evaluation of oxide systems relevant to fuel ashes and slags. Part 1: Alkali oxide–silica systems, Calphad 30(3) (2006) 270-276.
[235] Database GTOx, GTT-Technologies, Forschungszentrum Jülich, 2010-2025, GTT-Technologies.
[236] A.D. Pelton, A general “geometric” thermodynamic model for multicomponent solutions, Calphad 25(2) (2001) 319-328.
[237] M.W. Chase, N.I.S. Organization, NIST-JANAF thermochemical tables, American Chemical Society Washington, DC1998.
[238] A. Dworkin, M. Bredig, The heat of fusion of the alkali metal halides, The Journal of Physical Chemistry 64(2) (1960) 269-272.
[239] H.S. Roberts, Some new standard melting points at high temperatures, Physical Review 23(3) (1924) 386.
[240] N.B.S. US, Selected Values of Chemical Thermodynamic Properties, Circ. 500 (1952).
[241] G. Moore, Heat Contents at High Temperatures of the Anhydrous Chlorides of Calcium, Iron, Magnesium and Manganese1, Journal of the American Chemical Society 65(9) (1943) 1700-1703.
[242] I. Barin, G. Platzki, Thermochemical data of pure substances, Wiley Online Library1989.

[243] M. Tokareva, The reciprocal system of nitrates and chlorides of lithium and calcium, Journal of Inorganic Chemistry 2(7-9) (1957) 230.
[244] D.W. Green, R.H. Perry, Perry's chemical engineers' handbook, McGraw-Hill Education2008.
[245] G. Brodale, W. Giauque, Relation of crystalline forms I, III, IV, and V of anhydrous sodium sulfate as determined by the third law of thermodynamics, The Journal of Physical Chemistry 76(5) (1972) 737-743.
[246] L. Denielou, Y. Fournier, J. Petitet, C. Tequi, Étude calorimétrique des sulfates de sodium et de rubidium entre 400 et 1523K, CR Acad. Sc. Paris 269(12) (1969) 1577-1579.
[247] M. Popov, D. Ginzburg, Specific heats of Na_2CO_3, Na_2SO_4, NaOH at high temperatures, J. Gen. Chem USSR 26(4) 971-980.
[248] J.P. Coughlin, High temperature heat contents, heats of transition and heat of fusion of anhydrous sodium sulfate, Journal of the American Chemical Society 77(4) (1955) 868-870.
[249] M.N. May, Chemical reaction equilibria in the combustion of sodium-base pulping liquors, TAPPI (Tech. Assoc. Pulp Pap. Ind.) 35(11) (1952) 511-517.
[250] K.K. Kelley, Contributions to the data on theoretical metallurgy, XIII. High-temperature heat-content, heat-capacity, and entropy data for the elements and inorganic compounds, Bulletin 584 Bureau of Mines (1960).
[251] C.H. Shomate, B. Naylor, High-temperature heat contents of aluminum oxide, aluminum sulfate, potassium sulfate, ammonium sulfate and ammonium bisulfate1, Journal of the American Chemical Society 67(1) (1945) 72-75.
[252] E. Dewing, F. Richardson, Decomposition equilibria for calcium and magnesium sulphates, Transactions of the Faraday Society 55 (1959) 611-615.
[253] J. Torres, J. Mendez, M. Sukiennik, Transformation enthalpy of the alkali-earths sulfates ($SrSO_4$, $CaSO_4$, $MgSO_4$, $BaSO_4$), Thermochimica acta 334(1-2) (1999) 57-66.
[254] C. Pistorius, J. Boeyens, J. Clark, Phase diagrams of $NaBF_4$ and $NaClO_4$ to 40 kbar and the crystal-chemical relationship between structures of $CaSO_4$, $AgMnO_4$, $BaSO_4$ and high-$NaClO_4$, High Temp High Press 1 (1969) 41-52.
[255] G. Moore, K. Kelley, The Specific Heats at Low Temperatures of Anhydrous Sulfates of Iron, Magnesium, Manganese, and Potassium, Journal of the American Chemical Society 64(12) (1942) 2949-2951.
[256] D.H. Smith, M.R. Close, U. Grimm, $Mg_2Ca(SO_4)_3$: Correct Stoichiometry of the Coumpound Previuosly Reported as $Mg_3Ca(SO_4)_4$, Energy & Fuels 10 (1996) 1241-1244.
[257] M. Weil, Single crystal growth of $CaMg_2(SO_4)_3$ via solid- / gas-phase reactions and its Nasicon-related crystal structure, Crystal Research and Technology 42(11) (2007) 1058-1062.
[258] S.V. Krivovichev, E.P. Shcherbakova, T.P. Nishanbaev, The crystal structure of $CaMg_2(SO_4)_3$, a mineral phase from coal dumps of the Chelyabinsk coal basin, Russia, The Canadian Mineralogist 48(6) (2011) 1469-1475.
[259] https://gtt-technologies.de/data/.
[260] D. Kobertz, M. Müller, Experimental studies on $NiSO_4$ by thermal analysis and calorimetry, Calphad 45 (2014) 55-61.
[261] T.-C. Ong, E. Graham, G. Will, T.A. Steinberg, An innovative empirical method for the accurate identification of the eutectic point of binary salts for solar thermal energy storage, Materials Today Communications 26 (2021) 101864.
[262] I. Chojnacka, I. Rutkowska, J. Kapała, L. Rycerz, Phase equilibria in the AgCl–LnCl 3 (Ln= Ce, Nd, Sm, Gd) binary systems, Journal of Thermal Analysis and Calorimetry 138 (2019) 4541-4549.
[263] W. Eysel, Keester, PDF 29-1196, Inst. für Kristall., Technische Hochschule, Aachen, Germany, ICDD Grant-in-Aid (1975).
[264] A. Obaied, F. Tang, I. Roslyakova, M. to Baben, "2 1/2th" generation Calphad databases: Extrapolating heat capacities of elements and compounds to 0K, Calphad 75 (2021) 102352.
[265] (v6.3), aiMP - aiOQ databases, 2024.
[266] A.D. Pelton, A database and sublattice model for molten salts, Calphad 12(2) (1988) 127-142.

Appendix A

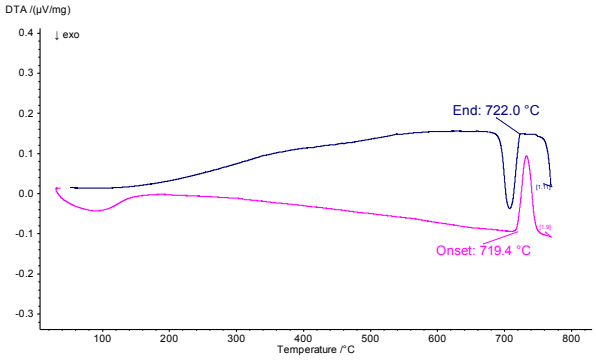


Figure A 1 *Heating and cooling DTA curves of $MgCl_2$ in sealed platinum tube.*

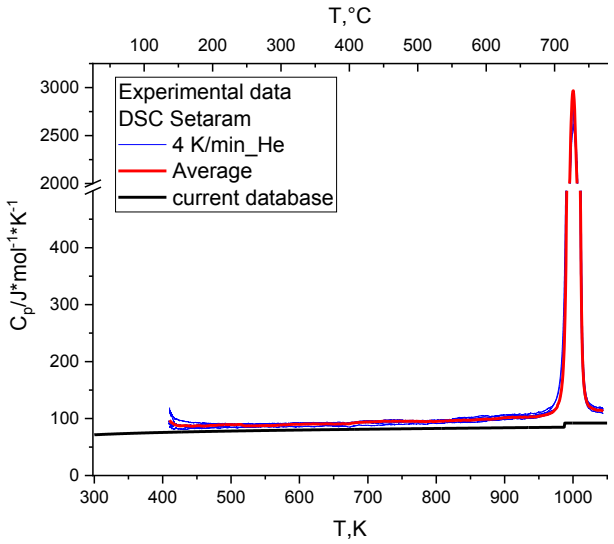


Figure A 2 *Comparison of heat capacity of the $MgCl_2$ from the experimental DSC measurements and the PCM2 database [4].*

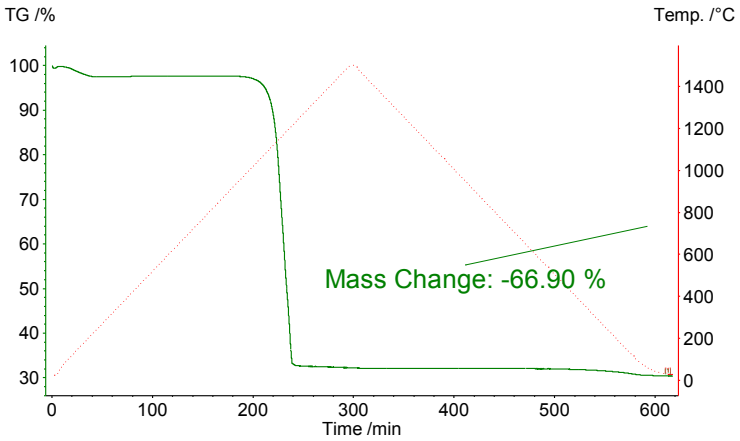
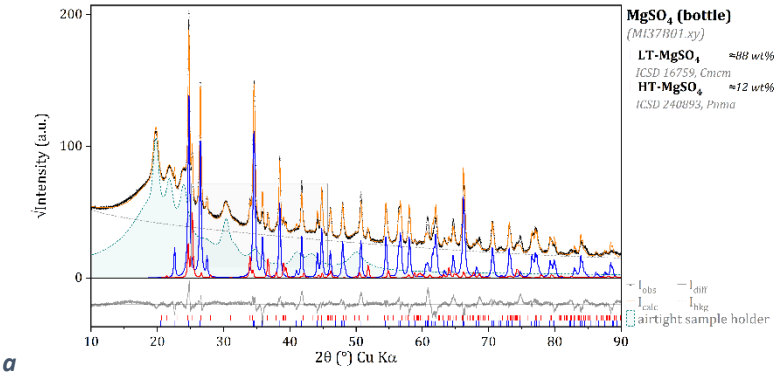
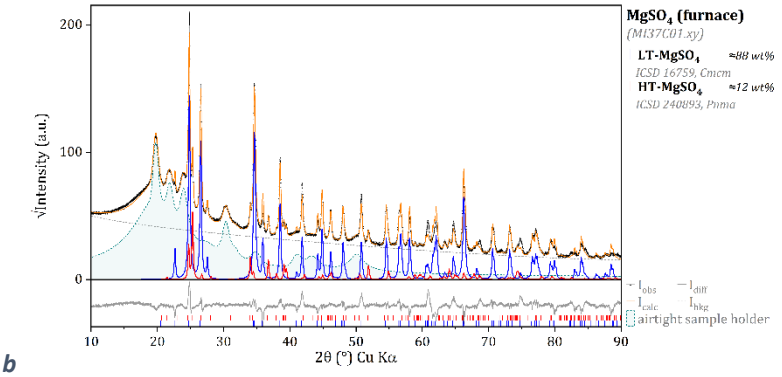


Figure A 3 *TG curve of $MgSO_4$ in open alumina crucible.*



a



b

Figure A 4 *X-ray diffractogram of $MgSO_4$ at room temperature:* ***a)*** *as purchased ($MgSO_4$ bottle);* ***b)*** *dried in furnace at 150 °C ($MgSO_4$ furnace).*

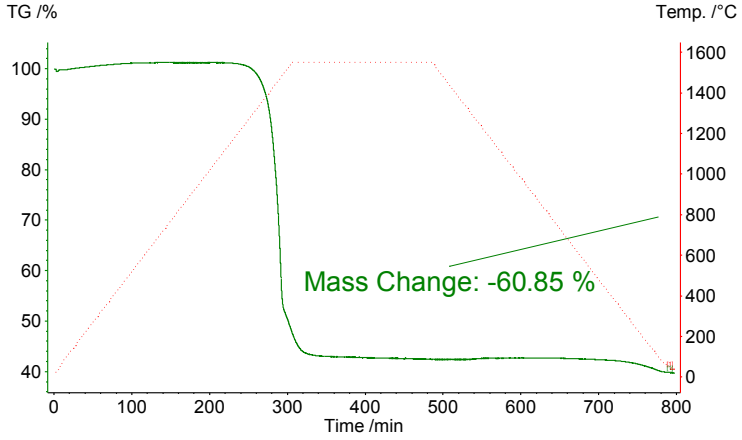


Figure A 5 *TG curve of $CaSO_4$ in open alumina crucible.*

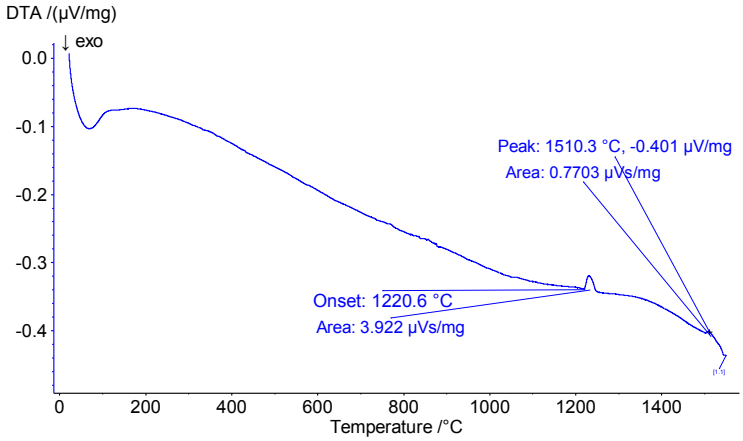


Figure A 6 *DTA curve of $CaSO_4$ in sealed platinum tube.*

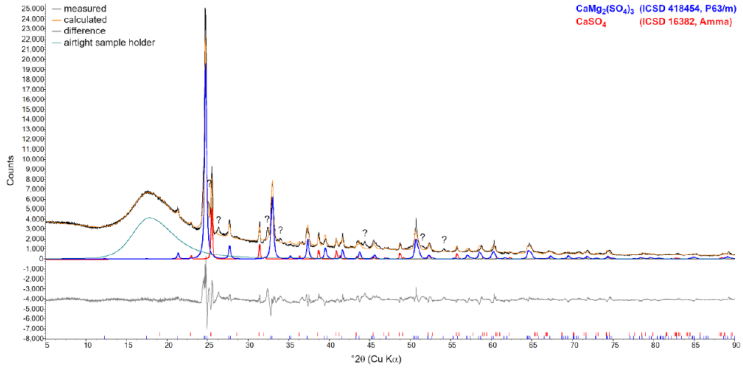


Figure A 7 *HTXRD $CaMg_3(SO_4)_4$. Weight ratio $CaMg_2(SO_4)_3$:$CaSO_4$ = 85:15. Lattice parameters of main phase: a = 8.349 Å, c = 7.158 Å, V = 432.09 $Å^3$ (sg P63/m).*

Table A 1 *Experimental conditions of HTXRD measurements of $CaMg_2(SO_4)_3$.*

	Atmosphere	Temperature profile	Heating and cooling rate	Diffractograms	
				Short scans	Long scans
HT1	Vacuum: P<10^{-4} mbar	25 °C → 350 °C → 25 °C	2 K/min	25 K steps	at 25, 100, 200, 300 and 350 °C
HT2	Vacuum: P<10^{-4} mbar	25 °C → 500 °C → 400 °C → 500 °C → 25 °C	50 K/min (25-450 °C); 10 K/min (450-500 °C); 5 K/min	at 400, 425, 450, 475 °C	at 500, 400, 300, 200, 100 and 25 °C
HT3	Synthetic air	25 °C → 500 °C → 25 °C	50 K/min (25-480 °C); 5 K/min (450-500 °C); 200 K/min (500-300 °C); 100 K/min (300-200 °C); 22 K/min (200-100 °C)		at 500 and 25 °C

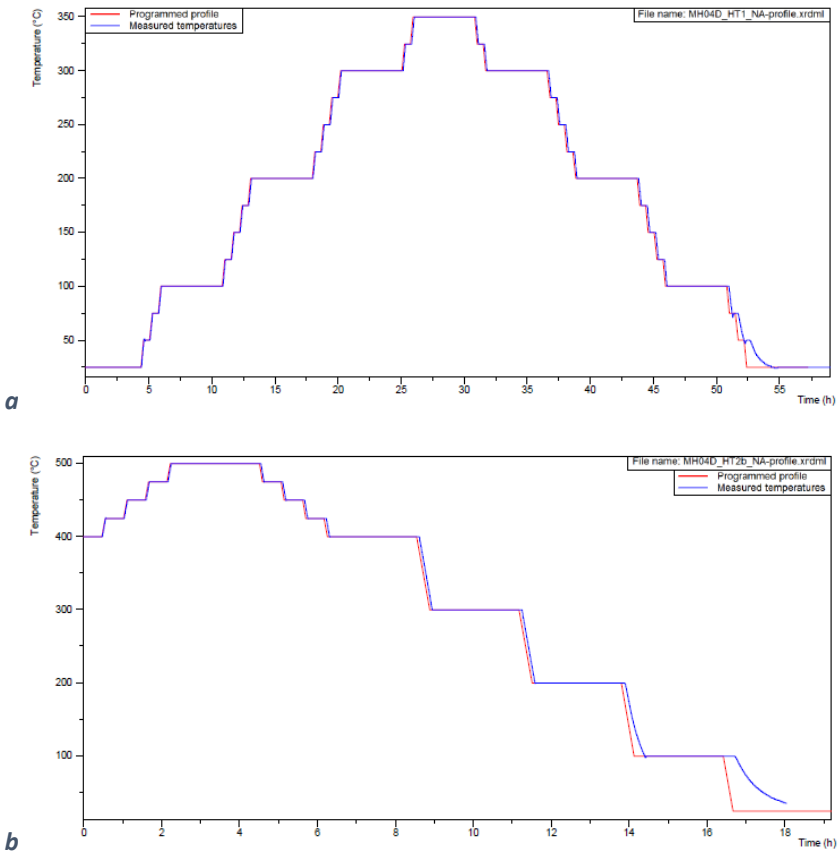


Figure A 8 *Temperature profile of HTXRD of $CaMg_2(SO_4)_3$:* ***a)*** *HT1 (25 °C → 350 °C);* ***b)*** *HT2 (25 °C → 500 °C).*

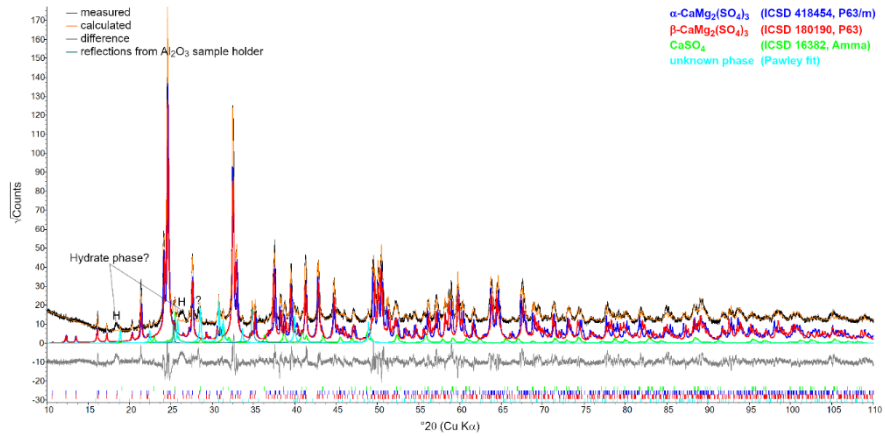


Figure A 9 *Diffractogram of $CaMg_2(SO_4)_3$ (HT1): initial state after placing in oven chamber (T = 25 °C / vacuum).*

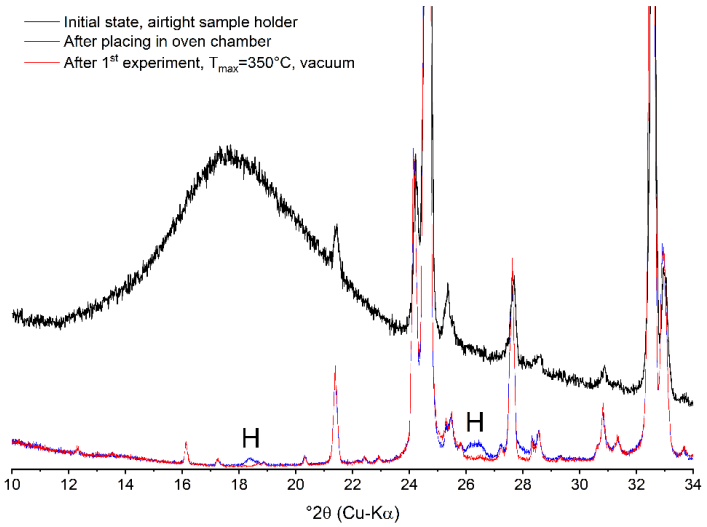
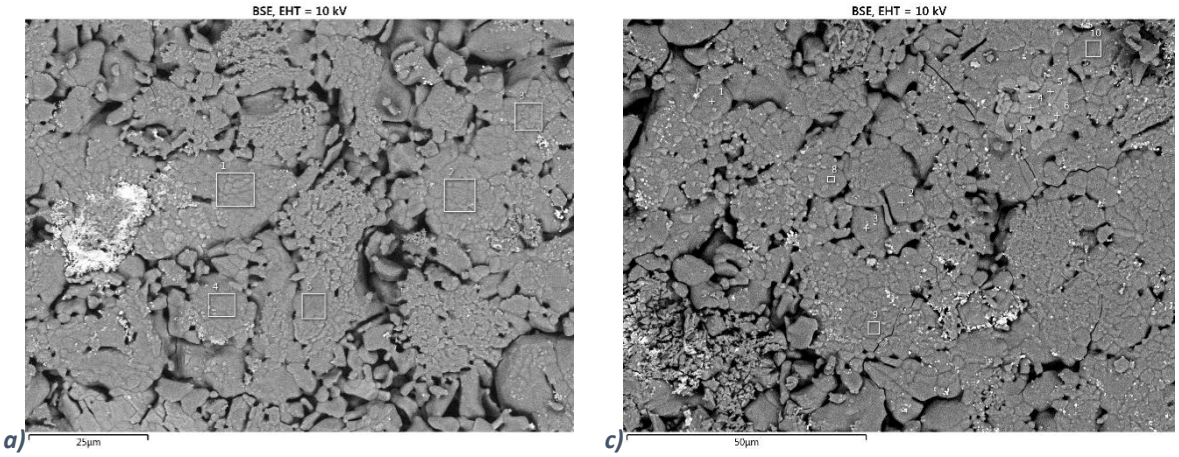


Figure A 10 *Presumed formation of a hydrate phase after contact with ambient air in $CaMg_2(SO_4)_3$ (HT1).*



a) c)

Figure A 11 *SEM-Images (Back Scatter Electrons) showing the grains and phases of $MgSO_4$(70 mol%)-$CaSO_4$(30 mol%) across the sample surface, highlighting areas analysed by Energy Dispersive X-Ray Spectroscopy (EDX). The areas analysed differ from those shown in* ***Figure 5-11****.*

Table A 2 *Molar percentages of elements detected in the analysed regions of the sample $MgSO_4$(70 mol%)-$CaSO_4$(30 mol%) by SEM-EDX.*

	Spectrum Label	O	Mg	S	Ca	Total (mol%)	$MgSO_4$:$CaSO_4$
Figure A 11a	Spectrum 1	66.6	11.4	16.6	5.4	100.0	2:1
	Spectrum 2	66.4	12.1	16.4	5.1	100.0	2:1
	Spectrum 3	66.6	11.8	16.6	5.1	100.0	2:1
	Spectrum 4	66.6	11.4	16.6	5.5	100.0	2:1
	Spectrum 5	66.5	12.0	16.5	5.0	100.0	2:1
Figure A 11b	Spectrum 1	66.5	11.7	16.5	5.3	100.0	2:1
	Spectrum 2	66.8	10.9	16.8	5.6	100.0	2:1
	Spectrum 3	64.1	17.1	14.1	4.8	100.0	3:1 ?
	Spectrum 4	66.9	0.3	16.9	16.0	100.0	0:1
	Spectrum 5	66.8	0.4	16.8	16.0	100.0	0:1
	Spectrum 6	66.8	0.3	16.8	16.2	100.0	0:1
	Spectrum 7	66.8	0.3	16.8	16.1	100.0	0:1
	Spectrum 8	66.6	11.2	16.6	5.6	100.0	2:1

	Spectrum 9	66.7	11.0	16.7	5.6	100.0	2:1
	Spectrum 10	66.6	11.6	16.6	5.3	100.0	2:1

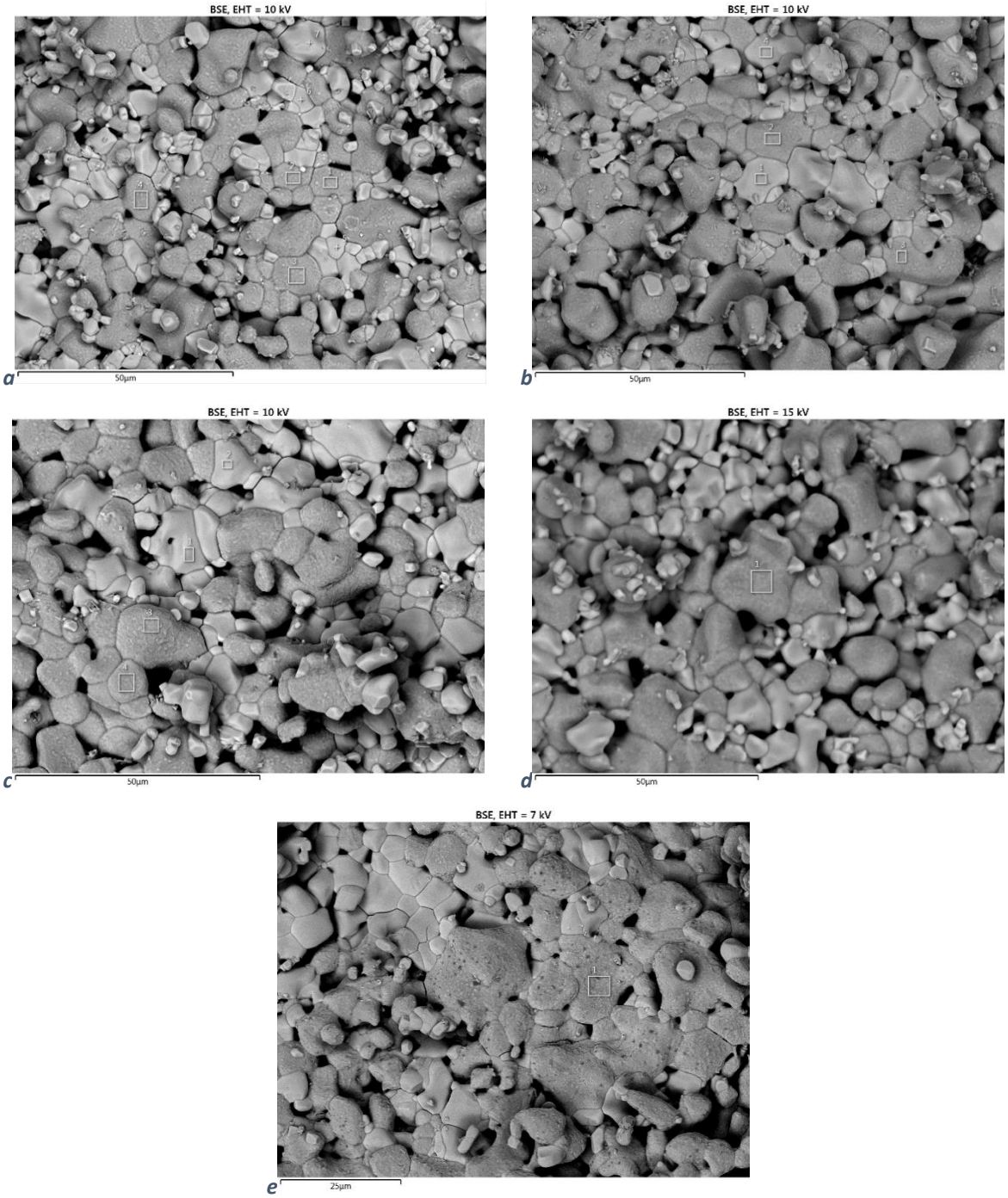


Figure A 12 *SEM-Images (Back Scatter Electrons) showing the grains and phases of $MgSO_4$(49.91 mol%)-$CaSO_4$(50.09 mol%) across the sample surface, highlighting areas analysed by Energy Dispersive X-Ray Spectroscopy (EDX).*

Table A 3 *Molar percentages of elements detected in the analysed regions of the sample $MgSO_4$(49.91 mol%)-$CaSO_4$(50.09 mol%) by SEM-EDX.*

	Spectrum Label	O	Mg	S	Ca	Total (mol%)	$MgSO_4$:$CaSO_4$
Figure A 12a	Spectrum 1	67.7	11.0	16.7	5.6	100.0	2:1

	Spectrum 2	66.6	11.3	16.6	5.6	100.0	2:1
	Spectrum 3	66.9	10.2	16.9	6.1	100.0	2:1
	Spectrum 4	66.7	10.9	16.7	5.8	100.0	2:1
	Spectrum 5	66.9	0.3	16.9	15.9	100.0	0:1
	Spectrum 6	66.7	0.3	16.7	16.4	100.0	0:1
	Spectrum 7	66.9	0.3	16.9	15.9	100.0	0:1
Figure A 12b	Spectrum 1	67.0	0.3	17.0	15.8	100.0	0:1
	Spectrum 2	66.6	11.3	16.6	5.6	100.0	2:1
	Spectrum 3	66.7	10.9	16.7	5.7	100.0	2:1
	Spectrum 4	66.6	0.4	16.6	16.5	100.0	0:1
Figure A 12c	Spectrum 1	66.6	0.5	16.6	16.3	100.0	0:1
	Spectrum 2	66.7	0.4	16.7	16.1	100.0	0:1
	Spectrum 3	67.0	10.1	17.0	6.0	100.0	2:1
	Spectrum 4	66.6	11.2	16.6	5.7	100.0	2:1
Figure A 12d	Spectrum 1 (15kV)	66.7	10.9	16.7	5.7	100.0	2:1
	Spectrum 1 (10kV)	66.8	10.7	16.8	5.7	100.0	2:1
Figure A 12e	Spectrum 1	66.6	11.2	16.6	5.7	100.0	2:1

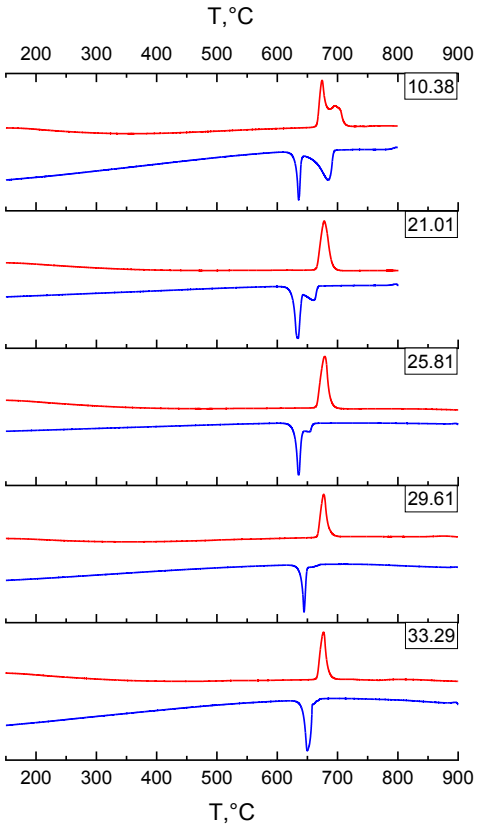


Figure A 13 *DTA curves of $MgCl_2$-$MgSO_4$ mixtures in alumina crucibles, expressed in molar percentage of $MgSO_4$: heating curves (red); cooling curves (blue).*

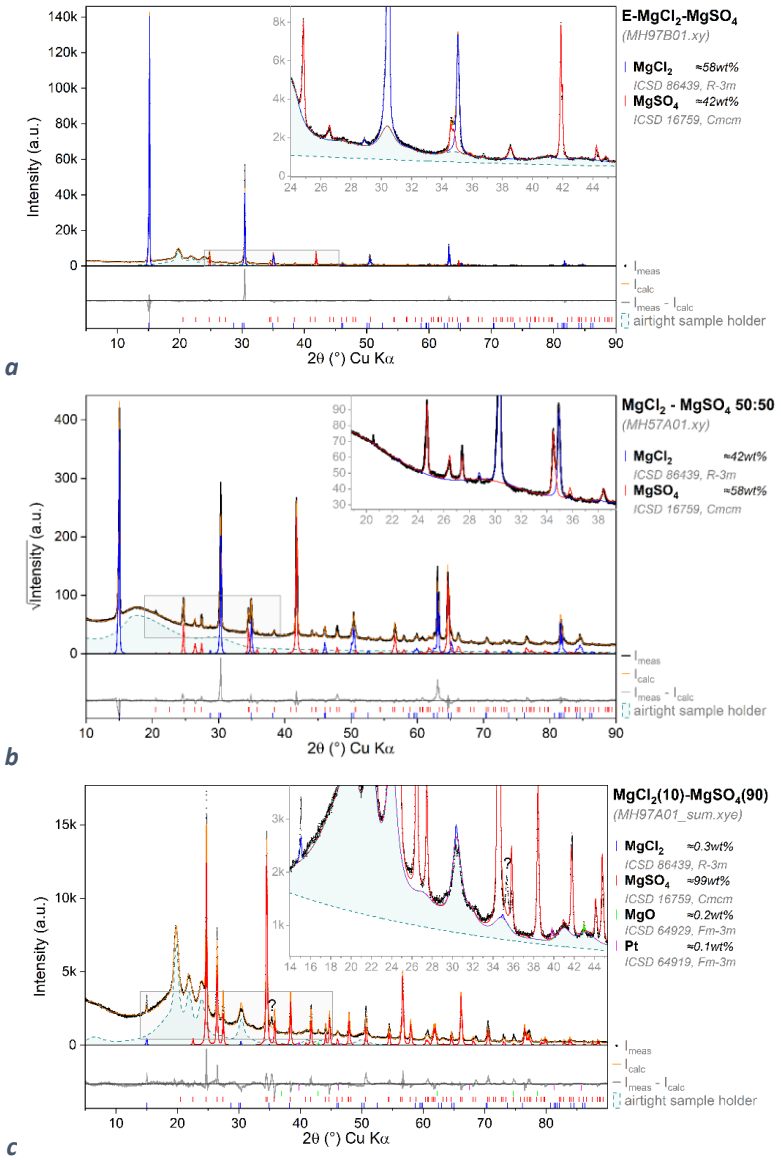


Figure A 14 *X-ray diffractogram of $MgCl_2$-$MgSO_4$ mixtures at room temperature:* ***a*** *$MgCl_2$(72 mol%)-$MgSO_4$(28 mol%);* ***b*** *$MgCl_2$(50 mol%)-$MgSO_4$(50 mol%);* ***c*** *$MgCl_2$(10 mol%)-$MgSO_4$(90 mol%).*

Table A 4 *Lattice parameters of $MgCl_2$(50 mol%)-$MgSO_4$(50 mol%) mixture.*

Phase	ICSD	wt%	SG	a (Å)	b (Å)	c (Å)
$MgCl_2$	86439	42	R-3m	3.642		17.682
$MgSO_4$	16759	58	Cmcm	5.176	7.878	6.503

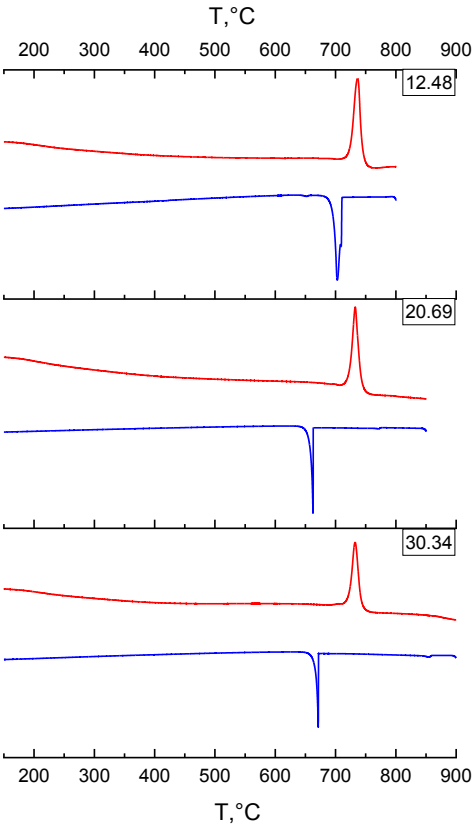


Figure A 15 *DTA curves of $CaCl_2$-$CaSO_4$ mixtures in alumina crucibles, expressed in molar percentage of $CaSO_4$: heating curves (red); cooling curves (blue).*

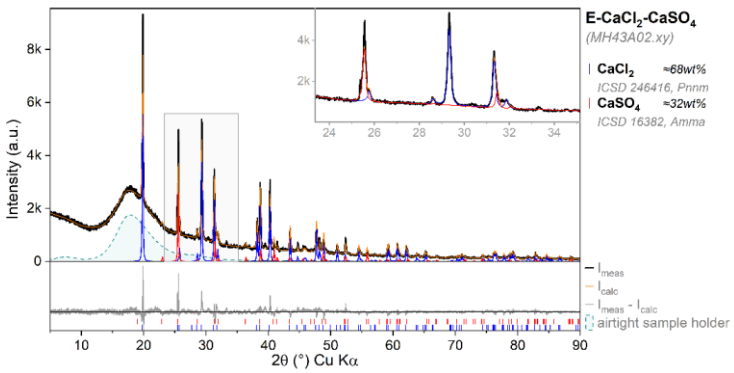


Figure A 16 *X-ray diffractogram of $CaCl_2$(86.01 mol%)-$CaSO_4$(13.99 mol%) mixture at room temperature*

Table A 5 *Lattice parameters of $CaCl_2$(86.01mol%)-$CaSO_4$(13.99mol%) eutectic mixture*

Phase	ICSD	wt%	SG	a (Å)	b (Å)	c (Å)
$CaCl_2$	246416	68	Pnnm	6.439	6.257	4.167
$CaSO_4$	16382	32	Amma	6.999	6.990	6.244

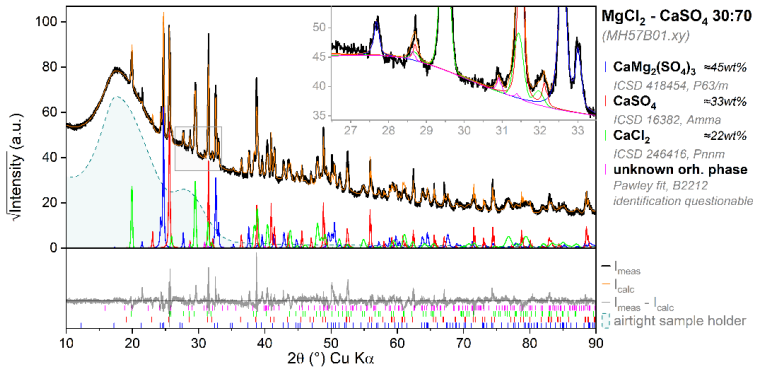


Figure A 17 *X-ray diffractogram of $MgCl_2$(30.80 mol%)-$CaSO_4$(69.20 mol%) mixture at room temperature.*

Table A 6 *Lattice parameters of MgCl2(30.80 mol%)-CaSO4(69.20 mol%) mixture.*

Phase	ICSD	wt%	SG	a (Å)	b (Å)	c (Å)
$CaMg_2(SO_4)_3$	418454	45	P63/m	8.315		7.362
$CaSO_4$	16382	33	Amma	6.992	6.987	6.242
$CaCl_2$	246416	22	Pnnm	6.420	6.246	4.140
Unknown orth. phase	Pawley fit	2	B2212	9.418	7.368	6.910

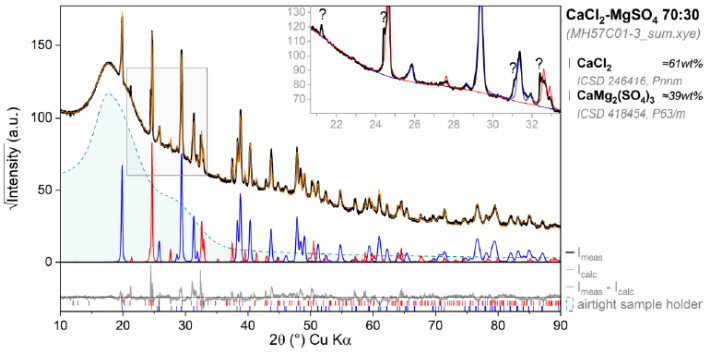


Figure A 18 *X-ray diffractogram of $CaCl_2$(71.70 mol%)-$MgSO_4$(28.30 mol%) mixture at room temperature.*

Table A 7 *Lattice parameters of CaCl2(71.70 mol%)-MgSO4(28.30 mol%).*

Phase	ICSD	wt%	SG	a (Å)	b (Å)	c (Å)
$CaCl_2$	246416	61	Pnnm	6.421	6.235	4.146
$CaMg_2(SO_4)_3$	418454	39	P63/m	8.314		7.322

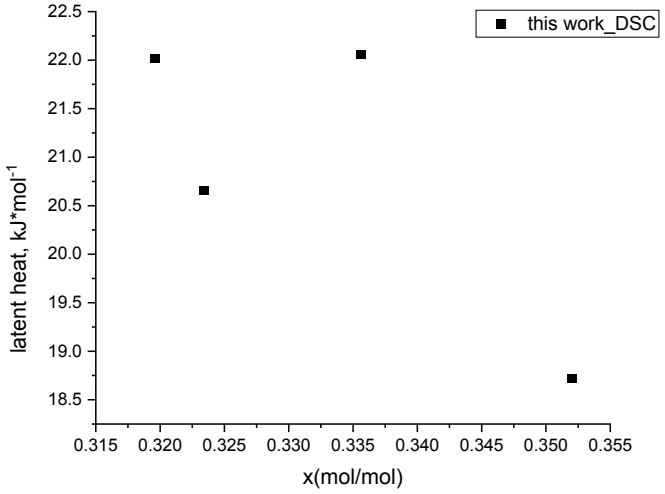


Figure A 19 *Latent heat as a function of composition, derived from cooling DSC curves for NaCl(100-x mol%)-$MgSO_4$(x mol%) mixtures (x= 31.96, 32.34, 33.56, 35.20).*

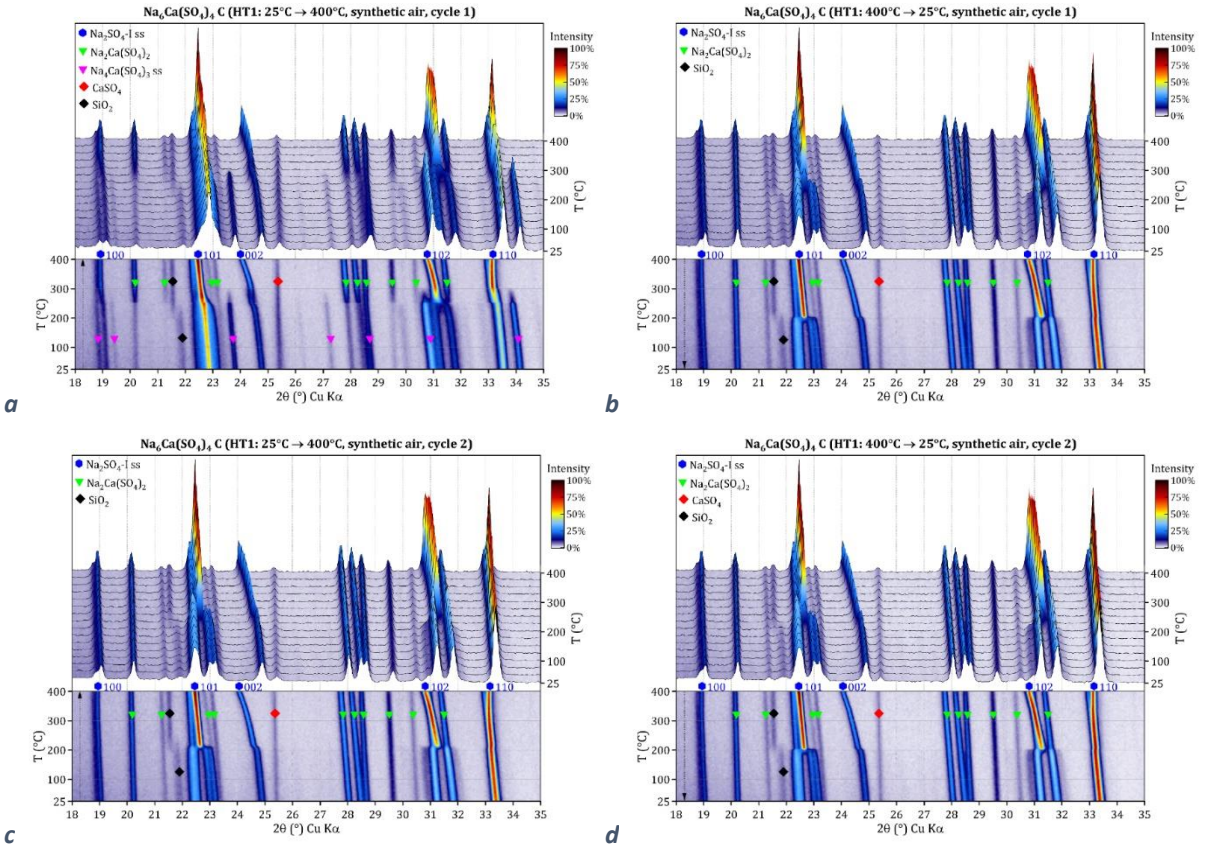


Figure A 20 *High temperature X-ray diffractogram of Na_2SO_4(75 mol%)-$CaSO_4$(25 mol%), i.e., $Na_6Ca(SO_4)_3$ mixture: **a** HT1-cycle 1 from 25 °C to 400 °C; **b** HT1-cycle 1 from 400 °C to 25 °C; **c** HT1-cycle 2 from 25 °C to 400 °C; **d** HT1-cycle 2 from 400 °C to 25 °C.*

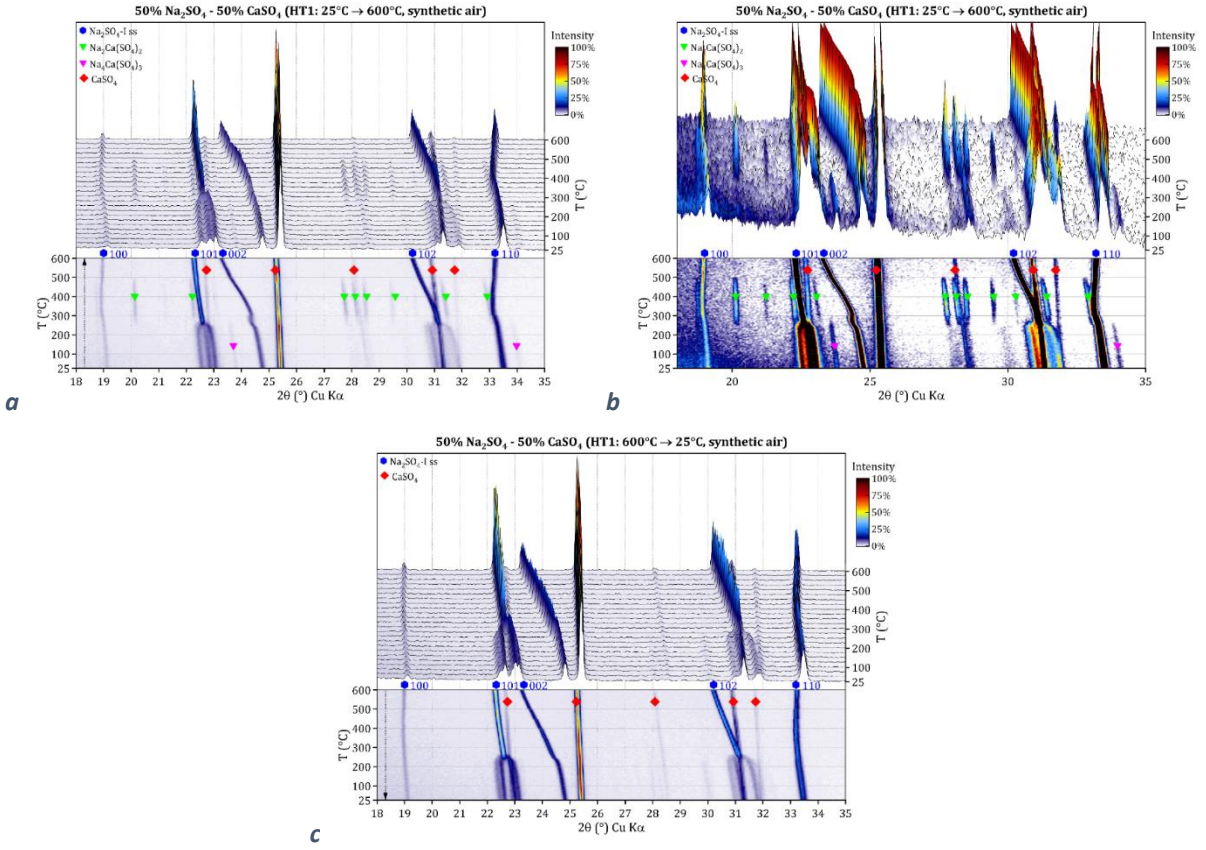


Figure A 21 *High temperature X-ray diffractogram of Na_2SO_4(50 mol%)-$CaSO_4$(50 mol%) mixture:* ***a*** *HT1 from 25 °C to 600 °C;* ***b*** *HT1 from 25 °C to 600 °C (intensity magnified);* ***c*** *HT1 from 600 °C to 25 °C.*

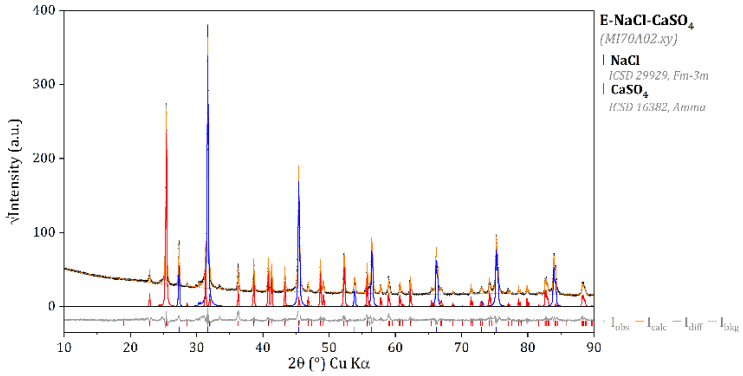


Figure A 22 *X-ray diffractogram of NaCl(83.10 mol%)-$CaSO_4$(16.90 mol%) mixture at room temperature.*

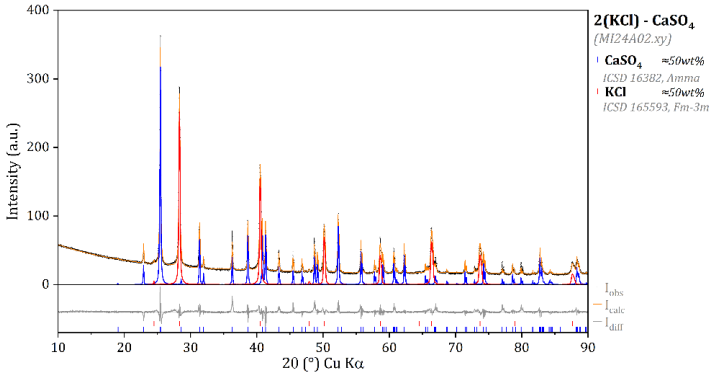


Figure A 23 *X-ray diffractogram of KCl(66.67 mol%)-$CaSO_4$(33.33 mol%) mixture at room temperature.*

Appendix B

Validation of the developed database

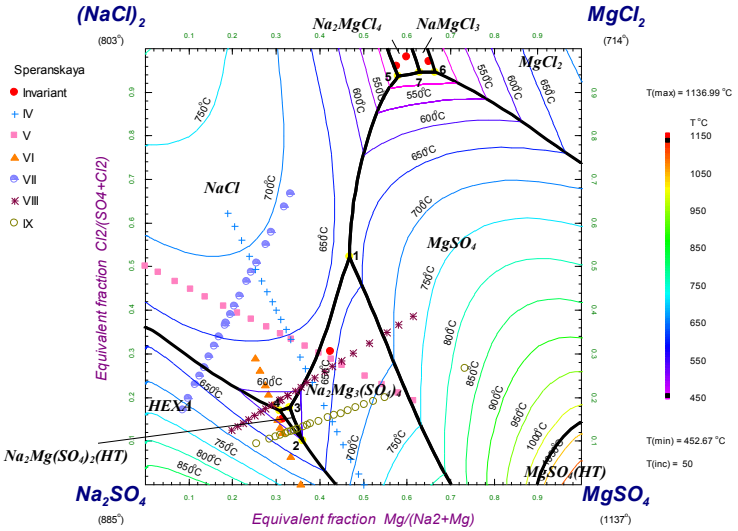
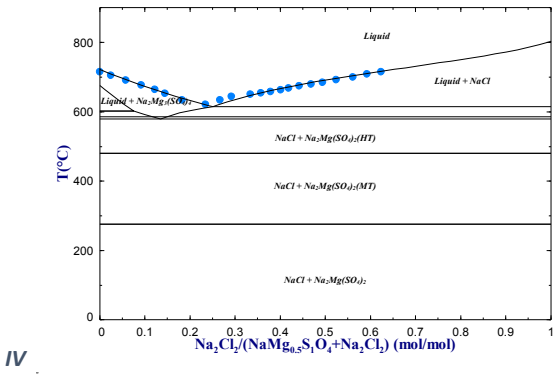
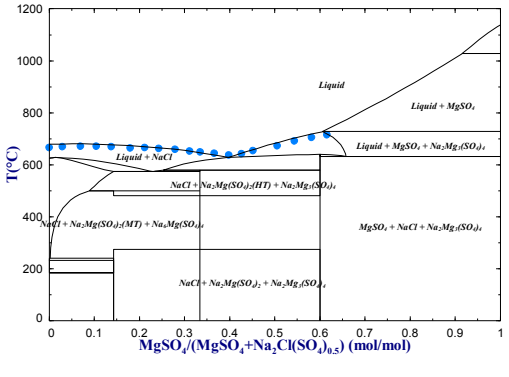


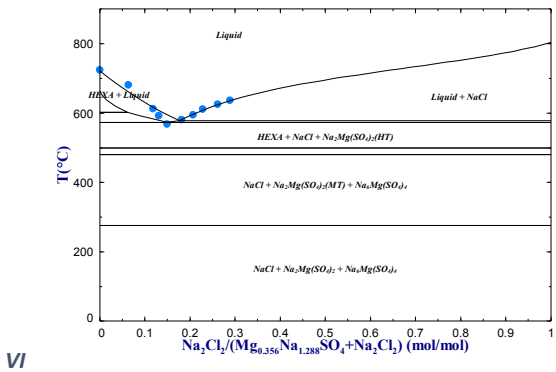
Figure A 24 *Liquidus surface of the reciprocal system Na^+, Mg^{2+} // Cl^-, SO_4^{2-} calculated with the developed database, and experimental data of Speranskaya [63] (sections IV-IX).*



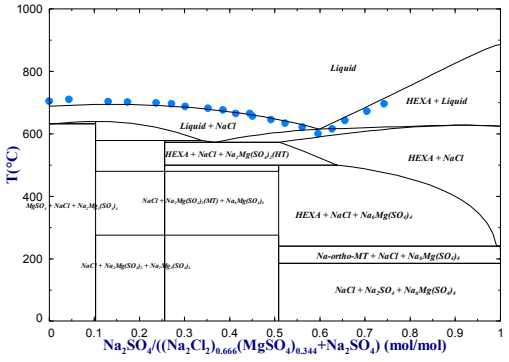
IV



V



VI



VII

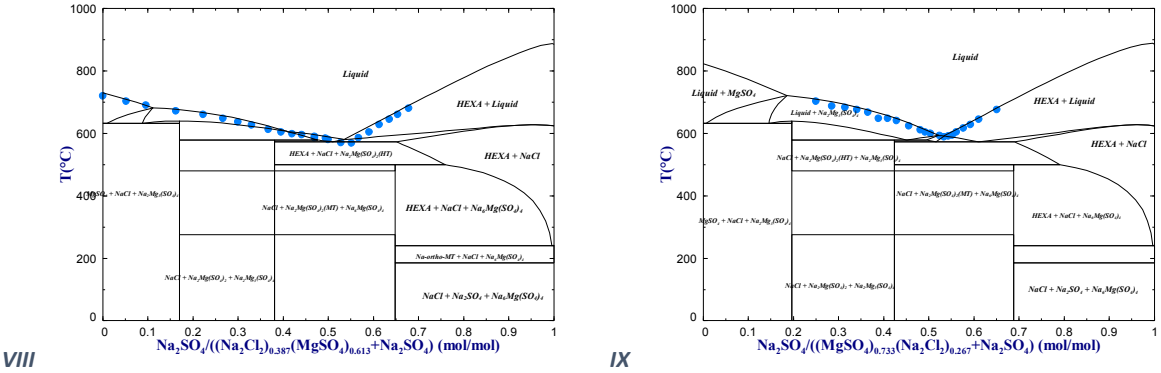


Figure A 25 *Phase diagrams of sections IV-IX in the frame of Na^+, Mg^{2+} // Cl^-, SO_4^{2-} system: comparison of the experimental points from Speranskaya [63] and the developed database. Sections* ***IV,VI****: (1-a)Na_2SO_4(a)$MgSO_4$-Na_2Cl_2 (with a: 0.5, 0.356); Sections* ***V****: (0.5)Na_2Cl_2(0.5)Na_2SO_4-$MgSO_4$; Sections* ***VII-IX****: (1-a-b)Na_2Cl_2(a)Na_2SO_4(b)$MgSO_4$ (with a: 0, 0, 0.25; b: 0.234, 0.631, 0.55).*

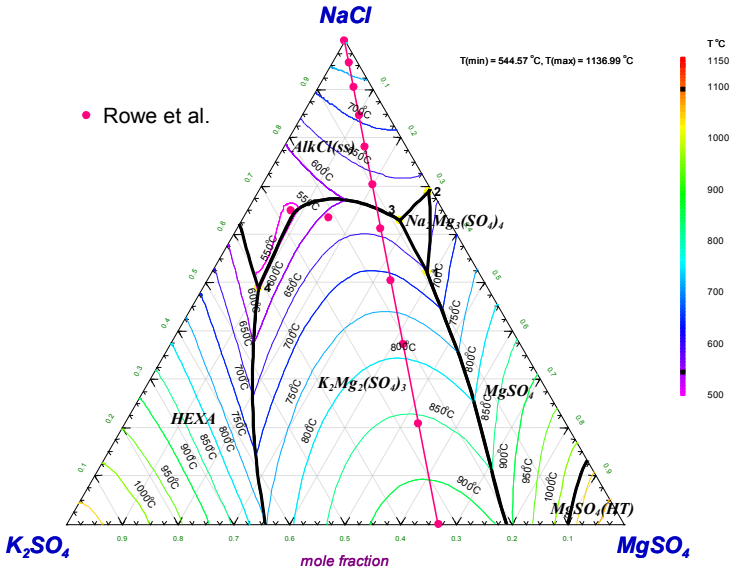


Figure A 26 *Phase diagram of NaCl-K_2SO_4-$MgSO_4$ system from the developed database and experimental points from Rowe et al. [49].*

Table A 8 *Calculated invariant points in the NaCl-K_2SO_4-$MgSO_4$ system.*

	NaCl, mol%	K_2SO_4, mol%	$MgSO_4$, mol%	T, °C	Solid phase
1	52.13	9.16	38.71	651.8	$MgSO_4$, $K_2Mg_2(SO_4)_3$, $Na_2Mg_3(SO_4)_4$
2	68.80	0.54	30.66	629.7	$MgSO_4$, $Na_2Mg_3(SO_4)_4$, AlkCl(ss)
3	62.88	8.70	28.42	600.6	$K_2Mg_2(SO_4)_3$, $Na_2Mg_3(SO_4)_4$, AlkCl(ss)
4	48.87	41.07	10.04	545.6	$K_2Mg_2(SO_4)_3$, AlkCl(ss), HEXA

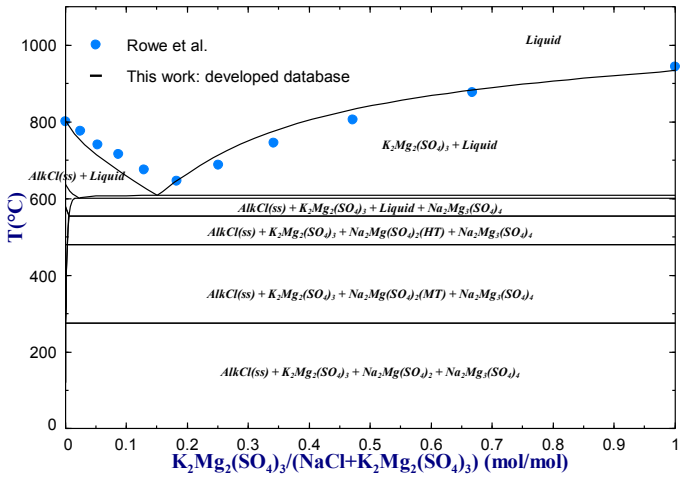


Figure A 27 *Phase diagram of NaCl-$K_2Mg_2(SO_4)_3$ system from the developed database and experimental points from Rowe et al. [49].*

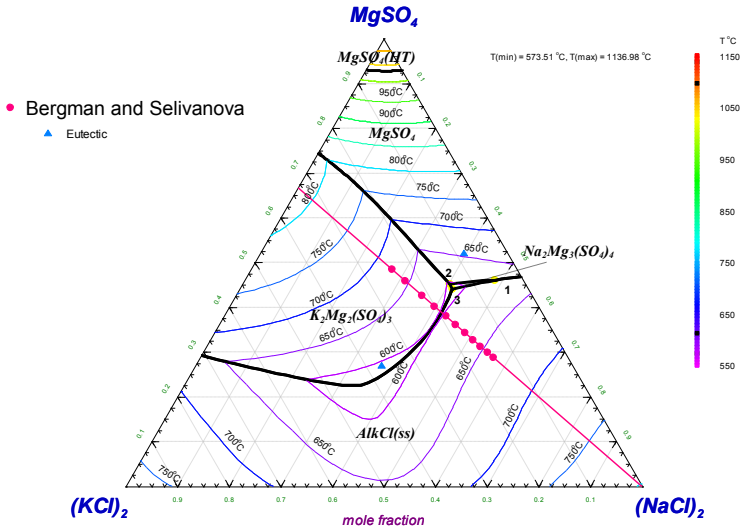


Figure A 28 *Phase diagram of $(NaCl)_2$-$(KCl)_2$-$MgSO_4$ system from the developed database and experimental points from Bergman and Selivanova (1938) in Voskresenskaya [133].*

Table A 9 *Calculated and experimental invariant points in the $(NaCl)_2$-$(KCl)_2$-$MgSO_4$ system.*

	$(NaCl)_2$, mol%	$(KCl)_2$, mol%	$MgSO_4$, mol%	T, °C	Solid phase	Ref.
1	48.56	5.40	46.04	617.9	$MgSO_4$, $Na_2Mg_3(SO_4)_4$, AlkCl(ss)	[a]
2	40.11	14.66	45.23	595.8	$K_2Mg_2(SO_4)_3$, $MgSO_4$, $Na_2Mg_3(SO_4)_4$	[a]
3	41.23	14.66	44.11	590.9	$K_2Mg_2(SO_4)_3$, $Na_2Mg_3(SO_4)_4$, AlkCl(ss)	[a]
1	39.5	8.5	52	624	NaCl, $MgSO_4$, KCl·$MgSO_4$	[133]
2	36	37	27	616	KCl, NaCl, KCl·$MgSO_4$	[133]

[a] this work

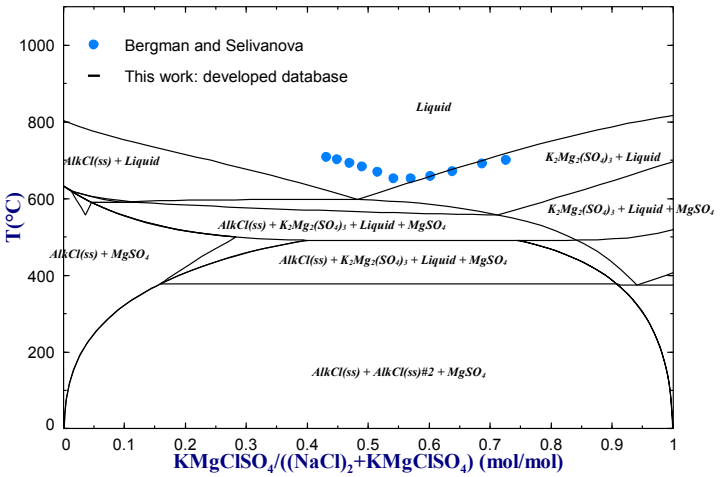


Figure A 29 *Phase diagram of $(NaCl)_2$-KCl·$MgSO_4$ system from the developed database and experimental points from Bergman and Selivanova (1938) in Voskresenskaya [133].*

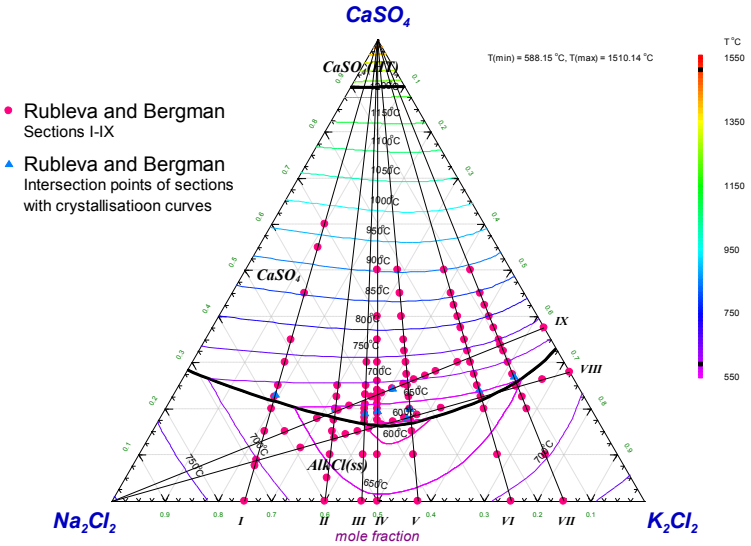


Figure A 30 *Phase diagram of $(NaCl)_2$-$(KCl)_2$-$CaSO_4$ system from the developed database and experimental points of sections I-IX from Rubleva and Bergman [135].*

Table A 10 *Calculated temperature minimum in the Na_2Cl_2-K_2Cl_2-$CaSO_4$ system.*

	Na_2Cl_2, mol%	K_2Cl_2, mol%	$CaSO_4$, mol%	T, °C
1	39.34	44.51	16.15	588.2

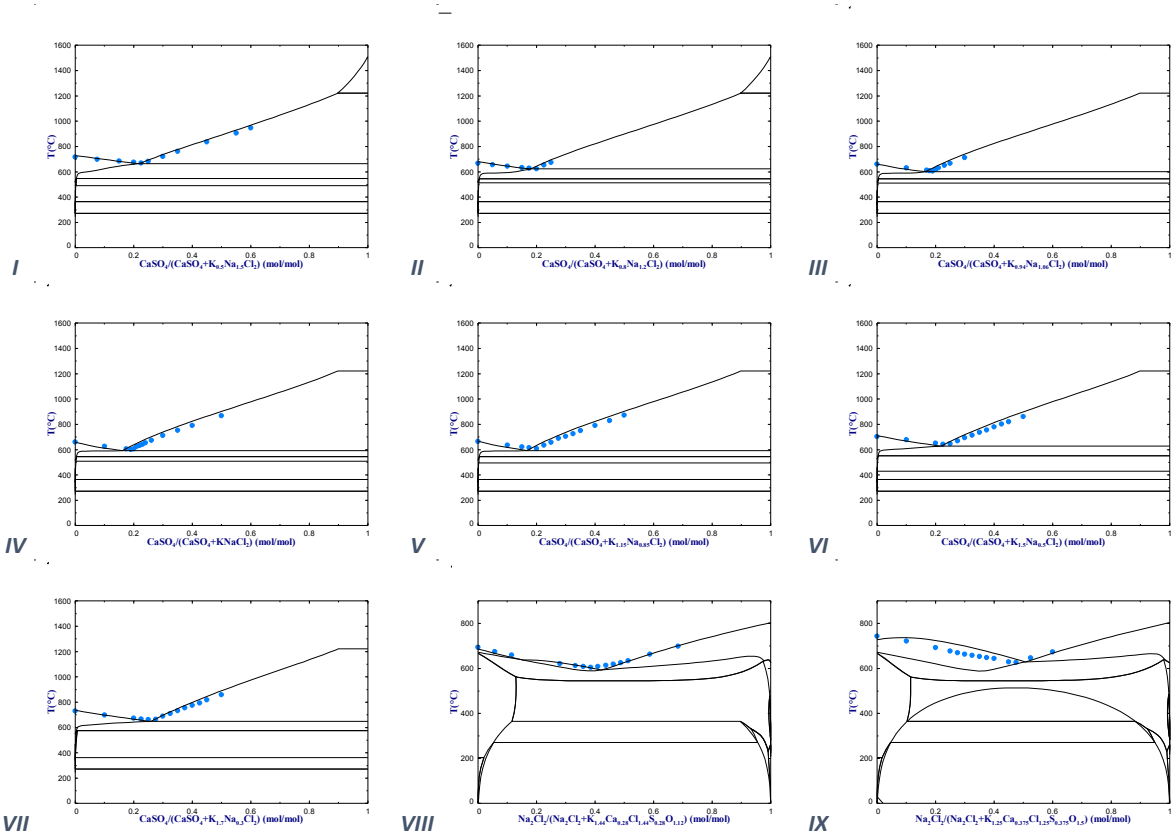


Figure A 31 *Phase diagrams of sections I-IX in the frame of $(NaCl)_2$-$(KCl)_2$-$CaSO_4$ system: comparison of the experimental points from Rubleva and Bergman [135] and the developed database. Sections* ***I-VII****: (100-a)K_2Cl_2(a)Na_2Cl_2-$CaSO_4$ (with a: 75, 60, 53, 50, 42.5, 25, 15 mol%); Sections* ***VIII-IX****: (100-a)$CaSO_4$(a)K_2Cl_2-Na_2Cl_2 (with a: 72, 62.5 mol%).*

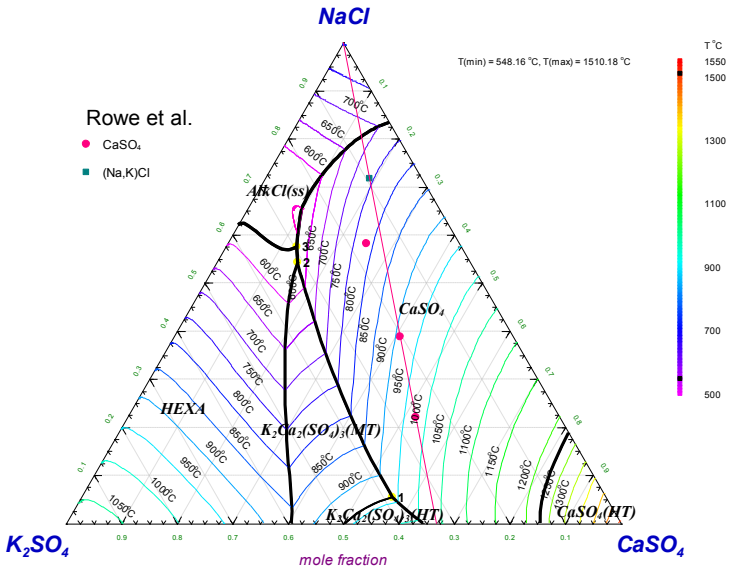


Figure A 32 *Phase diagram of NaCl-K_2SO_4-$CaSO_4$ system from the developed database and experimental points from Rowe et al. [49].*

Table A 11 *Calculated invariant points in the NaCl-K_2SO_4-$CaSO_4$ system.*

	NaCl, mol%	K_2SO_4, mol%	$CaSO_4$, mol%	T, °C	Solid phase
1	5.40	38.44	56.16	936.9	$CaSO_4$, $K_2Ca_2(SO_4)_3$(MT), $K_2Ca_2(SO_4)_3$(HT)
2	54.26	31.10	14.64	563.0	$CaSO_4$, $K_2Ca_2(SO_4)_3$(MT), HEXA
3	57.61	29.58	12.81	551.9	AlkCl(ss), $CaSO_4$, HEXA

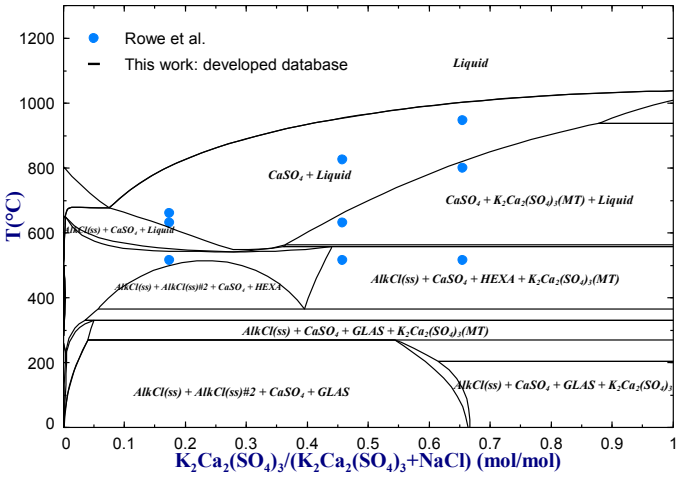


Figure A 33 *Phase diagram of NaCl-$K_2Ca_2(SO_4)_3$ system from the developed database and experimental points from Rowe et al. [49].*

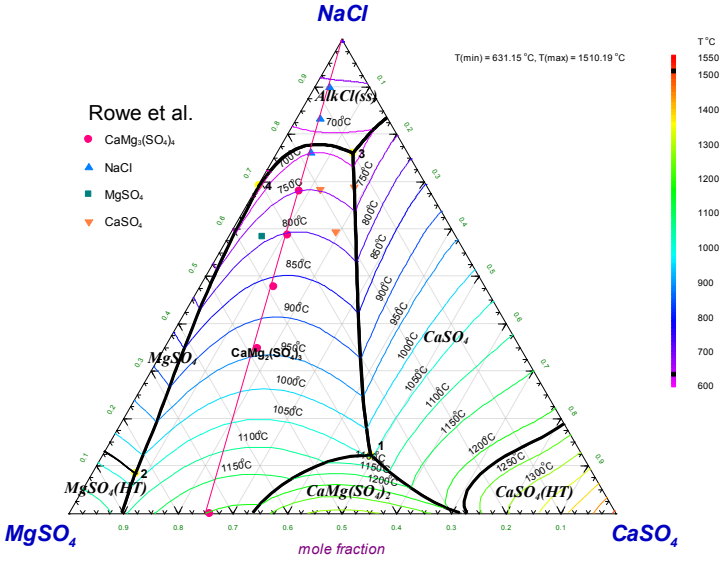


Figure A 34 *Phase diagram of NaCl-$MgSO_4$-$CaSO_4$ system from the developed database and experimental points from Rowe et al. [49].*

Table A 12 *Calculated invariant points in the NaCl-$MgSO_4$-$CaSO_4$ system.*

	NaCl, mol%	$MgSO_4$, mol%	$CaSO_4$, mol%	T, °C	Solid phase
1	12.18	38.61	49.21	1044.2	$CaSO_4$, $CaMg(SO_4)_2$, $CaMg_2(SO_4)_3$
2	8.38	83.63	7.99	1027.2	$MgSO_4$(LT), $MgSO_4$(HT), $CaMg_2(SO_4)_3$
3	75.95	10.05	14.00	681.7	AlkCl(ss), $CaSO_4$, $CaMg_2(SO_4)_3$
4	69.08	30.57	0.35	631.2	AlkCl(ss), $MgSO_4$, $CaMg_2(SO_4)_3$

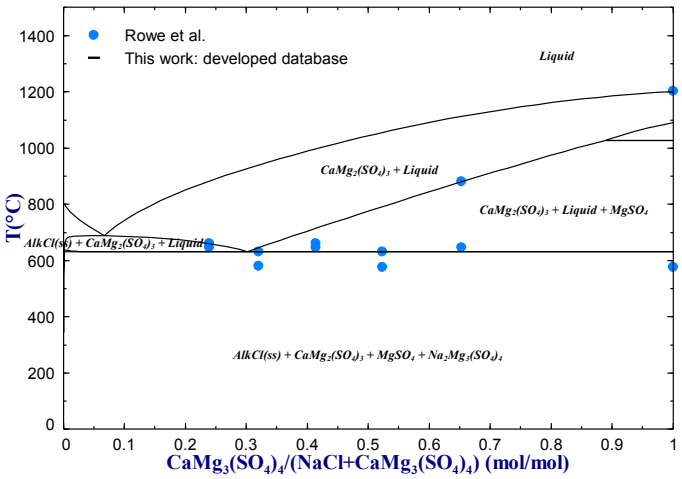


Figure A 35 *Phase diagram of NaCl-$CaMg_3(SO_4)_4$ system from the developed database and experimental points from Rowe et al. [49].*

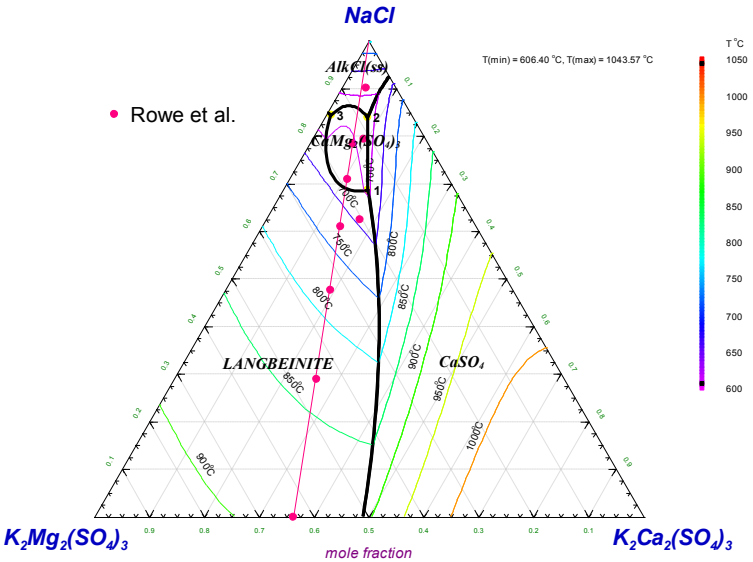


Figure A 36 *Phase diagram of NaCl-$K_2Mg_2(SO_4)_3$-$K_2Ca_2(SO_4)_3$ system from the developed database and experimental points from Rowe et al. [49].*

Table A 13 *Calculated invariant points in the NaCl-$K_2Mg_2(SO_4)_3$-$K_2Ca_2(SO_4)_3$ system.*

	NaCl, mol%	$K_2Mg_2(SO_4)_3$, mol%	$K_2Ca_2(SO_4)_3$, mol%	T, °C	Solid phase
1	68.71	15.79	15.49	641.4	$CaSO_4$, $CaMg_2(SO_4)_3$, LANGBEINITE
2	83.89	8.26	7.86	618.1	$CaSO_4$, $CaMg_2(SO_4)_3$, AlkCl(ss)
3	84.42	14.67	0.91	606.4	$CaMg_2(SO_4)_3$, AlkCl(ss), LANGBEINITE

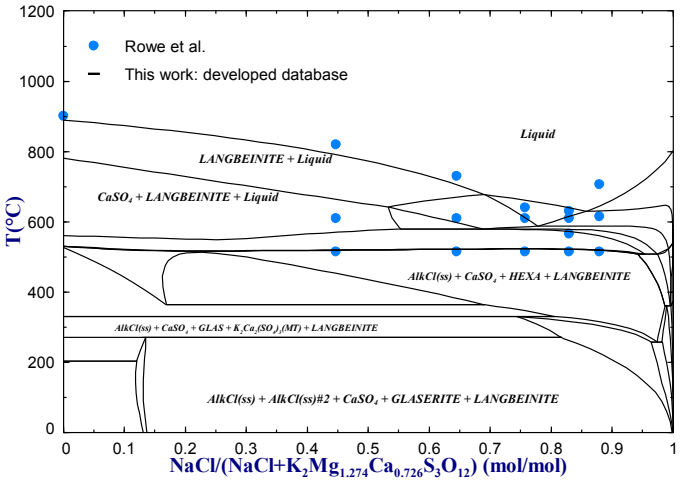


Figure A 37 *Phase diagram of NaCl-(0.637)$K_2Mg_2(SO_4)_3$(0.363)$K_2Ca_2(SO_4)_3$ system from the developed database and experimental points from Rowe et al. [49].*

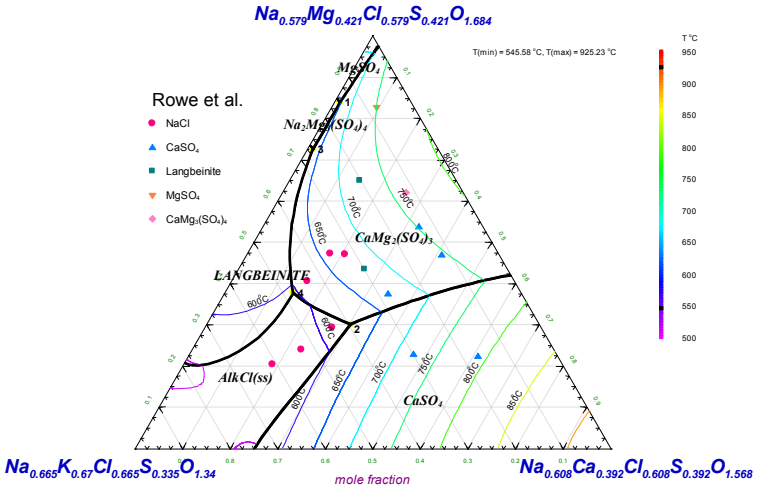


Figure A 38 *Phase diagram of 40-percent NaCl plane in the NaCl-K_2SO_4-$MgSO_4$-$CaSO_4$ system from the developed database and experimental points from Rowe et al. [49].*